A Non-destructive Damage Detection Method for Reinforced Concrete Structures Based on Modal Strain Energy

by

Yujue Wang

A thesis submitted in partial fulfilment
of the requirements for the degree of
Doctor of Philosophy

Faculty of Engineering and Information Technology
University of Technology, Sydney

February 2010

CERTIFICATE OF AUTHORSHIP/ORIGINALITY

I certify that the work in this thesis has not previously been submitted for a degree nor has it been submitted as part of requirement for a degree except as fully acknowledged within the text.

I also certify that the thesis has been written by me. Any help that I have received in my research work and preparation of the thesis itself has been acknowledged. In addition, I certify that all information sources and literature used are indicated in the thesis.

Signature of Candidate

_____

(Yujue Wang)

Sydney, February 2010

ABSTRACT

In recent years, much research and development has been carried out on the use of vibration characteristics to detect structural damage in various types of structures. Being a type of the widely developed methods, the vibrations based damage detection methods, in particular modal based methods, are found to be promising in assessing the "health" condition of a structure in terms of locating and quantifying damage.

However, despite of advances in vibration based damage detection methods of numerical simulations and some laboratory experimental implementations, very limited progress has been reported in field applications. The main obstacles in field applications are associated with the uncertainties, such as measurement noise, processing errors and error due to limited measurement points. In addition, the complexity of civil structures and/or materials further undermines the effectiveness and reliability of developed damage detection methods. This is evident by the fact that much less research and development has been reported for timber or reinforced concrete structures in terms of damage detection. It is therefore necessary to investigate effects of measurement noise, processing errors and errors due to limited measurement points on damage detection and develop a new robust and reliable method to locate and quantify damage in reinforced concrete structures.

The aim of this PhD research work is to formulate a new non-destructive modal based damage detection method that is robust and reliable to evaluate the "state of health" for a reinforced concrete (RC) structure by investigating its capability to locate and to estimate severity of damage based on modal strain energy of a RC beam before and after damage. The new method is based on combination of mode shapes and mode shape curvatures from the undamaged and damaged states making the method more robust and less vulnerable to noise compared with other existing modal based damage detection methods that are either based only on mode shape or mode shape curvature.

Numerical studies that utilises finite element (FE) models of reinforced concrete beams were employed to investigate the effectiveness and the reliability of the proposed damage detection method. The FE model of a reinforced concrete beam was created

incorporating laboratory tested material properties for concrete and steel reinforcement and then validated both statically and dynamically. Damage scenarios that are commonly found in reinforced concrete structures (i.e. cracks and honeycomb) were numerically simulated. Using 41-node mode shape data, the damage detection results without noise pollution demonstrate that the proposed damage detection method is capable of locating the damage accurately. To evaluate impact of noise on the proposed new damage detection method, various magnitudes of white Gaussian noise were added to the time response data obtained from FE transient analysis. The noise-added data were then processed using the virtual experimental modal analysis to obtain the modal parameters with the same number of measurement points as experiments (9-nodes). The damage detection results under influence of noise illustrate that the proposed method is also able to identify the location of damage, although it occasionally generated false positives. In terms of damage severity estimation, the proposed damage detection method was able to estimate the severity of damage with reasonable accuracy without noise pollution. However, when noise is present, the proposed method is less reliable in estimating the severity of damage.

In this study, comparison has been made between the results of the proposed method and two existing popular methods with and without the noise influence. The comparison results prove that the proposed method is more robust and reliable than the two other methods in identifying the location of damage. An improvement to the proposed damage detection method (DI-NI) was introduced to enhance its robustness and reliability. The improved method was applied to detect damage in a number of numerical cases, both with and without noise present. The results show that the improved method does not significantly improve the accuracy of damage detection in the absence of noise, since the original results identifying the location of damage are already accurate. However, when noise is present, the results illustrate that the method is able to significantly improve reliability of damage detection, i.e. false positives are reduced, and location of damage is identified more precisely.

The experimental verification of the proposed damage detection methods for reinforced concrete structures was also performed on five reinforced concrete beams in the UTS Structures Laboratory. The experimental modal parameters such as natural frequencies and mode shapes were obtained by modal testing and experimental modal analysis. The

Cubic Spline interpolation technique was employed to reconstruct a finer mode shapes (9-to-41-nodes) from the measured data (9-node mode shape) in order to enhance the capability of the damage detection method to evaluate damage. Based on the findings of the numerical work, the improved version of the proposed damage detection method was utilised to detect damage using the experimental data. From the measured natural frequencies, it is observed that the percentage of drop in frequency for all modes is non-linearly changing as the inflicted damage becomes more severe but there is no clear evidence that frequency change can be clearly correlated to damage severity. For damage localisation, the improved method shows that it is capable of locating the damage, even though some false positives may be generated. Comparing to the two existing popular damage detection methods, the improved method is more accurate than the two other methods in identifying the locating damage.

In summary, a new modal strain energy based damage detection method has been successfully developed to overcome shortcomings of existing methods. The numerical and experimental evaluation and verification have shown that the new method, especially the improved version of the method, is reliable and effective in locating single and multiple damage scenarios. The new method is also successful in estimating severity of damage to a certain extent.

Acknowledgement

This PhD project could not have been possible without the assistance, understanding and guidance rendered by numerous people throughout the project. The author would very much like to express his appreciation and gratitude to his supervisors, Associate Professor Jianchun Li, and Professor Bijan Samali, for their support and guidance throughout this work and for their patience with proof-reading this thesis. The author would also like to thank Dr. Fook Choon Choi, who had given the author invaluable advice and assistance in writing this thesis. Utmost gratitude is also due to Dr. Ravi Ravindrarajah, who helped the author for various aspects at different stages of the project. The author gratefully acknowledges the financial assistance provided by the University of Technology, Sydney (International Research Scholarship) and Centre for Built Infrastructure Research (CBIR) of the Faculty of Engineering and Information Technology, UTS.

Furthermore, the author would like to thank staff of the UTS Structures Laboratory for their help in the experimental work. The author also feels a deep sense of gratitude to all the academic and non-academic staff in the Faculty of Engineering and Information Technology for the help rendered. To friends at UTS, warm and special thanks must go to Yukari, Janitha, Peter, Fabil, Rong, Nikhil, Ulrike, Zelin, Amir, Yancheng, Othman, Chinu, Rijun, Zhinous, Debby, Chris and others who shared their time and friendship with the author and rendered invaluable help.

Finally, the author wishes to thank his parents for keeping supporting him for many years. The author would like to acknowledge Charlie Sheard for his reviews and comments and Gill Hewitt for her English classes. Without their endless help, support and love the completion of this thesis would not have been possible.

List of Publications Based on This Research

Refereed Journal Articles

1. Wang, Y., Li, J. & Samali, B. (2010), 'Modal Strain Energy Based Damage Detection Method for Reinforced Concrete Beams', *In Preparation.*
2. Wang, Y., Li, J. & Samali, B. (2010), 'Improved Damage Detection Method Based on Modal Strain Energy for Reinforced Concrete Beams', *In Preparation.*

Refereed Conference Papers

1. Wang, Y., Li, J., Samali, B. & Ravindrarajah, R. (2008), 'Non-destructive damage detection in reinforced concrete beams based on modal strain energy', *Proceedings of Australasian structural Engineering Conference,* 26-27 June 2008, The Sebel Albert Park, Melbourne Australia. Paper number: 102.
2. Wang, Y., Li, J., Samali, B. & Ravindrarajah, R. (2008), 'A New Damage Detection Method for Reinforced Concrete Beams Based on Modal Strain Energy', *Proceedings of the 9th International Conference on Motion and Vibration Control*, 15-18 September 2008, Technische Universitaet Muenchen, Munich, Germany.
3. Wang, Y., Li, J., Samali, B. & Choi, F. C. (2008) 'A New Non-destructive Damage Detection Method for Reinforced Concrete Beams Based on Modal Strain Energy', *Proceedings of the 20th Australasian Conference on the Mechanics of Structures and Materials*, 2-5 December 2008, Toowoomba, Australia. pp. 773-779.

LIST OF CONTENTS

LIST OF FIGURES

LIST OF TABLES

List of Notations

Δ	change in the flexibility matrix
ρ	density
$\mu_{\beta j}$	mean of β_j values for all j-th elements
$\sigma_{\beta j}$	standard deviation of β_j values for all j-th elements
λ_i	eigenvalue for mode i of undamaged beam
λ_i^*	eigenvalue for mode i of damaged beam
ω	natural frequency of system
ω_{Exp}	natural frequency of experimental result
ω_{FE}	natural frequency of finite element result
ϕ	mode shape vector
ϕ_i	mode shape or eigenvector of mode i
ϕ_{ij}	mode shape vector of the i^{th} mode and j^{th} element of undamaged beam
ϕ_{ij}^*	mode shape vector of the i^{th} mode and j^{th} element of damaged beam
ϕ_{ij}''	mode curvature vector of the i^{th} mode and j^{th} element of undamaged beam
$\phi_{ij}^{*''}$	mode curvature vector of the i^{th} mode and j^{th} element of damaged beam
$\{\hat{\phi}\}_{ij}''$	normalised mode curvature vector of the i^{th} mode and j^{th} element of undamaged beam
$\{\hat{\phi}^*\}_{ij}''$	normalised mode curvature vector of the i^{th} mode and j^{th} element of damaged beam
δ	deflection of the reinforced concrete beam
α_j	damage severity estimator
ε_{cu}	ultimate strain of concrete
ε_{tu}	ultimate strain of reinforcing bars
ε_{ts}	tensile strain in the analysis step
*	denoting damaged case
1L3M5S7L	cumulative damage scenario of light damage at 1/8 span,

	medium damage at 3/8 span, severe damage at 5/8 span, and light damage at 7/8 span
3-D	three-dimensional
41-nodes	41 measuring points taken from the MAF
9-nodes	9 measuring points taken from the VEMA
9-to-41-nodes	Reconstruct 9-nodes to 41-nodes using the Cubic Spine technique
ANN	artificial neural networks
C	system damping matrix
CFRP	carbon fibre reinforced polymer
CMSE	cross-modal strain energy
COMAC	coordinate modal assurance criterion
CWT	continuous wavelet transform
DD	damage detection
DDF	Digital Damage Fingerprints
$Denom_{ij}$	denominator of β_{ij}
$D.I._{compressive}$	compressive damage index of concrete
$D.I._{tensile}$	tensile damage index of concrete
DI-A	results of Damage Index A
DI-C	results of Damage Index C
DI-N	results of the proposed method
DI-NI	results of the improved damage detection method
DI-NO	results of the original damage detection method
DLV	damage locating vector
DOF	degree of freedom
DPD	Damage Parameters Database
DRC	damaged reinforced-concrete
DSD	dynamic steepest descent
E_c	modulus of elasticity of concrete
E_j	j^{th} equivalent elemental modulus of elasticity of undamaged beam
E_j^*	j^{th} equivalent elemental modulus of elasticity of damaged beam

EI	flexural stiffness
EMA	experimental modal analysis
EMD	empirical mode decomposition
E_s	Modulus of elasticity of reinforcement
EXPASS	Expansion Pass
F	system force vector
$f_c^{'}$	compressive strength of concrete
f_{ct}	tensile strength of concrete
FE	finite element
FEA	finite element analysis
FEM	finite element model
FFT	fast Fourier transform
FDPI	Frequency Direct Parameter Identification
FRF	frequency response function
FSD	fussy steepest descent
f_y	yield strength of reinforcement
GFI	global flexibility index
HB	honeycomb damage in the bottom of RC beam
HHT	Hilbert-Huang transform
HT	honeycomb damage at the top of RC beam
I	moment of inertia
IMFs	intrinsic mode functions
ISPPR	Intelligent Signal Processing and Pattern Recognition
K	system stiffness matrix
K_j	elemental stiffness matrix for j^{th} element
K_{jo}	baseline stiffness contribution of the same element due to undamaged geometry of structure
K_{jo}^{*}	baseline stiffness contribution of the same element due to damaged geometry of structure
L	lower triangular matrix
L (for damage)	light damage
LVDT	linear variable differential transformer
M	system mass matrix

M (for damage)	medium damage
M_j	mass of j^{th} element of undamaged beam
M_j^*	mass of j^{th} element of damaged beam
MAC	modal assurance criterion
MACerror	MAC error between FE and experimental models
MAF	Modal Analysis Function
MDI	modified damage index
MIMO	multiple-input-multiple-output
MLP	multi-layer perceptron
MSE	modal strain energy
MSE_{ij}	modal Strain Energy for the Euler-Bernoulli beam model of the j^{th} element of i^{th} mode before the occurrence of damage
MSE_{ij}^*	modal Strain Energy for the Euler-Bernoulli beam model of the j^{th} element of i^{th} mode after the occurrence of damage
MSEC	modal strain energy change
MSECR	modal strain energy change ratio
N_{2fc}	number of complete cycles to failure for concrete
N_{2fr}	number of complete cycles to failure for reinforcing bars
NDE	non-destructive evaluation
NDE	non-destructive testing
NFerror	natural frequency difference between FE and experimental models
Num_{ij}	numerator of β_{ij}
OF	objective function
P	Static load on reinforced concrete beams
RC	reinforced concrete
S (for damage)	severe damage
SDOF	single degree of freedom
SHM	structural health monitoring
SIMO	single-input-multiple-output
SISO	single-input-single-output

SWT	stationary wavelet transform
TSD	tunable steepest descent
VEMA	Virtual Experimental Modal Analysis
Z	system displacement vector
$\dot{Z}$	system velocity vector
$\ddot{Z}$	system acceleration vector
Z_j	damage location index

CHAPTER 1

OVERVIEW

1.1 Background

Reinforced concrete construction was introduced into Australia in the late nineteenth century. The first reinforced concrete structure built in Australia was the Johnstones Creek and White Creek Sewer Aqueduct built in Annandale in 1897 (Heritage Council of New South Wales 2009). Afterwards, they were taken up quickly and nowadays reinforced concrete structures are widely used in Australia.

Even though reinforced concrete structures are relatively durable and robust, they can be severely weakened by poor maintenance or a very harsh environment. A significant number of reinforced concrete structures in Australia are old, subject to increasing traffic loads and intensity, and some with functional deficiency. For example, it was reported that West Gate Bridge, the third longest in Australia, was initially designed to carry loads of up to 25 tonnes but now carries B-double trucks weighing up to 68 tonnes. The bridge was built to carry 40,000 vehicles per day, but volumes are now more than four times of the original amount, approximately 160,000 vehicles on an average day. Therefore, it was reported in 2007 that the Victorian Government was planning a $240 million project to identify and eliminate structural weaknesses in the bridge, with specific concerns including crash barriers, cracking, corrosion and potential buckling (Heinrichs 2007).

In order to strengthen or rehabilitate damaged reinforced concrete structures, identification of the nature and extent of damage, careful analysis of the remaining capacity of the structure, and then selection of the most efficient solution for treatment of the structure are essential. In this process, the critical phase is to reliably and robustly locate and quantify damage in an impaired structure at the earliest possible stage.

In the past, numerous damage detection methods, termed “local damage detection methods”, have been developed and commonly employed. All of these experimental

techniques require that the location of the damage is known a priori, and that the section of the structure being examined is readily accessible. In order to overcome the limitations of local damage detection methods, a large number of "global damage detection methods" have been rapidly developed in recent times.

In the light of current developments in global damage detection methods, the vibration-based methods have become the most promising non-destructive damage detection technique (Cao et al. 2006). Among the vibration-based methods, modal-based damage detection methods, taking advantage of changes in the modal parameters of structures for damage detection, have received considerable attention in civil engineering applications (Kim et al 2006). To date, an increasing quantity of research work has indicated that, derivatives or combination of derivatives (such as modal strain energy) of modal parameters are sensitive quantities to structural damage (Zhu and Xu 2005). Modal strain energy, based on mode shape curvature has been used to detect damage location and to estimate damage severity in field applications with certain degree of success.

Modal strain energy based damage detection methods were initially proposed by Kim & Stubbs (1995) and Doebling et al (1997) and later improved in underlying assumptions and formulation (Kim & Stubbs 2002). Shi et al. (1998) presented another method based on modal strain energy change in order to locate damage in structures. The authors further developed the method in 2000 (Shi et al. 2000) and in 2002 (Shi et al. 2002). Li et al. (2006) presented a modal strain energy decomposition method for damage detection in their research. In the same year, cross-modal strain energy method was presented (Hu et al 2006a). All these modal strain energy based damage detection methods will be reviewed in Chapter 2.

It should be noted that, despite the fact that much research work has been published on damage detection methods, not much research work has been reported on methods applicable to reinforced concrete structures. The slow development of damage detection methodology for reinforced concrete structures is due to the fact that reinforced concrete, unlike metals, is a non homogeneous material with varying composition, raw materials and complex binding behaviours between different materials. Therefore, many

damage detection methods that appear to work well on other structures might perform poorly when being applied to reinforced concrete structures.

Furthermore, in real field applications, there are many practical issues associated with the performance of damage detection including environmental influences, operational influences, measurement noise, processing error and limited number of sensors. In particular, modal based damage detection methods rely on Experimental Modal Analysis (EMA) to produce modal parameters for damage detection. The results of modal parameters estimation are heavily affected by imperfections or errors, and environmental and operational conditions during such process. For example, the changes in modal properties resulting from changes in environmental conditions can be as significant as the changes in these properties caused by damage. In addition, due to the limitation of the number of measurement points (sensors) the reconstruction of mode shapes is necessary for conducting damage detection. Reconstruction of mode shape may produce errors especially under noise influence. It is also worthwhile to point out that most sensitive damage indicators, such as mode shape curvatures, is also sensitive to these disturbances. This is part of the reason that most damage detection methods perform poorly in field applications. It is, therefore, important to develop a more reliable and robust damage detection method that is potentially suitable for field application.

In this thesis, a new non-destructive modal based damage detection method is formulated and proven to be robust and reliable by investigating its capability to locate and to estimate severity of damage based on modal strain energy of a RC beam. The new method is based on combination of mode shapes and mode shape curvatures from the undamaged and damaged states making the method more robust and less vulnerable to noise compared with other existing modal based damage detection methods that are either based only on mode shape or mode shape curvature.

1.2 Objective of the Study

The main objective of this thesis is to develop a reliable and robust modal strain energy based damage detection method, to identify location and to estimate severity of damage in reinforced concrete structures. The details of the research work are:

1. To develop and formulate a new modal strain energy based method for damage detection which is more robust and reliable than existing methods;
2. To perform property tests in order to provide the material property parameters for modelling of reinforced concrete beams and to perform static loading tests and dynamic tests on a reinforced concrete beam in order to validate the finite element modelling of the reinforced concrete beams;
3. To numerically evaluate and verify the performance of the developed damage detection method for detecting location and estimating severity of damage in reinforced concrete beams, using finite element models inflicted with single and multiple damage scenarios, including refining the damage detection method;
4. To investigate the influence of various levels of noise pollution on the proposed damage detection method, by adding various levels of noise to FE time response data before the virtual experimental modal analysis processes; and
5. To validate the reliability of the proposed damage detection method on reinforced concrete beams, using experimental data obtained from experimental modal analysis on simply supported reinforced concrete beams inflicted with single and multiple damage scenarios.

1.3 Scope of the Work

The research work presented in this thesis is concerned with damage detection on reinforced concrete structures. The damage considered here is of localised defects, such as honeycomb and cracks. Global damage or defects, such as general corrosion, in reinforced concrete structures are not included in the scope of this study.

In the light of complexity of reinforced concrete structures, the research started with a simply supported reinforced concrete (RC) beam, which is a basic but an important

element in many types of reinforced concrete structures, such as a bridge. An analytical model of a reinforced concrete beam was numerically developed using a commercial finite element analysis package (ANSYS 11.0 2007). For the FE modelling, the material properties input were obtained from the material property tests conducted in the laboratory. Localised damage was simulated by either local stiffness reduction method (to simulate honeycomb) or discontinuing element model method (to simulate crack). The finite element (FE) model is then validated by experimental results obtained from the experimental static loading and dynamic tests.

A new modal strain energy based damage detection method (DI-NO) is proposed in the research. The new method is based on a reasonable assumption that most damage will result in an equivalent stiffness change, other than the geometric property changes. After obtaining modal parameters (natural frequency and mode shape) calculated from the finite element model, the proposed damage detection method was employed to predict damage locations and to estimate damage severities for single and multiple damage scenarios.

In order to simulate the actual environmental conditions in numerical study, white Gaussian noise is added to the acceleration time history data obtained from ANSYS (2007) to examine whether or not the proposed damage detection method is sensitive to noise. The results of the proposed damage detection method are compared with the results of two well-established damage detection methods to verify its robustness and reliability. The proposed method is also refined to improve its capability to predict the locations of damage.

For the experimental work, Experimental Modal Analysis (EMA) is performed on five reinforced concrete beams before and after the beams was inflicted with various damage scenarios. In the experimental work, the honeycomb is simulated by putting a polystyrene hexahedron into the frame of the reinforcement of the beams before pouring the concrete and the crack is simulated by small cutting from the soffit of the reinforced concrete beams. The EMA is adopted to obtain modal parameter data from both the undamaged and damaged beams.

The proposed damage detection method is performed using the modal parameters of the five reinforced concrete beams obtained from experimental modal analysis. Comparison of results is also carried out using the experimental data between the improved version of the proposed method and the two other selected methods. The comparison between the numerical results and the experimental results of the improved version of the proposed method is also carried out to verify the effectiveness and reliability of the method.

1.4 Significance of the Research Work

In this study, a new modal strain energy based method (DI-NO) has been developed for damage detection aiming for improvement of the reliability and robustness of damage detection. The new method is formulated based upon more reasonable assumptions. After theoretical development of the method, the proposed damage detection method is numerically investigated using experimentally validated finite element reinforced concrete beam models. An improvement on the proposed method is also made by normalising the mode shape curvature resulting in great enhancement of its capability in more accurate evaluation of damage location. Corresponding to the numerical work, five reinforced concrete beams have been cast and then tested in the UTS Structures Laboratory to provide data for verification of the proposed damage detection method. The results of both numerical and experimental work have proven that the new proposed method is capable of locating and quantifying damage based upon the measured mode shapes from both undamaged and damaged states, and that the new proposed method is more robust and reliable than two other well-established methods.

The main contribution of this research is to develop a new modal strain energy based damage detection method that is more reliable and robust than current existing methods. The new method has been applied to detect damage in reinforced concrete structures, specifically, a reinforced concrete beam numerically and experimentally for evaluation and verification of the method. The original contributions of the thesis include:

1. From the literature review (Chapter 2), it is clear that there is limited published research on using modal strain energy to detect damage on reinforced concrete

structures. Furthermore, all published modal strain energy based damage detection methods have their shortcomings, such as generating many false positive (spurious damage) results, even though they have the potential to be employed as a damage localisation method. Therefore, to overcome the shortcomings mentioned above, a new modal strain energy based damage detection method is formulated first and then applied to reinforced concrete beams in this research.

2. In the process of performing the proposed damage detection method, there were fewer false positive results generated than the two well-established methods, which are deliberately reviewed in this thesis, due to their highly referenced status in many research works, to verify the robustness and reliability of the proposed method.
3. Both mode shapes and mode shape curvatures are incorporated in the formulation of the proposed damage detection method. Compared with other damage detection methods which usually employ only one modal parameter, the proposed method is still sensitive enough to damage but much less sensitive to the presence of noise. Thus, the results confirm that the proposed method is more robust and reliable than other methods in detecting damage.
4. The proposed damage detection algorithm has been further refined by normalising the mode shape curvature of each considered mode with respect to the maximum curvature value of the corresponding mode. The advantage of normalising the mode shape curvature is that the contribution of lower modes will not be underestimated when higher modes are considered in detecting damage.
5. The research described in this thesis is intended to predict the location of damage and estimate the severity of damage in reinforced concrete structures. The damage cases simulated in the research began with single damage location up to maximum of four damage locations, and three different levels of damage severity are considered in different damage cases. The coverage of the inflicted damage scenarios is considered quite thorough to verify the robustness and reliability of the proposed damage detection method.

1.5 Organisation of the Thesis

In Chapter 1, a general overview of the work, the objective of the study, the scope of the work and the significance of the research are given.

In Chapter 2, the background and the state-of-the-art in damage detection methods, specific to reinforced concrete structures, are outlined first. Subsequent to the introduction of the four levels of damage detection, global non-destructive vibration based damage detection methods are extensively reviewed. Moreover, the finite element modelling of reinforced concrete is also reviewed in this chapter.

In Chapter 3, test specimens are described first. Then material property tests are reported. The set-up of four point bending test is also described, followed by the discussion of the non-linear behaviour of the reinforced concrete beam. Finally, the least square method with two explanatory variables is adopted to process the measured test data.

In Chapter 4, the procedure of establishing reasonable and reliable finite element (FE) models of laboratory reinforced concrete beams is first detailed. Three approaches to simulate the damage in reinforced concrete and mesh density comparison are also briefly introduced in this chapter. After validating the RC beam, using results from the bending test and dynamic test, transient dynamic analysis used to determine the dynamic response of a structure under any general time-dependent loads, is briefly discussed in the chapter.

In Chapter 5, a new modal strain energy based damage detection method and its improvement, as well as two other selected methods are formulated. The advantages of the proposed method over the other damage detection methods are also addressed in the chapter.

In Chapter 6, two approaches of obtaining modal parameters (natural frequencies and mode shapes) are introduced first. Then a number of different damage scenarios are simulated. To simulate the real experimental situation, different levels of noise pollution

are added to the acceleration time history data. Then the proposed damage detection method is applied to the numerical work. Comparison is also made between the proposed method and two other selected methods. Finally, an improvement to the proposed algorithm is introduced to improve its reliability and effectiveness.

In Chapter 7, the procedure of experimental modal analysis is detailed at the beginning. Then the five reinforced concrete beams to be used in the experiment work are introduced. After applying the proposed method to the experimental work, the damage detection results are analysed and explained. The results are compared with results of two other selected methods. The experimental results are also compared with the numerical results.

In Chapter 8, conclusions and recommendations for future research are presented.

Chapter 8 is followed by the list of Reference and then by three appendices, namely, Appendix A, reporting on measured and estimated strain data, Appendix B, presenting, graphically, results of damage detection without noise and with simulated noise and finally Appendix C, presenting, graphically, results of the damage detection of the RC beam in the experimental work including comparisons with the numerical work.

CHAPTER 2

LITERATURE REVIEW

2.1 Introduction

This literature review details some of the most significant work regarding the development of non-destructive damage detection methods in civil engineering applications. This previous work, by other researchers, serves as the platform upon which the original research offered here (from Chapter 3) is founded.

This chapter opens with background information pertaining to reinforced concrete structures. This is followed by an outline of damage detection in such structures which has been a pre-eminent issue in civil engineering for decades. Before reviewing basics of damage detection methods, four levels of damage detection are introduced. Then, the main category of damage detection methods is explored, namely, global damage detection methods. This forms the main bulk of the chapter. Further to this, the finite element modelling of reinforced concrete is reviewed in this chapter. Finite element modelling enables accurate modelling of reinforced concrete beams, including damage. This will subsequently provide the basis for validation, in numerical work, of the damage detection method proposed in this thesis.

2.2 Background

Reinforced concrete (RC) structures are usually designed with a lifespan of about 50 to100 years. They are not built to last forever. Overtime, the structures are structurally weakened due to increase of external loading with changes in the design code, continuous exposure to harsh environmental conditions and wear and tear. The most commonly observed damage to RC structures was in the form of cracking (Kono & Tanaka, 2002). Typical examples are reinforced concrete bridges in which the cracks develop gradually when the bridges suffer from sudden overloading, seismic effects, corrosion and excessive temperature effects. Some of the cracks will develop into

functional damage with ageing of the reinforced concrete structures. Two typical types of damage in RC structures, namely crack and honeycomb, are illustrated in Figure 2.1. The damage detection method proposed in the research will focus on detecting these two forms of damage. More details regarding causes and types of damage in RC structures can be found in Hassoun et al. (2008) and Nawy (2009).

(a) (b)

Figure 2.1 (a) Crack and (b) honeycomb damage in reinforced concrete structures

In Australia, more than 60% of bridges for local roads are over 50 years and about 55% of all highway bridges are over 20 years old (Stewart, 2001). In Western Australia alone, there are over 2,800 bridges, many of them are old. Many of these bridges are RC slab bridges and have already shown sign of deterioration (Zanardo et al., 2007). In general, some reinforced concrete bridges in Australia may have the possibility of suddenly crumbling or may have to be put out of operation without any early warning. It is estimated that A$1 billion is urgently needed to strengthen or replace defective bridges in the state of New South Wales (Clucas, 1996). Therefore, damage detection in reinforced concrete structures at an early stage has become an important issue in civil engineering community. This allows maintenance and repair works to be timely programmed and thereby minimising the incurred costs and ensuring safety of our road network.

Current damage detection methods in use are either visual or localised experimental methods such as non-destructive evaluation (NDE) methods including, but are not limited to, ultrasonic pulse velocity method, magnetic method, electrical method, radioactive method, short-pulse radar method and stress wave propagation method. More details on local damage detection methods can be found in Bungey et al. (2006) and Malhotra & Cariono (2004). Although the local damage detection methods have been developed and used quite successfully in reinforced concrete structures, they have weaknesses: all these techniques usually require that the vicinity of damage is known prior to damage detection, and that the section of the structure in question is readily accessible for inspection (Maeck, 2003). Otherwise, the localised methods may not work effectively. In addition, the local methods are time consuming and very costly. To overcome the shortcomings inherent in local damage detection methods, increasing attention has been drawn to global damage detection methods for reinforced concrete structures.

Among various global damage detection methods, vibration based methods are useful and popular NDE tools, though they are more elaborate. Amongst the vibration techniques, modal based damage detection methods have shown great potential. The methods are established based on the principle that changes in modal parameters (particularly natural frequencies, mode shapes, and modal damping) are closely related to changes in the physical properties of a structure (mass, damping, and stiffness). This subject has received considerable attention in literature (Doebling, S. W. et al 1996). It is important to highlight that most researchers, in the literature, have dealt with homogeneous structural members, where damage is represented by localised stiffness reduction due to a crack or a cut. Not much attention has been paid to problems involving non-homogeneous members, such as reinforced concrete structures (Zhu & Law, 2007). This has prompted the research work in this thesis to fill the gap of knowledge for exploring and investigating better vibration based damage detection methods to evaluate typical damage found in reinforced concrete structures.

2.3 State-of-the-art

As mentioned earlier, progress has been made in using vibration based global NDE methods to detect damage. However, it remains difficult to obtain accurate damage detection results when applying such methods to reinforced concrete structures, for the following reasons:

1. Reinforced concrete is highly non-homogeneous with a complicated microstructure. Large numbers of micro defects and micro cavities are naturally present in concrete, and these can initiate micro-cracks/defects when loads are applied to any reinforced concrete structure. Although such tiny defects and micro cracks are not damage features in themselves, they progressively evolve into structural cracks under external loads. These structural cracks may be scattered and this will influence the dynamic characteristics of the structure, thus also affect the damage detection results.
2. Reinforced concrete by its very nature is highly variable. Therefore reinforced concrete structures with similar concrete mix proportion may not react identically, both dynamically and statically, using the same damage detection method to identify similar damage.
3. Reinforced concrete structures are usually huge and heavy compared to other building materials. This makes the structures relatively harder to be excited using vibration methods as huge impact energy is required. Thus, some vibration based global damage detection methods are as yet not widely used in reinforced concrete structures, because the output results may sometime not be reliable with weak output signals.
4. Some reinforced concrete structures are so complicated that measurement equipment can neither be easily placed nor well situated on the structures. Then again, even if measurement equipment can be placed on the structure, the measured dynamic responses can not be well analysed due to the high noise to signal ratio. Factors such as these contribute to the difficulty of performing global damage detection methods on reinforced concrete structures.

2.3.1 Non-destructive Damage Detection for Reinforced Concrete Structures

Despite the difficulties such as those mentioned above, researchers continue the development of non-destructive global damage detection methods for reinforced concrete structures. Following is a review of latest damage detection methods specific to reinforced concrete structures.

To evaluate damage severity, Kim et al. (2005) presented two damage indices, one termed compressive damage index of concrete, the other termed tensile damage index of reinforcing bars, to quantify the damage in reinforced concrete columns under earthquake loading. The two damage indices were formulated respectively as follows,

$$D.I._{compressive} = 1 - (1 - 0.3\sum \frac{1}{N_{2fc}})(\frac{2\varepsilon_{cu} - \varepsilon_{cs}}{2\varepsilon_{cu}})^2 \qquad \text{Equation 2.1}$$

$$D.I._{tensile} = 1.20(\frac{\varepsilon_{ts}}{2(1 - 0.3\sum \frac{1}{N_{2fr}})\varepsilon_{tu}})^{0.67} \qquad \text{Equation 2.2}$$

where N_{2fc} is the number of complete cycles to failure for concrete; N_{2fr} is the number of complete cycles to failure for reinforcing bars; ε_{cu} is the ultimate strain of concrete; ε_{cs} is the main compressive strain in the analysis step; ε_{tu} is the ultimate strain of reinforcing bars; and ε_{ts} is the tensile strain in the analysis step. The numerical results showed that the proposed damage indices were able to predict the severity of damage roughly, at different stages of loading. However, the indices were unable to predict the locations of damage, and were not suitable for other reinforced concrete structures.

After investigating fractal theory, Cao et al. (2006) then adopted it to extract the fractal damage characteristic factors of a reinforced concrete structure by characterizing its surface-crack assessment. The results from experimental testing, performed on a 100mm ×200mm×1500 mm reinforced concrete beam, revealed that approximate linear relationships existed between the fractal damage characteristic factors and the traditional damage characteristic factors, such as natural frequency and average carbonized depth. Therefore, the researchers concluded that the fractal damage characteristic factors could serve as an alternative damage detection factor. The researchers also mentioned that further studies were needed in order to explore the correlations between the fractal damage characteristic factors and the traditional damage

characteristic factors, before the fractal damage characteristic factors could reliably be employed in damage detection.

Zembaty et al. (2006) performed a dynamic test to study change of modal parameters in a reinforced concrete frame, due to development of crack in the concrete. A characteristic decrease of natural frequencies and an increase of structural damping were observed. During the dynamic test, the first cracks which caused a 15% loss of stiffness, could not be visually detected until the frequency dropped by 10%.

Zhu et al. (2007) performed a test on a four meter long reinforced concrete beam, 300mm×200 mm in cross section. The beam was initially subjected to three-point loading at mid-span to create crack damage. Then the beam was unloaded and impact hammer tests were conducted to obtain the different modal parameters of the beam. After comparison of results from modal analysis and Hilbert transform, it was observed that the acceleration-frequency relationship in one cycle of vibration showed nonlinear vibration characteristics. It was concluded that the damping ratio and frequency change could be two good indicators in damage detection for reinforced concrete beams.

Zhong et al (2007) presented a new approach for crack damage detection in beam-like structures. To verify the efficiency of the new approach, 36 cracked beams were modelled, using ABAQUS FE package. Then modal parameters were calculated, and the stationary wavelet transform (SWT) decomposition of the signals obtained from the mode shapes were studied. The results showed that the new method was able to provide evidence of crack existence at the correct location of the beam. So it was concluded that the proposed method had potential in the field of crack detection of beam-like structures. However, the use of SWT based method required fairly accurate data of the mode shapes, which was difficult to obtain in experimental work. The paper did not discuss estimation of severity of damage using the new method.

Faleiro et al (2008) formulated a member damage index, and a global damage index, to measure stiffness loss of structures due to damage. Two indices were employed to assess overall state of damage of structures. To verify the method, two reinforced concrete frames were modelled numerically and then applied to dynamic analysis. The two indices were unable to predict the locations of damage, and the results indicated

that they were able to provide a quantitative evaluation of the state of damage, for both members of structures and of overall structure.

Fang et al. (2008) developed a sensitivity-based updating method, for detecting damage in a reinforced concrete frame, by minimizing the discrepancies of modal frequencies and mode shapes. Initial to the detection, a modal test was performed to obtain the frequencies and mode shapes of the undamaged reinforced concrete frame. Then a static loading test was applied to the frame, to generate a visual crack in the beam section of the frame. Finally, the model test was carried out again, to obtain the frequencies and mode shapes of the damaged reinforced concrete frame. The results showed that the proposed method could locate the single damage site located at the mid span of the beam. However, it is not known yet if the proposed method could be applied in cases of multiple damage.

Baghiee et al. (2009) studied the correlation between the occurrence of damage and the dynamic characteristics of concrete beams. The researchers built nine reinforced concrete beams, with dimensions 150 mm (width), 200 mm (height) and 2200 mm (length) each. To introduce crack damage, increasing static loads were applied at different load steps to the nine beams. Then dynamic tests were carried out on the damaged beams, to obtain modal parameters after unloading. The results showed that the frequencies dropped with increasing severity of damage, but that the shifts of frequencies were not influenced by damage locations. The modal assurance criterion (MAC) could provide information about overall stiffness change of the structure due to damage, but could not determine the stiffness change at each degree of freedom. The coordinate modal assurance criterion (COMAC) was able to detect the changes in beam stiffness. COMAC was also more precise in identifying crack zone in reinforced concrete beams than with frequencies or MAC. However, the accuracy of the COMAC based damage detection method depended on the accuracy of technique used in calculating the curvatures.

2.3.2 Previous Literature Review and Surveys

An extensive literature review covering the period 1968 to 1996 has been done by Doebling et al. (1996). The review has covered a wide range of damage detection

methods using various vibration based damage detection methods. The focus of the review, modal based damage detection methods, was based on parameters including frequency changes, mode shape changes and its derivatives, as well as flexibility changes. It is important to note that methods using mode shape, mode shape curvatures, modal strain energy and their derivatives have been widely researched and found many applications in real life civil engineering structures such as bridges. This research work offers a new modal based damage detection method with advanced features for application in real life civil engineering structures, specifically for reinforced concrete structures. The authors also discussed some important areas such as intelligent system based methods and methods that are widely used in other engineering practice, which lately found application in civil engineering structures.

A number of review papers addressing damage detection and related issues have been published. Farrar and Doebling (1997) and Doebling at al. (1998) reported an overview of modal based damage detection methods. Salawu (1997) provides a thorough review on structural damage detection through changes in natural frequency. The main advantage of using natural frequency is that it can be easily and cheaply acquired. Bishop (1994) has reviewed several usage of neural networks, one of them being to solve inverse problem for pattern recognition and a guide to the neural literature was also appended. Housener et al. (1997) have reported an extensive review on the state-of–the-art in structural health monitoring (SHM) from 80's to 90's indicating the importance of damage detection especially in civil structures. Online damage detection and health monitoring techniques for delamination damage on composite structures were reviewed by Zou et al. (2000). Avitabile (2002) provided an overview of the developments in structural dynamic modification techniques for the past two to three decades, related to damage detection. The technique is useful to study the structural changes of a system. A comprehensive review of new techniques in SHM is undertaken by Sohn et al. (2003). The review reports on the state–of-the-art in SHM technologies and identifies the need to improve SHM application in real structures. Carden and Fanning (2004) also presented a review on vibration based condition monitoring, as an extension to the review done by Doebling et al. (1996). An overview of fault detection using intelligent systems was presented by Worden and Dulieu-Barton (2004). The work encompasses taxonomy of the relevant concepts in damage detection, operational

evaluation of a hierarchical damage detection scheme, sensor optimisation and data processing methodology based data fusion method.

2.4 Basics of Damage Detection

The basic concept of damage detection can be defined as ways or methods that are able to capture the changes in structural characteristics due to damage or degradation. Many damage detection methods are categorised as global NDE because they assess structures without removing any structural components and cause no harm to the integrity of the structures. Damage can be broadly defined as follows: changes occurring within a structural system which negatively impacts on the current or future performance of that system. Implicit in this definition is a conception that damage is not meaningful without a comparison between two different states of the same system, one of which is assumed to represent the intact, therefore undamaged state and the other one is the damaged state. For example, a crack that forms in a bridge element produces a change in its stiffness that alters the dynamic behaviour of the bridge. Depending on the size and the location of the crack, and the loads applied to the system, the negative effects of this damage may be immediate, or they may take some time to alter the system's performance.

To classify levels of damage, a system is presented by Rytter (1993), who defines four levels of damage detection as follows:
Level 1: Determination that damage is present in the structure
Level 2: Determination of the geometric location of the damage
Level 3: Quantification of the severity of the damage
Level 4: Prediction of the remaining service life of the structure

Local damage detection methods can only provide Level 1 damage detection. Global damage detection methods are able to provide information beyond Level 1 damage detection. For example, vibration based damage detection methods (which do not make use of some structural model) primarily provide Levels 1 and 2 damage detection. When vibration based methods are coupled with structure modelling, Level 3 damage detection can be obtained in some cases. Level 4 prediction is generally associated with the fields of fracture mechanics, fatigue-life analysis, or structural design assessment.

The damage detection at Levels 2, 3 and partly 4 using a modal based method is the aim of this study.

2.5 Non-destructive Global Damage Detection Methods

Local damage detection methods usually require that the vicinity of any damage is known before damage detection, and that the location of damage being inspected is easily accessible. Subject to such limitations, these local methods can detect damage on or near the surface of a structure. However, in the case of structural monitoring, and indeed in most damage detection applications, information regarding damage is not available before damage detection, and the location of damage may be inaccessible. This fact accounts for the development of an altogether different paradigm of methodology, the global detection methods. These methods were developed in order to facilitate analysis of complex structures (Sohn et al 2003). Hence in this chapter an extensive review of vibration based global damage detection methods is performed in the following section.

The author of this thesis decided to present the review in a few categories relevant to the focus of the research work or future developments of the work. The main categories are listed as follows:

- Methods Based on Vibration
- Methods Based on Artificial Intelligence
- Methods Based on Wavelet Analysis

The review focused on papers and articles published after 2000. However, any articles and papers considered relevant to the scope of this study prior to year 2000 were also included. Readers interested in the state-of–the-art in the damage detection area pre-2000 are referred to the reviews and surveys mentioned above.

2.5.1 Methods Based on Vibration

2.5.1.1 Frequency Response Functions

As a vibration signature of structures, FRF has been investigated as a sensitive indicator for the prediction of damage in different structures. Wang, Lin and Lim (1997) formulated a new damage detection algorithm using measured frequency response function data. Then the method was applied to an experimental 3-bay plane frame structure, made of mild steel square bars. The structure was designed to have two replaceable joint parts located in the middles of two horizontal bars, in order to then introduce different kinds of damage. Numerical studies showed that the method was capable of identifying the locations and severities of damage within reasonable margins of error. The results from experimental investigation, however, were less satisfactory in reflecting the facts. The authors also concluded that the proposed damage detection method may not be applicable to the identification of small scale damage (such as surface or internal cracks, flaws, voids, thin spots and so on), because the changes in vibration data caused by minor damage might not be detectable in the presence of noise.

Sampaio, Maia and Silva (1999) formulated a frequency response function curvature method, for the detection of damage in structures. Their method is based on the absolute difference of frequency response function curvatures when comparing damaged and undamaged structure. After numerical application to a free-free beam, the method was able to locate damage, even in the presence of noise. Furthermore, the results showed that the frequency response function method performed better in damage detection than the damage index method. Results from the experimental studies reiterated that the method was capable of detecting damage. The researchers pointed out, however, that the method was still in need of further development and better characterization.

Maia, Silver, Almas and Sampaio (2002) investigated the difference between mode shape based damage detection methods and frequency response function based damage detection methods. In their research work, a free-free beam, with 99 elements and 100 nodes, was constructed numerically. To simulate damage, three other models were generated with reductions of 25%, 50% and 75% of the Young's modulus at element 70. A force of 1 N was applied at node 34. After modal and harmonic analyses of the

beams, the results showed that all methods, with the exception of the mode shape method, were capable of pinpointing the correct damage location. However, there were some false damage indications at the boundaries, due to the interpolation method used to calculate the derivatives. In the experimental work, a steel beam with constant rectangular cross section was used. The results showed that only FRF-based mode shape curvature method, FRF-based mode shape curvature square method and FRF-based damage index method, were successful in locating the damage (saw cut in the beam), even though there were some false damage indications. The authors suggested that in order to get a better result from their method, improvements could be made in the following areas: to their interpolation process; by defining a noise level under which results are not considered; in their method for calculation of the maximum occurrences; in applying statistics to the results; and in the set-up of the experiment itself.

Owolabi et al. (2003) studied damage detection, using the measured changes in the first three frequencies, and the corresponding amplitudes of the measured acceleration frequency response functions. In their research, two sets of aluminium beams were used for the experimental investigation. Each set consisted of seven beam models. The first set had fixed ends, while the second set had simply supported ends. Each beam model was made of an aluminium bar of cross-sectional area 25.4 mm × 25.4 mm with a length of 650 mm. To simulate damage, cracks were generated to the desired depth using a thin saw cut. Crack depth varied from $0.1d$ to $0.7d$ (d was the depth of the beam) with an increment of $0.1d$ at each crack position. In the dynamic tests, it was observed that the fundamental frequency ratios showed a clear downward trend as the crack depth ratio increased. The amplitude of the FRF also showed a decreasing trend, as the crack grew in size. The reduction in the amplitude of the FRF of the second mode was similar to that of the first mode. The amplitude changes observed in the third mode did not follow the same pattern (Figure 2.2). Based on the changes of amplitudes of the FRFs, a contour line was plotted, representing the amplitude changes which resulted in a combination of different crack locations and crack depths (Figure 2.3). This contour was plotted as a curve, with crack location and crack depth as its axes. The contour detected crack with errors, and clearly required further development in the future.

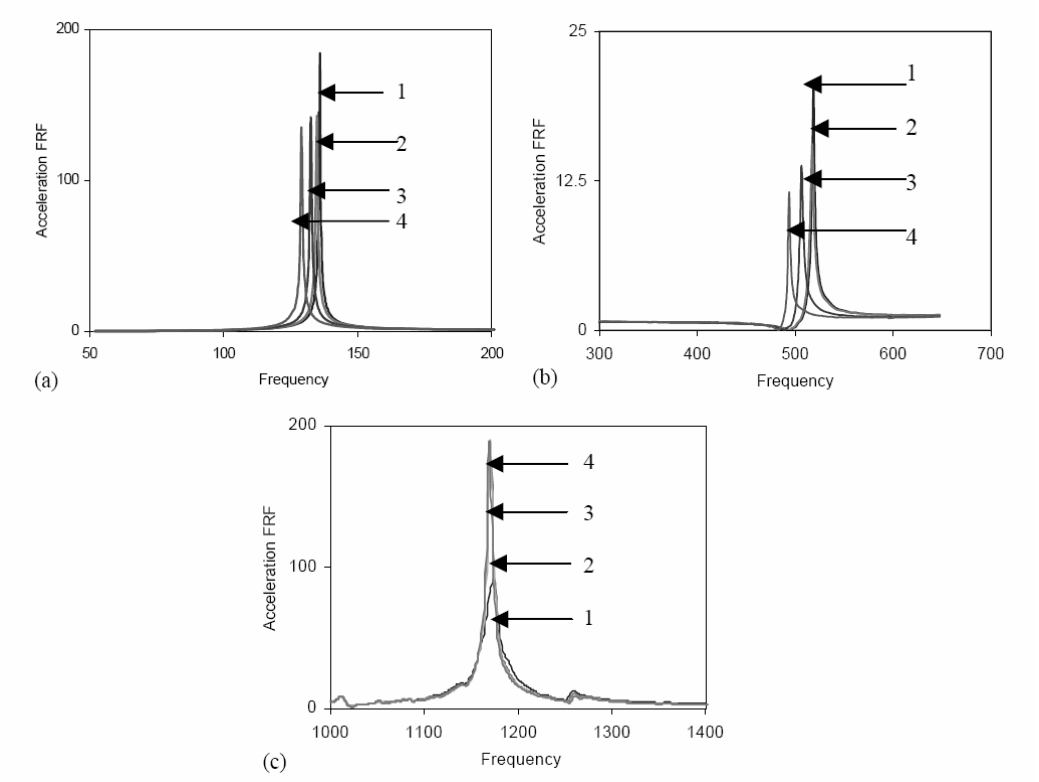

Figure 2.2 Natural frequency shifts and FRF amplitudes for a crack located at a crack length ration *c/l* of 5/16 of a simply supported beam for a various crack rations *a/h* – accelerometer located at quarter of the span of the beam from left (1: uncracked; 2: *a/h* = 0.1; 3: *a/h* = 0.2; 4: *a/h* = 0.4): (a) first natural frequency; (b) second natural frequency; and (c) third natural frequency (Owolabi et al. 2003)

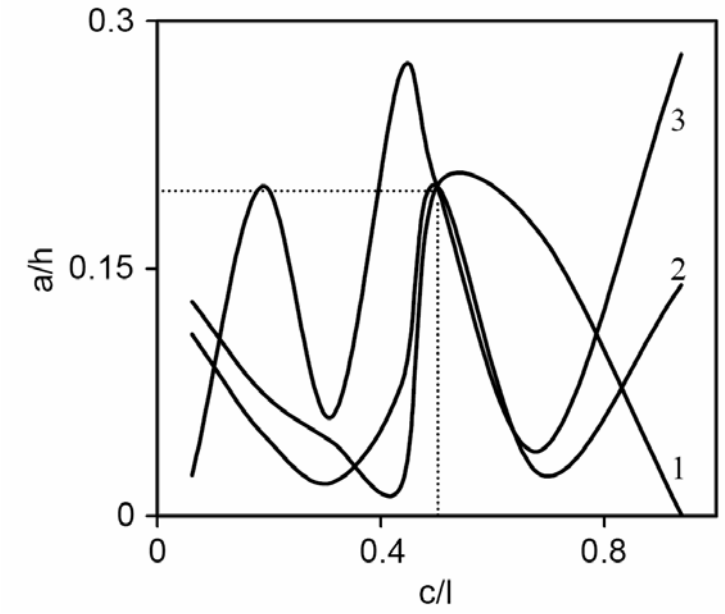

Figure 2.3 Crack identification techniques by using amplitude contours of the fist three modes of a simply supported beam - accelerometer located at 3/8 of the span of the

beam from left (1: model1, normalized amplitude (0.9998); 2: model2, normalized amplitude (0.9613); 3: model3, normalized amplitude (0.9575)) (Owolabi et al. 2003)

Furukawa and Otsuka (2006) presented a method which used frequency response functions data to detect damage. The research utilised hypothesis testing based on the bootstrap method, in order to minimize errors due to measurement noise. Then the method was applied to an aluminium beam, which was 50 cm long, 2 cm wide and 0.5 cm thick. The beam had 11 nodes and 10 elements. The damage was introduced into different elements by changing the value of stiffness. After numerical dynamic tests, the researchers claimed that the proposed method provided accurate damage detection with the presence of a large amount of noise.

2.5.1.2 Modal Parameters

The fundamental theory of modal parameters based damage detection methods is simple. Modal parameters (natural frequencies, mode shapes, and modal damping) are functions of the physical properties of a structure (mass, damping and stiffness). Therefore, changes in the physical properties will cause changes in the modal properties. Damage detection methods based on modal parameters, therefore, are methods in which modal properties are measured in order to reveal physical properties. Examples follow.

However, in real field applications, there are many practical issues associated with the performance of damage detection including environmental influences, operational influences, measurement noise, processing error and limited number of sensors. The results of modal parameters estimation are heavily affected by imperfections or errors, and environmental and operational conditions during such process. The changes in modal properties resulting from changes in environmental conditions can be as significant as the changes in these properties caused by damage. For example, the shift of frequency caused by damage can be covered by the shift of frequency resulting from temperature change, thus it is difficult to detect damage in this situation. This is part of the reason that most damage detection methods perform poorly in field applications.

2.5.1.2.1 Natural Frequencies

An important dynamic property of any elastic system is its natural frequency of vibration. For an intact/damaged beam of given dimensions, the natural frequency of vibration is mainly related to the equivalent modulus of elasticity or stiffness of the system. Hence, the equivalent modulus of elasticity of a material can be related to the measurement of the natural frequency of vibration. Based on this point, shifts in natural frequencies are considered as damage indicators. Use of natural frequency for damage detection has been very popular due to the fact that natural frequencies are relatively easy to determine, and that therefore a single sensor is sufficient for many applications.

It should be noted that measured natural frequencies in civil structures are normally lower modes of structures, and that it is therefore difficult for natural frequencies to provide local information about structural changes. For this reason, it is not ideal to use shifts in frequencies to identify more than the mere existence of damage. The location and severity of damage cannot be determined through natural frequencies in most cases.

There are large amounts of literature related to damage detection using shifts in natural frequencies. The greater part of the earliest work on natural frequencies was based on simple structures and structural elements. One of the papers most commonly quoted on the use of natural frequencies in damage detection is by Cawley and Adams (1979). Their paper demonstrated, both analytically and experimentally, that a single point in a structure can be used to detect and quantify damage. The main idea in their method is to use the ratio of frequencies in two modes as a function of the damage locations. The positions where this theoretically determined ratio equals the experimentally measured value are deemed possible damage sites. The locus for several pairs of modes may be superimposed and the actual damage site predicted by the intersection of the curves. The method was successfully applied to free-free carbon fibre reinforced polymer (CFRP) plates. The other objective of this study was to filter out the influence of temperature from the measured natural frequencies. However, a different opinion was presented by Banks et al. (1996), who stated that using natural frequency to detect damage is dependent on geometry of the damage. For some types of damage, the method may be appropriate for damage detection but for other configurations the method may not be.

Low sensitivity of frequency shifts to damage requires either very precise measurements or large levels of damage. For example, Farrar and Jauregui (1998) conducted tests on a steel plate girder bridge and the results demonstrated this point. In the test, four levels of damage were introduced to the middle span of the north plate girder close to the seat supporting the floor beam at mid-span. Damage was introduced by making various torch cuts in the web and flange of the girder. After vibration testing, the results showed that little change in the dynamic properties were observable until the final level of damage was introduced. At the final level of damage, the frequencies for the first two modes dropped to values 7.6% and 4.4% less, respectively, than those measured during the undamaged tests. For modes where the damage was introduced near a node (mode 3 and mode 5), no significant changes in frequencies were observed. The researchers concluded that standard modal properties such as frequencies are poor indicators of damage.

Even though frequencies change with the occurrence of damage, they are easily affected by environmental changes such as fluctuations in temperature and humidity. It is observed that changes in frequencies are small in comparison to fluctuations due to environmental conditions. Wahab and De Roeck (1997) investigated the effect of temperature on the modal parameters of a prestressed concrete highway bridge. The bridge, named B15 and built in 1971, was a three-span box-girder bridge with an overall length of 124.6 m (35.8+53.0+35.8). The box-girder was 9.4 m wide varying in depth between 1.0 and 2.5 m. The width of the bridge was 13.0 m with two traffic lanes. The structure was supported at the two outside abutments by neoprene bearings, which allow for lateral movements. The dynamic response of the bridge was measured twice: in the spring, May 1996 (temperature around 15ºC), and in the winter, January 1997 (temperature around 0ºC). The modal parameters of the bridge (i.e., the natural frequencies, damping ratios and mode shapes) were extracted from the measured data, using a time domain analysis in the form of a vector auto-regressive model. The results showed that the change in natural frequency, due to the increase in temperature, was a decrease of about 4-5%. The researchers made the conclusion that, when change in natural frequencies is used to evaluate damage in a structure, the effect of temperature should be taken into account.

Although using the natural frequencies to detect damage is practically difficult, some researchers have made great progress in this area. Kim and Stubbs (2003) formulated a crack-location model to locate and estimate size of crack in beams for which natural frequencies were available. The method can locate the crack and estimate the size of crack, both within only a small margin of error. However, the limitation of the method is that it has only been applied to crack in beams. It is not clear if the method will perform well if it is applied to different types of damage, or to different structures.

Morassi and Rocchetto (2003) presented the results of an experimental investigation into damage-induced changes in the modal parameters of steel-concrete composite beams subjected to small vibrations. The dynamic tests were performed on four composite beams, two having a partial connection and two having a total connection. The tests revealed that, flexural frequencies show a rather high sensitivity to damage, and flexural frequencies can be considered as a reasonable indicator in damage detection.

Recent development has been to couple the measurement and analysis of natural frequencies with that of other modal parameters, in order to obtain enhanced damage detection ability. Kosmatka and Ricles (1999) presented a method to detect damage in structural systems. Their experimental research was performed on a lightweight ten-bay statically indeterminate space truss consisting of 135 members and 44 joints. Each bay had the outer dimensions of 356 mm × 356 mm, with the truss having a total length of 3,327 mm. In the experimental model, damage was simulated by altering either one truss member, or the joints of the truss. Four different damage cases were generated in this way. As the first step in the process of damage detection and according to the method developed in the research, an experimental modal survey was performed on the undamaged structure. This was done in order to obtain measured system vibration properties Λ_o, which included the natural frequencies and mode shapes. The second step of the algorithm was then to conduct a modal survey on the structure after it had been damaged, in order to measure the vibration properties Λ_d, which also included natural frequencies and mode shapes. The difference in the measured modal properties (Λ_d) and the undamaged properties (Λ_o) was identified to locate damage; the severity of damage was determined by establishing a relationship between the measured vibration characteristics and the structural parameters, using a first-order Taylor series expansion.

The modal testing was performed using a small Kistler accelerometer, weighing 0.5 grams. The SMS STAR modal software package (STAR 1991) was used to reduce the measured data to acquire the frequency response functions. The results showed that the method was able to determine the location of damage.

Ndambi, Vantomme and Harri (2002) performed experimental tests in order to evaluate the following: the correlation between the progressive cracking process in reinforced concrete beams, and the resulting changes that can be observed in the dynamic system characteristics. In their test, two types of experiments were combined: the static loading test and the dynamic measurements test. The first experiment was performed so as to gradually introduce the crack in the RC beams. The second experiment was performed so as to determine the dynamic characteristics. In the experiment, after each loading step, the beams were unloaded and supports were removed. The beams were then suspended, using four elastic springs attached at the theoretical nodal points of the first bending mode during all the dynamic measurements. The springs were used to simulate the free-free boundary conditions. The results demonstrated that all the investigated eigenfrequencies were affected by accumulation of cracks in the RC beams, but that their evolutions were not influenced by the crack damage locations. It was also noted that the decrease of eigenfrequencies remained monotonical during the cracking process, which allowed the severity of the damage to be followed.

Garesci, Catalano and Petrone (2006) reported a methodology for identifying location of damage. In the method, damage location was determined through analysis of the eigenvectors corresponding to those eigenvalues which presented the highest percentage differences compared to the undamaged system. The method was applied first on rectangular plates which had a milled slot in different positions, and afterwards on mechanical components. The results showed that it was possible to identify the damaged zone using the developed method. However, to obtain clear evidence of damage, an appropriate choice of chromatic scale for the graphic output was required. The method requires further refinement.

2.5.1.2.2 Damping

Damping is a controversial factor in the damage detection, although there have been attempts to use damping ratios as a measure of damage. Salane and Baldwin (1988) performed a test on a steel girder bridge with concrete decking. In the test, the data acquisition system comprised an Ampex FM tape recorder and an external analog-to-digital converter. Severo-accelerometers were used to measure the steady-state response at the resonant frequencies. The results of the test showed that although damping ratios were affected by deterioration, they were unsuitable as a damage indicator, because the damping ratios initially increased, and then decreased with increasing damage. This finding is supported by Farrer and Jauregui (1998), who also found that the damping of a steel plate girder bridge did not consistently increase or decrease as damage increased.

Another structure, a 104 m six-span, two-lane reinforced concrete highway bridge, was tested before and after structural repairs by Salawu and Williams (1995). The tests were conducted to investigate any correlation that may exist between the repair works and changes in the dynamic characteristics of the bridge. The results showed that the damping ratios changed after the repair works, in the manner following: 50% in the first mode, no change in the second mode, 6% in the third mode, -6% in the fourth mode, -10% in the fifth mode, and no change in the sixth and seventh modes. There was no identifiable pattern to the changes in damping values caused by the repairs.

Four pairs of reinforced concrete beams (A_1, A_2, B_1, B_2, C_1, C_2, D_1 and D_2) were constructed by Casas and Aparicio (1994) for damage identification tests. Each of these beams had a total length of 1.8 m, a span length of 1.5 m, with constant depth of 0.07 m and width of 0.1 m in rectangular cross-section. In the four pairs of beams, number 1 indicated the undamaged beam, whilst beams numbered 2 had a region with different cracking characteristics. Damage was simulated by means of formwork dispositions during concrete pouring. In the vibration tests, the acceleration transducers were located at mid-span and quarter-span. Two dynamic channels were simultaneously recorded, so the vibration test was performed alternatively in undamaged and damaged beams. An impact hammer was used to excite the beams, by hitting at the quarter-point. The results of the test revealed no clear direct relationship between damage expansion and increase in damping.

Even though inconsistency in changes of damping values have been noted previously and many researchers believe that damping is an unreliable indicator for damage detection, Razak and Choi (2001) draw a different conclusion. Three reinforced concrete beams were cast for their research. One beam was used as an undamaged beam. The other two were subjected to different states of reinforcement corrosion, and were therefore used as damaged beams. The results of modal tests showed that with increase of severity of damage, the modal damping ratio for mode 2 increased by 18.8% and 49%, using transfer function method; by 42.5% and 141.4%, using normal mode method. For mode 3, the modal damping ratio increased by 36.5% and 15.3%, using transfer function method; and by 6.8% and 84.9%, using normal mode method. A conclusion was made that modal damping of the second and third modes reflected a pattern consistent with the severity of the corrosion damage.

2.5.1.2.3 Mode Shapes

An overwhelming majority of research suggests that modal shapes are a far more satisfactory damage detection indicator than natural frequencies and damping. A large number of methods for interpretation of mode shape data have been suggested. Amongst all these methods, most work on mode shapes has concentrated on looking at the modal assurance criterion (MAC) (Allemang & Brown 1983). MAC compares the damaged mode shape of mode *i* against the undamaged reference mode shape of mode *j*, for all the modes *i* and *j* measured, and then develops a correlation value between each damaged mode shape and each reference mode shape. For undamaged structures it would be expected that MAC is 1 when *i* equals *j* and MAC is 0 when *i* does not equal *j*.

A further development of MAC method is the coordinate modal assurance criterion (COMAC) (Lieven & Ewins 1988), which, like MAC, is also commonly used in damage detection. COMAC is used to identify the location where two sets of mode shape data disagree, and hence to find the location of the damage (Alampalli et al. 1997).

Ching and Beck (2004) studied damage detection and assessment of a test structure, using pre and post damage modal shapes data, which was collected in hammer impact and ambient vibration dynamic tests. The experimental tests were performed on nine

configurations. Configurations one to six were braced cases, with configuration one being the undamaged case. Configurations seven to nine were unbraced cases, with configuration seven being the undamaged case. For the braced cases, damage was simulated by removing braces. For the unbraced cases, the damage was simulated by decreasing the rotational stiffness of some beam column connections. In the results, the brace damage was detected and assessed, whether from hammer or ambient vibration data. However, the connection damage was much more difficult to reliably detect and assess, because the identified modal parameters were less sensitive to connection damage, allowing modelling errors to influence the results more strongly.

Zhu and Xu (2005) presented a sensitivity-based method for localization and assessment of damage in mono-coupled periodic structures. To verify the method, a mono-coupled periodic spring-mass system with 10 elements was analysed numerically, and a building model was experimentally constructed. The experimental model consisted of three steel plates of 850 mm × 500 mm × 25mm and four equally sized rectangular columns of 9.5 mm ×75 mm. The numerical results showed that, among natural frequencies, mode shapes, slopes and curvatures, the mode shape curvatures were the most sensitive to damage, but the slopes of mode shapes were more indicative of damage location. Larger changes in the natural frequencies implied higher sensitivity of these modes to damage. The numerical results also showed that single and multiple damage, whether slight or severe, could be localized using a few of the slopes and curvatures of the lower mode shapes. For single or multiple damage of the same size, size of damage could be identified using only the first frequency. Regarding multiple damage in different sizes, accuracy in identifying damage size depended on the number of used frequencies. The experimental results showed that the proposed method was able to detect either slight or severe damage, in either single or multiple locations, in mono-coupled periodic structures.

Choi, Park and Stubbs (2005) presented a methodology to render location and size of damage in a structure, using a compliance index, utilizing the change in the distribution of the compliance of a structure due to damage. The change in the compliance distribution was obtained using the changes in the mode shapes of a structure. A simply supported beam and a continuous two span beam were tested numerically, and a free-free beam was tested experimentally, to verify the proposed method. The results

revealed that the compliance index could identify single and multiple damage locations, and the method yielded less damage identification error than the other existing energy methods. The researchers also suggested that performance of both damage localization and severity estimation may be improved, by using the composite damage indices which utilize multiple mode shapes simultaneously.

Ismail, Razak and Rahman (2006) formulated an indicator for determining the location of damage due to single crack and honeycomb. This indicator was obtained by rearranging the equation for free transverse vibration of a uniform beam, and applying the fourth order centred finite-divided difference formula to the regressed mode shape data. In the research, five reinforced concrete beams were cast in the laboratory, in order to investigate the method. The results revealed that the indicator was able to locate the damage and estimate the severity of damage, with error. The poor results in the vicinity of the supports implied that the technique was unable to detect damage close to the supports.

Kim, Park and Voyiadjis (2006) proposed a vibration-based damage evaluation method utilizing a few of the lower mode shapes. The proposed method attempted to resolve the mode selection problem, the singularity problem, the axial force problem, and the absolute severity estimation problem, all of which remained unsolved in earlier research. However, their results showed that the proposed method did not locate the damage in a real structure in all levels of damage, and that the proposed method was successful only in estimating the relative severity of damage. The researchers also addressed two weaknesses of the proposed method. One was dense measurement of gird, and the other was accurate extraction of the mode shapes.

2.5.1.2.4 Modal Strain Energy

Even though mode shapes are unique characteristics of a structure, and are known as an indicator in damage detection, an increasing quantity of research work has shown that derivatives of mode shapes are more sensitive to damage than mode shapes themselves (Zhu and Xu 2005). Mode shape curvatures can be obtained by differentiating mode shapes twice and modal strain energy is a function of mode shape curvature. Therefore, modal strain energy has been widely investigated as an indicator in damage detection.

Kim and Stubbs presented a non-destructive damage detection algorithm to locate and estimate damage from a few mode shapes of structures (Kim and Stubbs 1995). Their research is based on an initial assumption that the fraction for modal strain energy is the same for both damaged and undamaged structures. Based on the assumption, a damage index β_{ji} of i^{th} mode and j^{th} member was obtained:

$$\beta_{ji} = \frac{E_j}{E_j^*} = \frac{\phi_i^{*T} C_{jo} \phi_i^*}{\phi_i^T C_{jo} \phi_i} = \frac{NUM}{DEN} \qquad \text{Equation 2.3}$$

In Equation 2.3, E_j and E_j^* are parameters representing the material stiffness properties associated with undamaged and damaged states, respectively; $\varnothing_i$ and $\varnothing_i^*$ are the i^{th} modal shapes associated with undamaged and damaged states, respectively; C_{jo} denotes geometric quantities; and superscript "T" denotes transpose of a vector.

For NM vibrational modes, a damage index β_i of j^{th} member was obtained:

$$\beta_j = \frac{\sum_{i=1}^{NM} NUM}{\sum_{i=1}^{NM} DEN} \qquad \text{Equation 2.4}$$

where $\beta_j \geq 0$ and damage is indicated at the j^{th} member if $\beta_j > 1$.
Moreover, the predicted location j was defined as follows:

$$Z_j = \frac{(\beta_j - \overline{\beta})}{\sigma_\beta} \qquad \text{Equation 2.5}$$

where $\overline{\beta}$ was the mean of the collection of β_j values and σ_β was the standard deviation of the collection of β_j values respectively. Finally, the severity of damage in the j^{th} member was estimated in the research work as follows:

$$\alpha_j = \frac{1}{\beta_j} - 1; \quad \alpha_j \geq -1 \qquad \text{Equation 2.6}$$

To verify the proposed damage detection method, a two span (4.5+4.5 m) aluminium model plate girder was tested. The structure had three supports: a pin support 0.15 m from the left edge, a roller support at the middle, and another roller support 0.15 m from the right edge. Damage was inflicted in the structure by cracking the girder at a location which was 1.02 m to the left of the right support. Eleven accelerometers were placed along the deck of the structure, and excited by ambient forces from lightweight traffic,

in order to extract modal responses of the structure. The experimental results indicated that the method located damage with both false negative error (missing detection of true damage location) and false positive error (prediction of locations that were not damaged). The method generated severity estimation error as well in quantifying the severity of damage.

This damage detection method was further developed by the same researchers in 2002 (Kim and Stubbs 2002). In the new research, new methods (Damage Index A, Damage Index B and Damage Index C) were formulated. This was done in order to improve the accuracy of both damage localization and severity estimation, by eliminating erratic assumptions and limits of the previous method. Then a two span continuous beam was constructed numerically and ten different damaged beams, with different locations and severities of damage, were simulated. After that, pre- and post-damage modal parameters of the first three modes were obtained from modal analysis of the test beams. The results showed that the newly formulated method was able to locate damage and estimate severity of damage with reasonable accuracy. However, the entire research was performed with purely numerical data. In the paper, the authors discussed neither the influence of noise presence, nor any results relating to testing of their method in laboratory environment.

Choi et al. (2007) presented a modified damage index (MDI) method, based on modal strain energy, for detecting damage to a timber beam. The sawn timber beam was of treated radiata pine measuring 45mm×90mm in cross section, with a span length of 4,500 mm. In the damage detection process, a cubic spline data interpolation function was used to perform mode shapes reconstruction of the experimental data. The reconstructed mode shapes were then differentiated to obtain mode shape curvatures, which were then normalised for damage index calculation. The proposed MDI method was capable of detecting the damage location from the experimental data with false positive error. However, using a combination of high and low modes proved to be more favourable for detecting multiple damage locations. Regarding the estimation of severity of damage, the authors claimed that it will be possible to further explore the MDI method, especially in regard to multiple damage scenarios.

Shi et al. (1998) presented a modal strain energy based method for damage detection. The method made use of the change of modal strain energy in each structural element, before and after the occurrence of damage. In their research, the stiffness matrix K^d, the i^{th} modal eigenvalue λ_i^d, and the i^{th} mode shape $\varnothing_i^d$ of the damaged system were represented as follows:

$$K^d = K + \sum_{j=1}^{L} \Delta K_j = K + \sum_{j=1}^{L} \alpha_j K_j \qquad (-1<\alpha_j\leq 0) \qquad \text{Equation 2.7}$$

$$\lambda_i^d = \lambda_i + \Delta\lambda_i \qquad \text{Equation 2.8}$$

$$\phi_i^d = \phi_i + \Delta\phi_i = \phi_i + \sum_{j=1}^{m} c_{ij}\phi_j \qquad \text{Equation 2.9}$$

where α_j is coefficient defining a fractional reduction in the j^{th} elemental stiffness matrices; c_{ij} is coefficient defining a fractional change of the mode shape vector; m is the number of modes considered, and L is the total number of elements in the system. So the elemental modal strain energy change (*MSEC*) for the j^{th} element in the i^{th} mode is expressed as

$$MSEC_{ij} = \phi_i^{dT} K_j \phi_i^d - \phi_i^T K_j \phi_i \qquad \text{Equation 2.10}$$

Then the modal strain energy change ratio (*MSECR*) was defined in the research as an indicator for detecting location of damage:

$$MSECR_j^i = \frac{\left| MSE_{ij}^d - MSE_{ij} \right|}{MSE_{ij}} \qquad \text{Equation 2.11}$$

where j and i denote the element number and mode number respectively; and *MSE* and MSE^d denote the modal strain energy before and after the occurrence of damage. If the modal strain energy for several modes were considered together, the $MSECR_j$ of the j^{th} element was defined as the average of the summation of $MSECR_j^i$ for all the modes normalized with respect to the largest value $MSECR^i_{max}$ of each mode.

$$MSECR_j = \frac{1}{m}\sum_{i=1}^{m} \frac{MSECR_j^i}{MSECR_{\max}^i} \qquad \text{Equation 2.12}$$

Subsequently in 2000 (Shi, Law and Zhang), the modal strain energy change method was further developed by the same authors. In this further development, the method is the same for damage localization, but a new parameter is developed to estimate severity of damage:

$$MSEC_{ij} = \sum_{p=1}^{L} -2\alpha_p \phi_i^T K_j \sum_{r=1}^{n} \frac{\phi_r^T K_p \phi_i}{\lambda_r - \lambda_p} \phi_r \qquad \text{Equation 2.13}$$

In Equation 2.13, the left hand side is the element modal strain energy change of the j^{th} element in the i^{th} mode, which was calculated from Equation 2.10 by using the mode shape of the undamaged and damaged states. The right side of Equation 2.13 consists of known information from the undamaged system, except for α_p. Thus the severity of damage, α_p, was calculated by solving Equation 2.13.

The modal strain energy change method was developed further again by the same authors in 2002 (Shi, Law and Zhang 2002). In this research, a weighting factor was introduced into the calculation of damage detection parameters, in order to improve computation accuracy. To verify the modal strain energy change method, a fixed end beam was constructed numerically. The beam consisted of 12 two-dimensional beam elements, 13 nodes and 39 degrees of freedom. The damage was simulated by decreasing the stiffness of the elements. The experimental test was performed on a two-storey steel plane frame, 2.82 m high and 1.41 m wide. Damage was simulated by removing angles at the joint. This release of restraints only affected the bending stiffness of the horizontal member, retaining the original connectivity of the structure. Both numerical and experimental results proved that the method was capable of locating damage and estimating damage. However, the method was sensitive to noise presence and the convergence property of the method presented great obstacles to satisfactory performance of the method.

Li et al. (2006) presented a modal strain energy decomposition method for damage localization. The method was based on decomposing the modal strain energy of each structural element into two parts, one of which was associated with the element's axial coordinates, and the other was associated with the element's transverse coordinates. Therefore, two damage indicators (axial damage indicator and transverse damage indicator) were formulated for each element of the structure. The two indicators were obtained from axial as well as transverse modal strain energy, respectively. Both numerical and experimental work indicated that the axial damage indicator was able to locate damage occurring in horizontal elements, and that the transverse damage indicator was able to locate damage occurring in vertical elements. However, the

method generated false positive error during the procedure of damage detection. Nor did it perform well in estimating severity of damage.

Hu et al. (2006a) presented cross-modal strain energy (CMSE) method for estimating severity of damage. In this research, a definition of stiffness matrix of damaged structures was made as follows:

$$K^* = K + \sum_{n=1}^{N_d} \alpha_n K_{\ln} \qquad \text{Equation 2.14}$$

where N_d was the total number of the damaged elements; α_n and l_n were the damage extent and the element number of the n^{th} damaged element, respectively; K was the stiffness matrix for the undamaged structure. The structural cross-modal strain energy between the i^{th} mode of the baseline structure and the j^{th} mode of the damaged structure was defined by the authors as:

$$C_{ij} = (\phi_i)^T K \phi_j^* \qquad \text{Equation 2.15}$$

where ϕ_i denotes the i^{th} eigenvector and ϕ_j^* denotes the j^{th} eigenvector respectively. The corresponding elemental cross-modal strain energy for the stiffness matrix was defined as:

$$C_{n,ij} = (\phi_i)^T K_{\ln} \phi_j^* \qquad \text{Equation 2.16}$$

After many steps of derivation, Equation 2.14 was rewritten as Equation 2.17:

$$\sum_{n=1}^{N_d} \alpha_n C_{n,ij} = \left(\frac{\lambda_j^*}{\lambda_i} - 1\right) C_{ij} \qquad \text{Equation 2.17}$$

Therefore, the parameter α_n was calculated by solving Equation 2.17, and was then used to estimate severity of damage. A three-dimensional five-storey frame structure was built numerically to verify the proposed method. Damage was simulated by decrease of stiffness of elements. The numerical results showed that the cross-modal strain energy method was capable of estimating the severity of damage under noise free measurement, if avoiding the numerical singularity problem. However, according to the authors, the method was not able to identify the location of damage. The authors are currently developing the CMSE method as a combined scheme for damage localization and damage severity estimation.

The modal strain energy based methods have been widely used by many researchers in various fields and applications. Worden, Manson and Allamn (2001) applied the strain

energy method to experimentally detecting and locating damage in an aluminium sheet. Damage was simulated by a saw cut on the stringer, ranging from 10% to 90% depth of cut. The mode shape was normalised. Using the strain energy method, the damage index (using nine measurement points) was unable to localise the damage at a non-sensor location. A cubic convolution polynomial interpolation was used to estimate the mode shape at 19 equally spaced points between sensors. Utilising the reconstructed mode shape, the damage indices of modes 1 to 5 gave poor results; only the highest levels of damage gave results for modes 1, 3 and 5. Furthermore, the results showed many false indications at undamaged locations. When all the modes were used, the two highest damage levels were detected. However, there was false positive damage generated in the damage detection, due to the limitation of sensor locations, and to the sampling of the mode shapes.

Hu et al. (2006b) presented an approach for detecting surface cracks in various composite laminates. In the research, the energy associated with sub-region (*i, j*) for the k^{th} mode was given first:

$$U_{k,ij} = \frac{1}{2}\int_{y_j}^{y_{j+1}}\int_{x_i}^{x_{i+1}} [D_{11}(\frac{\partial^2 \phi_k}{\partial x^2})^2 + D_{22}(\frac{\partial^2 \phi_k}{\partial y^2})^2 + 2D_{12}\frac{\partial^2 \phi_k}{\partial x^2}\frac{\partial^2 \phi_k}{\partial y^2} + 4(D_{16}\frac{\partial^2 \phi_k}{\partial x^2} + D_{26}\frac{\partial^2 \phi_k}{\partial y^2}) \times (\frac{\partial^2 \phi_k}{\partial x \partial y}) + 4D_{66}(\frac{\partial^2 \phi_k}{\partial x \partial y})^2]dxdy \quad \text{Equation 2.18}$$

Then a fractional energy before and after damage was defined as:

$$F_{k,ij} = \frac{U_{k,ij}}{U_k} \quad \text{Equation 2.19}$$

$$F^*_{k,ij} = \frac{U^*_{k,ij}}{U^*_k} \quad \text{Equation 2.20}$$

where U_k and U^*_k were the modal strain energy associated with the mode shape ϕ_k before and after damage, respectively. Considering all measured modes *m*, a damage index in sub-region *(i, j)* was defined as:

$$\beta_{ij} = \frac{\sum_{k=1}^{m} F^*_{k,ij}}{\sum_{k=1}^{m} F_{k,ij}} \quad \text{Equation 2.21}$$

A normalized damage index was given by

$$Zi_j = \frac{\beta_{ij} - \overline{\beta}_{ij}}{\sigma_{ij}} \qquad \text{Equation 2.22}$$

where $\overline{\beta}_{ij}$ and σ_{ij} represented the mean and standard deviation of the damage indices, respectively.

To verify the method, a FE model was established to simulate a laminated plate. Eight-node linear solid element (SOLID 46) was adopted for the numerical modelling using the ANSYS program. To simulate surface crack, the nodes at the location of surface crack were replaced by separated nodes. In the experiment, a 209 mm × 126 mm × 2.4 mm laminated plate was built, and a 25 mm long and 1 mm deep surface crack was created near the centre by using a laser cutting machine. The test plate was excited by an impact hammer with a force transducer throughout all gird points. The dynamic responses were measured by an accelerometer fixed to the corner of the test plate. ME'Scope (software for general purpose curve fitting) was used to extract modal parameters. Even though the numerical results indicated that the proposed method was able to localise the damage, the experimental results showed that the method located the damage with a large degree of false positive error. Furthermore, the method was not applicable in case of multiple damages, and no information was made available in the paper regarding estimation of severity of damage.

A damage indicator method based on modal strain energy for plate-like structures was presented by Lee and Yun (2006). In their research, the coarse mode shapes obtained from field testing were interpolated into finer grids by using cubic polynomial function. Employing neural network techniques, the differences in mode shapes before damage and mode shapes after damage were used as the error-insensitive input data. Various damage scenarios were inflicted on the flange and web of the bridge. A success rate (SR) was employed for screening process out of 100 randomly perturbed cases for each damage case. In general, a SR of 43% was achieved in locating damage for single and two damage scenarios. It may seem to be quite low. However, it is difficult to consistently recognise an actually damaged member using the DIM-MSE with the presence of a significant noise level.

2.5.1.2.5 Dynamic Flexibility

An approach presented by Pandey and Biswas (1994) is one of the mostly frequently cited articles on using flexibility to detect damage. In their research, the flexibility matrix F was defined as

$$F = \Phi\Omega^{-1}\Phi^T = \sum_{i=1}^{n} \frac{1}{\omega_i^2}\Phi_i\Phi_i^T \qquad \text{Equation 2.23}$$

where Φ=[Φ_1, Φ_2, ... Φ_n] is the mode shape matrix, Φ_i is the i^{th} mode shape, Ω =diag(ω^2_i) is the modal eigen vector, ω_i is the i^{th} modal frequency. Based on the flexibility matrices, change in the flexibility matrix Δ can be obtained as

$$\Delta = F_i - F_d \qquad \text{Equation 2.24}$$

where F_i and F_d are the flexibility matrices for the intact and damaged cases, respectively. For each degree of freedom j, $\bar{\delta}_j$ is the maximum absolute value of the elements in the corresponding column of Δ, i.e.,

$$\bar{\delta}_j = \max_i \left|\delta_{ij}\right| \qquad \text{Equation 2.25}$$

where δ_{ij} are elements of Δ. Thus, in the research, $\bar{\delta}_j$ was used as the measure of change of flexibility for each measurement location, in order to be able to detect and locate damage in a structure.

In the numerical research, three types of beams, (a simply supported beam, a cantilever beam and a free-free beam) were used to study how presence of damage affected the flexibility matrix, and to demonstrate how this change of flexibility matrix can be used to identify and locate damage in a structure. Damage was simulated by reduction of the modulus of elasticity of the elements. In the experimental component of the research, a (U.S. Standard) W12×16 beam was used, which was of identical dimensions to those of the numerically modelled beams. The damage was simulated by loosening bolts from the splice plates, which were located at the bottom of the beam. The result of single damage testing of both numerical and experimental examples was successful: the location of damage was identified from just the first two measured modes of the structure.

Maeck et al. (2000) presented a technique for calculating direct stiffness of reinforced concrete beams, for application in damage detection. In the experimental program, two reinforced concrete beams were constructed, and damage was introduced by increasing static load. Then the beams were excited by hammer impact. Accelerometers were placed every 0.2 m at both longitudinal edges of the upper side of the beam (62 measurement points in total) to extract the modal parameters, and to obtain the dynamic response of the beam. The experimental results showed that the method located the damaged region with reasonable success. However, this damage detection procedure required a rather dense measurement gird, in order to enable accurate identification of the higher mode shapes for curvature calculation.

A method, designated as damage locating vector (DLV), was presented to locate damage in structures that could be treated as linear in regard to pre- and post-damage by Bernal (2002). His basic concept was as follows: lack of deterministic information on the input can be partially compensated for, by knowledge of the structure of the mass matrix. He proposed the DLV for location of damage by inspecting stress fields created by vectors that were contained in the null space of the change in flexibility. The method was then applied to a planar truss, consisting of 44 bars and a total of 39 DOF. All the bars in the truss were made of steel and the section area was 64.5 cm^2. The results indicated that the DLV method only identified small sets containing the damaged elements. The author suggested that a final assessment on robustness, therefore, awaits experimental validation.

Gao et al. (2006) extended the DLV method for continuous structure health monitoring. The essence of the proposed method was to construct an approximate flexibility matrix for the damaged structure, utilizing the modal normalization constants from the undamaged structure. In the numerical simulation, a planar truss structure, which consisted of 53 steel bars, was adopted to verify the method. Damage was simulated by reducing the stiffness in one element of the truss. The numerical example indicated that the proposed method located the damage, by showing that the normalized cumulative stress value of the damaged element was smaller than that of the undamaged elements. However, false positive error was generated in the processing of damage detection, because a number of normalized cumulative stress values of the undamaged element were smaller than the normalized cumulative stress value of the damaged element.

A global flexibility index (GFI) was proposed for health monitoring of highway bridges by Patjawit et al. (2005). The index was the spectral norm of the modal flexibility matrix, obtained in association with selected reference points sensitive to the deformation of the bridge structures. In the experiment, a simple steel beam and a reinforced concrete beam were selected to verify the method. The test simulated different degrees of deterioration by introducing cuts in the bottom flanges at the middle span of the beam. The results showed that the GFI decreased as the single cut size increased. The GFI value of a bridge was also measured, and the authors concluded that the regular monitoring of a bridge would provide an advanced warning for any sharp decay in its GFI, which was directly related to the global weakening of the bridge.

Maeck, J. and De Roeck, G. (2003) presented a vibration based damage assessment method, which made use of the calculation of modal bending moments and curvatures to derive the bending stiffness at each location. In the method, it was assumed that damage can be directly related to a decrease of stiffness in a structure. To validate the method, experimental work was performed on Z24 Bridge in Canton Bern, Switzerland. The bridge was a prestressed bridge, with three spans, two lanes and 60 m overall length. The experimental results indicated that even though the method was able to predict the location of damage, the results of higher modes gave bad indications. The authors concluded that the direct stiffness calculation might be a good alternative for other sensitivity-based updating damage detection methods.

2.5.2 Methods Based on Time Domain Vibration

Time domain based damage detection methods can provide spatial information relating to damage in structures. These methods can also provide precise information regarding time of damage as listed below.

The Hilbert-Huang transform (HHT) method is a time domain based method which has been investigated in damage detection for this reason. There are two steps in the Hilbert-Huang transform data analysis method. The first step is the empirical mode decomposition (EDM), which can decompose any data set into several intrinsic mode functions (IMFs) by a procedure called sifting process. The second step of HHT method is implemented by performing the Hilbert transform to each IMFs component (Zhang et al 2003).

Nari er al (2006) presented a time serious algorithm for damage identification and localization. The vibration signals obtained from sensors are modelled as autoregressive moving average (ARMA) time series. In their research, a new damage-sensitive feature, DSF, was defined as a function of the first three auto regressive (AR) components. It is found that the mean values of the DSF for the damaged and undamaged signals were different. Thus, a hypothesis test involving the t-test was used to obtain a damage decision. Two localization indices, LI_1 and LI_2, defined in the AR coefficient space were also introduced. The damage detection methodologies were test on the analytical and experimental results of the ASCE benchmark structure. The result of the damage detection indicated that the method was able to detect the existence of all damage pattens corresponds to removal of single brace, removal of all braces in a story and removal of all braces in two stories, respectively. The researchers also addressed that represent initial testing of the algorithm and further investigations will be needed to test the validity of the damage detection method.

Xu et al (2003) firstly applied the HHT method to a set of measured data to identify dynamic characteristics of a building, and then compared the results with those from the fast Fourier transform (FFT) based method. The building was located in downtown Sheng Zhen city in China and had sixty nine storeys. The set of measured data recorded the wind velocity and structural dynamic response of the building during Typhoon York, between 17:20 (Hong Kong time) on 15 September 1999, and 8:20 (Hong Kong time) on 17 September 1999. Then the HHT method was applied to the measured data to obtain dynamic characteristics of the building. According to the test results, the natural frequencies identified by the HHT method were almost the same as those rendered by the FFT method. The first two modal damping ratios given by the HHT method were lower than those of the FFT method. Chen et al (2004) performed similar research, using the HHT method to identify the natural frequencies and modal damping ratios of Tsing Ma suspension bridge during Typhoon Victor. Chen et al. drew the same conclusion as Hu et al., which the HHT method and the FFT based method produce almost identical natural frequencies, but that the FFT based method gives higher damping ratios than the HHT method.

After researching the use of the HHT method to identify dynamic characteristics of a structure, Xu et al. (2004) further investigated the use of the HHT method applied to

identification of structural damage caused by a sudden change of structural stiffness. The experimental research was performed on a model three-storey building, consisting of three steel plates 850 mm × 500 mm × 25 mm, and four rectangular columns of cross section 9.5mm×75mm. Damage was simulated by pulling out a pin which connected the floor plate and the spring, thereby releasing the spring during the vibration of the building. The results showed that the method was able to identify the damage time instant, by observing the occurrence time of damage spikes appearing in the first IMF component of the acceleration response. However, the method was not robust in locating damage, and no quantitative relationship between the spike amplitude and the damage severity was established by the experiment. The authors suggested that further investigation was therefore required.

Zhang et al (2003) examined the rationale of HHT for analysing dynamic and earthquake motion recording in studies of seismology and engineering. Their study showed that HHT was suitable for analysing non stationary dynamic and earthquake motion recordings, due to the following: the grouped IMF components were capable of capturing both the low frequency pulse like wave signals, and the high frequency wave signals, from the original data. Therefore, their paper concluded that HHT performed better than some conventional Fourier data processing techniques for extracting some features of recording in studies of seismology and earthquake engineering.

Yang et al. (2004) proposed two methods to extract damage information from measured time history data obtained from a structure. The first method, based on the EMD, was designed to extract damage spikes of a sudden change in structural stiffness, and thereby to detect the damage time instants. The second method, based on EMD and Hilbert transform, was designed to detect the damage time instants as well as to detect the natural frequencies and damping ratios of the structure before and after damage. To demonstrate the two proposed methods, the four-storey ASCE benchmark building was used in the numerical study. The first method was found to be able to detect the damage time instants only if the noise pollution level was very small and the changes in the structure were not abrupt. In general, if the level of noise pollution was high or the damage was small, the first method might not produce satisfactory results. The simulation results from the second method showed that it was capable of determining the time instant of damage occurrence, and also of identifying the natural frequencies

and damping ratios of the structure, both before and after damage. However, with only a single record, the location and the severity of damage in the structure were not identified. In the same paper, the authors suggest that they have already extended their second method in order to identify system matrices, which they plan to report on in the future.

Zhou et al. (2006) used HHT method for system identification and damage detection in their research. A three-storey structure, 90 cm tall and 64.6 kg in weight, was built in the laboratory. Damage was simulated by removing two columns of the structure. The experimental results indicated that the HHT method was capable of identifying the structure characteristics, such as stiffness matrices, and therefore was capable of detecting the damage by comparing the stiffness of each storey unit before and after damage. It is worth mentioning that the experimental structure consisted of only six supporting columns on each level, and that damage was simulated by removing two out of these six columns. This degree of damage is quite extreme, and the stiffness of the damaged storey unit decreased sharply after damage.

2.5.3 Methods Based on Artificial Intelligence

Neural networks are computational models derived from understanding of the structures and operations of the human brain. They are an assembly of connected processing units called neurons. The strength of the connection is represented by the "weights" or parameters, which are determined in the training process. Since neural networks provide a range of powerful new techniques for solving problems in pattern recognition, data analysis and control, they have been adopted in engineering contexts for the detection of damage in various structures.

Yam et al. (2003) presented an integrated method for damage detection of composite structures using the wavelet transform and artificial neural networks (ANN) identification. In this numerical study, a PVC sandwich plate, 295 mm in length, 98 mm in width and 8 mm in thickness, was modelled and then employed in the damage detection. Damage was simulated by using different nodal coordinates to generate the length, width and depth of crack. A neural network with 32 inputs and 4 outputs was designed for application to the numerical model. Then, among the acquired 120 sets of

vibration response of the sandwich plate with different crack damage, 108 sets of data were taken as samples for training the ANN, and the remaining twelve sets of samples were taken for performance verification of the trained ANN. The results indicated that the damage location detected by the trained ANN was close to the real location. However, the output error of the ANN gradually increased as the crack length decreased. Clearly, the accuracy of damage detection using the ANN in this research was influenced by the severity of damage. Furthermore, it was found that the noise disturbance had a key effect, influencing the results of damage detection.

Su et al. (2004) proposed another artificial neural network based damage detection method. Initial to the research, an Intelligent Signal Processing and Pattern Recognition (ISPPR) package was developed, using wavelet transform and artificial neural network. Then the spectrographic characteristics of simulated Lamb wave signals were extracted and digested as Digital Damage Fingerprints (DDF), in order to construct a Damage Parameters Database (DPD) based on ISPPR. Finally, the DPD was employed to train a multi-layer feed forward artificial neural network to detect damage. The damage location predicted by the method was close to the actual location. However, the research did not mention either multiple damage detection cases or damage severity estimation.

Suresh et al. (2004) utilised modal frequencies of a cantilever beam having transverse surface crack, for training a neural network to predict both crack location and depth. The structure was created analytically. Various crack locations and depths were inflicted, using a fracture mechanics based crack model with an effective spring at the crack location. In the research, multi-layer perceptron (MLP) and radial basis function (RBF) networks were utilised for damage detection. The results showed that the RBF network performed better than the MLP network; the former required longer training time however.

Fang et al. (2005) proposed a tunable steepest descent (TSD) algorithm to detect damage by using frequency response functions as input data to the neural network. A cantilevered beam was simulated to verify the accuracy of the proposed method. The dimensions of the simulated beam were 0.5 m in length, 0.04 m in width and 0.002 m in thickness. The frequency response functions of both the undamaged and the damaged beams were used as input data in construction of the TSD based neural network, which was a three-layer feed forward network with 78 input nodes, 40 hidden nodes and 5 output nodes. The network outputs were designed to render the relative stiffness ratio of

the damaged structures in comparison to the relative stiffness ratio of the undamaged structure. In the numerical work, the results from the TSD based artificial neural network were compared to those from a DSD (dynamic steepest descent) based artificial neural network and from a FSD (fussy steepest descent) based artificial neural network. It was found that the TSD based neural network outperformed both the DSD and the FSD based neural networks, since the TSD method improved the convergence performance.

In 2008, Gonzalez et al. presented a method for damage identification in buildings with steel moment-frame structure. Their method is based on artificial neural network and modal variables. In the research, a simplified finite element model (a five storey building) was used to generate the data needed to train the neural network. The five storey building was 16m in width and 18m in length, with a height of 4m for the first floor and 3m for the following floors. The input to the neural network was the first flexural modes (natural frequencies and mode shapes) at each principal direction of the structure; the outputs were the spatial variables (mass and stiffness). Then a damage index at each storey was determined by comparing the initial and final stiffness. The proposed method was able to ascertain which storey of the building was damaged. However, the results were sensitive to both noise presence and to modal errors.

Sazonov et al (2002) presented a fuzzy logic expert system designed to mimic the human decision process. An expert system allows for easy encoding of expert knowledge as a set of rules. “Fuzziness” of the expert system allows better treatment of the uncertainties of the problem and to simplify the expert system itself. In the research, the fuzzy expert system was designed based on a finite element model of a simply beam and provided reliable detection of damage for every tested damage scenario. The system recognized damages with 100% accuracy, and not false positives or negatives on mode shapes acquired by impact testing and/or non-contact laser vibrometer techniques.

2.5.4 Methods Based on Wavelet Analysis

Wavelet analysis is a common tool for analysing localized variations of power within a time series. By decomposing a time series into time-frequency space, it is possible to determine the dominant modes of variability, and also how those modes vary in time

(Torrence & Compo 1997). Therefore, wavelet analysis has recently emerged as a tool both for damage detection and for structural health monitoring, that is, for measuring the difference between pre- and post-damaged states.

Hou et al. (2000) proposed a wavelet-based approach for structural damage detection. Their research numerically simulated a single-degree-of-freedom mass-damper-spring system. In the system, each spring was pre-assigned a threshold value, and a spring broke if the structural response exceeded its corresponding threshold value. After wavelet analysis of the time history data from the system under harmonic excitation, the results demonstrated that their wavelet-based approach was able to detect the damage time instant by showing spikes in the details of wavelet decomposition. However, the numerical model (a single-degree-of-freedom mass-damper-spring system) used in the research was very simple; it is not yet known whether or not the method can successfully be applied to structures of normal complexity.

Melhem et al. (2003) investigated the effectiveness of vibration-based methods in damage detection by using FFT and continuous wavelet transform (CWT) analysis. As part of the experimental work which constituted their research, a Portland cement concrete pavement (15.2 cm thick, 609.6 cm long and 167.6 cm wide) and a prismatic prestressed concrete beam (335.3 cm long, 30.5 cm deep and 16.5 cm wide) were built in the laboratory. The cement concrete pavement was subjected to degradation induced by a truck axle, loaded to 4994 kg. A total of nine linear variable displacement transducers (LVDTs) were installed to measure the slab deflection due to the impulse loads. The damage in the prismatic prestressed concrete beam was introduced by applying a static load on top of the beam. Response acceleration data of the beam was measured using two accelerometers installed at the bottom of the beam. Results showed that FFT analysis was able to detect the damage in the beam but not in the slab, while the CWT was able to detect the damage for both structures. Furthermore, even though both FFT and CWT identified which frequency components existed in the signal, only CWT analysis showed when a particular frequency occurred. However, damage location was not accurate and no research into damage severity was performed during the experiment.

Hera et al. (2004) presented an application of wavelet analysis for damage detection using ASCE structural health monitoring benchmark data. The structure used in the benchmark study was a four storey; two-bay by two-bay steel-frame scale model structure with a total hight of 3.6 m and plan dimensions of 2.5 m×2.5 m. Damage was simulated by removing bracing elements in the structural model. The results indicated that the damage time was detected by spikes in the wavelet details. However, the effectiveness of the wavelet approach was relative to the measurement noise level and the damage severity.

Han et al. (2005) proposed a wavelet packet energy rate index for damage detection on beam structures. In their research, the measured dynamic signals were firstly decomposed into the wavelet packet components, and then the wavelet energy rate index was computed to detect the damage. Five simply supported beams (one undamaged beam and four damaged beams) were numerically modelled using ANSYS, and damage was simulated by reducing the stiffness of specific elements. Further, in experimental work, four different steel beams were built in the laboratory and damage was simulated by cutting part of an element at the bottom of the beam. The results showed that the wavelet energy rate index was able to locate the damage in different beams in both numerical and experimental research. Unfortunately, damage severity was not able to be estimated in the research.

2.6 Finite Element Modelling of Reinforced Concrete

In developing a theory of non-destructive damage detection, it is crucial to validate the theory by the use of numerical work. Finite element modelling of reinforced concrete structures are briefly reviewed here. In Chapter 4, finite element modelling will be used for the numerical modelling of concrete beams, in order to verify the novel damage detection method proposed in this thesis.

2.6.1 Modelling of the Reinforced Concrete Beam and Its Nonlinearity

Reinforced concrete structures are widely employed in civil engineering because of the benefits of combining the two construction materials (steel and concrete). However, the

inelastic behaviour of composite members in reinforced concrete is not yet thoroughly understood. Therefore, it is difficult to simulate nonlinearities in the response of reinforced concrete, a difficulty related to inelasticity of materials.

To investigate the question of how to model the nonlinearities in the response of reinforced concrete, Liang et al. (2005) developed a three-dimensional finite element model to account for geometric and material nonlinear behaviour of reinforced concrete beams. In their finite element modelling, steel reinforcing bars in concrete were modelled as smeared layers with a constant thickness in shell elements, and a bilinear stress-strain relationship was used for steel bars in both compression and tension zones. The concrete in compression was modelled as an elastic-plastic material with strain softening. Then the finite element model was verified by experimental data. The finite element model, as developed in this research, predicted the ultimate strength of composite beams in combined bending and shear. It was concluded in the paper that the design model was applicable to simply supported composite beams with any section.

Spacone et al. (2004) proposed two models to simulate the bond condition between concrete and steel. The first model used concentrated springs to simulate the connection between concrete and steel, which were modelled by different elements. This concentrated spring model was simple to use, but presented a number of disadvantages. First of all, it required a large number of elements, and therefore a large number of degrees of freedom were generated, which required huge computational resources. Secondly, fibre elements were used as part of the modelling, which accounted for the softening behaviour of concrete under large compressive strains, which might lead to strain localization problems. The second model was based on distributed bond. Assumptions were made in the second simulation that bond stress and bond slip were continuous along the contact surface, and also that the steel and the concrete had the same vertical displacement and curvature. It was found that the second model simulated the bond condition between steel and concrete more accurately than the first model.

Paepegem et al. (2005) investigated the relationship between degradation of bending stiffness and damage in a beam. It was found that the relationship was not linear, and that a nonlinear correction term was required for application to classic beam theory. The

nonlinear relationship between the degradation of the bending stiffness and the damage was expressed as follows:

$$EI(x) = E_0[\int_{-\frac{h}{2}}^{\frac{h}{2}}(1-D)y^2dy - \frac{(\int_{-\frac{h}{2}}^{\frac{h}{2}}(1-D)ydy)^2}{\int_{-\frac{h}{2}}^{\frac{h}{2}}(1-D)dy}] \qquad \text{Equation 2.26}$$

where $EI(x)$ is the degraded bending stiffness, E_0 is the original elastic modulus, D is the scalar damage ($0 \leq D \leq 1$), h is the total thickness of the beam. The results from a displacement-controlled bending test showed that the experimental data agreed with the relationship expressed in Equation 2.26. However, more research needs to be performed to investigate if the theory is valid on structures other than beams.

2.6.2 Modelling of Damage in Reinforced Concrete

Modelling of damage in reinforced concrete beams is a central concern when studying the vibration behaviour of reinforced concrete beam. Often the damage is represented by cracks, and numerous models of beams with cracks have been developed. These generally include either a crack that is permanently open, or a "breathing" crack which opens and closes during vibration.

Many models simulate cracking in beams by either a massless rotational spring at the joint between two of the beam elements, or by reducing the stiffness in one element. Narkis (1994) proposed a method for calculation of natural frequencies of a cracked simply supported uniform beam. The crack was simulated by an equivalent linear spring, connecting the two segments of the beam. Then the data on the variation of the first two natural frequencies was processed to detect damage. By comparing the experimental results to the numerical finite element calculations, the authors concluded that the procedure of damage detection was simple and accurate.

The method was extended to a beam with a series of cracks by Shifrin and Ruotolo (1999), who proposed a new technique to calculate natural frequencies of a vibrating beam with an arbitrary finite number of transverse open cracks. In the research, the cracks were represented by massless springs. Nandwana and Maiti (1997) also used a rotational spring to simulate crack in their research, developing a method based on

measurement of natural frequencies for detection of the location and size of a crack in a stepped cantilever beam.

While the research mentioned above used rotational springs to simulate cracks in different beams, Fernanadez-Saez et al. (1999) suggested a different approach. Their research presented a simplified method of evaluating the fundamental frequency for the bending vibration of cracked beams. The method was based on the approach of representing the crack in a beam by a spring, but in their work the transverse deflection of the cracked beam was constructed by adding polynomial functions to that of the uncracked beam. The coefficients in the polynomials were calculated using the boundary conditions and slope discontinuity (caused by the spring representing the damage) at the cracked position.

Since most cracks open and close during vibrations, unless a static load is applied, much research has been performed to simulate this kind of "breathing crack". Ballo (1998) modelled a cracked rotating shaft with a breathing crack represented by a rotational spring element. This element had different properties, depending on whether the curvature was positive or negative. Cheng et al (1999) modelled the breathing crack as a non-linear spring, but their model was limited to the fundamental mode. This was because they had to assume that the changes in the spring's properties occurred at the fundamental frequency, to enable the equation of motion for the beam to be solved. Kisa and Brandon (2000) proposed a finite element model of a steel beam with a fatigue crack with varying degrees of closure. They then used modal superposition to model the transition region, and to calculate the natural frequency of the cracked beam. These models included crack non-linearity, to enable a better prediction of the natural frequency of a cracked beam. Any changes in frequency due to a change in amplitude of vibration were not investigated. Instead, the vibration was assumed to be linear with amplitude.

Many damage detection methods have been performed numerically by using stiffness reduction in elements to simulate damage. Kim and Stubbs (2002) simulated damage in beams by reducing the elastic modulus of the appropriated elements, as part of the verification of their proposed modal strain energy based damage detection method; Shi et al. (2002) reduced the elastic modulus elements in their modal strain energy change

damage detection method; and Li, Yang and Hu (2006) also used the loss of elastic modulus to simulate damage, when performing their modal strain energy decomposition method for damage localization in 3D frame structures. Choi, Park and Stubbs (2005) proposed a damage index, based on changes in the distribution of the compliance of the structure, for damage identification. In the modelling of the two beams, damage was numerically simulated by reducing the elastic moduli of the appropriated elements. Kim et al (2006) also simulated a damaged beam by reducing the elastic moduli for specific elements, in order to verify a damage detection method in their numerical study.

An alternative method to simulate damage was proposed by Soh et al. (2003), who investigated the damage in concrete around a reinforcement bar, and defined three types of damage, in concrete and at the concrete-rebar interface. Based on their definitions, a three-dimensional damaged reinforced-concrete (DRC) element (Figure 2.4) was proposed, then implemented as a user defined element of MSC MARC2000 (a commercial finite element analysis software package). The element consisted of a 10 node concrete element, a two node rebar element, and a four node concrete-rebar interface element. Numerical results showed that the DRC element was able to simulate the bond deterioration in reinforced-concrete structural members. However, only one bar was considered in the model, and its direction was only along an axis of the coordinate system. The size of the element was also limited to a certain length. These limitations, on the size of the element, the number of the rebar and the direction of the rebar, hindered the further use of the modelling. Garesci et al (2006) presented a method to detect damage using variations in modal parameters. In the research, a rectangular plate of homogeneous and isotropic material, under free-free constraint conditions, was modelled in order to verify the method. Damage was simulated by a milled slot, 3mm wide and of various lengths. This kind of damage simulation in numerical research was suitable for simulation of void materials in structures.

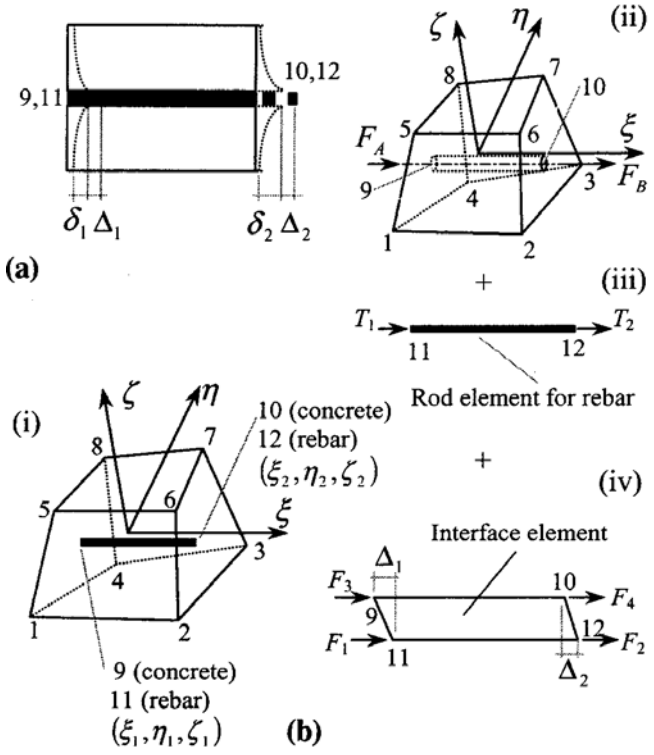

Figure 2.4 Construction of 12-node DRC element: (a) deformation of DRC element; (b) assembly of DRC element (i = ii+iii+iv)

2.7 Conclusions

This chapter opened with a brief introduction followed by the background and state-of-the-art of damage detection methods, specific to reinforced concrete structures. A brief description of previous reviews and surveys of vibration based damage detection was introduced and some basics of damage detection were briefed, including the important definition of the four levels of damage detection. Then the gist of this research work, namely global non-destructive vibration based damage detection methods, was extensively reviewed. Some relevant work using finite element (FE) to model reinforced concrete structures was also highlighted as FE modelling forms part of the important contribution and advancement to knowledge in the thesis, especially in the non-linear simulation.

It is clear from the literature review that although promising research has been performed on non-destructive vibration based damage detection in reinforced concrete structures, there are still many challenges before making them practical. These include,

particularly selection of a sensitive index to damage severity and the effects of presence of noise and problems due to limited sensors. Therefore, a non-destructive modal based damage detection method which is sensitive to the presence of damage, but much less sensitive to the presence of noise, need to be developed. The work presented in this thesis is developed out of the following issues:

1. Many vibration based damage detection methods, as reviewed in this chapter, have only been applied to examples of single damage sites. Also, damage detection results have commonly been compromised due to presence of noise. Moreover, it is found from the literature review that derivatives of modal parameters are more sensitive to damage than the original modal parameters themselves. Therefore, a novel modal based damage detection method, namely, modal strain energy based method, which is more robust than existing methods, needs to be developed and proposed in the research. Furthermore, the newly developed method requires to be less mode dependant, and to work in cases of both single and multiple damage in real environments including in presence of noise. The proposed method should be capable of estimating severity of damage as well.
2. To solve the problem of limited number of sensors in the experimental work, appropriate mode shape reconstruction techniques should be adopted, thus improving damage detection ability of the proposed method. The proposed damage detection method should be verified by using numerical data, both with and without the presence of noise.
3. In the literature review, most proposed damage detection methods were not performed on reinforced concrete structures, due to the complexity of the materials of reinforced concrete. Therefore, a new robust damage detection method is developed specifically for reinforced concrete structures. To verify the proposed damage detection method, numerical models of reinforced concrete beams should be developed as part of the research, and then applied in the detection of different scenarios of damage in reinforced concrete beams.
4. To verify the proposed method, modal testing and modal analysis on reinforced concrete beams should be performed as experimental work. The proposed damage detection method should then be applied to the experimental results. To verify its accuracy and robustness, the results of the proposed damage detection

CHAPTER 3

DESIGN OF RC SPECIMENS AND ASSOCIATED PROPERTY TESTING AND STATIC TESTING

3.1 Introduction

This chapter presents the details of the reinforced concrete (RC) beam test specimens, which will be used for the experimental damage detection investigation in Chapter 7. Some basic knowledge of the material properties of both concrete and reinforced steel are briefly introduced and the results of property testing are discussed. These properties will be utilised for the finite element (FE) modelling of a reinforced concrete (RC) beam in Chapter 4. The four-point bending test on a reinforced concrete beam specimen is also described and the non-linear mechanical behaviour of the RC beam is analysed. The results of the bending test will be used for validating the numerical modelling of the RC beam. Finally, in order to process the measured strain data from the test, least square technique for best fit strain plane is introduced. The estimated strains at middle span are also illustrated. These results will also be used to validate the numerical model.

3.2 Dimensions of the RC Test Beams

Six reinforced concrete beams were cast in the UTS Structures Laboratory. Among the six beams, one beam was employed to perform a four-point bending test to destruction, in order to capture relevant characteristics of the beam for validating the finite element model. The remaining five beams were used for experimental modal analysis (EMA), followed by damage detection studies. Among these beams, subsequently, some of them were subjected to static load test to destruction in order to obtain their remaining strength capacity.

The dimensions of the reinforced concrete beams are shown in Figure 3.1. The beams were cast with cross sectional dimensions of 300 mm in height, 150 mm in width and

with an overall length of 3,560 mm. The concrete for the test beams were of ready-mixed concrete ordered from a nearby concrete batching plant. The concrete was of Grade 25 with 150 mm slump to provide the desired workability. The beams were singly reinforced with high tensile steel bars, i.e., two 16 mm diameter tension bars (one layer on bottom), two 16 mm diameter compression bars (one layer on top), and 10 mm diameter mild steel stirrups at a spacing of 200 mm centre-to-centre. The concrete cover to the stirrups was nominal 50 mm thick.

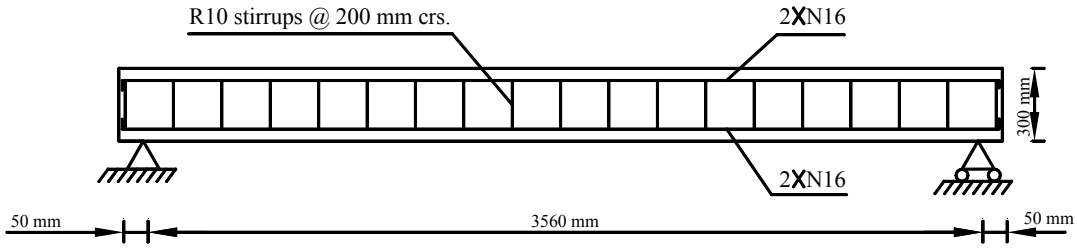

Figure 3.1 The dimensions of the reinforced concrete beams

3.3 Properties of Concrete and Steel and Property Testing

3.3.1 Properties of Concrete and Steel

Concrete is made from cement, aggregates and water, as well as admixtures. Therefore, concrete can be regarded as a complex mixture of materials, each component of which may, in itself, vary in their properties. The material properties of concrete include compressive strength, tensile strength, shear strength, stress-strain relationship, modulus of elasticity, creep and shrinkage.

The compressive strength, f_c', is usually in the range of 20 MPa to 70 MPa. The tensile strength (f_{ct}) of concrete is low. A good approximation for the tensile strength is 0.10 $f_c' < f_{ct} < 0.20\ f_c'$ (Bungey et al 2006). Shear strength is more difficult to determine experimentally than tensile strength, due to the difficulty of isolating shear from other stresses. Shear strength may be considered as 20% to 30% greater than the tensile strength of concrete, or about 12% of its compressive strength.

Typical stress-strain curves for concretes of different strength are shown in Figure 3.2. The curves are obtained by testing concrete cylinders to rupture at the age of 28 days, and by recording the strains at different load increments (1psi=6.89×10^3 Pa) (Hassoun & Al-manaseer 2008). All the curves consist initially of a relatively straight elastic portion, reaching maximum stress at a strain of about 0.002; rupture then occurs at a strain of about 0.003.

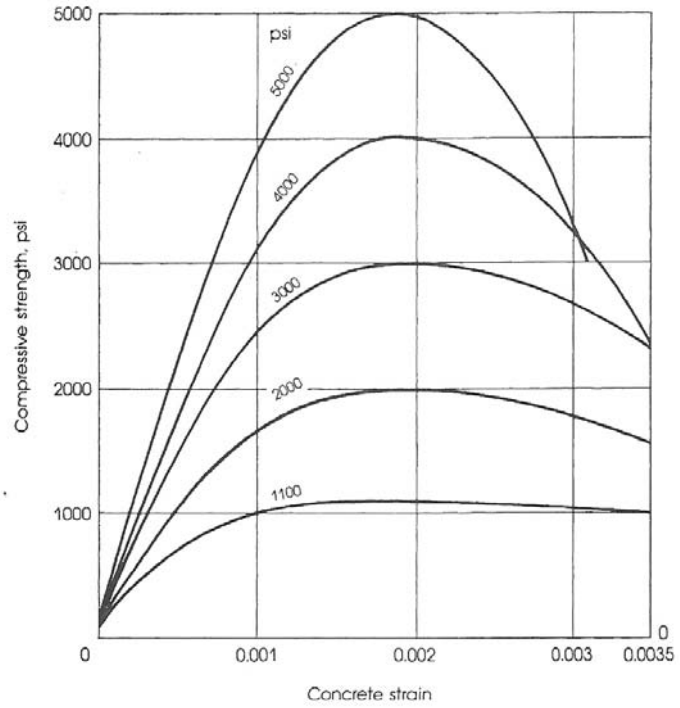

Figure 3.2 Typical stress-strain curves of concrete (Hassoun & Al-manaseer 2008)

One of the most important elastic properties of concrete is its modulus of elasticity, which can be obtained from a compressive test on concrete cylinders. The modulus of elasticity can be defined as the change of stress with respect to strain in the elastic range. Shrinkage and creep in concrete are not discussed here, since they are not covered in the research scope of this thesis.

Steel is a homogeneous and isotropic material with a large linear elastic region in its stress-strain curve. Unlike concrete, which is much weaker in tension than in compression, steel behaves in the same manner in either the tension or the compression zones. Reinforcing steel is placed therefore mainly in the tension zone of a concrete member, in order to resist the tensile forces resulting from external loads on that

member. However, when applied force is sufficiently high, steel will exceed its yield point, and will begin to behave plastically until fracture failure.

The most important properties of reinforcing steel are Young's modulus (E_s) and yield strength (f_y). The modulus of elasticity is the slope of the stress-strain curve in the elastic range, up to the proportional limit. For most structural steels, the Young's modulus is taken as 2×10^5 MPa. The yield strength can be obtained from the stress-strain curve for most reinforcing steels. However, in high-tensile steel, ultimate strength is reached gradually under an increase of stress, and a definite yield point may not be identifiable on the stress-strain curve. In this case, the yield strength may be considered as the stress corresponding to a total strain of 0.5% to 0.6% under load.

3.3.2 Results of Property Testing

Nine concrete cylinder samples of 150 mm in diameter and 300 mm in height were cast together with the test beams in the laboratory. These samples were used to determine the properties of concrete for material properties input in the finite element modelling (Chapter 4). The cylinders were moulded in accordance with AS 1012.8 (2000).

Three concrete cylinders were used for the compressive strength test. The test was performed in accordance with AS 1012.9 (1999). For test preparation, the cylinders were cured in water (20ºC) until testing, and were capped with dental plaster on top loading surfaces in the testing. Another three concrete cylinders were used for the estimation of concrete density. The density of concrete was calculated from these test samples using the ratio of self weight over the volume. The remaining three concrete cylinders were used for the determination of modulus of elasticity. The modulus of elasticity was calculated based on AS 3600 (2001). The results of the concrete property testing are given in Table 3.1.

The tensile stress of concrete is usually estimated by assuming it to be one tenth of the compressive stress (Hassoun & Al-manaseer 2008). Based on the material test results, the estimated concrete tensile stress is 2.9 MPa. The information gathered from the material tests will be used in the numerical modelling in Chapters 4 and 6. Shrinkage

and creep of concrete are not considered in the modelling of reinforced concrete beams, thus these properties were not investigated in the laboratory.

Table 3.1 Properties of concrete used in the RC beams

Specimens	Compressive Strength (f_c') (MPa)	Density (ρ) (kg/m^3)	Modulus of elasticity (E_c) (GPa)
1	28.1	-	-
2	27.7	-	-
3	30.8	-	-
Average	**28.9**	-	-
Standard Deviation	**1.3**	-	-
4	-	2505	-
5	-	2405	-
6	-	2395	-
Average	-	**2435**	-
Standard Deviation	-	**49.6**	-
7	-	-	28.5
8	-	-	26.7
9	-	-	28.0
Average	-	-	**27.7**
Standard Deviation	-	-	**0.75**

The young modulus, the density and the yield strength of reinforcing steel are available from the laboratory tests in accordance with AS 4100 (1998) as is listed in Table 3.2.

Table 3.2 Properties of reinforcement used in the RC beams

Specimens	Yield Strength (f_{sy}) (MPa)	Density (ρ) (kg/m^3)	Modulus of elasticity (E_s) (GPa)
1	505	7983	209
2	492	7908	215
3	518	7824	191
Average	**505**	**7905**	**205**
Standard Deviation	**10.6**	**112.4**	**10.1**

3.4 Four-point Bending Test for the RC Beam

In order to validate the modelling of reinforced concrete (RC) beams, a four-point bending test was performed on a RC beam in the laboratory. Results of the test will be compared with the numerical results in Chapter 4.

3.4.1 Set-up of the Test

The experimental set up for the four-point bending test is illustrated in Figure 3.3. Two point loads are applied on the top of the beam at one third span from both end supports.

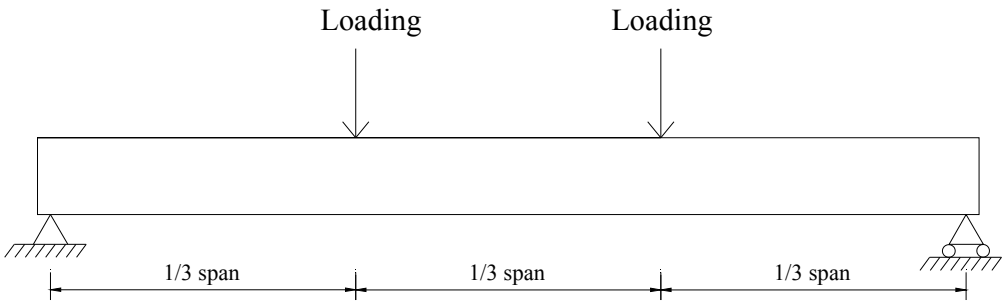

Figure 3.3 Experimental set up of four point bending test for the beam

In the static loading test, two 5mm strain gauges (S1 and S2) were instrumented on the compression bars (top layer) to record the compressive strain. Four 5mm strain gauges (S3, S4, S5 and S6) were instrumented on the tension bars (bottom layer) to record the tensile strain. The strain gauges S1, S3 and S4 were placed at quarter span, while the strain gauges S2, S5 and S6 were placed at middle span. All strain gauge locations are illustrated in Figure 3.4 and three typical strain gauges are shown in Figure 3.5.

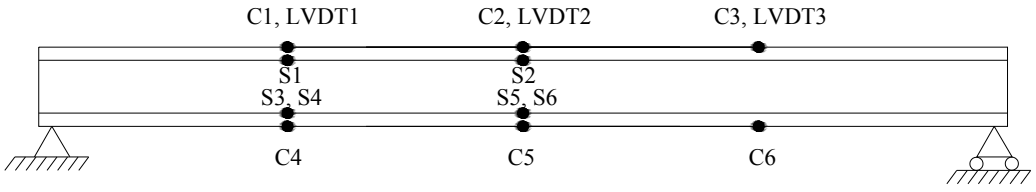

Figure 3.4 the locations of strain gauges and LVDT

Figure 3.5 Strain gauges for recording strain in the steel bars

Three 60mm strain gauges C1, C2 and C3 were instrumented on top surface of the beam to record the strain of the concrete in compression area. Three 60mm strain gauges C4, C5 and C6 were instrumented on the soffit of the beam to record the strain of the concrete in tension area. The strain gauges C1, C3, C4 and C6 were placed at quarter span and the strain gauges C2 and C5 were placed at middle span. All 60mm strain gauge locations are shown in Figure 3.4 and a typical strain gauge of this kind is shown in Figure 3.6.

Figure 3.6 A strain gauge for recording strain of concrete

Three displacement transducers or LVDTs (LVDT1, LVDT2 and LVDT3) were positioned on top of the beam to monitor the deflections of midspan and quarter span of the beam. The transducers LVDT1 and LVDT3 were placed at quarter span, while the transducer LVDT2 was placed at midspan. All LVDT locations are shown in Figure 3.4 and one typical transducer is shown in Figure 3.7.

Figure 3.7 A displacement transducer (LVDT) used for displacement monitoring

3.4.2 Response of the RC Beam under Different Stages of Static Load

Figures 3.8 shows the load-deflection curves at quarter span, midspan and three quarter span. Three main stages of the beam's behaviour under the static loads are observed in the reinforced concrete beam prior to failure. They are detailed as below.

Stage 1.

The applied load increased from 0 to 10 kN and no cracks were observed. At this beginning stage, tensile stresses started to develop at the bottom of the beam. The entire concrete section was effective, with the steel bars at the tension side sustaining a strain equal to that of the corresponding concrete. At any given section, the entire concrete and the steel reinforcement jointly resisted the bending moment and shearing force. At the end of this stage, maximum tensile stress at the bottom of the beam caused by applied

load was equal to the tensile strength of the concrete. The strain in the steel bars was equal to the strain in the adjacent concrete. On the other hand, the compressive stress of concrete at the top was much lower than the ultimate concrete compressive strength. Thus, the load-deflection relationship of the RC beam remained linear, as shown in Figure 3.8.

Stage 2.

The applied load increased from 10 kN to 70 kN. At the beginning of this stage, tensile stresses in the concrete started to increase to a point where cracks started to develop. This happened mainly at the midspan, where the highest stress occurred. The deflection of the beam also increased considerably. Since the concrete had cracked, only the steel bars were effective in resisting the tensile force. With cracks propagating, the neutral axis of the beam shifted upward. The concrete below the neutral axis did not participate much in resisting external moment. Thus the moment of inertia at cracked section decreased, and the stiffness of the beam also decreased. Therefore, as seen in Figures 3.8, the slopes of load-deflection curves for Stage 2 are relatively smaller than that of Stage 1.

Stage 3.

The applied load increased from 70 kN until the failure of the beam. At the initial portion of this stage, tensile strains increased rapidly until the maximum load was reached. The steel bars yielded, and cracks widened sharply. Both midspan deflection of the beam and the compressive strain in the concrete increased greatly. With the increase of load, strain hardening occurred in the steel and concrete reached its maximum strain. The concrete in the compressive zone started to crush prior to the failure of the beam as depicted in Figure 3.9. The beam was further damaged at this stage, the slopes of the curve at this stage are much smaller than those of Stage 2 as shown in Figure 3.8.

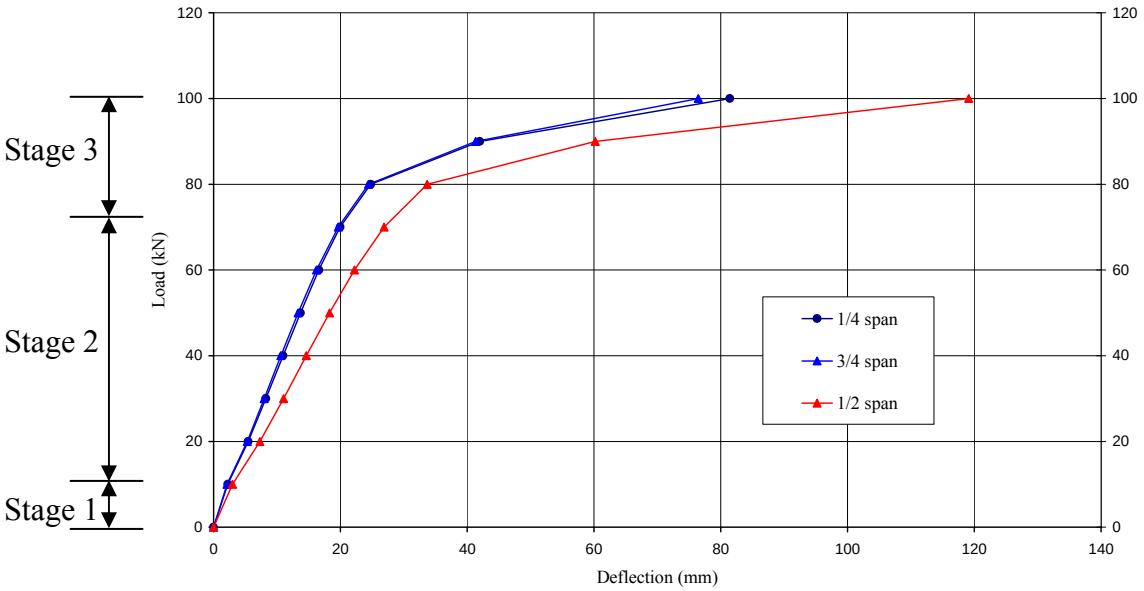

Figure 3.8 Load-deflection curves of the beam

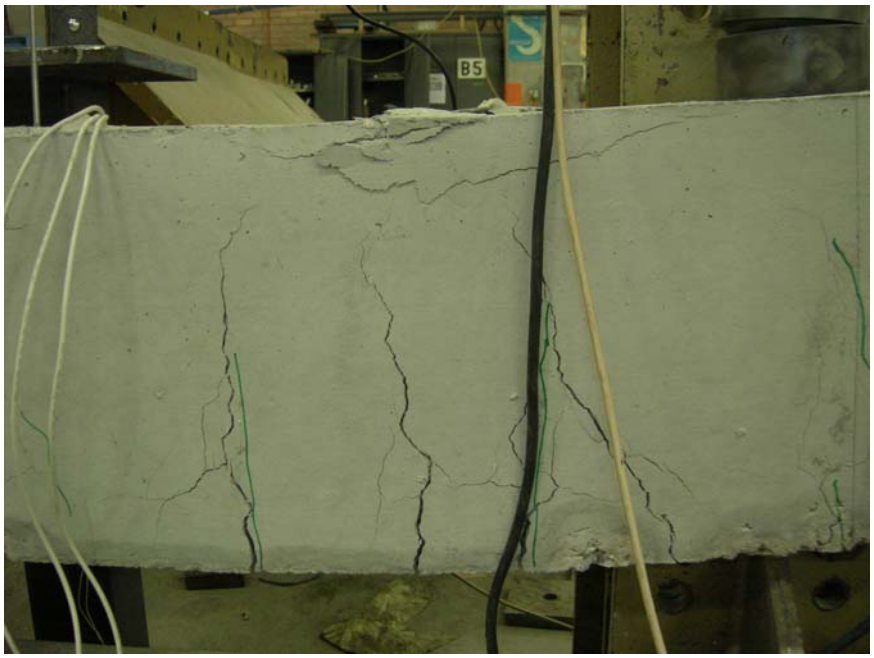

Figure 3.9 The failure of the RC beam

3.4.3 Analysis of Non-linear Behaviour of Reinforced Concrete Beam

The question of how to model the behaviour of concrete and reinforcing steel, especially in the tension zone, has become an important issue in civil engineering research. The tensile stress-strain relationship is one of the major concerns in modelling reinforced

concrete beams (Liang et al. 2005).For finite element modelling of reinforced concrete structures it is quite common to use a linear stress-strain relationship as shown in Figure 3.10 for concrete in tension. In Figure 3.10, f_{ct} is the tensile strength of concrete, e_{to} is the concrete strain corresponding to the beginning of concrete cracking, and, e_{tu} is the concrete strain corresponding to concrete softening. Hence, to establish an accurate reinforced concrete beam model, it is essential to understand the non-linear behaviour of the beam under increasing load and the reasons for the beam to behave non-linearly. Some possible causes of non-linear behaviour in reinforced concrete beams are discussed below.

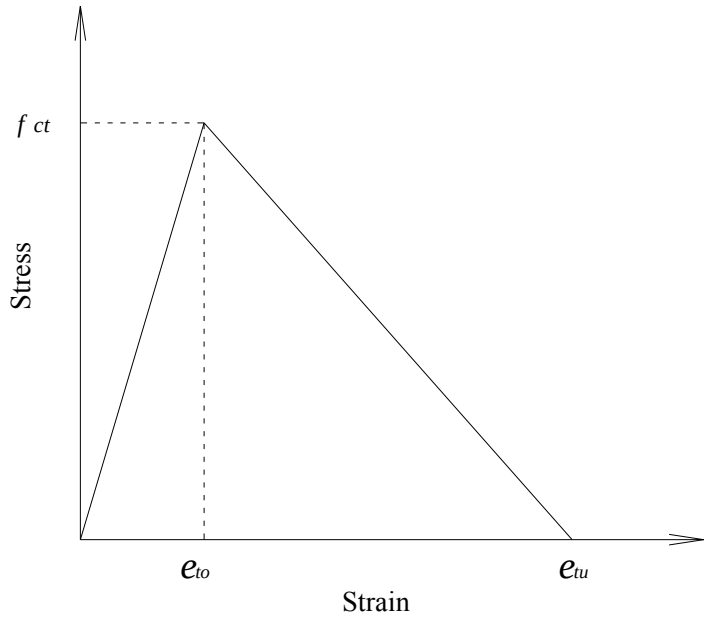

Figure 3.10 Stress-strain relationship for concrete in tension (Liang et al. 2005)

3.4.3.1 Cracking of Concrete

It is inevitable for concrete to crack when the tensile stress of concrete reaches its tensile strength. Increase in crack length causes decrease in flexural stiffness, which has a close relationship with the non-linearity of the beam. When a crack is opened during external loading, aggregate in the concrete may prevent the cracks from closing after the load is removed. Furthermore, the interaction between steel and concrete must also be considered. If there is localised slip of the steel relative to the concrete, due to debonding at the crack, it is possible that, once unloaded, a proportion of the relative slip will remain. When this happens, the crack may not close, as the stresses are not

large enough to overcome the residual slip. Therefore, it may not be possible for crack to close in a cracked concrete beam when unloading (Neild 2002). These factors may cause non-linear behaviour in a reinforced concrete beam.

3.4.3.2 Concrete in Compression

Concrete is considered a non-linear material in compression. For medium strength concrete subjected to uniaxial compressive loading, there are four major stages in the development of micro-cracking in the failure process (Nawy 2009):

1. Up to a stress level of about 30% of ultimate strength, the extent of micro cracking is very limited. As a result, the stress-strain response is almost linear.
2. With a stress level of between 30% and 75% of the ultimate strength, the new cracks are still limited to the aggregate-cement interface, and the growth of such bond cracks is accompanied by a gradual softening of the stress-strain response.
3. From 75% to about 90% of the ultimate strength, the cracks begin to extend noticeably into the mortar phase and to form continuous crack plane by connecting the bond cracks along the large aggregate particles. At this point, strain increases rapidly with increasing stress.
4. Beyond the 90% stress level, crack growth becomes unstable and causes rapidly increasing inelastic deformations, with failure strain being between 0.002 and 0.003. This final phase is accompanied by significant expansion in volume.

3.4.3.3 Failure of Concrete in Tension

As concrete is a brittle material, it is particularly vulnerable in the tension zone and will crack when tensile stress reaches its limit. Direct tension tests are not reliable for obtaining the tensile strength of concrete, since the results are heavily affected by minor misalignment and stress concentrations in the gripping devices. In general, the tensile strength of concrete is around 10% of its compressive strength.

3.5 Strain Distribution in RC Beam at Various Loading

In order to validate the modelling of reinforced concrete beams, the measured strains at different locations of the beam under increasing loading are first analysed in this section and then compared to the numerical work in Chapter 4. Therefore, calculation of the internal forces and moments and strain at the designated sections is essential. Due to limited strain data available from the bending test, estimated and projected strain values are necessary. A method using strain plane was established to obtain the missing strain data. The purpose of establishing the strain planes are:

(1) Gaining an insight into stress-strain distribution in the reinforced concrete beam during loading;
(2) Verifying and exploring measurement error and nonlinearity in sections;
(3) Estimating the neutral axis location at various loading stages, therefore confirming behaviour of the RC beam described in section 3.4.2; and
(4) Providing data for validating and calibrating the finite element models.

3.5.1 Measured Strain of Concrete and Reinforced Bars

Figure 3.11 shows the development of concrete strain with increasing load at different locations of the beam (C1, C2, C3, C4, C5 and C6). The locations of strain gauges are shown in Figure 3.4. In general, the compressive strain values of concrete (C1, C2 and C3) increase with the increase of external loading. The amplitude of the strain shift in C2 is much larger than that in either C1 or C3, because the stress in the middle span of the beam is much larger than the stress in the quarter span. When the loading reaches around 90 kN, the strains of the concrete in the compressive zone (C1 and C2) stop increasing, due to the occurrence of crushing.

The strain gauges C4, C5 and C6 were used to record the concrete strains in tensile area. During the static test, strain gauge C5 was broken two minutes into the start of the test, when the applied load was only 6.4 kN, due to tension. As external loading increased, cracks developed at the bottom of the beam, which caused local stress relaxation.

Therefore, strain gauges C4 and C6 may not accurately reflect the strain of concrete in the tensile zone.

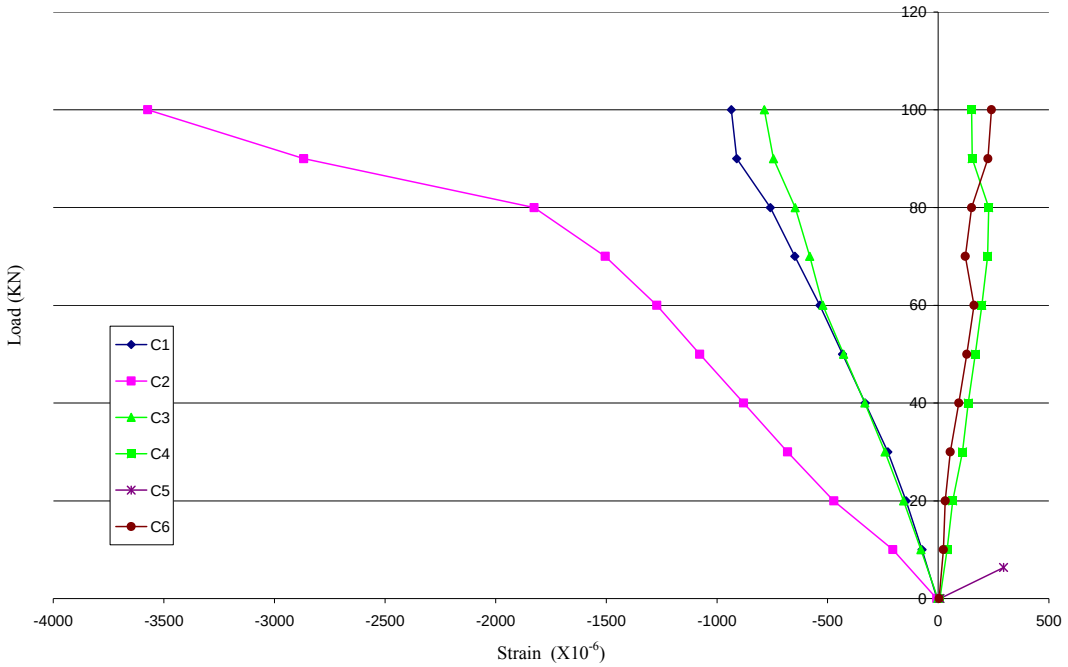

Figure 3.11 The measured strains of concrete

Figure 3.12 shows the development of strain in compressive and tensile steel bars with the increasing load (S1, S2, S3, S4, S5 and S6). The locations of the strain gauges are shown in Figure 3.4. Typically, all the strains increase with the increase of the applied load. From Figure 3.12, it is observed that the compressive strains (S1 and S2) increased marginally, while the tensile strains (S5 and S6) increased significantly. This is due to the fact that with the increase of the load, the neutral axis shifted upward. Therefore, the distance between the neutral axis and tension bars increased and the tensile strains increased significantly. In theory, the strain values of S5 and S6 should be identical. However, in the real world, cracks in RC beams do not propagate evenly through depths and crack paths are neither straight nor regular, which resulted in different strain measurements on the reinforcement bars. In addition, the asymmetric crack patterns in concrete will also disturb the loading causing imperfect loading condition. Similar phenomena can be observed when comparing S3 and S4.

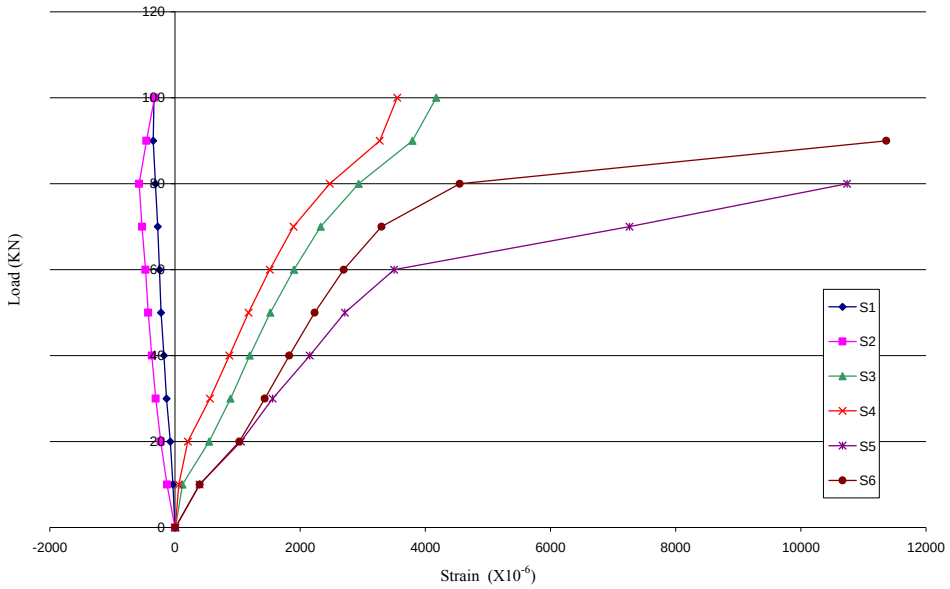

Figure 3.12 The measured strains of steel bar reinforcement

3.5.2 Least Square Method with Two Explanatory Variables

To process the measured strains on a given cross section, it is assumed that the strains at a given cross section can be represented by a strain plane (Li et al. 2002). Under this assumption, least square method with two explanatory variables is adopted. This makes it possible to obtain the strain plane at each given cross section, using data measured from the static loading test. The theory for obtaining a best fit strain plane is explained in the following equations.

The least-square plane method with two explanatory variables uses a linear plane

$$S = a + bx + cy \qquad \text{Equation 3.1}$$

to approximate the given set of data, (x_1, y_1, S_1), (x_2, y_2, S_2), …, (x_n, y_n, S_n), where $n \geq 3$. The best fit plane $f(x, y)$ has the least square error, ie,

$$\delta = \sum_{i=1}^{n} [S_i - f(x_i, y_i)]^2 = \sum_{i=1}^{n} [S_i - (a + bx_i + cy_i)]^2 = \min \qquad \text{Equation 3.2}$$

Please note that *a*, *b*, and *c* are coefficients to be determined by the process, while all x_i, y_i and S_i are given. To minimise the least square error, the unknown coefficients *a*, *b* and *c* must yield zero first derivatives.

$$\frac{\partial \delta}{\partial a} = 2\sum_{i=1}^{n}[S_i - (a + bx_i + cy_i)] = 0 \qquad \text{Equation 3.3}$$

$$\frac{\partial \delta}{\partial b} = 2\sum_{i=1}^{n} x_i[S_i - (a + bx_i + cy_i)] = 0 \qquad \text{Equation 3.4}$$

$$\frac{\partial \delta}{\partial c} = 2\sum_{i=1}^{n} y_i[S_i - (a + bx_i + cy_i)] = 0 \qquad \text{Equation 3.5}$$

Expanding the above equations gives the following:

$$\sum_{i=1}^{n} S_i = a\sum_{i=1}^{n} n + b\sum_{i=1}^{n} x_i + c\sum_{i=1}^{n} y_i \qquad \text{Equation 3.6}$$

$$\sum_{i=1}^{n} x_i S_i = a\sum_{i=1}^{n} x_i + b\sum_{i=1}^{n} x_i^{\,2} + c\sum_{i=1}^{n} x_i y_i \qquad \text{Equation 3.7}$$

$$\sum_{i=1}^{n} y_i S_i = a\sum_{i=1}^{n} y_i + b\sum_{i=1}^{n} x_i y_i + c\sum_{i=1}^{n} y_i^{\,2} \qquad \text{Equation 3.8}$$

Let:

$$[A]_{3\times 3} = \begin{bmatrix} A_{11} & A_{12} & A_{13} \\ A_{21} & A_{22} & A_{23} \\ A_{31} & A_{32} & A_{33} \end{bmatrix} = \begin{bmatrix} \sum_{i=1}^{n} n & \sum_{i=1}^{n} x_i & \sum_{i=1}^{n} y_i \\ \sum_{i=1}^{n} x_i & \sum_{i=1}^{n} x_i^2 & \sum_{i=1}^{n} x_i y_i \\ \sum_{i=1}^{n} y_i & \sum_{i=1}^{n} x_i y_i & \sum_{i=1}^{n} y_i^2 \end{bmatrix} \qquad \text{Equation 3.9}$$

$$[B]_{3\times 1} = \begin{bmatrix} B_{11} \\ B_{12} \\ B_{13} \end{bmatrix} = \begin{bmatrix} \sum_{i=1}^{n} S_i \\ \sum_{i=1}^{n} x_i S_i \\ \sum_{i=1}^{n} y_i S_i \end{bmatrix} \qquad \text{Equation 3.10}$$

Equations 3.6, 3.7 and 3.8 can be expressed in the following:

$$[A]_{3\times3}\begin{Bmatrix}a\\b\\c\end{Bmatrix}=[B]_{3\times1} \qquad \text{Equation 3.11}$$

The unknown coefficients *a*, *b* and *c* can therefore be obtained:

$$\begin{Bmatrix}a\\b\\c\end{Bmatrix}=[A]^{-1}_{3\times3}[B]_{3\times1} \qquad \text{Equation 3.12}$$

Finally, the best fit strain plane is obtained and described as in Equation 3.1:

$$S = a + bx + cy$$

3.5.3 Results and Discussions on Strain Distribution

In order to generate strain planes, at least four variables are needed to perform least square method. In the experimental tests, there are five variables at both quarter span and middle span. The five variables are one concrete tensile strain, two reinforcement tensile strains, one concrete compressive strain and one reinforcement compressive strain. Since the concrete tensile strains (C4, C5 and C6) were not recorded accurately, these results were not considered in the analysis. At the quarter span, the concrete strain in the compression zone (C1), the steel strain in the compression zone (S1) and steel strain in the tensile zone (S3 and S4) were employed in the analysis. At the midspan, the concrete strain in the compression zone (C2), the steel strain in the compression zone (S2) and steel stain in the tensile zone (S5 and S6) were employed in analysis.

Using Equation 3.1, three strain planes at midspan of the beam are calculated and depicted in Figures 3.13, 3.14 and 3.15, corresponding to 10 kN, 40 kN and 70 kN loads, respectively. In these figures, the strain planes are marked by A, B, C and D. On these strain planes, the experimental data (C2, S2, S5 and S6) are marked by red asterisks, while the estimated data (C2, S2, S5 and S6) are marked by blue circles. A straight line is employed to connect the experimental data and estimated data, denoting

the difference between them. Close-up views of these data are shown in Figures 3.13, 3.14 and 3.15. Both measured and estimated data are also tabulated in Table 3.3.

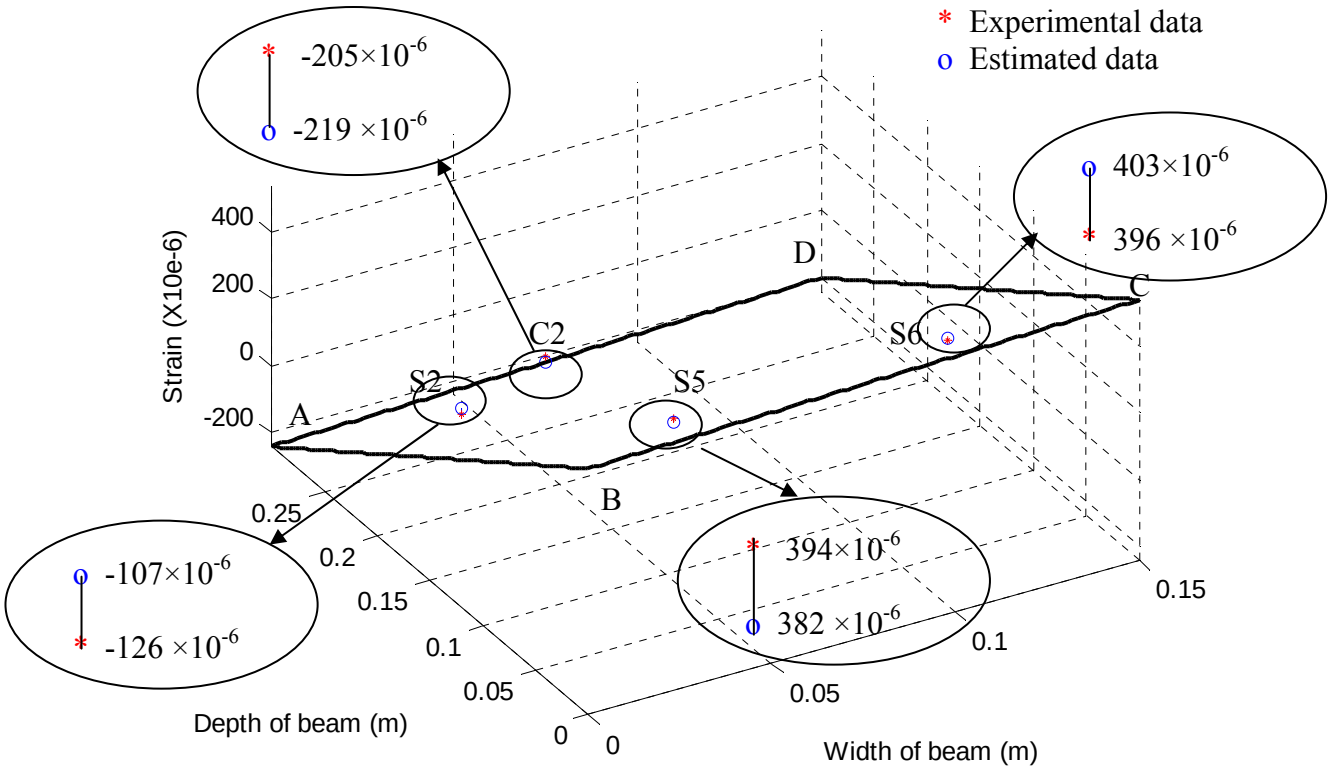

Figure 3.13 A strain plane at midspan (10 kN)

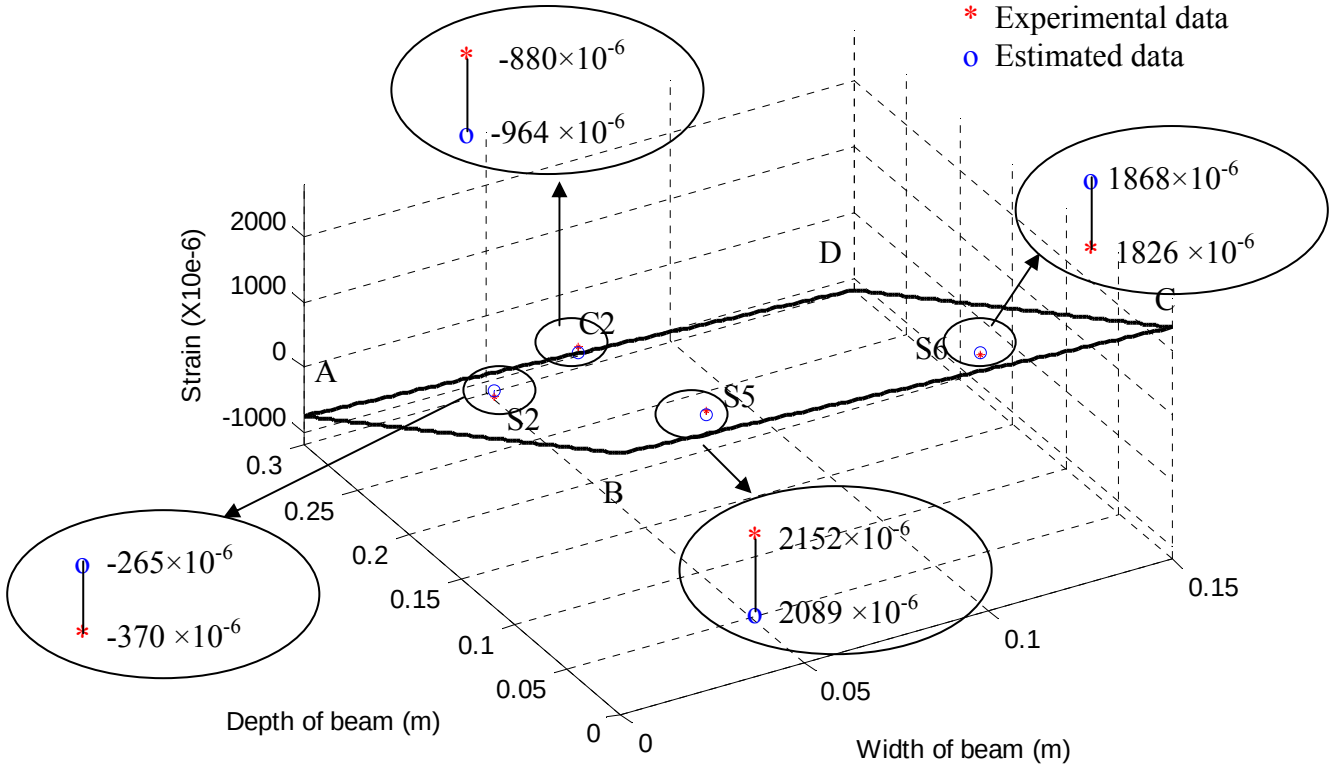

Figure 3.14 A strain plane at midspan (40 kN)

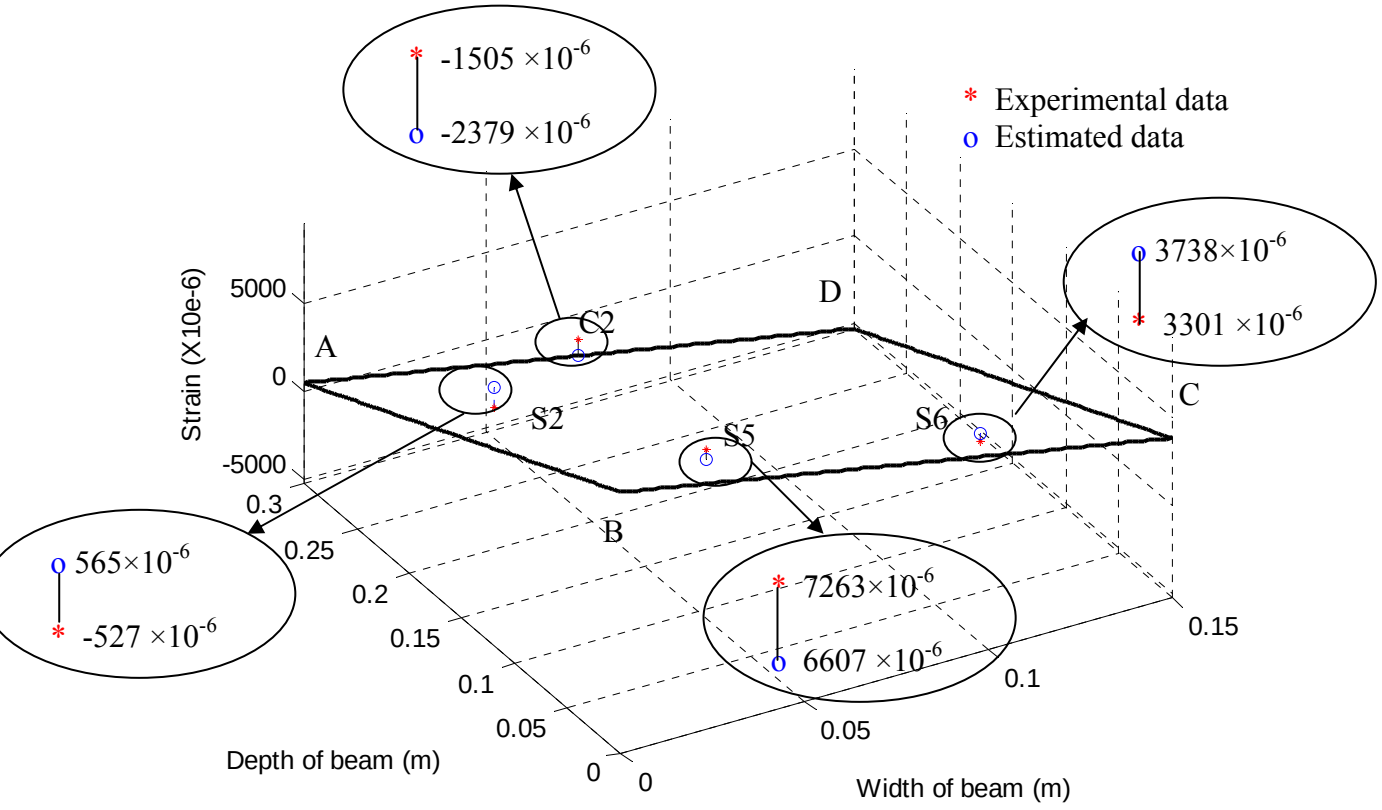

Figure 3.15 A strain plane at midspan (70 kN)

Table 3.3 Measured and estimated micro strain data ($\times 10^{-6}$) of the three strain plains at midspan

Measured and estimated strains at different locations		Applying loads		
		10 kN	40 kN	70 kN
Compressive strain of concrete (C2)	Measured	-205	-880	-1505
	Estimated	-219	-964	-2379
	| % Difference |	7	9	37
Compressive strain of rebar (S2)	Measured	-126	-370	-527
	Estimated	-107	-265	565
	| % Difference |	17	40	193
Tensile strain of rebar (S5)	Measured	394	2152	7263
	Estimated	382	2089	6607
	| % Difference |	3	3	10
Tensile strain of rebar (S6)	Measured	396	1826	3301
	Estimated	403	1868	3738
	| % Difference |	2	2	12

As shown in Table 3.3, the differences between the measured and the estimated strain data increase as applied loading increases during the test. For example, in the case C2, as the load increases from 10 to 70 kN, the percentage differences between the measured and estimated strains also increase from 7% to 37%, respectively. This is due to the fact that when applied loading increases, the reinforcement steel bars and concrete begin to exhibit non-linearity. After the development of cracks and when concrete crushes, the strain gauges slip off from the concrete and reinforcement steel, and are unable to record the accurate strain values. Meanwhile, the beam starts to twist. Therefore, the estimated strain plane exhibits a greater divergence from the measured data the longer the experiment is continued.

Likewise, the strain planes at quarter and three quarter span subjected to various loads (from 10 kN to 80 kN) can be established, using the experimental data from the four-point bending test. Subsequently, the estimated strain data can be produced. All measured, estimated strain data and their differences can be seen in Appendix A.

Figure 3.16 shows all estimated strains at the midspan of the beam with increment of 10 kN applied load from 10 kN to 80 kN. The compressive concrete strains (C2) and the compressive steel strains (S2) can be directly obtained from the strain plane, while the tension steel strains are obtained by averaging the two tensile steel strains (S5 and S6). It can be seen clearly that the strains increase with the increase of the applied load. When the applied load reaches 60 kN, the strain relationship between the concrete and rebar become significantly non-linear with the development of cracking and crushing. As depicted in Figure 3.16, when the applied load reaches 70 kN and 80 kN, the strains of the concrete and rebar at midspan are not in the same plane any more. Hence, the strain planes (from 10 kN up to 60 kN) can be considered to be planes, while the strain planes (70 kN and 80 kN) can not be considered to be planes any more. The strain data in Figure 3.16 also clearly illustrate that the neutral axis shifts upwards marginally when the applied load increases from 10 kN to 60 kN. The neutral axis shifts upward markedly after the applied load exceeds 60 kN.

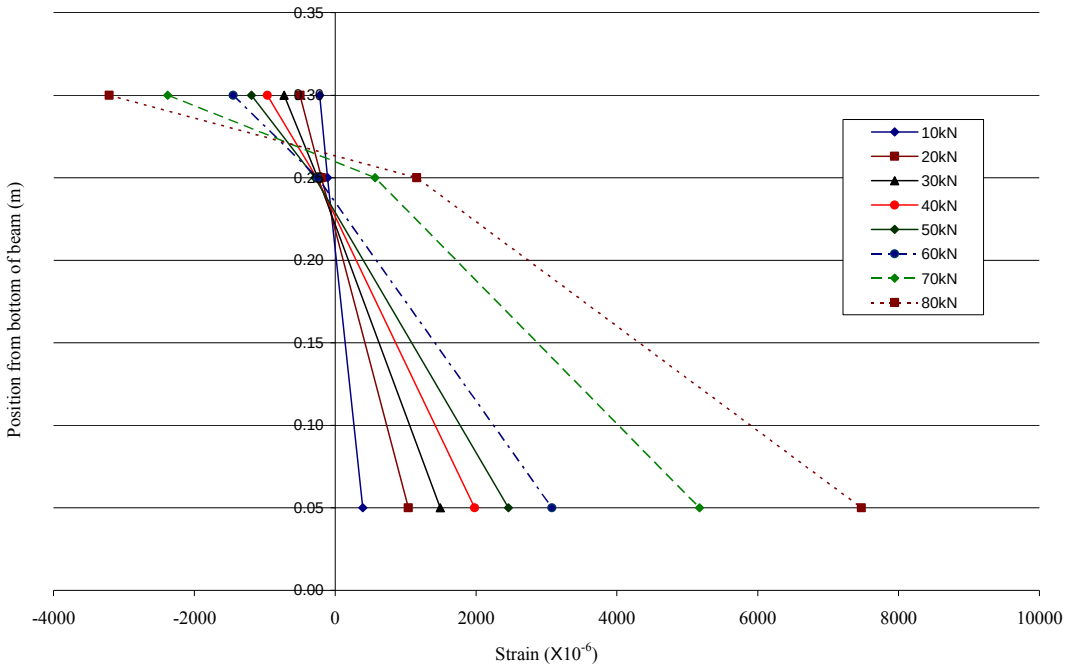

Figure 3.16 Estimated strains versus loads at midspan

3.6 Summary

At the beginning of this chapter, the details of a test specimen were described. Properties of concrete and steel were briefly introduced. The results of property testing will be used in the numerical modelling in Chapters 4 and 6.

Then, the set-up of the four-point bending test was outlined. It was observed that there were three main stages prior to the failure of the beam during the test. The causes of non-liner behaviour in the beam during the test were also discussed in the chapter.

Finally, the measured strains at different locations of the beam were obtained and illustrated in Figures 3.11 and 3.12. The least square method with two explanatory variables was employed to process the measured data. The results showed that the strains increase and the neutral axis shifts upward as the load increases.

CHAPTER 4

FINITE ELEMENT MODELLING

4.1 Introduction

This chapter presents the procedure of establishing reasonable and reliable Finite Element (FE) models of a laboratory reinforced concrete (RC) beam. Instead of modelling the RC beam using a straight forward linear FE model, a more sophisticated non-linear RC beam FE model is adopted to achieve a reasonably good result. Many challenges in FE modelling of non-linearity in reinforced concrete structures are due mainly to the complex inhomogeneous nature of the concrete materials and also the complex combined interactive behaviour of RC structures. Some of these non-linearity features come from, for example, cracked concrete and debonded concrete cover as well as yielded reinforcing bar.

In this study, the built FE beam model adopts material testing data for concrete and reinforcing steel as input of material properties. The geometry of the FE model is based on the experimental test beam as discussed in Chapter 3. Some important input features of non-linearity in the FE analysis are also listed. Then, modelling of inflicted damage such as crack and honeycomb is discussed. Such inflicted damage features will be used for creating various damaged FE beams, numerically, which will be used together with an intact beam for damage detection in Chapter 6. A mesh density study was performed in order to obtain a reasonable and an optimal mesh size for an accurate model. The final FE model was, statically, validated with the experimental data of four-point bending results, while for its dynamic characteristics, the model was validated using modal data obtained from the dynamic testing. The validated FE model is used for numerical study of the new damage detection method proposed in Chapter 5.

4.2 Finite Element Model of Intact Reinforced Concrete Beam

For reinforced concrete beam modelling, element Solid 65 in ANSYS was chosen to simulate concrete. Element Solid 65 is specially designed for the three dimensional (3-D) modelling of solids with or without reinforcing bars and is capable of cracking in tension and crushing in compression. In general, the element Solid 65 is defined by eight nodes having three degrees of freedom (DOF) at each node, namely, translations in the nodal X, Y, and Z directions. The most important contribution of the element Solid 65 is the treatment of nonlinear material properties. When concrete is modelled with this element, the modelled concrete is capable of cracking (in three orthogonal directions), crushing, plastic deformation, and creep. The rebar elements are capable of tension and compression, but not shear. They are also capable of plastic deformation and creep. The geometry, node locations, and the coordinate system for element Solid 65 are shown in Figure 4.1.

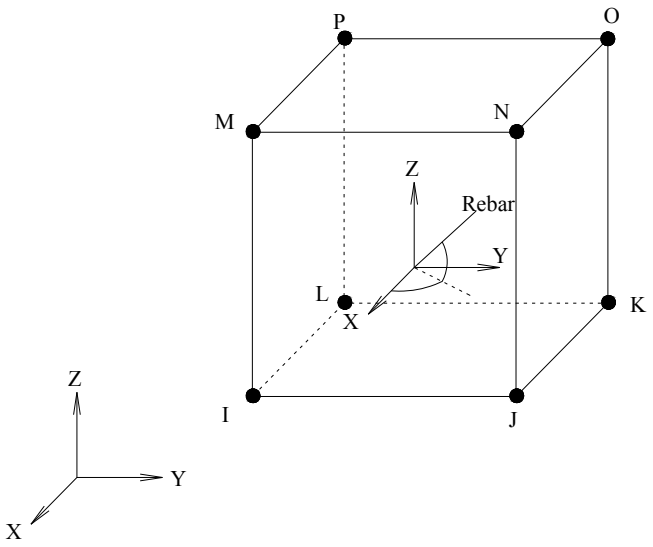

Figure 4.1 The geometric properties of Solid 65 (ANSYS Inc. 2007)

In order to model the main reinforcement and stirrup more accurately in the concrete, element Link 8 was employed in the numerical work. Element Link 8 is a spar which can be used in a variety of engineering applications such as trusses, sagging cables, etc. Element Link 8 is a uniaxial tension-compression element with three degrees of freedom (DOF) at each node, namely, translations in the nodal X, Y, and Z directions.

The bending of this element is not considered. However, plasticity, creep, swelling, stress stiffening, and large deflection capabilities are included (ANSYS Inc. 2007).

After the elements were selected, a typical reinforced concrete beam was modelled, using the ANSYS program. A typical finite element (FE) model of an intact reinforced concrete beam is illustrated in Figure 4.2.

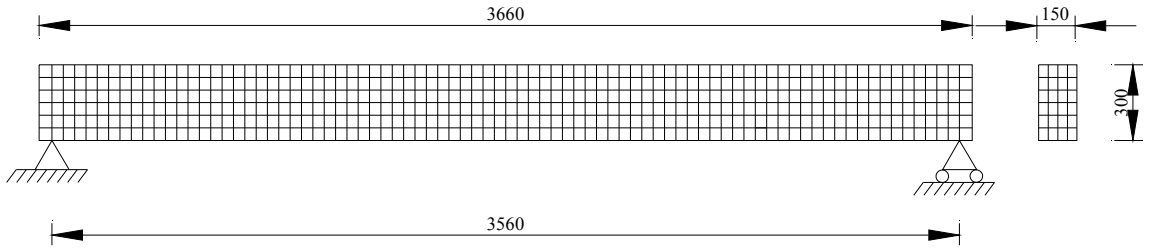

All dimensions are in mm.

Figure 4.2 A typical FE model of a reinforced concrete beam

4.2.1 Geometry and Material Properties

The dimensions of the FE beam were identical to the experimental beam (Chapter 3) with 3,660 mm in length, 300 mm in height and 150 mm in width, as shown in Figure 4.2. The beam was divided into 82 elements along the length, 6 elements along the height and 4 elements along the width. The pin-roller boundary condition was set at the second bottom node from both ends of the beam as depicted in Figure 4.2. The FE model, in total, consisted of 2,905 nodes. With this mesh configuration, the beam modal had 8,715 degrees of freedom (DOF). The reinforcement consisted of two top compression bars (82 elements each), two bottom tension bars (82 elements each) and twenty-one reinforced stirrup bars (12 elements each) with a spacing of 200 mm as shown in Figure 4.3. Therefore, there were 1,968 elements (82 × 6 × 4) for concrete and 580 elements (164 + 164 + 252) for reinforcement. In total 2,548 elements were used for the reinforced concrete beam modelling.

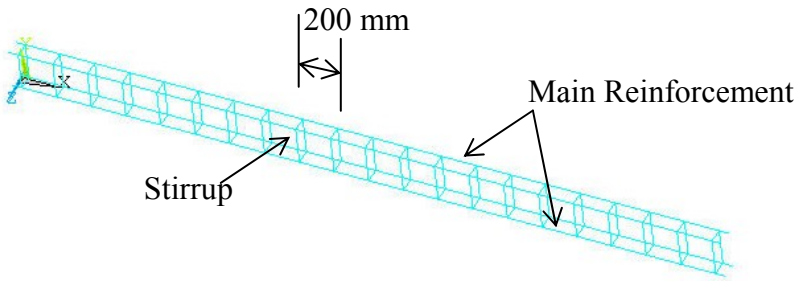

Figure 4.3 Reinforcing bars in the beam

The material property data used in the FE modelling were obtained from concrete and steel reinforcement property tests detailed in Chapter 3. The input value for the modulus of elasticity of concrete was 27.7 GPa, and the concrete compressive and tensile strength were 28.9 MPa and 2.9 MPa, respectively. The density of concrete was 2,435 kg/m^3. The modulus of elasticity for the reinforcement was 205 GPa, the yield strength of reinforcement was 505 MPa and the density of reinforcement was 7,905 kg/m^3. All material property input data are summarised in Table 4.1.

Table 4.1 Material properties used in the FE modelling of the RC beam

Materials	Input data of material properties	
Concrete	Compressive strength (MPa)	28.9
	Tensile strength (MPa)	2.9
	Density (kg/m^3)	2,435
	Modulus of elasticity (GPa)	27.7
Reinforcement	Yield strength (MPa)	505
	Density (kg/m^3)	7,905
	Modulus of elasticity (GPa)	205

4.2.2 Non-linear Features Used in the FEA

For non-linear solutions in the FE beam model using the ANSYS (2007) programs, there are several important features to be specified in order to obtain reasonable outputs. The solution controls used for the non-linear analysis are listed in Table 4.2.

Table 4.2 Solution controls used in the non-linear analysis

Solution Controls	**Option Used**
Analysis Option	Large Static Displacement
Time Control	Automatic Time Stepping
Number of Substeps	40
Maximum Number of Substeps	1,000
Minimum Number of Substeps	1
Solver	Full Newton-Raphson
Convergence Value	0.05

In ANSYS code, for non-linear solution, the presence of crack damage at an integration point for an element was characterised by modifying the stress-strain relations through introducing a plane of weakness in a direction normal to the crack face. The stress-strain relation for concrete that has cracked in one direction can be represented by Figure 4.4.

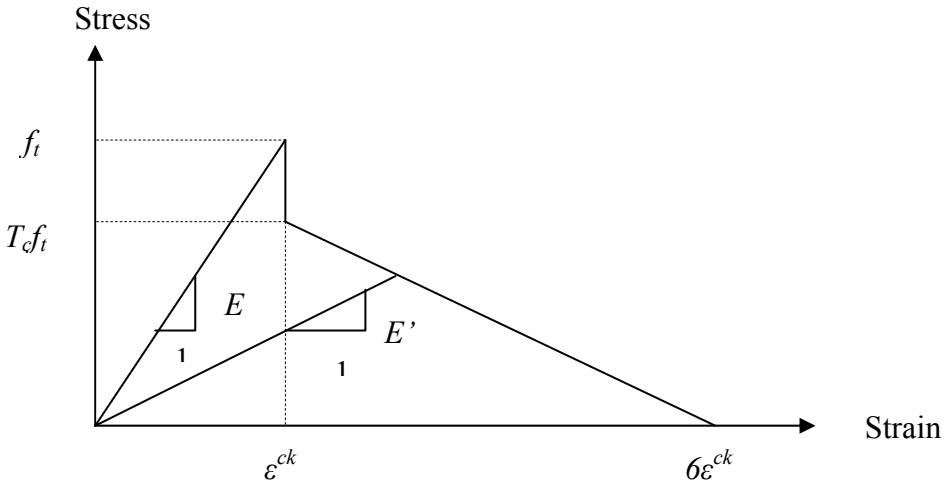

Figure 4.4 Strength of cracked condition

Where f_t is uniaxial tensile cracking stress, T_c is a multiplier for the amount of tensile stress relaxation (defaults to 0.6 in the ANSYS code), ε^{ck} is the strain associated with cracking stress and $6\varepsilon^{ck}$ is the failure strain.

4.3 Methods of Modelling Damage in Reinforced Concrete Beam

The modelling of the inflicted damage, numerically, will be used for developing finite element (FE) models of damaged reinforced concrete (RC) beams. The inflicted damage in the damaged beam models is similar to that of actual experimental RC beams. Subsequently, the damaged beam FE models and the intact beam FE model (mentioned in Section 4.2) will be employed for damage detection studies in Chapter 6.

There are many types of damage in reinforced concrete structures. In general, crack and honeycomb are two major types of damage that most often appear in reinforced concrete structures (Zhong & Oyadiji 2007; Dilek 2007). Therefore, these two types of damage were chosen in this study for the numerical and experimental work. Numerically, there are three main approaches to model such damage: (1) equivalent stiffness reduction method; (2) discrete spring model method; and (3) discontinuing element model method (Friswell & Penny 2002).

Firstly, equivalent stiffness reduction method is the simplest method to apply to finite element models. The method reduces the stiffness locally, for example, by reducing element stiffness by a small percentage to simulate a light damage. This approach is easy to perform and the local stiffness can be reduced accordingly depending on the severity of damage. The second method, discrete spring model method, divides a beam type structure into two parts that are pinned at the crack location, where the crack is simulated by the addition of a rotational spring. This approach is a gross simplification of crack dynamics, and it does not involve the damage size and location directly. For the third approach, discontinuing element model method, the technique is to imitate the geometry of actual damage. For example, if there is a loss of section in a real structure, elements of similar damage size and location will be omitted from the numerical model.

Based on the nature of the damage, discontinuing element model method was employed to simulate a crack by introducing a notch in the reinforced concrete beam. On the other hand, the honeycomb was simulated using equivalent stiffness reduction method, whereby stiffness of the designated damaged elements was reduced. In order to investigate the effects of damage locations and damage severities, 18 different damaged

cases were created in the numerical work. These damage cases are described in Chapter 6.

4.3.1 Simulation of Crack Damage

In the numerical work, three different severities (light, medium and severe) of damage were introduced to the reinforced concrete beams to simulate various kinds of cracks in the experiment. All simulated damage were of notch type with the same length of 45 mm and width of 150 mm, but with different depths, i.e. a depth of 50 mm for light damage, 100 mm for medium damage and 150 mm for severe damage. Figure 4.5 shows a typical severe damage. The damage was created in various locations to simulate single and multiple damage scenarios for the study of damage detection using the newly proposed damage detection algorithm in this thesis.

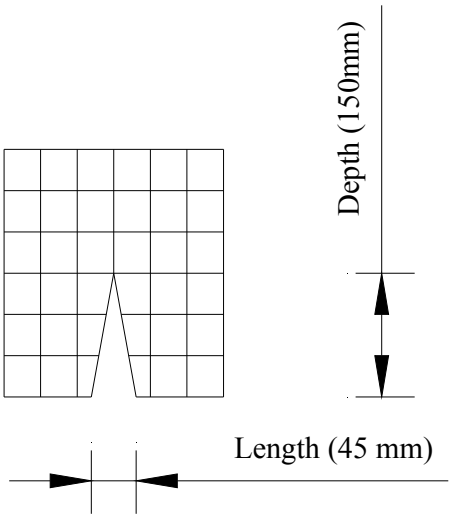

Figure 4.5 The side elevation of a severe crack damage

4.3.2 Simulation of Honeycomb Damage

Besides the crack damage simulated by a notch, another type of defect typically found in reinforced concrete structures, namely honeycomb, was also studied in this research. The honeycomb damage was simulated by two layers of four elements each (Figure 4.6) set with modulus of elasticity (E) close to zero. This value of E is chosen as in the experimental work, where a block of polystyrene hexahedron (89 mm long, 75 mm wide and 100 mm deep) was used to simulate honeycomb in reinforced concrete

structures, where its stiffness can be ignored compared to that of concrete. The honeycomb damage was modelled at different locations to simulate various single honeycomb damage scenarios.

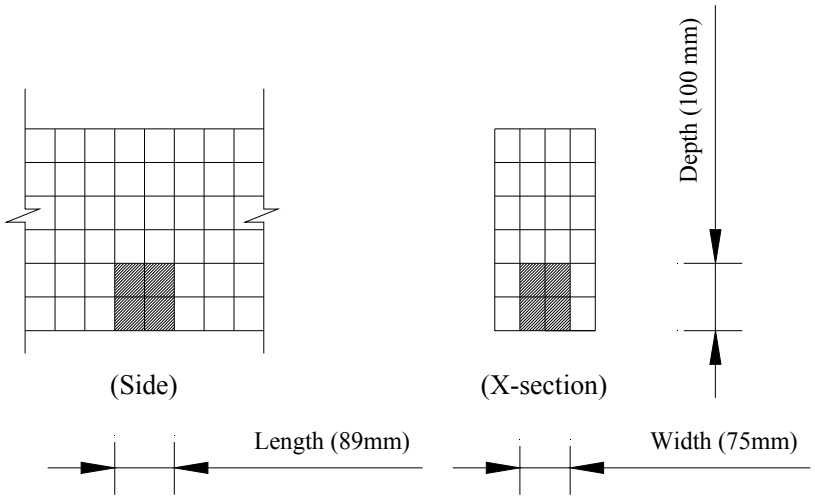

Figure 4.6 The side elevation and cross sectional view of a bottom honeycomb damage

4.4 Mesh Density

It is widely acknowledged that the quality of finite element analysis (FEA) depends on mesh and this will heavily influence the validity of the analysis results (Dittmer et al. 2006). A high-quality mesh, or usually also a more dense mesh, is often time consuming and costly. Therefore, it is important to establish a finite element (FE) model with optimum mesh size to generate valid results, while not consuming too much time and resources.

4.4.1 Meshes Considered For Modelling

In FE modelling, the mesh size can be easily controlled for a simple structure. Hence, it is essential to be able to use a reasonable mesh size for the FE model to work efficiently. Three types of mesh size were created for comparison, i.e. coarse, fine and very fine, as depicted in Figure 4.7.

Referring to Figure 4.7(a), the coarsely meshed model of a reinforced concrete beam was divided into 42 elements along the length, 6 elements along the height and 4 elements along the width. The coarsely meshed FE model, in total, consisted of 1,505

nodes (43 nodes along the length × 7 nodes along the height × 5 nodes along the width) and 1,428 elements (including elements of compression bars, tension bars and stirrup bars).

For the fine mesh density model as shown in Figure 4.7(b), there were 83 nodes along the length, 7 nodes along the height and 5 nodes along the width. Hence, the fine mesh model comprised 1,968 elements (82 × 6 ×4) for concrete, 580 elements (164 + 164 + 252) for reinforcement and in total 2,548 elements were used for the reinforced concrete beam model.

The very fine meshed model of reinforced concrete beam, as shown in Figure 4.7(c), was divided into 164 elements along the length, 6 elements along the height and 4 elements along the width. Therefore, the very fine meshed model consisted of 5,775 nodes (165 nodes along the length × 7 nodes along the height × 5 nodes along the width) and 4,816 elements (including elements of compression bars, tension bars and stirrup bars).

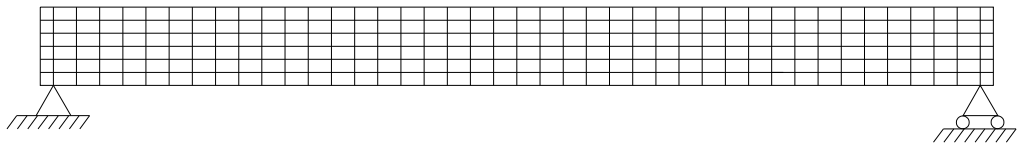

(a) Coarse

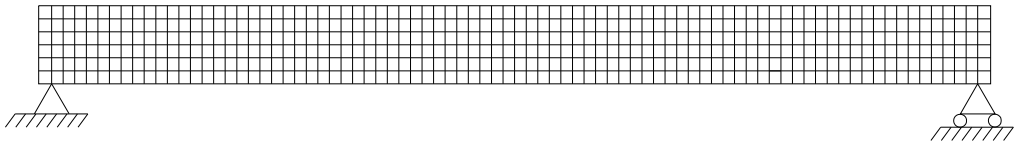

(b) Fine

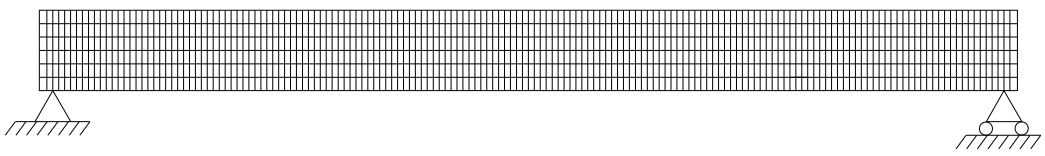

(c) Very fine

Figure 4.7 Different mesh models of the RC beam

4.4.2 Comparison of Different Mesh Densities

Figures 4.8(a) to (e) show the results of the first five mode shapes obtained from the three different meshed models of the reinforced concrete beam. In each figure, the legend of 165 Nodes, 83 Nodes and 43 Nodes denote number of nodes used along the length of the beam corresponding to the very fine meshed model (Figure 4.7 (c)), fine mesh model (Figure 4.7 (b)) and coarse mesh model (Figure 4.7 (a)), respectively. All mode shape data were collected evenly from 41 nodes on the top of the beam within the span length.

Referring to Figures 4.8(a) to (c), the difference of mode shape (1 to 3) results between different mesh densities (165 Nodes, 83 Nodes and 43 Nodes) is insignificant. The difference of mode shapes between very fine mesh model (165 Nodes) and fine mesh model (83 Nodes), for example, area around node 6, as illustrated in Figure 4.8(d) (mode 4), is insignificant, while the difference of mode shapes between fine (83 Nodes) and coarse mesh (43 Nodes) is noticeable. Likewise, similar phenomenon occurs in Figure 4.8(e) (mode 5), for example, area around node 14. However, these differences are fairly small and it can be said that the first five mode shapes are not sensitive to mesh densities tested here. Based on the comparison, it can be concluded that all meshed models are comparable and they are deemed good enough for the numerical work required in this study. Considering the time and cost, the fine meshed model with 82 elements along the length, 6 elements along the height and 4 elements along the width as shown in Figures 4.2 and Figure 4.7(b), was adopted for all subsequent analysis and discussions.

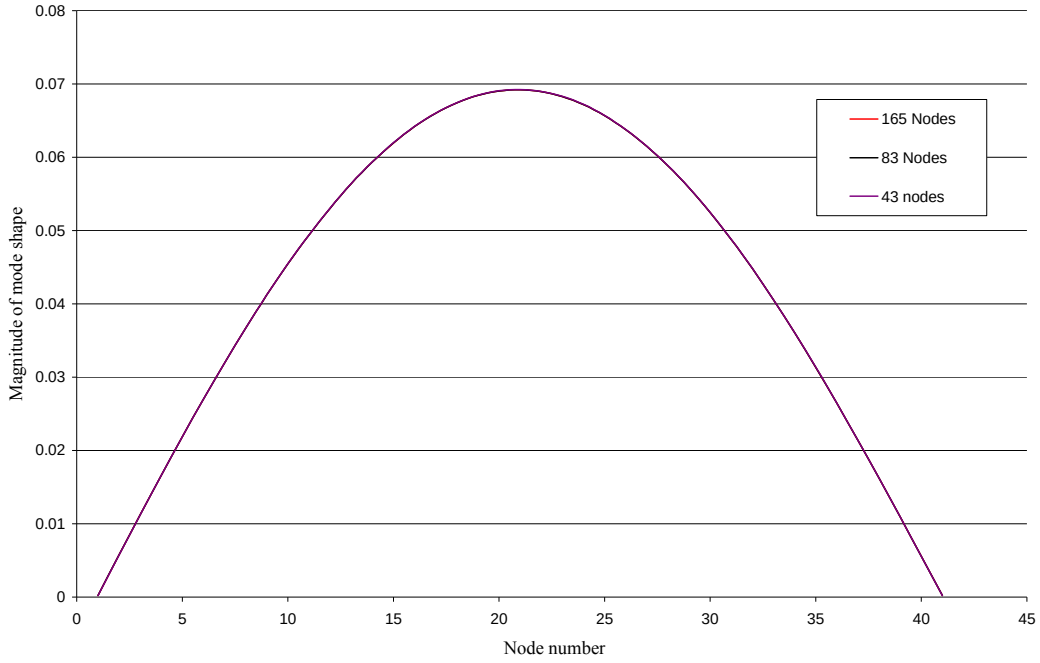

(a) The first mode

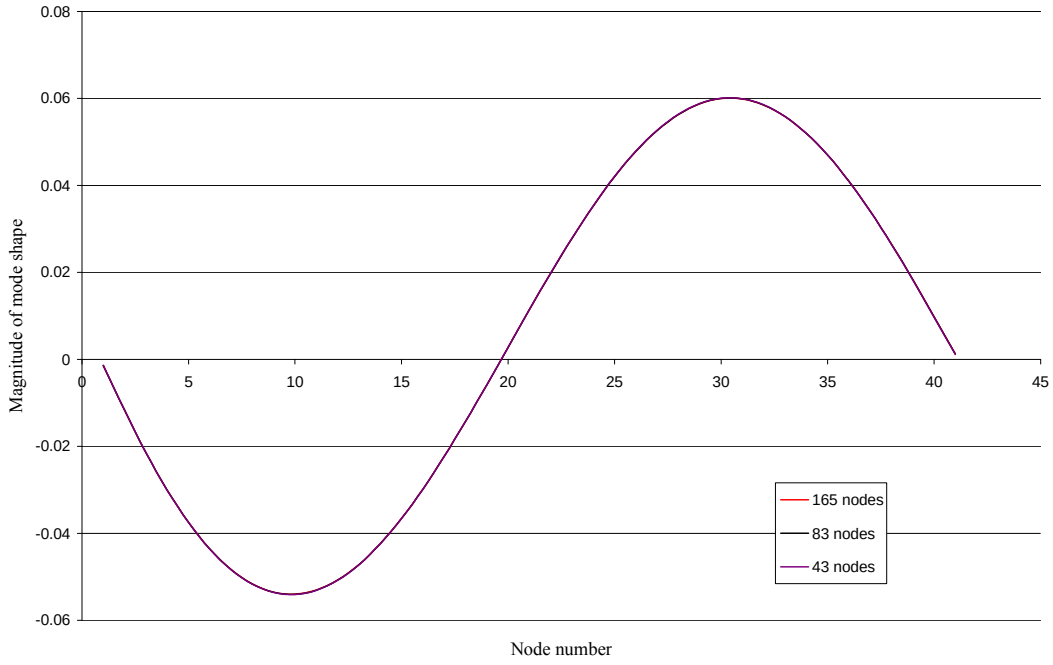

(b) The second mode

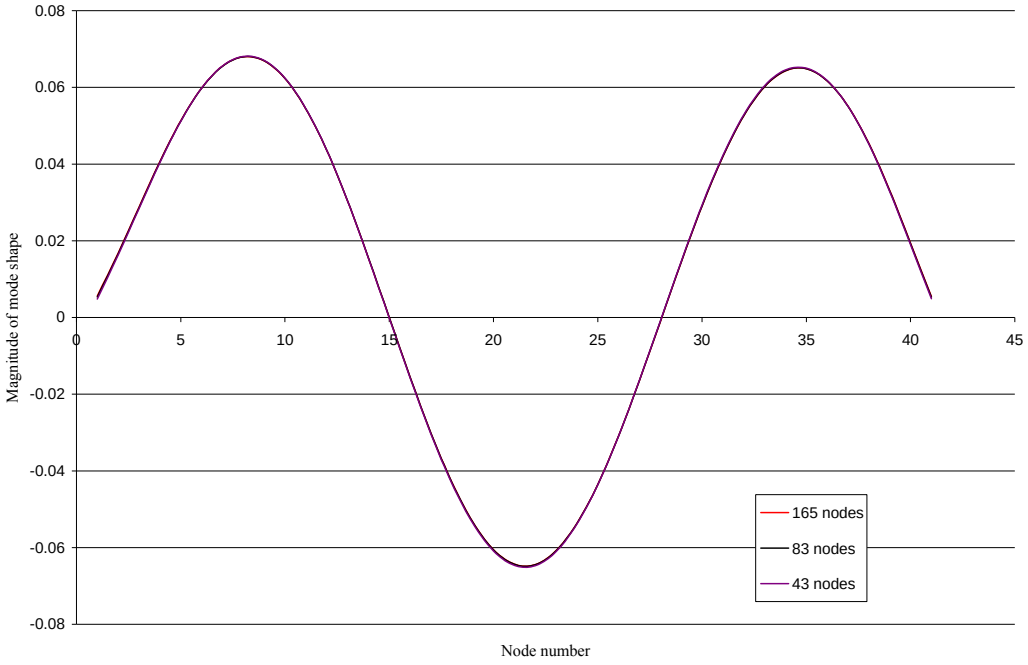

(c) The third mode

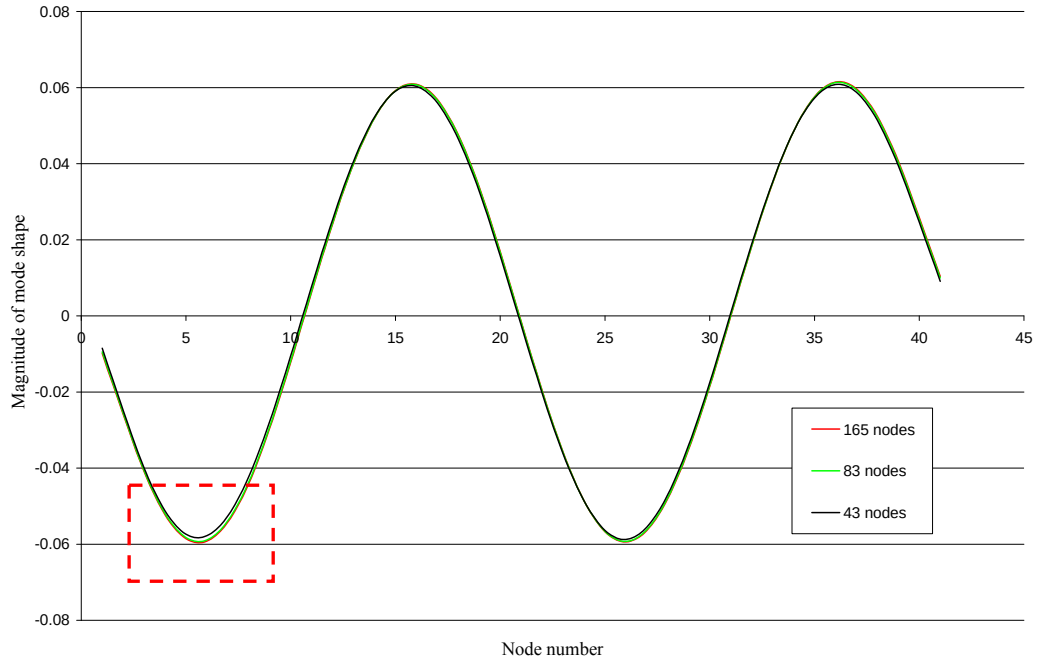

(d) The fourth mode

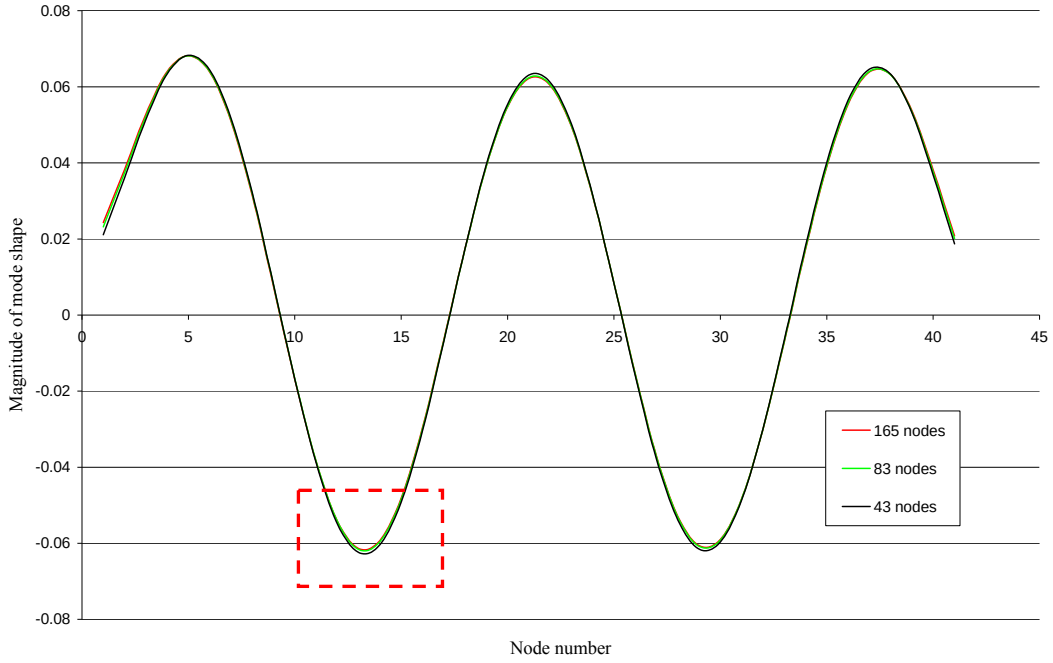

(e) The fifth mode

Figure 4.8 The mode shapes of intact FE beam with different mesh densities

4.5 Numerical Simulation of Four-point Bending Test

Subsequent to establishing an optimum meshed model, the designated reinforced concrete beam FE model was subjected to static load test, numerically, to study its non-linear characteristics, as well as to validate the model with the experimental results. A simply supported reinforced concrete beam, as illustrated in Figure 4.9, subjected to four-point loading was constructed, tested and analysed,

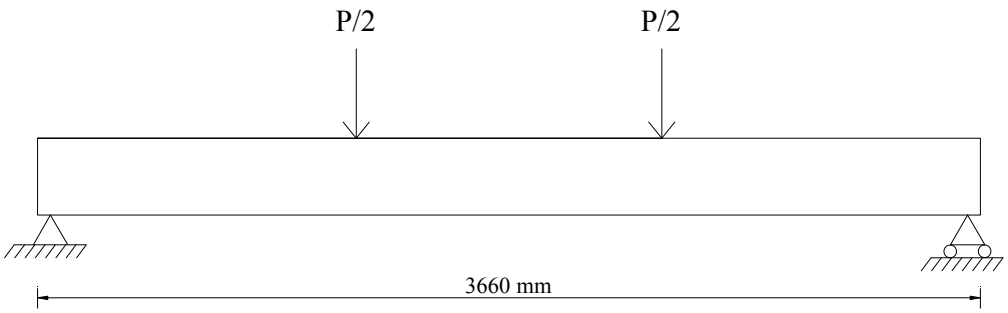

Figure 4.9 The RC beam FE model subjected to four-point being test

4.5.1 The Results and Discussions on Load-deflection Relationship

Figure 4.10 shows the relationship between the Load (P) and the deflection (δ) of the reinforced concrete beam at ¼ span, ½ span and ¾ span. As shown in the figure, the loading and deflection relationship of the reinforced concrete beam experiences three major stages of change.

The first stage takes place when the load increases from 0 to 10kN. Using the theory of bending stress, the estimated first cracking load of the beam is 10.9kN. Hence, for loads less than 10kN or before the first cracking, the response of the model is expected to be linear. At this stage, the compressive stress is mainly imposed onto the concrete in the compression area, while the tensile stress is resisted by both the concrete and the reinforcement in the tension area. This relationship continues with the increase of the load until the principal stress in the major principal direction exceeds the maximum tensile strength, and the first crack occurs at the bottom of the beam. The maximum deflections at this first stage, occurring when load reaches 10kN, are 0.528 mm, 0.744mm and 0.528 mm, for ¼ span, middle span (½ span) and ¾ span, respectively.

The second stage takes place when the load increases from 10kN to 70kN, and the beam undergoes changes from the uncracked state to cracked state. During this stage, the neutral axis moves up, and increasing number of cracks develops and begins to extend noticeably. The compressive stress is still resisted by the concrete in the compression area, while the tensile stress is mainly carried by the reinforcement, due to cracking in concrete in tensile zone. As a result, the flexural stiffness of the beam decreases as seen in Figure 4.10, whereby slopes of the curves decrease. The maximum deflections at this stage, when load reaches 70kN, are 19.7 mm at ¼ span, 28.4 mm at middle span (½ span) and 19.7 mm at ¾ span.

The final stage takes place after the load reaches and goes beyond 70kN. In this stage, crack growth becomes increasingly unpredictable and the results are of immense inelastic nature. Meanwhile, the neutral axis shifts up faster than previous stages. Stress in the steel reinforcement passes the yield strength and continue to increase until the concrete is crushed in compression, resulting in the final collapse of the beam. The

maximum deflections at this stage, when load reaches 110 kN, are 70.2 mm, 104 mm and 70.2 mm, for ¼ span, middle span (½ span) and ¾ span, respectively.

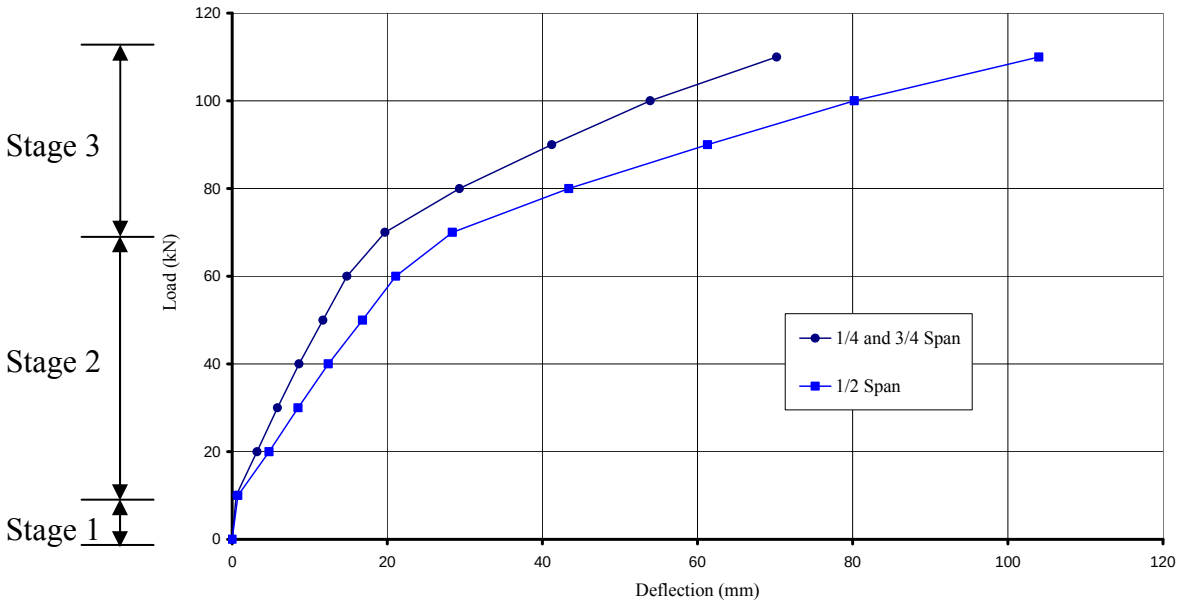

Figure 4.10 Load-deflection curves at the ¼, ½ and ¾ span of the FE model of a reinforced concrete beam

4.5.2 Comparison between Numerical and Experimental Load-deflection Results

Figure 4.11 compares the load-deflection curves obtained from FE analysis with those obtained from experimental testing in Chapter 3. It can be observed in the figure that when the load increases from 0 kN to 10 kN, the relationships between the load and deflection remain linear. After the load reaches 10 kN, the beam experiences a sudden loss of stiffness, due to initiation of cracking in concrete. Therefore, the slope of curves decreases suddenly from this point on. When the steel bars start to yield and concrete begins to crush, the beam experiences another loss of stiffness and the slope of the curves decreases again.

The load-deflection response of the experimental RC beam is captured accurately by the numerical simulation. The ultimate load achieved in the numerical model, 110 kN, is within 10% of the ultimate test load of 100kN. The difference in deflection is only 6% when the load is 70 kN. Furthermore, both the numerical and experimental curves exhibit the three major stages of beam behaviour as detailed in Section 4.5.1. It is also

worth mentioning that some researchers experienced convergence problem in their simulation of nonlinear model of reinforced concrete. For example, Fanning (2001) used ANSYS to simulate a reinforced concrete beam and in the numerical model the increased deflection was such that converged solutions were not achieved beyond about 27 mm deflection at midspan of the beam. However, the modelling presented here has successfully solved the convergence problem in the calculations. Therefore, it is demonstrated that the simulation of non-linearity in the RC beam presented in this chapter is fairly accurate and reliable.

In general, the load-deflection curves show that numerical and experimental results are close with only small differences, except at the final stages approaching failure. Both curves also exhibit similar behaviours, i.e. possessing similar changes at the three main loading stages. The differences between the numerical and experimental results are manifested in the deflections and stiffness of the beam. Since the real materials and the bonding between materials are naturally imperfect, the experimental results are not expected to be identical to the numerical results. It can, therefore, be concluded that the RC beam FE model is able to represent, statically, the experimental RC beam for the study of damage detection in the following chapters.

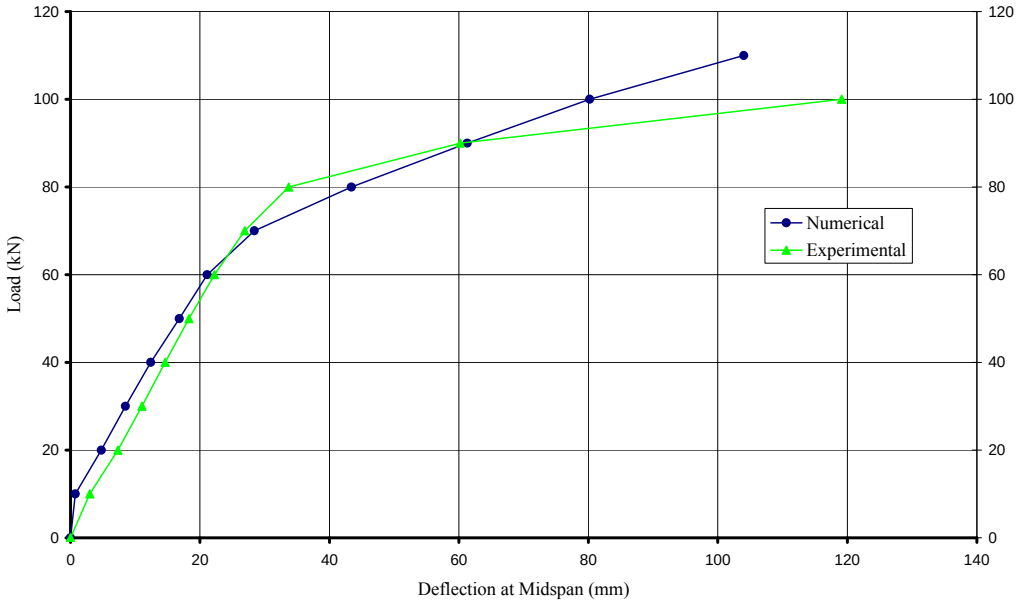

Figure 4.11 Load-deflection curves of both numerical and experimental results at midspan (½ span)

4.6 Validation Using Dynamics Results

After the reinforced concrete (RC) beam finite element (FE) model was validated, statically, using the four-point bending test results, it is also important to validate the model, dynamically, as the newly developed damage detection method is based mainly on the dynamic characteristics of the RC beam.

4.6.1 Correlation Analysis

Correlation analysis is a technique to examine quantitatively and qualitatively the correspondence and difference of modal parameters between analytical and experimental research (Brownjohn et al. 1999). This analysis gives a platform for modal parameters selection related to dynamic responses in model updating. In the beam analysis, dynamic responses (natural frequencies and mode shapes) are used as the indices for the objective function (*OF*) for the correlation analysis. The goal of updating or calibration process of the finite element (FE) model was to minimise the objective function. The global objective function used is given in Equation 4.1.

$$OF = f\left(NFerror, MACerror\right) \qquad \text{Equation 4.1}$$

NFerror and *MACerror* are given by Equation 4.2 and 4.3 as discussed later.

Regarding mode shapes, two criteria (the order of mode shape and compatibility between modes) are adopted for comparison between all possible mode shape pairs. Numerical mode shape correlation techniques such as the Modal Assurance Criterion (*MAC*) can be used to check all possible mode shape pairs and calculate a quantity that expresses the level of compatibility.

The dynamic responses (natural frequencies and mode shapes) of both numerical and experimental research are adopted in the correlation analysis. The numerical results are obtained from finite element modelling performed in this chapter and Chapter 6. The experimental results are obtained from experimental dynamic tests performed in the laboratory, which will be explained in Chapter 7.

4.6.2 Natural frequencies

Regarding Natural Frequency (*NF*), the relative error or difference between the analysis (finite element model) and experiments (modal tests) can be computed in order to check their correlation. In order to gauge the relative error in natural frequencies more clearly, an error index for the *NF* is suggested. The *NFerror* given in the *OF* is a function of natural frequency difference between FE and experimental models and is given as follows:

$$NFerror = \frac{\left|\omega_{Exp} - \omega_{FE}\right|}{\omega_{Exp}} \times 100 \qquad \text{Equation 4.2}$$

where ω is the natural frequency. Its subscripts *Exp* and *FE* denote experimental and finite element results, respectively. The values of the natural frequency and *NFerror* are displayed in Table 4.3. The *NFerror* in general is less than 7%, except for mode 2. The reason for slightly larger *NFerror* value for mode 2 may be due to the fact that impact location falls on the anti-node point of this mode. Table 4.3 shows that the FE model is able to represent the experimental model well.

Table 4.3 Comparison of natural frequencies of the RC beam

Mode	FE (Hz)	Experimental (Hz)	Absolute Difference (Hz)	*NFerror* (%)
1	36.60	34.46	2.14	6.21
2	128.81	115.22	13.59	11.79
3	320.27	337.45	17.18	5.09
4	502.57	525.34	22.77	4.33
5	756.06	743.66	12.4	1.67

4.6.3 Mode shapes

Modal Assurance Criterion (*MAC*) (Allemang & Brown 1983) is one of the most popular measures of correlating two sets of mode shapes. This parameter provides a measure of the least-squares deviation of the points from the straight-line correlation. The *MACerror* utilises *MAC* for indicating the correlation between finite element (*FE*) and experimental (*Exp*) model results.

$$MACerror\left(\varphi_{Exp},\varphi_{FE}\right)=1-\frac{\left|\left\{\varphi_{Exp}\right\}^{T}\left\{\varphi_{FE}\right\}\right|^{2}}{\left(\left\{\varphi_{Exp}\right\}^{T}\left\{\varphi_{Exp}\right\}\right)\left(\left\{\varphi_{FE}\right\}^{T}\left\{\varphi_{FE}\right\}\right)} \qquad \text{Equation 4.3}$$

where φ is the mode shape vector. A value close to 1 indicates poor correlation between the mode shapes, whilst a value close to 0 indicates good correlation. The extent of calibration can be determined through the evaluation of change in the correlation between the mode shapes. The *MACerror* results are shown in Table 4.4. For the first four modes, the *MACerror* values are generally lower than 0.09. This means that both sets of mode shapes match very well as the *MACerror* values are less than 0.1 (or 90% for MAC), which are considered acceptable (Brownjohu & Xia 1999; Maia & Silva 1997). The first five modes (can be found in Chapter 6) were employed in the analysis. The correlation between the numerical and experimental mode shapes is really good with errors of less than 10%. However, in the fifth mode, the *MACerror* value is 0.21 or 21% error. This is due to the fact that the fifth mode of the RC beam, experimentally, is 743.66 Hz and this is considered a high frequency mode for civil engineering applications. It is commonly known that in a dynamic test, it is usually easier to excite lower modes of lower frequencies rather than that of higher frequencies. Higher frequencies require a lot of energy to excite. This is even more obvious for reinforced concrete structures as they are usually large and heavy. Therefore, the frequency response function obtained may not be as good as that of lower frequencies. Considering the fifth frequency of the RC beam is relatively high, it is not surprising to obtain the *MACerror* value as high as 0.21.

Table 4.4 Mode shapes correlation between FE and experimental models

Mode	*MAC*	% *MAC*	*MACerror*	% *MACerror*
1	1.00	99.54	0	0
2	0.91	90.51	0.09	9
3	0.98	97.90	0.02	2
4	0.94	94.12	0.06	6
5	0.79	78.68	0.21	21

In conclusion, the results of the *NFerror* and *MACerror* generally infer that the finite element (FE) model simulates the experimental model quite well. Therefore, this FE model can be used in damage detection methods proposed in this thesis.

4.7 Response Time History under Impulse Loading

In real field application, noise is always present in any form of data acquisition. Thus, the damage detection results using the experimental data will naturally inherit noise. In order to study the impact of noise on damage detection, numerically, which will be performed in Chapter 6, it is necessary to obtain the response time history of reinforced concrete beam with added noise under impulse loading. A method, namely, transient dynamic analysis (sometimes called time-history analysis) was employed to acquire the dynamic characteristic of the RC beam FE model under various levels of noise. In general, this is a numerical technique used to determine the dynamic response of a structure under the action of any general time-dependent load. It can be used to determine the time-varying displacements, strains, stresses, and forces in a structure as it responds to any combination of static and transient loads. A simple formulation of the technique is listed below and the details of using this technique to acquire modal parameters can be found in Chapter 6.

The basic equation of motion solved by transient dynamic analysis is

$$[M]\{\ddot{Z}\}+[C]\{\dot{Z}\}+[K]\{Z\}=\{F(t)\} \qquad \text{Equation 4.4}$$

where [*M*] is mass matrix, [*C*] is damping matrix, [*K*] is stiffness matrix, {*Z*} is nodal displacement vector, $\{\dot{Z}\}$ is nodal velocity vector, $\{\ddot{Z}\}$ is nodal acceleration vector and {*F(t)*} is load vector.

These equations are treated as a set of equilibrium equations that take into account inertia forces $[M]\{\ddot{Z}\}$ and damping forces $[C]\{\dot{Z}\}$ when calculation is performed. The Newmark time integration method, or an improved method called Hilbert Huang Transform method, is used to solve these equations at discrete time points in transient dynamic analysis.

Transient dynamic analysis was carried out on the intact reinforced concrete beam and damaged beams. A typical acceleration response at midspan for the intact beam is shown in Figure 4.12. When the beam was impacted by an impulse load, the displacements measured by the sensors, which were evenly placed on the top of the beam, were obtained. Then these accelerations were calculated by double differentiation of the displacement and were subsequently used to obtain the mode shapes of the beams to compare with the experimental results.

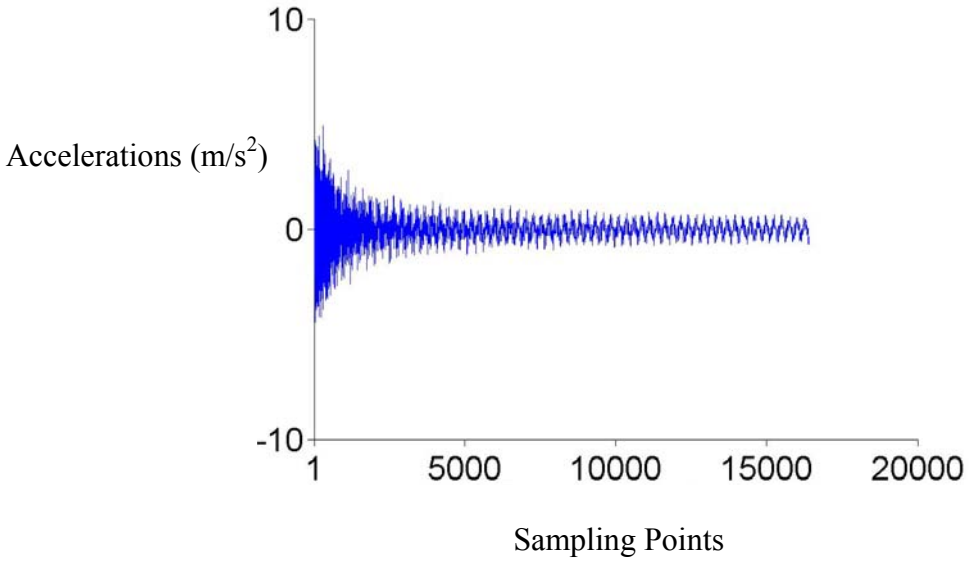

Figure 4.12 A typical acceleration response at midspan for an intact RC beam FE model

4.8 Summary

This chapter presented the procedure of establishing reasonable and reliable Finite Element (FE) models of laboratory reinforced concrete beams. Firstly, Solid element 65 and Link element 8 were selected in the FE model, simulating an actual reinforced concrete beam. After the elements were selected, an intact reinforced concrete beam FE model was developed. Three approaches to simulate the damage in reinforced concrete were also briefly introduced in this chapter. Of these three approaches, the first approach (equivalent stiffness reduction method) was employed to simulate honeycomb in the reinforced concrete beams, and the third approach (discontinuing element model method) was employed to simulate crack in the reinforced concrete beams. Mesh density comparison was also discussed in the chapter.

After the deemed optimum meshed model was finalised, the FE beam model was subjected to four-point bending loading, numerically, tested and then analysed in order to study the nonlinear behaviour of a reinforced concrete beam under increasing load. The beam model was subsequently validated with the experimental results. The load-deflection curves obtained from FE analysis were compared with the ones obtained from experimental testing. It is found that the FE model is, statically, close to the real test beam.

The statically validated RC beam FE model was then subjected to dynamic test to investigate its validity in terms of dynamics. The correlation analysis results showed that the natural frequencies and mode shapes for the numerical model are close to the experimental ones. Therefore, the RC beam FE model can be used to represent the experimental RC test beams.

In order to study the influence of noise in damage detection (Chapter 6), transient dynamic analysis, used to determine the dynamic response of a structure under any general time-dependent load, was briefly discussed here.

CHAPTER 5

DEVELOPMENT OF A NEW DAMAGE DETECTION METHOD BASED ON MODAL STRAIN ENERGY

5.1 Introduction

This Chapter presents details of a new damage detection algorithm used in this study to identify damage locations and to estimate the severities. The formulation of the new algorithm is enlisted in Section 5.3, while other damage detection algorithms are discussed in Section 5.4 for comparison purposes. The advantages of the new damage detection algorithm are also briefly discussed here.

5.2 Background

A great deal of recent research has focused on developing algorithms concerning the detection, localisation and characterisation of structural damage via various techniques. The current techniques used in structural damage detection can be categorised into two main groups. One group, namely "model based" methods, makes use of finite-element model updating techniques, and damage detection problems can be considered as a special case of the general model updating problem. The methods in this group solve for the updated matrices by forming a constrained optimisation problem based on the structural equations of motion, the nominal model, and the measured data. Comparing the updated matrices to the original correlated matrices provides an indication of damage, which can be used to detect the location and to quantify the extent of damage. The other group of techniques used for locating structural damage makes use of some damage indicators based on measured structural information, such as modal parameters of a structure. The methods in this group require measurements before and after occurrence of damage for damage detection. This group of methods are often referred as

"model free" methods and the damage detection method to be developed in this thesis is of this group.

Among both model based and model free techniques, a group of damage detection methods have been developed for the identification of damage based on directly measured mode shapes and/or their derivatives. Mode shapes are unique characteristics of a structural system and are known as the spatial description of the amplitude of each corresponding resonant frequency. It is commonly acknowledged that local damage will cause changes to the mode shapes in the vicinity of the damage. One of the earliest methods using mode shape method for damage identification was modal assurance criterion (MAC) (Allemang & Brown 1983), which was based on correlations between two sets of mode shape data. A further development of MAC method, the coordinate modal assurance criterion (COMAC) (Lieven & Ewins 1988), was commonly used in damage detection (Alampalli et al. 1997). Nowadays, these two methods are in use mainly in the model updating process or calibration of finite element models with experimental modal data. The direct comparison of mode shapes, combined with other modal-based damage detection methods, is also used for structural health monitoring.

To date, an increasing trend of research work using derivatives of modal parameters (such as mode shape) has indicated that these derivative parameters are more sensitive to damage than modal parameters themselves (Zhu & Xu 2005). For example, modal strain energy, as a function of mode shape curvature (i.e. the second derivative of mode shape), has been quite successfully used to detect location of damage and to estimate the severity of damage. The following are some examples.

In 1995, a non-destructive damage detection algorithm was proposed to identify location and size of damage in structures using a small number of modal responses of the structures (Kim & Stubbs 1995). After making an assumption in the research work that the fraction of modal energy was the same for both damaged and undamaged structures, a damage index β_{ji} of i^{th} mode and j^{th} member was obtained:

$$\beta_{ji} = \frac{E_j}{E_j^*} = \frac{\phi_i^{*T} C_{jo} \phi_i^*}{\phi_i^T C_{jo} \phi_i} \qquad \text{Equation 5.1}$$

In Equation 5.1 E_j and E_j^* are parameters representing the material stiffness properties associated with undamaged and damaged states, respectively; ϕ_i and ϕ_i^* are the i^{th} modal shapes associated with undamaged and damaged states, respectively; C_{jo} denotes geometric quantities; and superscript "T" denotes transpose of a vector.

For NM vibrational modes, a damage index β_i of j^{th} member is obtained:

$$\beta_j = \frac{\sum_{i=1}^{NM} \phi_i^{*T} C_{jo} \phi_i^*}{\sum_{i=1}^{NM} \phi_i^T C_{jo} \phi_i} \qquad \text{Equation 5.2}$$

where $\beta_j \geq 0$ and damage is indicated at the j^{th} member if $\beta_j > 1$.

Let the fractional change in the stiffness of the j^{th} member be given by the severity estimator, α_j, then, $E_j^* = E_j(1+\alpha_j)$. So, combining with Equation 5.2, the severity of damage in the j^{th} member is estimated as follows:

$$\alpha_j = \frac{1}{\beta_j} - 1; \quad \alpha_j \geq -1 \qquad \text{Equation 5.3}$$

Another damage localization method based on modal strain energy was presented in 1998 (Shi et al. 1998). This method made use of the change of modal strain energy in each structural element before and after the occurrence of damage. Information required in the identification was the measured mode shapes and elemental stiffness matrix. Then the method was further developed by the same authors in 2000 (Shi et al. 2000) and in 2002 (Shi et al. 2002). In their research work, Modal Strain Energy Change Ratio (MSECR) was presented for damage localization (as follows).

$$MSECR_j^i = \frac{\left| MSE_{ij}^d - MSE_{ij} \right|}{MSE_{ij}} \qquad \text{Equation 5.4}$$

where j and i denote the element number and mode number respectively. If the modal strain energy (MSE) for several modes are considered together, the $MSECR_j$ of the j^{th} element is defined as the average of the summation of $MSECR^i_j$ for all the modes normalized with respect to the largest value $MSECR^i_{max}$ of each mode.

$$MSECR_j = \frac{1}{m}\sum_{i=1}^{m}\frac{MSECR_j^i}{MSECR_{\max}^i} \qquad \text{Equation 5.5}$$

A recently developed damage severity estimation method, termed as cross-modal strain energy (*CMSE*) method, and capable of estimating the damage magnitude of multiple damaged members, was presented in 2006 (Hu et al. 2006). The *CMSE* method was a non-iterative, exact solution method which used both the mode shapes and modal frequencies for the damage severity estimation. While traditional modal strain energy methods must compare the modal information from the same i^{th} mode for the baseline and damaged structures, there was no such need for the *CMSE* method. Since many *CMSE* equations could be formulated from a single measured mode with as many analytical modes, minimal modal information from measurements was required. The method did not require the analytical and measured modes to be consistent in scale, or to be normalized in any particular way. In the research, a parameter developed to estimate the severity of damage is presented here in Equation 5.6.

$$\hat{\alpha} = (C^T C)^{-1} C^T b \qquad \text{Equation 5.6}$$

where $\hat{\alpha}$ is the parameter to estimate severity of damage after applying least squares approach; C is a matrix of cross-modal strain energy between the mode of the baseline structure and the mode of the damaged structure and b is the size of column vector.

The algorithms given above are able to detect the location or estimate the severity of damage in structures to a certain extent. However, they have various shortcomings. The method given by Kim and Stubbs (1995) generates error in both locating and estimating damage when only limited measurements are available, especially under influence of noise. The method given by Shi et al (1998, 2000 and 2002) also appears to be noise sensitive, while in real field environments, noise is inevitable as part of experimental measurements. Furthermore, the convergence property of Shi's algorithm presents great

difficulty in performance of the method. In the method proposed by Hu et al (2006), even though the parameter $\hat{\alpha}$ was proposed to estimate the severity of damage, one weak point of the parameter was that it was unable to identify the location of damage. The authors, therefore, concluded that the method needed to be further developed to be employed as a damage localization method. The authors also recommended development of the CMSE method as a combined scheme for damage localization and damage severity estimation, which they are presently working on.

In order to overcome the shortcomings of the existing modal strain energy based damage detection methods mentioned above, a new damage detection algorithm based on modal strain energy is proposed in this research work. The new proposed algorithm is capable not only of identifying the location of damage, but also of quantifying the severity of damage.

5.3 Formulation of the Proposed Method

For a structure, the equation of motion is presented in Equation 5.7 in terms of global coordinates.

$$[M]\{\ddot{Z}\}+[C]\{\dot{Z}\}+[K]\{Z\}=\{F\} \qquad \text{Equation 5.7}$$

where $[M]$ denotes the $n\times n$ system mass matrix, $[C]$ denotes the $n\times n$ system damping matrix, $[K]$ denotes the $n\times n$ system stiffness matrix, $\{Z\}$ denotes the system displacement vector, $\{\dot{Z}\}$ denotes the system velocity vector, $\{\ddot{Z}\}$ denotes the system acceleration vector and $\{F\}$ denotes the system force vector.

Based on the fact that the frequencies and mode shapes are properties of the given structure and thus unaffected by the applied forces, if neglecting the damping in the system, frequencies and mode shapes can be obtained from the 'homogeneous' equations given by omitting the external forces (Thorby, 2008) i.e. state of free vibration:

$$[M]\{\ddot{Z}\}+[K]\{Z\}=0 \qquad \text{Equation 5.8}$$

or, say,

$$\begin{bmatrix} m_{11} & m_{12} & \dots \\ m_{21} & m_{22} & \dots \\ \dots & \dots & \dots \end{bmatrix} \begin{Bmatrix} \ddot{z}_1 \\ \ddot{z}_2 \\ \dots \end{Bmatrix} + \begin{bmatrix} k_{11} & k_{12} & \dots \\ k_{21} & k_{22} & \dots \\ \dots & \dots & \dots \end{bmatrix} \begin{Bmatrix} z_1 \\ z_2 \\ \dots \end{Bmatrix} = 0 \qquad \text{Equation 5.9}$$

Since there is no damping, if the system is assumed to have been set in motion at frequency ω, all elements of the vector $\{z\}$ will vibrate in phase with each other. The response at points z_1, z_2, etc. can be considered as horizontal or vertical projection of a rotating, complex unit vector, $e^{i\omega t}$, multiplied by the real constants $ø_1$, $ø_2$, etc. Then the response of all the points $ø_1$, $ø_2$, etc., are given by

$$\{z\} = \begin{Bmatrix} z_1 \\ z_2 \\ \dots \end{Bmatrix} = \begin{Bmatrix} \phi_1 \\ \phi_2 \\ \dots \end{Bmatrix} e^{i\omega t} = \{\phi\} e^{i\omega t} \qquad \text{Equation 5.10}$$

The vector of accelerations, $\{\ddot{z}\}$, is given by differentiating Equation 5.10 twice with respect to time:

$$\{\ddot{z}\} = \begin{Bmatrix} \ddot{z}_1 \\ \ddot{z}_2 \\ \dots \end{Bmatrix} = -\omega^2 \begin{Bmatrix} \phi_1 \\ \phi_2 \\ \dots \end{Bmatrix} e^{i\omega t} = -\omega^2 \{\phi\} e^{i\omega t} \qquad \text{Equation 5.11}$$

Substituting Equation 5.10 and Equation 5.11 into Equation 5.9 and dividing through by $e^{i\omega t}$ gives

$$-\omega^2 \begin{bmatrix} m_{11} & m_{12} & \dots \\ m_{21} & m_{22} & \dots \\ \dots & \dots & \dots \end{bmatrix} \begin{Bmatrix} \phi_1 \\ \phi_2 \\ \dots \end{Bmatrix} + \begin{bmatrix} k_{11} & k_{12} & \dots \\ k_{21} & k_{22} & \dots \\ \dots & \dots & \dots \end{bmatrix} \begin{Bmatrix} \phi_1 \\ \phi_2 \\ \dots \end{Bmatrix} = 0 \qquad \text{Equation 5.12}$$

Or

$$(-\omega^2 [M] + [K]) \{\phi\} = 0 \qquad \text{Equation 5.13}$$

Or writing $\lambda=\omega^2$

$$[K]\{\phi\} = \lambda[M]\{\phi\} \qquad \text{Equation 5.14}$$

where as before $[K]$ denotes the $n\times n$ system stiffness matrix, $[M]$ denotes the $n\times n$ system mass matrix, $\{\phi\}$ denotes the mode shape vector and λ denotes the associated eigenvalue. So Equation 5.14 can be expressed as the following for the i^{th} mode.

$$[K]\{\phi\}_i = \lambda_i[M]\{\phi\}_i \qquad \text{Equation 5.15}$$

Now, let's subdivide the entire beam structure into N elements as shown in Figure 5.1.

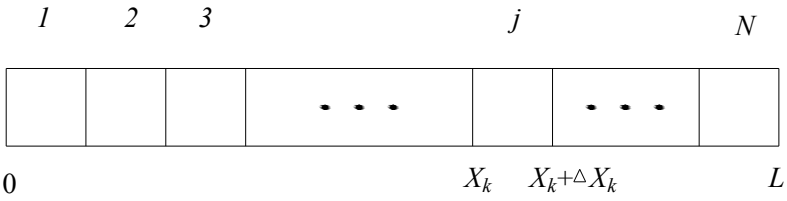

Figure 5.1 Drawing of subdivisions of a beam

Then, for the j^{th} element of the i^{th} mode of the structure, Equation 5.15 yields Equation 5.16 for each single element (Kim et al. 2002; Shi et al. 2002).

$$[K]_j\{\phi\}_{ij} = \lambda_i[M]_j\{\phi\}_{ij} \qquad \text{Equation 5.16}$$

where $[K]_j$ denotes the j^{th} elemental stiffness matrix, $[M]_j$ denotes the mass of j^{th} element and $\{\phi\}_{ij}$ denotes j^{th} element of the i^{th} mode shape vector.

When damage occurs in a structure, it often changes the stiffness of the damaged area, rather than changing the material properties of the area. Based on this point, an assumption is made that $[K]_j$ can be written as follows:

$$[K]_j = E_j[K]_{jo} \qquad \text{Equation 5.17}$$

where E_j denotes j^{th} equivalent elemental modulus of elasticity, which relates to the true stiffness of the j^{th} element, and matrix $[K]_{jo}$ represents a baseline stiffness of the same element due to geometry of structure. By substituting Equation 5.17 into Equation 5.16, a new equation is derived.

$$E_j[K]_{jo}\{\phi\}_{ij} = \lambda_i[M]_j\{\phi\}_{ij} \qquad \text{Equation 5.18}$$

Premultiplying Equation 5.18 by $\{\phi_{ij}\}^T$ yields Equation 5.19 and then 5.20.

$$E_j\{\phi\}_{ij}{}^T[K]_{jo}\{\phi\}_{ij} = \lambda_i\{\phi\}_{ij}{}^T[M]_j\{\phi\}_{ij} \qquad \text{Equation 5.19}$$

$$E_j = \frac{\lambda_i\{\phi\}_{ij}{}^T[M]_j\{\phi\}_{ij}}{\{\phi\}_{ij}{}^T[K]_{jo}\{\phi\}_{ij}} \qquad \text{Equation 5.20}$$

When the j^{th} element of i^{th} mode shape vector $\{ø\}_{ij}$ is approaching zero, $\{ø\}_{ij}{}^T[K]_{jo}\{ø\}_{ij}$ will also become zero, which leads to singularity problem. So, Equation 5.20 is only valid when $\{ø\}_{ij}{}^T[K]_{jo}\{ø\}_{ij}$ is not zero.

After the beam is inflicted with damage, an equation similar to Equation 5.20 can be written as follows in the same way:

$$E_j^* = \frac{\lambda_i^*\{\phi^*\}_{ij}{}^T[M^*]_j\{\phi^*\}_{ij}}{\{\phi^*\}_{ij}{}^T[K^*]_{jo}\{\phi^*\}_{ij}} \qquad \text{Equation 5.21}$$

In Equation 5.21, superscript '*' is used to indicate damaged state of the beam. As in the case of the undamaged beam model, Equation 5.21 is only valid when $\{ø^*\}_{ij}{}^T[K^*]_{jo}\{ø^*\}_{ij}$ is not zero. Dividing Equation 5.20 by Equation 5.21, a new damage indicator, β_{ij}, can be obtained:

$$\beta_{ij} = \frac{E_j}{E_j^*} = \frac{\dfrac{\lambda_i\{\phi\}_{ij}{}^T[M]_j\{\phi\}_{ij}}{\{\phi\}_{ij}{}^T[K]_{jo}\{\phi\}_{ij}}}{\dfrac{\lambda_i^*\{\phi^*\}_{ij}{}^T[M^*]_j\{\phi^*\}_{ij}}{\{\phi^*\}_{ij}{}^T[K^*]_{jo}\{\phi^*\}_{ij}}} \qquad \text{Equation 5.22}$$

It is worthwhile to note that terms in Equation 5.22 have clear physical meaning. Modal Strain Energy (MSE) for the Euler-Bernoulli beam model of the j^{th} element of i^{th} mode before (Equation 5.23) and after (Equation 5.24) the occurrence of damage is defined as (Shi, et al. 2002):

$$MSE_{ij} = \{\phi\}_{ij}^{T}[K]_j\{\phi\}_{ij} \qquad \text{Equation 5.23}$$

$$MSE_{ij}^{*} = \{\phi^{*}\}_{ij}^{T}[K^{*}]_j\{\phi^{*}\}_{ij} \qquad \text{Equation 5.24}$$

The Modal Strain Energy (MSE) of the subdivided beam for element j at mode i between two locations $(x_k,\ x_k+\Delta x_k)$ is given in the following form (before and after damage in Equation 5.25 and Equation 5.26, respectively):

$$MSE_{ij} = \{\phi\}_{ij}^{T}[K]_j\{\phi\}_{ij} = \frac{1}{2}\{\phi\}_{ij}^{T}\left(\int_{x_k}^{x_k+\Delta x_k} E_j I_j [\{\phi\}_{ij}^{''}]^2\, dx\right)\{\phi\}_{ij} \qquad \text{Equation 5.25}$$

$$MSE_{ij}^{*} = \{\phi^{*}\}_{ij}^{T}[K^{*}]_j\{\phi^{*}\}_{ij} = \frac{1}{2}\{\phi^{*}\}_{ij}^{T}\left(\int_{x_k}^{x_k+\Delta x_k} E_j^{*} I_j [\{\phi^{*}\}_{ij}^{''}]^2\, dx\right)\{\phi^{*}\}_{ij} \qquad \text{Equation 5.26}$$

Based on the assumption in Equation 5.17, Equation 5.27 and Equation 5.28 can be defined as follows:

$$\overline{MSE}_{ij} = \frac{MSE_{ij}}{E_j} = \frac{\{\phi\}_{ij}^{T}[K]_j\{\phi\}_{ij}}{E_j} = \{\phi\}_{ij}^{T}\frac{I_j}{2}\left(\int_{x_k}^{x_k+\Delta x_k} [\{\phi\}_{ij}^{''}]^2\, dx\right)\{\phi\}_{ij} \qquad \text{Equation 5.27}$$

$$\overline{MSE}_{ij}^{\ *} = \frac{MSE_{ij}^{*}}{E_j^{*}} = \frac{\{\phi^{*}\}_{ij}^{T}[K^{*}]_j\{\phi^{*}\}_{ij}}{E_j^{*}} = \{\phi^{*}\}_{ij}^{T}\frac{I_j^{*}}{2}\left(\int_{x_k}^{x_k+\Delta x_k} [\{\phi^{*}\}_{ij}^{''}]^2\, dx\right)\{\phi^{*}\}_{ij}$$

Equation 5.28

Also note that the mass of the j^{th} element of the beam does not change when damage does occur, which means $[M]_j = [M^{*}]_j$, and we also assume that the size of the j^{th} element of the beam does not change as damage has been taken into account by the equivalent elemental modulus of elasticity, which means $I_j=I_j^{*}$. Therefore Equation 5.22 can be rewritten as follows:

$$\beta_{ij} = \frac{E_j}{E_j^*} = \frac{\dfrac{\lambda_i \{\phi\}_{ij}{}^T \{\phi\}_{ij}}{\overline{MSE}_{ij}}}{\dfrac{\lambda_i^* \{\phi^*\}_{ij}{}^T \{\phi^*\}_{ij}}{\overline{MSE}_{ij}{}^*}} \qquad \text{Equation 5.29}$$

To avoid singularity in Equation 5.29, all available modes are employed to calculate the damage indicator. Therefore, for all available modes, *NM*, the damage indicator value for a single element j, is given as:

$$\beta_j = \frac{\sum_{i=1}^{NM} Num_{ij}}{\sum_{i=1}^{NM} Denom_{ij}} \qquad \text{Equation 5.30}$$

where Num_{ij} = numerator of β_{ij} and $Denom_{ij}$ = denominator of β_{ij} in Equation 5.29, respectively. Assuming that the collection of the damage indicators, β_j, represents a sample population of a normally distributed random variable, thus, transforming the damage indicator values into the standard normal space, the normalised damage index Z_j is obtained:

$$Z_j = \frac{\beta_j - \mu_{\beta j}}{\sigma_{\beta j}} \qquad \text{Equation 5.31}$$

where $\mu_{\beta j}$ = mean of β_j values for all *j* elements and $\sigma_{\beta j}$ = standard deviation of β_j for all *j* elements.

Let the damaged elemental equivalent stiffness be a fractional change of the undamaged one, bounded by the severity estimator, α_j; then

$$E_j^* = E_j(1 - \alpha_j) \qquad \text{Equation 5.32}$$

Rewriting Equation 5.32 in terms of α_j yields

$$\alpha_j = 1 - \frac{E_j^*}{E_j} = 1 - \frac{1}{\beta_j} \qquad \text{Equation 5.33}$$

In this research work, Z_j is proposed as a damage location index to indicate the location of damage for given modes, and α_j is proposed as a damage severity estimator to quantify the severity of damage for given modes. The basic principle is that damage will alter the stiffness of the j^{th} element, E_j, due to the damage in the element. Generally speaking, the values of the proposed damage detection index will increase clearly at the damaged element(s) and surrounding elements due to the decrease of the stiffness of the damaged element(s).

5.4 Discussion on the New Method in Comparison with Other Methods

The principle of modal strain energy based damage detection methods is to find a damage sensitive parameter, which relates to modal strain energy and clearly varies due to the change of local stiffness of structures, from which one can identify the location of damage and estimate severity of damage. The parameters used in the modal strain energy based damage detection methods are different, and therefore they perform quite differently in various methods.

Kim & Stubbs (1995) presented a non destructive damage detection technique to locate and size damage from few mode shapes of structures. In their research, a damage index β_{ji} of the i^{th} mode and the j^{th} member was obtained to identify the location of damage as follows (as given in Equation 5.1):

$$\beta_{ji} = \frac{E_j}{E_j^*} = \frac{\phi_i^{*T} C_{jo} \phi_i^*}{\phi_i^T C_{jo} \phi_i} = \frac{NUM}{DEN} \qquad \text{Equation 5.34}$$

where E_j and E_j^* are parameters representing the material stiffness properties for both undamaged and damaged structures, respectively; ϕ_i and ϕ_i^* are the i^{th} modal vectors for both undamaged and damaged structures, respectively; and C_{jo} involves only geometric quantities.

Based on β_{ji}, the estimator of severity of damage in the j^{th} member was given as following (as given in Equation 5.3):

$$\alpha_j = \frac{1}{\beta_j} - 1; \qquad \text{Equation 5.35}$$

After applying the method to a test structure, a two-span aluminium model plate girder, the authors made the following conclusions: (1) That damage can be confidently located to within a fraction of 0.13 of the length of the span; (2) That the magnitude of damage can be evaluated with a severity-estimation error of about 24%; (3) That seven of ten predicted locations could be false positive (i.e., prediction of location that are not damaged) errors; and (4) that four of ten damage locations could be false-negative (i.e., missing detection of true damage locations) errors.

In their research, an assumption was made that the fraction of modal energy is the same for both damaged and undamaged structures. However, in real life, the fraction of modal energy changes due to the change of stiffness of structures. This may be one of reasons that their results might not be accurate in some damage detection cases.

In 2002, Kim & Stubbs (2002) improved their original damage detection method. In their new research, a new damage detection algorithm was formulated to overcome limitations of the previous method (Kim & Stubbs 1995), and to thereby improve the accuracy of damage localization and severity estimation. Three damage indices (referring as Damage Index A, Damage Index B and Damage Index C) were presented in their new algorithm.

For Damage Index A:

$$\beta_j = \frac{E_j}{E_j^*} = \frac{\sum_{i=1}^{nm} \gamma_{ij}^* K_i}{\sum_{i=1}^{nm} \gamma_{ij} K_i^*} \qquad \text{Equation 5.36}$$

$$\alpha_j = \frac{\sum_{i=1}^{nm} \gamma_{ij} K_i^*}{\sum_{i=1}^{nm} \gamma_{ij}^* K_i} - 1 \qquad \text{Equation 5.37}$$

where K_i and K_i^* are the i^{th} modal stiffness of the arbitrary structure before and after damage; $\gamma_{ij}=\varnothing_i^T C_{jo}\varnothing_i$; $\gamma_{ij}^* = \varnothing_i^{*T} C_{jo}\varnothing_i^*$; $\varnothing_i$ and $\varnothing_i^*$ are the i^{th} modal vector before and after damage, respectively. Damage is indicated at j^{th} member if $\beta_j>1$ and damage severity is indicated as the reduction in stiffness in the j^{th} member if $\alpha_j<0$.

For Damage Index B:

$$\beta_j = \frac{E_j}{E_j^*} = \frac{\sum_{i=1}^{nm}(\gamma_{ij}^* + \sum_{k=1}^{ne}\gamma_{ik}^*)K_i}{\sum_{i=1}^{nm}(\gamma_{ij} + \sum_{k=1}^{ne}\gamma_{ik})K_i^*} \qquad \text{Equation 5.38}$$

$$\alpha_j = \frac{\sum_{i=1}^{nm}(\gamma_{ij} + \sum_{k=1}^{ne}\gamma_{ik})K_i^*}{\sum_{i=1}^{nm}(\gamma_{ij}^* + \sum_{k=1}^{ne}\gamma_{ik}^*)K_i} - 1 \qquad \text{Equation 5.39}$$

For Damage Index B based damage detection method, damage is indicated at the j^{th} location if $\beta_j>1$ and damage severity is indicated as the reduction in stiffness in the j^{th} member if $\alpha_j<0$.

For Damage Index C:

$$\beta_{ji} = \frac{E_j}{E_j^*} = \frac{\gamma_{ij}^*}{\gamma_i g_i(\lambda,\phi) + \gamma_{ij}} = \frac{Num}{Den} \qquad \text{Equation 5.40}$$

$$\beta_j = \frac{\sum_{i=1}^{nm} Num}{\sum_{i=1}^{nm} Den} \qquad \text{Equation 5.41}$$

$$\alpha_j = \frac{dE_j}{E_j} = \frac{1}{\beta_j} - 1 \qquad \text{Equation 5.42}$$

where $\gamma_{ij} = \varnothing_i^T C_{jo}\varnothing_i$ and $\gamma_{ij}^* = \varnothing_i^{*T} C_{jo}\varnothing_i^*$; dE_j/E_j is the fractional changes in the stiffness of the j^{th} member; $g_i(\lambda, \varnothing)$ is the dimensionless factor representing the systematic change in modal parameters of the i^{th} mode due to the damage. The same as before, damage is indicated at the j^{th} location if $\beta_j>1$ and damage severity is indicated as the reduction in stiffness in the j^{th} member if $\alpha_j<0$.

After applying these damage detection methods to the numerical work, the results of the three damage indices were as follows. The use of Damage Index A for the damage prediction resulted in (1) relatively small false-negative error (false detection of true damage locations); (2) small localisation error; (3) relatively high false-positive error (prediction of locations that are not damaged); and (4) high severity estimation error. Damage Index A consistently overestimated severity of damage by about 1.75 times the actual damage size. The use of Damage Index B resulted in little error related to damage localisation but high severity of estimation error. It consistently underestimated severity by about 0.15 times the true damage size. The use of Damage Index C resulted in little error related to damage localisation and very small severity estimation error. Finally, the authors concluded that compared to the two other Damage Indices, Damage Index C enhanced the accuracy of the damage localisation and severity estimation results. However, all the results were obtained from numerical studies, and the results from experimental work have not been available as yet.

To evaluate the performance of the damage detection algorithms proposed by Kim and Stubbs (2002) in their research and the performance of algorithm newly proposed in this research, comparison studies have been carried out in both numerical and experimental work (Chapter 6 and Chapter 7). Only Damage Index A and Damage Index C are employed in the comparison work. Damage Index A is chosen because it is highly regarded and, as such, has been referred to in many research work; Damage Index C is chosen because Damage Index C is more accurate than Damage Index A and Damage Index B.

As mentioned in section 5.1, Shi et al. (1998) presented a different damage localisation method based on modal strain energy change in 1998. The method was improved in 2000 (Shi, et al. 2000) and improved again in 2002 (Shi, et al. 2002). In their research work, the stiffness matrix K^d, the i^{th} modal eigenvalue λ_i^d, and the i^{th} mode shape ϕ_i^d of the damaged system were defined as follows:

$$K^d = K + \sum_{j=1}^{L} \Delta K_j = K + \sum_{j=1}^{L} \alpha_j K_j \qquad (-1<\alpha_j\leq 0) \qquad \text{Equation 5.43}$$

$$\lambda_i^d = \lambda_i + \Delta\lambda_i \qquad \text{Equation 5.44}$$

$$\phi_i^d = \phi_i + \Delta\phi_i = \phi_i + \sum_{j=1}^{m} c_{ij}\phi_j \qquad \text{Equation 5.45}$$

where α_j is coefficient defining a fractional reduction in the j^{th} elemental stiffness matrices; c_{ij} is coefficient defining a fractional change of the mode shape vector; m is the number of modes considered and L is the total number of elements in the system. So the elemental modal strain energy change (MSEC) for the j^{th} element in the i^{th} mode is expressed as:

$$MSEC_{ij} = \phi_i^{dT} K_j \phi_i^d - \phi_i^T K_j \phi_i \qquad \text{Equation 5.46}$$

Then the modal strain energy change ratio (MSECR) was defined in the research as an indicator to detect damage location:

$$MSECR_j^i = \frac{\left| MSE_{ij}^d - MSE_{ij} \right|}{MSE_{ij}} \qquad \text{Equation 5.47}$$

where j and i denote the element number and mode number, respectively; MSE and MSE^d denote the modal strain energy before and after the occurrence of damage.

Regarding the severity of damage, another equation was developed in the research:

$$MSEC_{ij} = \sum_{p=1}^{L} [-2\alpha_p \phi_i^T K_j (\sum_{r=1}^{n} \frac{\phi_r^T K_p \phi_i}{\lambda_r - \lambda_p} \phi_r)] \qquad \text{Equation 5.48}$$

where P is the number of element and L is the total number of elements in the system. The term on the left-hand side of Equation 5.48 is the element modal strain energy change of the j^{th} element in the i^{th} mode, which can be calculated from Equation 5.46 by using the experimental mode shape of the undamaged and damaged states. All the terms on the right-hand side of Equation 5.48 except α_p are all known information of the undamaged system. Thus the severity of damage, α_p, can be calculated by solving Equation 5.48.

In the processing of damage detection by using modal strain energy change based method, although the refined method reduced the truncation error in computation, it avoided the finite element modelling error in higher modes, and improved the rate of convergence in the computation, the refined method had the following weaknesses: (1) both measured mode shapes and analytical system matrices were required in the performance of damage localization and quantification approach. Analytical system matrices were difficult to obtain in performing the method; and (2) the convergence property of the method presents great difficulty in performance of the method.

The third method as mentioned in section 5.1 was presented by Hu et al (2006). These authors presented a different algorithm, namely cross modal strain energy (CMSE) method, to estimate the damage magnitude of multiple damaged members. In their research, a definition of stiffness matrix of damaged structures was made as follows:

$$K^* = K + \sum_{n=1}^{N_d} \alpha_n K_{\ln} \qquad \text{Equation 5.49}$$

where N_d is total number of the damaged member; α_n and l_n are damage extent and the element number of the n^{th} damaged element, respectively; K is the stiffness matrix for the undamaged structure. Then the structural cross-modal strain energy between the i^{th} mode of the baseline structure and the j^{th} mode of the damaged structure was defined as:

$$C_{ij} = (\phi_i)^T K \phi_j^* \qquad \text{Equation 5.50}$$

where ϕ_i denotes the i^{th} eigenvector and ϕ_j^* denotes the j^{th} eigenvector of the damaged structure, respectively. The corresponding elemental cross-modal strain energy for the stiffness matrix was defined as:

$$C_{n,ij} = (\phi_i)^T K_{\ln} \phi_j^* \qquad \text{Equation 5.51}$$

After many steps of derivation, Equation 5.49 can be rewritten as Equation 5.52:

$$\sum_{n=1}^{N_d} \alpha_n C_{n,ij} = (\frac{\lambda_j^*}{\lambda_i} - 1) C_{ij} \qquad \text{Equation 5.52}$$

Therefore, the severity of damage, α_n, can be calculated by solving Equation 5.52.

Even though the authors mentioned merits of the CMSE method, the method was not able to identify the location of damage. Developing the CMSE method as a combined scheme for damage localization and damage severity estimation is currently underway.

The features of the new damage detection algorithm proposed in this research are summarized as follows: (1) both mode shapes and mode shape curvature are utilised in the new method. Many research works have indicated that mode shape curvature is very sensitive to damage. However, it also means that mode shape curvature is very vulnerable to unwanted disturbance in real life applications such as noise, error due to reconstruction of mode shapes due to limited measurements and imperfection of mode shapes obtained from Experimental Modal Analysis. Based on mode shapes and modal strain energy formulation, the new method combining mode shape and mode shape curvature is capable of identifying the location of damage and quantifying the severity of damage more robustly and accurately than the other methods; and (2) the new method has no difficulty in convergence and is most suited to the complex problem at hand.

5.5 Summary

Firstly, some typical modal strain energy based damage detection methods were introduced in the chapter. Then a new algorithm for damage detection was derived. The advantages of the new algorithm are summarised here:

1. The new algorithm is based on a more reasonable assumption, that is, most damage change the stiffness of the affected area, other than changing the mass of the structure.
2. The change in indicator proposed in the new algorithm is more robust and less noise sensitive than that of other methods, due to the fact that the formulation of

the damage indicator includes both mode shape and mode shape curvature. Thus the new algorithm is expected to be more reliable than other methods to locate damage and quantify its severity.

3. The new algorithm should not have problem in convergence property and therefore has no difficulty in performing the approach.

In this chapter, the differences between the new method and the methods proposed by other researchers was also analysed and the advantages of the new method are proven in both numerical work (Chapter 6) and experimental work (Chapter 7).

CHAPTER 6

APPLICATION OF THE NEW DAMAGE DETECTION METHOD (NUMERICAL STUDIES)

6.1 Introduction

This chapter presents a comprehensive numerical study of damage detection on reinforced concrete beams using the newly developed algorithm in Chapter 5. Firstly, the methods of acquiring modal parameters (natural frequencies and mode shapes), which are essential to the proposed damage detection, are introduced in the chapter. The proposed damage detection method is implemented for detecting damage location and estimating damage severity on a series of numerical cases with single and multiple damage scenarios under various combinations of location and severity of damage. Subsequently, the proposed damage detection method is compared with two existing popular damage detection methods. Finally, some further improvements are proposed to enhance the capacity of the proposed damage detection method to assess damage. A number of numerical cases have been used to demonstrate the effectiveness of such improvements.

6.2 Modal Analysis

For given structural vibration responses, the vibrational characteristics (natural frequencies, mode shapes and modal damping or stiffness, damping and mass matrices) can be obtained from the modal analysis. These characteristics are important parameters in performing damage detection using modal based methods. In this study, mode shape will be the main modal parameter used in the newly developed damage detection method. In general, there are two different approaches to, numerically, determine the modal parameters. One approach is to obtain the modal parameters by directly solving the eigenproblem when stiffness, mass and damping matrices of the given system are available, such as using the Modal Analysis Function (MAF) under the Structural Analysis Package in ANSYS 11 (2007). The other approach is Experimental Modal

Analysis (EMA), which the modal parameters are obtained from vibrational response time histories (either numerically simulated or experimentally measured). The EMA is based on curve fitting techniques and consists of signal processing, frequency response function (FRF) calculation and modal parameter estimation.

A description of the Modal Analysis Function in the ANSYS program is briefly introduced. More detailed information on this technique can be obtained by referring to ANSYS Inc. (2007). The procedure of performing the EMA, numerically, is also introduced. It is worth noting that whether time history data is obtained, numerically or experimentally, EMA requires similar steps to acquire the modal parameters.

6.2.1 Obtaining Modal Parameters by Solving Eigenproblem

In most FEA softwares such as ANSYS (2007), the eigenvalue and eigenvector problem is solved by analysing Equation 6.1.

$$[K]\{\phi\} = \lambda[M]\{\phi\} \qquad \text{Equation 6.1}$$

where $[K]$ is structural stiffness, $\{\phi\}$ is eigenvector, λ is eigenvalue and $[M]$ is structural mass matrix. For the procedure, the system of equations is first condensed down to those degrees of freedom (DOFs) associated with the master DOFs by Guyan reduction. The set of n master DOFs characterise the natural frequencies of interest in the system. The number of master DOFs selected should usually at least be equal to twice the number of frequencies of interest. Next, the actual eigenvalue extraction is performed. The extraction technique employed is the Householder-Bisection-Inverse Iteration (HBI) extraction technique which is explained in the following five steps:

(A) Transformation of the Generalised Eigenproblem to a Standard Eigenproblem

Equation 6.1 is transformed to the desired standard eigenproblem form with $[A]$ being symmetric, i.e.

$$[A]\{\psi\} = \lambda\{\psi\} \qquad \text{Equation 6.2}$$

This is accomplished by premultiplying both sides of Equation 6.1 by $[M]^{-1}$.

$$[M]^{-1}[K]\{\phi\} = \lambda\{\phi\} \qquad \text{Equation 6.3}$$

Decompose $[M]$ into $[L][L]^T$ by Cholesky decomposition, where $[L]$ is a lower triangular matrix. Combining with Equation 6.3,

$$[L]^{-T}[L]^{-1}[K]\{\phi\} = \lambda\{\phi\} \qquad \text{Equation 6.4}$$

It is convenient to define:

$$\{\phi\} = [L]^{-T}\{\psi\} \qquad \text{Equation 6.5}$$

Combing Equation 6.4 and Equation 6.5, and reducing yields:

$$[L]^{-1}[K][L]^{-T}\{\psi\} = \lambda\{\psi\} \qquad \text{Equation 6.6}$$

Or

$$[A]\{\psi\} = \lambda\{\psi\} \qquad \text{Equation 6.7}$$

where: $[A]=[L]^{-1}[K][L]^{-T}$.

Note that the symmetry of $[A]$ has been preserved by this procedure.

(B) Reduction [*A*] to Tridiagonal Form

This step is performed by Householder's method through a series of similarity transformations yielding

$$[B] = [T]^T[A][T] \qquad \text{Equation 6.8}$$

where:

$[B]$=tridiagonaised form of $[A]$

$[T]$= matrix constructed to tridiagonalise $[A]$

The eigenproblem is reduced to:

$$[B]\{\psi\} = \lambda\{\psi\} \qquad \text{Equation 6.9}$$

Note that the eigenvalues *(λ)* have not changed through these transformations, but the eigenvectors are related by

$$\{\phi\} = [L]^{-T}[L]\{\psi\} \qquad \text{Equation 6.10}$$

(C) Eigenvalue Calculation

The Sturm sequence (a finite sequence of polynomials) is used to check with the bisection method to determine the eigenvalues.

(D) Eigenvector Calculation

The eigenvectors are evaluated using inverse iteration with shifting. The eigenvectors associated with multiple eigenvalues are evaluated using initial vector deflation by Gram-Schmidt orthogonalisation in the inverse iteration procedure.

(E) Eigenvector Transformation

After the eigenvectors $\{\psi\}$ are evaluated, mode shapes $\{\phi\}$ are recovered through Equation 6.10. Using the EXPASS (Expansion Pass) command to obtain a complete solution, the eigenvectors are expanded from the master DOFs to the total DOFs.

6.2.2 Obtaining Modal Parameters by Experimental Modal Analysis (EMA)

Experimental modal analysis (EMA) is the process of determining the modal parameters of a linear, time invariant system by reconstruction of a modal model from measured or simulated experimental data. When using experimental data, EMA can be costly and time consuming if it is required for parametric studies. Hence, EMA often uses numerical data first before costly experiments start. The numerical way of performing the EMA sometimes is named Virtual Experimental Modal Analysis (VEMA) (Elliott & Richardson, 1998). In this chapter, the VEMA includes modelling of a test structure, simulation of excitation force, acquisition of output acceleration and modal parameters

estimation. Since VEMA is derived from the EMA, most of the detailed description of the major parts of the method is discussed in the experimental chapter, Chapter 7.

Before proceeding, some basic assumptions used for VEMA or even EMA need to be established. There are four basic assumptions concerning any structure developed in order to perform an experimental modal analysis:

(1) The structure is assumed to behave linearly i.e., the response of the structure to any combination of forces, simultaneously applied, is the sum of the individual response to each of the forces acting alone.
(2) The structure is time invariant i.e. the parameters that are to be determined are constants with time. In general, a system which is not time invariant will have components composed of mass, stiffness, or damping depending on factors that are not measured or are not included in the model. For example, some components may be temperature dependent. In this case the temperature of the component is viewed as a time varying signal, and, hence the component has time varying characteristics.
(3) The structure obeys Maxwell's reciprocity i.e. a force applied at degree-of-freedom (DOF) *m* causes a response at DOF *n* that is the same as the response at DOF *m* caused by the same force applied at DOF *n*.
(4) The structure is observable i.e. the input-output measurements that are generated contain enough information to create an adequate behavioural model of the structure. Structures, which have degree-of-freedom of motion that are not measured, are not completely observable, for example, considering the motion of a partially filled tank of liquid when complicated sloshing of the fluid occurs.

Following are step-by-step procedures of obtaining modal parameters using the VEMA.

(A) Modelling the test structure

A finite element (FE) model of a laboratory reinforced concrete (RC) beam was developed. The model was validated with the experimental results. The details of the modelling are given in Chapter 4.

(B) Applying the impact loading

Using the FE beam model, a transient dynamic analysis was performed. The "full method" (details given in ANSYS (2007)), which uses the full system matrices to calculate the transient response, was adopted for the transient dynamic analysis. In the transient dynamic analysis, an impact loading, detailed in Figure 6.1, was applied on the top of the beam, at 3/8 span from the left support. The location of the impact loading is chosen to be the same as the one in the experimental work.

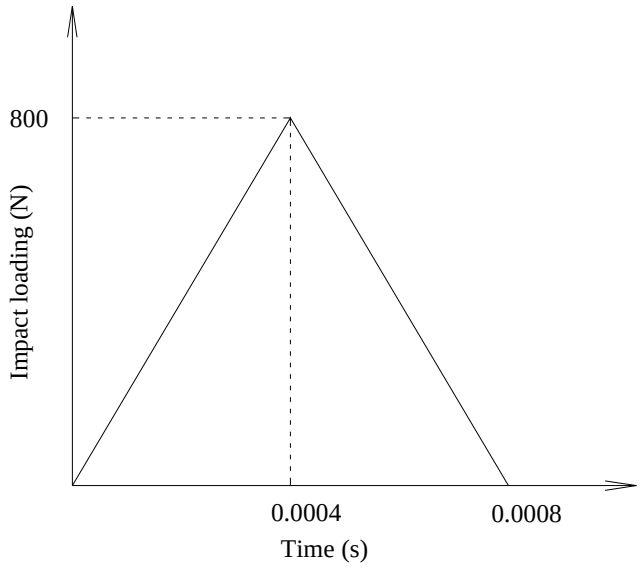

Figure 6.1 The applied impact loading in the transient dynamic analysis

(C) Obtaining the output results

From the transient dynamic analysis, the displacements at nine measurement points (abbreviated as 9-points), chosen evenly on the top of the beam, were obtained. These measuring locations correspond to the experimental ones. Using an in-house software written in MATLAB (2007) code, the accelerations of the 9-points were obtained by performing double differentiations on the displacements. In order to investigate the influence of noise presence on the proposed damage detection method, various levels of white Gaussian noise of 0%, 2% and 10% were added to the acceleration data. From the noisy acceleration data, the fast Fourier transform (FFT) and frequency response function (FRF) data of the RC beam were subsequently computed.

(D) Estimating the modal parameters

A commercial modal analysis program, namely LMS (1992), was used to identify the modal parameters from the obtained FRF data. Finally, the modal parameters of the RC beam (natural frequencies and mode shapes) were obtained. Damping ratio was not acquired as it was not considered in the numerical work. The details of the above-mentioned processes can be found in Chapter 7.

6.3 Damage Localisation for Reinforced Concrete Beams

Finite element (FE) reinforced concrete (RC) beam models were constructed for damaged beams with different types of damage scenarios. These models were utilised to evaluate the effectiveness and reliability of the proposed damage detection method formulated in Chapter 5. Details of the FE modelling can be found in Chapter 4. For the intact FE beam model, the first five flexural modes were extracted as depicted in Figure 6.2. All mode shapes considered are mass normalised. Mode shapes for the damaged beams were also extracted to be used together with the intact beam ones in the damage detection algorithms.

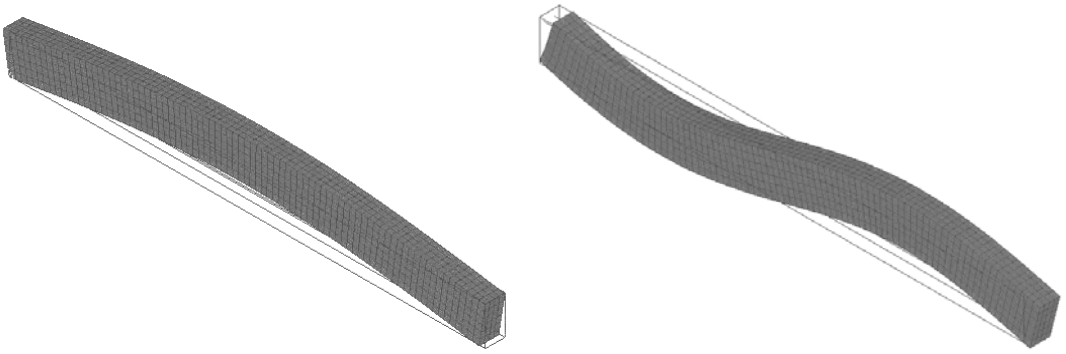

(a) Mode 1 (36.60 Hz) (b) Mode 2 (128.81 Hz)

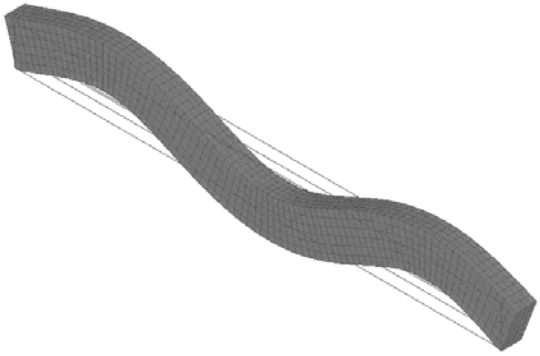

(c) Mode 3 (320.27 Hz)

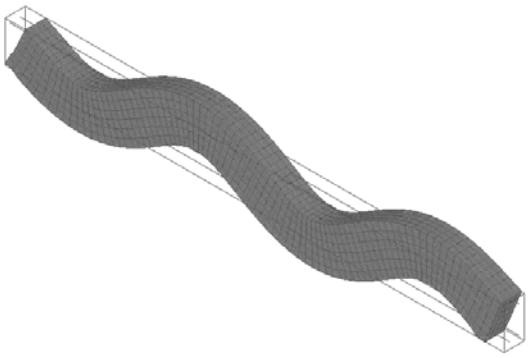

(d) Mode 4 (502.57 Hz)

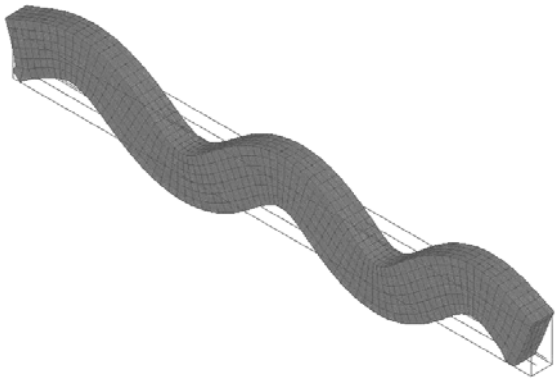

(e) Mode 5 (756.06 Hz)

Figure 6.2 The first five flexural mode shapes of the reinforced concrete beam

In the following discussion, mode shapes named as “Results without Noise” refer to results obtained from the eigenproblem solution using the Modal Analysis Function (MAF) (ANSYS, 2007) with 41 measuring points (abbreviated as 41-nodes) taken from the top of the beam with even spacing. “Results with Noise” refers to the results obtained from the virtual experimental modal analysis (VEMA). These mode shapes were originally taken from 9 measuring points (abbreviated as 9-nodes) on top of the beam with even spacing, which correspond to measurements in the experimental work. The 9-points mode shapes were then reconstructed using a numerical technique, namely Cubic Spline, to generate mode shapes with 41 measuring points. These reconstructed mode shapes are called “9-to-41-nodes”. The reconstruction technique creates more measuring points, hence enhancing the capability of damage detection methods based on mode shape and its derivatives (Choi et al., 2006). The advantage of using the

experimental modal analysis (EMA) to obtain modal parameters from the numerical outputs rather than using eigensolution directly is that it simulates real experimental condition.

It is important to highlight that the results obtained from the eigenproblem solution using the Modal Analysis Function (MAF) in ANSYS (2007) is obviously not the same as the one acquired from the virtual experimental modal analysis (VEMA) with 0% noise present. This is due to the fact that although noise level is set at 0%, it still simulates the results obtained from the VEMA and still stimulates the imperfection of modal analysis and error of reconstruction of mode shapes from limited number of sensors. A summary guide to interpret the results is listed in Table 6.1.

Table 6.1 A summary guide to interpret the results

Results	Description of Mode Shape	Abbreviation
Without Noise	41 measuring points taken from the MAF	41-nodes
With Noise Levels of 0%, 2% and 10%	9 measuring points taken from the VEMA	9-nodes
	Reconstruct 9-nodes to 41-nodes using the Cubic Spine technique	9-to-41-nodes

6.3.1 Different Cases of Damaged Beams

In the numerical studies, three different levels of severity of damage (light, medium and severe) were introduced to the reinforced concrete beams to simulate various kinds of cracks inflicted in the experimental studies. All cracks were of notch type with the same thickness of 45 mm, width of 150 mm and with various depths, i.e. 50 mm for light damage (**L**), 100 mm for medium damage (**M**) and 150 mm for severe damage (**S**), corresponding to 36.03%, 58.86% and 71.27% loss of cross sectional moment of inertia (**I**), respectively. In order to locate the damage, the reinforced concrete beams were divided into eight regions evenly by their length as shown in Figure 6.3. In this research work, the following notations are used for indicating different regions: 1 stands for the

region on 1/8 span of the beam, 2 stands for 2/8 span of the beam, 3 stands for 3/8 span of the beam, and so on. In terms of damage severity, **L** stands for light damage, **M** stands for medium damage and **S** stands for severe damage. A numbering system is created to recognise damage characteristics of a damaged beam. For example, 1L3M5S7L denotes a beam with four damage locations on 1/8 span, 3/8 span, 5/8 span and 7/8 span corresponding to damage severity of light, medium, severe and light, respectively. Figure 6.3 depicts the damaged beam 1L3M5S7L. As mentioned earlier, the 41 nodes on the top of numerical beams were selected evenly as coordinates of mode shapes, so the 1/8 span ends at node 6, the 2/8 span ends at node 11, the 3/8 span ends at node 16, the 4/8 span ends at node 21, the 5/8 span ends at node 26, the 6/8 span ends at node 31, and the 7/8 span ends at node 36. The pin and roller supports correspond to zero span and full span as well as node 1 and node 41, respectively. The details of the numbering system are illustrated in Figure 6.3.

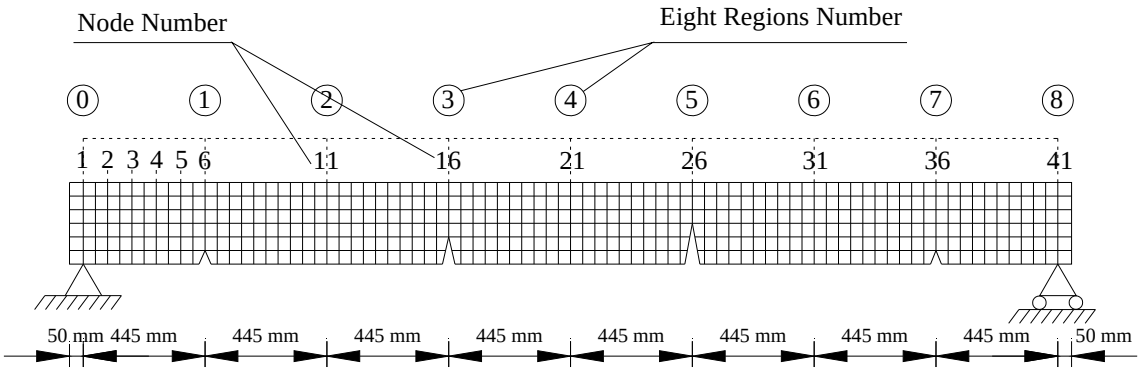

Figure 6.3 1L3M5S7L Damaged beam

To simulate the honeycomb damage at the bottom of the RC beam, eight elements (four elements were at the first level and four elements at the second level from the soffit of the beam) were chosen and their modulus of elasticity was decreased close to zero in the modelling of reinforced concrete beam as shown in Figure 6.4 by the “red” circle. The centre of the modelled honeycomb was 2.72 meters from the left side of the beam (pin support) and ended at node 31. This damage is named HB. For honeycomb damage at the top of the beam, similar process and location of modelling for HB was adopted but the damage starts from the top of the beam. The damaged beam with honeycomb at the top is denoted HT. The details of modelling the damage can be found in Chapter 4.

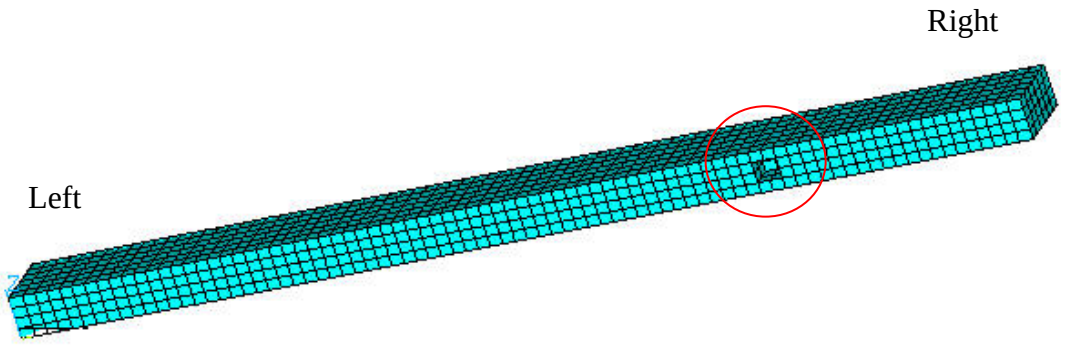

Figure 6.4 Damaged beam with honeycomb at the bottom (HB)

In order to investigate the effects of damage locations and damage severities on the reinforced concrete beams, 18 different damaged cases were employed in the numerical work with combination of different locations and levels of damage severity. The damage cases in experimental investigation will be a subset of the numerical cases. All damage cases are described in Table 6.2.

Table 6.2 Numerical damage scenarios

Damage case	Damage scenario	Damage location with respect to 41 nodes	Thickness (mm)	Depth (mm)	Width (mm)
0	Undamaged	-	-	-	-
1	2L	11	45	50	150
2	2M	11	45	100	150
3	2S	11	45	150	150
4	3L	16	45	50	150
5	3M	16	45	100	150
6	3S	16	45	150	150
7	4L	21	45	50	150
8	4M	21	45	100	150
9	4S	21	45	150	150
10	1L4L	6, 21	45	50, 50	150
11	3S7S	16, 36	45	150, 150	150
12	2M5M	11, 26	45	100, 100	150
13	3M7S	16, 36	45	100, 150	150

14	1L2L3L	6, 11, 16	45	50,50,50	150
15	2M4M6M7M	11,21,31,36	45	100, 100, 100, 100	150
16	2M3S5M7S	11,16,26,36	45	100, 150, 100,150	150
17	HB	31	89	100	750
18	HT	31	89	100	750

6.3.2 Damage Detection without Noise

For damage localisation in this research, impacts of different combination of mode shapes, ranging from using only the first flexural mode to using all first five flexural modes on the proposed damage detection method has been investigated. The choice of the first five flexural modes used in the damage detection method is mainly due to the constraint of the number of modes that can reliably be obtained from the experimental work. The mode shapes used in this section, named "Without Noise", were from the eigenproblem solution through the Modal Analysis Function (MAF) of ANSYS (2007) with no noise present. The 41-node mode shapes were employed in the damage detection method.

In the numerical investigation presented in the following section, the damage location indices (Z_j) are plotted against the node number of the reinforced concrete beam. In principle, when the damage location index (Z_j) of a given location is greater than zero there exists a possibility that damage occurs at that location. In the following figures, the actual damage locations are indicated with vertical red dashed lines.

6.3.2.1 Damage Simulation by Single Notch/Crack

Figures 6.5 and 6.6 show the results of the proposed damage detection algorithm applied to the reinforced concrete beam models with a single damage. Each group of figures consists of five diagrams from (a) to (e), showing damage detection results of using cumulative of modes from the first one up to the fifth, in the damage detection algorithm. Diagram (a) gives the result of using only the first mode shape (mode 1); diagram (b) gives the result of using both the first and the second mode shapes (modes 1+2); diagram (c) gives the result of using the first three mode shapes (modes 1+2+3);

and so on. The two Figures 6.5 (2L) and 6.6 (4S) depict the damage detection results of two different levels of damage severity, i.e., light and severe damage at the location 2/8 span (node 11) and 4/8 span (node 21), respectively. The damage detection results of other single damage scenarios (2M, 2S, 3L, 3M, 3S, 4L and 4M) are shown in Appendix B.1.

From Figures 6.5 and 6.6, the single damage is distinctly identified for all combination of modes. It can also be observed that the magnitude of the damage location index (Z_j) increases with the severity of damage indicating the increased probability of damage existence. For example, using all five modes (modes 1+2+3+4+5) in the method for case 2L, the Z_j is about 3.3, while for case 2S is higher with a value of about 4.0 as shown in Figures 6.5(e) and 6.6(e), respectively. From the damage detection results for single damage cases, it is apparent that the proposed damage detection method using different combination of modes preforms effectively in locating damage for reinforced concrete beams. It is also possible to deduce that, by using only the first mode and all the first five modes in the algorithm, they are of similar effectiveness in detecting the location of single damage at different locations in the numerical studies.

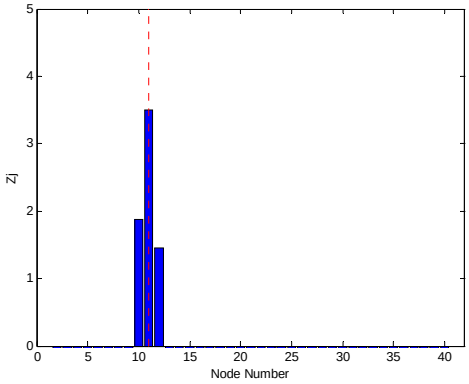

(a) Mode 1

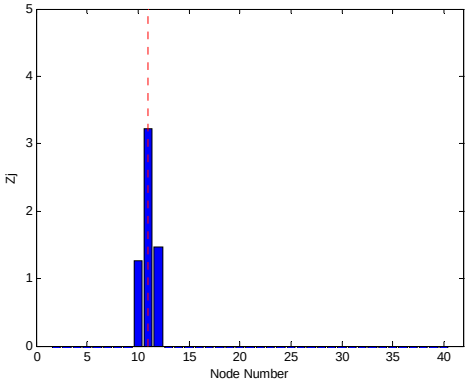

(b) Modes 1+2

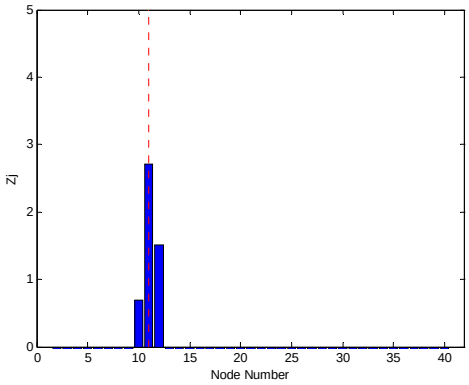

(c) Modes 1+2+3

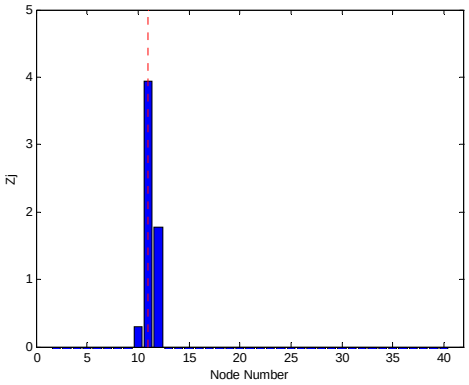

(d) Modes 1+2+3+4

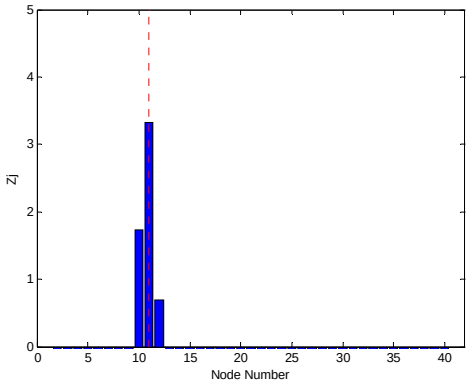

(e) Modes 1+2+3+4+5

Figure 6.5 Damage localisation with single light damage (2L)

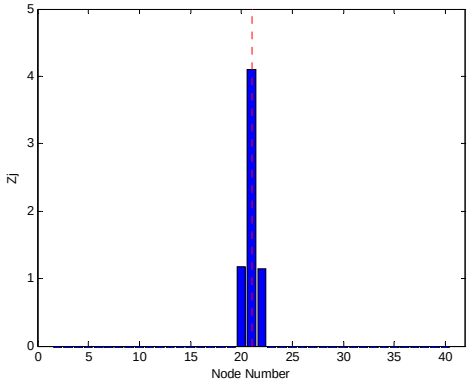

(a) Mode 1

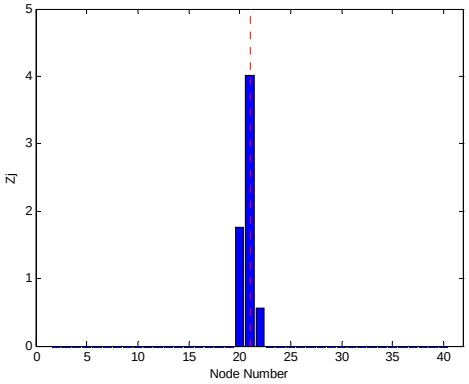

(b) Modes 1+2

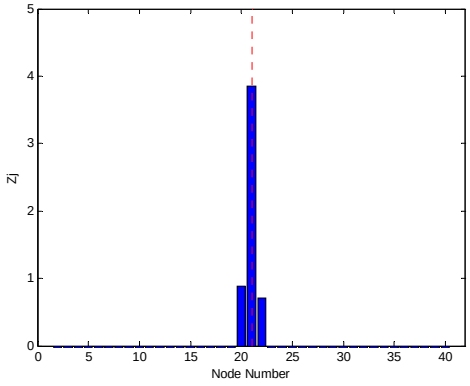

(c) Modes 1+2+3

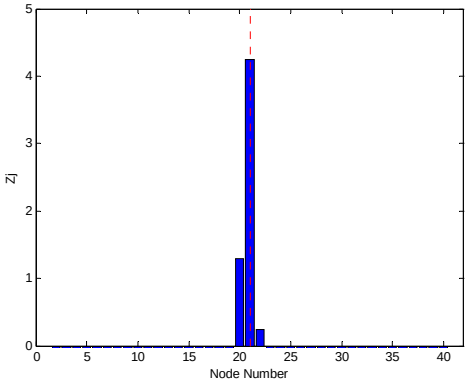

(d) Modes 1+2+3+4

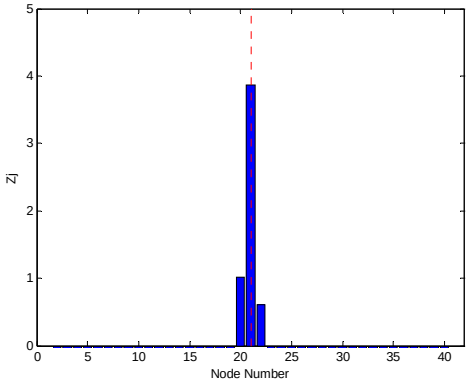

(e) Modes 1+2+3+4+5

Figure 6.6 Damage localisation with single severe damage (4S)

6.3.2.2 Multiple Notch/Cracks Types of Damage

Figures 6.7 and 6.8 demonstrate two applications of the proposed damage detection algorithm for multiple damage cases for cases 3M7S and 2M4M6M7M, respectively. The damage detection results of other multiple damage scenarios (1L4L, 3S7S, 2M5M,

1L2L3L and 2M3S5M7S) are shown in Appendix B.2. Similar to the single damage cases, five diagrams in each figure represent the results from five different combinations of mode shapes.

From Figures 6.7 and 6.8, all damage locations were accurately identified. For example, the medium and severe damage at node 16 and node 36, respectively, were clearly located by the proposed method as shown in Figure 6.7. This also applies to the four damage location case as shown in Figure 6.8, for damage locations at node 11, node 21, node 31 and node 36. It is worthy of mentioning that Figures 6.8(a) and (e) using only the first mode shape and using all the first five modes, respectively, show that the magnitude of Z_j for the four damage locations are quite similar indicating the actual situation of the beam inflicted with four medium damage locations. However, in the other figures (in which damage location index was calculated with different combination of mode shapes), the magnitudes vary a lot, which are different to the actual inflicted damage scenario. For the case of 3M7S (Figure 6.7), the aforementioned observations appear in all combination of mode shapes used in the algorithm to detect damage. It is, therefore, concluded that the proposed damage detection algorithm is effective in identifying damage location of reinforced concrete beam for both single and multiple damage cases. It is recommended, based on the above findings, that it is reasonable to use two types of combination of mode shapes, i.e. using only mode 1 (Mode 1 can be abbreviated as 1-Mode) and using the first five modes (Modes 1+2+3+4+5 can be abbreviated as 5-Modes), in the proposed damage detection for the following discussions.

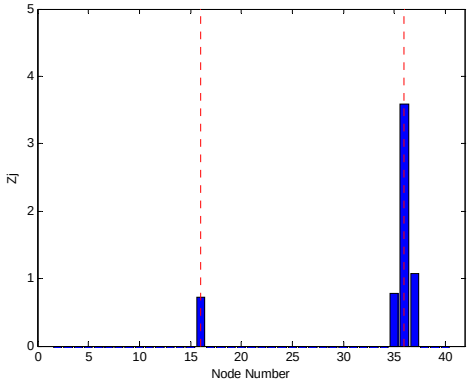

(a) Mode 1

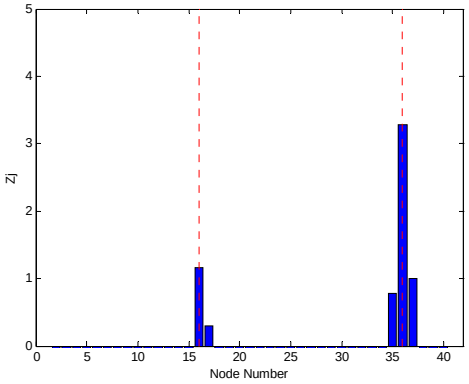

(b) Modes 1+2

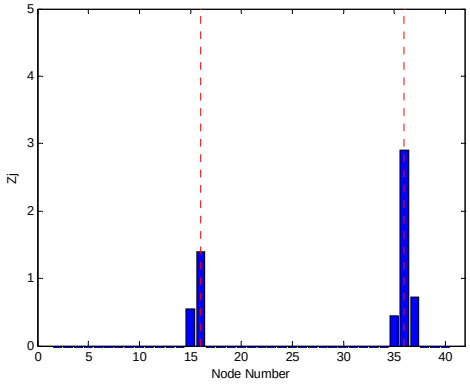

(c) Modes 1+2+3

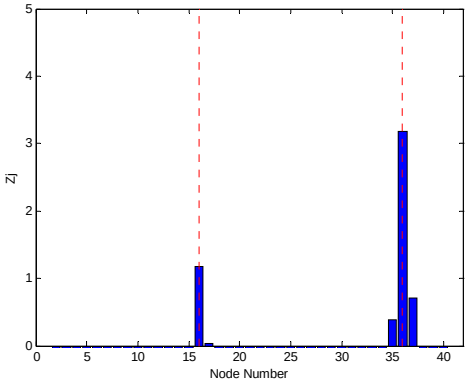

(d) Modes 1+2+3+4

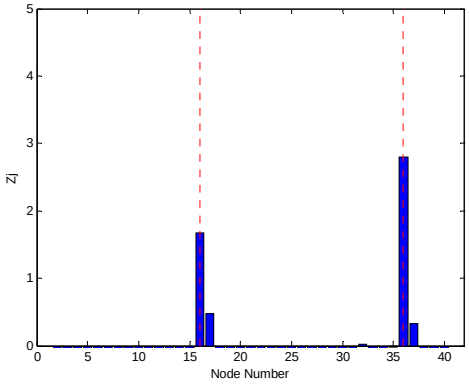

(e) Modes 1+2+3+4+5

Figure 6.7 Damage localisation with two damage locations (3M7S)

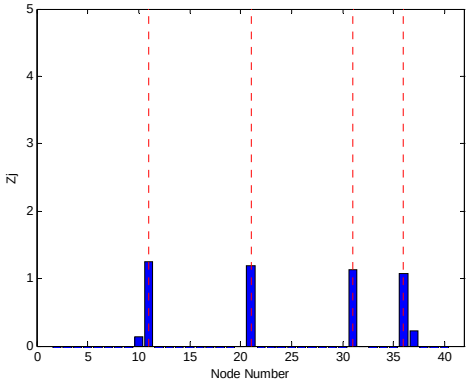

(a) Mode 1

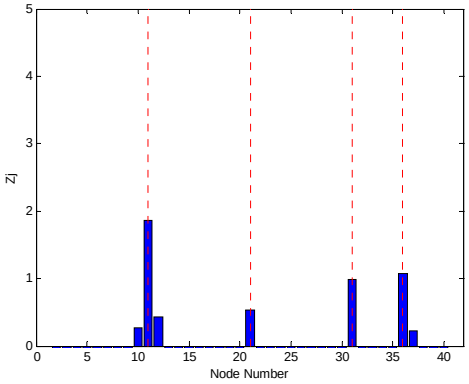

(b) Modes 1+2

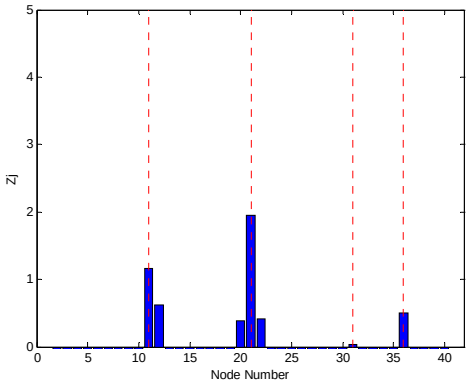

(c) Modes 1+2+3

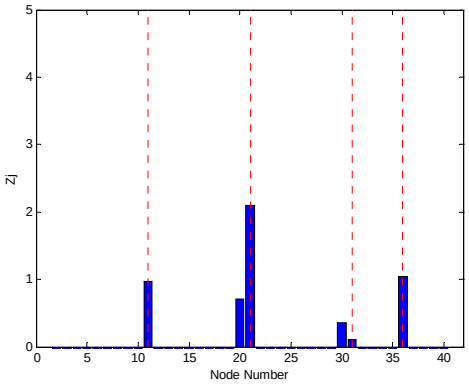

(d) Modes 1+2+3+4

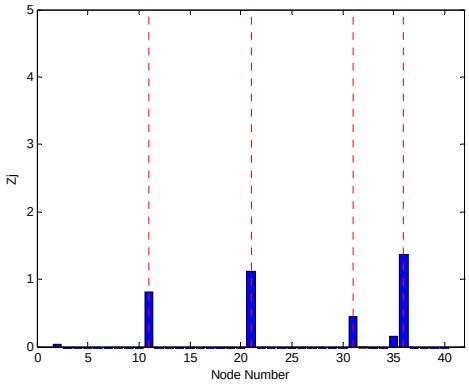

(e) Modes 1+2+3+4+5

Figure 6.8 Damage localisation with four damage locations (2M4M6M7M)

6.3.2.3 Honeycomb Type of Damage

Figure 6.9 shows the application of the proposed damage detection method to another type of damage commonly found in RC structures, i.e. honeycomb or void type of damage. This section will focus the discussion mainly on the HT case, i.e., the

honeycomb damage found on the top part of the beam. The damage detection results of using the proposed method with honeycomb in the bottom are shown in Appendix B.3. From Figures 6.9(a) to (e), it was observed that by applying the proposed damage detection method, the damage was accurately located for all combination of mode shapes. This again proves the effectiveness of proposed damage detection method as well as the appropriateness of using the combination of modes for 1-Mode (Mode 1) and 5-Modes (Modes 1+2+3+4+5) in the proposed method for damage detection.

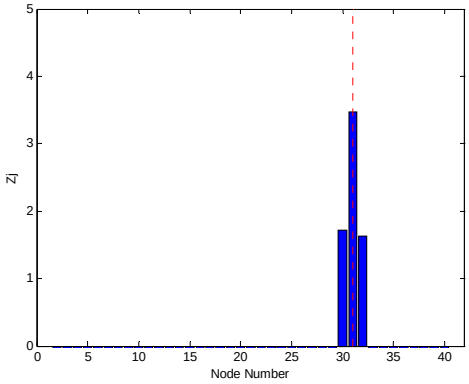

(a) 1-Mode (Mode 1)

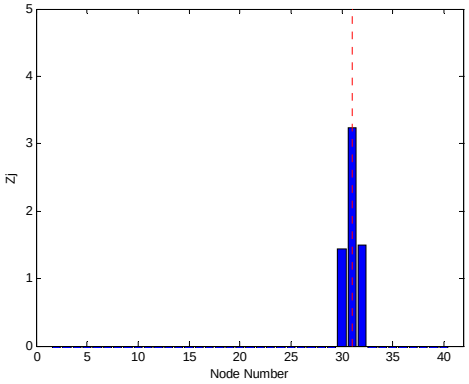

(b) Modes 1+2

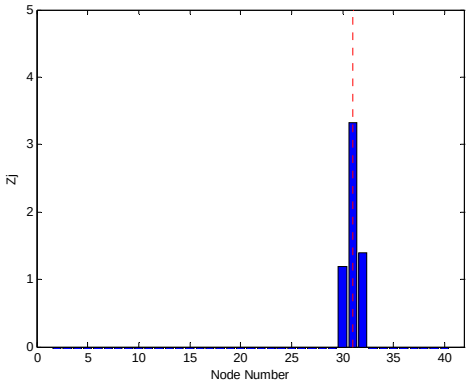

(c) Modes 1+2+3

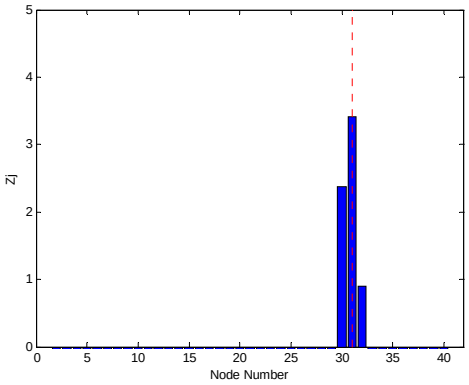

(d) Modes 1+2+3+4

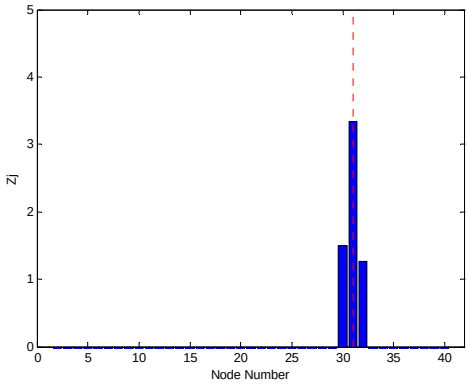

(e) 5-Modes (Modes 1+2+3+4+5)

Figure 6.9 Damage localisation with honeycomb damage on top of the beam (HT)

6.3.3 Damage Detection under Simulated Noise

As mentioned earlier, there are two different approaches to determining vibration characteristics of a structure. One approach determines vibration characteristics from given mass, stiffness and damping matrices of structure, by utilising the Modal Analysis

Function (MAF) under the Structural Analysis Package in ANSYS (2007) by solving an eigenproblem. This method is employed to obtain mode shapes from eigensolution of FE models as outlined previously. The second approach determines the vibration characteristics of a structure through the virtual experimental modal analysis (VEMA), which utilises the response time histories and input force to produce frequency response function (FRF) and Modal Parameter Estimation.

The second approach, namely VEMA, is utilised to acquire mode shapes of the FE reinforced concrete beam model. Nine nodes on the top of the numerical beam were selected evenly for collecting the acceleration data of the beam consistent with the measuring points employed in the experimental work. After Signal Processing, Post Processing and Modal Parameter Estimation, the mode shapes of the beam were obtained.

To closely simulate the actual experimental condition, white Gaussian noise was added to the acceleration time history data obtained from ANSYS. White Gaussian noise was chosen because white Gaussian noise has a random and normal distribution of instantaneous amplitudes over time and therefore can simulate noise in experimental environment very well. Further more, white Gaussian noise is a random signal with a flat power spectral density. By having power at all frequencies, the total power of such a signal is infinite and therefore impossible to generate. Therefore, the signal contains equal power within a fixed bandwidth at any central frequency. In this research work, in order to investigate effects of noise, imperfection of modal analysis and error of mode shape reconstruction on the damage detection results, 0%, 2% and 10% added White Gaussian noise were considered in the study.

From both the original acceleration time history data (0% noise) and the noisy (2% and 10%) acceleration time history data, five flexural vibration modes and natural frequencies ranging from 10 Hz to 1,000 Hz were captured. The nine-point mode shape coordinates can be reconstructed using cubic spline interpolation technique (O'Neill 2002) to obtain mode shape vectors with 41 point coordinates. The mode shapes with finer coordinates have shown better results in detecting damage location, compared to the use of coarse coordinates (Choi et al., 2006). The reconstructed mode shapes were

then used in the proposed damage detection algorithms for locating and evaluating the inflicted damage in reinforced concrete beams.

6.3.3.1 Results of Damage Detection Subjected to Simulated Noise

In this research work, the acceleration time history data from four different damage cases (2L, 4M, 4S and 2M4M) were polluted with white Gaussian noise. 0%, 2% and 10% noise cases were considered. In total, 12 different cases were generated. The results of single damage 4S with three levels of noise pollution of 0%, 2% and 10% are shown in Figures 6.10 to 6.12. The results for all other cases are shown in Appendix B.4.

From Figures 6.10 to 6.12, the single severe damage at location 2/8 span or node 11 was clearly identified using only the first flexural mode (1-Mode) in the method. This observation also applies to the case of using the first five flexural modes (5-Mode), except there was a false positive (spurious damage location) appearing as shown in Figures 6.10(b), 6.11(b) and 6.12(b). The results show that the proposed damage detection algorithm is effective in locating damage for the single damage case with different levels of noise. However, presence of noise, imperfection of modal analysis and coarse measurement coordinates (even after the mode shapes being reconstructed) jeopardise the effectiveness and accuracy of damage localisation using the proposed damage detection method. This can be observed from false positive damage detection produced in diagrams (b) of Figures 6.10 to 6.12. This false positive damage detection is generated around node 26 or 5/8 span. This is due to the fact that the frequency of fifth mode of the RC beam is relatively high (about 750 Hz) and it is very difficult to obtain a high quality frequency response function (FRF), thus generating less accurate mode shapes. In addition, for higher modes like the fifth mode, its curvature value is high and thus making it more prone to disturbance of any error, even though, in principle, it may have higher possibility to detect a local damage well.

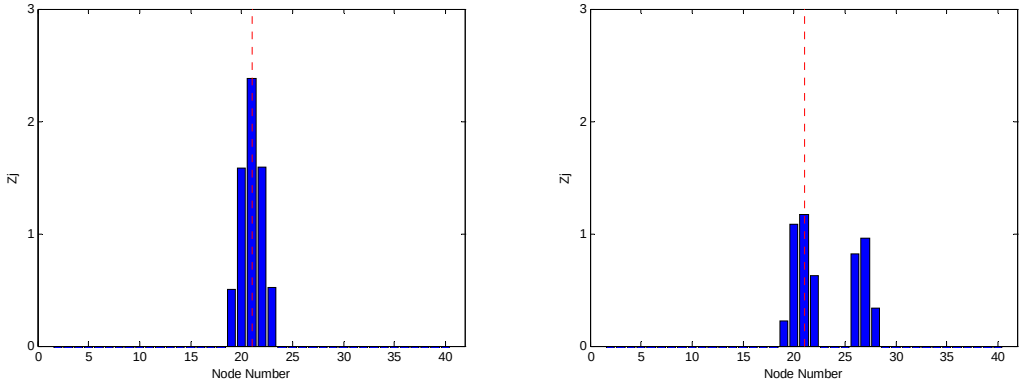

(a) 1-Mode (b) 5-Modes

Figure 6.10 Damage localisation of single damage (4S) with 0% noise

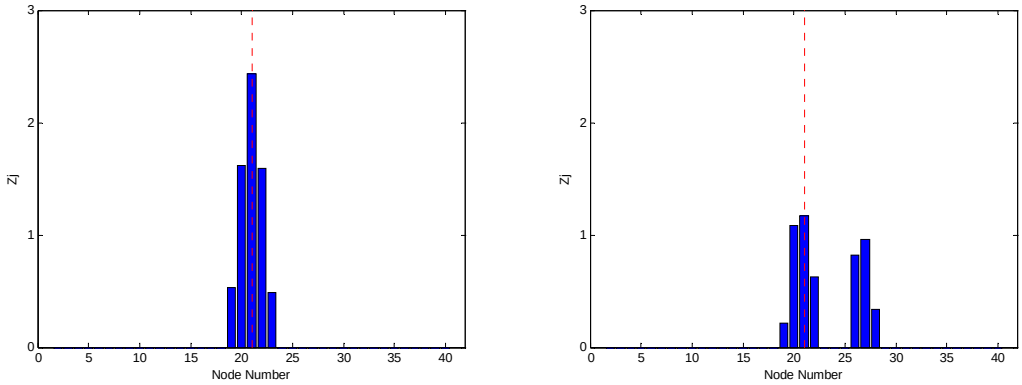

(a) 1-Mode (b) 5-Modes

Figure 6.11 Damage localisation of single damage (4S) with 2% noise

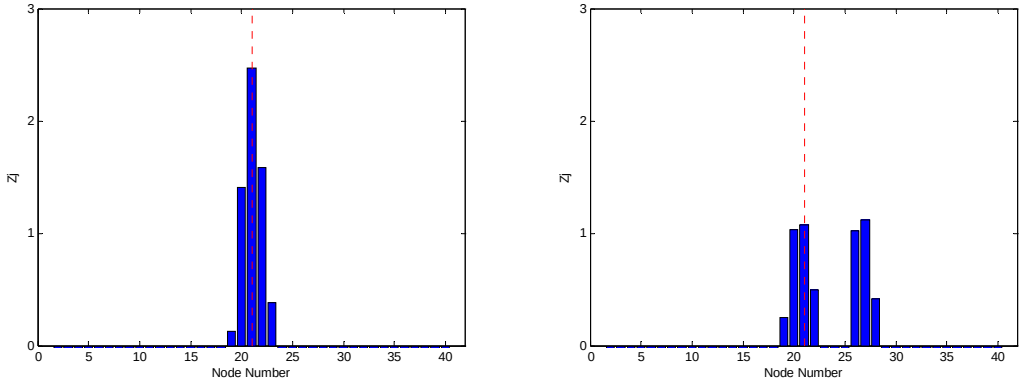

(a) 1-Mode (b) 5-Modes

Figure 6.12 Damage localisation of single damage (4S) with 10% noise

6.4 Estimation of Severity of Damage

There are four levels in damage detection as mentioned in Chapter 2. Determination of the geometric location of a damage is of Level 2, while Level 3 is quantification of severity of damage.The proposed damage detection algorithm is capable of determining the geometric location of damage efficiently in various damage cases. Since the locations of damage are already identified, the processing of estimation of severity of damage only focuses on the damaged node and nodes in the vicinity of the damage. For damage severity estimation, the proposed damage detection algorithm uses the first five flexural modes. The formulations of the proposed damage estimation algorithm used in the following discussions were presented in details in Chapter 5.

6.4.1 The Result without Noise Pollution

The proposed damage detection method is capable of estimating the severity of damage qualitatively with reasonable confidence as mentioned earlier. It is more beneficial if the quantity of damage is also provided. Hence, 11 different damage cases with different locations and severities of damage were created to investigate the effectiveness of the proposed damage detection method in estimating physical quantity of a damage. The damage cases are listed in Table 6.3. The results of estimation of damage severity are also presented in the same table.

Table 6.3 Estimation of severity of damage without noise pollution

Cases	Damage scenario	Damaged node No.	Simulated Damage Severity (Loss of 'I') (%)	Estimated Severity (Loss of 'I') (%)	Error (%)
1	2L	11	36.03	29.72	17.5
2	2M	11	58.86	58.41	0.7
3	2S	11	71.27	74.22	-4.1
4	3L	16	36.03	28.45	21.0
5	3M	16	58.86	55.34	5.9
6	3S	16	71.27	70.53	1.0
7	4L	21	36.03	26.22	27.2

8	4M	21	58.86	51.87	11.8
9	4S	21	71.27	66.66	6.4
10	2M5M	11, 26	58.86, 58.86	57.86, 44.13	1.6, 25.0
11	3S7S	16, 36	71.27,71.27	72.51, 66.34	-1.7, 6.9

In the numerical investigation presented in the following section, the damage severity estimators (α_j) are plotted against the node number of the reinforced concrete beam. The actual damage locations are indicated with vertical red dashed lines and the actual level of the severity of damage is indicated with horizontal green dash-dotted line in all figures. The results of 3M and 3S are shown in Figures 6.13 and 6.14, respectively, while the results for all other cases are shown in Appendix B.5.

From Table 6.3, it is obvious that for medium and severe single damage, the estimated severity of damage is very close to the inflicted damage with less than 10% error. For example, for the cases 2M and 3S, the difference between the simulated and the estimated severity of damage is very small, practically negligible. The estimated severity of damage for cases 2S, 3M, 4M and 4S is very close to the simulated severity of damage and the percentage differences are -4.1%, 5.9%, 11.8% and 6.4%, respectively. However, for the light damage cases (2L, 3L and 4L), the damage severity estimator quantify the severity of damage with quite a large margin of error, ranging from 15% to 30%. Similar trend is observed in the two damage cases (2M5M and 3S7S). For two damage scenarios, the medium damage has already shown errors up to 25% and is much higher than that of single cases. Nevertheless, the severe damage cases are still being predicted with less than 7% error. For light damage, the estimation of severity of damage is much less accurate than the severe damage, because light damage alters the mode shape and its derivatives to a much lesser extent compared to the severe damage case. Hence, the light damage case would have a higher noise-to-signal ratio compared to the severe damage cases.

In summary, the proposed damage severity estimator is able to quantify the severity of damage with reasonable accuracy. Significantly, the damage severity estimator is more accurate in the cases of medium damage and severe damage than in cases of light damage for pure numerical results without noise.

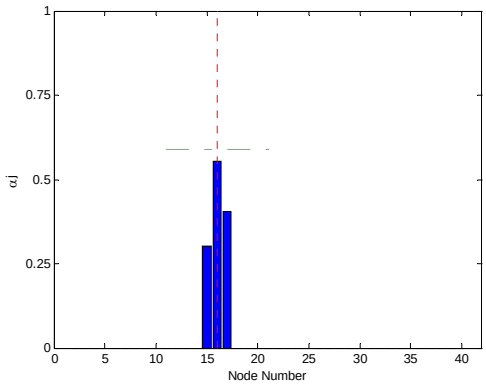

Figure 6.13 Damage severity estimation of case 3M (5-Mode)

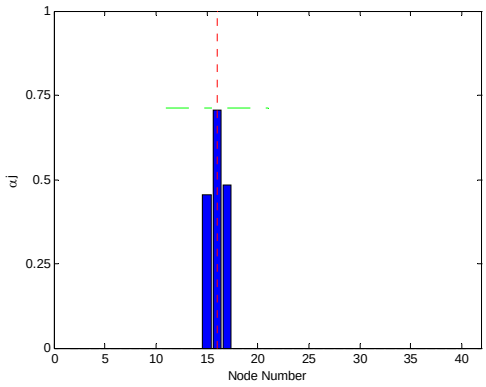

Figure 6.14 Damage severity estimation of case 3S (5-Mode)

6.4.2 The Results of Damage Severity Estimation with Noise

In order to investigate the sensitivity of the proposed damage severity estimator to noise pollution, three damaged cases (2L, 2M and 2S) were simulated with different levels of noise pollution (0%, 2% and 10%). Table 6.4 describes these nine cases and the results of the estimation of damage severity are also presented in the same table.

Table 6.4 Estimation of severity of damage with noise presence

Cases	Damage scenario	Noise Level	Simulated Damage Severity (Loss of 'I') (%)	Estimated Severity (Loss of 'I') (%)	Error (%)
1	2L	0%	36.03	19.31	46.4
2	2L	2%	36.03	20.19	43.9
3	2L	10%	36.03	16.77	53.4

4	2M	0%	58.86	43.32	26.4
5	2M	2%	58.86	43.23	26.5
6	2M	10%	58.86	44.43	24.5
7	2S	0%	71.27	57.98	18.6
8	2S	2%	71.27	58.52	17.8
9	2S	10%	71.27	55.10	22.6

Figures 6.15 to 6.17 depict the results of damage severity estimation for the case of 2S with 0%, 2% and 10% noise. The results for all other cases are shown in Appendix B.6. Referring to Tables 6.3 and 6.4, it can be seen that the damage cases of 2L, 2M and 2S showing the proposed damage severity estimation has been affected by both presence of noise and reconstruction of mode shapes. The damage severity estimator did not quantify well even for the severe damage case of 2S (with 20% error in Table 6.4) compared to the case without the presence of noise (with 4% error in Table 6.3). It is also observed that the damage estimation is less affected by noise for severe damage cases than light damage cases. This is proven in the cases of 0% noise, where the estimation of severity of 2S (18.6%) is more accurate than that of 2M (26.4%), which in turn is more accurate than 2L (46.4%). Similar pattern is noticed in the case of 2% noise and 10% noise for cases 2L, 2M and 2S. In the case of 2% noise, the damage severity of 2S (17.89%) is more accurate than that of 2M (26.55%), which in turn is more accurate than 2L (43.96%). In the case of 10% noise, the damage severity of 2S (22.69%) is more accurate than that of 2M (24.52%), which in turn is more accurate than 2L (53.46%). On the other hand, the more noise added to the original data, the less accurate the damage severity estimation becomes. This is proven by the fact that the estimation indices with 10% noise pollution are less accurate than those with 2% noise pollution.

In summary, even though the proposed damage severity estimator is able to estimate the severity of damage with reasonable accuracy in cases with no noise pollution, accuracy of severity estimation decreases when dealing with real testing conditions, such as noise presence and imperfection of modal analysis and mode shape reconstruction. However, these factors impact the severe damage less than light damage. In all cases, the presence of noise results in underestimation of damage severity.

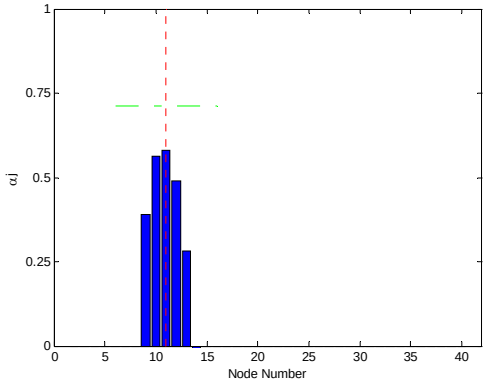

Figure 6.15 Damage severity estimation of case 2S with 0% noise

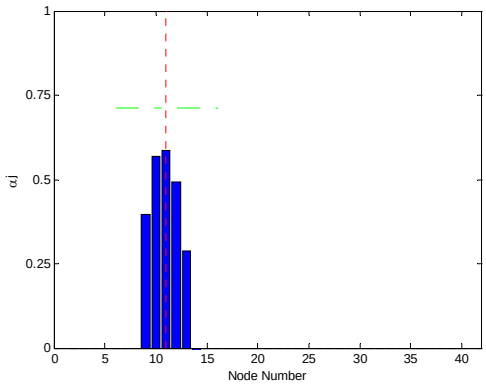

Figure 6.16 Damage severity estimation of case 2S with 2% noise

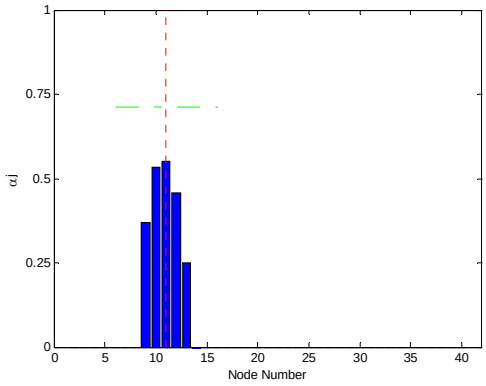

Figure 6.17 Damage severity estimation of case 2S with 10% noise

6.5 Comparison of the Proposed Method with Other Methods

To investigate the effectiveness of the new damage detection method, the results of the proposed method (abbreviated as DI-N) are compared with the results of Damage Index A (abbreviated as DI-A) and Damage Index C (abbreviated as DI-C) presented by Kim and Stubbs (2002) as detailed in Chapter 5. The reasons for choosing to work with Damage Index A and Damage Index C have been previously outlined in Chapter 5.

6.5.1 The Results with No Noise Pollution

Figures 6.18 and 6.19 enlist damage detection results for the cases of 1L4L and 3M7S, employing Damage Index A and Damage Index C, for the purpose of comparing the newly developed damage detection method (DI-N) in this study. The results for all other cases are shown in Appendix B.7. It is quite obvious from the results that both Damage Index A (Figures 6.18(a) and (d) and Figures 6.19(a) and (d)) and Damage Index C (Figures 6.18(b) and (e) and Figures 6.19(b) and (e)) produce many false-positive errors. These errors greatly reduce the reliability in damage detection results. However, in the results obtained by the newly proposed damage detection method, there are far fewer or virtually no false-positive errors present (Figures 6.18(c) and (f) and Figures 6.19(c) and (f)). It can also be observed in Figures 6.18 and 6.19 that the higher the number of modes used in the damage detection methods, the more false-positive errors are generated in the results given by both Damage Index A and Damage Index C. This is due to the fact that higher mode shapes have higher curvatures, and provide larger errors if uncertainties are present.

In summary, the damage detection algorithm proposed in this thesis is more reliable in identifying the location of damage than both Damage Index A and Damage Index C, since it generates relatively less false-positive (spurious damage location) and false-negative (actual damage location was not detected) in the cases with no noise present.

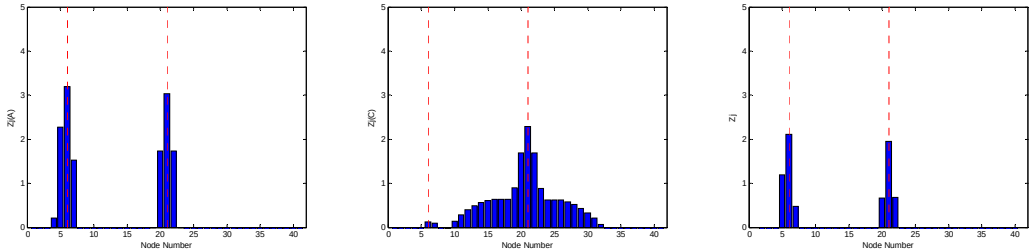

(a) DI-A (1-Mode) (b) DI-C (1-Mode) (c) DI-N(1-Mode)

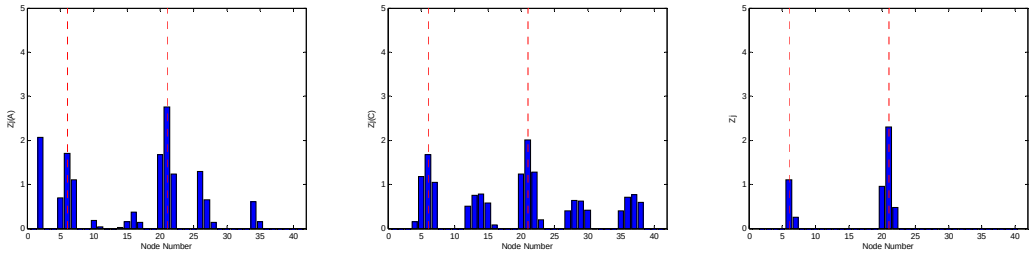

(d) DI-A (5-Modes) (e) DI-C (5-Modes) (f) DI-N (5-Modes)

Figure 6.18 Damage detection from the proposed damage detection method, Damage Index A and Damage Index C for case 1L4L without noise pollution

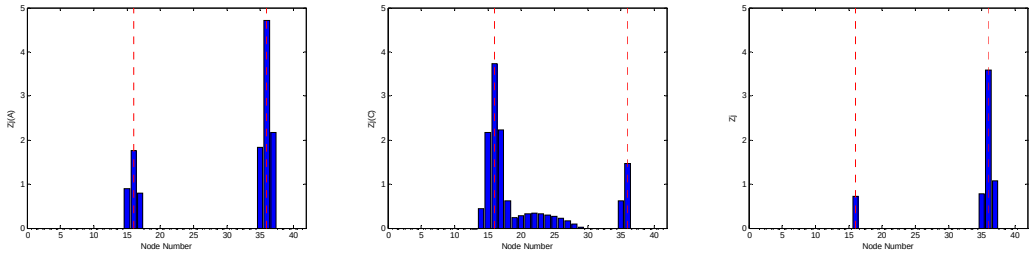

(a) DI-A (1-Mode) (b) DI-C (1-Mode) (c) DI-N(1-Mode)

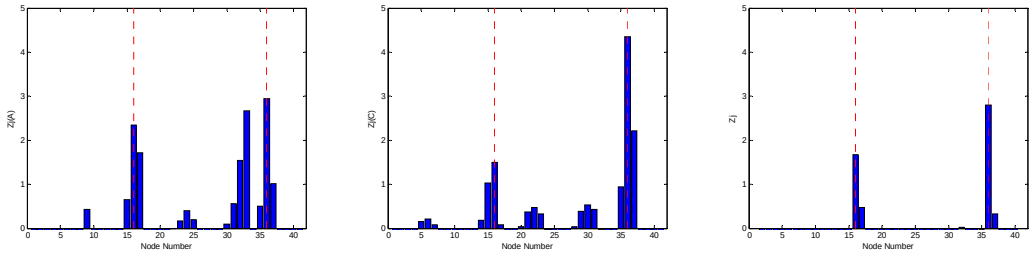

(d) DI-A (5-Modes) (e) DI-C (5-Modes) (f) DI-N (5-Modes)

Figure 6.19 Damage detection from the proposed damage detection method, Damage Index A and Damage Index C for case 3M7S without noise pollution

6.5.2 Damage Detection with Simulated Noise

For the purpose of comparison, four different cases (2L, 4M, 4S and 2M4M) have been considered, with 0%, 2% and 10% noise pollution. Figures 6.20 and 6.21 depict the results of damage detection from Damage Index A (DI-A), Damage Index C (DI-C) and the new damage detection method (DI-N) for two separate cases, i.e. 4S with 2% noise present and 2M4M with 10% noise present. The results for other cases are shown in Appendix B.8.

Once again, under the influence of noise, Damage Index A and Damage Index C produce more false-positives. It is also observed that higher mode shapes used in the damage detection produce more false-positives as shown in Figures 6.20(d) and (e), and Figures 6.21 (d) and (e). Comparing the results from Damage Index A and Damage Index C, the results obtained from the newly proposed damage detection algorithm identify the location of damage with higher accuracy and reliability as depicted in Figures 6.20(c) and (f). In all numerical cases, the proposed damage detection method identifies the location of damage more accurately and it is less noise sensitive than Damage Index A and Damage Index C methods.

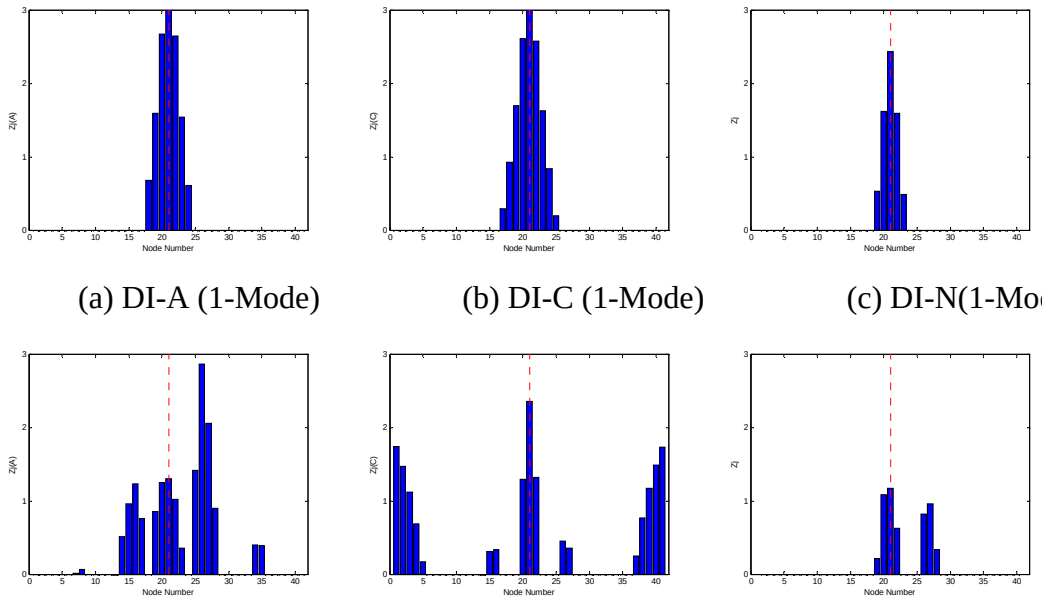

(a) DI-A (1-Mode) (b) DI-C (1-Mode) (c) DI-N(1-Mode)

(d) DI-A (5-Modes) (e) DI-C (5-Modes) (f) DI-N (5-Modes)

Figure 6.20 Damage detection from the proposed damage detection method, Damage Index A and Damage Index C for case 4S with 2% noise pollution

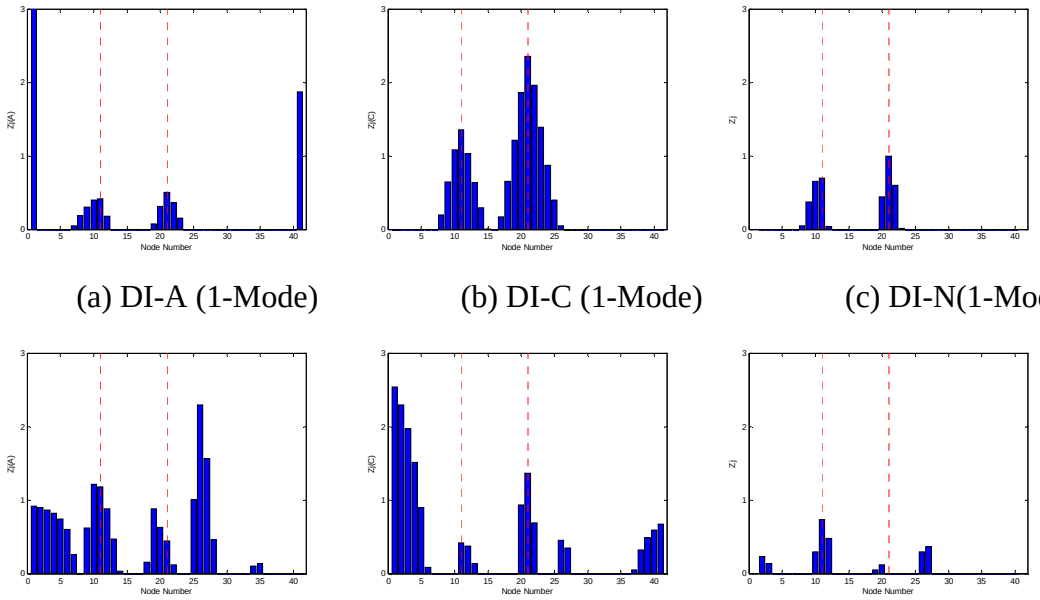

(a) DI-A (1-Mode) (b) DI-C (1-Mode) (c) DI-N(1-Mode)

(d) DI-A (5-Modes) (e) DI-C (5-Modes) (f) DI-N (5-Modes)

Figure 6.21 Damage detection from the proposed damage detection method, Damage Index A and Damage Index C for case 2M4M with 10% noise pollution

6.6 Improvement of the Proposed Method

The proposed damage detection method introduced in Chapter 5 has been successful in locating damage but some false positives have been generated when higher modes are involved, especially under the presence of noise. One of the reasons is the fact that Equation 5.30 accounts for all available mode shapes through the summation and combination of mode shape curvatures. Mode shape vectors have been normalised instead of the mode shape curvatures used for the damage index calculation. Values of mode shape curvature are dependant on the shapes of each individual mode shape. Instead of reflecting the changes in the curvature due to damage, the summation of non-normalised mode shape curvatures will distort the damage index in favour of higher modes, which results in spurious damage identifications. To solve this problem, the following algorithm is proposed in this investigation, whereby mode shape curvatures for the i^{th} mode of a given beam are normalised with respect to the maximum value of the corresponding mode (Choi et al., 2007).

After implementing these modifications, Equations 5.27 and 5.28 can be rewritten as follows:

$$\overline{MSE}_{ij} = \frac{MSE_{ij}}{E_j} = \frac{\{\phi\}_{ij}^T [K]_j \{\phi\}_{ij}}{E_j} = \{\phi\}_{ij}^T \frac{I_j}{2} (\int_{x_k}^{x_k+\Delta x_k} [\{\hat{\phi}\}_{ij}^{''}]^2 dx) \{\phi\}_{ij} \qquad \text{Equation 6.11}$$

$$\overline{MSE}_{ij}^{\ *} = \frac{MSE_{ij}^*}{E_j^*} = \frac{\{\phi^*\}_{ij}^T [K^*]_j \{\phi^*\}_{ij}}{E_j^*} = \{\phi^*\}_{ij}^T \frac{I_j^*}{2} (\int_{x_k}^{x_k+\Delta x_k} [\{\hat{\phi}^*\}_{ij}^{''}]^2 dx) \{\phi^*\}_{ij}$$

Equation 6.12

where $\{\hat{\phi}\}_{ij}^{''}$ and $\{\hat{\phi}^*\}_{ij}^{''}$ are normalised curvature vectors for undamaged and damaged states, respectively. Once again a damage location index can be obtained by using Equation 5.31 in Chapter 5.

6.6.1 The Results without Noise Pollution

To evaluate the accuracy of the improved damage detection algorithm formulated above, four different damage cases (3L, 3M, 3S and 2M5M) were employed in the numerical work to detect the location of damage. Figure 6.22 demonstrates the results of the original and improved damage detection method for case 2M5M, abbreviated as DI-NO and DI-NI, respectively. The results for other cases are shown in Appendix B.9. Referring to Figure 6.22, both methods are capable of predicting the location of damage accurately. Nevertheless, there is a slight difference between the results of the two methods. For multiple damages with similar extent of severity, the magnitudes of the two damage location indices (Z_j) of the improved method (Figure 6.22(b)) show a more equal set of indices than that of the original method (Figure 6.22(a)). An equal magnitude of Z_j means that similar probability of damage existed in that location. However, the improved method does not improve the accuracy of predicting location of damage significantly. The improved method prevails more in the experimental results in Chapter 7.

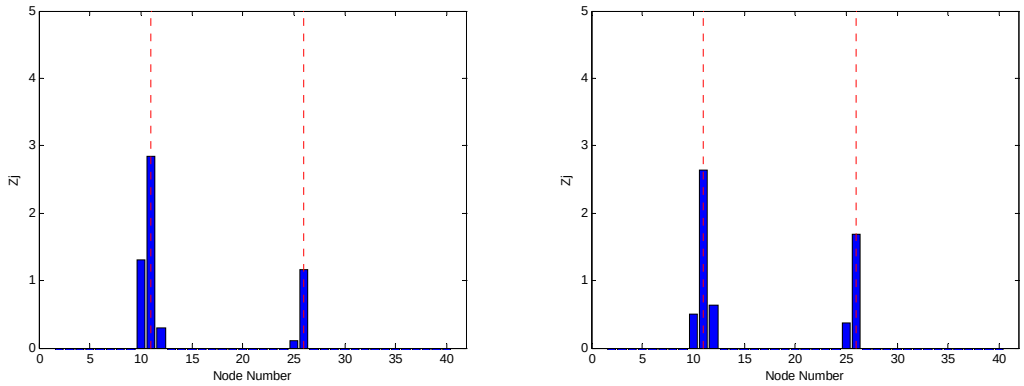

(a) DI-NO (5-Modes) (b) DI-NI (5-Modes)

Figure 6.22 Damage detection of the original and improved DI-N methods (2M5M)

6.6.2 The Damage Detection Results with Simulated Noise

Four different cases (2L, 2M, 4S and 2M4M) with different levels of noise were employed in the numerical work to demonstrate the enhanced accuracy of the improved algorithm when simulated noise has been added to time history data. Figures 6.23, 6.24 and 6.25 depict the results of the improved method for the cases of 2L under 0% noise, 4S under 2% noise and 2M4M under 10% noise. The results for all other cases are shown in Appendix B.10.

The results in the case of single damage in diagrams (b) and (a) of Figures 6.23 and 6.24 demonstrate that the results of the improved method are more accurate than those of the original method with no false positives (indicated by “red” circle) appearing. Hence, the improved method is able to detect the location of damage more reliably than the original method. Figure 6.25 illustrates the results of damage detection in the cases of multiple damage locations. Again, it can be observed that the improved method (Figure 6.25(b)) is more reliable in damage detection than the original method (Figure 6.25(a)). Most false-positives disappear in the results of the improved method. The improved method takes into account even contributions of all mode shapes used in the computation, which reduces errors from higher modes and at the same time incorporates its ability to detect damage better.

It is also worth noting that there is a false positive appearing in the case of 2L as shown in Figure 6.23(a) with 0% noise for the investigation of “With Noise Pollution”.

However, in the more damage case of 2M5M as shown in Figure 6.22(a), there was no false positive appearing for the investigation of "Without Noise Pollution". This may due to the fact that for the investigation of "Without Noise Presence", the results were from modal parameters obtained from the eigensolution which has no noise pollution. While for the "With Noise Pollution", the results were from modal parameters obtained from virtual experimental modal analysis polluted with noise, imperfection of modal analysis and error of mode shape reconstruction.

Based on the results of both single damage and multiple damage cases, it can be concluded that the improved proposed method is capable of identifying the location of damage more accurately and reliably than the originally proposed method in the presence of noise, even though the two methods produce similar results for the cases without noise pollution. The method does improve the results significantly when it is applied to the cases with noise present, which is closer to the real experimental environment.

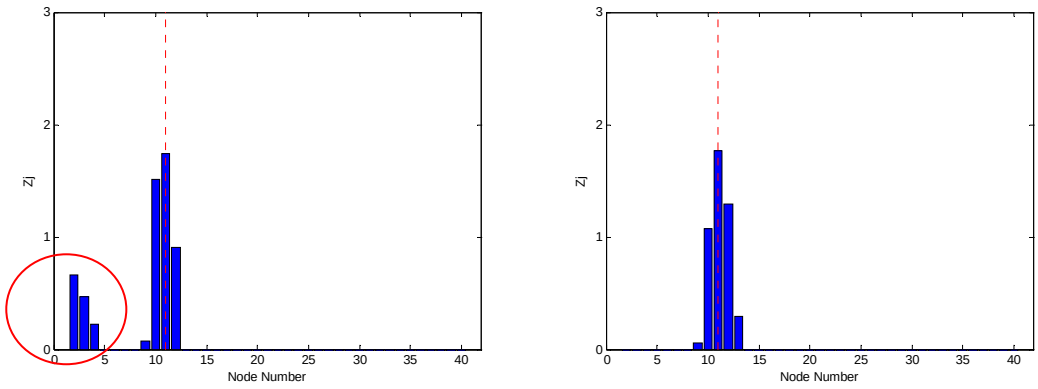

(a) DI-NO (5-Modes) (b) DI-NI (5-Modes)

Figure 6.23 Damage detection of the original and improved DI-NI methods for case 2L with 0% noise

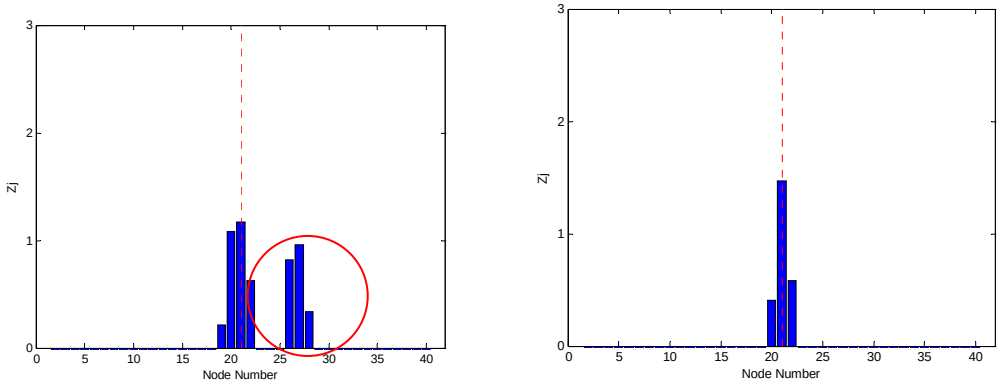

(a) DI-NO (5-Modes) (b) DI-NI (5-Modes)

Figure 6.24 Damage detection of the original and improved DI-NI methods for case 4S with 2% noise

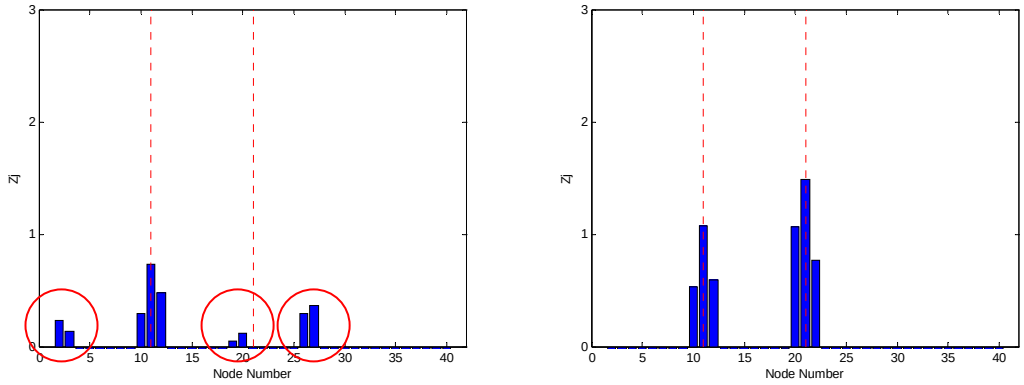

(a) DI-NO (5-Modes) (b) DI-NI (5-Modes)

Figure 6.25 Damage detection of the original and improved DI-NI methods for case 2M4M with 10% noise

6.7 Summary

In this chapter, finite element (FE) models of a reinforced concrete beam were employed to investigate, numerically, the effectiveness and the robustness of the proposed damage detection using different combination of the first five flexural mode shape data. Firstly, two approaches of obtaining modal parameters (natural frequencies and mode shapes) were introduced in the chapter. One approach of determining vibrational characteristics of a structure was to utilise Modal Analysis Function of the Structural Analysis Package in ANSYS by solving eigenproblem. The other approach obtained modal parameters by experimental modal analysis performing by the computer

including signal processing, calculation of Frequency Response Function and Modal Parameter Estimation.

Secondly, in order to investigate the effectiveness and the reliability of the proposed damage detection algorithm, a number of different damage scenarios were simulated. The results without noise present demonstrated that the proposed damage detection method was capable of identifying the location of damage. To simulate the real experimental situation, different levels of noise pollution were added to the acceleration time history data. The damage detection results under influence of noise illustrated that the proposed method was able to identify the location of damage, although it occasionally generated false positives. In terms of damage severity estimation, the proposed damage detection algorithm was able to estimate the severity of damage with reasonable accuracy in the cases without noise pollution. However, the proposed method was not able to estimate the severity of damage when noise existed as reliably as in the case without noise pollution.

Thirdly, in this chapter, comparison was also made between the proposed method and two well-established methods with and without the noise influence, and both results proved that the proposed method was more reliable and effective than the other two methods in identifying the location of damage.

Finally, an improvement to the proposed algorithm was introduced to improve its reliability and effectiveness. The improved method was used to detect damage in a number of numerical cases, both with and without noise present. The results show that the improved method did not significantly improve the accuracy of damage detection without the presence of noise, since the original results identifying the location of damage were accurate enough. However, when noise was present, the results illustrated that the method could significantly improve reliability of damage detection, i.e. false positives were reduced and location of damage could be evaluated more precisely.

CHAPTER 7

APPLICATION OF THE NEW DAMAGE DETECTION METHOD (EXPERIMENTAL STUDIES)

7.1 Introduction

This chapter reports on a full experimental investigation on the new damage detection method, and it also provides background to Experimental Modal Analysis (EMA) for reinforced concrete beams in order to acquire the modal parameters. The chapter begins with introduction of the experimental set up and modal testing procedures, followed by the output of experimental modal analysis (such as natural frequencies and mode shapes). These parameters are then used for application of the damage detection algorithm proposed in Chapter 5 to identify the location and to estimate the severity of damage. Following the system established in Chapter 6, the results of this new damage detection method are compared with two existing popular methods. Finally, comparisons are made between the results obtained from the numerical studies and those from the experimental studies.

7.2 Experimental Modal Analysis

Experimental modal analysis (EMA) is a process to determine the modal parameters of a linear and time invariant system from time history data usually measured from experimental tests such as modal testing. The procedure for experimental modal testing and modal analysis used in this research work can be described as follows:

- Experimental set up,
- Selection of equipment and sensors,
- Data acquisition by modal test, and
- Modal parameters estimation.

7.3 Experimental Set Up

The geometrical details of the reinforced concrete (RC) test beams are described in Chapter 3. It is followed by the design of a set of special supports to simulate a real pin-roller support as close as possible. Since cracks and honeycomb are two types of damage typically found in reinforced concrete structures (Zhong & Oyadiji 2007; Dilek 2007), the details of crack (notch-type) and honeycomb (area filled with material of very low stiffness) damage scenarios are considered and they are used for verifying, experimentally, the proposed damage detection method in this experimental study.

7.3.1 The Dimensions of the Test Beams

Five reinforced concrete beams were cast in the UTS Structures Laboratory. The dimensions of the beams were the same, i.e. 3660 mm (length), 300 mm (height) and 150 mm (width). The beams were reinforced with high yield steel bars: two 16mm tension bars (one layer on bottom), two 16mm compression bars (one layer on top) and 10mm mild steel stirrups at a spacing of 200mm centre-to-centre. The properties of concrete and reinforcement used in the RC beams were detailed in Chapter 3. The dimensions of the reinforced beams are depicted in Figure 7.1.

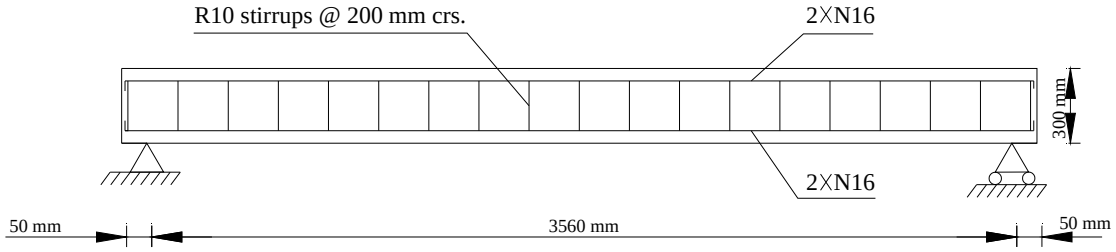

Figure 7.1 The dimensions of the reinforced concrete beams

7.3.2 A Specially Designed Support

A special support system was designed to provide the best possible boundary condition for modal testing. It is shown in Figure 7.2 and its details are illustrated in Figure 7.3. As commonly known, when flexural vibration is involved it is difficult to simulate a

perfect pin or roller condition. With this special support design, one can reduce the bouncing and separation effects at the supports during the vibration tests which can greatly reduce distortion on modal parameter estimation. Structurally, comparing the natural frequencies of the numerical and experimental results, the modal frequency results of FE model with “pin-roller” boundary condition comes closer to that from the current experimental setting. For example, the first two natural frequencies of the experimental RC beam with the specially designed support system are 34.46 Hz and 115.22 Hz, respectively. While for the FE model with “pin-roller” support, the first two natural frequencies are 36.60 Hz and 128.81 Hz, respectively. These two sets of results are fairly close with less than 12% difference. However, the first two natural frequencies for the FE model with “pin-pin” support are 59.84 Hz and 142.91 Hz, respectively. They are quite different compared with the experimental results with more than 24% difference. Since in real experimental environment there is neither a perfect “pin-roller” support, nor a perfect “pin-pin” support, therefore, it is quite reasonable to make an assumption that the specially designed support is the best presentation of a “pin-roller” boundary condition supporting of the current FE model.

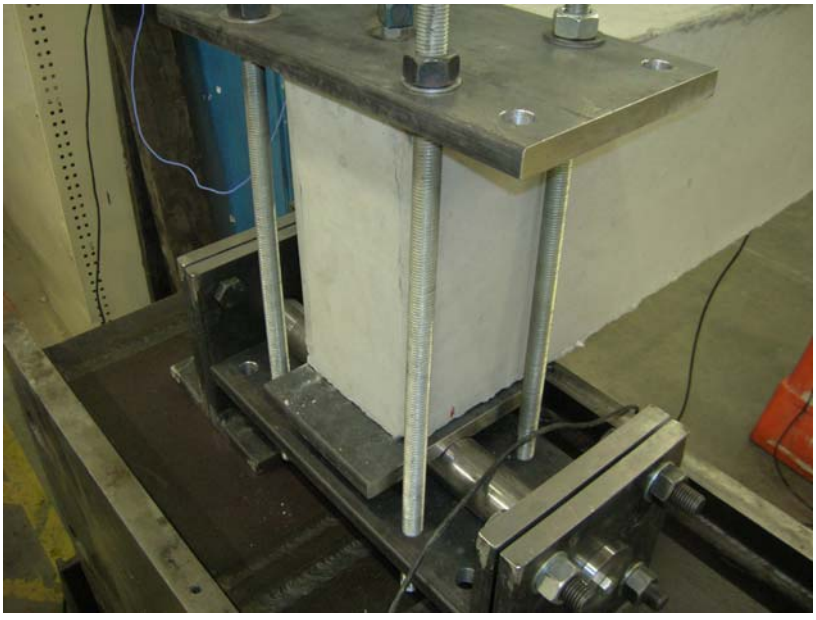

Figure 7.2 The specially designed support

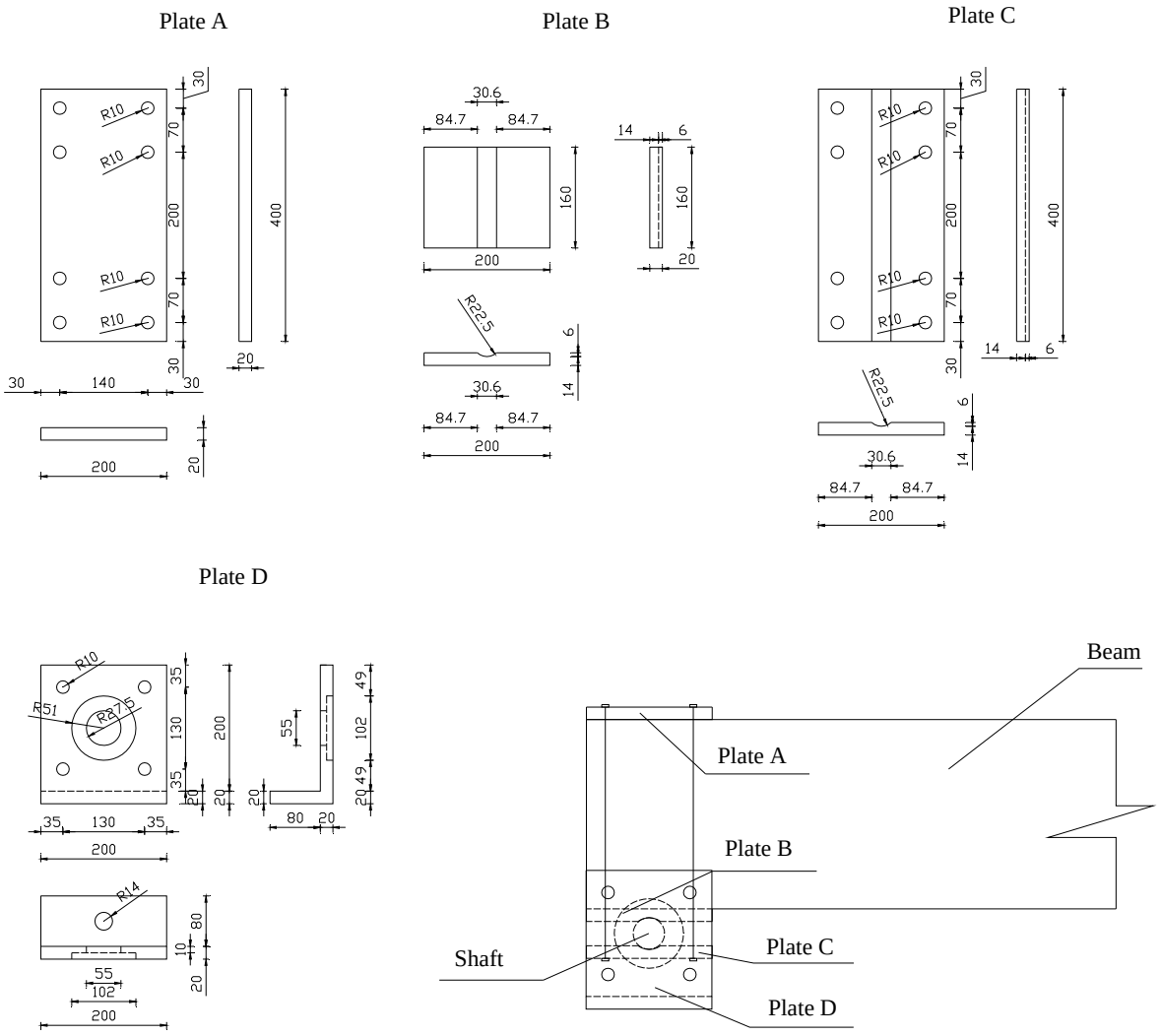

Figure 7.3 Details of the special support

7.3.3 Inflicted Damage in Test Beams

Among the five reinforced concrete beams cast, four beams were used as damaged beams, whilst the remaining one was used as a baseline (intact/undamaged) beam. The four beams were subjected to different damage scenarios, such as crack and honeycomb, as described in Table 7.1. In the experimental work, crack and honeycomb were created to investigate the robustness of the proposed damage detection method. In different scenarios of simulated damage, the severity of the inflicted damage is interpreted by loss of cross sectional moment of inertia (I). Using the convention previously proposed in Chapter 6, the locations of damage and the loss of cross sectional moment of inertia (I) are summarised in Table 7.1.

Table 7.1 Details of damage inflicted in the RC beams

Beam Number	Damage Case	Damage Scenario	Location per 8^{th} of span length	Length (mm)	Depth (mm)	Loss of I (%)
Beam 1	1	4L	4	5	50	36.03
	2	4M	4	5	100	58.86
	3	4S	4	5	150	71.27
	4	2S4S	2, 4	5	150, 150	71.27
Beam 2	5	3L	3	5	50	36.03
	6	3M	3	5	100	58.86
	7	3S	3	5	150	71.27
	8	3SBar	3	5	150	75.06
Beam 3	9	HB	6	100	80	23.18
Beam 4	10	HT	6	100	80	23.18

Regarding the crack damage, three levels of damage severity, namely light (L), medium (M) and severe (S) damage, were adopted in the experimental work. The light damage was created by a saw-cut of 5mm long and 50mm deep, while for medium and severe damage the cuts were 5 mm × 100 mm and 5 mm × 150 mm, respectively. For all three cases the cuts were made across the entire width of the beams, namely, 150 mm without cutting the reinforcing steel bars. The cracks are located at 2/8, 3/8, and 4/8 span of the beam. Typical inflicted crack damage is depicted in Figure 7.4. Regarding the damage scenario of 3SBar (Beam 2), it was only introduced in the experimental work. Simulation of the 3SBar damage starts with creating the severe damage (3S), and then one of the bottom reinforcing bars was cut half way through its cross section.

Figure 7.4 An elevation of a typical inflicted crack damage

The honeycomb damage was created by replacing a concrete area with a polystyrene hexahedron block of size 89 mm (length) × 75 mm (width) × 100 mm (height). It is located at 6/8 span of the beam. An inflicted honeycomb damage used in this study is shown in Figure 7.5. The stiffness of the block is expected to be very low compared with the concrete and it can be assumed to be zero.

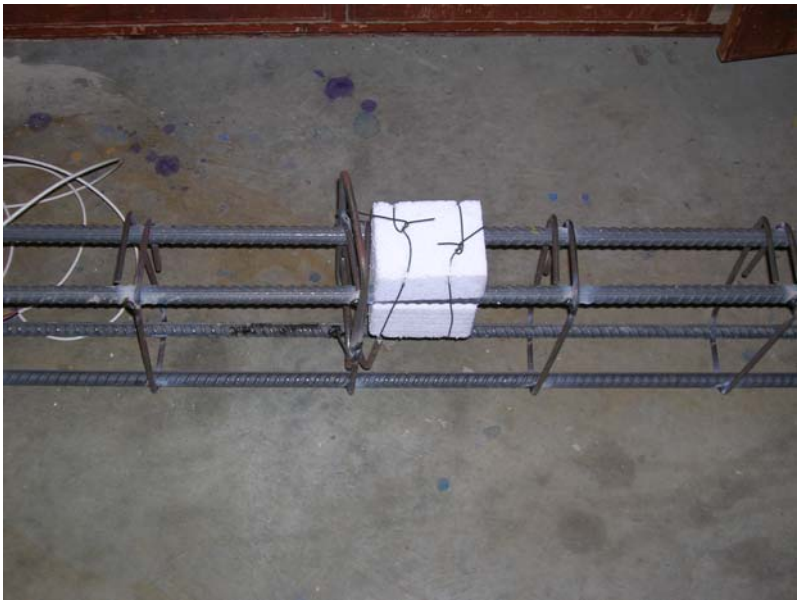

Figure 7.5 A polystyrene hexahedron block used to simulate honeycomb

7.4 Equipment and Sensors

As a preamble to modal test in Section 7.5, it is essential to introduce suitable equipment and sensors used in the dynamic test namely, modal test, to obtain modal parameters for the RC test beams.

7.4.1 Sensors

In this study, the vibration output signals of the test beams are acceleration response time histories. The signal acquisition is part of the process of experimental modal analysis (EMA). The acceleration data is acquired using a piezoelectric transducer.

The most widely used transducers for measurement of acceleration response of a structure are accelerometers and these devices operated very well over a fairly wide frequency range. In the experimental work for modal testing, a total of nine piezoelectric accelerometers were used to measure the response signals (acceleration). The two types of accelerometers used in this research are shown in Figure 7.6 (model PCB356A08 and PCB 337A26) and their sensitivity range is from 94mV/g to 100mV/g, respectively. The response signals were amplified and conditioned using a multi-channel signal conditioner (model PCB 483B03). The multi-channel signal conditioner is shown in Figure 7.7. The nine accelerometers are placed evenly on top of the RC test beams and the details can be found in Section 7.5.

Model PCB 356A08

Model PCB 337A26

Figure 7.6 Piezoelectric accelerometers

Figure 7.7 Multi-channel signal conditioner

7.4.2 Excitation Methods and Device

In order to obtain the response signals from a test structure, the structure has to be excited. In general, there are two categories of excitation methods, namely controlled excitation and ambient excitation, for modal testing. The controlled excitation method is a method that excitation forces are usually applied in a controlled manner and are measured accordingly. On the other hand, for the ambient excitation, the input excitation to a system can not be measured and only responses are measured. As a standard modal analysis procedure, the controlled excitation methods can produce a high quality frequency response function (FRF) for the subsequent modal estimation, while although the output-only modal analysis procedure is able to produce modal parameters from the ambient vibration, the quality of the estimated modal parameters is compromised (Yousaf, 2007). Hence, most research on vibration based damage detection use the controlled excitation method. In this thesis, one of the controlled excitation methods, namely impulse method imparted by a modal hammer, is adopted to excite the test structure, as shown in Figure 7.8. More details on the techniques used in the controlled excitation methods to impart and measure excitation force can be found in Sohn et al. (2002).

Figure 7.8 A large 12 lb modal hammer

7.5 Modal Test

A schematic drawing of the modal test set up and the arrangement of instruments are shown in Figure 7.9. In the modal test, a modal hammer (Figure 7.8) was employed to excite the test beams at a reference point (at Number 3 as illustrated in Figure 7.9). The reference point was set at 3/8 span of the beams in order to excite as many modes simultaneously as possible. The input force, generated by the hammer, was measured by means of a force transducer in the hammer, and was then amplified and conditioned by a signal conditioner. The response signals of the vibrating beams were captured by the nine piezoelectric accelerometers. There were two different types of piezoelectric accelerometers used in the modal test to measure the acceleration response of the vibrating beams as shown in Figure 7.6. After the acceleration response signals were captured, they were amplified and conditioned in a multi-channel signal conditioner (model PCB 480E06), as shown in Figure 7.7. Nine measuring points were set on the top of the tested beams as depicted in Figure 7.9. Nine measuring locations were selected optimally to reconstruct the first five flexural mode shapes with the required accuracy using interpolation techniques. One of the accelerometers provided the driving point measurement at Number 3 as shown in Figure 7.9 for the mode shapes to be mass normalised. Each accelerometer was attached onto a small piece of steel plate, and glued to the top of the concrete beam to provide firm and solid contact between

accelerometers and the specimens. The dimensions of the small square steel plate were 40 mm × 40 mm × 1 mm. The distance between the accelerometers was 445 mm, as depicted in Figure 7.9. The signal processing techniques used are quite common and details can be found in many literatures (Maia & Silva 1997).

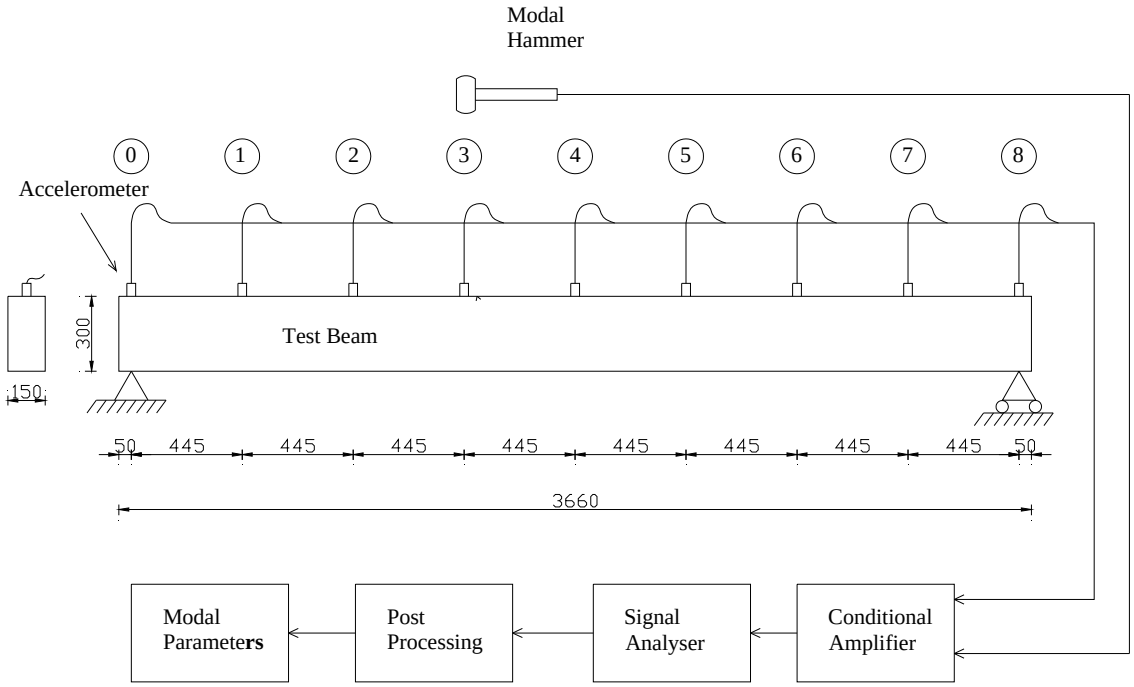

Figure 7.9 Schematic diagram of modal test

After the input (impact force) and output (acceleration) data are acquired, these data went through a post-processing process. In the post-processing, the time domain data can be converted into frequency domain data using the fast Fourier transform (FFT) technique. Subsequently, the frequency data can be used to obtain the frequency response functions (FRFs) of the test beam using transfer function techniques. More details on frequency response function can be found in Craig & Kurdila (2006).

With frequency response function (FRF) being computed, modal parameter estimation technique was then performed to estimate the modal parameters. The modal parameter estimation is often referred to as curve fitting usually carried out using commercial softwares.

7.6 Modal Parameter Estimation

Modal parameter estimation is a key step in Experimental Modal Analysis (EMA). This technique is also known as a complex curve-fitting technique. Numerous modal parameter estimation methods have been developed and many different approaches have been published based on modal parameter estimation (Avitabile 2006). Modal parameter estimation determines the three modal parameters, i.e. natural frequency, damping ratio and mode shape, from the experimental time history of a test structure data. The obtained modal parameters form modal model describing the dynamic behaviour of the structure.

7.6.1 Types of Modal Parameter Estimation

The purpose of modal parameter estimation is to identify dynamic properties of a structure from the measured time history data based on complex curve-fitting techniques. There are three main categories of modal estimation/identification methods, namely, time domain, frequency domain and tuned-sinusoidal methods as shown in Figure 7.10.

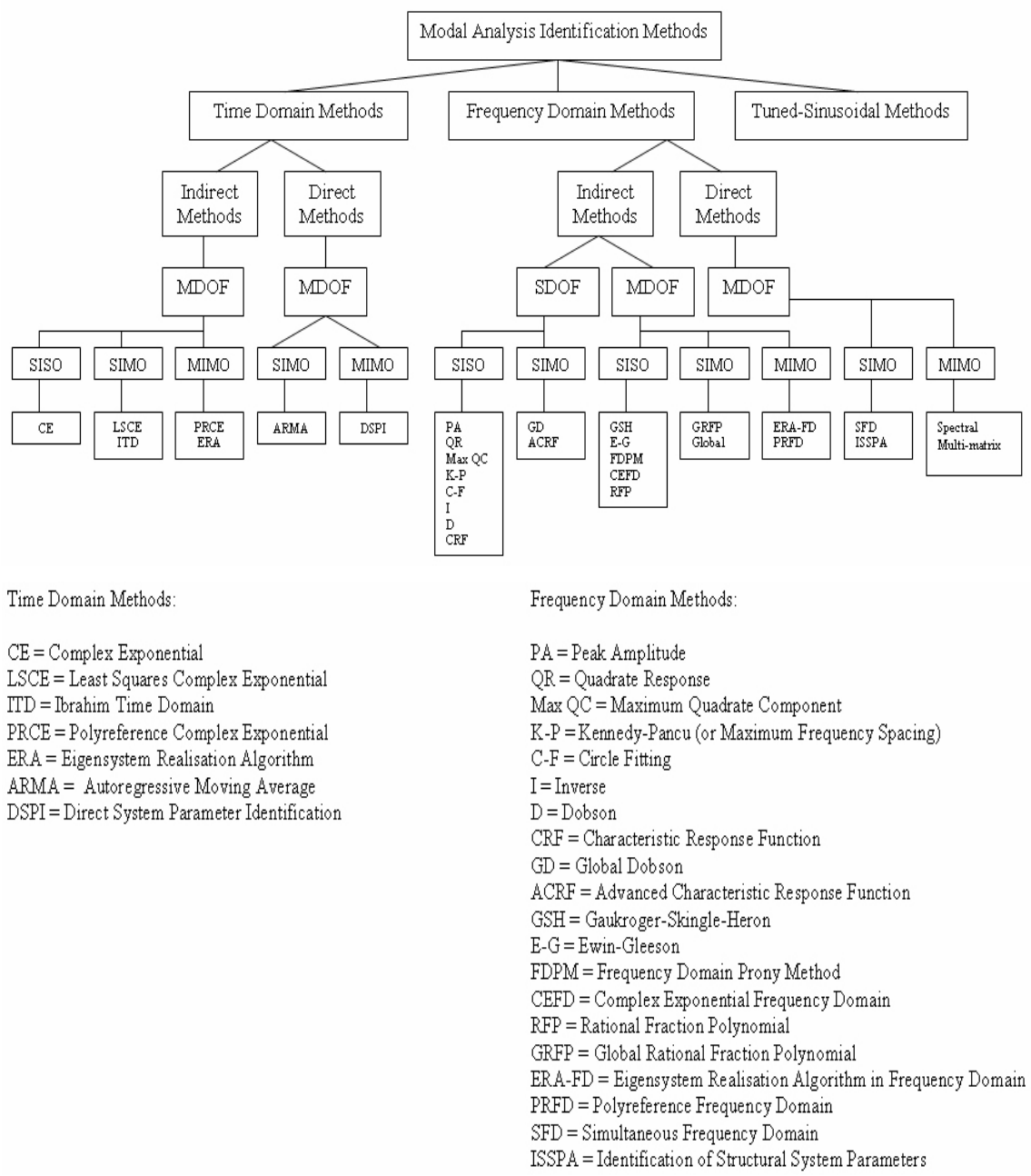

Figure 7.10 Classification of modal estimation methods (Maia &Silva 1997)

Time domain methods use the time response data directly for estimation of modal parameters, while frequency domain methods mainly rely on measured frequency response function (FRF) data obtained from post processing time response data. The time domain methods tend to provide the best results when a large frequency range or large number of modes exists in the data. For frequency domain methods, they tend to provide the best results when the frequency range of interest is limited and the number of modes is relatively small. Frequency domain methods are also capable of taking into

account the effects of modes outside the frequency band of analysis that can improve the analysis results.

Tuned-sinusoidal methods (Cunha & Caetane 2006) are a special class of modal identification methods in general. They are essentially based upon the experimental 'isolation' or tuning of real modes of vibration, by means of the excitation of the structure at each natural frequency by a set of exciters appropriately distributed in space and time. This category of methods can not be considered as genuine identification methods. Nevertheless, these methods constitute one of the oldest approaches to the study of the dynamic properties of structures and are still used nowadays in the aeronautical industry (Maia &Silva 1997).

Both time domain and frequency domain methods can be subdivided into two categories namely, indirect and direct methods. The indirect method means that the identification of the modal parameters is based on a modal model, while the direct method is directly based on the spatial model.

Indirect and direct methods can be further subdivided into single degree of freedom (SDOF) and multiple degree of freedom (MDOF) methods. Time domain analysis is available only for MDOF for both indirect and direct methods. While, in the frequency domain, the SDOF and MDOF are applicable to indirect methods but direct methods only apply to MDOF analysis. In real applications, a system is usually MDOF, thus the most common methods employ multiple mode analytical models (see Figure 7.11). However, in some circumstances, the FRF of a MDOF system can be separated into many SDOF systems for the analysis when the modes are relatively isolated from each other. For these circumstances, the single mode methods will produce reasonably good results for most engineering analyses.

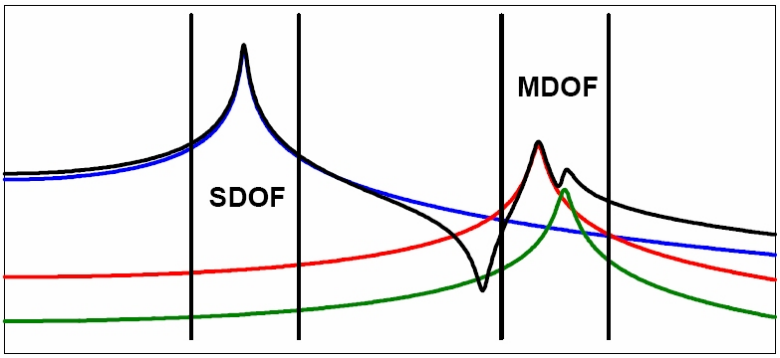

Figure 7.11 Curve fitting different bands using different methods (Avitabile 2001)

The identification methods that only use FRF data from one excitation and one output are called single FRF or single-input-single-output (SISO) methods. Similarly, single-input-multi-output (SIMO) methods permit several FRFs to be analysed simultaneously, with responses taken at various points on the structure using just one excitation point. Finally, there are methods that can process all available FRFs simultaneously, from various excitation and response locations. These methods are called polyreference or multi-input-multi-output (MIMO) methods.

7.6.2 Modal Analysis

Modal analysis is a subsequent step after modal tests to estimate modal parameters from the measured data such as FRFs spectrum. The modal parameter estimation is often referred to as curve-fitting. This is implemented using computer software that utilises mathematical algorithms to estimate the modal characteristics from the measured data. The basic parameters extracted are frequency, damping and mode shape. To enable curve-fitting, the measured FRFs are usually broken into many single degree of freedom (DOF) systems. There are varieties of curve-fitting techniques, i.e. some techniques employ time domain data while others use frequency domain data. In this experimental modal analysis, the Frequency Direct Parameter Identification (FDPI) technique was employed to estimate the natural frequencies, damping values and mode shapes of several modes simultaneously (LMS International 1992). This technique operates directly on frequency domain data. Hence, it is capable of taking into account the effects of modes outside the frequency band of analysis, which improves the analysis results. The basis of FDPI method is the second order differential equation for mechanical structures. When transformed into frequency domain, the differential equation can be

reformulated in terms of measured FRFs. The measurement data can be described by a second order linear model with constant matrix coefficients. From the identified matrices, the system's pole and mode shapes can be estimated through an eigenvalue and eigenvector decomposition of the system matrix. The details can be found in LMS CADA-X Modal Analysis manual (LMS International 1992).

After modal parameter estimation, the first five flexural vibration modes were captured at the natural frequency ranging from 10 Hz to 1,000 Hz. The measured nine-point (9-node) mode shapes were then reconstructed into forty-one-point (9-to-41-node) mode shapes, using cubic spline interpolation technique. The mode shape with finer coordinates can identify the location of damage much more accurately than the mode shape with coarse coordinates (Choi et al., 2006). In this thesis, the reconstructed mode shapes were used by the proposed damage detection algorithm to identify the, and to estimate the severity of damage.

7.7 Results and Discussion of the Experimental Work

7.7.1 Natural Frequency

In this research, as outlined above, five reinforced concrete beams were cast in the laboratory, four of which were used to carry out various damage scenarios. It is important to mention that for each damaged beam, a set of intact or undamaged modal data was collected before inflicting the damage. This intact/undamaged modal data is used for comparison with the corresponding damaged modal data in the following discussions.

Table 7.2 shows the results of natural frequency of Beam 1 at different modes under different damage scenarios. Table 7.3 depicts the percentage of shifts in natural frequency of Beam 1, whereby the percentage of reduction in natural frequency is defined as the percentage of difference between natural frequencies of the intact and damaged data. As can be seen from Table 7.2, the frequencies of the damaged beams decrease after damage occurs. However, despite overall trend of frequency decrease after damage, the frequency drop does not correlate well with the inflicted severity of

damage. This may be due to the fact that frequency can easily be influenced by noise and environmental factors. Figure 7.12 illustrates the percentage of drops in the first five natural frequencies of damage cases 4L, 4M and 4S. It is observed that the percentage of drop in frequency for all modes non-linearly changes as the inflicted damage becomes more severe but there is no clear evidence that frequency change can be clearly correlated to damage severity.

Table 7.2 Comparison of natural frequencies of Beam 1

Damage cases	Natural frequencies (Hz)				
	Mode 1	Mode 2	Mode 3	Mode 4	Mode 5
Undamaged	30.34	107.19	300.67	479.49	760.74
4L	26.39	95.30	273.96	442.86	580.26
4M	26.31	94.48	272.98	425.65	576.97
4S	26.25	94.26	266.55	394.44	570.73
2S4S	25.75	92.12	260.77	392.82	567.93

Table 7.3 Comparison of percentage of drop in frequency of Beam 1

Damage	Percentage of drop in natural frequency (%)				
cases	Mode 1	Mode 2	Mode 3	Mode 4	Mode 5
4L	13.02	11.09	8.88	7.64	23.72
4M	13.28	11.86	9.21	11.23	24.16
4S	13.48	12.06	11.35	17.74	24.98
2S4S	15.13	14.06	13.27	18.08	25.35

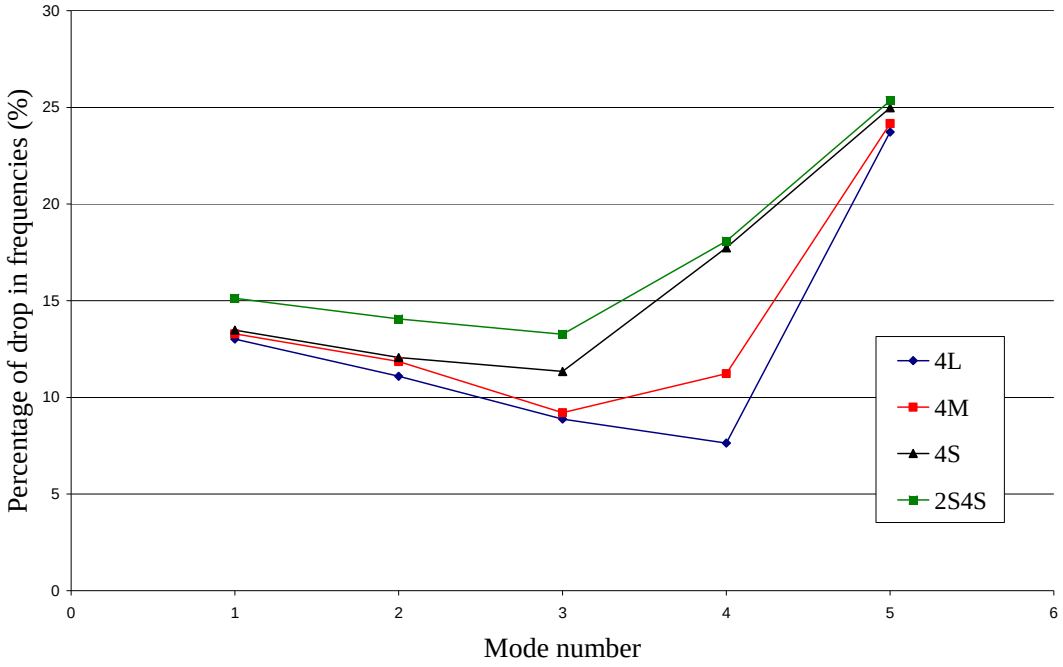

Figure 7.12 Percentage of drops of first five natural frequencies of Beam 1

The results from Beam 2, Beam 3 and Beam 4 follow the same pattern as that established in Beam 1, and the corresponding results are listed in Tables 7.4, 7.6 and 7.8, and Tables 7.5, 7.7 and 7.9, for shifts in frequency and their percentage, respectively. In general, the frequencies of damaged beams decrease with the increase of severity of damage. However, the magnitudes of frequency drop for every mode are different without an obvious trend.

In summary, the drop in natural frequencies corresponds to the severity of inflicted damage. It can be used as one good indicator to identify the existence of damage but not for assessing the extent of damage in reinforced concrete beams.

Table 7.4 Comparison of natural frequencies of Beam 2

Damage cases	Natural frequencies (Hz)				
	Mode 1	Mode 2	Mode 3	Mode 4	Mode 5
Undamaged	34.31	114.99	342.33	525.34	809.27
3L	32.87	113.14	331.59	521.35	801.05
3M	31.51	112.14	324.26	494.37	799.24
3S	30.68	109.68	315.93	489.62	789.79
3SBar	30.16	109.25	303.41	458.89	726.99

Table 7.5 Comparison of percentage of drop in frequency of Beam 2

Damage	Percentage of drop in natural frequency (%)				
cases	Mode 1	Mode 2	Mode 3	Mode 4	Mode 5
3L	4.20	1.61	3.14	0.76	1.02
3M	8.16	2.48	5.28	5.90	1.24
3S	10.58	4.62	7.71	6.80	2.41
3SBar	12.10	4.99	11.37	12.65	10.17

Table 7.6 Comparison of natural frequencies of Beam3

Damage	Natural frequencies (Hz)				
cases	Mode 1	Mode 2	Mode 3	Mode 4	Mode 5
Undamaged	34.46	115.22	337.45	525.34	743.66
HB	31.63	106.21	314.80	485.11	742.63

Table 7.7 Comparison of percentage of drop in frequency of Beam 3

Damage cases	Percentage of drop in natural frequency (%)				
	Mode 1	Mode 2	Mode 3	Mode 4	Mode 5
HB	8.21	7.82	6.71	7.66	0.14

Table 7.8 Comparison of natural frequencies of Beam 4

Damage	Natural frequencies (Hz)				
cases	Mode 1	Mode 2	Mode 3	Mode 4	Mode 5
Undamaged	34.46	115.22	337.45	525.34	743.66
HT	27.65	101.86	276.29	460.87	595.62

Table 7.9 Comparison of percentage of drop in frequency of Beam 4

Damage cases	Percentage of drop in natural frequency (%)				
	Mode 1	Mode 2	Mode 3	Mode 4	Mode 5
HT	19.76	11.60	18.12	12.27	19.91

.

7.7.2 Damage Localisation

In order to locate damage, a large number of measurement points are desirable. However, considering practicality in real applications, the number of measurement points (i.e. the number of sensors) is always limited. Due to limited number of sensors used in the test, the coarse mode shape and its derivatives used in the damage detection may not generate accurate results (Choi et al, 2007). In order to obtain better results, cubic spline interpolation technique was used for the reconstruction of finer mode shapes, expanding the initial 9 point (9-node) mode shapes to the reconstructed 41 points (9-to-41-node) mode shapes. For further details of mode shape reconstruction techniques refer to Peterson et al. (2003), Peterson et al. (2001a, 2001b), Stubbs & Parks (1996).

In the experimental studies, the improved version of the newly proposed damage detection method employed the first five flexural modes for damage detection. The improved damage detection method (DI-NI) was adopted because it can produce better damage detection results as concluded in the numerical work (Chapter 6). All mode shapes considered in the experimental work have been mass normalised. In addition to the mass normalised mode shapes, mode shape curvatures are also normalised with respect to the maximum mode shape curvature value of each corresponding mode. In the following figures, the damage location index (Z_j) is plotted against the reconstructed node number of the reinforced concrete beam. In principle, when the damage location index value (Z_j) is larger than zero there is a possibility that damage occurs at that location. The actual damage locations are indicated with vertical red dashed lines in all figures for reinforced concrete beams.

Figures 7.13 and 7.14 illustrate the results of the damage cases of 4S and 2S4S using the proposed damage detection method for Beam 1. The results of the other two cases (4L and 4M) are shown in Appendix C.1. It is observed that the method is capable of locating the damage, both in single damage (4S) and in multiple damage (2S4S) cases. However, in the case of single damage, the damage index has generated misleading representation of the probability of existence of damage (false positive damage) when higher modes are used in the method. There are some reasons why false positives were generated. First of all, for node point of a mode shape where the displacement is

approaching zero, the equation in the proposed damage detection method most probably generates singularity at that position. Therefore, false positive damage may happen. For example, in Figure 7.13 (c) of case 4S, the nodal point of third mode shape is located nearby node 16 where the false positive happens. Secondly, during the dynamic test, the accelerometers were attached to a small piece of steel plate, which was in turn glued on the top of the reinforced concrete beam. There is a possibility that the acceleration response data acquired was actually from the steel plate and not from the test beam. This would affect the reconstruction of the mode shapes, and subsequently jeopardise the results of damage detection. Lastly, the inconsistency of materials in the reinforced concrete beam and the noise in the laboratory may be the reasons that false positives were generated.

For case 2S4S with multiple damage locations as depicted in Figures 7.14 (a) and (b) for the first mode and up to combination of two modes, respectively the method is able to detect all locations of severe damage accurately at nodes 11 and 21. However, for combinations of mode shapes up to the 3^{rd}, 4^{th} and 5^{th} modes as shown in Figures 14 (c), (d) and (e), respectively, the method is able to identify the two locations of damage but it was not distinct for the damage at node 11 with the peak shifted slightly to the right. Nevertheless, it is still possible to conclude that the method is capable of locating single and multiple damage well. It also tallies with the findings of the numerical work that using just Mode 1 (abbreviated as 1-Mode) and combination of modes up to 5^{th} mode (abbreviated as 5-Modes) in the method would detect location of damage well. Hence, only the results of 1-Mode (Mode 1) and 5-Modes (Modes 1+2+3+4+5) are presented in the following discussions.

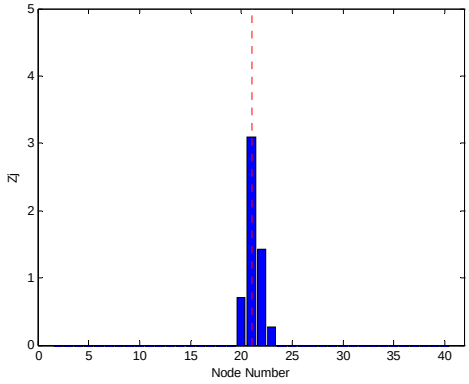

(a) Mode 1 (1-Mode)

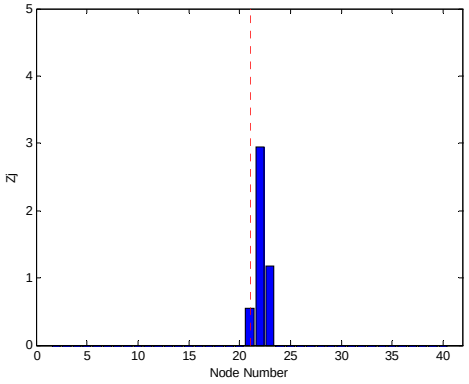

(b) Modes 1+2

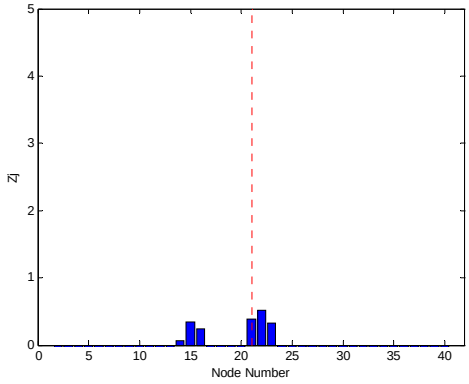

(c) Modes 1+2+3

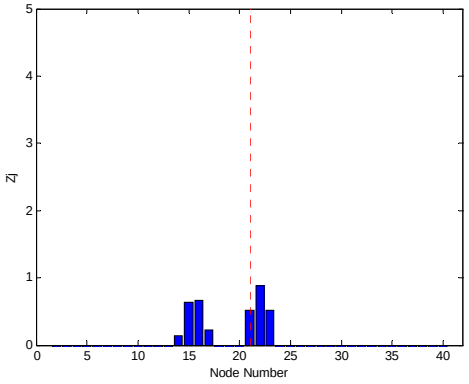

(d) Modes 1+2+3+4

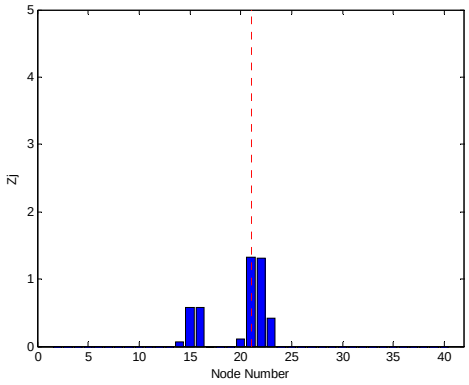

(e) Modes 1+2+3+4+5 (5-Modes)

Figure 7.13 Damage localisation for single damage case 4S

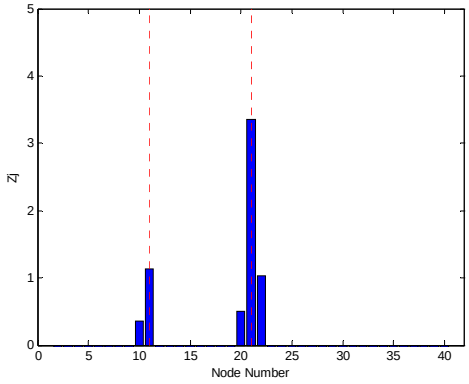

(a) Mode 1 (1-Mode)

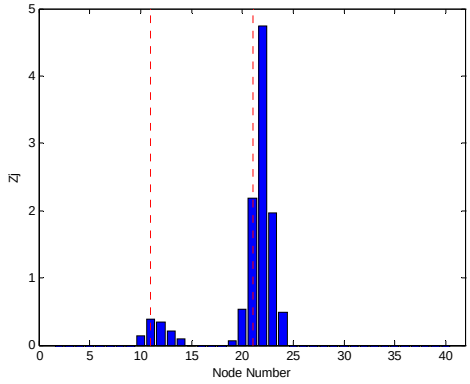

(b) Modes 1+2

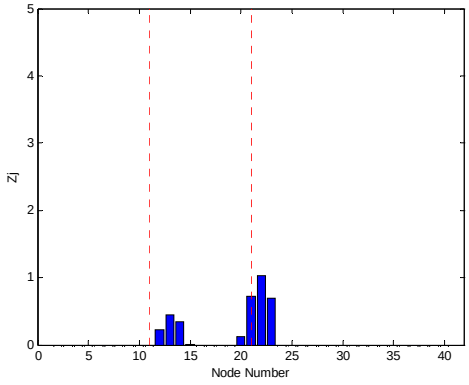

(c) Modes 1+2+3

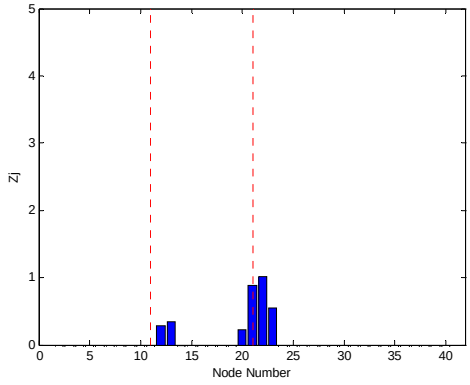

(d) Modes 1+2+3+4

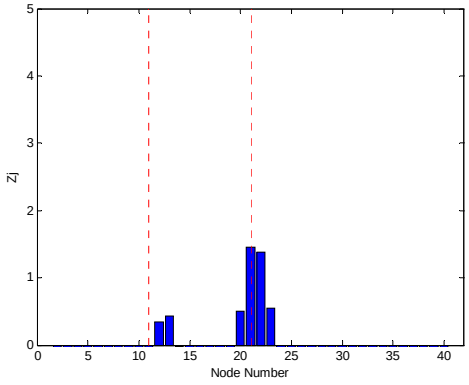

(e) Modes 1+2+3+4+5 (5-Modes)

Figure 7.14 Damage localisation for two damage case 2S4S

The second beam (Beam 2) has four different scenarios of inflicted damage (3L, 3M, 3S and 3SBar). Figure 7.15 depicts the results of the improved version of the proposed damage detection method (DI-NI) using the damage case of 3Sbar. The results of the other cases are shown in Appendix C.1. It is again seen that the method is able to locate the damage. However, false positive appears near one of the supports. As mentioned

earlier, the false positive may be due to imperfections in the boundary conditions. In the experiment, the support system will never be an ideal pin-roller boundary condition as compared with the numerical ones. Instead of having zero displacement at the support, which occurs in the numerical simulation, the experimental support system is subjected to very small displacement under vibration. The magnitude of the displacement is close to the level of measured noise. Therefore, the measured modal displacement at the supports is strongly affected by measurement noise. Hence, the results of damage detection are affected by the noise polluted data. In practice, it is more important to have detected the damage, even though there may have been some spurious damage location, rather than not detecting the damage. This would help to reduce the risk of a catastrophic failure.

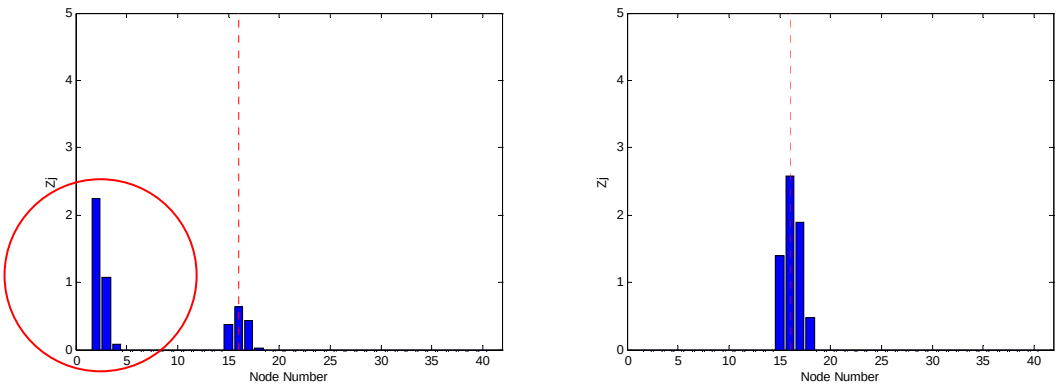

(a) 1-Mode (b) 5-Modes

Figure 7.15 Damage localisation for steel bar damage case 3SBar

The damage simulated in the third (Beam 3) and fourth beam (Beam 4) is honeycomb type of damage, which is located at the soffit and top of the beam, respectively, at 2.72 m from the left side of the beam namely, node 31. The results of damage detection for Beam 3 are presented in Figure 7.16, and the results of Beam 4 are shown in Appendix C.1. Referring to Figure 7.16, the damage detection method identifies the location of damage very accurately and reliably, without any false positives.

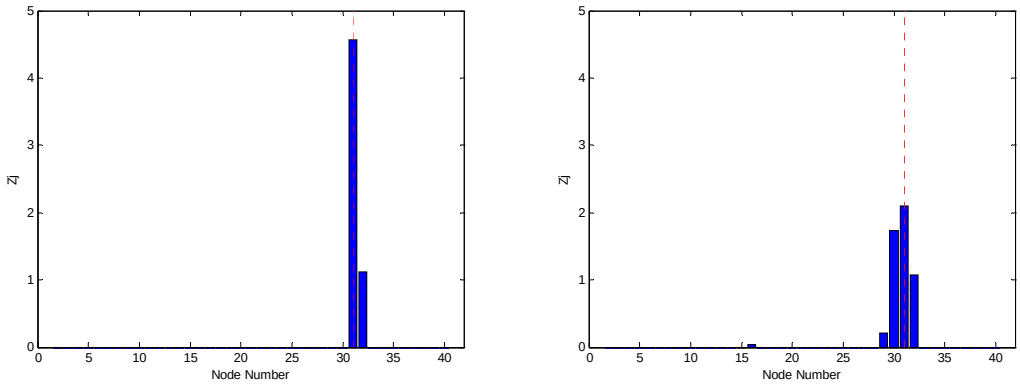

(a) 1-Mode (b) 5-Modes

Figure 7.16 Damage localisation for honeycomb damage case HB

In summary, the improved version of the proposed damage detection method shows promising capability of identifying the location of damage, especially for honeycomb type of damage. However, due to uncertainties associated with measurement and processing errors, false positive or spurious damage location might be generated during performance of damage detection. They are explained as follows:

1. As discussed above, in the experimental work, a specially designed support system was used to simulate a better boundary condition that was very close to a pin-roller boundary condition of the FE model. However, the support system could never generate an ideal pin-roller boundary condition. Instead of having zero displacement, as occurs in the numerical simulation, the 'real' supports are subjected to very small modal displacement under vibration, at which the magnitude of displacement is close to the level of measurement noise. Such small measured modal displacement at the supports is strongly affected by measurement noise. For any modal testing, in the case of both intact/undamaged and damaged beams, the modal displacements obtained at the supports were mostly influenced by noise, rather than by the actual vibrations. The noise-polluted mode shape data at the supports was then employed in the reconstruction of the mode shape from coarse coordinates to a finer coordinates. This rendered distorted reconstructed results as compared to the ideal mode shape results. On the other hand, the principle behind the proposed damage detection method identifies damage by utilising the difference of mode shapes and mode shape curvatures (second derivative of mode shape) between the

undamaged and damaged cases. Therefore, the false positive at locations near the supports was identified as damage only because of the difference in magnitude of modal displacement for the undamaged and damaged cases due to noise. This accounts for the fact that some false positives were produced around the location of supports, and also for the phenomenon that the magnitudes of these false positives are sometimes larger than the magnitudes of real damage. However, even though some false positives were generated in the process of damage detection, the experimental results can still identify the location of inflicted damage.

2. During the modal test, some of the accelerations obtained may have contributions from the local vibration of the mounting steel plates rather than the test beam. This may attribute to generating false positives.

3. In the modal test, nine accelerometers were used to obtain the acceleration data of the reinforced concrete beams. After modal analysis, the measured nine-point (9-node) mode shapes were then reconstructed into forty-one point (9-to-41-node) mode shapes, using cubic spline interpolation technique. The reconstructed mode shapes were used in the proposed damage detection method to identify the location of damage, and to estimate its severity. However, the reconstructed mode shapes were not real mode shapes and there are always some differences between the real ones and reconstructed ones. Even though the difference between the real mode shapes and reconstructed mode shapes were small, the difference between the mode shape curvatures and modal strain energy were not ignorable after derivation. All these contributed to generating false positives.

7.7.3 The results in Comparison with Two Other Methods

To evaluate the accuracy of the damage detection method proposed in the research, the experimental results of the improved version of the new damage detection method (DI-NI) are compared with the results of two existing popular methods namely, Damage Index A (DI-A) and Damage Index C (DI-C). Similar comparison was also done,

numerically, in Chapter 6. The reason that Damage Index A and Damage Index C were selected has been addressed in Chapter 5.

Figures 7.17 and 7.18 present damage detection results employing Damage Index A method, Damage Index C method and the improved method proposed in this thesis, using the same data generated from EMA on the RC beams. The results for all other cases are shown in Appendix C.2. The results show that both selected methods produce many false positives and some false negatives. False positive is the incorrect prediction of locations that are not damaged, and false negative is that true damage locations are not identified. They both affect the reliability and robustness of a damage detection method. However, false negative is more serious than false positive, because it is dangerous to ignore damage if it is there in a structure. All these errors seriously undermine the reliability of damage detection results. In contrast, the results given by the newly improved damage detection method provide no false negatives at all and remarkably reduced number of false-positives.

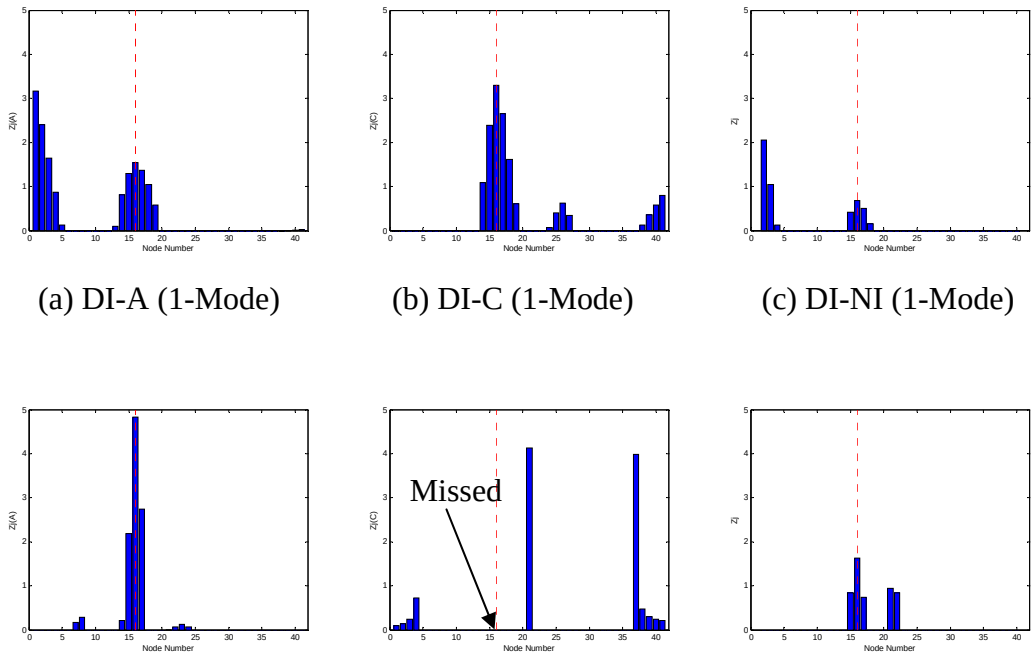

(a) DI-A (1-Mode) (b) DI-C (1-Mode) (c) DI-NI (1-Mode)

(d) DI-A (5-Modes) (e) DI-C (5-Modes) (f) DI-NI (5-Modes)

Figure 7.17 Damage detection comparisons between DI-A, DI-C and DI-NI for single damage case 3M

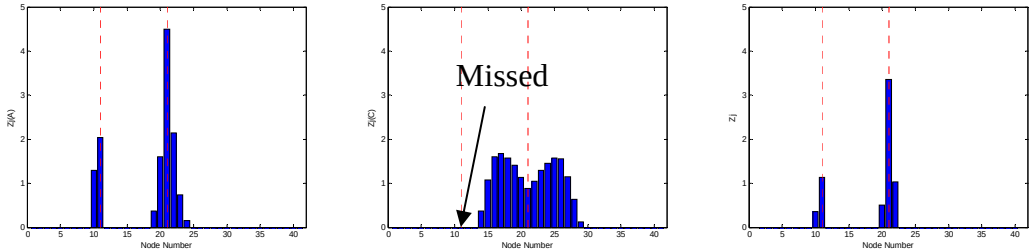

(a) DI-A (1-Mode) (b) DI-C (1-Mode) (c) DI-NI (1-Mode)

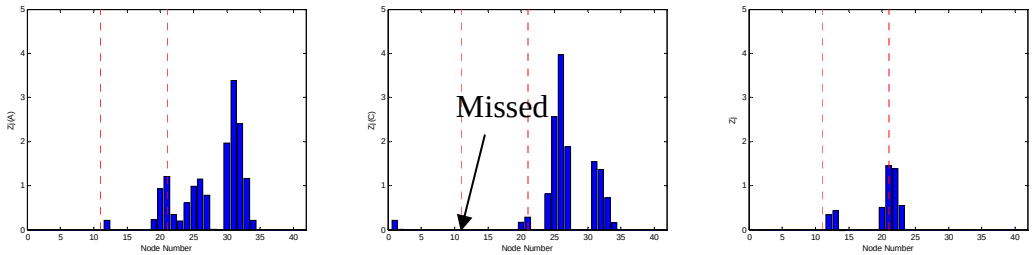

(d) DI-A (5-Modes) (e) DI-C (5-Modes) (f) DI-NI (5-Modes)

Figure 7.18 Damage detection comparisons between DI-A, DI-C and DI-NI for two damage case 2S4S

In summary, the results from experimental investigation show that the improved damage detection method (DI-NI) proposed in this research is more reliable and robust in identifying the location of damage than Damage Index A (DI-A) method and Damage Index C method (DI-C).

7.7.4 Estimation of Severity of Damage

Chapter 6 has shown that the proposed damage detection method is capable of estimating the severity of damage with reasonable confidence by using numerically simulated data. However, it is challenging when the experimental data is to be used in estimation of damage severity in the proposed method, considering measurement noise, imperfect boundary conditions, uncertainties in materials and structures.

To evaluate the effectiveness of the proposed damage detection method in the damage severity estimation, the method is applied to data obtained experimentally from the five reinforced concrete beams. The formulation of the proposed damage detection method used in the following discussions has been presented in Chapter 5. As discussed in

Chapter 6, since the locations of damage are already available, the processing of estimation of severity of damage only focuses attention on the damaged node and nodes around the damage. This approach is also adopted in the experimental results. The first five flexural modes are chosen for application in the damage severity estimation. The damage severity estimators (α_j) are plotted against the node number of the reinforced concrete beam. The actual damage locations are indicated with vertical red dashed lines and the actual level of the severity of damage is indicated with horizontal green dash-dotted line in all the following figures.

Table 7.10 presents the simulated and the estimated damage severities. Each damage corresponds to the percentage of loss of "I", as shown in Table 7.10.

Table 7.10 Estimation of severity of damage in experiment

Damage Cases		Damage Scenario	Damaged Node	Simulated Severity (Loss of "I", %)	Estimated Severity (Loss of "I", %)	Error (%)
Beam 1	1	4L	21	36.03	56.2	-55.98
	2	4M	21	58.86	51.9	11.82
	3	4S	21	71.27	53.57	24.83
	4	2S4S	11, 21	71.27, 71.27	23.15, 56.73	67.51, 20.4
Beam 2	5	3L	16	36.03	27.1	24.78
	6	3M	16	58.86	41.64	29.25
	7	3S	16	71.27	49.29	30.84
	8	3SBar	16	75.06	64.97	13.44
Beam 3	9	HB	31	23.18	34.02	-46.76
Beam 4	10	HT	31	23.18	65.06	-180.67

Figures 7.19 and 7.20 illustrate the results of estimation of damage severity in two damage cases of 4M and 3Sbar. The results for all other cases are shown in Appendix C.3. Even though the proposed damage detection method is able to estimate the severity of damage with reasonable confidence using the numerical data, the method estimates the severity of damage with higher percentage of errors using the experimental data. For example, the difference between simulated severity and estimated severity is 12%, 25%,

25%, 30% and 13% for cases of 4M, 4S, 3L, 3M and 3SBar, respectively. In some cases, the error is quite large. For example, in the cases of 4L and HB, the errors are 56% and 47%, respectively. It is worth pointing out that in the case HT, the error between simulated and estimated damage severity is extremely large, around 180%. There are quite a number of factors causing the errors. Besides the factors discussed in Section 7.7.2, another reason is that in the experimental set up, an accelerometer was located directly on the top of the damage, i.e. the polystyrene hexahedron block, in this case (HT). It is difficult to establish a rigid connection between the block and the accelerometer as it is too soft, thus generating a highly inaccurate acceleration data. Therefore, the proposed damage detection method over estimated the severity of damage.

In summary, the improved version of the proposed damage detection method is able to identify the location of damage accurately. However, the proposed method predicts the severity of damage with larger errors in the experimental study, due to the uncertainties in the experimental set up, imperfection in the modal analysis and presence of noise. This slight shortcoming of the method can be compensated for, either by use of other NDE techniques which work well in this area, or by further refinement of the estimation of the proposed method, which are not included in the scope of work of this thesis.

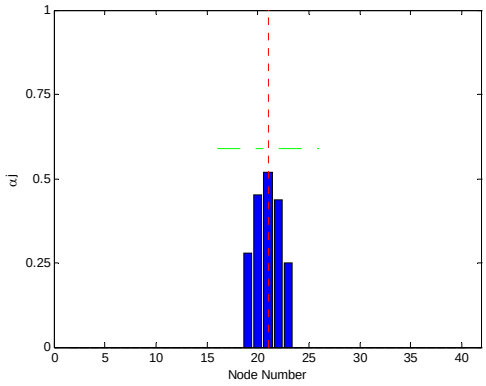

Figure 7.19 Damage estimation index (4M)

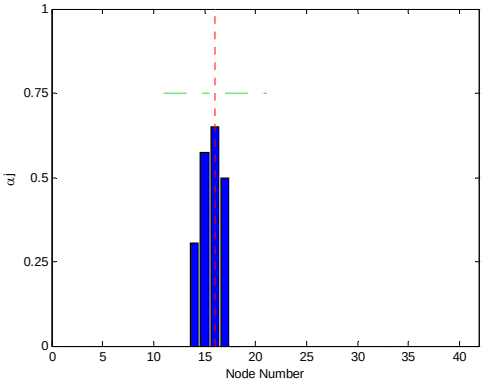

Figure 7.20 Damage estimation index (3SBar)

7.8 Comparison between Numerical and Experimental Results

A comparison has been performed between the numerical and experimental results of damage detection on reinforced concrete beams, using the improved version of the proposed damage detection method (DI-NI). The damage cases discussed in this section are summarised in Table 7.11 with details given in Chapter 6 and Section 7.7.

Table 7.11 Different damaged beams in comparison work

Beam Number	Damage Scenario	Damaged node No.	Loss of I (%)
Beam 1	4L	21	36.03
	4M	21	58.86
	4S	21	71.27
Beam 2	3L	16	36.03
	3M	16	58.86
	3S	16	71.27
Beam 3	HB	31	23.18
Beam 4	HT	31	23.18

7.8.1 Comparison between Noise-free Numerical and Experimental Results

To investigate the difference between numerical and experimental results, eight different cases, namely, 4L, 4M, 4S, 3L, 3M, 3S, HB and HT, as listed in Table 7.11,

were used in the comparison. Figures 7.21 and 7.22 illustrate the results of the location of damage using both numerical and experimental data for two damage cases of 3S and HB, respectively. The case 3S is crack (notch type) damage, while case HB is honeycomb (area filled with very soft material type) damage. The results for all other cases are shown in Appendix C.4.

The results show that the simulated damage in the reinforced concrete beam can be identified in both numerical work and experimental work. The results of the numerical work are distinct and clear without any false identification. This is because the numerical data is pure, not polluted by noise and free from errors of the imperfection of modal analysis. In the results of the experimental work, due to noise pollution, environmental uncertainties and imperfection of modal analysis, some false positives were generated. Nevertheless, it is important to note that, in the experimental results, the damage was not missed and this would provide a safe and conservative assessment results and reduce any possibility of a catastrophic failure. It is possible to conclude that the proposed damage detection method is capable of detecting damage of crack and honeycomb types in reinforced concrete beams, numerically and experimentally.

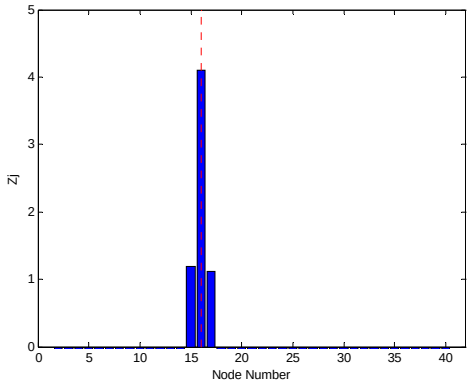

(a) Numerical (1-Mode)

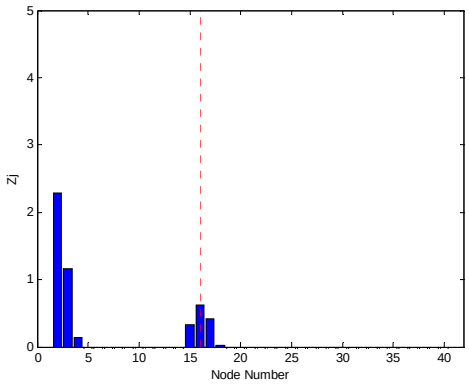

(b) Experimental (1-Mode)

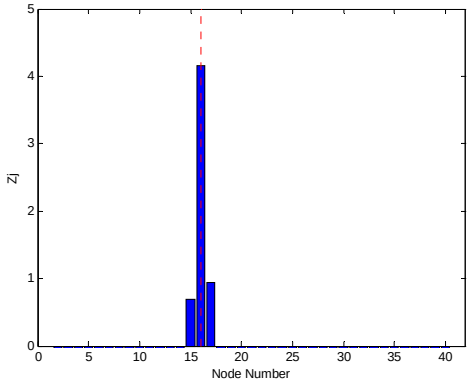

(c) Numerical (5-Modes)

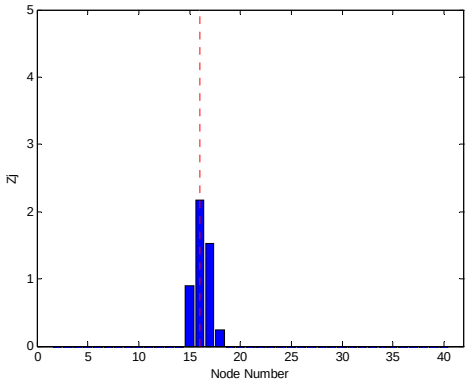

(d) Experimental (5-Modes)

Figure 7.21 Comparison between noise-free numerical and experimental results (3S)

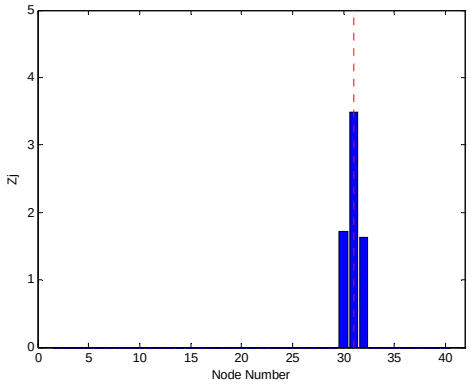

(a) Numerical (1-Mode)

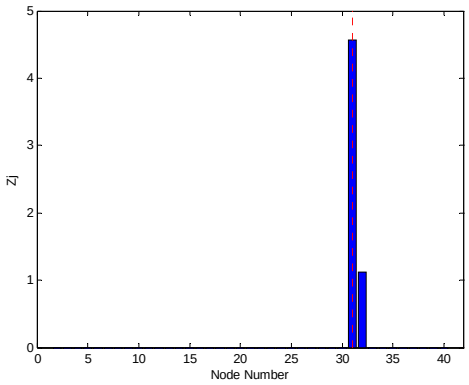

(b) Experimental (1-Mode)

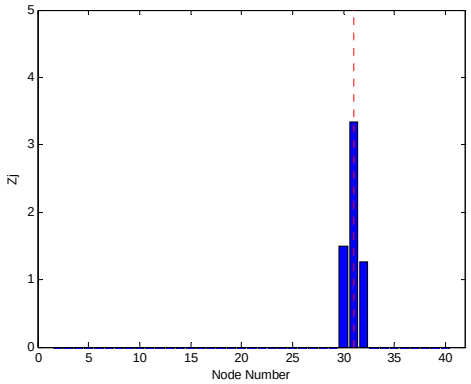

(c) Numerical (5-Modes)

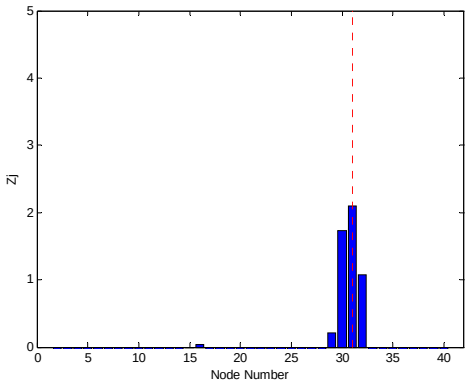

(d) Experimental (5-Modes)

Figure 7.22 Comparison between noise-free numerical and experimental results (HB)

7.8.2 Comparison between Numerical and Experimental Results with Noise Pollution

Figures 7.23 and 7.24 present comparison of damage detection results between numerical data with noise and experimental data. In each figure, the first column diagram depicts the results of using the numerical data with 2% noise (NUM-2%); the second column diagram shows the results of using the numerical data with 10% noise (NUM-10%) and the third column diagram illustrates the results of using the experimental data (EXP). For the number of modes employed in the method, we denote "1-Mode" for the first flexural mode being used, while "5-Modes" denotes the first five flexural modes being used.

The results show that with the increase of noise level in the numerical data, the proposed damage detection algorithm becomes less effective in detecting the location of damage. For example, this can be seen from the decrement of the damage index (Z_j) (probability of damage existence) and from the results of 2% and 10% noise pollution, of Figures (a) and (b), respectively. This is because, when the numerical data is more polluted by noise there will be less difference in the generated mode shapes and its derivatives between the undamaged and damaged beams.

Comparing both numerical results polluted with 2% and 10% white Gaussian noise to the experimental ones, it can be seen that the numerical results with 10% noise present looks more similar to the experimental results. For example, Figure 7.23(c) of EXP result is more similar to Figure 7.23(b) of NUM-10% rather than Figure 7.23(a) of NUM-2%. This is quite reasonable as in real applications of civil engineering structures, the noise level is usually assumed to be from 10-20% of the signal.

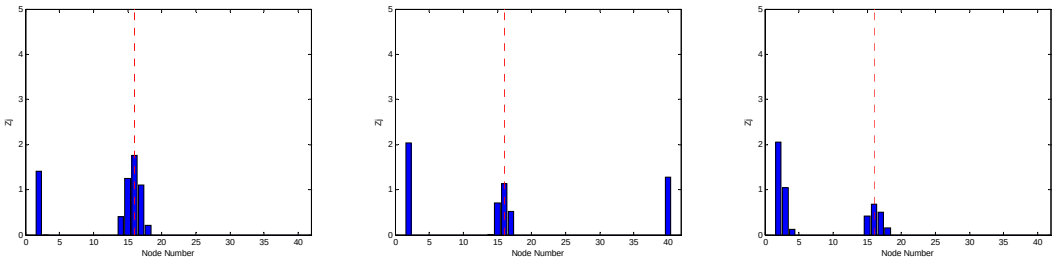

(a) NUM-2% (1-Mode) (b) NUM-10% (1-Mode) (c) EXP (1-Mode)

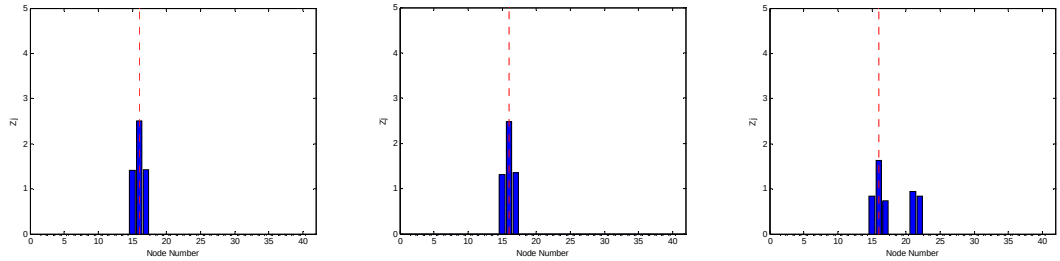

(d) NUM-2% (5-Modes) (e) NUM-10% (5-Modes) (f) EXP (5-Modes)

Figure 7.23 Comparison between noise present numerical and experimental results (3M)

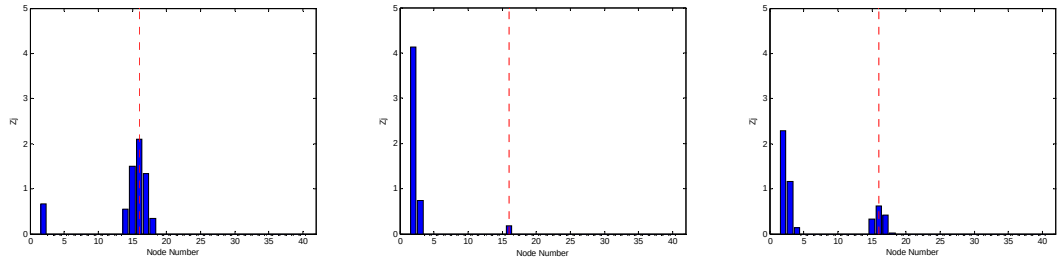

(a) NUM-2% (1-Mode) (b) NUM-10% (1-Mode) (c) EXP (1-Mode)

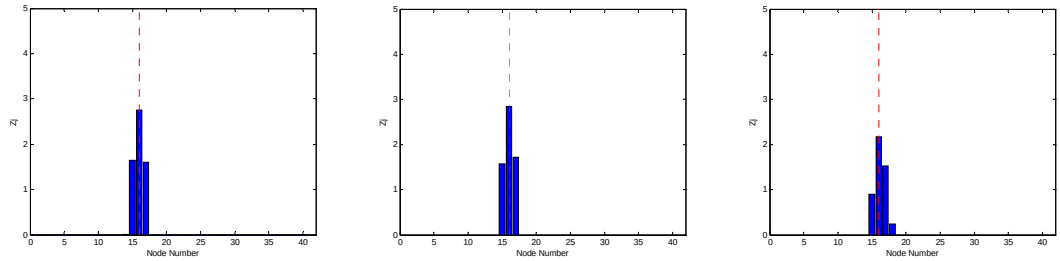

(d) NUM-2% (5-Modes) (e) NUM-10% (5-Modes) (f) EXP (5-Modes)

Figure 7.24 Comparison between noise present numerical and experimental results (3S)

7.8.3 Comparison of Damage Severity Estimation Results

In this section, six different cases, namely, 4L, 4M, 4S, 3L, 3M and 3S, are considered to illustrate the difference in estimation of severity of damage between the numerical and the experimental results. The numerical data without noise are adopted for the severity estimation. Both numerical and experimental results were obtained using the first five flexural modes (5-Modes) in the proposed damage severity estimator. The predicted damage severity is given in Table 7.12. Figures 7.25 and 7.26 depict the difference of estimation of severities between numerical and experimental research in two damage cases of 4M and 4S.

Table 7.12 Estimation of severity of damage of numerical and experimental results

Beam Number	Damage Scenario	Simulated Damage Severity (%)	Predicted Numerical Damage Severity (%)	Predicted Experimental Damage Severity (%)
Beam 1	4L	36.03	26.22	56.20
	4M	58.86	51.87	51.90
	4S	71.27	66.66	53.57
Beam 2	3L	36.03	28.45	27.10
	3M	58.86	55.34	41.64
	3S	71.27	70.53	49.29

Table 7.12 shows that numerical results are closer to the simulated ones compared with the predictions from the experimental data. For example, the percentage of differences, between simulated damage severity and both predicted numerical and experimental damage severity, are about 6% and 25% for the case 4S, respectively. It is also observed that for some damage cases in both the numerical and experimental damage severity prediction results, the light damage cases are not as accurate as the results of the medium and severe damage cases. For example, for the light damage case 4L, the percentage of difference between simulated and predicted experimental damage severity is overestimated by 56%, while for damage cases 4M and 4S they are underestimated by 12% and 25%. This may be due to the fact that lighter damage will change the mode shape at the damage location to a lesser extent compared with the medium and severe damage. Thus, the light damage results may be affected more by noise than the medium and severe damage results.

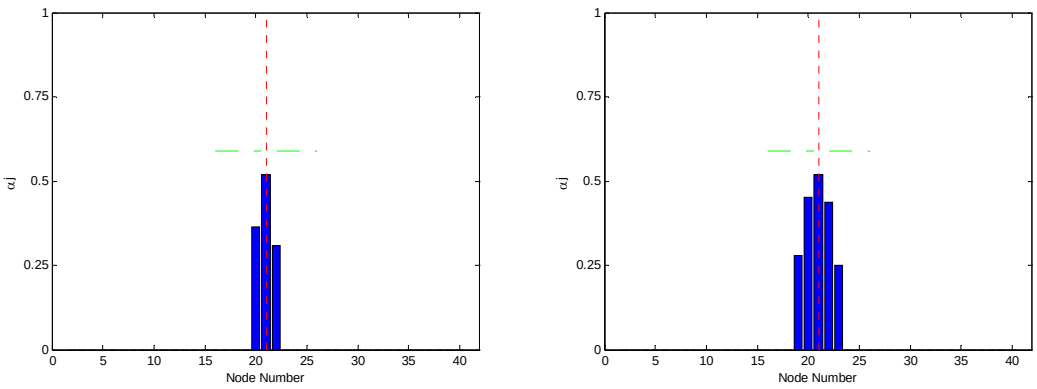

Figure 7.25 Comparison results between numerical and experimental severity estimation (4M)

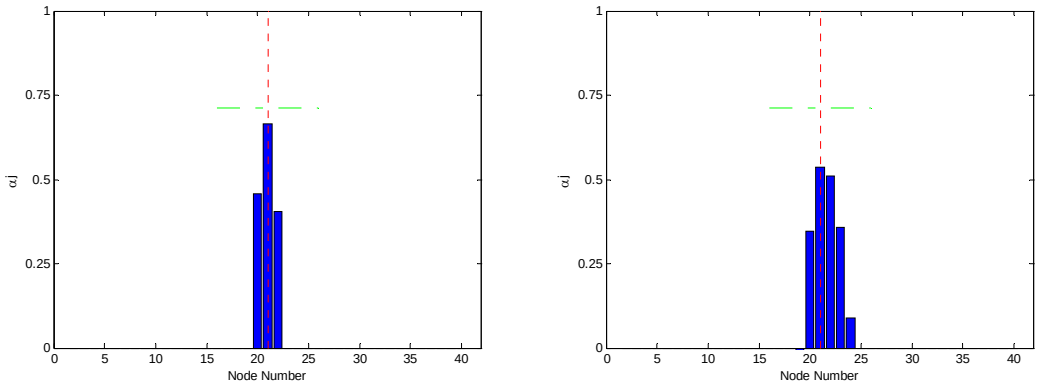

Figure 7.26 Comparison results between numerical and experimental severity estimation (4S)

7.9 Summary

This chapter presented the evaluation and verification of the improved version of the newly proposed damage detection method for damage detection on several experimental reinforced concrete beams inflicted with different damage scenarios typically found in reinforced concrete structures.

Firstly, the procedures of experimental modal analysis (EMA) were outlined. Then, the details of five reinforced concrete beams cast in the laboratory, and the design of the supports, were presented. The simulation of two typical damage cases often found in reinforced concrete, namely, crack and honeycomb, was described. Ten damage cases, i.e. 4L, 4M, 4S, 2S4S, 3L, 3M, 3S, 3SBar, HB and HT, were created and together with the corresponding intact/undamaged cases used for experimental evaluation of the proposed damage detection method.

The results of natural frequency of both undamaged and damaged beams showed that even though the overall tendency of frequency was to decrease after the occurrence of damage, there was no obvious correlation between the severities of damage and drops of frequencies. Therefore, natural frequency might be used only as one indicator to detect existence of damage. However, feasibility of using frequency for quantifying the severity of damage, or locating damage, requires further investigation.

The results of damage localisation showed that the improved version of the proposed damage detection method (DI-NI) was capable of identifying the location of damage in both single and multiple damage cases in a laboratory environment. The results also confirmed that the more severe the damage, the higher is the confidence in locating the damage. However, during the procedure of damage detection, false positive damage was generated. The reasons that caused false positives were discussed in Section 7.7.2. To evaluate the reliability of the proposed damage detection method, the results of the proposed method were compared to two existing popular methods namely, Damage Index A (DI-A) and Damage Index C (DI-C). The comparison results again proved that the proposed method was more reliable and robust than the two other methods in identifying the location of damage.

Comparison was made firstly between the experimental work and noise free numerical work, and then between the experimental work and noise present work. The proposed damage detection method is capable of locating the damage, regardless of using the experimental data, the noise free numerical data, or the noise present numerical data. However, false positive damage was generated when the experimental data and noise present numerical data were employed. The comparison results showed that the noise free numerical results were more accurate in identifying the location of damage than experimental results. The higher percentage the noise, the more difficult it became on the proposed method to detect damage.

Regarding the severity of damage, the results of estimating the severity of damage in experimental work were not as good as the results in numerical work, due to presence of measurement noise, imperfections of modal analysis and boundary conditions and uncertainties in materials and structures. Even though the method was capable of estimating the severity of damage with reasonable confidence using numerical data, the proposed damage detection method estimated the severity of damage less accurately using the experimental data. The shortcomings of the proposed method in estimation of severity of damage can be compensated for either by combination with other NDT methods that work well on the area, or by refinement of the estimation method as future research work.

CHAPTER 8

CONCLUSIONS AND RECOMMENDATIONS

8.1 Conclusions

This thesis focused on the development and verification of a new modal based damage detection method for locating and evaluating damage in reinforced concrete (RC) structures. The work consisted of numerical modelling using finite element analysis (FEA) and experimental testing of reinforced concrete beams. Finite element model has validated using load-deflection curves and modal parameters. Material testing of various elements of a reinforced concrete beam as part of the experimental work was performed to assist in development of accurate FE model. An extensive experimental program employing experimental modal analysis for reinforced concrete beams formed a major portion of this study. Developing a new damage detection method and refining the method through damage detection applications for single and multiple damage scenarios, numerically and experimentally formed the core of this research.

In addition to series of material testing for different elements used in the reinforced concrete beams, namely, concrete and reinforcing steel, four point bending static tests and impulse dynamic tests were performed and their results were used for validating the finite element (FE) modelling of the RC beams. The least square method with two explanatory variables was employed to process the measured experimental strain data.

Based on the material properties obtained from the material testing, numerical modelling using finite element analysis (FEA) of reinforced concrete beams was performed. The FE models comprise an intact/undamaged beam and beams with damage at different locations and severities. The inflicted damage introduced was typically found in reinforced concrete structures, i.e. crack and honeycomb. In the FE modelling, discontinuing element model method was employed to simulate crack and equivalent stiffness reduction method was employed to simulate honeycomb. The intact beam FE model was verified using static and dynamic experimental test results. From the four point bending test (static), it is found that the results of load-deflection curves

obtained from the FE analysis are very close to the ones from experimental testing. For the dynamic test, the correlation analysis results also show that the natural frequencies and mode shapes obtained from the numerical model are very close to the experimental ones, with errors of less than 12% and 10% (except for mode 5), for *NFerror* and *MACerror*, respectively. It is, therefore, concluded that the FE modelling of the RC beam can be used to represent the experimental RC test beam.

A new modal based damage detection method namely, DI-NO, was proposed for damage detection of reinforced concrete beams. The method is based upon reasonable assumptions and it utilises advantages from both mode shapes and mode shape curvatures in damage detection. Even though many research works have indicated that mode shape curvature is very sensitive to damage, mode shape curvature is also very vulnerable to disturbance in real life applications, which results in low reliability in damage detection. The newly proposed method, which is based on combination of mode shape and mode shape curvature, is capable of identifying the location of damage and quantifying the severity of damage with more robustness and reliability than the other methods. The DI-NO method was later refined by normalising the mode shape curvature for damage localisation. It was noted that values of mode shape curvature are dependant on the shapes of each individual mode shape, and calculation of damage index by the summation of non-normalised mode shape curvatures will distort the damage index in favour of higher modes, which results in false damage identifications. To evaluate and verify the proposed new method, two existing popular damage detection methods namely, DI-A and DI-C, by Kim and Stubbs (2000) were adopted for comparison purpose.

Numerical studies of damage detection using a finite element model of reinforced concrete beams with the proposed new methods were performed. Results of the numerical investigation show that the proposed damage detection method using different combination of the first five flexural modes is reliable and robust in locating damage for reinforced concrete beams, for both single and multiple damage scenarios. When noise was added to the time response data to simulate real experimental environment, the results show that the proposed damage detection method was still effective in locating damage for the single damage case inflicted with different levels of noise. However, presence of noise, imperfection of modal analysis and limited

measurement points may jeopardise the reliability and accuracy of damage localisation in multiple damage cases.

For estimating the severity of damage, when noise is absent, the proposed new damage detection method was capable of quantifying the severity of damage with high accuracy for medium and severe damage. In the FE modelling, it was found that the accuracy of severity estimation decreases when real testing conditions, such as presence of noise, imperfection of modal analysis and mode shape reconstruction errors, are encountered. The presence of noise results in underestimation of damage severity. The comparison results of the proposed method with two existing popular methods proved that the proposed method was able to identify the location of damage with higher reliability and more robustness than the other methods, with and without the presence of noise. The results of the proposed method underwent refinement to illustrate that the improved method could significantly improve reliability and robustness of damage detection. It is recommended for use in the experimental studies.

The improved version of the proposed damage detection method was applied to detect damage experimentally using the reinforced concrete beams. The results show that the method was capable of identifying the location of damage, especially for honeycomb type of damage. However, due to uncertainties associated with measurement and processing errors, false positive (spurious damage location) might be generated. However, the comparison results of the proposed method with two existing popular methods have shown that the proposed new method was still more accurate and reliable in damage detection. The proposed damage detection method predicts the severity of damage with error in the experimental results, due to the uncertainties in the experimental set up, imperfection of the modal analysis and presence of noise.

In summary, a new damage detection method and its improved version based on a combination of the mode shape and mode shape curvature has been developed in this thesis. The new method was capable of detecting the location of damage and estimating the severity of damage, for single and multiple damage scenarios. Through extensive numerical and experimental investigations, it was found that the new method is more reliable and robust than the two existing popular methods.

8.2 Recommendations and Future Work

Further work and some refinements are recommended to make this research work more practical for application. Hence, the purpose of this section is to focus on the issues that should be addressed by future researchers to make use of this method as a practical tool for damage detection in reinforced concrete structures, as well as its application to general structural health monitoring.

First of all, since the number and spacing of sensors are critical to the damage detection results, it is recommended that using a beam system, parametric studies on sensitivity of number of sensors and spacing be carried out. Besides, it is also recommended to study the threshold of damage that can be detected using different combination of number of sensors and spacing.

Secondly, mode shape plays an important role in damage detection. In this research, mode shape was reconstructed using Cubic Spline interpolation technique. Since there are still differences between the reconstructed and the real mode shapes, it is recommended that research should be carried out on how to reconstruct mode shape in order to further minimise the difference between the reconstructed mode shape and the real mode shape.

Finally, the proposed damage detection method is based upon the modal parameters of both undamaged and damaged states. Often, the lack of availability of the baseline data makes the method impractical for certain applications. Therefore, one major challenge is to develop methods in order to minimise the dependence on baseline information.

References

Abdul Rahman, A.G. 1999, *Notes of Signal Processing*, Mechanical Engineering Department, Faculty of Engineering, University of Malaya.

Agilent Technologies 2000, *The fundamentals of modal testing*, Agilent Technologies, US.

Alampalli, S. Fu, G. & Dillon, E.W. 1997, 'Signal versus Noise in Damage Detection by Experimental Modal Analysis', *Journal of Structural Engineering*, Vol. 123, No.2, February, 1997. 237-245.

Allemang, R.J. & Brown, D.L. 1983, 'Correlation coefficient for modal vector analysis', *Proceedings of 1st International Modal Analysis Conference*, Society for Experimental Mechanics, Inc., pp. 690-695.

ANSYS Inc. 2007, *ANSYS release 11.0*.

ANSYS Inc. 2007, *ANSYS release 11.0 documentation*, Canonburg, US.

Avitabile, P. 2001, 'Experimental modal analysis', *Sound and Vibration Magazine*, January 2001, pp. 1-11.

Avitabile, P. 2002, 'Twenty years of structural dynamic modification- A review', *Proceedings of IMAC-XX: A Conference on Structural Dynamics*, vol. 1, Society for Experimental Mechanics, Inc. , The Westin Los Angeles Airport, Los Angeles, California, pp. 356-372.

Avitabile, P. 2006, 'Modal Space in Our Little World', *Sound and Vibration Magazine*, Modal Analysis and Controls Laboratory, University of Massachusetts Lowell.

Baghiee, N., Esfahani, M.R. & Moslem, K. 2009, 'Studies on Damage and FRP Strengthening of Reinforced Concrete Beams by Vibration Monitoring', Engineering Structures, 31 (2009) 875-893.

Ballo, I. 1998, 'Non-linear effects of vibration of a continuous transverse cracked slender shaft', *Journal of Sound and Vibration*, 217(2) 321-333.

Banks, H.T., Inman, D.J., Leo, D.J. & Wang, Y. 1996, 'An experimentally validated damage detection theory in smart structures', *Journal of Sound and Vibration*, vol. 191, no. 5, pp. 859-880.

Barbosa, A. F. & Ribeiro, G. O. 1998, 'Analysis of Reinforced Concrete Structures using Ansys Nonlinear Concrete Model', *COMPUTATIONAL MECHANICS*, New Trends and Applications, CIMNE, Barcelona, Spain.

Bernal, D. 2002, 'Load vectors for damage localisation', *Journal of Engineering Mechanics*, vol. 128, no. 1, pp. 7-14.

Bishop, C.M. 1994, 'Neural networks and their applications', *Review of Scientific Instruments*, vol. 65, no. 6, pp. 1803-1832.

Borsaikia, A., Talukdar, S. & Dutta, A. 2006, 'Study of Modal Parameters and Vibraiton Signatures of Notched Concrete Prisms', *Cement and Concrete Research*, 36(2006) 592-598.

Bovsunovsky, A.P. & Matveev, V.V. 2000, 'Analytical Approach to the Determination of Dynamic Characteristics of a Beam with a Closing Crack', *Journal of Sound and Vibration*, (2000), 235 (3), 415-434.

Brownjohn, J.M.W. & Xia, P. 1999, 'Finite element model updating of a damaged structure', *Proceedings of the 17th International Modal Analysis Conference*, Society for Experimental Mechanics, Inc., Hyatt Orlando Hotel, Kissimmee, Florida, US, pp. 457-462.

Bungey, J.H., Millard, S.G. & Granthan, M.G. 2006, *Testing of Concrete in Structures*. ISBN10: 0-415-26301-8, ISBN 13: 978-0-415-26301-6.

Cao, M., Ren, Q. & Qiao, P 2006, 'Non-destructive Assessment of Reinforced Concrete Structures Based on Fractal Damage Characteristic Factors', *Journal of Engineering Mechanics*, Vol. 132, No. 9, September 1, 2006. 924-931.

Carden, P., E & Fanning, P. 2004, 'Vibration based condition monitoring: a review', *Structural Health Monitoring*, vol. 3, no. 4, pp. 355-377.

Casas, J.R. & Aparicio, A.C. 1994, 'Structural Damage Identification from Dynamic-test Data', *Journal of Structural engineering*, Vol. 120, No. 8, August, 1994. Paper No. 3439.

Cawley, P. & Adams, R.D. 1979, 'The location of defects in structures from measurements of natural frequencies', *Journal of Strain Analysis*, vol. 14, No. 2, pp. 49-57.

Chen, J., Xu, Y.L. & Zhang, R.C. 2004, 'Modal parameters identification of Tsing Ma suspension bridge under typhoon victor: EMD-HT method', *Journal of wind Engineering and Industrial Aerodynamics*, 92 (2004) 805-827.

Cheng, S.M., Wu, X.J. & Wallace, W. 1999, 'Vibration Response of a Beam with a Breathing Crack', *Journal of Sound and Vibration*, (1999), 225 (1), 201-208.

Ching, J. & Beck, J.L. 2004, 'Bayesian Analysis of the Phase II IASC-ASCE Structural Health Monitoring Experimental Benchmark Data', *Journal of Engineering Mechanics*, vol. 130, No. 10, October 1, 2004, pp. 1233-1244.

Choi, F.C., Li, J., Samali, B. & Crews, K. 2006, 'Impact of Different Numerical Techniques on Damage Identification in Structure', *Tenth East Asia-Pacific Conference on Structural Engineering and Construction*, August 3-5, 2006, Bangkok, Thailand, pp. 111-116.

Choi, F.C., Li, J., Samali, B. & Crews, K. 2007, 'An Experimental Study on Damage Detection of Structures Using a Timber Beam', *Journal of Mechanical Science and Technology*, 21 (2007), pp 903-907.

Choi, S., Park, S.& Stubbs, N. 2005, 'Non-destructive Damage Detection in Structures using Changes in Compliance', *International Journal of Solids and Structures*, 42 (2005) 4494-4513.

Clucas, J. 1998, 'Crunch time for bridges'. Public Works Engineering: 15-16.

Craig, R.R.J. & Kurdila, A.J. 2006, *Fundamentals of structural dynamics*, 2nd edition edn, John Wiley & Sons, Hoboken, New Jersey, US.

Cunha, A. & Caetano, E. 2006, 'Experimental Modal Analysis of Civil Engineering Structures', *Sound and Vibration*, June, 2006.

Dilek, U. 2007, 'Assessment of Fire Damage to a Reinforced concrete structure during Construction', *Journal of Performance of Constructed Facilities*, Vol. 21, No. 4, August 1, 2007. pp257-263.

Ditter, J. P., Jensen, C. G., Gottschalk, M. & Almy T, 2006, 'Mesh optimization using a genetic algorithm to control mesh creation parameters', *Computer-Aided Design & Application*, Vol. 3, No. 6, pp 731-740

Doebling, S.W., Hemez, F. M., Peterson, L. D., and Farrar, C. 1997, 'Improved damage location accuracy using strain energy based on mode selection criteria', *AIAA J*, 35 (4), pp. 693-699.

Doebling, S.W., Farrar, C.R. & Prime, M.B. 1998, 'A summary review of vibration-based damage identification methods', *The Shock and Vibration Digest*, vol. 30, no. 2, pp. 91-105.

Doebling, S.W., Farrar, C.R., Prime, M.B. & Shevitz, D.W. 1996, *Damage identification and health monitoring of structural and mechanical systems from changes in their vibration characteristics: A literature review*, Report Number Report LA-13070-MS, Los Alamos National Laboratory, New Mexico.

Doherty, J.E., “Nondestructive Evaluation”, Chapter 12 in Handbook on Experimental Mechanics, A. S. Kobayashi Edt., Socity for Experimental Mechanics, Inc., 1987.

Elliott, A. S. & Richardson, M. H. 1998, 'Virtual Experimental Modal Analysis', *IMAC XVI*, February, 1998. pp. 1-7.

Ewins, D.J. 2000, *Modal testing: theory, practice and application*, vol. 2, Research Studies Press Ltd, England.

Faleiro, J., Oller, S. & Barbat, A.H. 2008, 'Plastic-damage seismic model for reinforced concrete frames', *Computers and Structures*, 86 (2008) 581-597.

Fang, S.E., Perera, R. & Roeck, G.D.. 2008, 'Damage Identification of a Reinforced Concrete Frame by Finite Element Model Updating Using Damage Parameterization', *Journal of Sound and Vibration*, 313 (2008) 544-559.

Fang, X. Luo, H. & Tang, J. 2005, 'Structural damage detection using neural network with learning rate improvement', *Computers and Structures*, 83 (2005) 2150-2161.

Fanning, P. 2001, 'Nonlinear Models of Reinforced and Post-tensioned Concrete Beams', *Electronic Journal of Structural Engineering*, Vol. 2, pp.111-119.

Farrar, C.R., Baker, W.E., Bell, T.M., Cone, K.M., Darling, T.W., Duffey, T.A., Eklund, A. & Migliori, A. 1994, *Dynamic characterization and damage detection in the I-40 bridge over the Rio Grande*, Report Number Report LA-12767-MS, Los Alamos National Laboratory, New Mexico.

Farrar, C.R. & Doebling, S.W. 1997, 'Lessons learned from applications of vibration-based damage identification methods to a large bridge structure', *Proceedings of the International Workshop on Structural Health Monitoring*, Stanford, California, US, pp. 351-370.

Farrar, C.R. & Juaragui, D. 1996, Damage detection algorithms applied to experimental and numerical modal data from the I-40 bridge, Los Alamos National Laboratory, Los Alamos, New Mexico, US.

Farrar, C.R. & Juaragui, D. 1998, 'Comparative study of damage identification algorithms applied to a bridge: I. Experimental', *Smart Materials and Structures*, No.7, 704-719.

Feng, M.Q., Liu, C., He, X. & Shinozuka, M. 2000, 'Electromagnetic Image Reconstruction for Damage Detection', *journal of Engineering Mechanics*, Vol. 126, No. 7, July, 2000.

Feng, M.Q., Flaviis, F.D., & Kim, Y.J. 2002, 'Use of Microwaves for Damage Detection of Fiber Reinforced Polymer-Wrapped Concrete Structures', *Journal of Engineering Mechanics*, Vol. 128, No. 2, February 1, 2002.

Fernandez-Saez, J. Rubio, L. & Navarro, C. 1999, 'Approximate Calculation of the Fundamental Frequency for Bending Vibrations of Cracked Beams', *Journal of Sound and Vibration*, (1999), 225 (2), 345-352.

Friswell, M. I. & Penny, J. E. T. 2002, 'Crack Modelling for Structural Health Monitoring', *Structural Health Monitoring*, Vol. I(2). Pp 139-148.

Furukawa, A & Otsuka, H. 2006, 'Structural Damage Detection Method Using Uncertain Frequency Response Functions', *Computer-Aided Civil and Infrastructure Engineering*, 21 (2006) 292-305.

Gao, Y. & Spencer, B.F.J. 2006, 'Online damage diagnosis for civil infrastructure employing a flexibility-baed approach', *Smart Materials and Structures*, vol. 15, pp. 9-19.

Garcia, G.V., Osegueda, R. & Meza, D. 1998, 'Comparison of the damage detection results utilizing an ARMA model and a FRF model to extract the modal parameters', *Smart Structures and Materials 1998*, SPIE-The International Society for Optical Engineering, San Diego, California, US, pp. 244-252.

Garesci, F., Catalano, L. & Petrone, F. 2006, 'Experimental Results of a Damage Detection Methodology using Variations in Modal Parameters', *Experimental Mechanics*, Vol. 46, pp 441-451.

Gonzalez, M.P. & Zapico, J.L. 2008, 'Seismic damage identification in buildings using neural networks and modal data', *Computers and Structures*, 86 (2008) 416-426.

Han, J.G., Ren, W.X. & sun, Z.S. 2005, 'Wavelet packet based damage identification of beam structures', *International Journal of Solids and Structures*, 42 (2005) 6610-6627.

Hassoun, M.Nadim & Al-Manaseer, A. 2008, 'Structural Concrete: Theory and Design', 4th ed. Includes bibliographical references and index. ISBN 978-0-470-17094-6.

Heinrichs, P. (2007). "$240m West Gate facelift to bridge safety fears". *The Age*. (August 5, 2007) www.theage.com.au.. Retrieved on 2009-06-18.

Hera, A. & Hou, Z. 2004, 'Application of Wavelet Approach for ASCE Structural Health Monitoring Benchmark Studies', *Journal of Engineering Mechanics*, Vol. 130, No. 1, January 1, 2004. 96-104.

Hou, Z. Noori, M. & Amand, R.S. 2000, 'Wavelet-based Approach for Structural Damage Detection', *Journal of Engineering mechanics*, Vol. 126, No. 7, July, 2000, 677-683.

Housner, G.W., Bergman, L.A., Caughey, T.K., Chassiakos, A.G., Claus, R.O., Masri, S.F., Skelton, R.E., Soong, T.T., Spencer, B.F. & Yao, J.T.P. 1997, 'Structural control: Past, present, and future', *Journal of Engineering Mechanics*, vol. 123, no. 9, pp. 897-971.

Hu, S-L. J., Wang, S. & Li, H. 2006a, 'Cross-modal strain energy method for estimating damage severity', *Journal of Engineering Mechanics*, vol. 132, no. 4, April 1, 2006.

Hu, H., Wang, B.T. Lee, C.H. & Su, J.S. 2006b, 'Damage Detection of Surface Cracks in Composite Laminates Using Modal Analysis and Strain Energy Method', *Composite Structures*, 74 (2006) 399-405.

Ismail, Z., Abdul Razak, H. & Abdul Rahman, A.G. 2006, 'Determination of damage location in RC beams using mode shape derivatives', *Engineering Structures*, vol. 28, pp. 1566-1573.

Kisa, M. & Brandon, J. 2000, 'The Effect of Closure of Cracks on the Dynamics of a Cracked Cantilever Beam', *Journal of Sound and Vibration*, (2000), 238 (1), 1-18.

Kim, B.H., Park, T. & Voyiadjis, G.Z. 2006, 'Damage Estimation on Beam-like Structures using the Multi-resolution Analysisr', *International Journal of Solids and Structures*, 43 (2006) 4238-4257.

Kim, J.-T. & Stubbs, N. 1995, 'Model-uncertainty and damage-detection accuracy in plate girder', *Journal of Structural Engineering*, vol. 121, no. 10, pp. 1409-1417.

Kim, J.-T. & Stubbs, N. 2002, 'Improved damage identification method based on modal information', *Journal of Sound and Vibration*, vol. 252, no. 2, pp. 223-238.

Kim, J.-T. & Stubbs, N. 2003, 'Crack detection in Beam-type Structures using frequency Data', *Journal of Sound and Vibration*, vol. 259, no.1, pp. 145-160.

Kim, T.-H., Lee, K.-M., Chung, Y.-S. & Shin, H.M. 2005, 'Seismic Damage Assessment of Reinforced Concrete Bridge Columns', *Engineering Structures*, 27 (2005) 576-592.

Kosmatka, J.B. & Ricles, J.M. 1999, 'Damage Detection in Structures by Modal Vibration Characterization', *Journal of Structural Engineering*, vol. 125, no.12, pp. 1384-1392.

Lee, J.J. & Yun, C.B. 2006, 'Damage diagnosis of steel girder bridges using ambient vibration data', *Engineering Structures*, vol. 28, pp. 912-925.

Li, H., Yang, H. & Hu, S.L.J. 2006, 'Modal Strain Energy Decomposition Method for damage Localization in 3D Frame Structures', *Journal of Engineering Mechanics*, vol. 132, No. 9, September 1, 2006. pp941-951.

Li, J., Samali, B., Ye, L. & Bakoss, S. 2002, 'Behaviour of Concrete Beam-column Connections Reinforced with Hybrid FRP Sheet', *Composite Structures*, 57 (2002) 357-365.

Liang, Q. Q., Uy, B., Bradford, M. A. & Ronagh, H. R. 2005, 'Strength analysis of steel-concrete composite beams in combined bending and shear', *Journal of Structural Engineering*, Vol. 131, No. 10, October 1, 2005.

Lieven, N.A.J. & Ewins, D.J. 1988, 'Spatial correlation of modespaces: the corridnate modal assurance criterion (COMAC)', *6th International Modal Analysis Conference*, Kissimmee, Florida, US, pp. 1063-1070.

Lim, T.W., & Kashangaki, T.A.I. 1994, 'Structural damage detection of space truss structures using best achievable eigenvectors', *AIAA J.*,, 32 (5), pp 1049-1057.

Lin, R.J., & Cheng, F.P. 2008, 'Multiple Crack Identification of a Free-free Beam with Uniform Material Property Variation and Varied Noised Frequency', *Engineering Structures*, 30 (2008) 909-929.

LMS International 1992, *LMS CADA-X modal analysis manual*, LMS International, Belgium.

Malhotra, V.M. & Carino, N.J. Nondestructive, 2004, Testing of Concrete, Second Edition, ISBN: 0-8031-2099-0.

Maeck, J. 2003, 'Damage assessment of civil engineering structures by vibration monitoring', PhD thesis, Katholieke Universiteit Leuven, Belgium.

Maeck, J. & De Roeck G. 2003, 'Damage Assessment Using Vibration Analysis on the Z24-Bridge', *Mechanical and Signal Processing*, Vol. 17, No. 1, pp. 133-142.

Maeck, J., Wahab, M.A., Peeters, B., Roeck, G.D., Visschere, J.D., Wilde, W.P., Ndambi, J.M. & Vantomme, J. 2000. 'Damage identification in reinforced concrete structures by dynamic stiffness determinaition', *Engineering Structures*, 22 (2000) 1339-1349.

Maia, N.M.M. & Silva, J.M.M.e 1997, *Theoretical and Experimental Modal Analysis*, Research Studies Press Ltd, Somerset.

Maia, N.M.M., Silva, J.M.M.. Almas, E.A.M. & Sampaio, R.P.C. 2003, 'Damage Detection in Structures: from Mode Shape to Frequency Response Function Methods', *Mechanical Systems and Signal Processing*, (2003) **17**(3), 489-498.

Melhem, H. & Kim, H. 2003, 'Damage Detection in Concrete by Fourier and Wavelet Analysis', *Journal of Engineering Mechanics*, Vol. 129, No. 5, May 1, 2003. 571-577.

Morassi, A. & Rocchetto, L. 2003, 'A Damage Analysis of Steel-concrete Composite Beams Via Dynamic Methods: Part I. Experimental Results', *Journal of vibration and Control*, 9:507-527.

Nair, K.K., Kiremidjian, A.S. & Law, K.H.. 2006, 'Time series-based damage detection and localization algorithm with application to the ASCE benchmark structure', *Journal of Sound and Vibration*, (2006), 291 (3), 346-368.

Nandwana, B.P., Maiti, S.K. 1997, 'Detection of the Location and size of a Crack in Stepped Cantilever Beams Based on Measurement of Natural Frequency', *Journal of Sound and Vibration*, (1997), 203 (3), 435-446.

Nawy, Edward.G. 2009, *Reinforced Concrete a Fundamental Approach*. Sixth Edition. ISBN-13:978-0-13-241703-7.

Narkis, Y. 1994, 'Identification of Crack Location in Vibration Simply Supported Beams', *Journal of Sound and Vibration*, (1994) 172 (4), 549-558.

Neild, S. A., Williams, M. S. & McFadden, P. D. 2002, 'Non-linear behaviour of reinforced concrete beams under low-amplitude cyclic and vibration loads', *Engineering Structures*, 24 (2002), pp 707-718.

Ndambi, J.M., Vantomme, J. & Harri, K. 2002, 'Damage Assessment in Reinforced Concrete Beams using Eigenfrequencies and mode shape derivatives', *Engineering Structures*, vol. 24, pp 501-515.

O'Neill, C. 2002, 'Cubic Spline Interpolation'.

Owolabi, G.M., Swamidas, A.S.J. & Seshadri, R. 2003, 'Crack Detection in Beams using Changes in Frequencies and Amplitudes of Frequency Response Functions', *Journal of sound and vibration*, vol. 265(2003), 1-22.

Paepegem, W.V., Dechaene, R. & Degrieck, J. 2005, 'Nonlinear correction to the Bending Stiffness of a Damaged Composite Beam', *Composite Structures*, 67 (2005) 359-364.

Pandey, A.K., Biswas, M. & Samman M. M. 1991, 'Damage detection from changes in curvature mode shapes', *Journal of sound and vibration*, vol. 145(2), 321-332.

Pandey, A.K. & Biswas, M. 1994, 'Damage detection in structures using changes in flexibility', *Journal of Sound and Vibration,* vol. 169, no. 1, pp. 3-17.

Patjawit, A. & Kanok-Nukulchai, W. 2005, 'Health monitoring of highway bridges based on a global flexibility index', *Engineering Structures,* vol. 27, no. 9, pp. 1385-1391.

Peterson, S.T., McLean, D.I. & Pollock, D.G. 2003, 'Application of dynamic system identification to timber bridges', *Journal of Structural Engineering,* vol. 129, no. 1, pp. 116-124.

Peterson, S.T., McLean, D.I., Symans, M.D., Pollock, D.G., Cofer, W.F., Emerson, R.N. & Fridley, K.J. 2001a, 'Application of dynamic system identification to timber beams I', *Journal of Structural Engineering*, vol. 127, no. 4, pp. 418-425.

Peterson, S.T., McLean, D.I., Symans, M.D., Pollock, D.G., Cofer, W.F., Emerson, R.N. & Fridley, K.J. 2001b, 'Application of dynamic system identification to timber beams II', *Journal of Structural Engineering*, vol. 127, no. 4, pp. 426-432.

Pugno, N. & Surace, C. 2000, 'Evaluation of the Non-linear Dynamic Response to Harmonic Excitation of a Beam with Several Brathing Cracks', *Journal of Sound and Vibration,* (2000), 235 (5), 749-762.

Ramsey, K.A. 1983, 'Experimental modal analysis, structural modifications and FEM analysis on a desktop computer', *Sound and Vibration*, February, p. 10.

Razak, H.A. & Choi, F.C. 2001, 'The Effect on Corrosion on the Natural Frequency and Modal Damping of Reinforced Concrete Beams', *Engineering Structures*, 23 (2001), 1126-1133.

Rytter, A. 1993, 'Vibration based inspection of civil engineering structures', Ph. D thesis, Aalborg University, Denmark.

Salawu, O.S. 1997, 'Detection of structural damage through changes in frequency: a review', *Engineering Structures*, vol. 19, no. 9, pp. 718-723.

Schechinger, B. & Vogel, T. 2007, 'Acoustic emission for monitoring a reinforced concrete beam subjected to four-point-bending', *Construction and Building materials*, 21 (2007) 483-490.

Shifrin, E.I. & Ruotolo, R. 1999, 'Natural Frequencies of a Beam with an Arbitrary Number of Cracks', *Journal of Sound and Vibration*, (1999) 222 (3), 409-423.

Shinozuba, M., Ghanem, R., Houshmand, B. and Mansouri, B. (2000), 'Damage Detection in Urban Areas by SAR Imagery', *Journal of Engineering Mehcanics*, Vol. 126, No. 7, July, 2000.

Sohn, H., Farrar, C.R., Hemez, F.M., Shunk, D.D., Stinemates, D.W. & Nadler, B.R. 2003, *A review of structural health monitoring literature: 1996-2001*, Report Number LA-13976-MS, Los Alamos National Laboratory, New Mexico.

Stubbs, N. & Park, S. 1996, 'Optimal sensors placement for mode shapes via Shannon's sampling theorem', *Microcomputers in Civil Engineering*, vol. 11, pp. 411-419.

Suresh, S., Omkar, S.N., Ganguli, R. & Mani, V. 2004, 'Identification of crack location and depth in a cantilever beam using a modular neural network.' *Smart Materials and Structures*, vol. 13, pp. 907-915.

Razak, H. & Choi, F.C. 2001, 'The effect of corrosion on the natural frequency and modal damping of reinforced concrete beams', *Engineering Structures*, 23 (2001) 1126-1133.

Salane, H.J. & Baldwin, J.W. 1990, 'Identification of Modal Properties of Bridge', *Journal of Structural Engineering*, Vol. 116, No. 7, July, 1990. Paper no. 24877.

Salawu, O.S. & Williams, C. 1995, 'Bridge Assessment using Forced-vibration Testing', *Journal of Structural Engineering*, Vol. 121, No. 2, February, 1995. Paper no. 6940.

Sampaion, R.P.C., Maia, N.M.M. & Silva, J.M.M. 1999, 'Damage Detection Using the Frequency Response Function Curvature Method', *Journal of Sound and Vibration*, Vol. **226**(5), 1029-1042.

Sazonov, Edward S., Kilinkhachorn, P., Gangarao, H.V.S. & Halabe, U.B. 2002, 'Fuzzy logic expert system for automated damage detection from changes in strain energy mode shapes', *Non-destructive Testing and Evaluation*, Vol. **18**(1), p.p.1-20.

Sánchez, J.C.H. 2005, 'Evaluation of structural damage identification methods based on dynamic characteristics', PhD thesis, University of Puerto Rico, Mayagüez.

Shi, Z.Y., Law, S.S. & Zhang, L.M. 1998, 'Structural damage localization from modal strain energy change', *Journal of Sound and Vibration*, vol. 218, no. 5, pp. 825-844.

Shi, Z.Y., Law, S.S. & Zhang, L.M. 2000, 'Damage localization by directly using incomplete mode shapes', *Journal of Engineering Mechanics*, vol. 126, no. 6, pp. 656-660.

Shi, Z.Y., Law, S.S. & Zhang, L.M. 2002, 'Improved damage quantification from elemental modal strain energy change', *Journal of Engineering Mechanics*, vol. 128, no. 5, pp. 521-529.

Soh, C.K., Liu, Y. Dong, Y.X. & Lu, X.Z. 2003, 'Damage Model Based Reinforced-concrete Element', *Journal of Materials in Civil Engineering*, Vol. 15, No. 4, August 1, 2003. 371-380.

Sohn, H., Farrar, C.R., Hemez, F.M., Shunk, D.D., Stinemates, D.W. & Nadler, B.R. 2003, *A review of structural health monitoring literature: 1996-2001*, Report Number LA-13976-MS, Los Alamos National Laboratory, New Mexico.

Spacone, E. & EI-Tawil, S. 2004, 'Nonlinear Analysis of Steel-Concrete Composite Structures: State of the Art', *Journal of Structure Engineering*, Vol. 130, No. 2, February 1, 2004. 159-168.

Stewart M. G., 2001, 'Reliability-based assessment of ageing bridges using risk-ranking and life cycle cost decision analysis', *Reliability Engineering and System Safety*, Vol, 74, pp. 263-273

Su, Z. & Ye, L. 2004, 'Lamb wave-based quantitative identification of delamination in CF/EP composite structures using artificial neural algorithm', *Composite Structures*, 66 (2004) 627-637.

Thorby, D.2008, *Structure dynamics and vibration in practice an engineering hand book*. Library of Congress Catalog Number: 2007941701, ISBN: 978-0-7506-8002-8.

Tom Irvine, 2000, *an Introduction to Frequency Response Functions*

Torrence, C. & Compo, G.P. 1997, 'A Practical Guide to Wavelet Analysis', *American Meteorological Society*.

Toutanji, H. 2000, 'Ultrasonic wave velocity signal interpretation of simulated concrete bridge decks', *Materials and Structures*, Vol. 33, April 2000, pp 207-215

Tsyfansky, S.L. & Beresnevich, V.L. 2000, 'Non-linear Vibration Method for Detection of Fatigue Cracks in Aircraft Wings', *Journal of Sound and Vibraiton*, (2000) 236 (1), 49-60.

Unger, J., Teughels, A. & Roeck, G.D. 2005, 'Damage Detection of a Prestressed Concrete Beam Using Modal Strains', *Journal of Structural Engineering*, Vol. 131, No.9, September 1, 2005, pp 1456-1463.

Wahab, M.A. & Roeck, G. 1997. 'Effect of Temperature on Dynamic System Parameters of a Highway Bridge'. *Structural Engineering International* 4, 266-270.

Wang, Z., Lin, R.M. & Lim, M.K. 1997, 'Structural Damage Detection using Measured FRF Data'. *Computer Methods in Applied Mechanics and Engineering*, 147, 187-197.

Warner, R F, Rangan, B V, Hall, A S & Faulkes K A 1998, *Concrete Structures*, Includes index. ISBN 0 582 80247 4.

Worden, K. & Dulieu-Barton, J.M. 2004, 'An overview of intelligent fault detection in systems and structures', *Structural Health Monitoring*, vol. 3, no. 1, pp. 85-98.

Worden, K., Manson, G. & Allman, D.J. 2001, 'An experimental appraisal of the strain energy damage location method', *Proceedings of the 4th International Conference on Damage Assessment of Structures*, eds K.M. Holford, J.A. Brandon, J.M. Dulieu-Barton, M.D. Gilchrist & K. Worden, Trans Tech Publications Ltd, Cardiff, Wales, UK, pp. 35-46.

Xu, Y.L. & Chen, J. 2004, 'Structural Damage Detection Using Empirical Mode Decomposition: Experimental Investigation', *Journal of Engineering Mechanics*, Vol. 130, NO. 11, November 1, 2004. 1279-1288.

Xu, Y.L., Chen, S.W. & Zhang, R.C. 2003, 'Modal Identification of Di Wang Building under Typhoon York Using the Hilbert-huang Transform Method'. *The Structural Design of Tall and Special Buildings*, 12, 21-47 (2003), Published online in Wiley InterScience.

Yam, L.H., Yan, Y.J. & Jiang, J.S. 2003, 'Vibration-based damage detection for composite structures using wavelet transform and neural network identification', *Composite Structures*, 60 (2003) 403-412.

Yang, J.N., Lei, Y., Lin, S. & Huang, N. 2004, 'Hilbert-Huang based approach for structural damage detection', *Journal of Engineering Mechanics*, vol. 130, no. 1, pp. 85-95.

Yankelevsky, D. Z. 1985, New finite element for bond-slip analysis', *Journal of Structural engineering*, vol. 111, no. 7, July, 1985 pp. 1533-1542.

Yousaf, E., 2007, Master of Science Thesis, 'Output only modal analysis', Department of Mechanical Engineering, Blekinge Institute of Technology, Karslkrona, Sweden: pp 64.

Zanardo, G., Hao, H., Xia, Y. & Deeks, A.J. 2007, 'Evaluation of the effectiveness of strengthening intervention by CFRP on MRWA Bridge', *Journal of Composites for Construction*, No. 3014,11(4): 363-374.

Zembaty, Z., Kowalski, M. & Pospisil, S. 2006, 'Dynamic Identification of a Reinforced Concrete Frame in Progressive States of Damage', *Engineering Structures*, 28 (2006) 668-681.

Zhang, R.R., Ma, S., Safak, E. & Hartzell, S. 2003, 'Hilbert-Huang Transform Analysis of Dynamic and Earthquake Motion Recordings'. *Journal of Engineering Mechanics*, Vol. 129, NO. 8, August 1, 2003. 861-875.

Zhong, S. & Oyadiji, S.O. 2007, 'Crack Detection in Simply Supported Beams without Baseline Modal Parameters by Stationary Wavelet Transfrom'. *Mechanical Systems and Signal Processing* , 21 (2007) 1853-1884.

Zhou, L.L. & Yan, G. 2006, 'HHT method for system identification and damage detection: an experimental study'. *Smart Structures and System*, Vol. 2, No. 2 (2006) 141-154.

Zhu, H.P. & Xu, Y.L. 2005, 'Damage detection of mono-coupled periodic structures based on sensitivity analysis of modal parameters'. *Journal of Sound and Vibration*, 285, 365-390.

Zhu, X.Q. & Law, S.S. 2007, 'Nonlinear Characteristics of Damaged Reinforced Concrete Beam from Hilbert-Huang Transform'. *Journal of Structure Engineering*, Vol. 133, No. 8, August 1, 2007. 1186-1191.

Zou, Y., Tong, L. & Steven, G.P. 2000, 'Vibration-based model-dependent damage (delamination) identification and health monitoring for composite structures- A review', *Journal of Sound and Vibration*, vol. 230, no. 2, pp. 357-378.

Zwonlinski, B. 1998, *Notes of vibration measurements*, Kistle Instrument Corporation.

APPENDICES

APPENDIX A: Measured Strain Data and Estimated Strain Data

Table A1 Compression strain of concrete at middle span ($\times 10^{-6}$) (C2)

Load (kN)	Measured	Estimated	Difference
5	-75	-86.9	-13.6%
10	-205	-219.8	-6.7%
15	-359	-378.3	-5.1%
20	-472	-499.1	-5.4%
25	-575	-606.3	-5.2%
30	-681	-726.4	-6.3%
35	-782	-863.7	-9.5%
40	-880	-964.0	-8.7%
45	-978	-1068.9	-8.5%
50	-1078	-1189.7	-9.4%
55	-1168	-1293.3	-9.7%
60	-1272	-1447.9	-12.1%
65	-1391	-2104.3	-33.9%
70	-1505	-2379.2	-36.7%
75	-1645	-2724.7	-39.6%
80	-1826	-3208.7	-43.1%

Table A2 Tension strain of reinforced steel at middle span ($\times 10^{-6}$) (S5)

Load (kN)	Measured	Estimated	Difference
5	129	120.1	7.4%
10	394	382.9	2.9%
15	785	770.6	1.9%
20	1055	1034.7	2.0%
25	1277	1253.6	1.9%
30	1559	1524.9	2.2%
35	1936	1874.7	3.3%
40	2152	2089.0	3.0%
45	2401	2332.8	2.9%
50	2715	2631.2	3.2%
55	3016	2922.0	3.2%
60	3502	3370.1	3.9%
65	6207	5672.1	9.4%
70	7263	6607.3	9.9%
75	8652	7842.2	10.3%
80	10737	9699.9	10.7%

Table A3 Tension strain of reinforced steel at middle span ($\times 10^{-6}$) (S6)

Load (kN)	Measured	Estimated	Difference
5	86	91.9	-6.4%
10	396	403.4	-1.8%
15	797	806.6	-1.2%
20	1028	1041.6	-1.3%
25	1227	1242.6	-1.3%
30	1435	1457.7	-1.6%
35	1631	1671.9	-2.4%
40	1826	1868.0	-2.2%
45	2022	2067.4	-2.2%
50	2230	2285.9	-2.4%
55	2452	2514.7	-2.5%
60	2697	2784.9	-3.2%
65	2974	3330.6	-10.7%
70	3301	3738.1	-11.7%
75	3780	4319.9	-12.5%
80	4550	5241.4	-13.2%

Table A4 Compression strain of concrete at quarter span ($\times 10^{-6}$) (C1)

Load (kN)	Measured	Estimated	Difference
5.0	-32.0	-28.4	12.8%
10.0	-73.0	-80.2	-9.0%
15.0	-111.0	-162.4	-31.7%
20.0	-145.0	-219.7	-34.0%
25.0	-185.0	-270.6	-31.6%
30.0	-228.0	-324.8	-29.8%
35.0	-281.0	-381.3	-26.3%
40.0	-330.0	-434.4	-24.0%
45.0	-379.0	-491.4	-22.9%
50.0	-432.0	-551.2	-21.6%
55.0	-479.0	-598.7	-20.0%
60.0	-535.0	-665.8	-19.6%
65.0	-591.0	-730.0	-19.0%
70.0	-648.0	-795.2	-18.5%
75.0	-699.0	-860.2	-18.7%
80.0	-759.0	-934.6	-18.8%

Table A5 Tension strain of reinforced steel at quarter span ($\times 10^{-6}$) (S3)

Load (kN)	Measured	Estimated	Difference
5.0	47.0	49.7	-5.5%
10.0	120.0	114.6	4.7%
15.0	361.0	322.4	12.0%
20.0	546.0	489.9	11.4%
25.0	726.0	661.8	9.7%
30.0	889.0	816.4	8.9%
35.0	1045.0	969.8	7.8%
40.0	1194.0	1115.7	7.0%
45.0	1354.0	1269.7	6.6%
50.0	1524.0	1434.6	6.2%
55.0	1699.0	1609.2	5.6%
60.0	1901.0	1802.9	5.4%
65.0	2114.0	2009.8	5.2%
70.0	2329.0	2218.6	5.0%
75.0	2609.0	2488.1	4.9%
80.0	2933.0	2801.3	4.7%

Table A6 Tension strain of reinforced steel at quarter span ($\times 10^{-6}$) (S4)

Load (kN)	Measured	Estimated	Difference
5.0	36.0	34.2	5.3%
10.0	63.0	66.6	-5.4%
15.0	100.0	125.7	-20.4%
20.0	207.0	244.4	-15.3%
25.0	396.0	438.8	-9.8%
30.0	559.0	607.4	-8.0%
35.0	721.0	771.1	-6.5%
40.0	869.0	921.2	-5.7%
45.0	1017.0	1073.2	-5.2%
50.0	1175.0	1234.6	-4.8%
55.0	1345.0	1404.9	-4.3%
60.0	1516.0	1581.4	-4.1%
65.0	1701.0	1770.5	-3.9%
70.0	1894.0	1967.6	-3.7%
75.0	2160.0	2240.6	-3.6%
80.0	2474.0	2561.8	-3.4%

APPENDIX B

B.1 Results of Damage Detection without Noise (Single Damage)

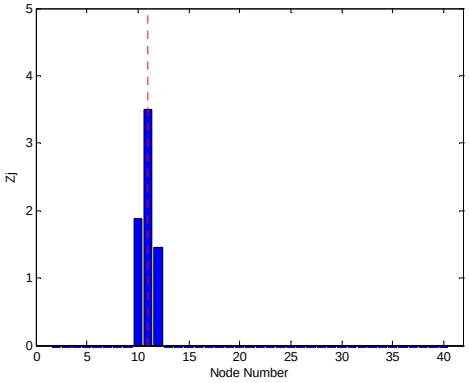

(a) Mode 1

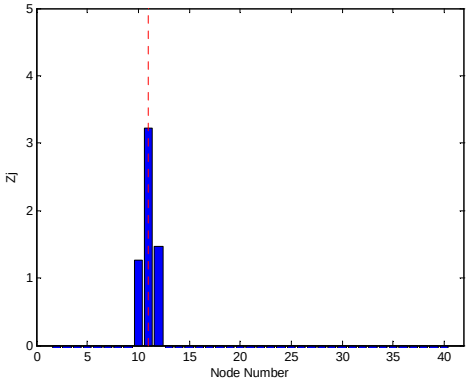

(b) Modes 1+2

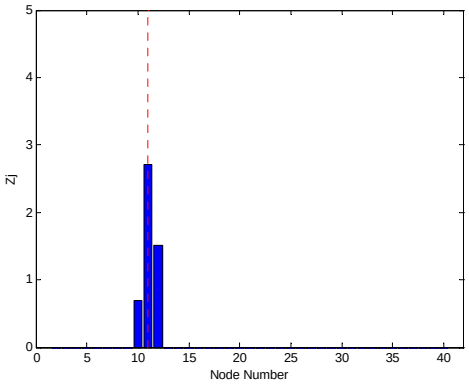

(c) Modes 1+2+3

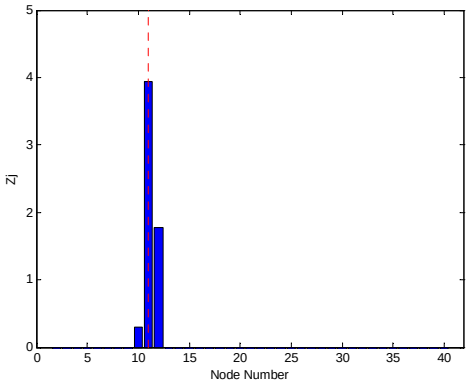

(d) Modes 1+2+3+4

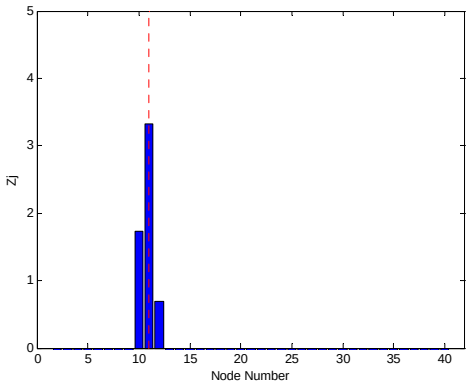

(e) Modes 1+2+3+4+5

Damage Detection without Noise (2L)

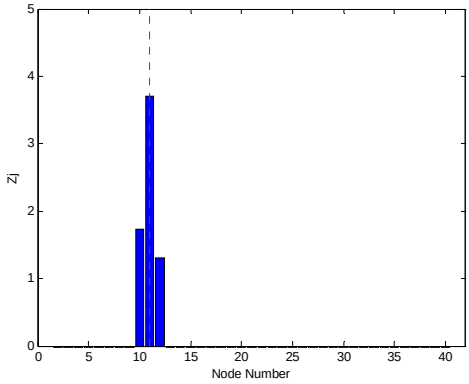

(a) Mode 1

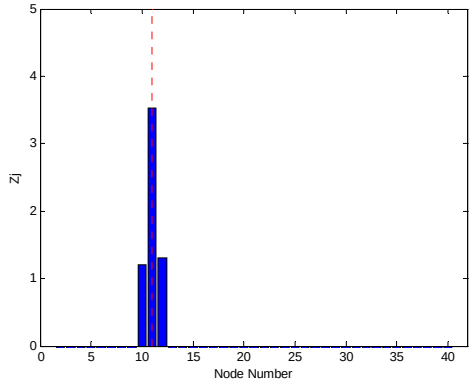

(b) Modes 1+2

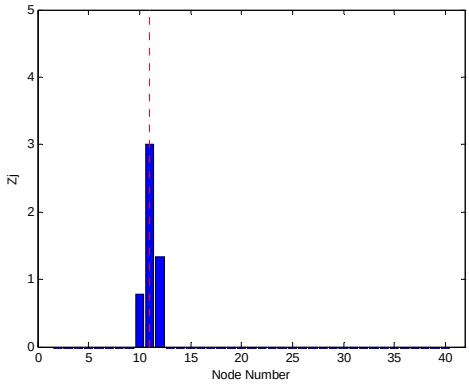

(c) Modes 1+2+3

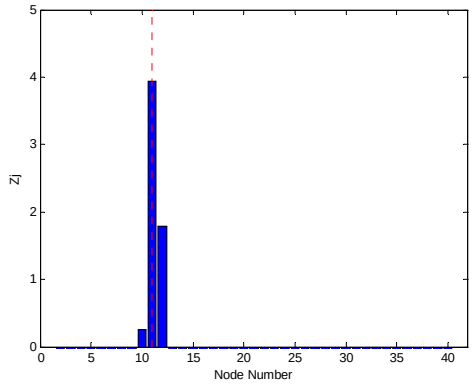

(d) Modes 1+2+3+4

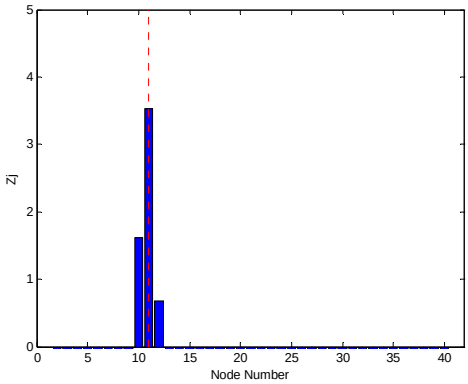

(e) Modes 1+2+3+4+5

Damage Detection without Noise (2M)

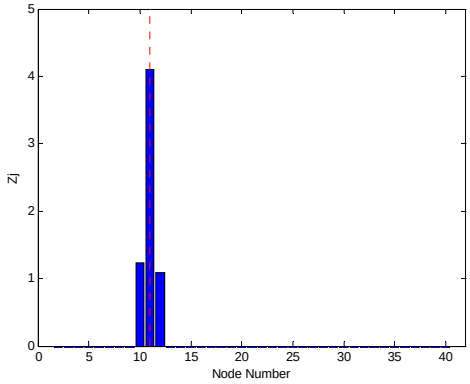

(a) Mode 1

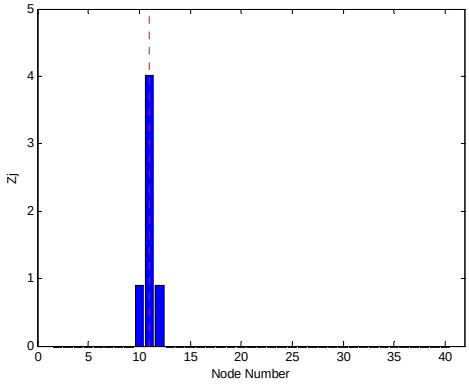

(b) Modes 1+2

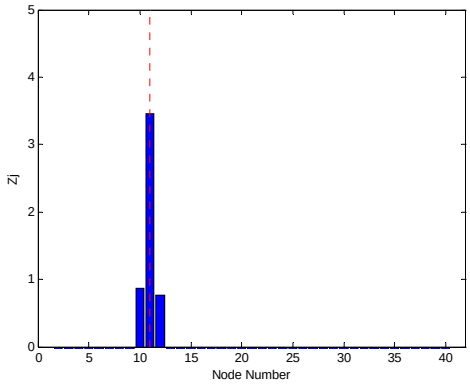

(c) Modes 1+2+3

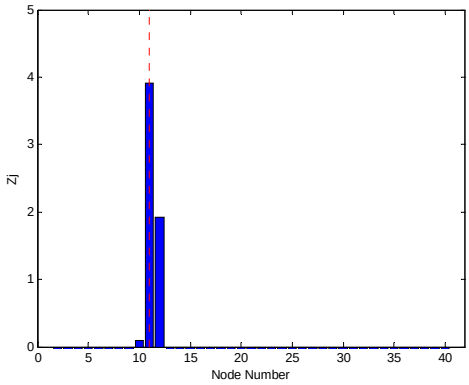

(d) Modes 1+2+3+4

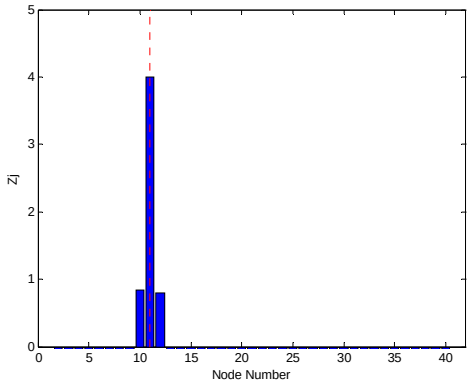

(e) Modes 1+2+3+4+5

Damage Detection without Noise (2S)

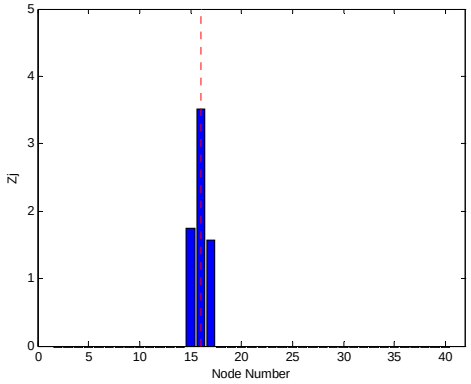

(a) Mode 1

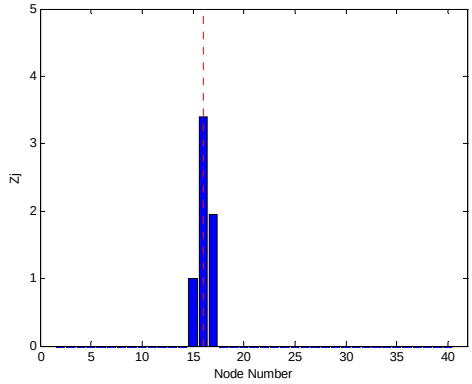

(b) Modes 1+2

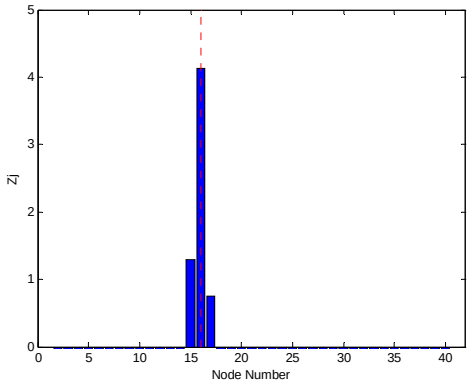

(c) Modes 1+2+3

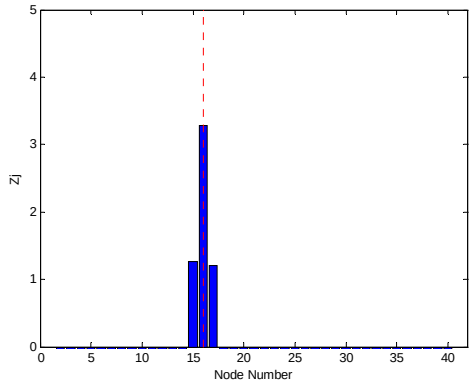

(d) Modes 1+2+3+4

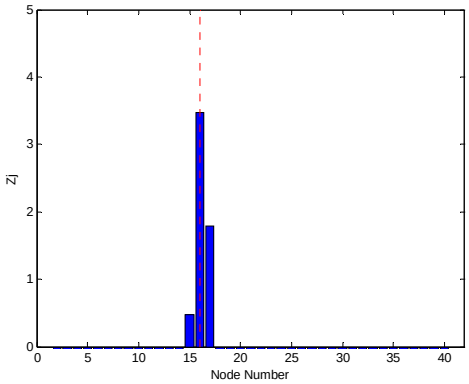

(e) Modes 1+2+3+4+5

Damage Detection without Noise (3L)

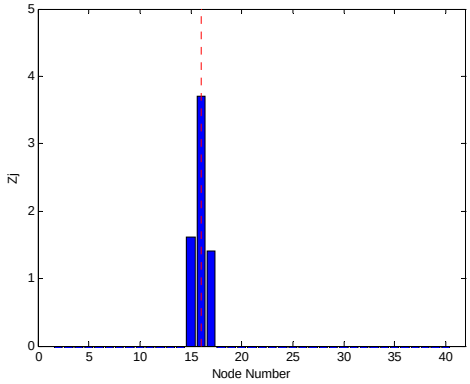

(a) Mode 1

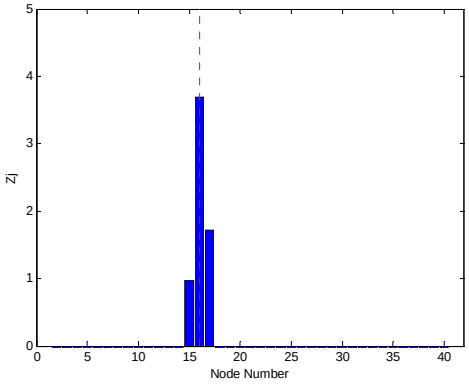

(b) Modes 1+2

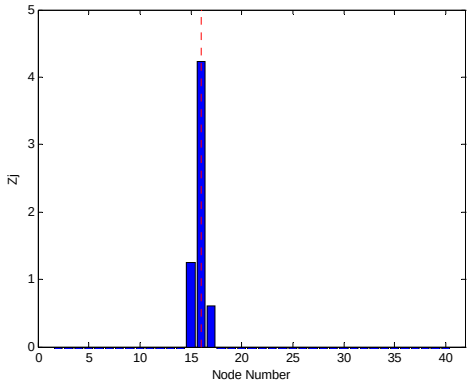

(c) Modes 1+2+3

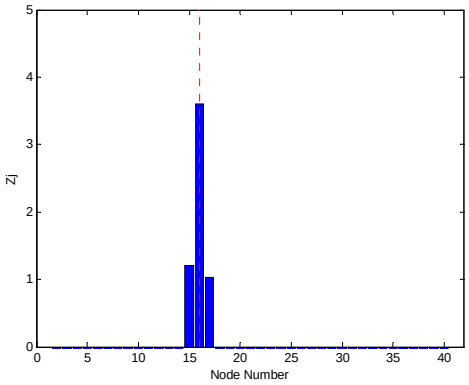

(d) Modes 1+2+3+4

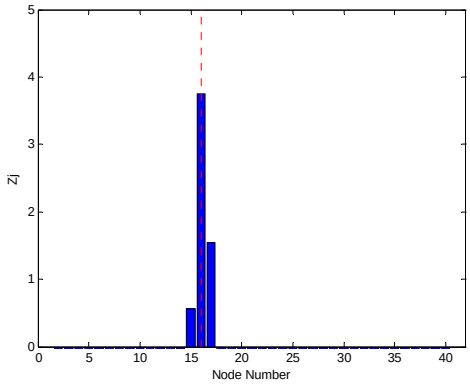

(e) Modes 1+2+3+4+5

Damage Detection without Noise (3M)

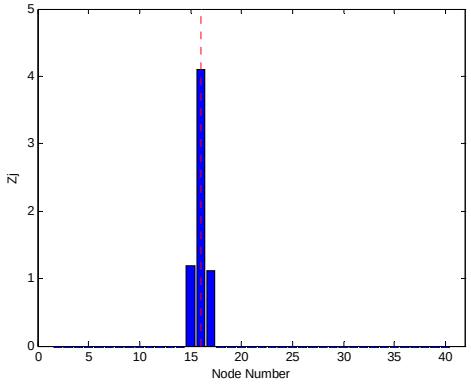

(a) Mode 1

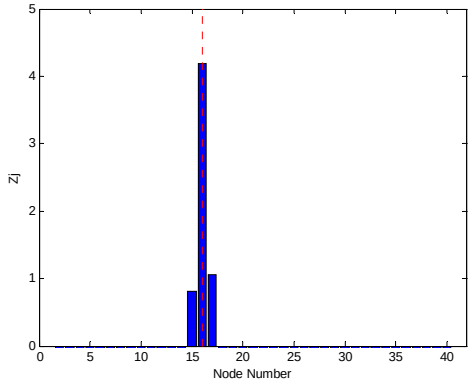

(b) Modes 1+2

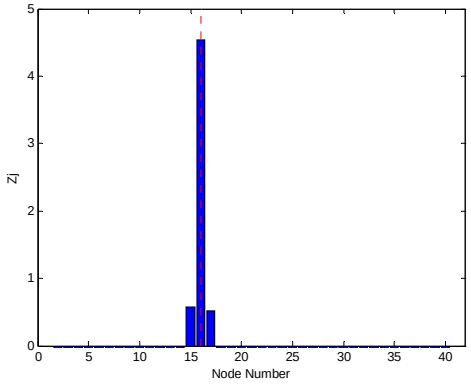

(c) Modes 1+2+3

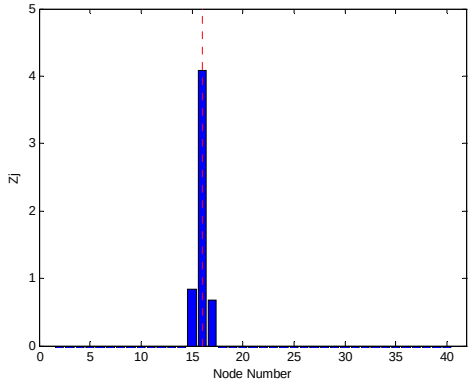

(d) Modes 1+2+3+4

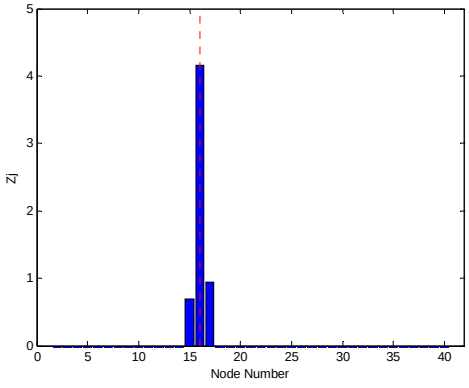

(e) Modes 1+2+3+4+5

Damage Detection without Noise (3S)

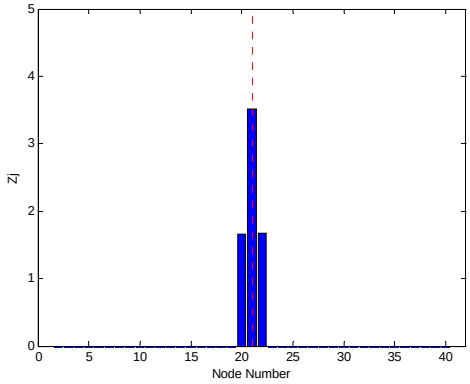

(a) Mode 1

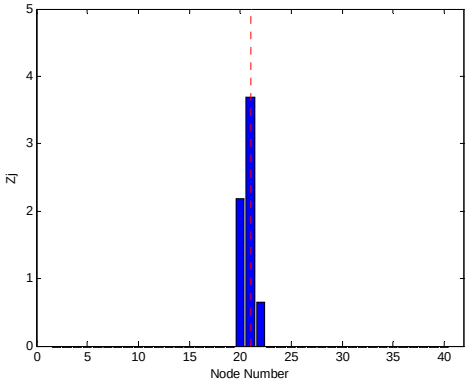

(b) Modes 1+2

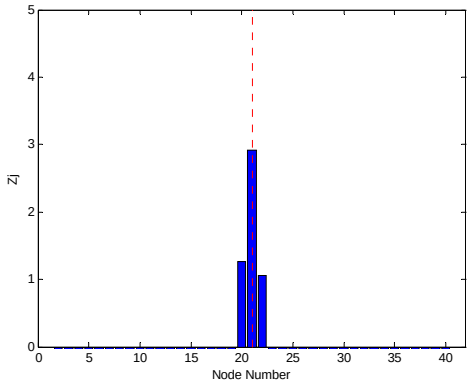

(c) Modes 1+2+3

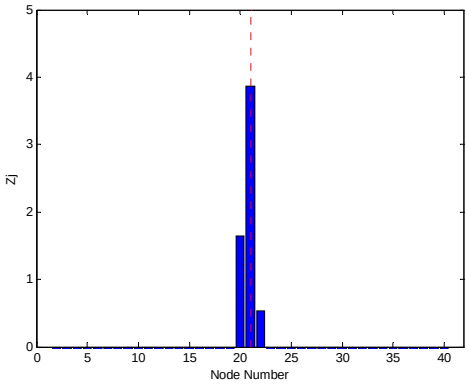

(d) Modes 1+2+3+4

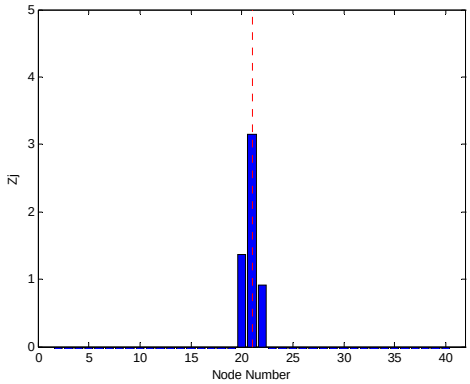

(e) Modes 1+2+3+4+5

Damage Detection without Noise (4L)

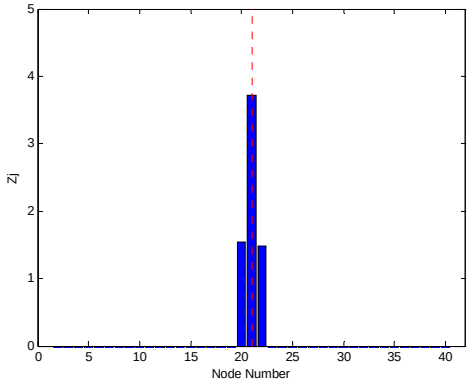

(a) Mode 1

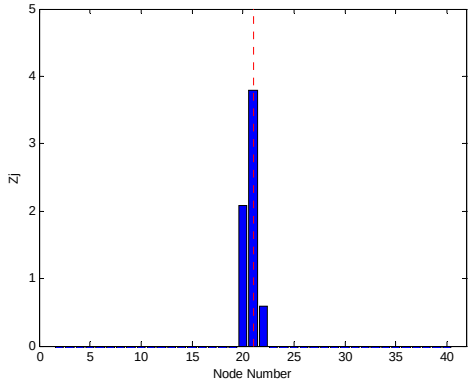

(b) Modes 1+2

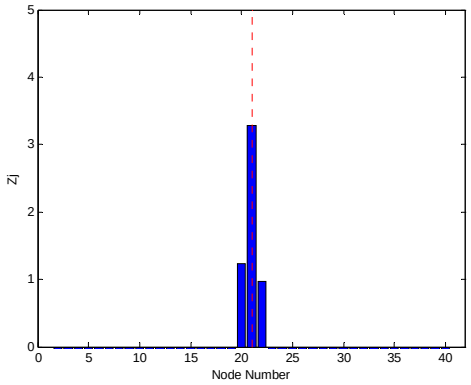

(c) Modes 1+2+3

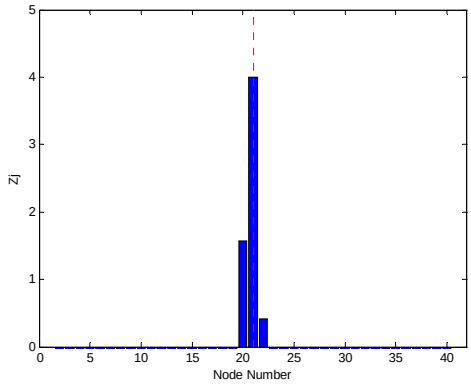

(d) Modes 1+2+3+4

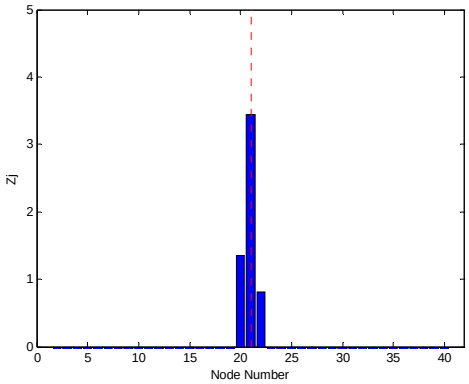

(e) Modes 1+2+3+4+5

Damage Detection without Noise (4M)

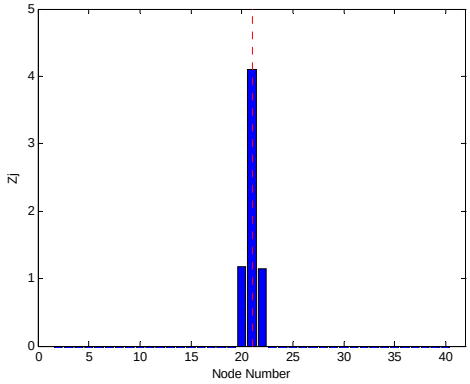

(a) Mode 1

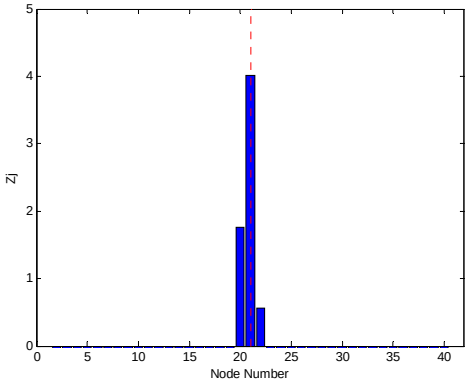

(b) Modes 1+2

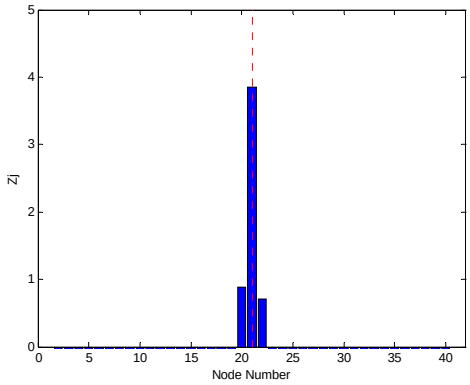

(c) Modes 1+2+3

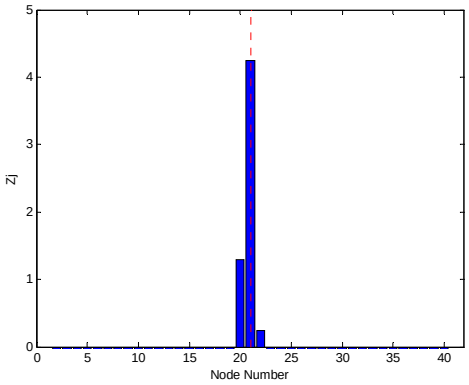

(d) Modes 1+2+3+4

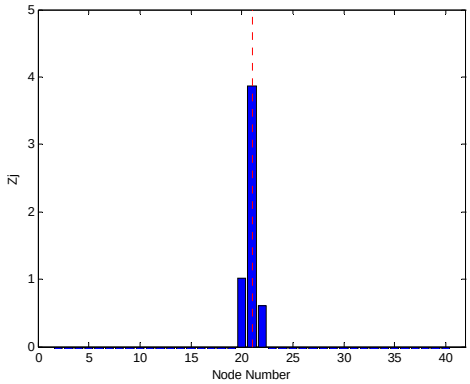

(e) Modes 1+2+3+4+5

Damage Detection without Noise (4S)

B.2 Results of Damage Detection without Noise (Multiple Damage)

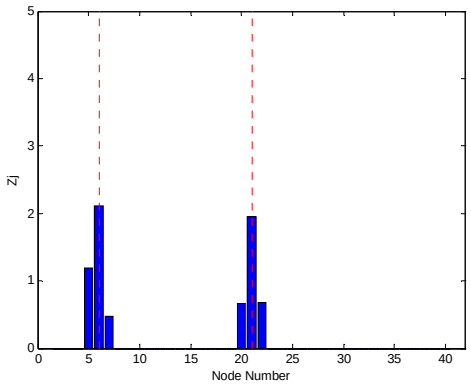

(a) Mode 1

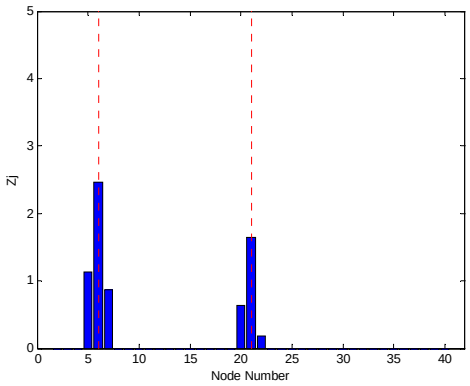

(b) Modes 1+2

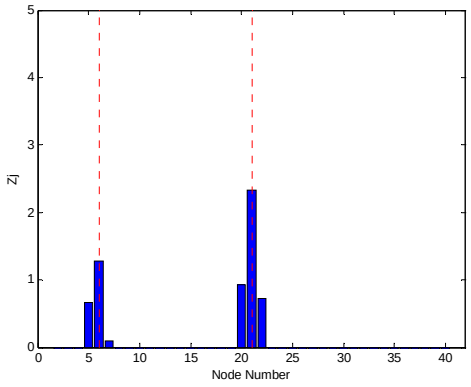

(c) Modes 1+2+3

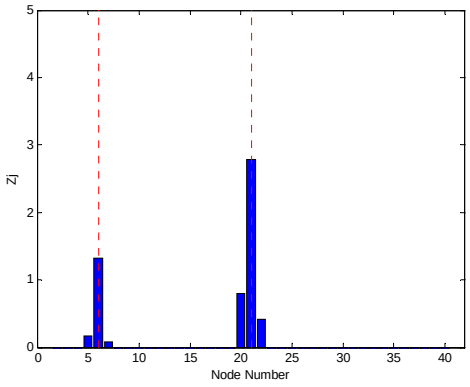

(d) Modes 1+2+3+4

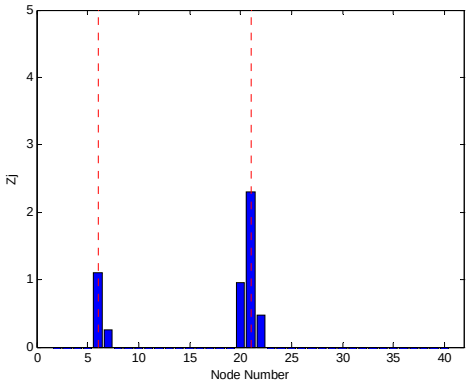

(e) Modes 1+2+3+4+5

Damage Detection without Noise (1L4L)

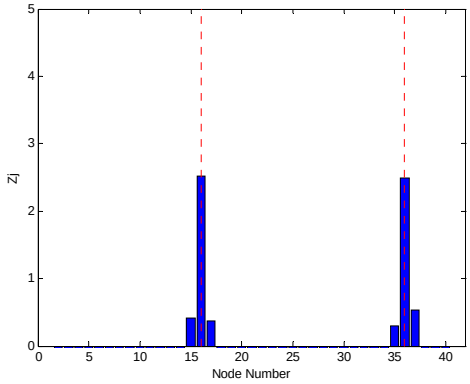

(a) Mode 1

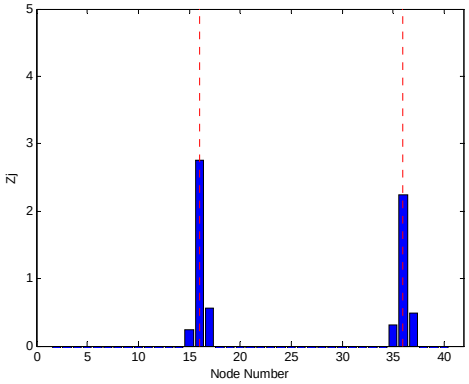

(b) Modes 1+2

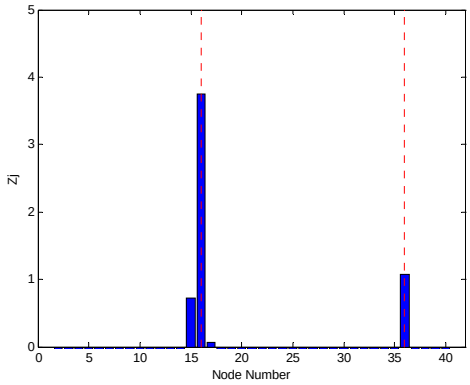

(c) Modes 1+2+3

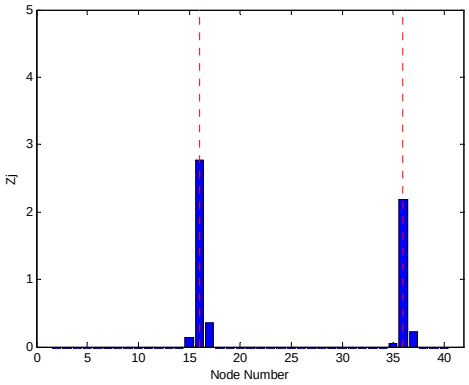

(d) Modes 1+2+3+4

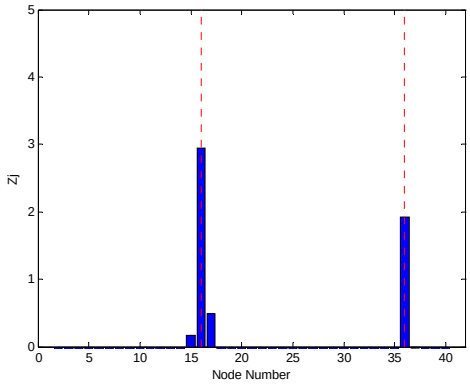

(e) Modes 1+2+3+4+5

Damage Detection without Noise (3S7S)

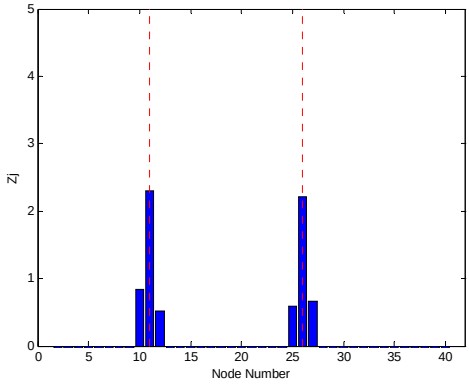

(a) Mode 1

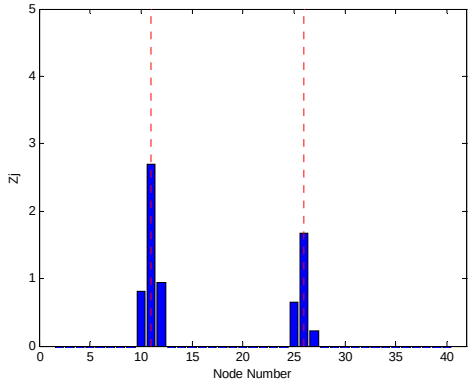

(b) Modes 1+2

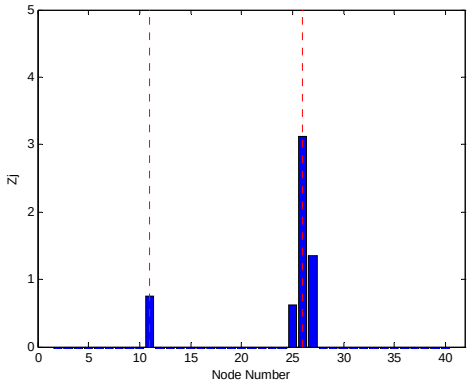

(c) Modes 1+2+3

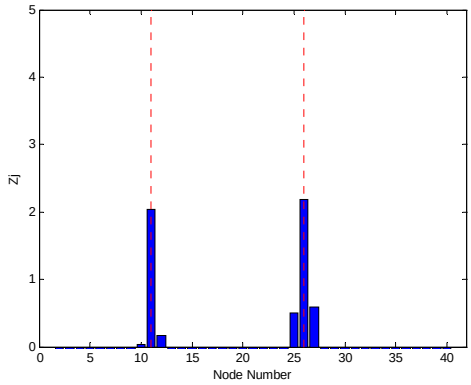

(d) Modes 1+2+3+4

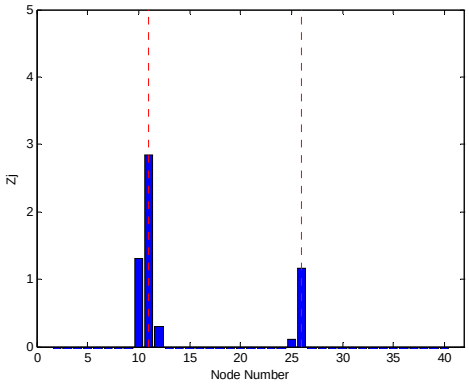

(e) Modes 1+2+3+4+5

Damage Detection without Noise (2M5M)

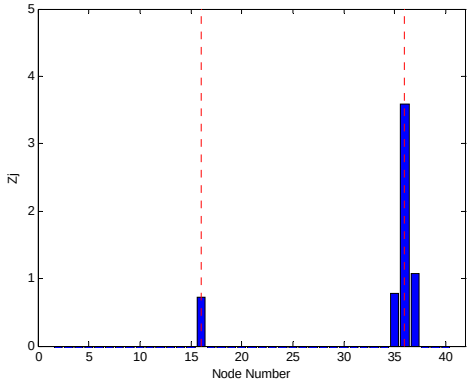

(a) Mode 1

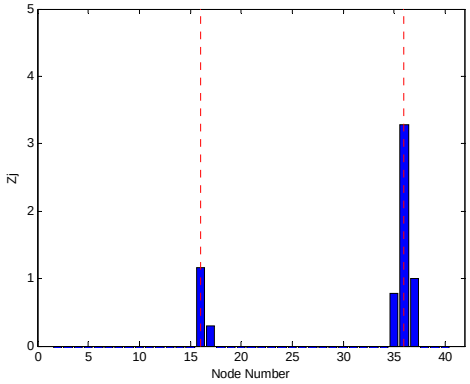

(b) Modes 1+2

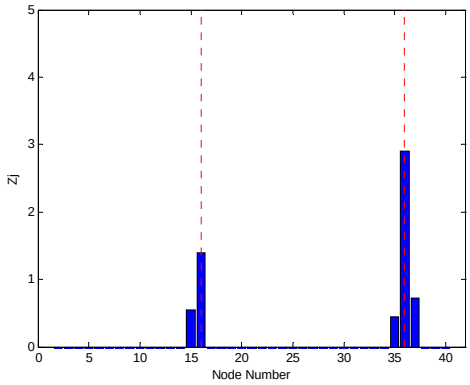

(c) Modes 1+2+3

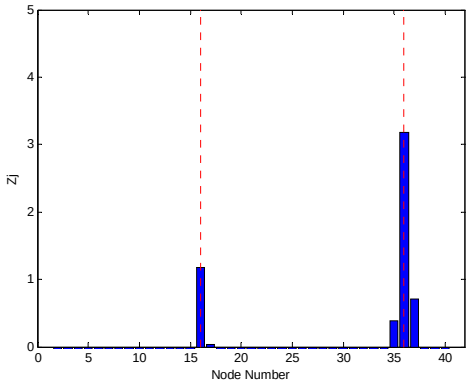

(d) Modes 1+2+3+4

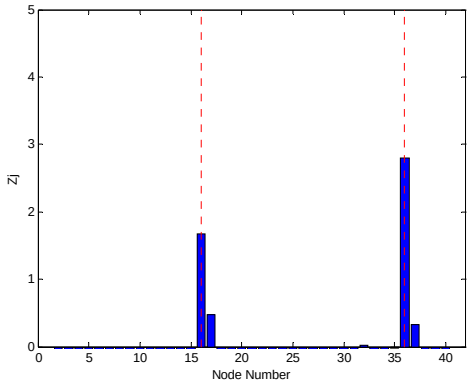

(e) Modes 1+2+3+4+5

Damage Detection without Noise (3M7S)

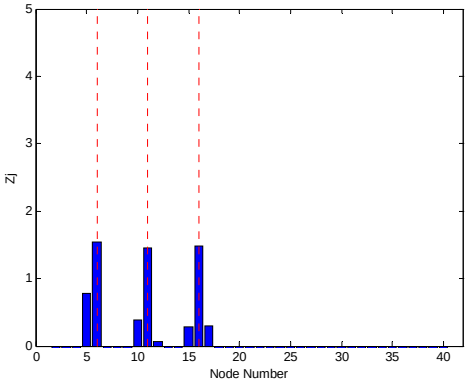

(a) Mode 1

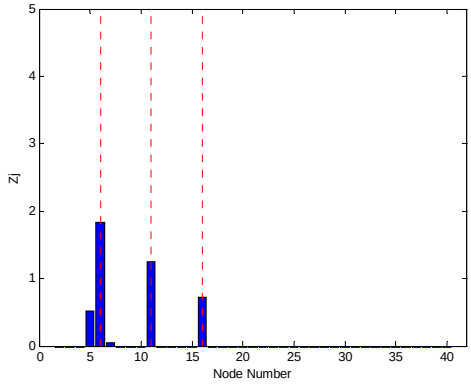

(b) Modes 1+2

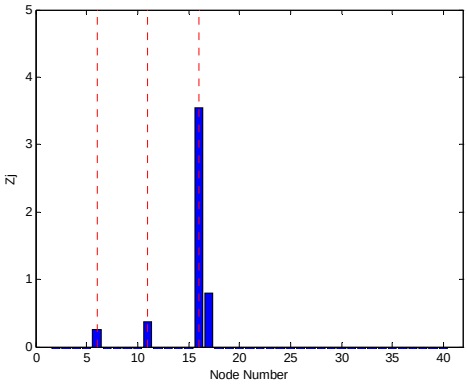

(c) Modes 1+2+3

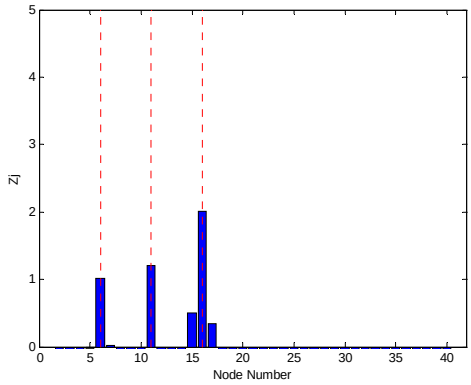

(d) Modes 1+2+3+4

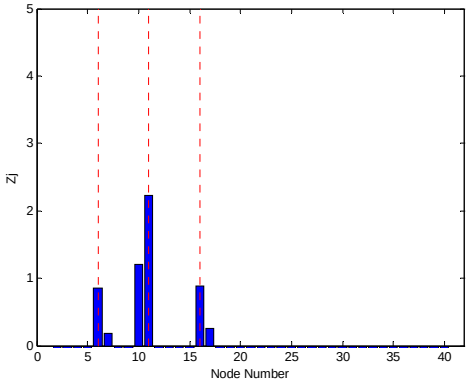

(e) Modes 1+2+3+4+5

Damage Detection without Noise (1L2L3L)

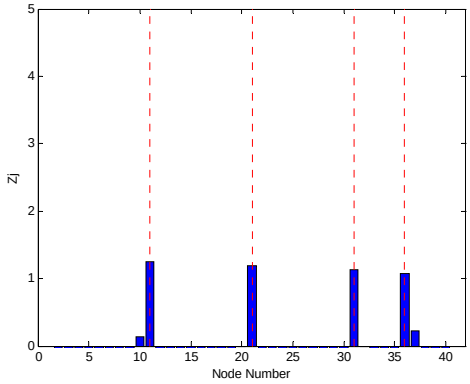

(a) Mode 1

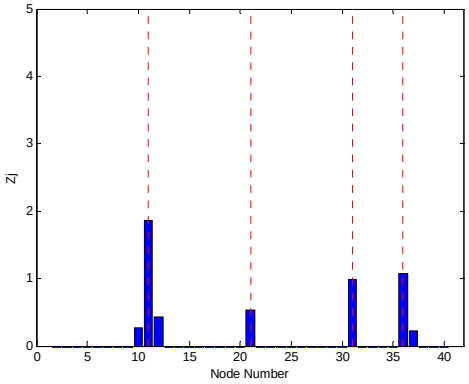

(b) Modes 1+2

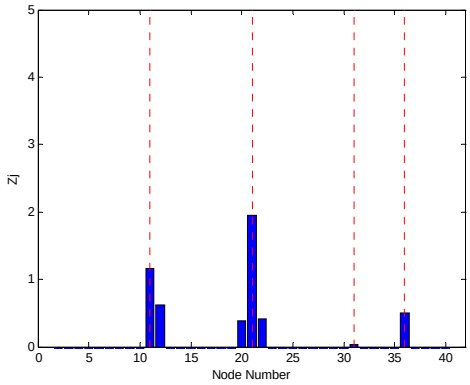

(c) Modes 1+2+3

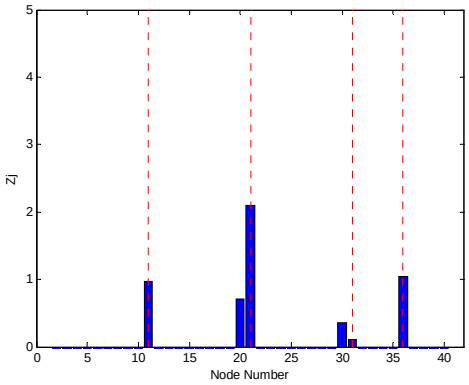

(d) Modes 1+2+3+4

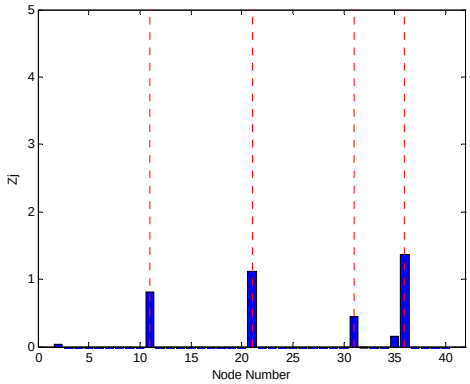

(e) Modes 1+2+3+4+5

Damage Detection without Noise (2M4M6M7M)

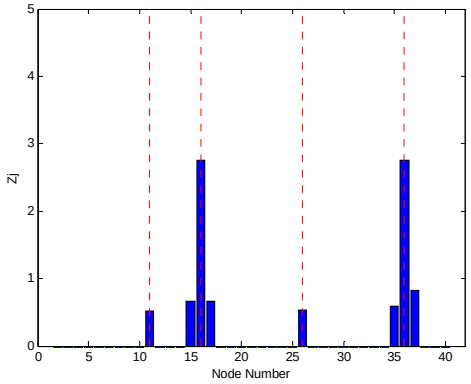

(a) Mode 1

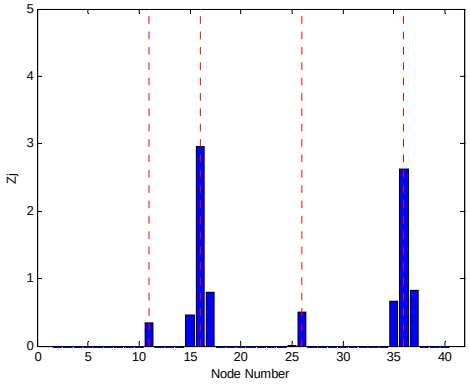

(b) Modes 1+2

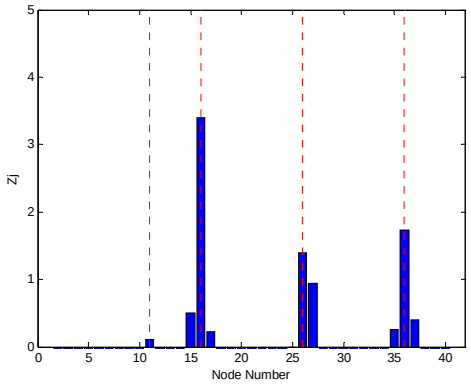

(c) Modes 1+2+3

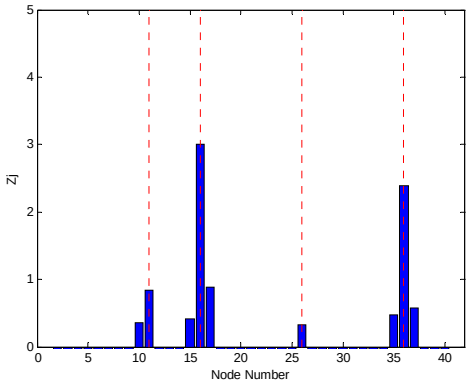

(d) Modes 1+2+3+4

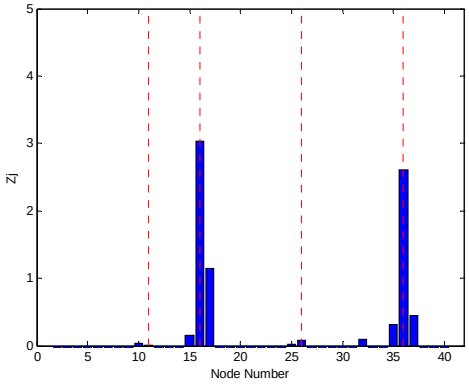

(e) Modes 1+2+3+4+5

Damage Detection without Noise (2M3S5M7S)

B.3 Results of Damage Detection without Noise (Honeycomb Damage)

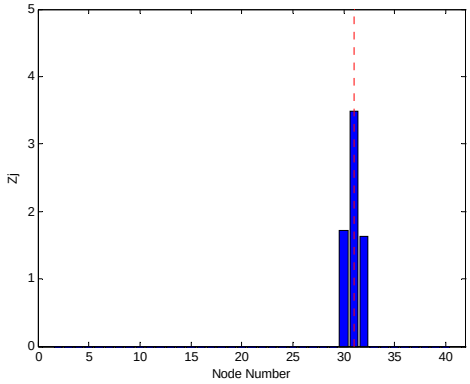

(a) Mode 1

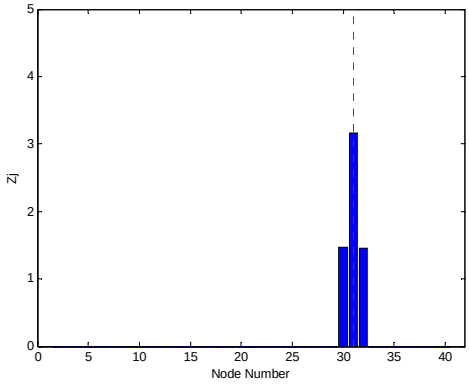

(b) Modes 1+2

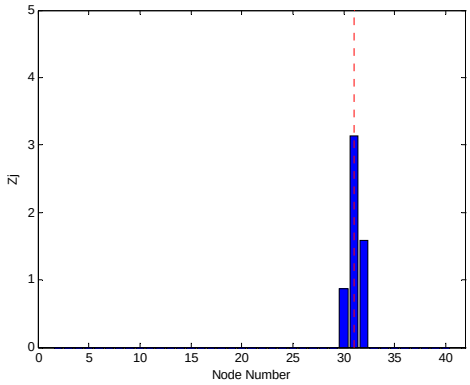

(c) Modes 1+2+3

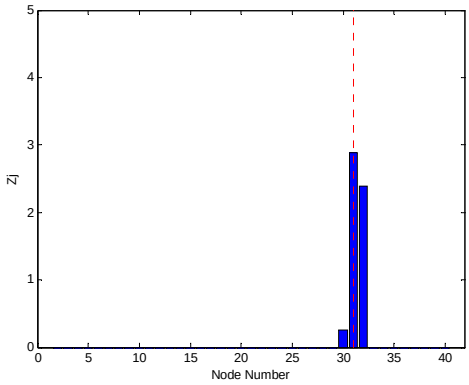

(d) Modes 1+2+3+4

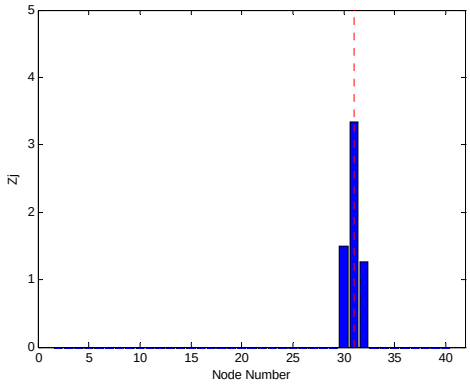

(e) Modes 1+2+3+4+5

Damage Detection without Noise (HB)

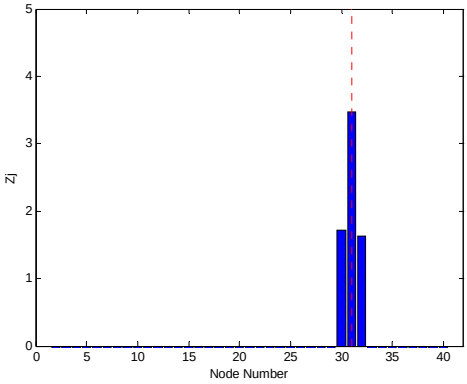

(a) Mode 1

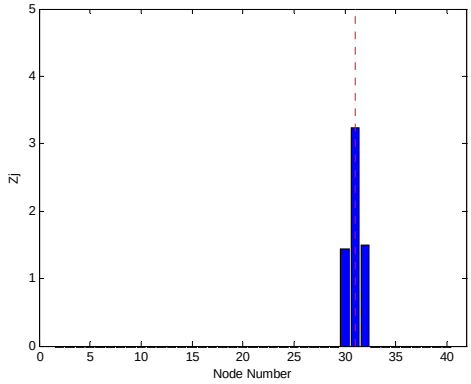

(b) Modes 1+2

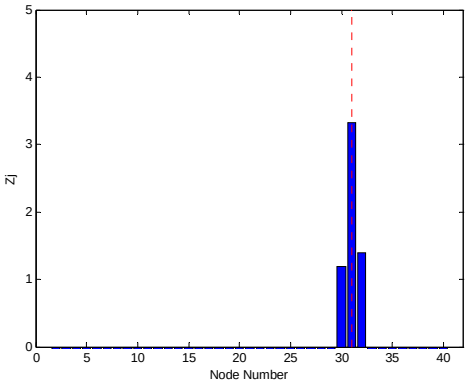

(c) Modes 1+2+3

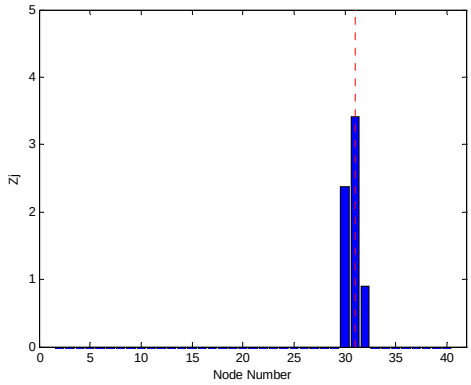

(d) Modes 1+2+3+4

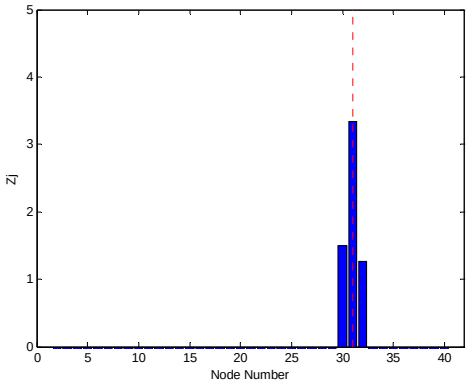

(e) Modes 1+2+3+4+5

Damage Detection without Noise (HT)

B.4 Results of Damage Detection Subjected to Simulated Noise

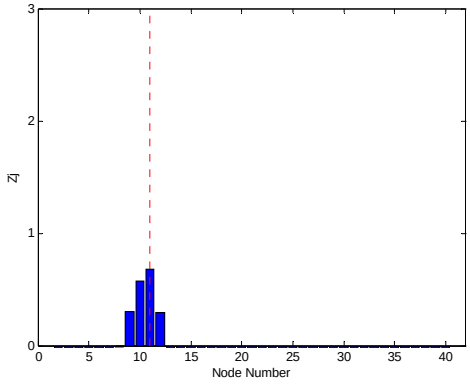

(a) Mode 1

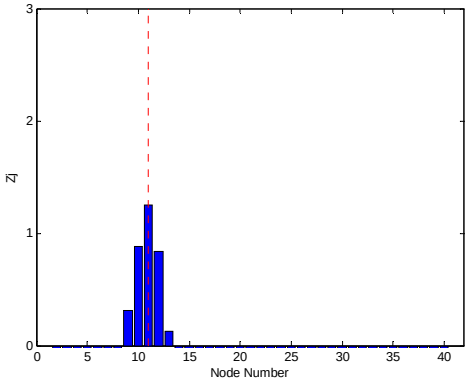

(b) Modes 1+2

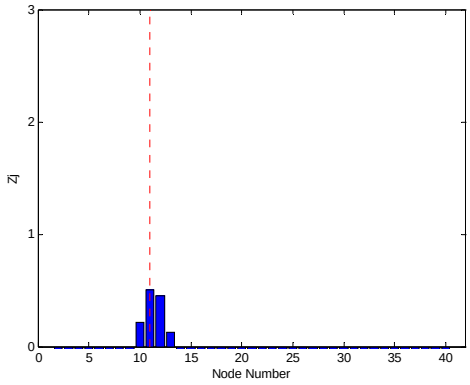

(c) Modes 1+2+3

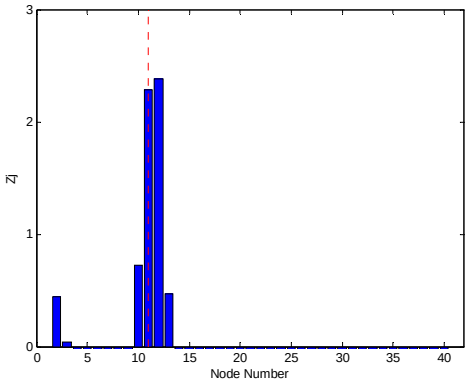

(d) Modes 1+2+3+4

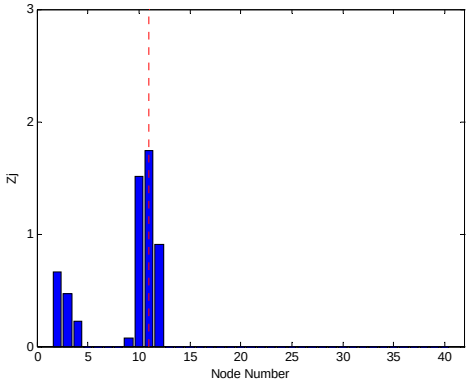

(e) Modes 1+2+3+4+5

Damage Detection with Noise (2L with 0% noise)

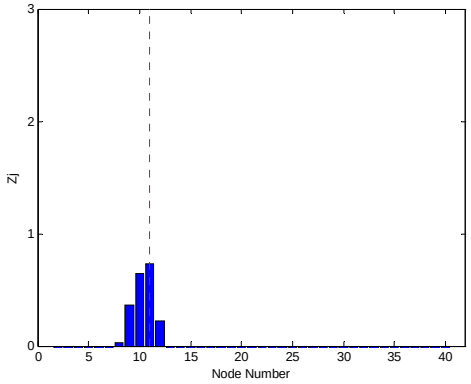

(a) Mode 1

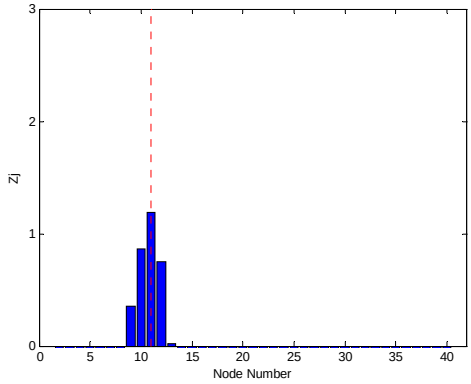

(b) Modes 1+2

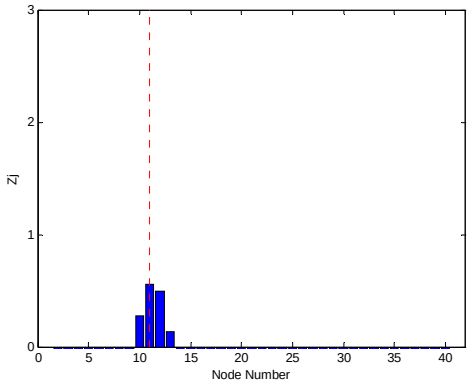

(c) Modes 1+2+3

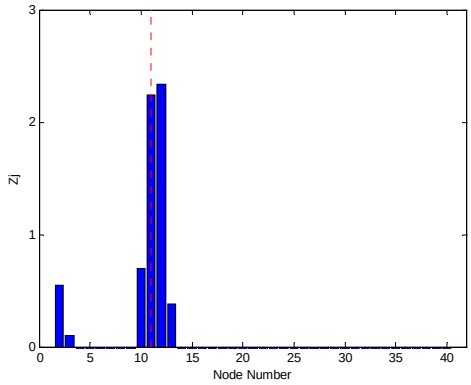

(d) Modes 1+2+3+4

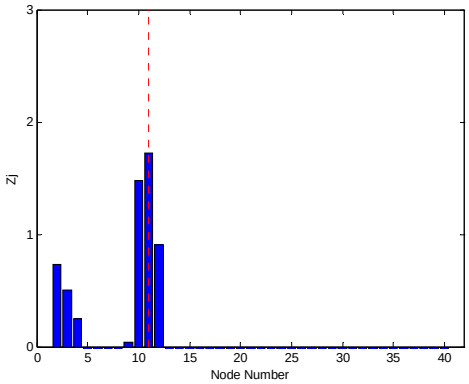

(e) Modes 1+2+3+4+5

Damage Detection with Noise (2L with 2% noise)

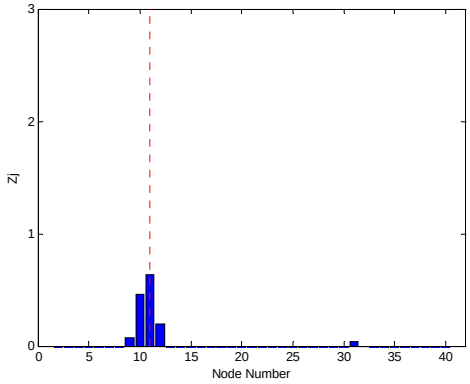

(a) Mode 1

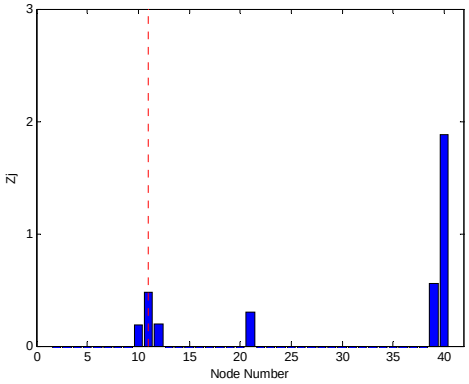

(b) Modes 1+2

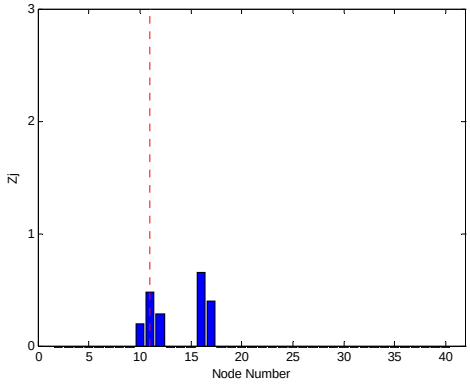

(c) Modes 1+2+3

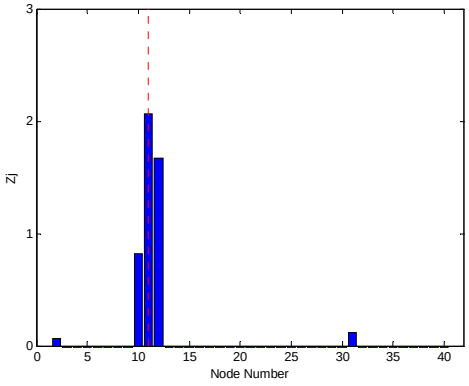

(d) Modes 1+2+3+4

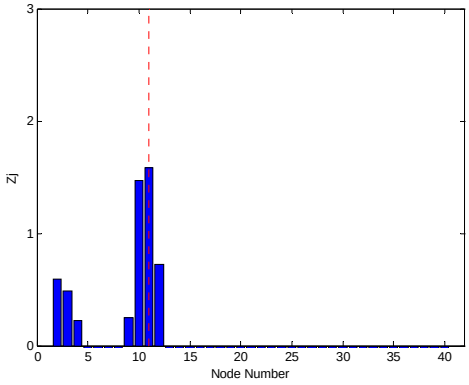

(e) Modes 1+2+3+4+5

Damage Detection with Noise (2L with 10% noise)

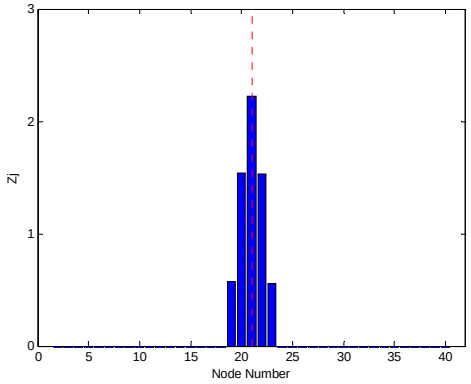

(a) Mode 1

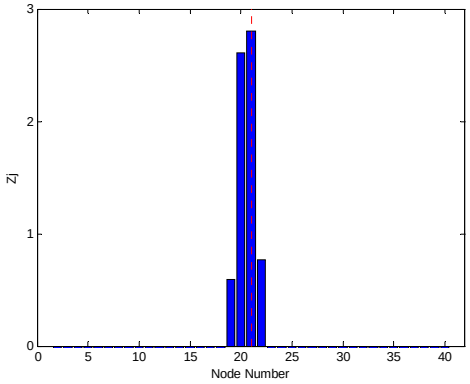

(b) Modes 1+2

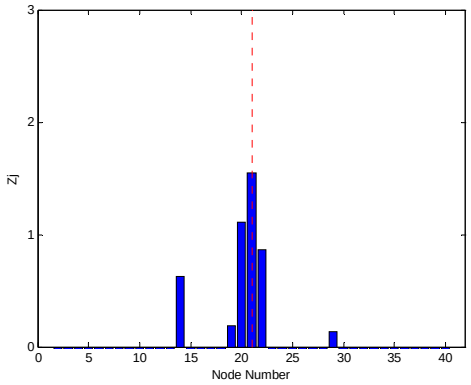

(c) Modes 1+2+3

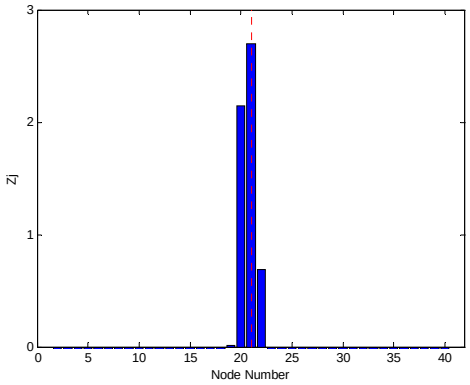

(d) Modes 1+2+3+4

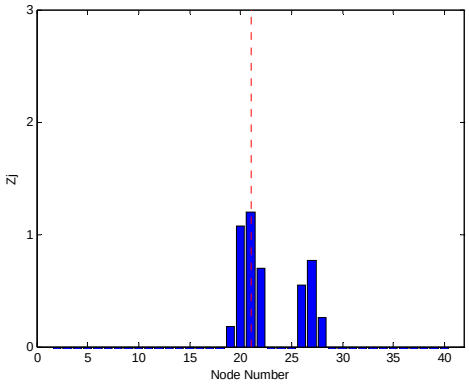

(e) Modes 1+2+3+4+5

Damage Detection with Noise (4M with 0% noise)

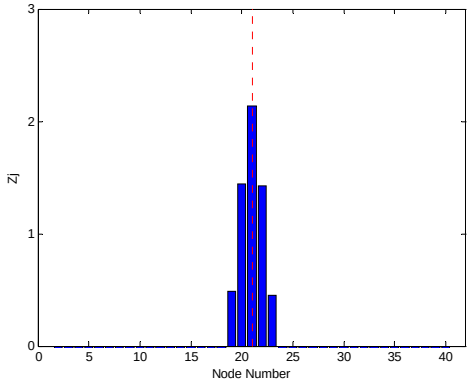

(a) Mode 1

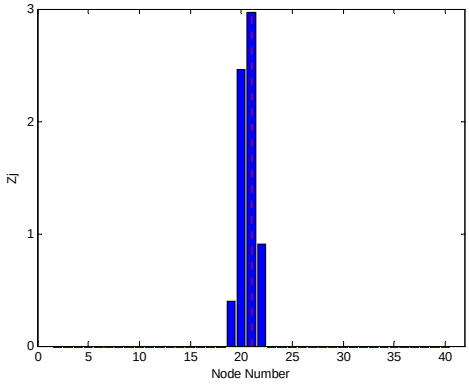

(b) Modes 1+2

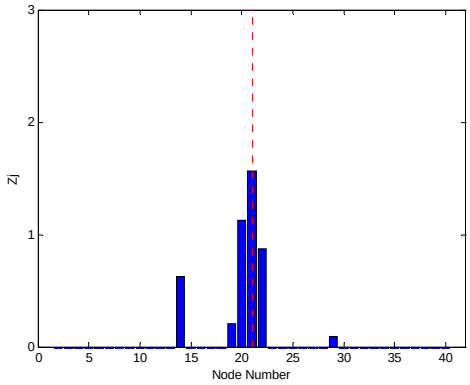

(c) Modes 1+2+3

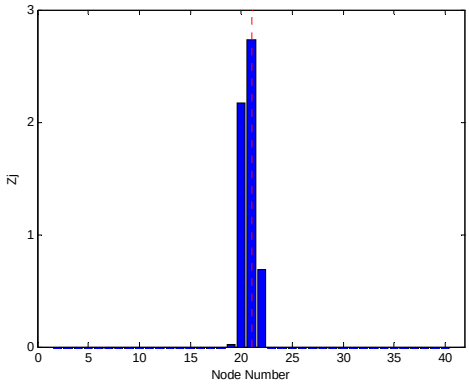

(d) Modes 1+2+3+4

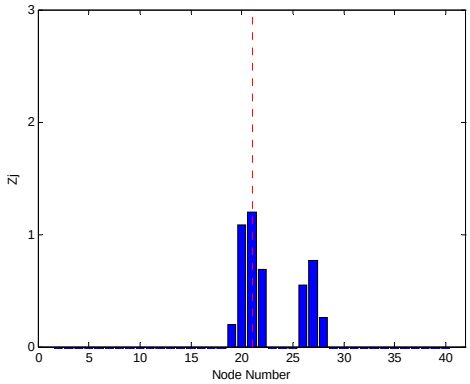

(e) Modes 1+2+3+4+5

Damage Detection with Noise (4M with 2% noise)

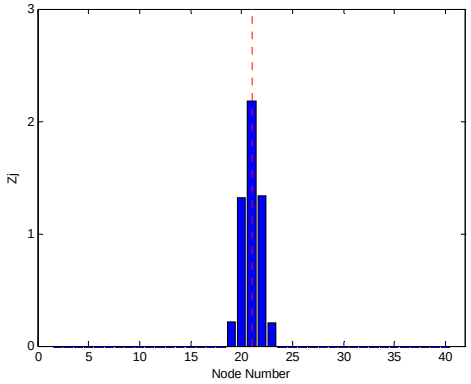

(a) Mode 1

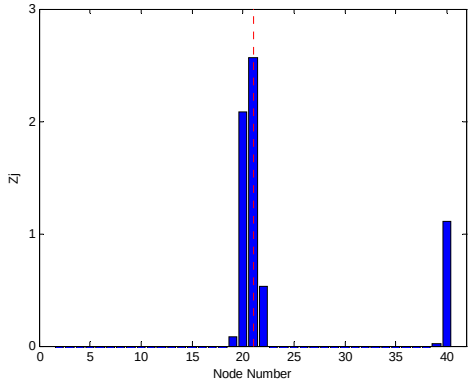

(b) Modes 1+2

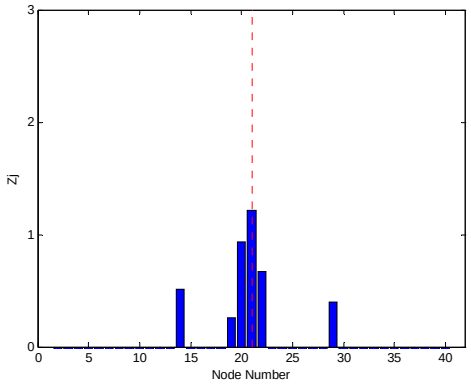

(c) Modes 1+2+3

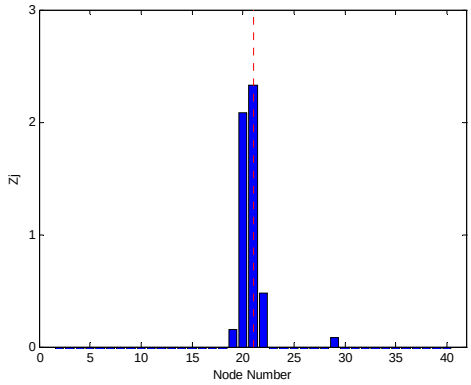

(d) Modes 1+2+3+4

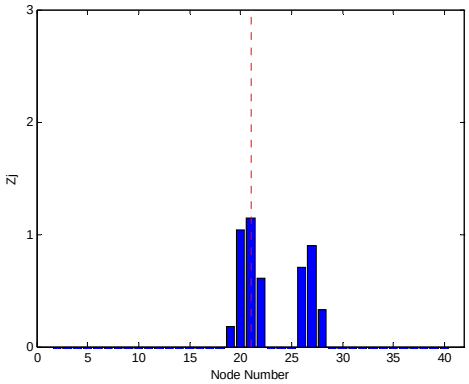

(e) Modes 1+2+3+4+5

Damage Detection with Noise (4M with 10% noise)

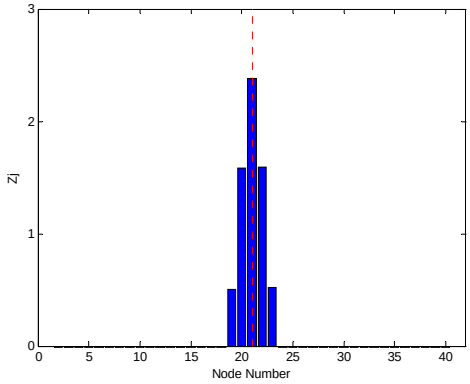

(a) Mode 1

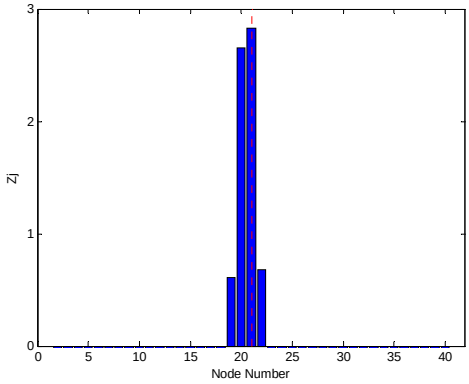

(b) Modes 1+2

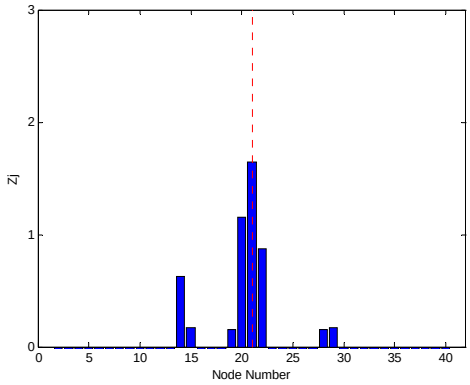

(c) Modes 1+2+3

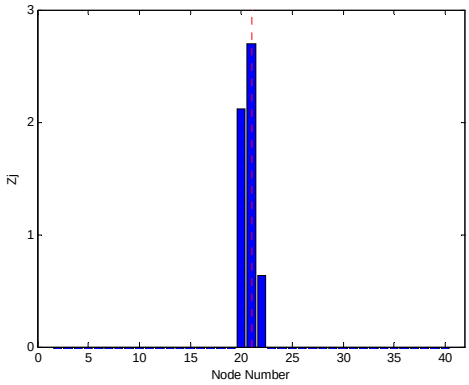

(d) Modes 1+2+3+4

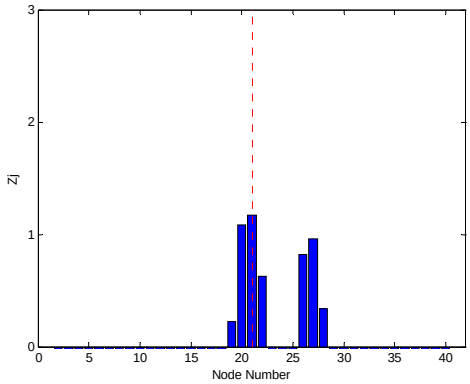

(e) Modes 1+2+3+4+5

Damage Detection with Noise (4S with 0% noise)

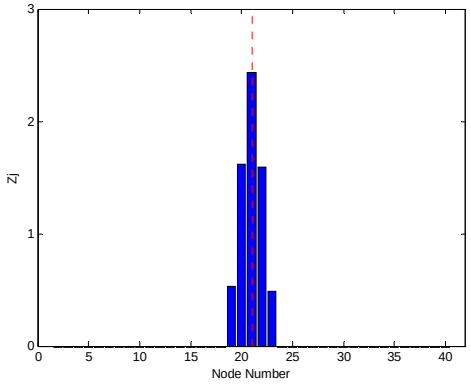

(a) Mode 1

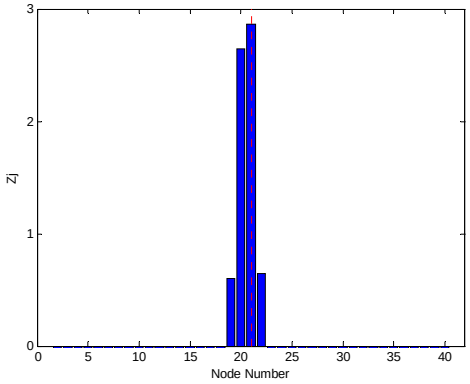

(b) Modes 1+2

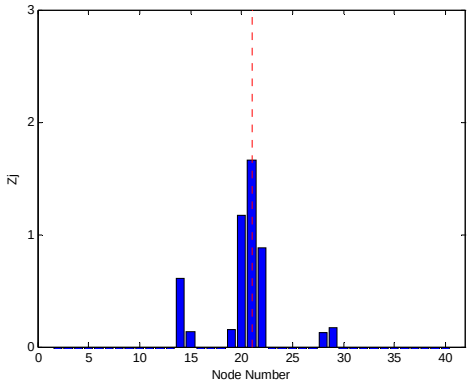

(c) Modes 1+2+3

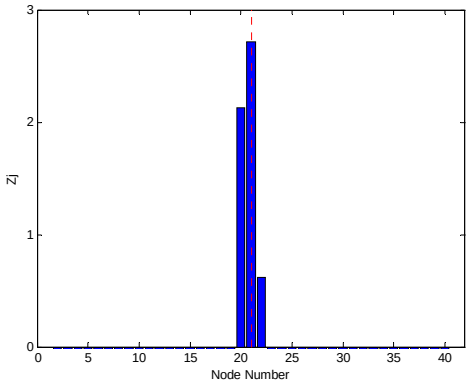

(d) Modes 1+2+3+4

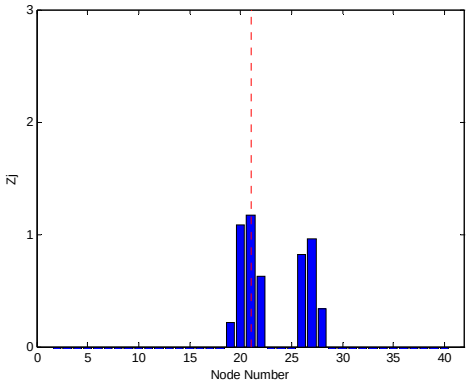

(e) Modes 1+2+3+4+5

Damage Detection with Noise (4S with 2% noise)

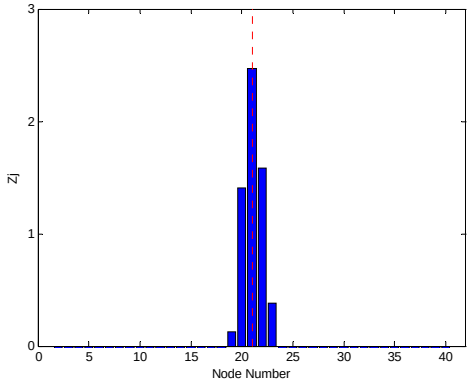

(a) Mode 1

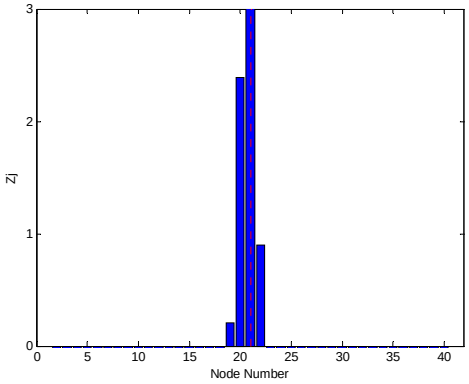

(b) Modes 1+2

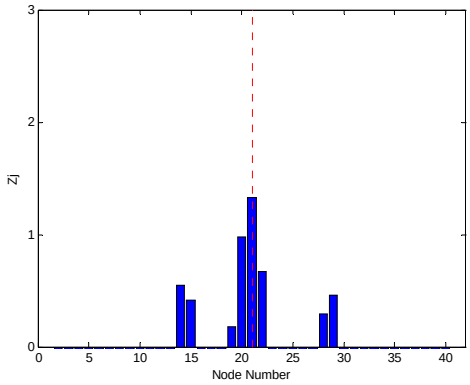

(c) Modes 1+2+3

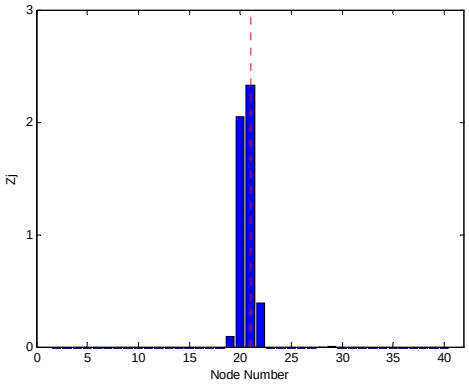

(d) Modes 1+2+3+4

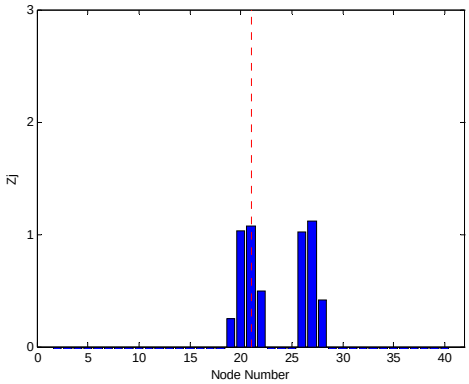

(e) Modes 1+2+3+4+5

Damage Detection with Noise (4S with 10% noise)

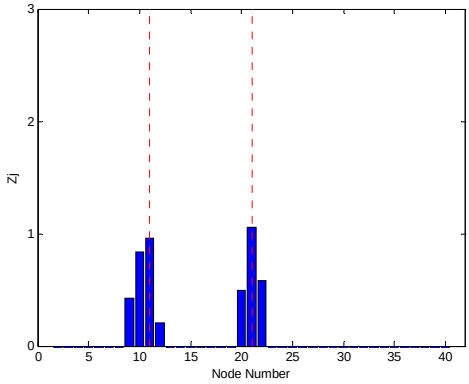

(a) Mode 1

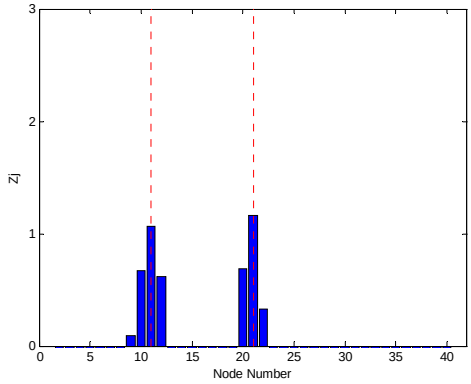

(b) Modes 1+2

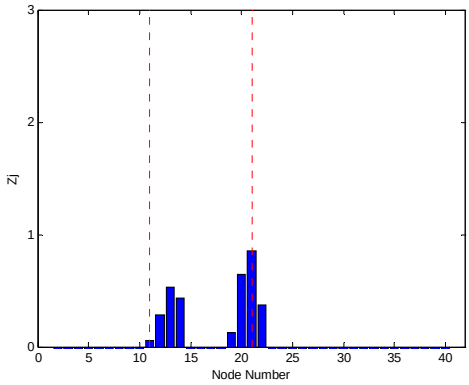

(c) Modes 1+2+3

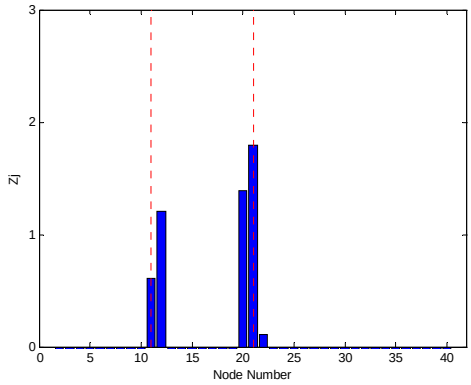

(d) Modes 1+2+3+4

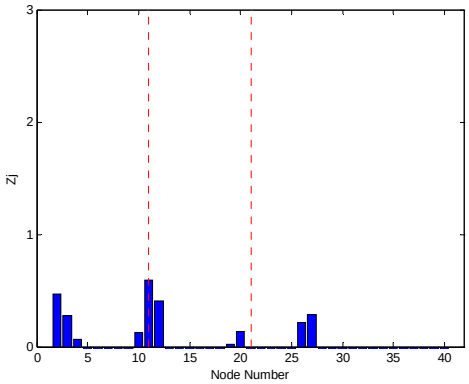

(e) Modes 1+2+3+4+5

Damage Detection with Noise (2M4M with 0% noise)

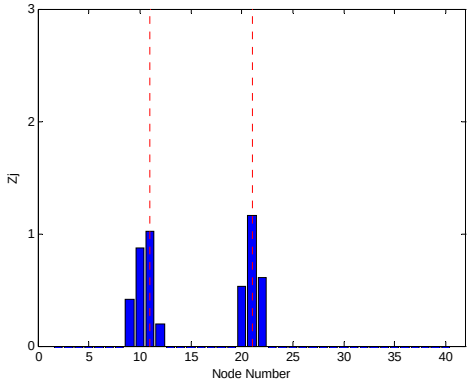

(a) Mode 1

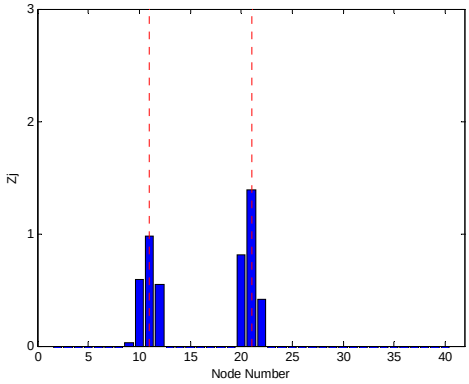

(b) Modes 1+2

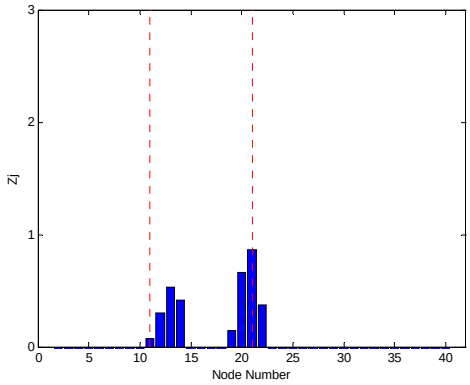

(c) Modes 1+2+3

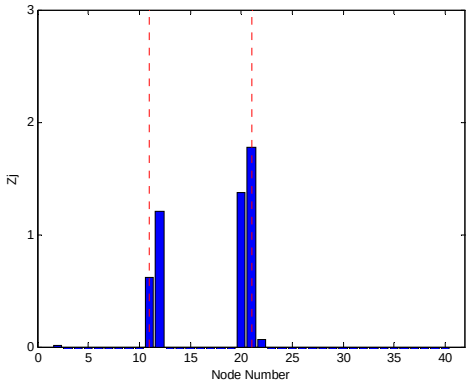

(d) Modes 1+2+3+4

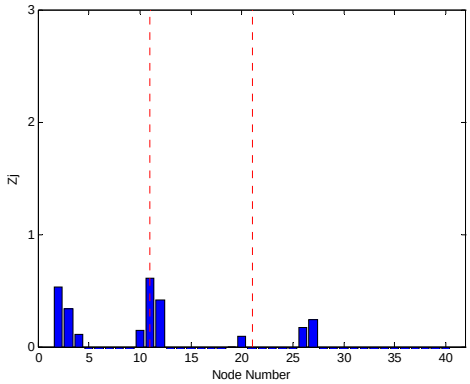

(e) Modes 1+2+3+4+5

Damage Detection with Noise (2M4M with 2% noise)

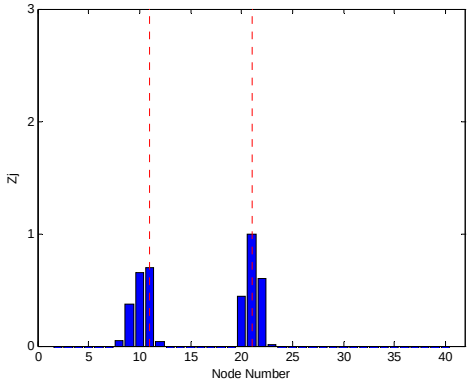

(a) Mode 1

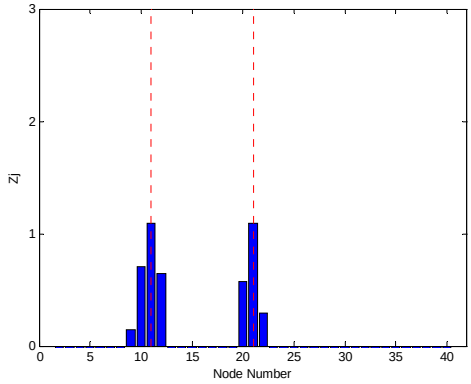

(b) Modes 1+2

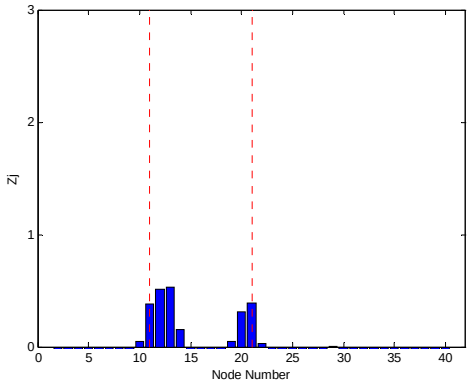

(c) Modes 1+2+3

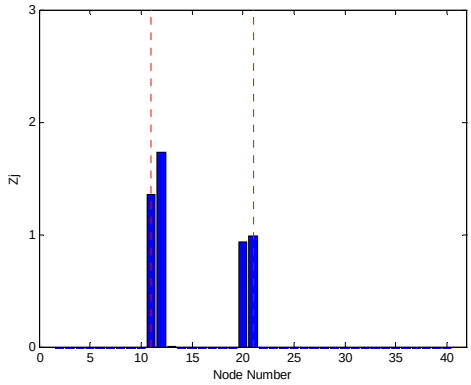

(d) Modes 1+2+3+4

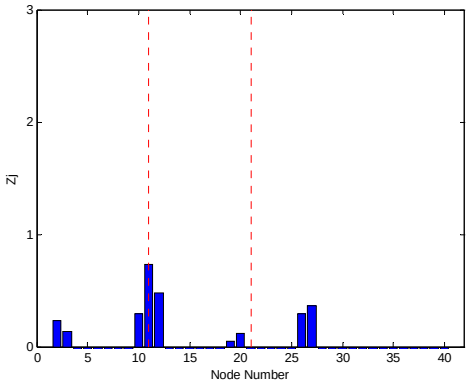

(e) Modes 1+2+3+4+5

Damage Detection with Noise (2M4M with 10% noise)

B.5 Results of Estimation of Damage Severity without Noise Pollution

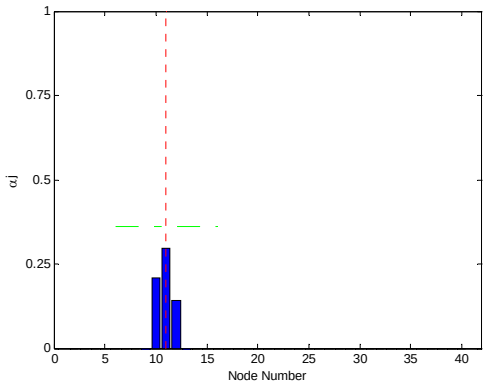

Estimation of Damage Severity without Noise (2L 5-Modes)

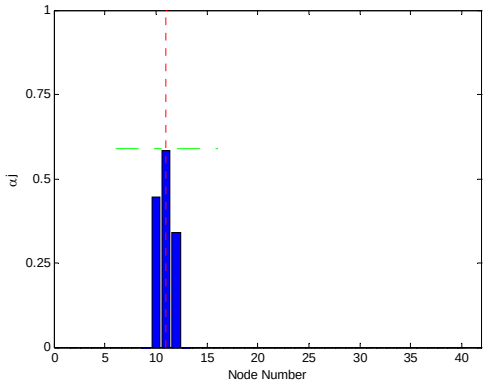

Estimation of Damage Severity without Noise (2M 5-Modes)

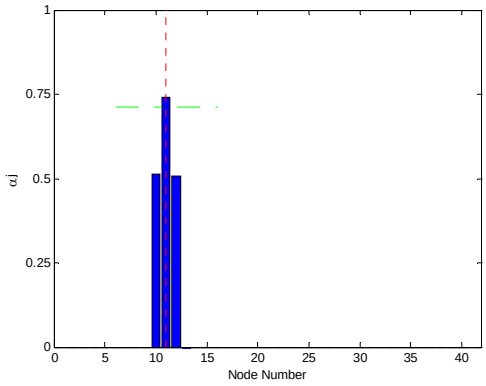

Estimation of Damage Severity without Noise (2S 5-Modes)

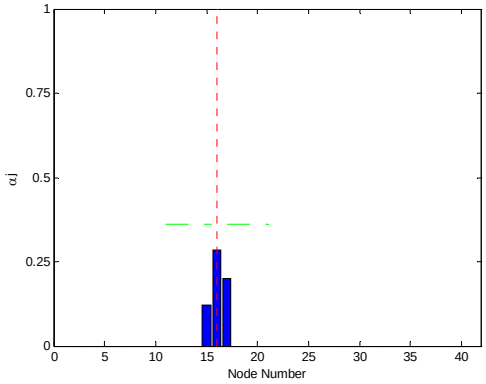

Estimation of Damage Severity without Noise (3L 5-Modes)

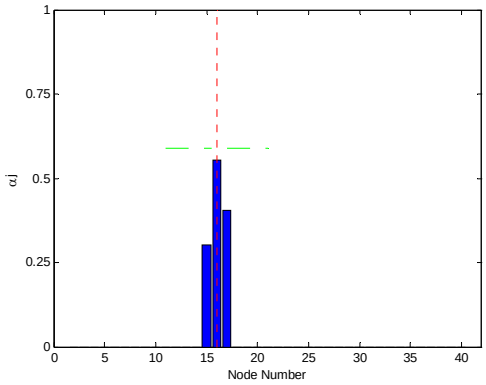

Estimation of Damage Severity without Noise (3M 5-Modes)

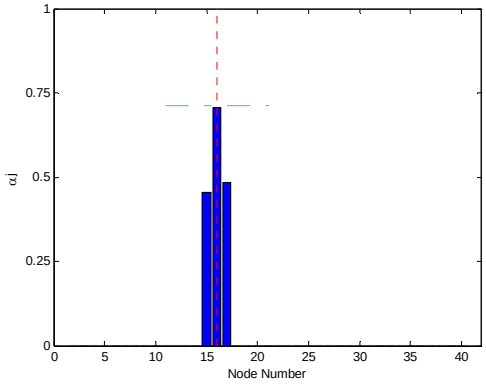

Estimation of Damage Severity without Noise (3S 5-Modes)

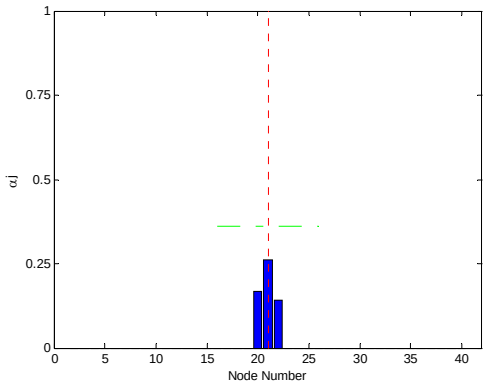

Estimation of Damage Severity without Noise (4L 5-Modes)

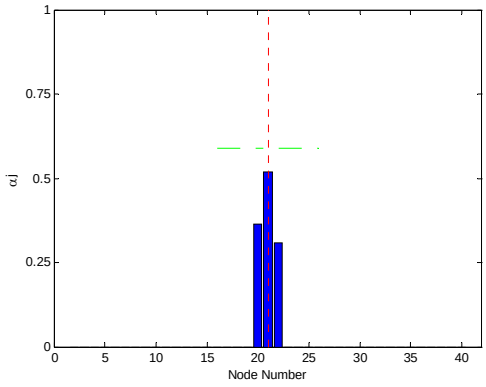

Estimation of Damage Severity without Noise (4M 5-Modes)

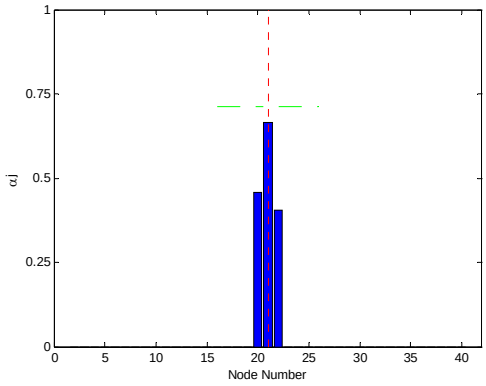

Estimation of Damage Severity without Noise (4S 5-Modes)

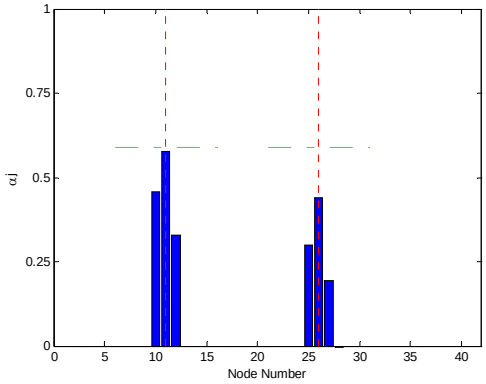

Estimation of Damage Severity without Noise (2M5M 5-Modes)

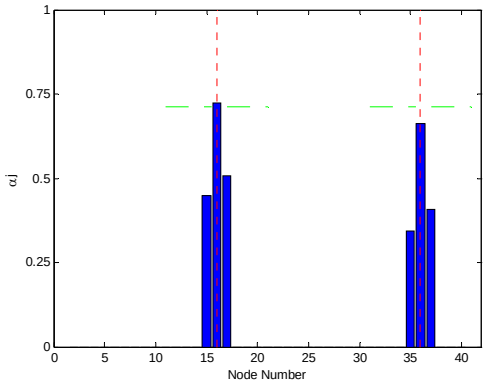

Estimation of Damage Severity without Noise (3S7S 5-Modes)

B.6 Results of Estimation of Damage Severity with Noise Pollution

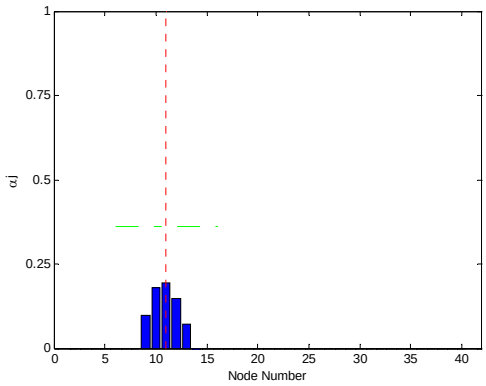

Estimation of Damage Severity with Noise (2L with 0% noise 5-Modes)

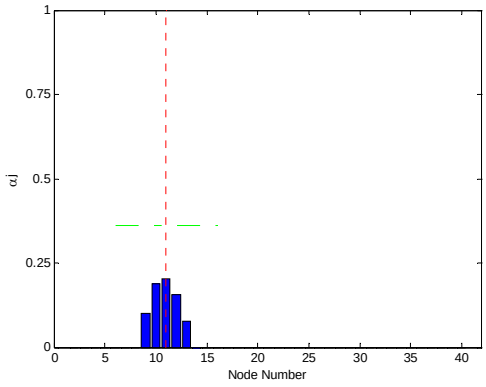

Estimation of Damage Severity with Noise (2L with 2% noise 5-Modes)

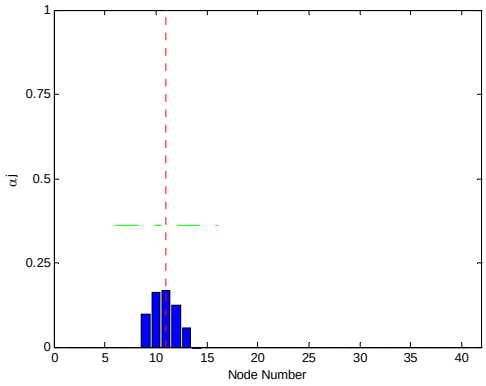

Estimation of Damage Severity with Noise (2L with 10% noise 5-Modes)

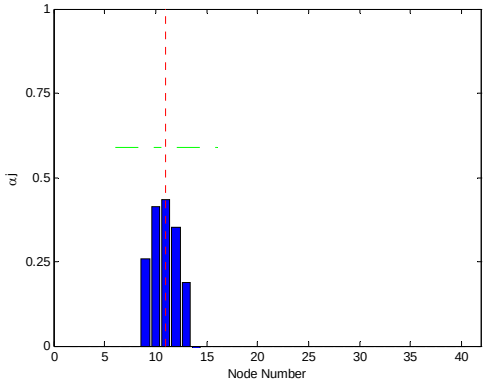

Estimation of Damage Severity with Noise (2M with 0% noise 5-Modes)

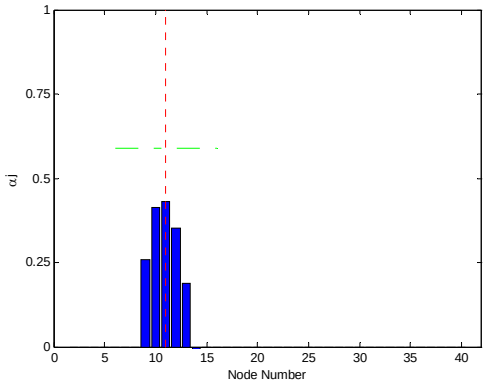

Estimation of Damage Severity with Noise (2M with 2% noise 5-Modes)

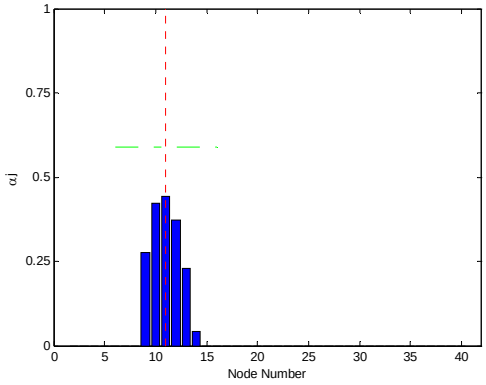

Estimation of Damage Severity with Noise (2M with 10% noise 5-Modes)

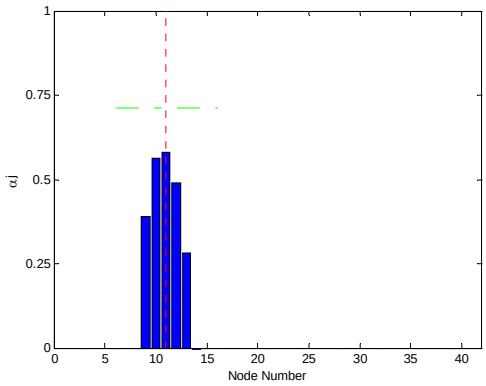

Estimation of Damage Severity with Noise (2S with 0% noise 5-Modes)

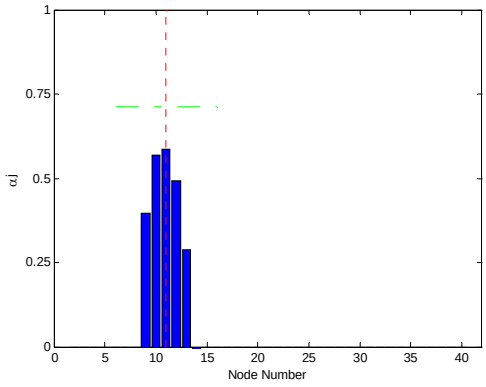

Estimation of Damage Severity with Noise (2S with 2% noise 5-Modes)

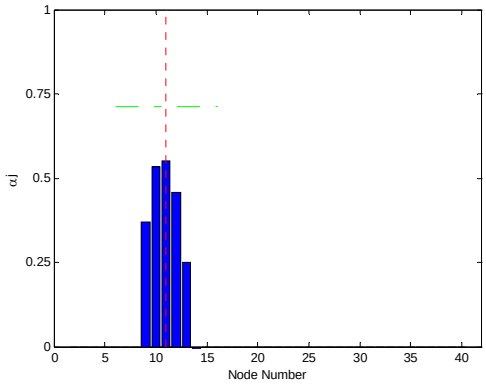

Estimation of Damage Severity with Noise (2S with 10% noise 5-Modes)

B.7 Comparison Results with No Noise Pollution

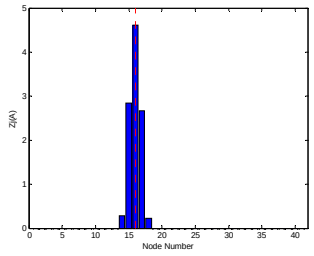

DI-A (1-Mode)

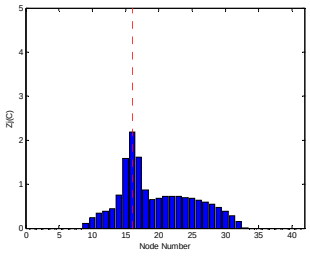

DI-C (1-Mode)

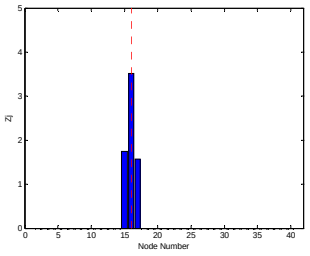

DI-N (1-Mode)

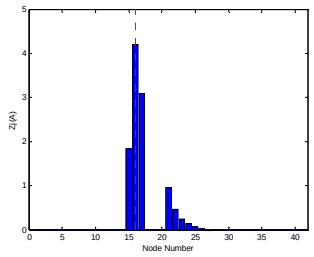

DI-A (2-Modes)

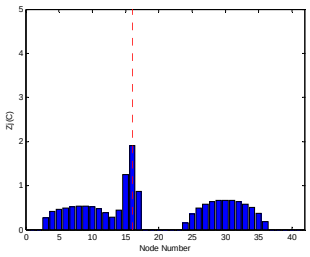

DI-C (2-Modes)

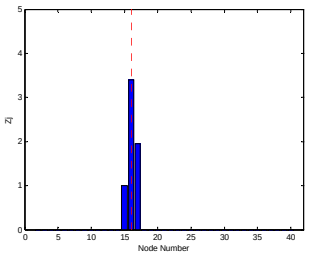

DI-N (2-Modes)

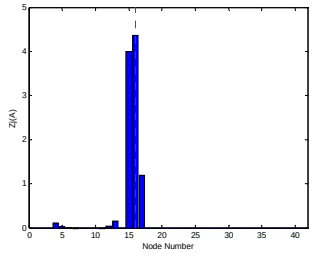

DI-A (3-Modes)

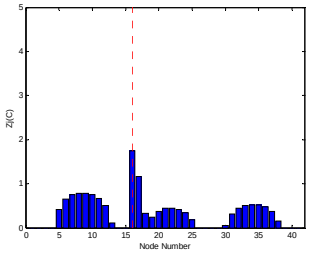

DI-C (3-Modes)

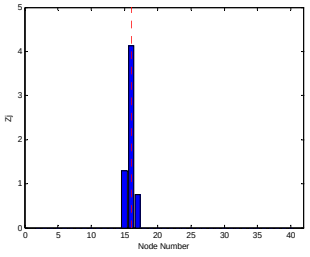

DI-N (3-Modes)

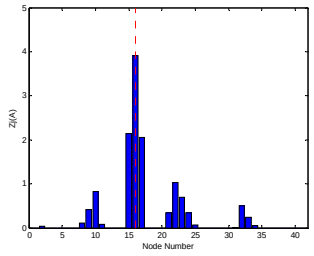

DI-A (4-Modes)

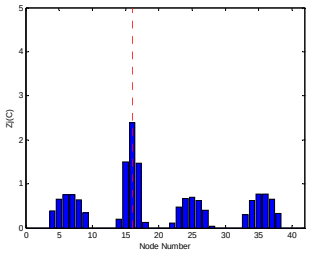

DI-C (4-Modes)

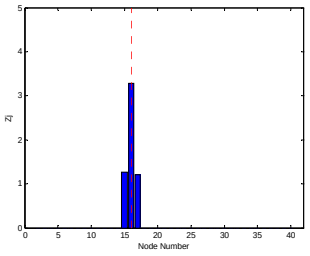

DI-N (4-Modes)

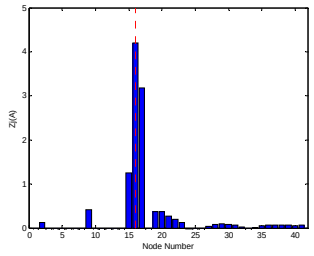

DI-A (5-Modes)

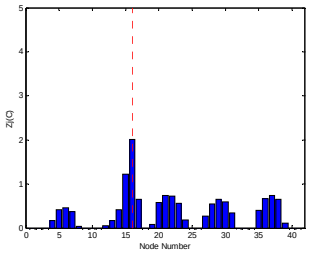

DI-C (5-Modes)

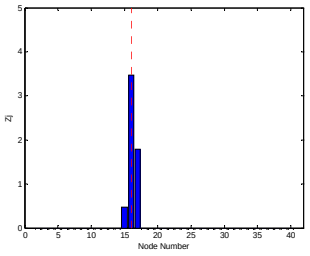

DI-N (5-Modes)

Comparison Results without Noise (3L)

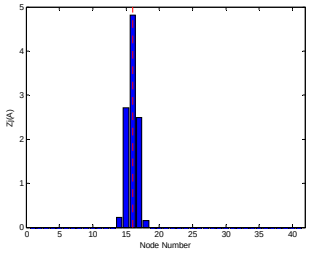

DI-A (1-Mode)

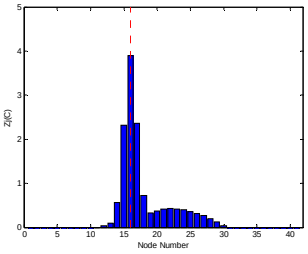

DI-C (1-Mode)

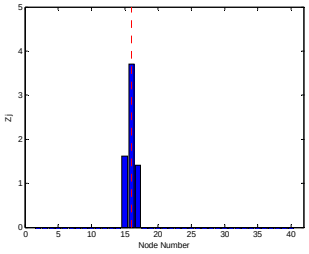

DI-N (1-Mode)

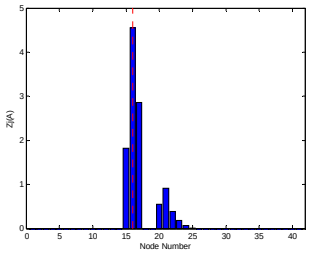

DI-A (2-Modes)

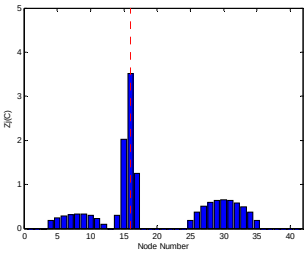

DI-C (2-Modes)

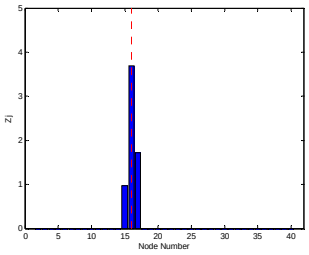

DI-N (2-Modes)

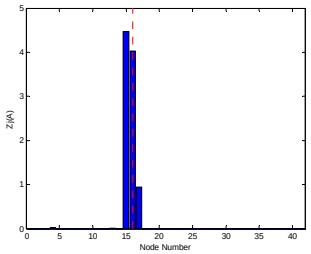

DI-A (3-Modes)

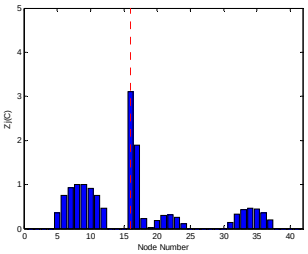

DI-C (3-Modes)

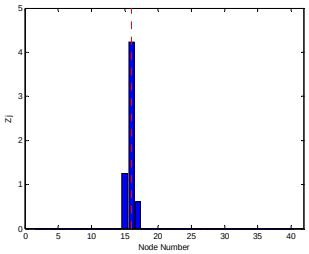

DI-N (3-Modes)

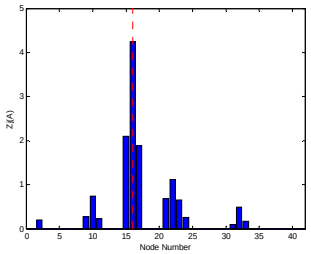

DI-A (4-Modes)

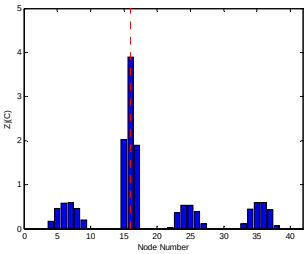

DI-C (4-Modes)

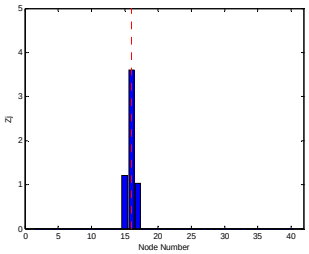

DI-N (4-Modes)

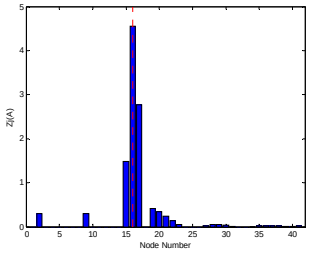

DI-A (5-Modes)

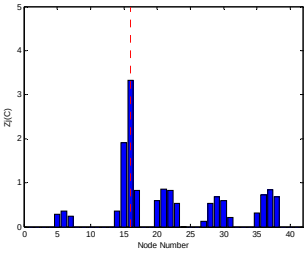

DI-C (5-Modes)

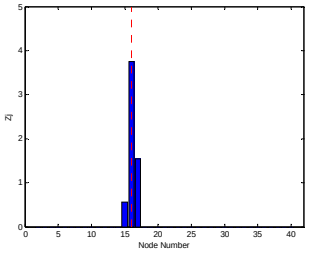

DI-N (5-Modes)

Comparison Results without Noise (3M)

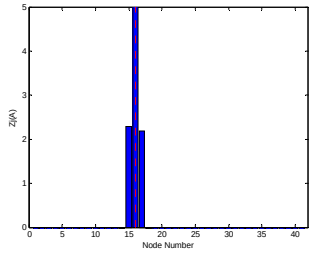

DI-A (1-Mode)

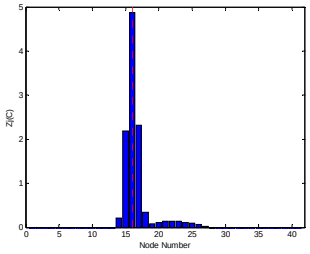

DI-C (1-Mode)

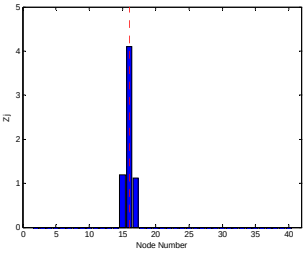

DI-N (1-Mode)

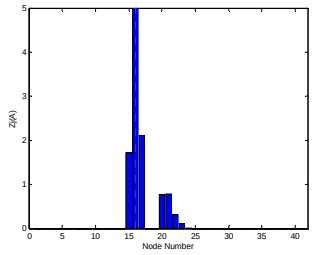

DI-A (2-Modes)

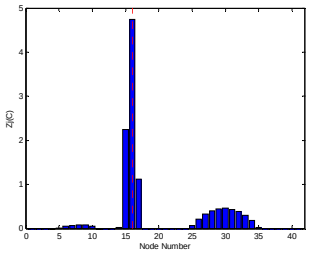

DI-C (2-Modes)

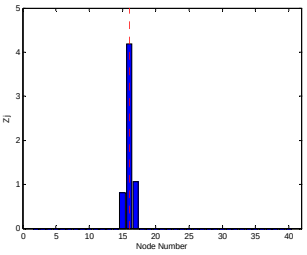

DI-N (2-Modes)

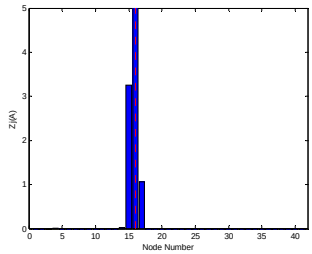

DI-A (3-Modes)

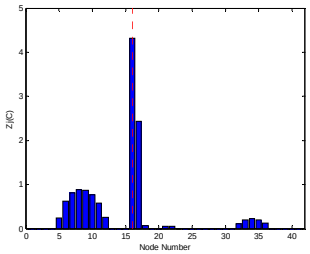

DI-C (3-Modes)

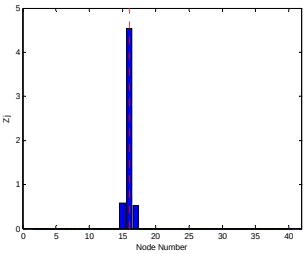

DI-N (3-Modes)

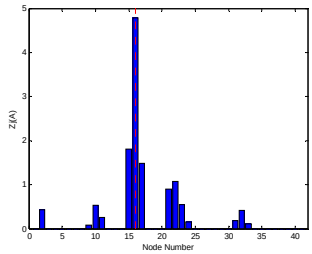

DI-A (4-Modes)

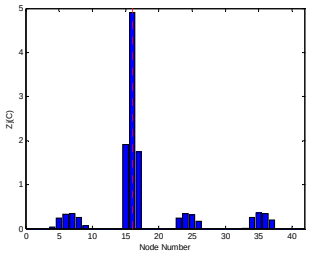

DI-C (4-Modes)

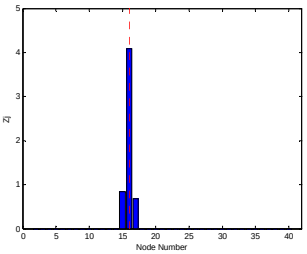

DI-N (4-Modes)

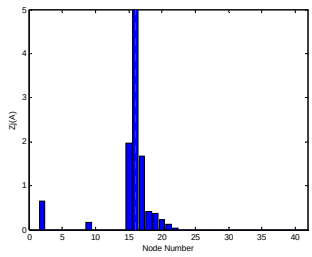

DI-A (5-Modes)

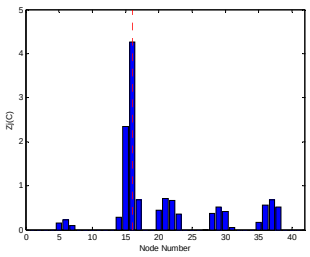

DI-C (5-Modes)

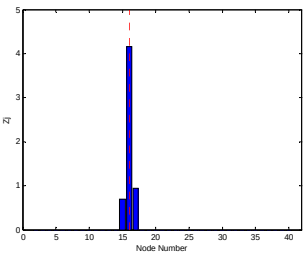

DI-N (5-Modes)

Comparison Results without Noise (3S)

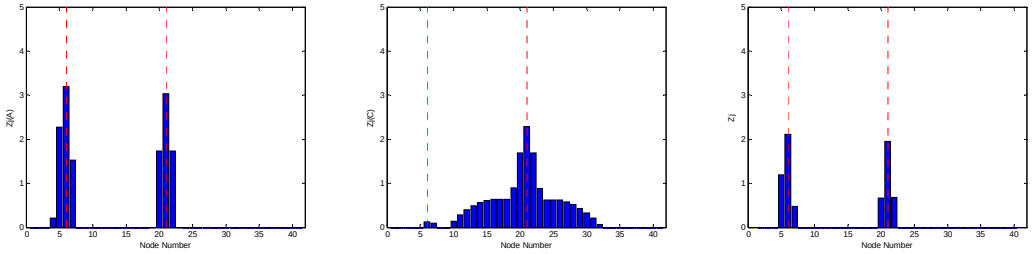

DI-A (1-Mode) DI-C (1-Mode) DI-N (1-Mode)

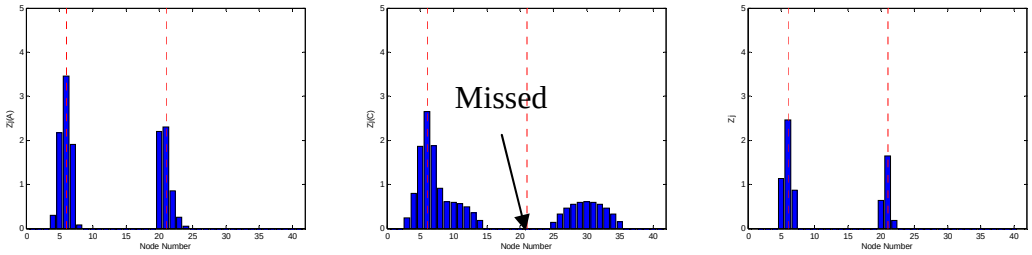

DI-A (2-Modes) DI-C (2-Modes) DI-N (2-Modes)

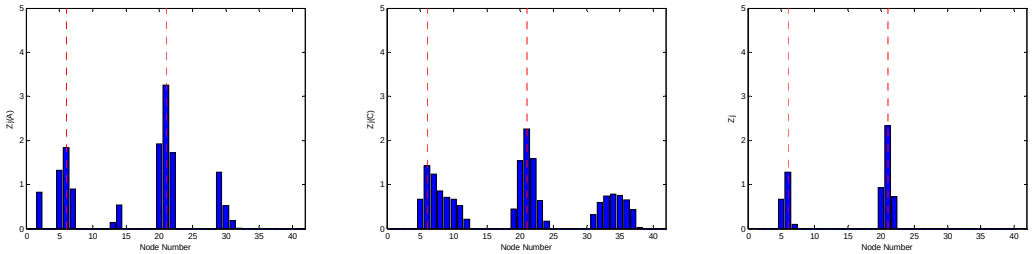

DI-A (3-Modes) DI-C (3-Modes) DI-N (3-Modes)

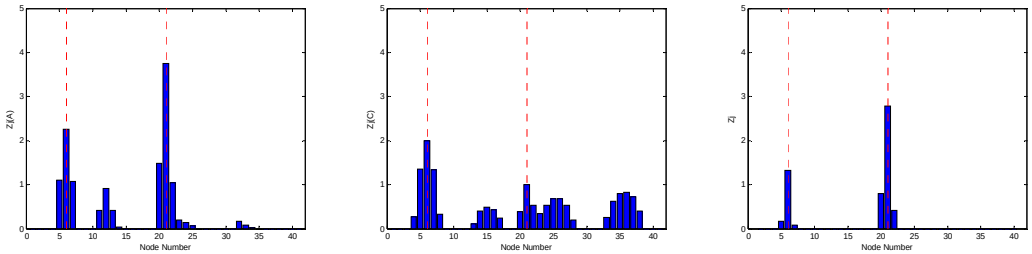

DI-A (4-Modes) DI-C (4-Modes) DI-N (4-Modes)

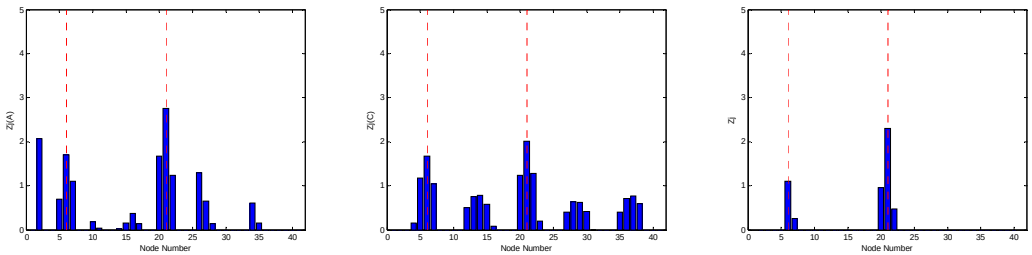

DI-A (5-Modes) DI-C (5-Modes) DI-N (5-Modes)

Comparison Results without Noise (1L4L)

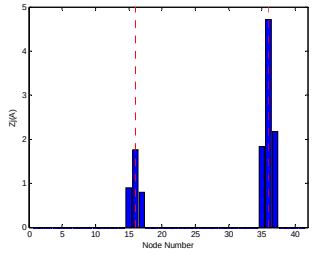

DI-A (1-Mode)

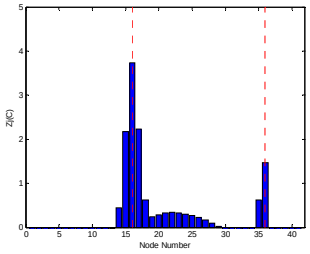

DI-C (1-Mode)

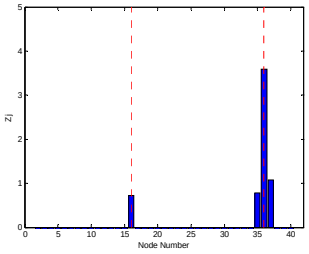

DI-N (1-Mode)

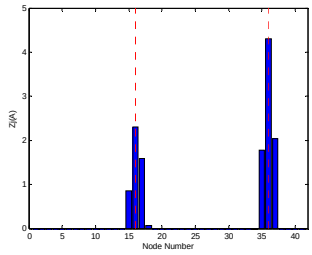

DI-A (2-Modes)

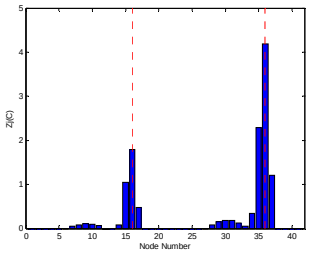

DI-C (2-Modes)

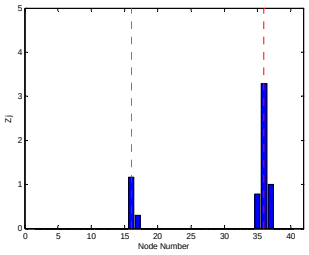

DI-N (2-Modes)

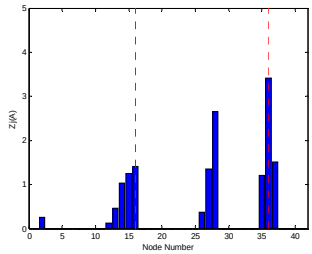

DI-A (3-Modes)

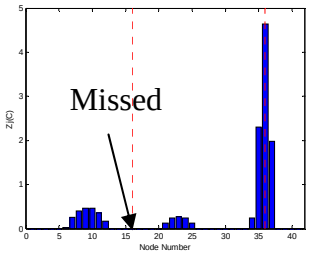

DI-C (3-Modes)

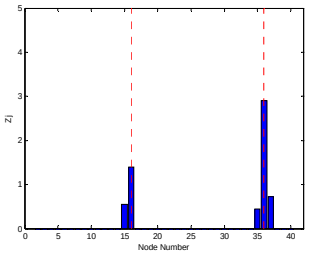

DI-N (3-Modes)

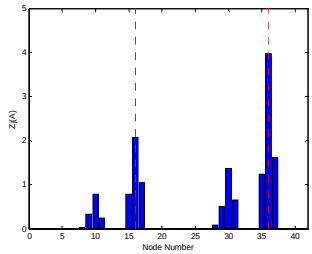

DI-A (4-Modes)

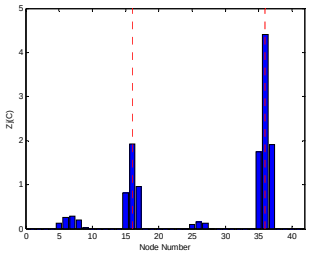

DI-C (4-Modes)

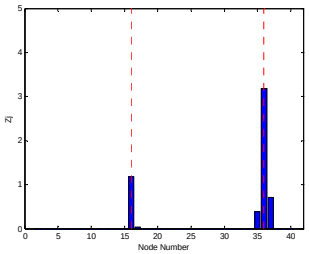

DI-N (4-Modes)

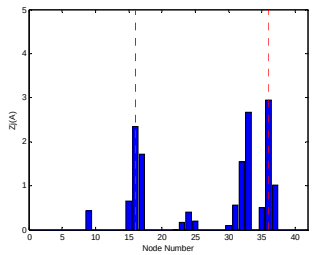

DI-A (5-Modes)

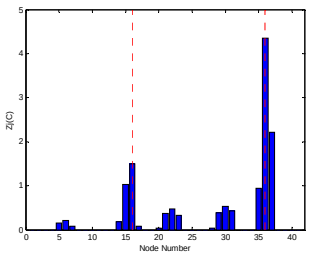

DI-C (5-Modes)

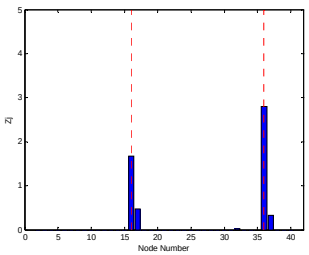

DI-N (5-Modes)

Comparison Results without Noise (3M7S)

B.8 Comparison of Results with Simulated Noise

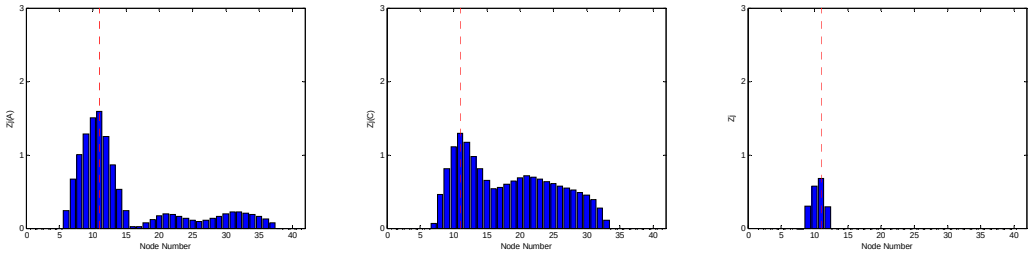

DI-A (1-Mode) DI-C (1-Mode) DI-N (1-Mode)

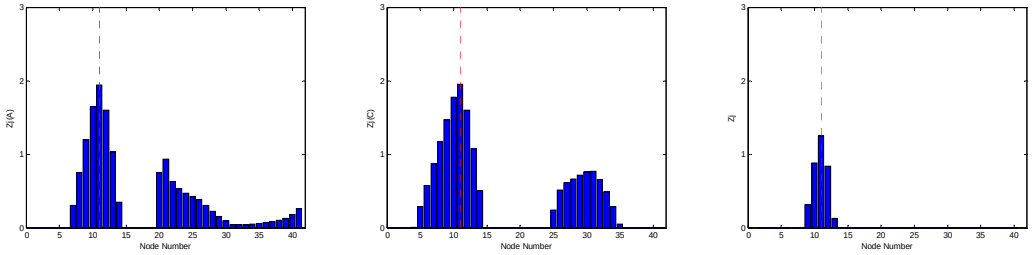

DI-A (2-Modes) DI-C (2-Modes) DI-N (2-Modes)

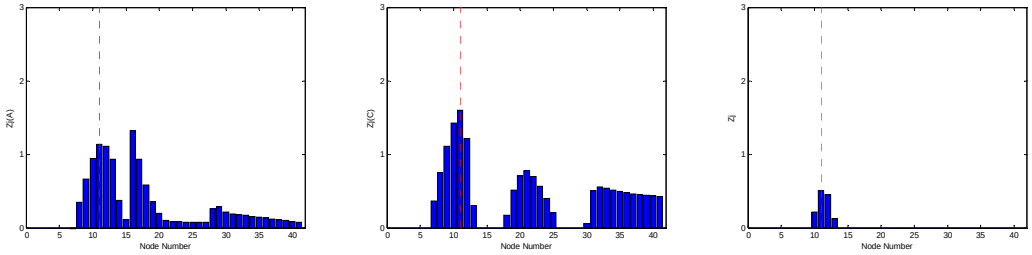

DI-A (3-Modes) DI-C (3-Modes) DI-N (3-Modes)

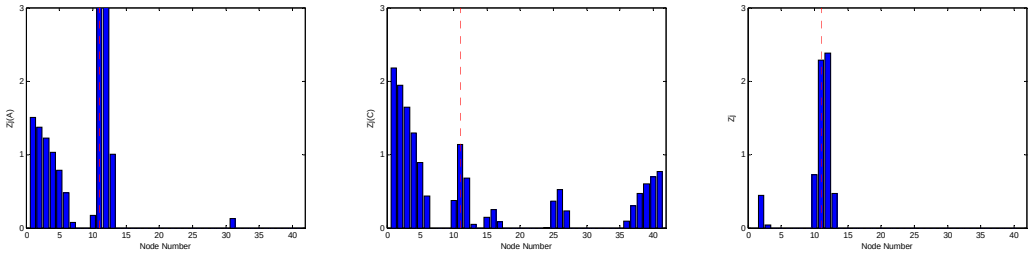

DI-A (4-Modes) DI-C (4-Modes) DI-N (4-Modes)

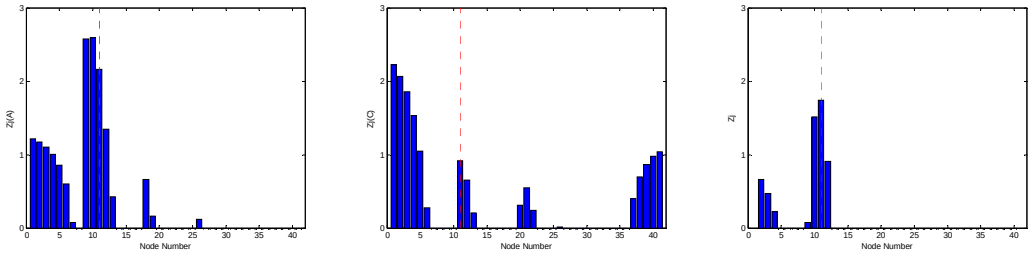

DI-A (5-Modes) DI-C (5-Modes) DI-N (5-Modes)

Comparison Results with Noise (2L with 0% noise)

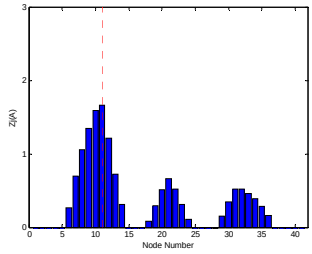

DI-A (1-Mode)

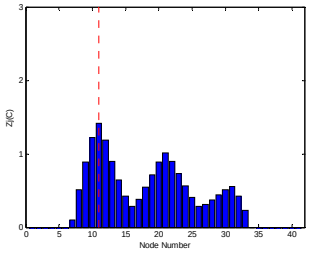

DI-C (1-Mode)

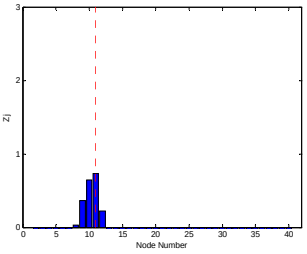

DI-N (1-Mode)

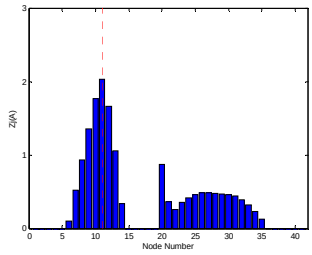

DI-A (2-Modes)

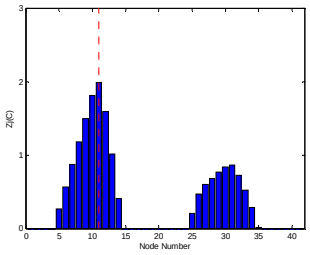

DI-C (2-Modes)

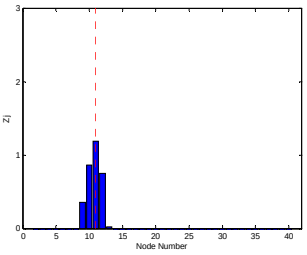

DI-N (2-Modes)

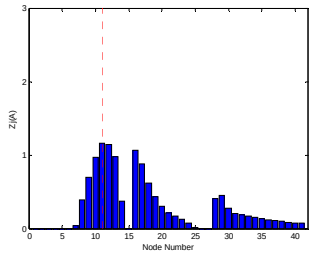

DI-A (3-Modes)

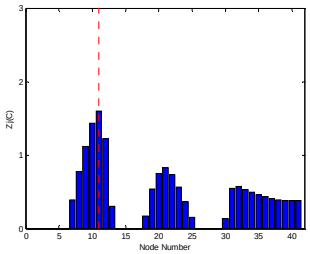

DI-C (3-Modes)

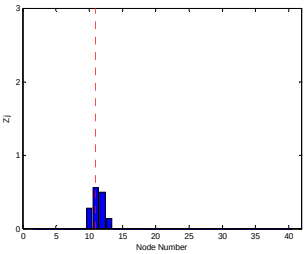

DI-N (3-Modes)

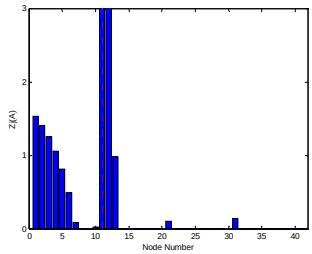

DI-A (4-Modes)

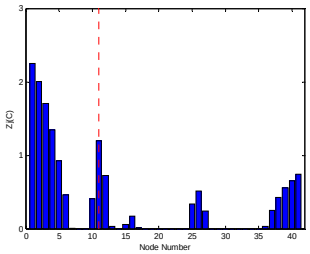

DI-C (4-Modes)

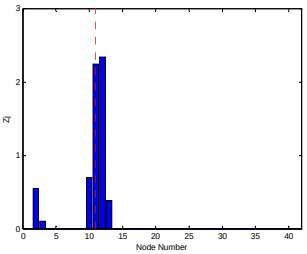

DI-N (4-Modes)

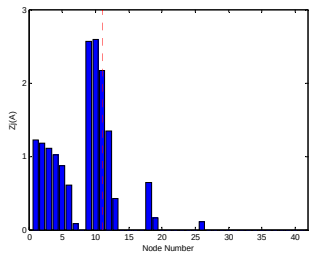

DI-A (5-Modes)

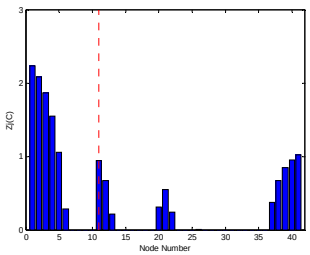

DI-C (5-Modes)

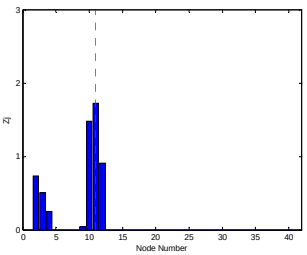

DI-N (5-Modes)

Comparison Results with Noise (2L with 2% noise)

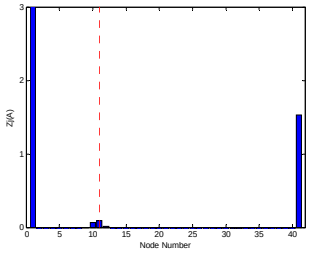

DI-A (1-Mode)

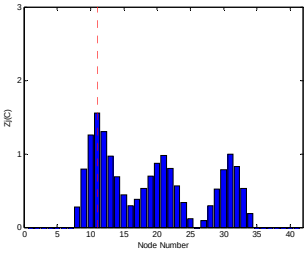

DI-C (1-Mode)

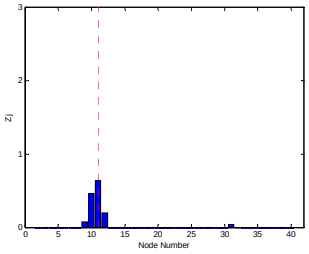

DI-N (1-Mode)

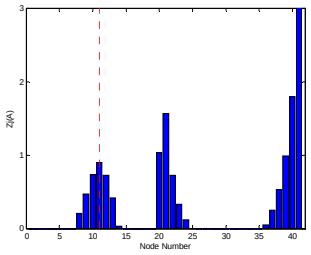

DI-A (2-Modes)

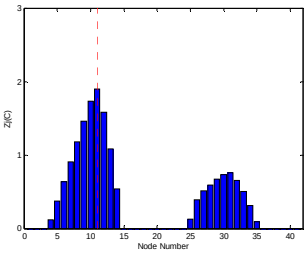

DI-C (2-Modes)

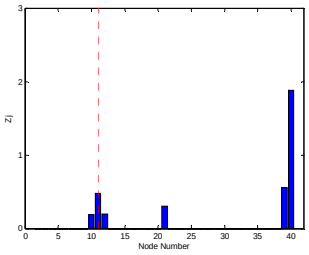

DI-N (2-Modes)

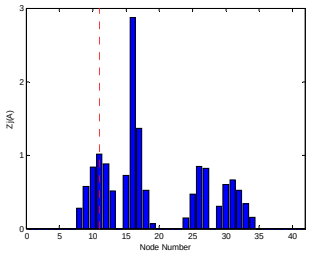

DI-A (3-Modes)

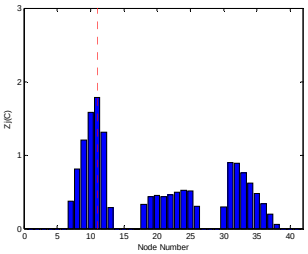

DI-C (3-Modes)

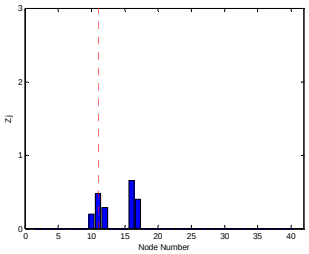

DI-N (3-Modes)

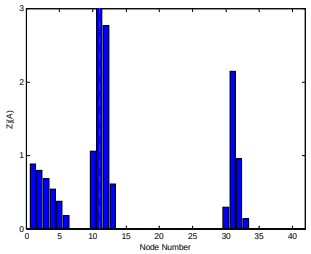

DI-A (4-Modes)

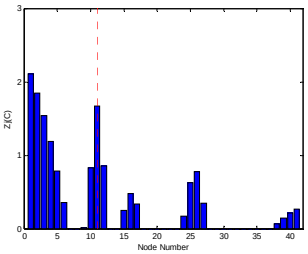

DI-C (4-Modes)

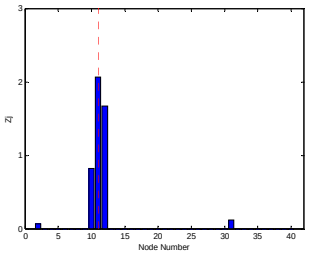

DI-N (4-Modes)

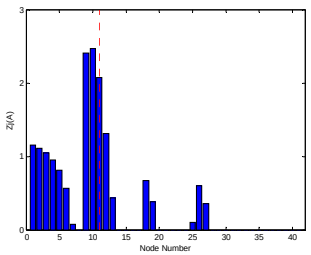

DI-A (5-Modes)

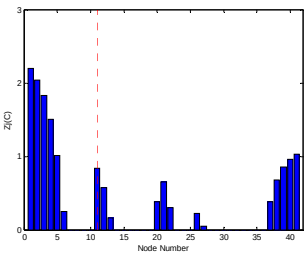

DI-C (5-Modes)

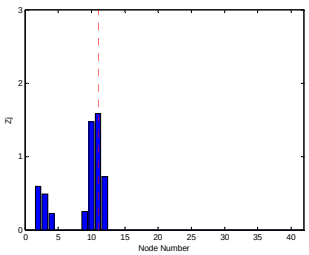

DI-N (5-Modes)

Comparison Results with Noise (2L with 10% noise)

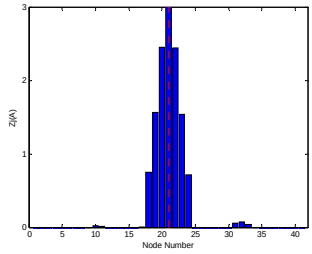

DI-A (1-Mode)

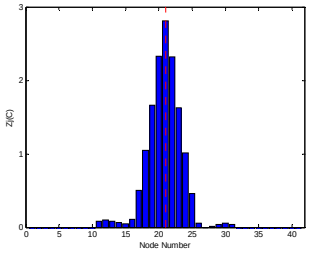

DI-C (1-Mode)

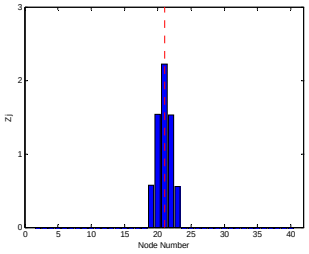

DI-N (1-Mode)

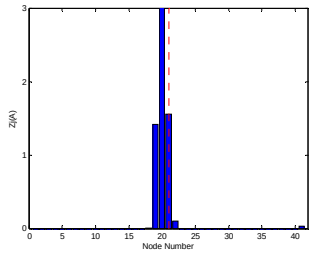

DI-A (2-Modes)

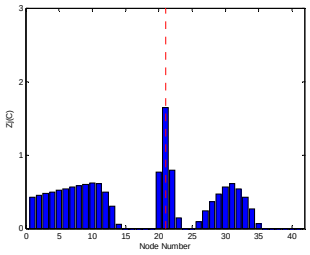

DI-C (2-Modes)

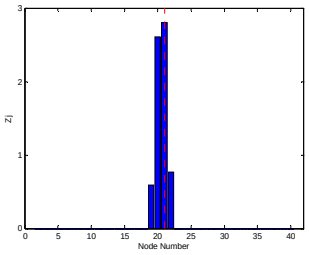

DI-N (2-Modes)

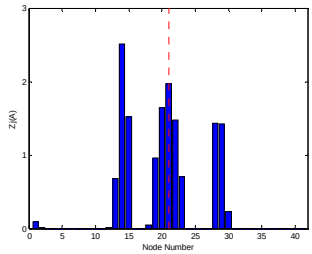

DI-A (3-Modes)

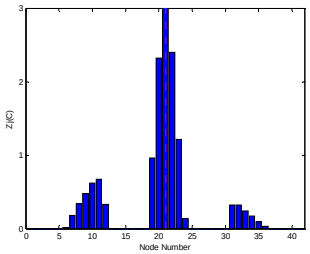

DI-C (3-Modes)

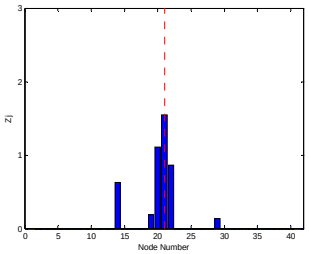

DI-N (3-Modes)

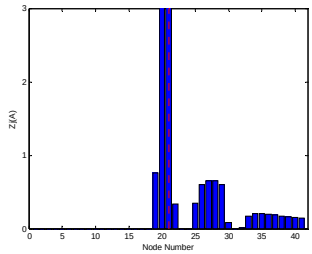

DI-A (4-Modes)

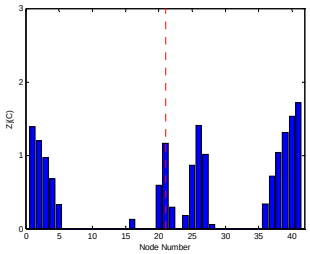

DI-C (4-Modes)

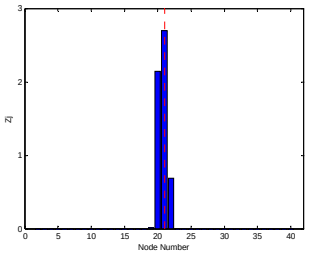

DI-N (4-Modes)

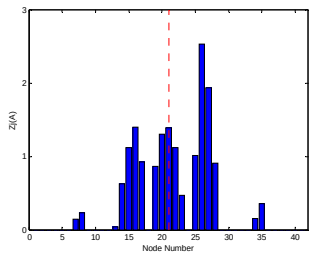

DI-A (5-Modes)

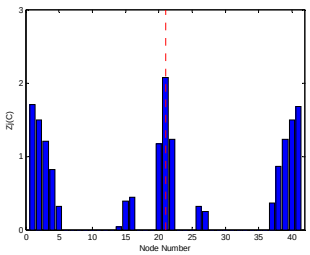

DI-C (5-Modes)

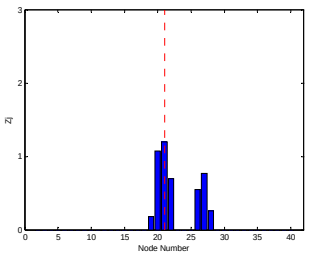

DI-N (5-Modes)

Comparison Results with Noise (4M with 0% noise)

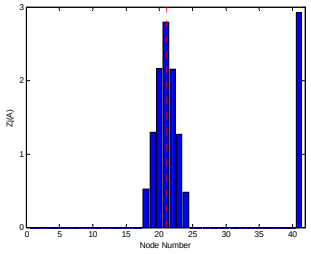

DI-A (1-Mode)

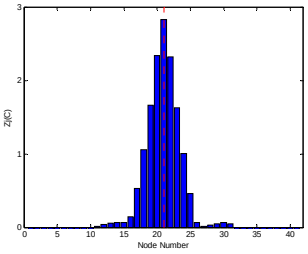

DI-C (1-Mode)

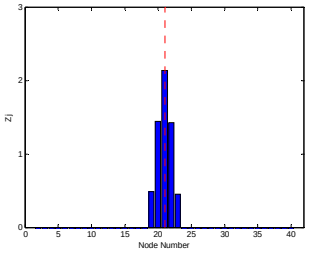

DI-N (1-Mode)

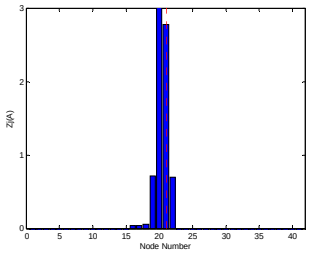

DI-A (2-Modes)

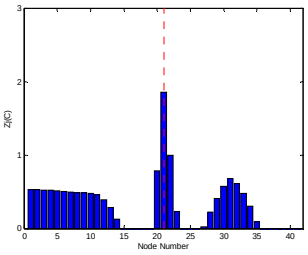

DI-C (2-Modes)

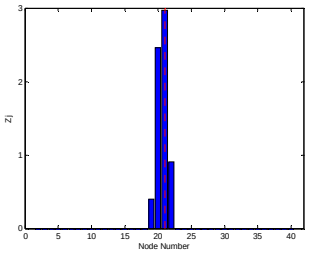

DI-N (2-Modes)

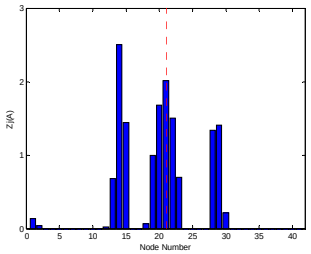

DI-A (3-Modes)

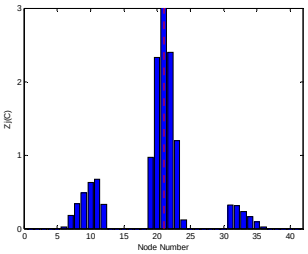

DI-C (3-Modes)

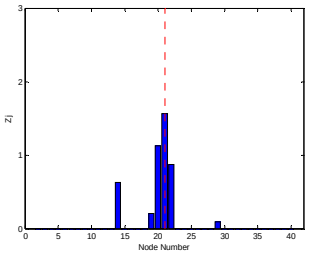

DI-N (3-Modes)

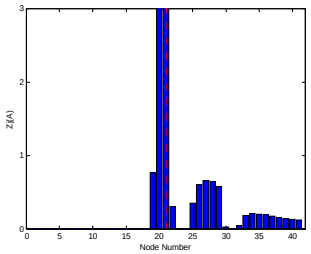

DI-A (4-Modes)

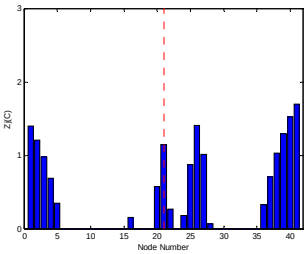

DI-C (4-Modes)

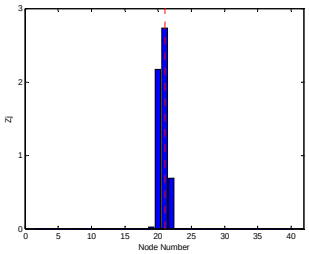

DI-N (4-Modes)

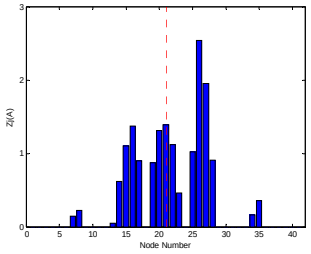

DI-A (5-Modes)

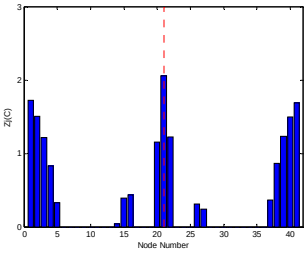

DI-C (5-Modes)

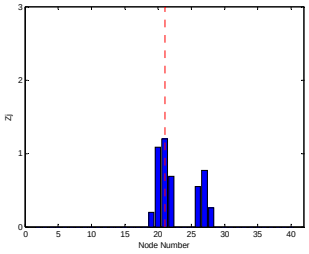

DI-N (5-Modes)

Comparison Results with Noise (4M with 2% noise)

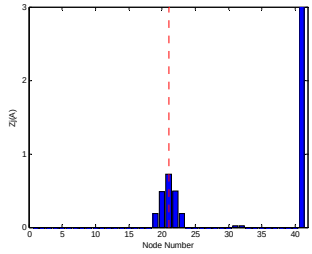

DI-A (1-Mode)

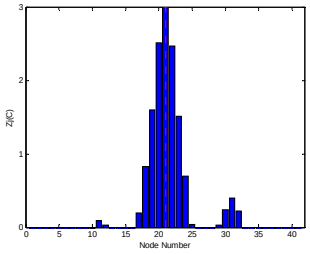

DI-C (1-Mode)

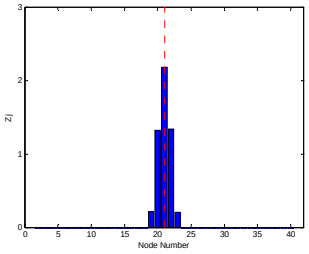

DI-N (1-Mode)

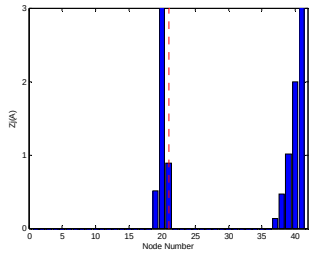

DI-A (2-Modes)

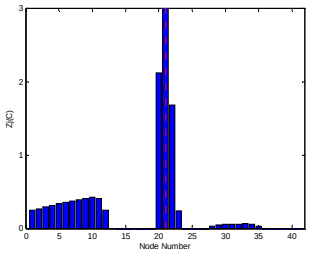

DI-C (2-Modes)

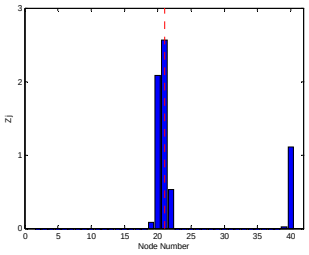

DI-N (2-Modes)

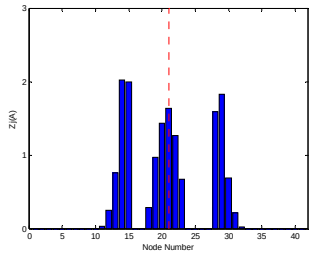

DI-A (3-Modes)

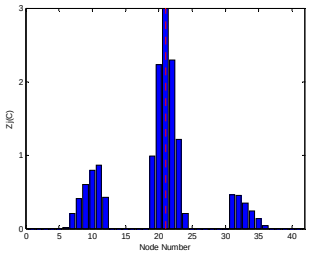

DI-C (3-Modes)

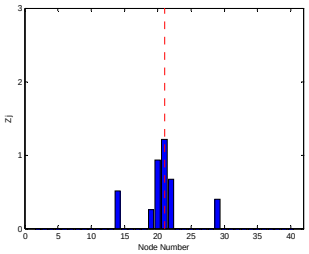

DI-N (3-Modes)

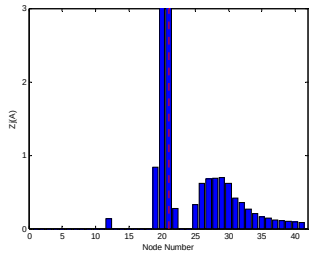

DI-A (4-Modes)

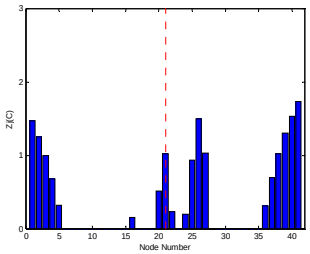

DI-C (4-Modes)

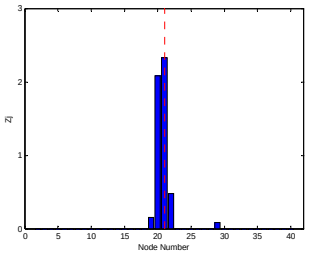

DI-N (4-Modes)

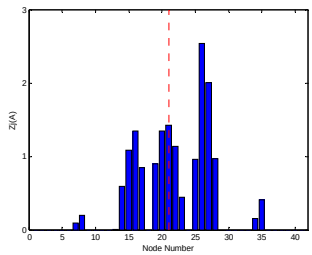

DI-A (5-Modes)

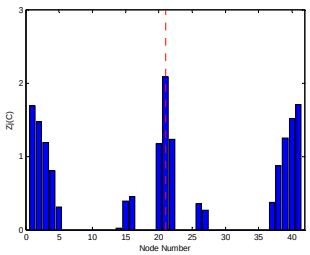

DI-C (5-Modes)

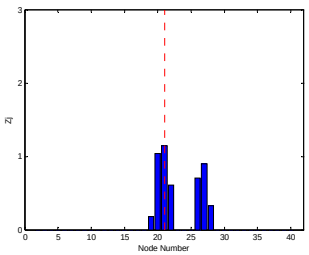

DI-N (5-Modes)

Comparison Results with Noise (4M with 10% noise)

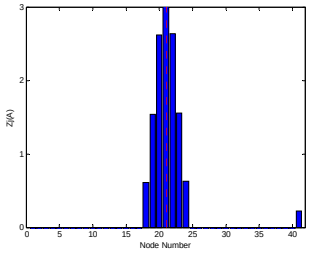

DI-A (1-Mode)

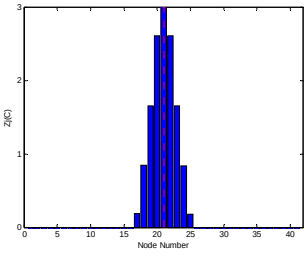

DI-C (1-Mode)

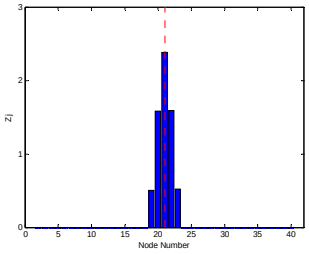

DI-N (1-Mode)

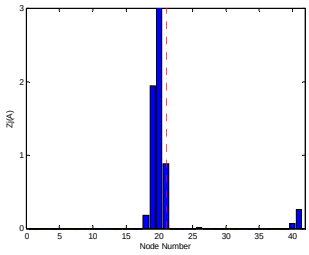

DI-A (2-Modes)

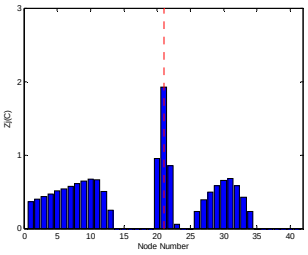

DI-C (2-Modes)

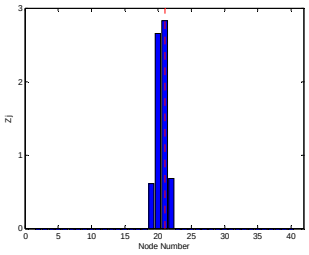

DI-N (2-Modes)

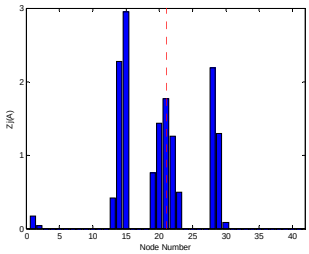

DI-A (3-Modes)

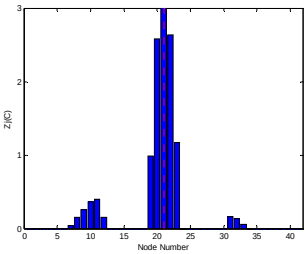

DI-C (3-Modes)

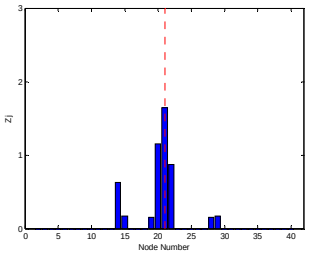

DI-N (3-Modes)

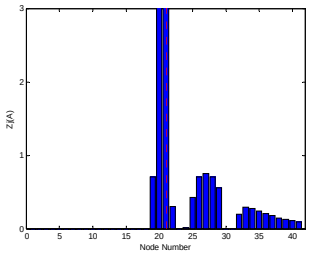

DI-A (4-Modes)

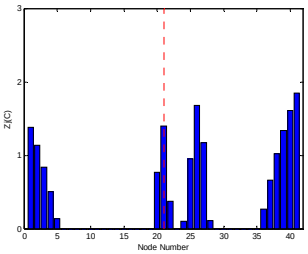

DI-C (4-Modes)

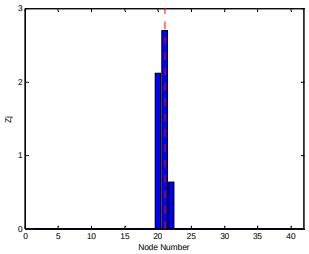

DI-N (4-Modes)

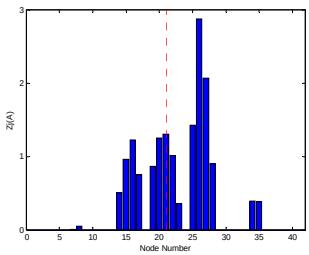

DI-A (5-Modes)

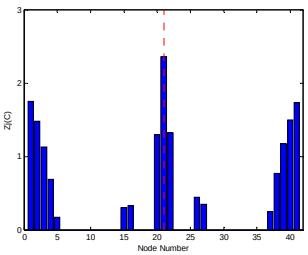

DI-C (5-Modes)

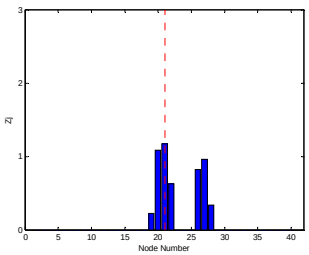

DI-N (5-Modes)

Comparison Results with Noise (4S with 0% noise)

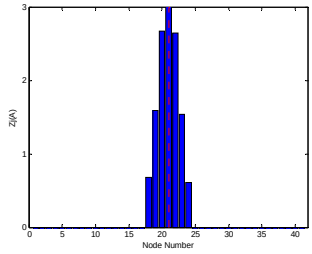

DI-A (1-Mode)

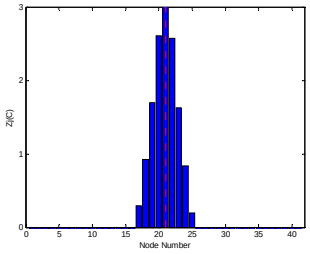

DI-C (1-Mode)

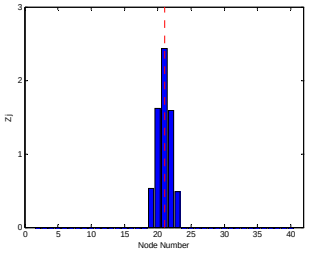

DI-N (1-Mode)

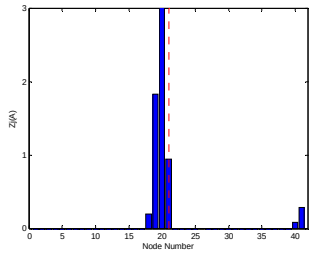

DI-A (2-Modes)

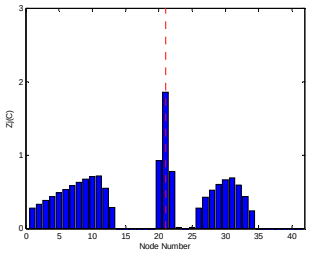

DI-C (2-Modes)

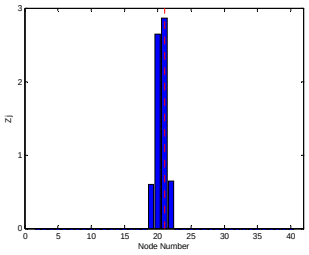

DI-N (2-Modes)

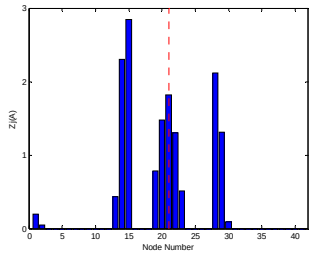

DI-A (3-Modes)

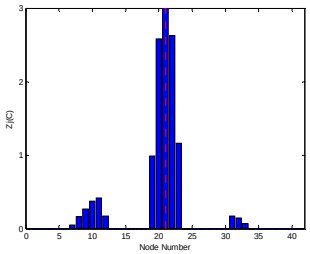

DI-C (3-Modes)

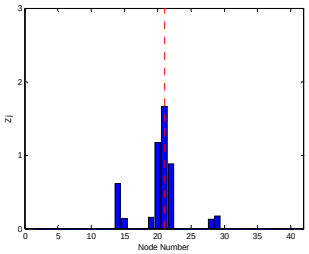

DI-N (3-Modes)

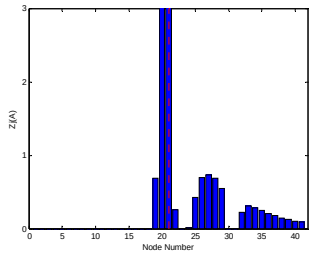

DI-A (4-Modes)

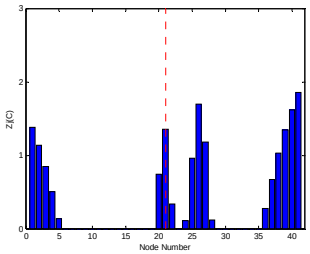

DI-C (4-Modes)

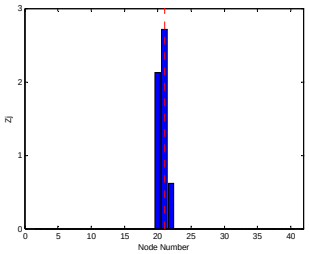

DI-N (4-Modes)

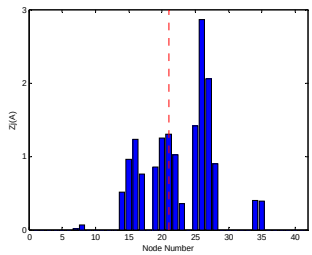

DI-A (5-Modes)

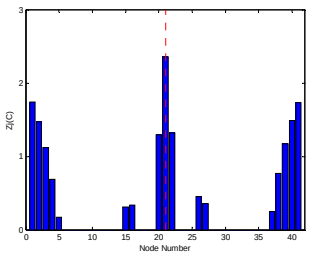

DI-C (5-Modes)

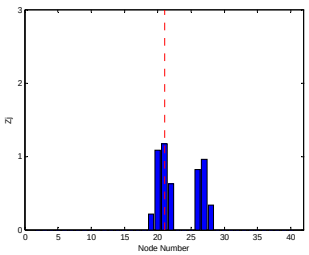

DI-N (5-Modes)

Comparison Results with Noise (4S with 2% noise)

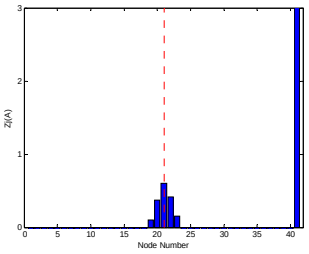

DI-A (1-Mode)

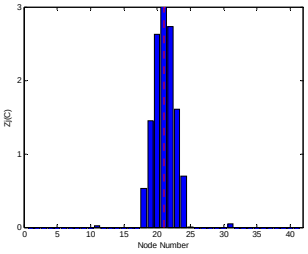

DI-C (1-Mode)

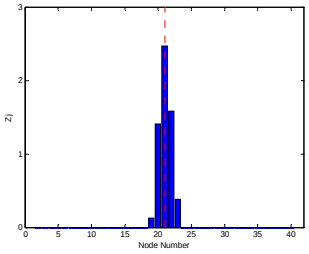

DI-N (1-Mode)

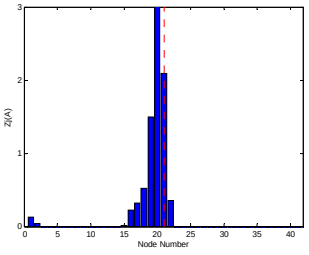

DI-A (2-Modes)

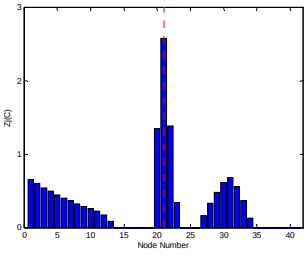

DI-C (2-Modes)

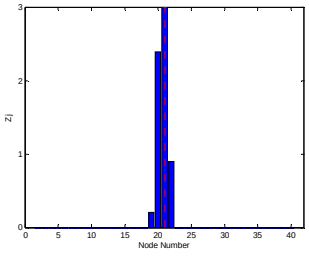

DI-N (2-Modes)

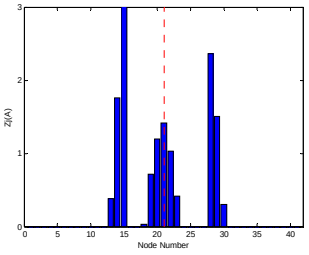

DI-A (3-Modes)

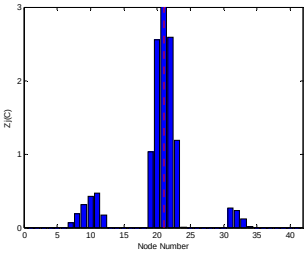

DI-C (3-Modes)

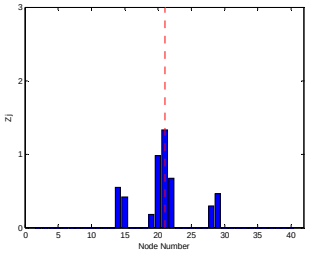

DI-N (3-Modes)

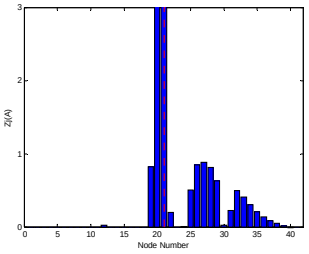

DI-A (4-Modes)

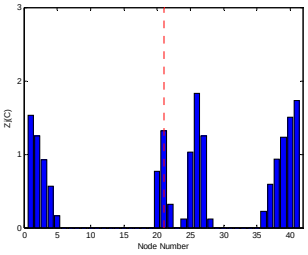

DI-C (4-Modes)

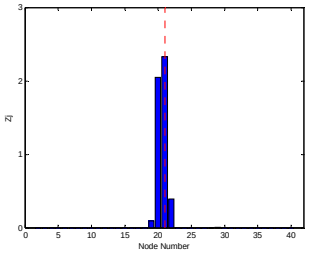

DI-N (4-Modes)

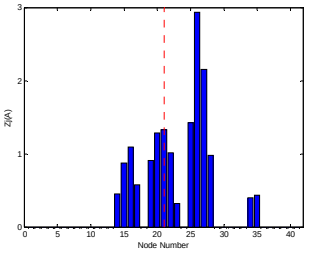

DI-A (5-Modes)

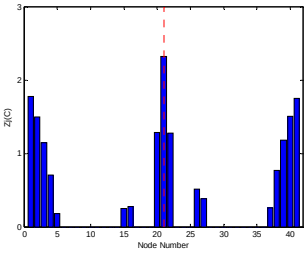

DI-C (5-Modes)

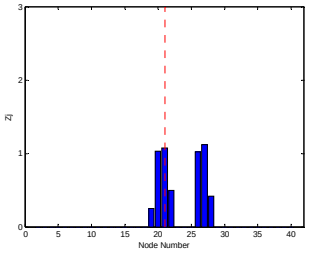

DI-N (5-Modes)

Comparison Results with Noise (4S with 10% noise)

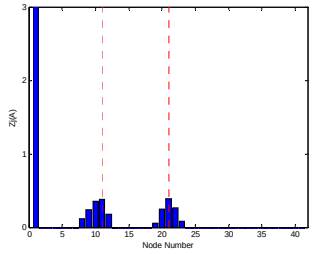

DI-A (1-Mode)

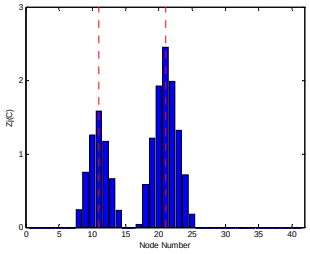

DI-C (1-Mode)

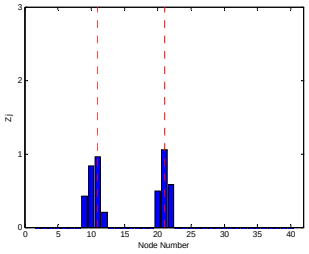

DI-N (1-Mode)

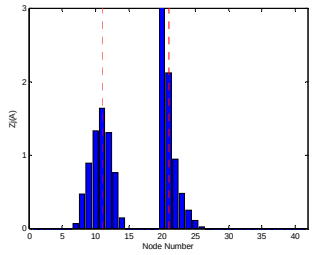

DI-A (2-Modes)

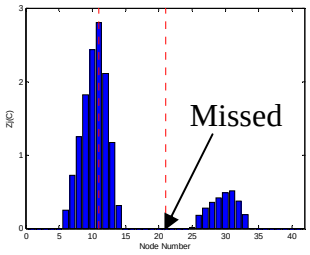

DI-C (2-Modes)

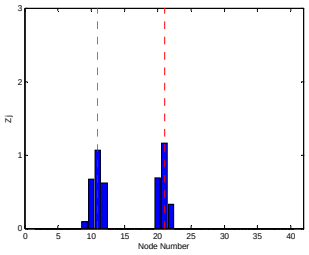

DI-N (2-Modes)

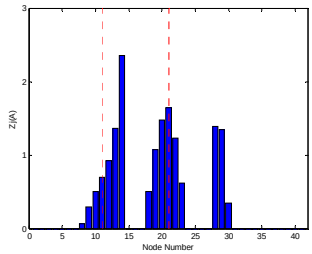

DI-A (3-Modes)

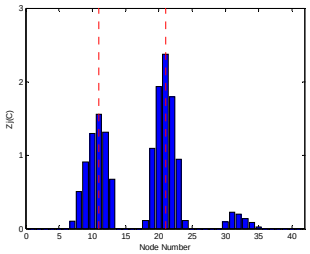

DI-C (3-Modes)

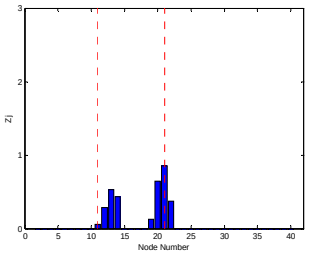

DI-N (3-Modes)

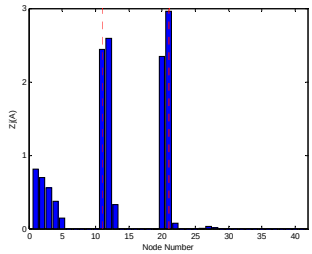

DI-A (4-Modes)

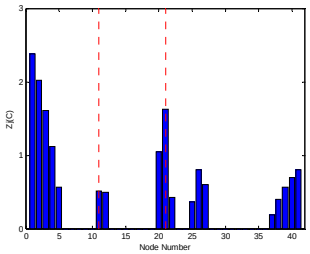

DI-C (4-Modes)

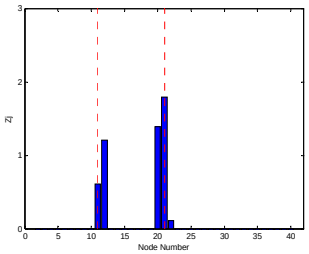

DI-N (4-Modes)

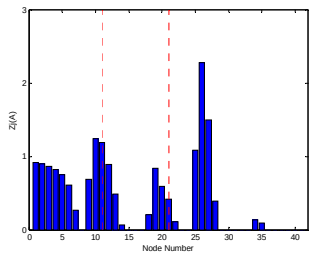

DI-A (5-Modes)

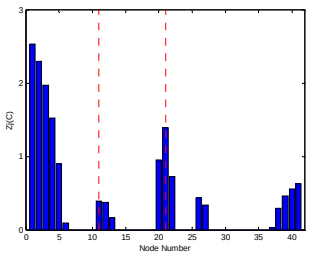

DI-C (5-Modes)

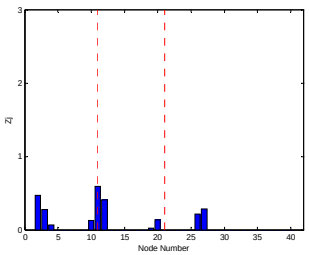

DI-N (5-Modes)

Comparison Results with Noise (2M4M with 0% noise)

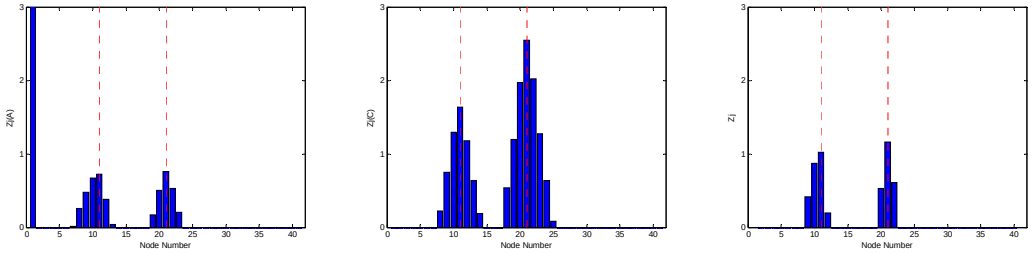

DI-A (1-Mode) DI-C (1-Mode) DI-N (1-Mode)

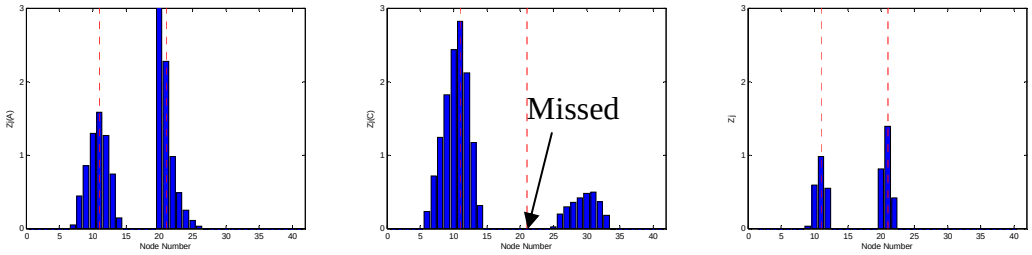

DI-A (2-Modes) DI-C (2-Modes) DI-N (2-Modes)

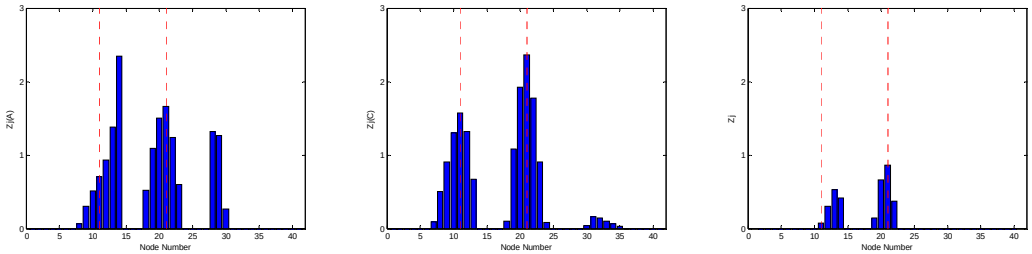

DI-A (3-Modes) DI-C (3-Modes) DI-N (3-Modes)

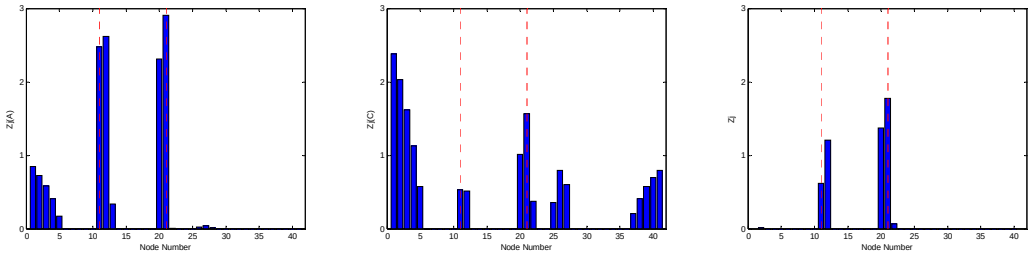

DI-A (4-Modes) DI-C (4-Modes) DI-N (4-Modes)

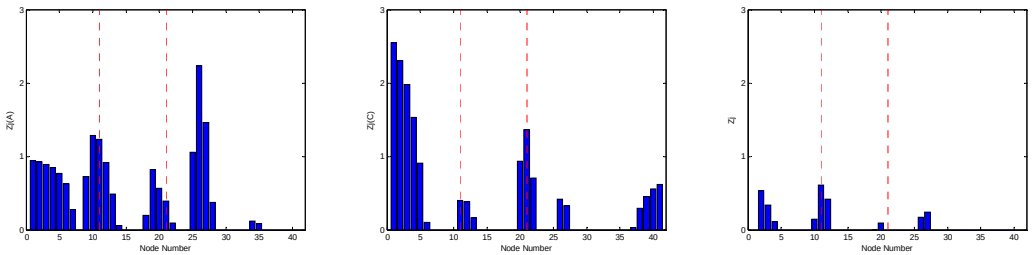

DI-A (5-Modes) DI-C (5-Modes) DI-N (5-Modes)

Comparison Results with Noise (2M4M with 2% noise)

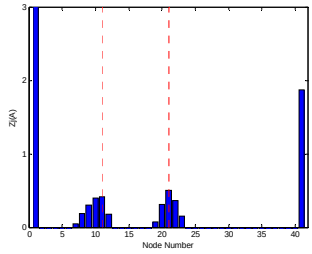

DI-A (1-Mode)

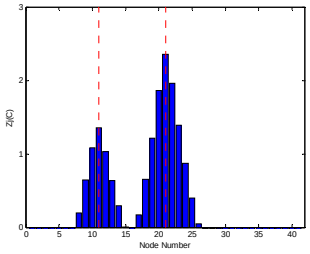

DI-C (1-Mode)

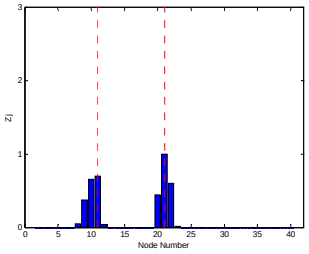

DI-N (1-Mode)

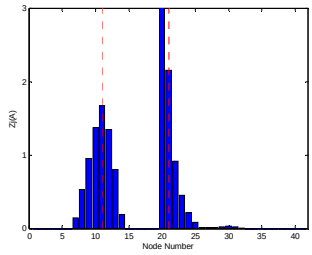

DI-A (2-Modes)

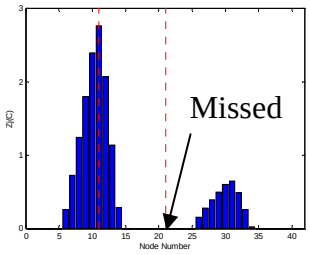

DI-C (2-Modes)

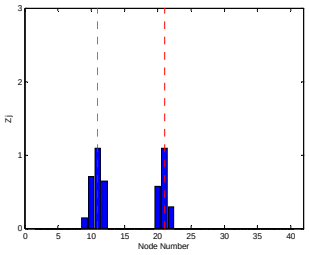

DI-N (2-Modes)

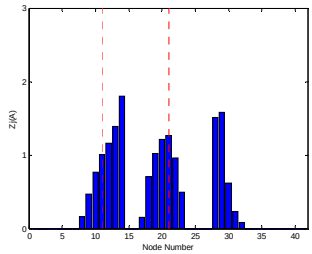

DI-A (3-Modes)

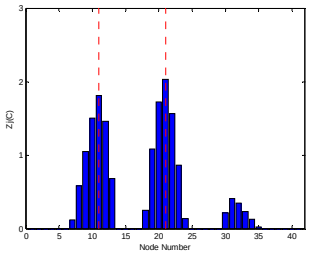

DI-C (3-Modes)

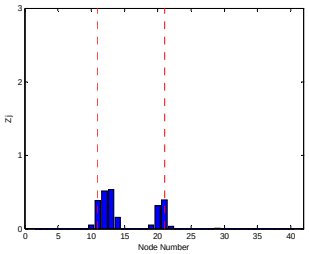

DI-N (3-Modes)

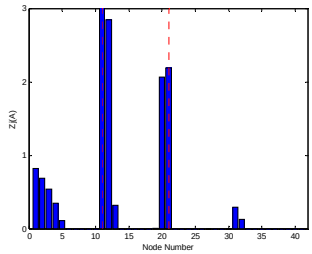

DI-A (4-Modes)

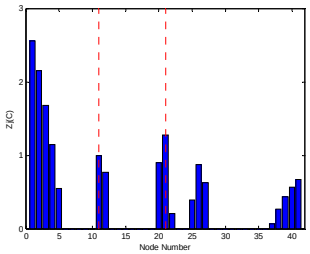

DI-C (4-Modes)

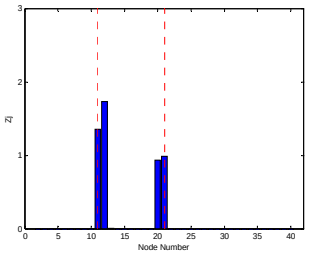

DI-N (4-Modes)

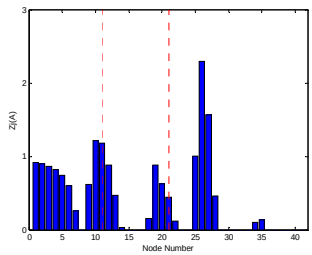

DI-A (5-Modes)

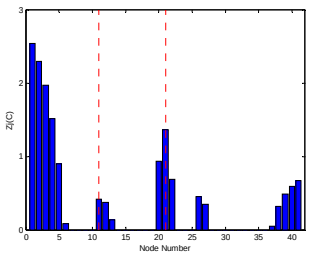

DI-C (5-Modes)

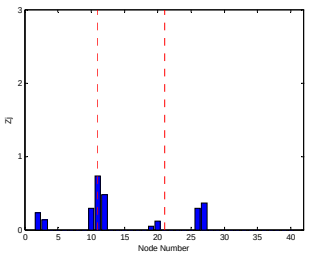

DI-N (5-Modes)

Comparison Results with Noise (2M4M with 10% noise)

B.9 Results of the Improved Method without Noise Pollution

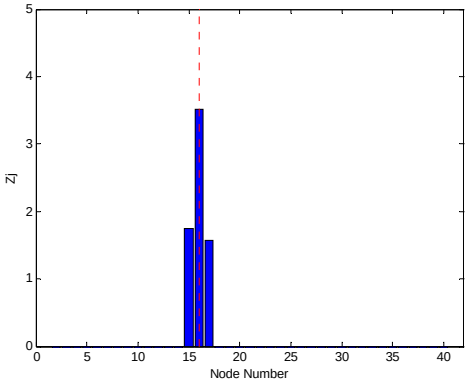

DI-NO (1-Mode)

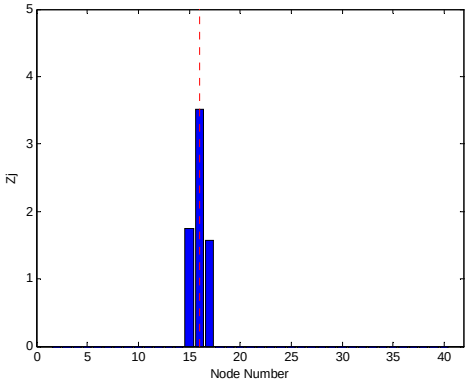

DI-NI (1-Mode)

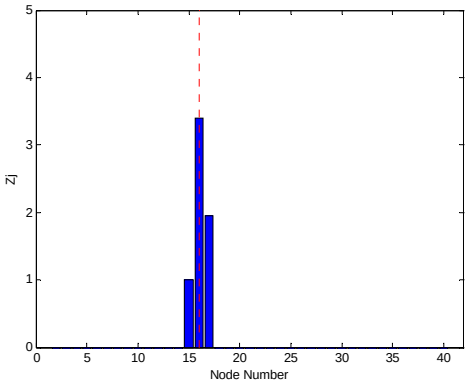

DI-NO (2-Modes)

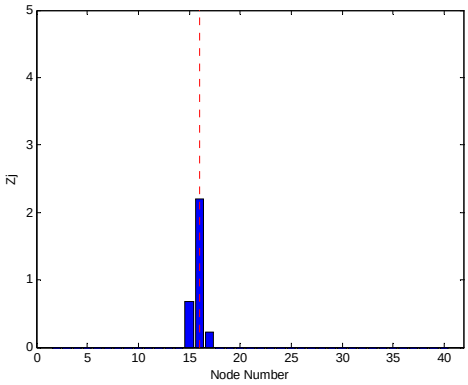

DI-NI (2-Modes)

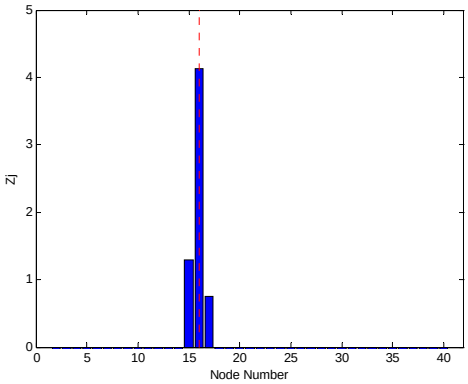

DI-NO (3-Modes)

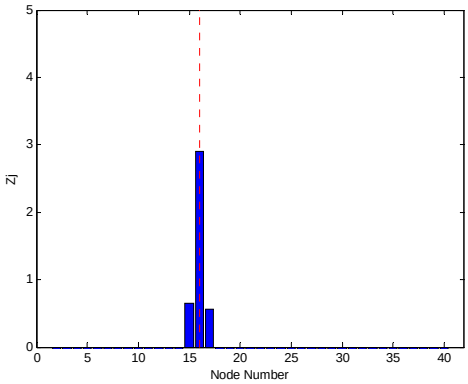

DI-NI (3-Modes)

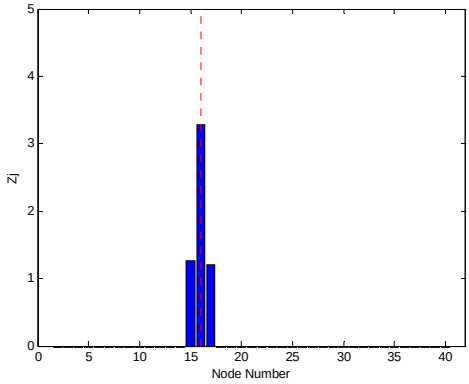

DI-NO (4-Modes)

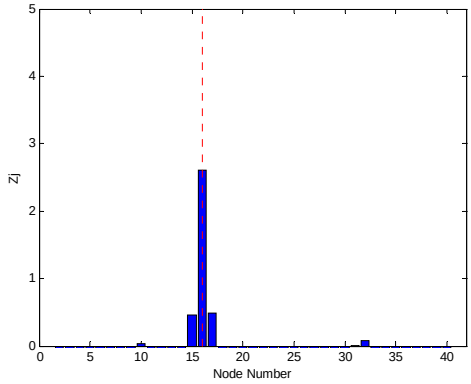

DI-NI (4-Modes)

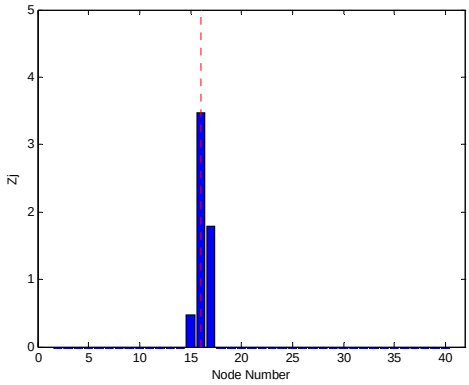

DI-NO (5-Modes)

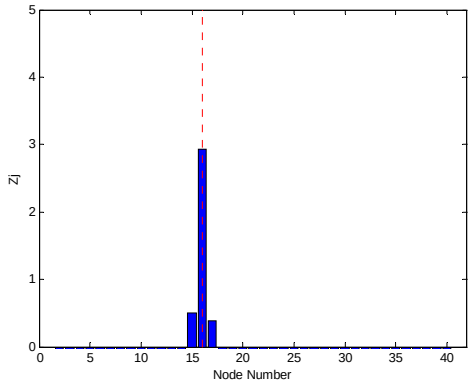

DI-NI (5-Modes)

Results of the Improved Method without Noise (3L)

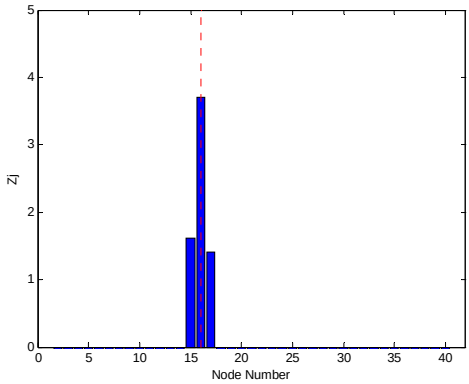

DI-NO (1-Mode)

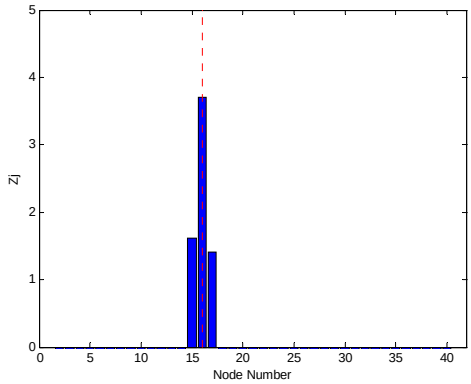

DI-NI (1-Mode)

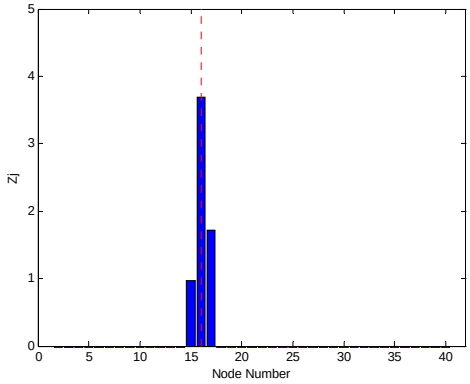

DI-NO (2-Modes)

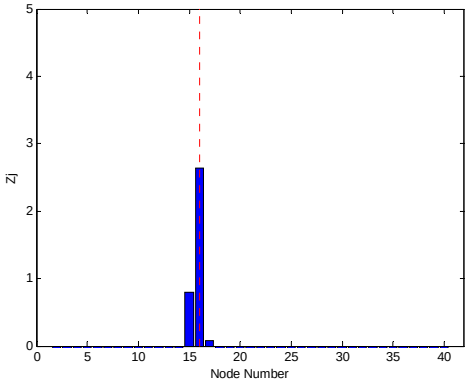

DI-NI (2-Modes)

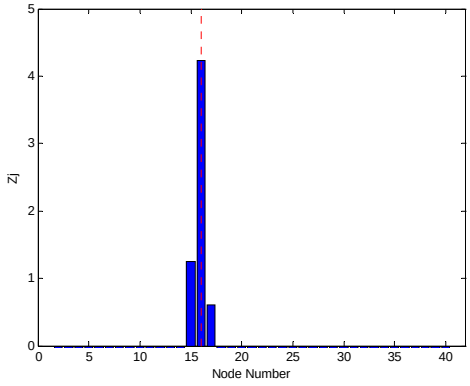

DI-NO (3-Modes)

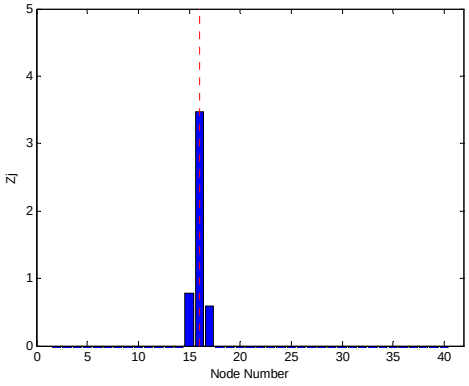

DI-NI (3-Modes)

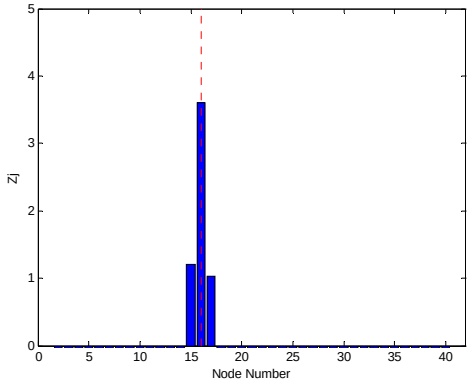

DI-NO (4-Modes)

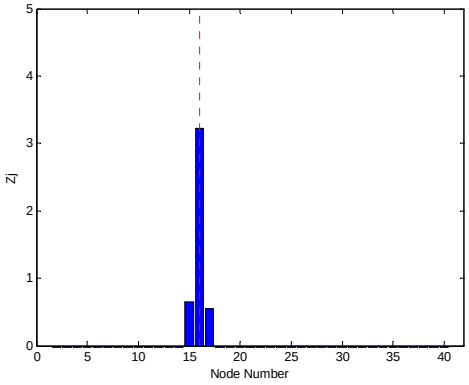

DI-NI (4-Modes)

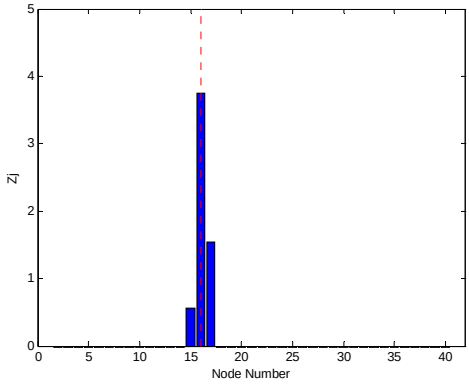

DI-NO (5-Modes)

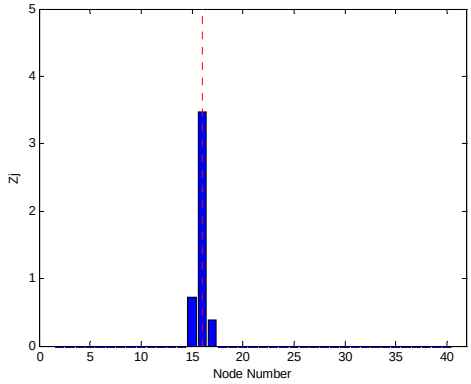

DI-NI (5-Modes)

Results of the Improved Method without Noise (3M)

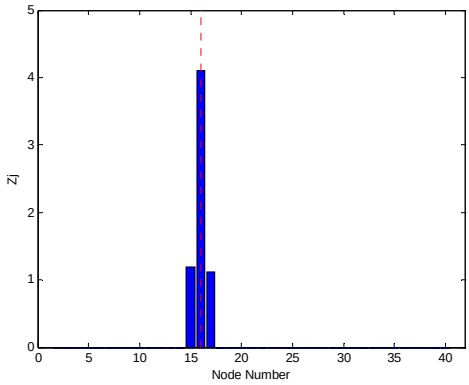

DI-NO (1-Mode)

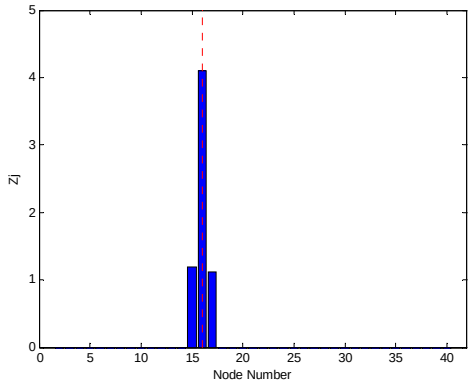

DI-NI (1-Mode)

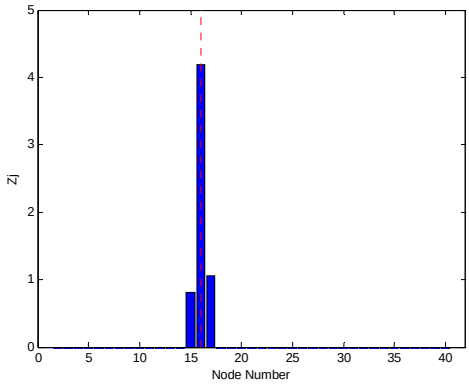

DI-NO (2-Modes)

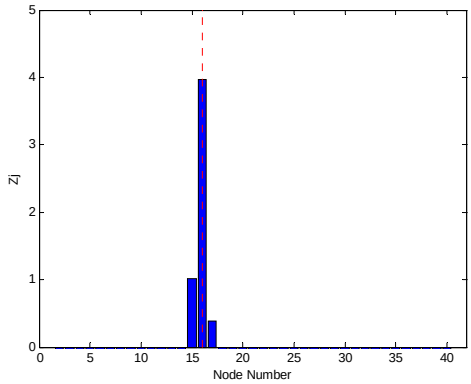

DI-NI (2-Modes)

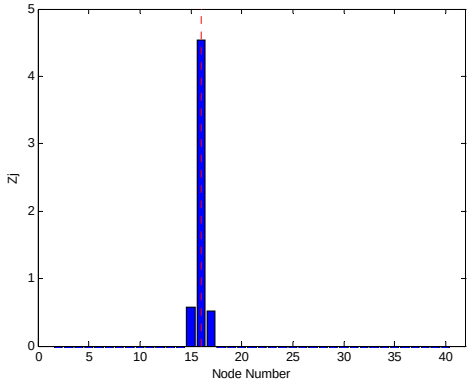

DI-NO (3-Modes)

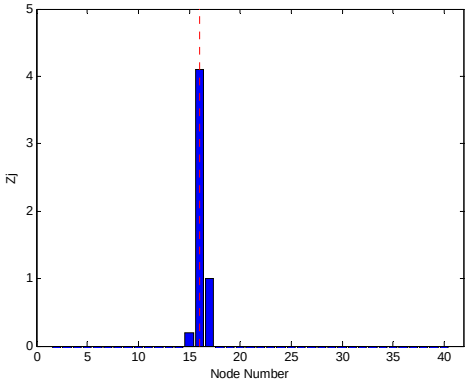

DI-NI (3-Modes)

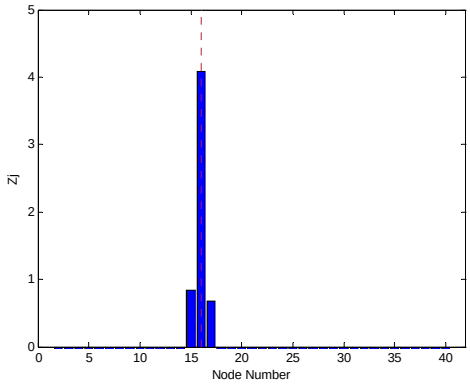

DI-NO (4-Modes)

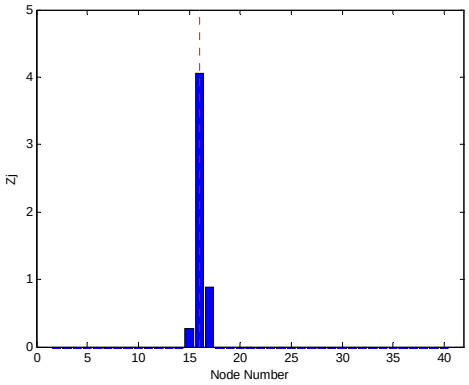

DI-NI (4-Modes)

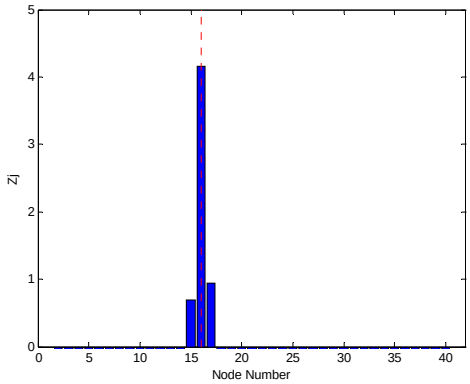

DI-NO (5-Modes)

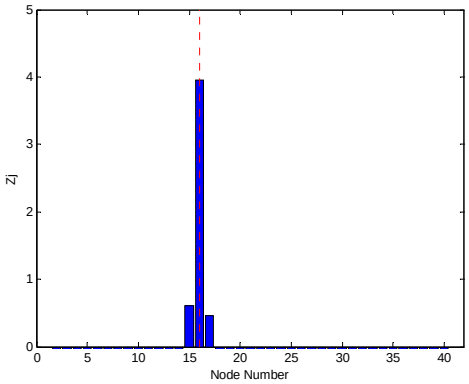

DI-NI (5-Modes)

Results of the Improved Method without Noise (3S)

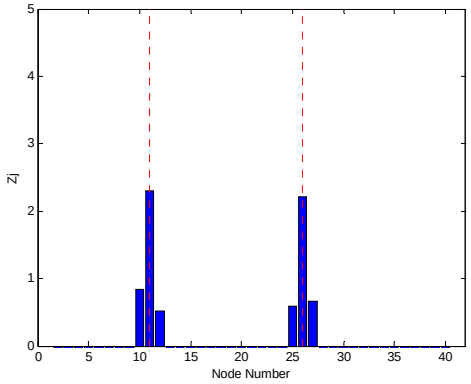

DI-NO (1-Mode)

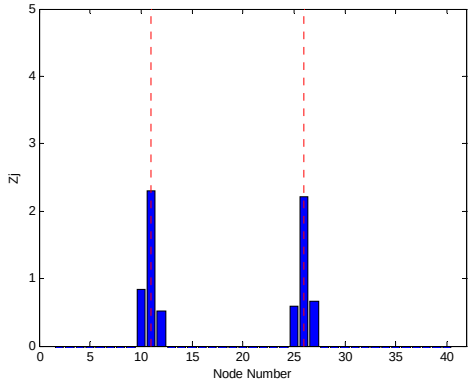

DI-NI (1-Mode)

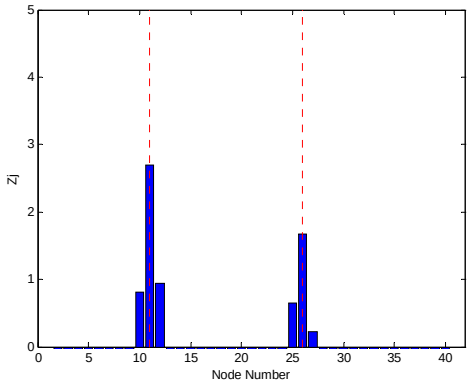

DI-NO (2-Modes)

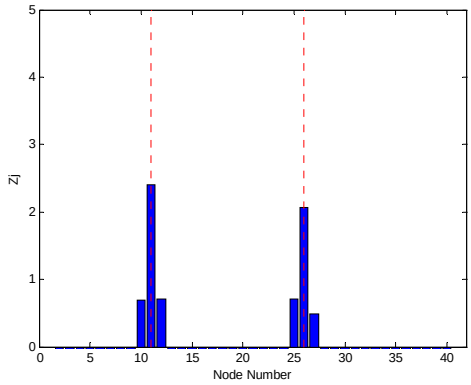

DI-NI (2-Modes)

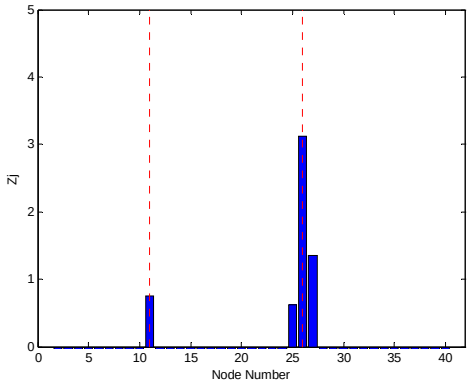

DI-NO (3-Modes)

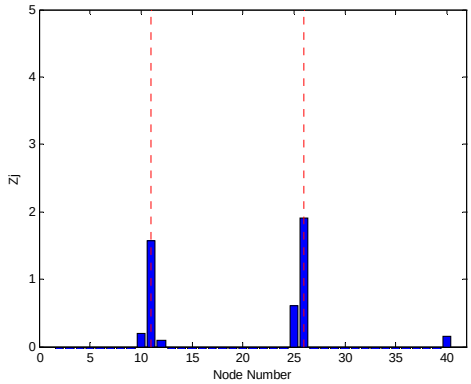

DI-NI (3-Modes)

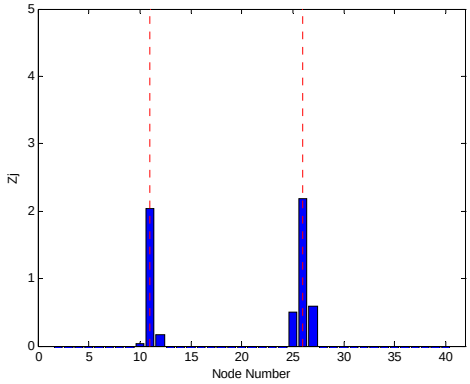

DI-NO (4-Modes)

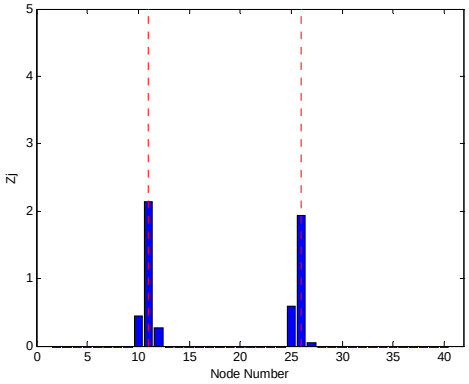

DI-NI (4-Modes)

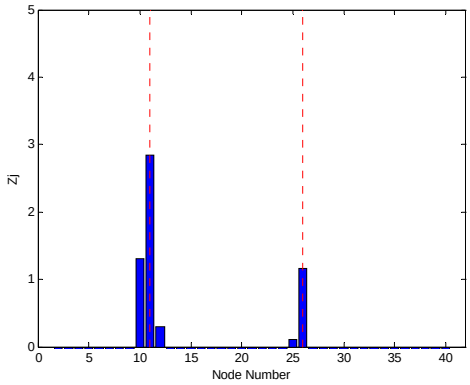

DI-NO (5-Modes)

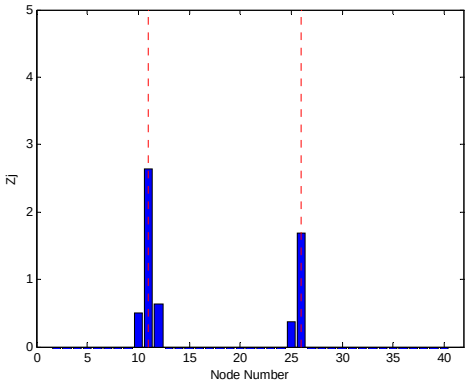

DI-NI (5-Modes)

Results of the Improved Method without Noise (2M5M)

B.10 Results of the Improved Method with Simulated Noise

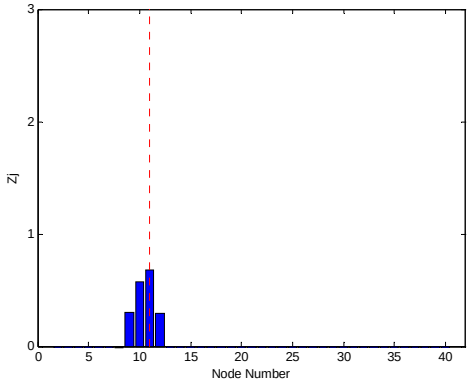

DI-NO (1-Mode)

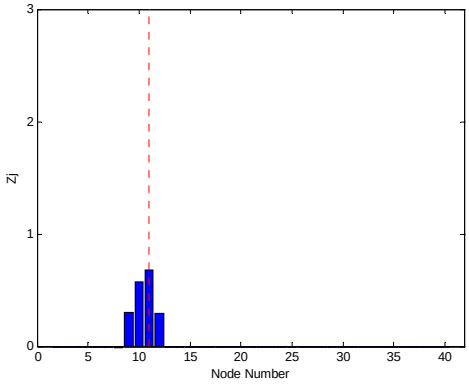

DI-NI (1-Mode)

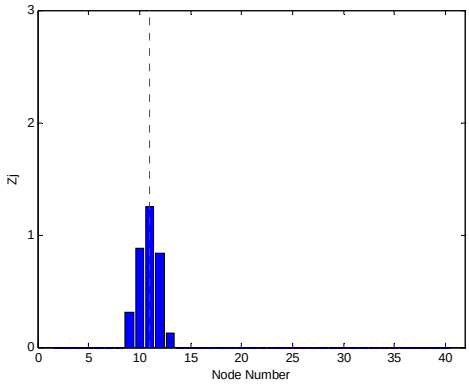

DI-NO (2-Modes)

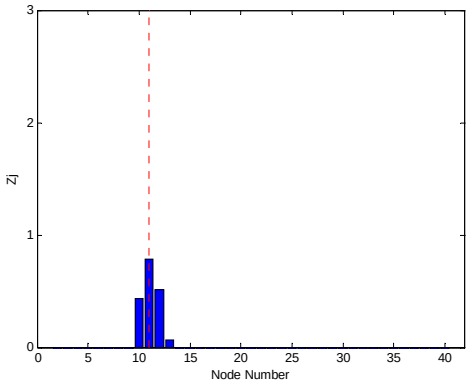

DI-NI (2-Modes)

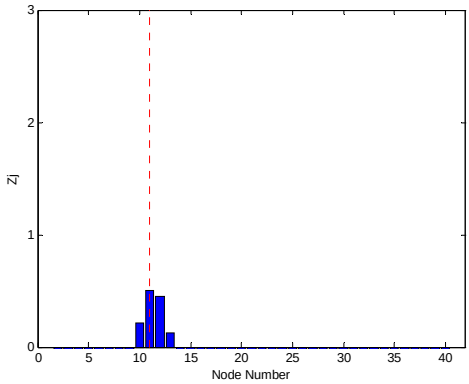

DI-NO (3-Modes)

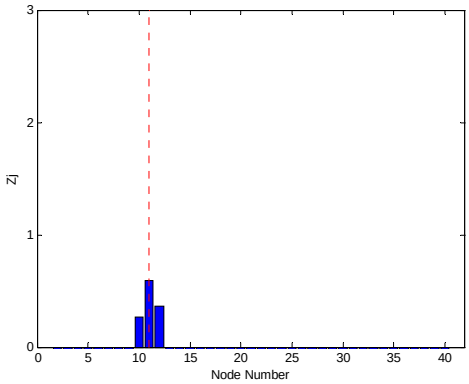

DI-NI (3-Modes)

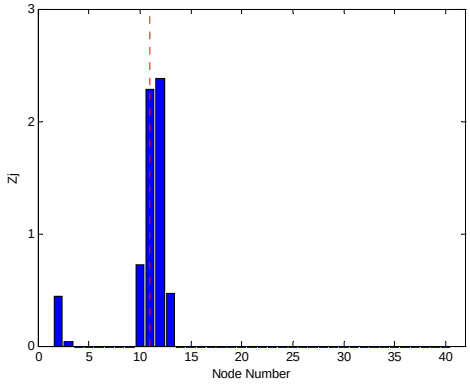

DI-NO (4-Modes)

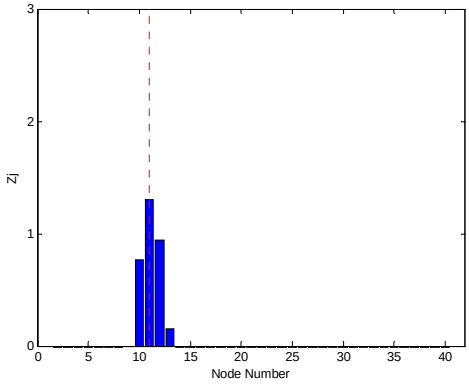

DI-NI (4-Modes)

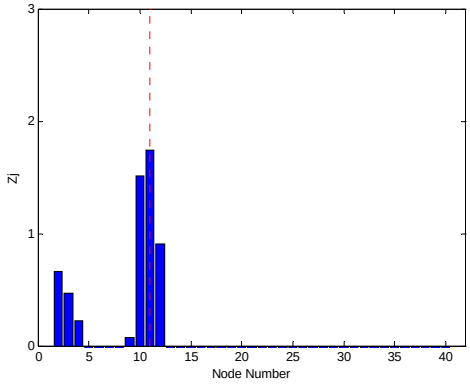

DI-NO (5-Modes)

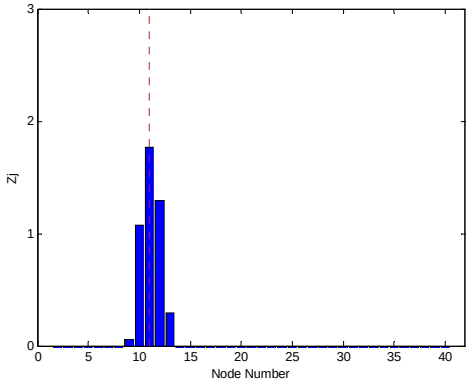

DI-NI (5-Modes)

Results of the Improved Method with Noise (2L with 0% noise)

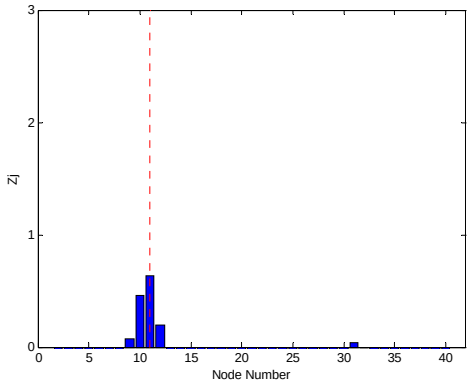

DI-NO (1-Mode)

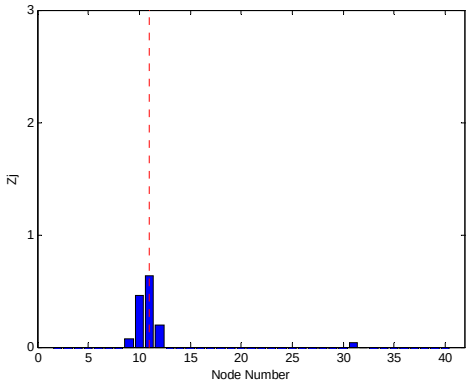

DI-NI (1-Mode)

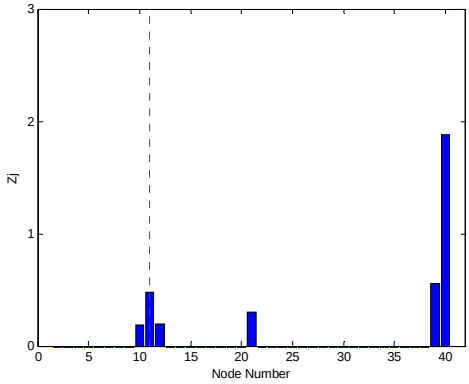

DI-NO (2-Modes)

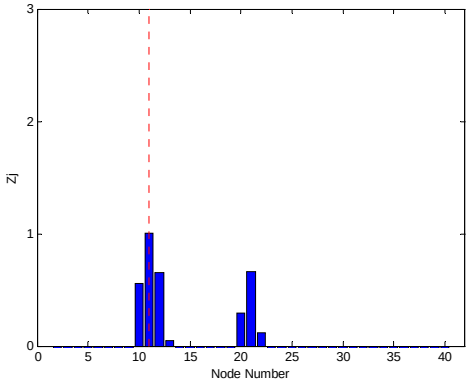

DI-NI (2-Modes)

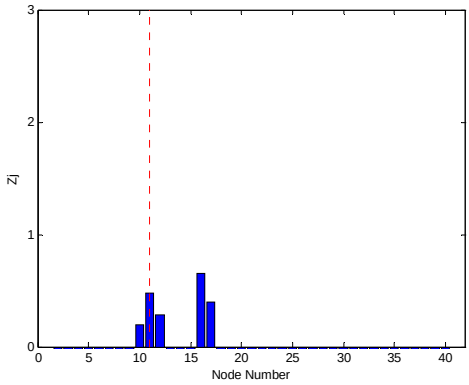

DI-NO (3-Modes)

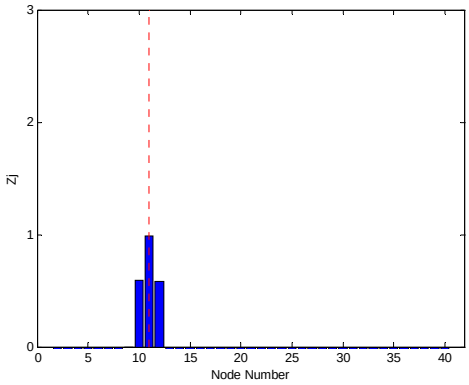

DI-NI (3-Modes)

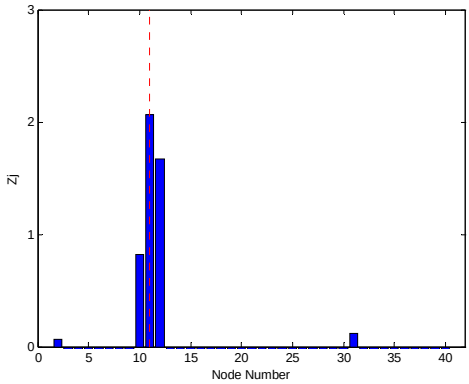

DI-NO (4-Modes)

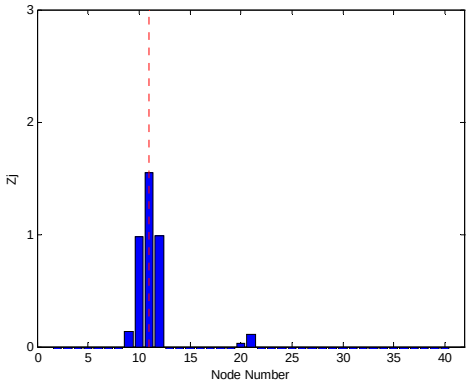

DI-NI (4-Modes)

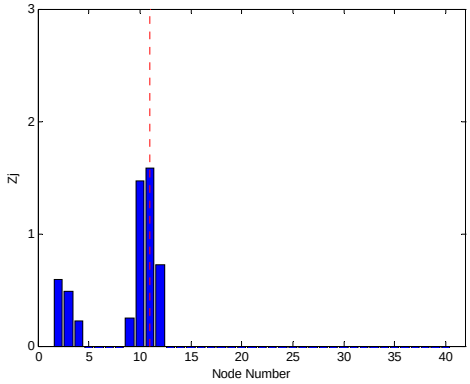

DI-NO (5-Modes)

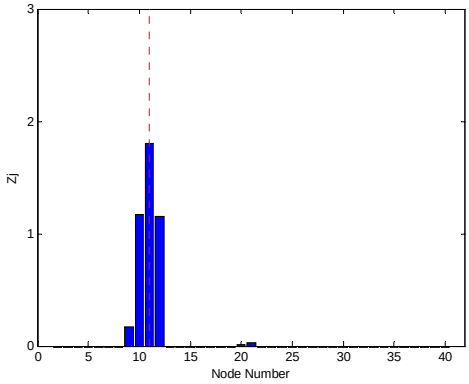

DI-NI (5-Modes)

Results of the Improved Method with Noise (2L with 10% noise)

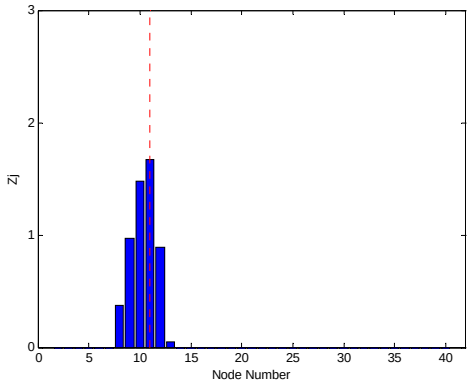

DI-NO (1-Mode)

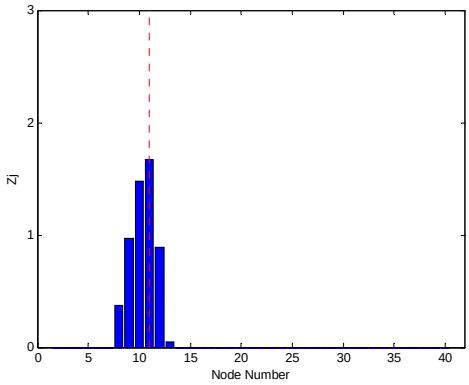

DI-NI (1-Mode)

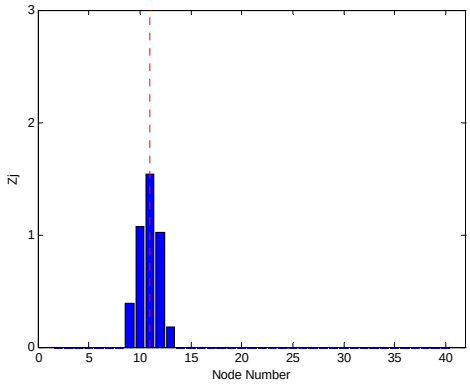

DI-NO (2-Modes)

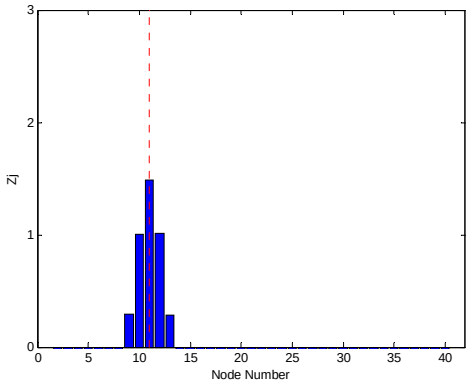

DI-NI (2-Modes)

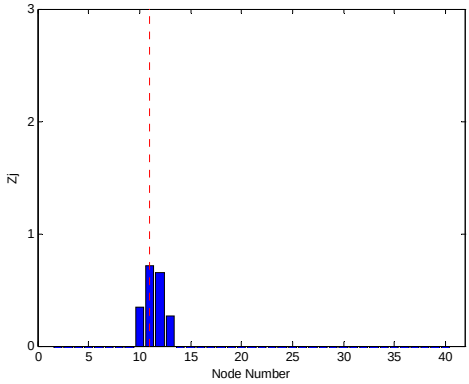

DI-NO (3-Modes)

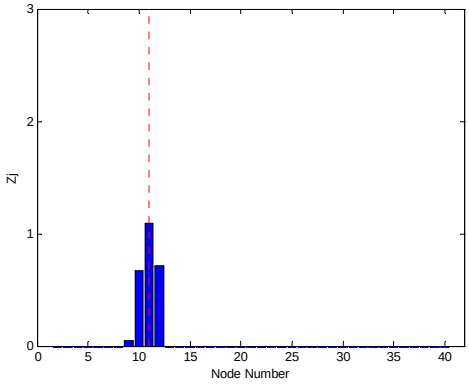

DI-NI (3-Modes)

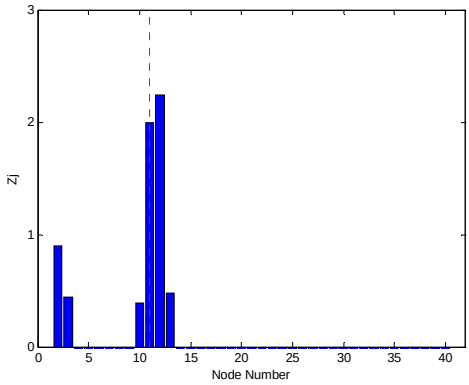

DI-NO (4-Modes)

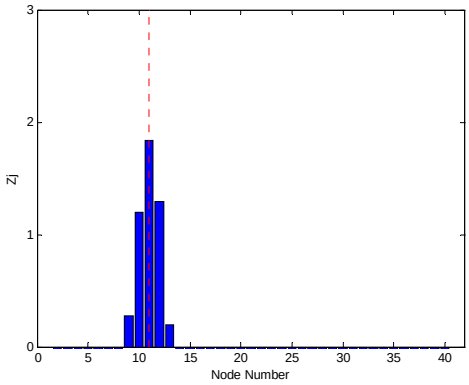

DI-NI (4-Modes)

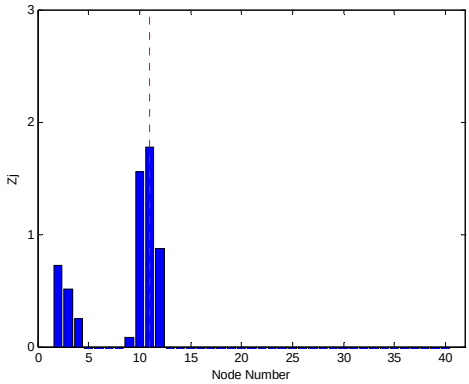

DI-NO (5-Modes)

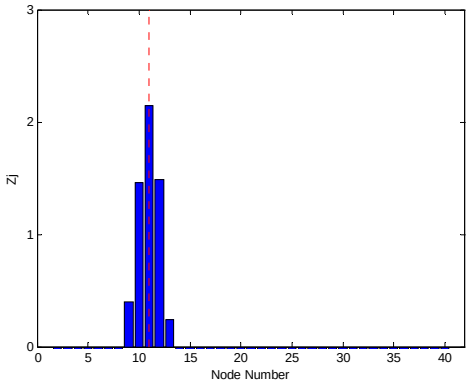

DI-NI (5-Modes)

Results of the Improved Method with Noise (2M with 0% noise)

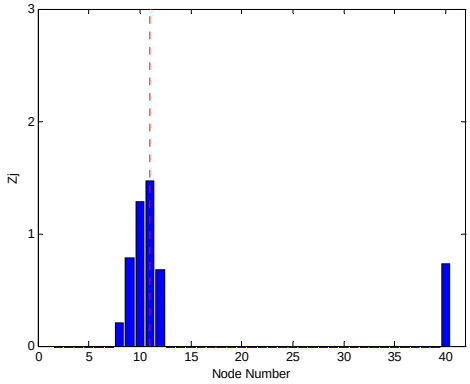

DI-NO (1-Mode)

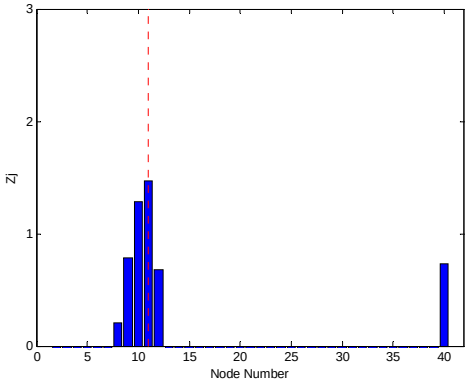

DI-NI (1-Mode)

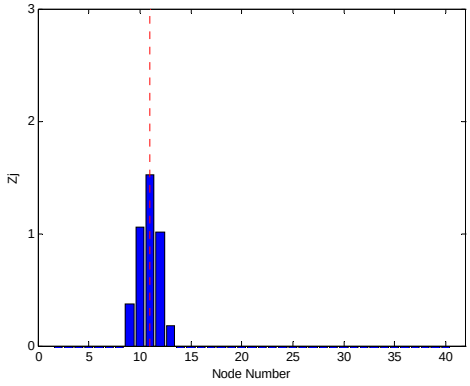

DI-NO (2-Modes)

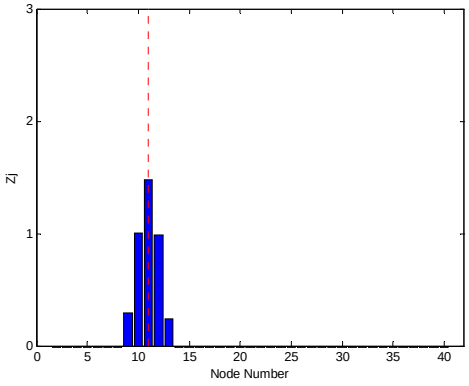

DI-NI (2-Modes)

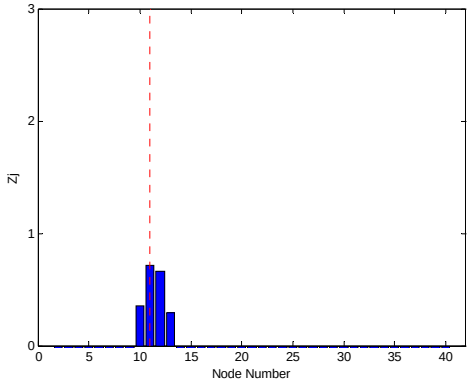

DI-NO (3-Modes)

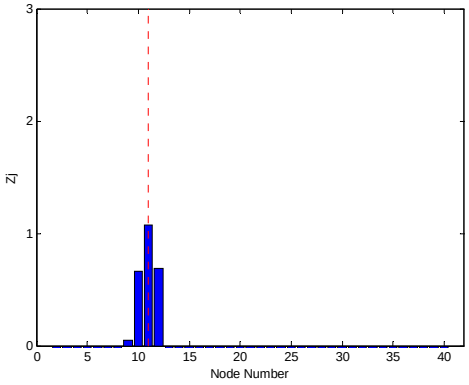

DI-NI (3-Modes)

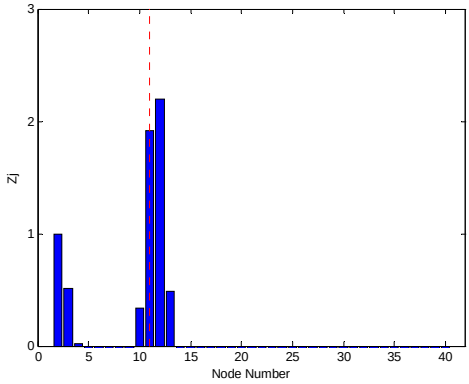

DI-NO (4-Modes)

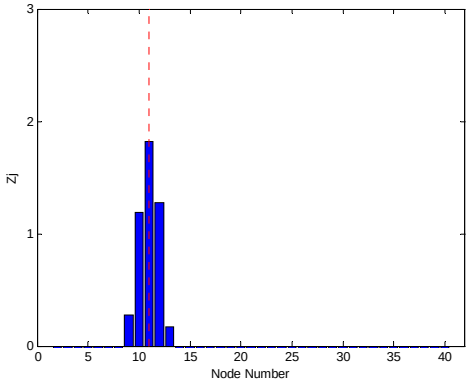

DI-NI (4-Modes)

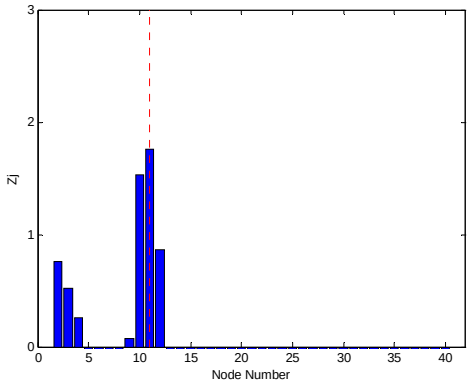

DI-NO (5-Modes)

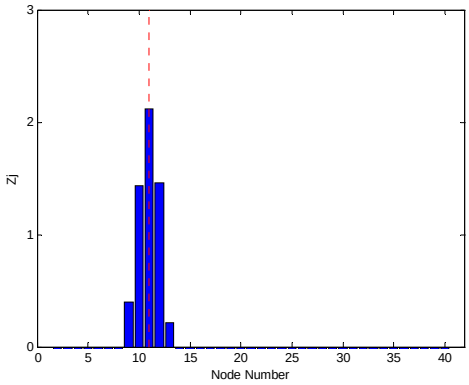

DI-NI (5-Modes)

Results of the Improved Method with Noise (2M with 2% noise)

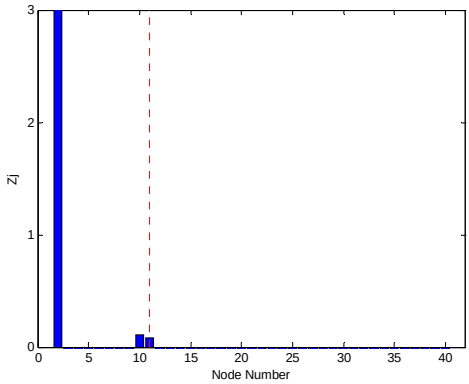

DI-NO (1-Mode)

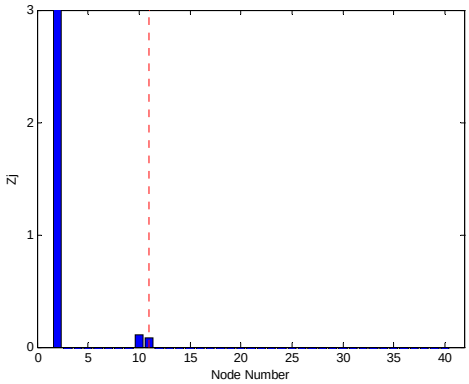

DI-NI (1-Mode)

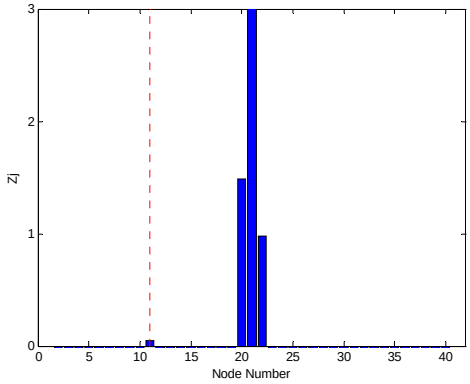

DI-NO (2-Modes)

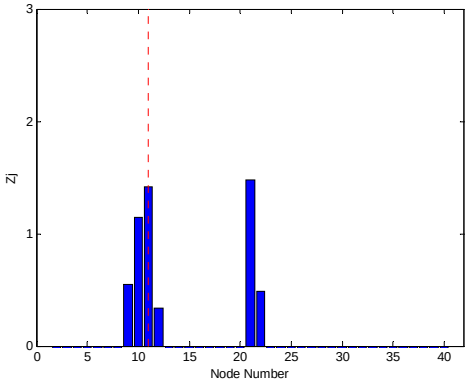

DI-NI (2-Modes)

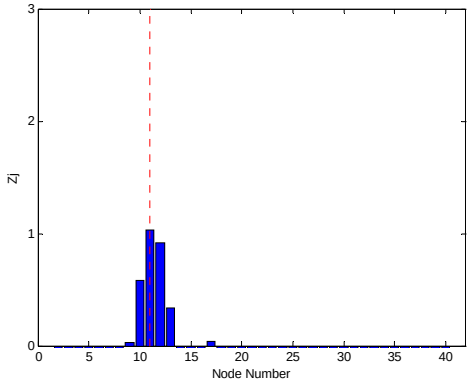

DI-NO (3-Modes)

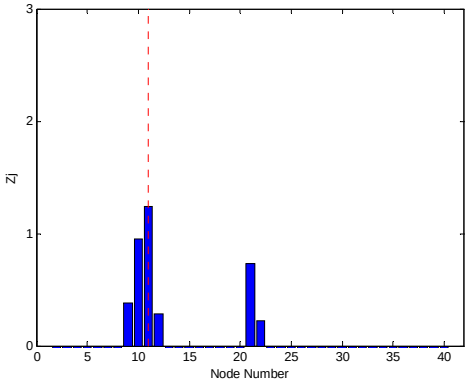

DI-NI (3-Modes)

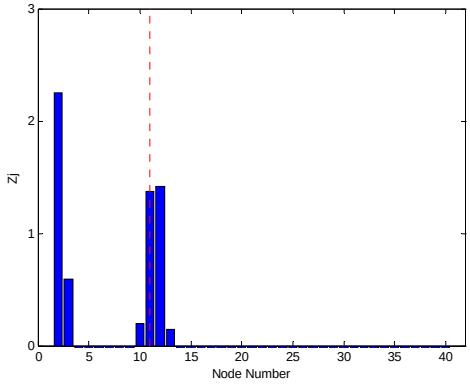

DI-NO (4-Modes)

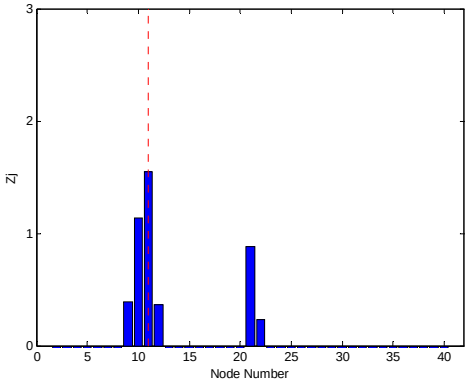

DI-NI (4-Modes)

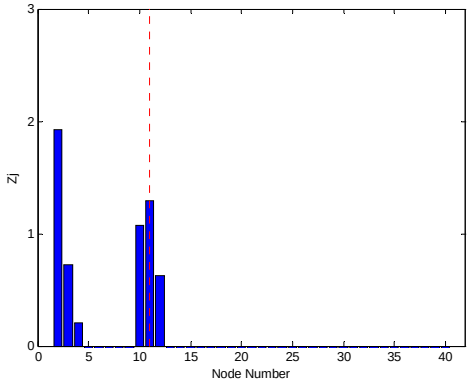

DI-NO (5-Modes)

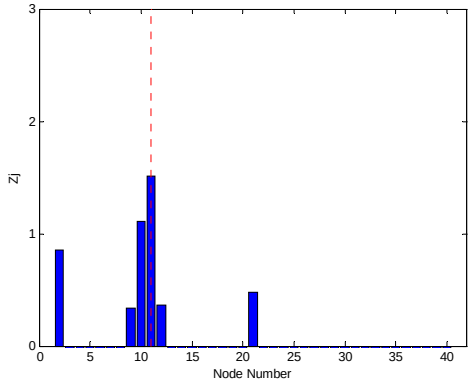

DI-NI (5-Modes)

Results of the Improved Method with Noise (2M with 10% noise)

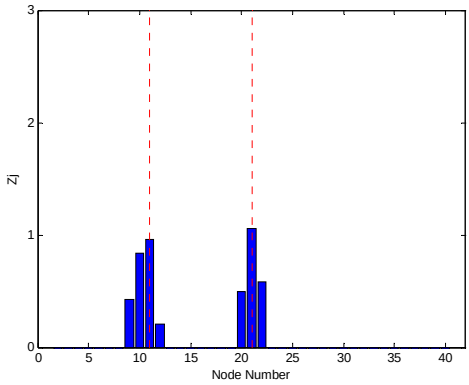

DI-NO (1-Mode)

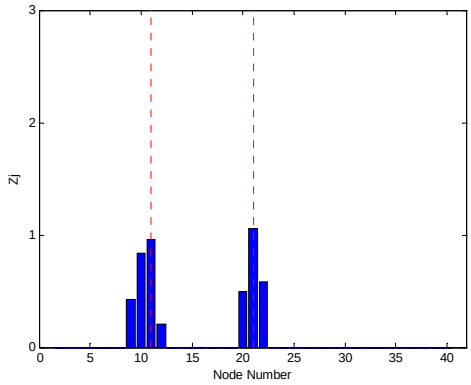

DI-NI (1-Mode)

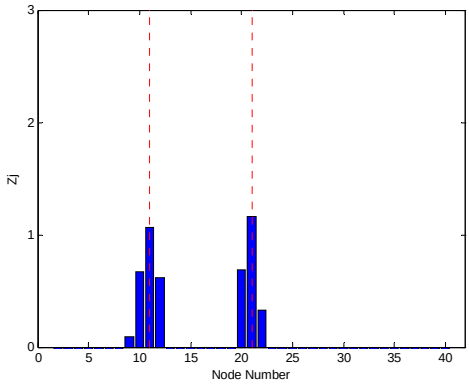

DI-NO (2-Modes)

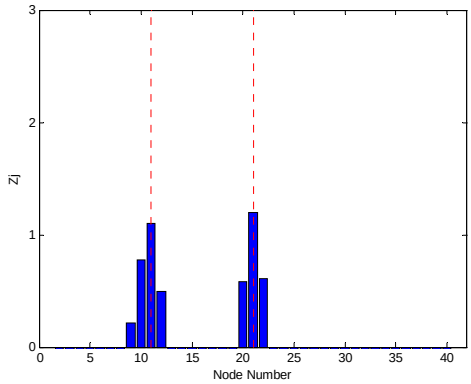

DI-NI (2-Modes)

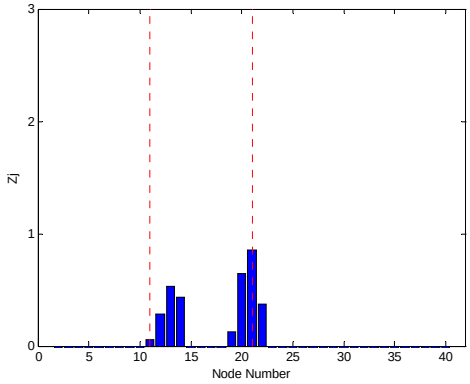

DI-NO (3-Modes)

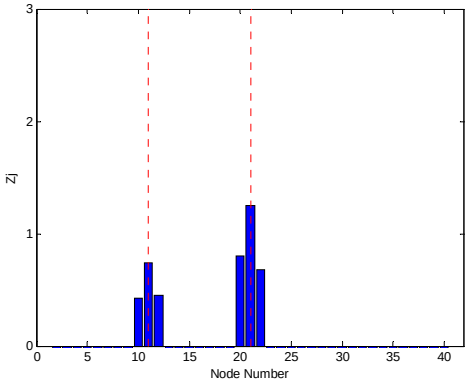

DI-NI (3-Modes)

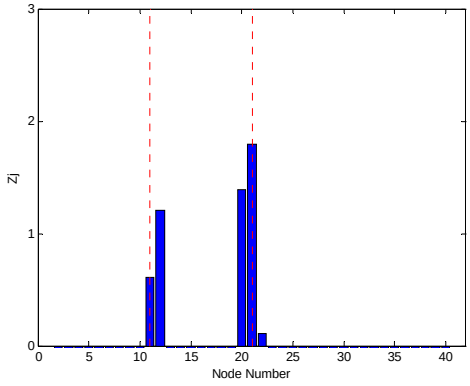

DI-NO (4-Modes)

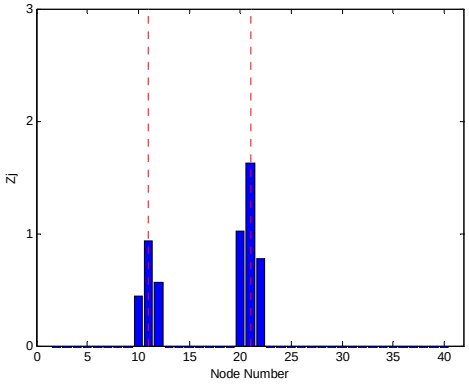

DI-NI (4-Modes)

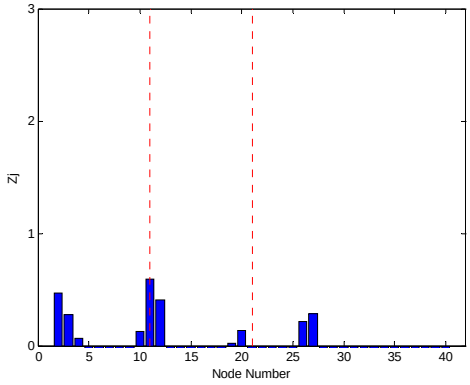

DI-NO (5-Modes)

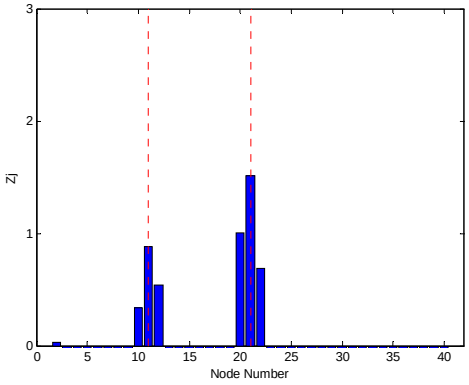

DI-NI (5-Modes)

Results of the Improved Method with Noise (2M4M with 0% noise)

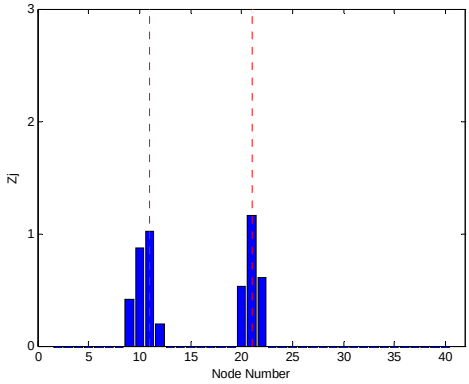

DI-NO (1-Mode)

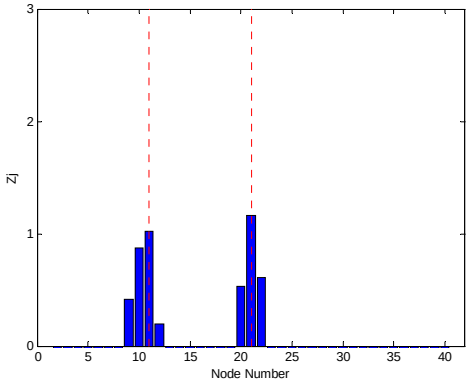

DI-NI (1-Mode)

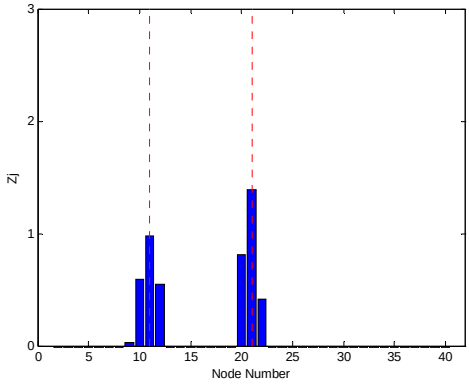

DI-NO (2-Modes)

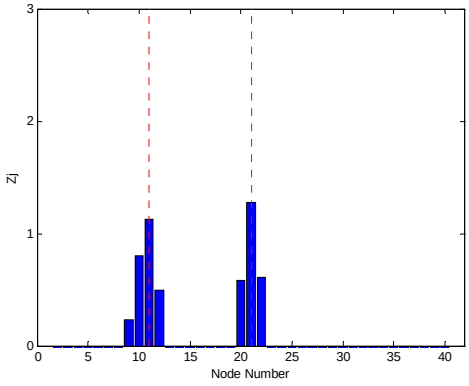

DI-NI (2-Modes)

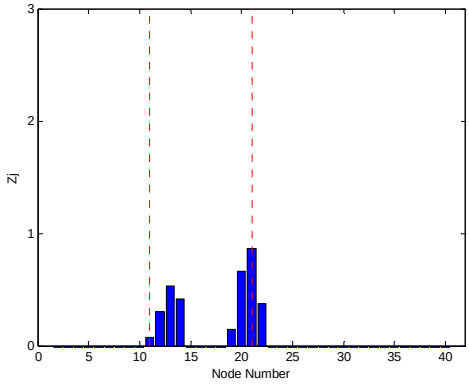

DI-NO (3-Modes)

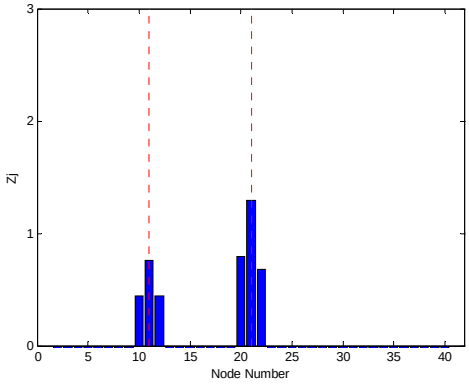

DI-NI (3-Modes)

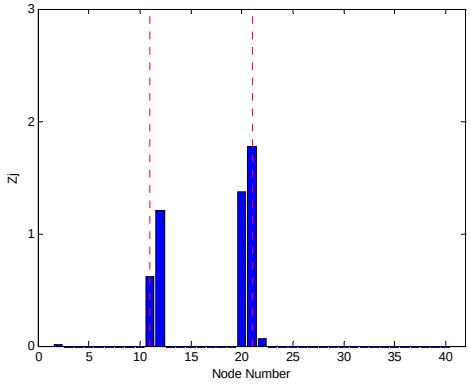

DI-NO (4-Modes)

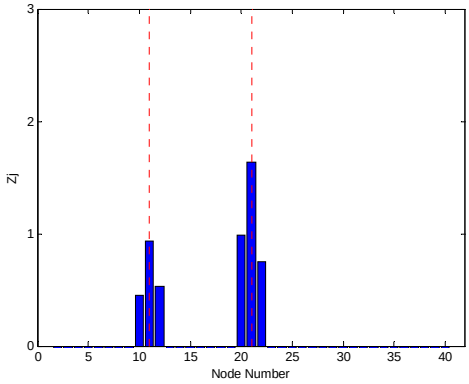

DI-NI (4-Modes)

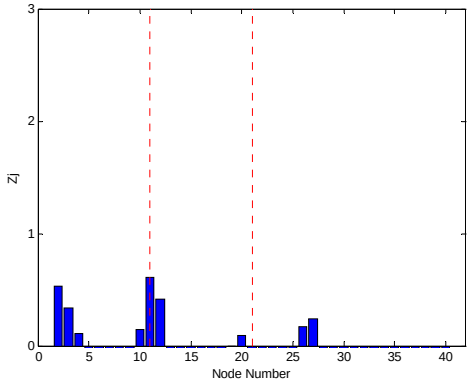

DI-NO (5-Modes)

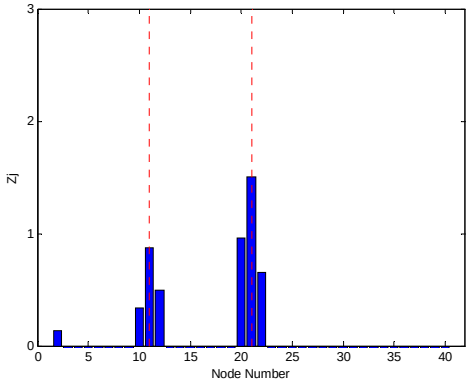

DI-NI (5-Modes)

Results of the Improved Method with Noise (2M4M with 2% noise)

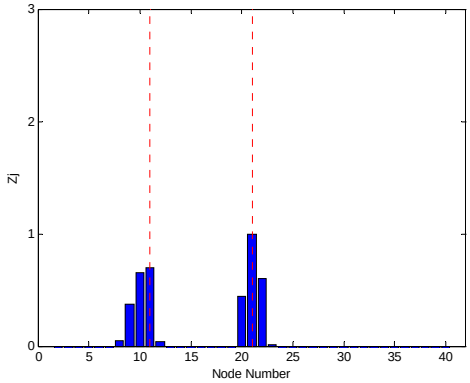

DI-NO (1-Mode)

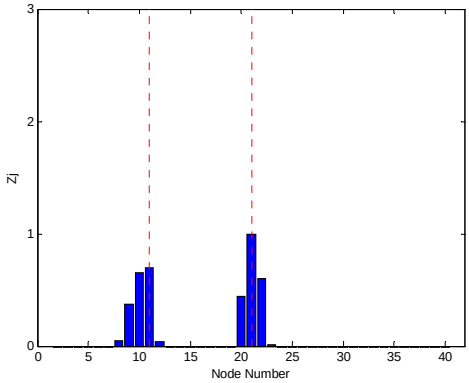

DI-NI (1-Mode)

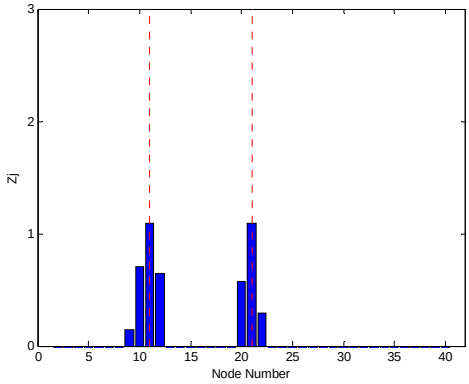

DI-NO (2-Modes)

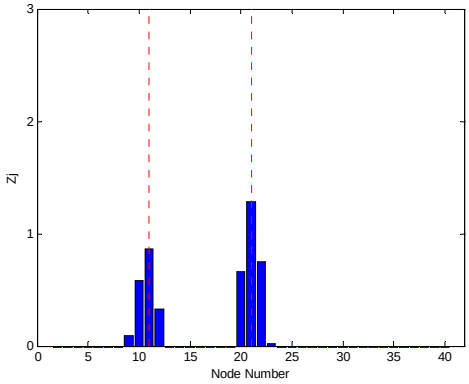

DI-NI (2-Modes)

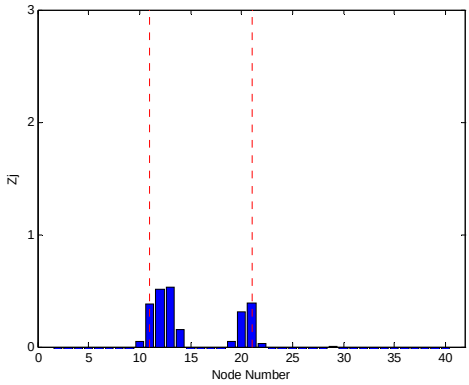

DI-NO (3-Modes)

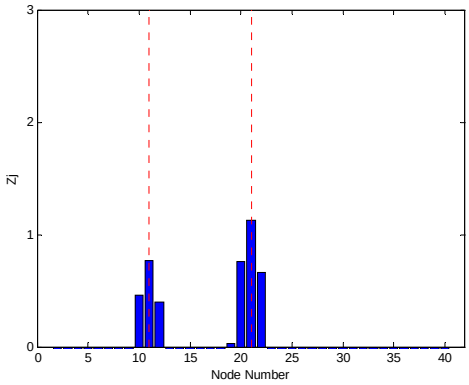

DI-NI (3-Modes)

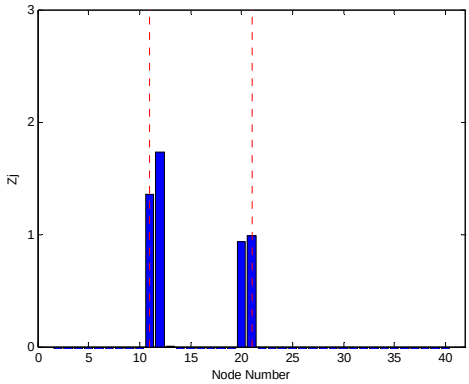

DI-NO (4-Modes)

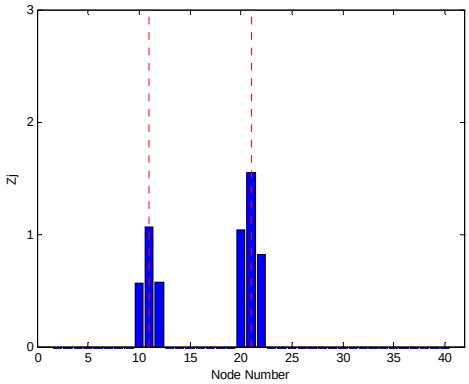

DI-NI (4-Modes)

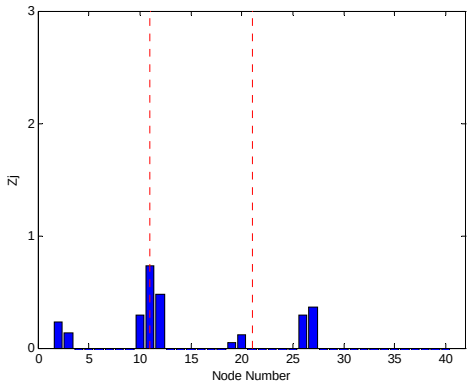

DI-NO (5-Modes)

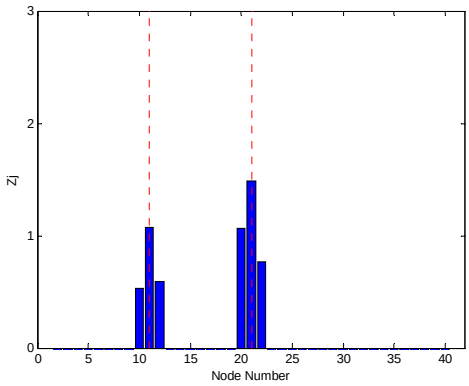

DI-NI (5-Modes)

Results of the Improved Method with Noise (2M4M with 10% noise)

APPENDIX C

C.1 Results of Damage Detection of the RC Beams in the Experimental Work

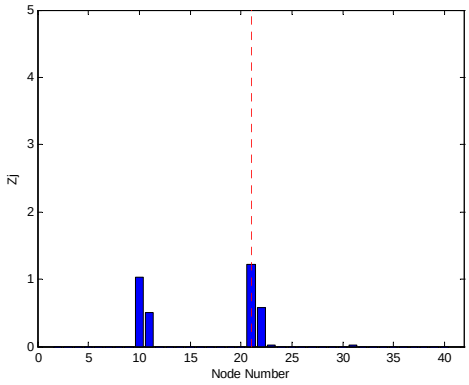

(a) Mode 1

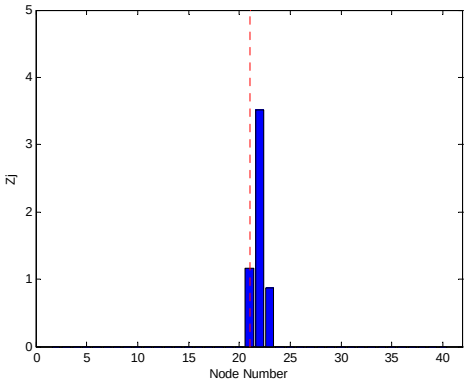

(b) Modes 1+2

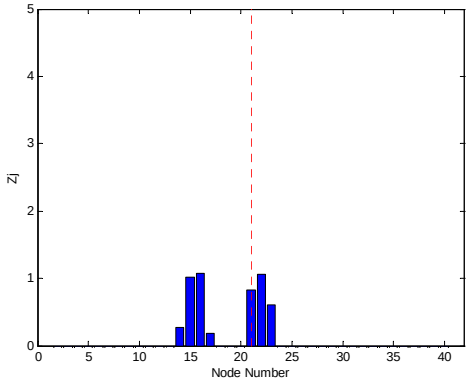

(c) Modes 1+2+3

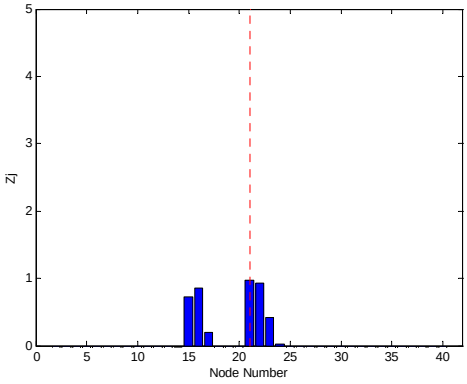

(d) Modes 1+2+3+4

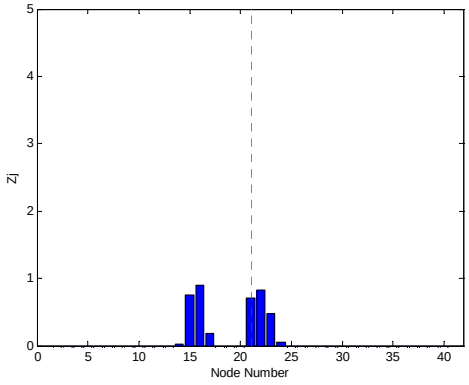

(e) Modes 1+2+3+4+5

Damage Detection of the RC Beams (4L)

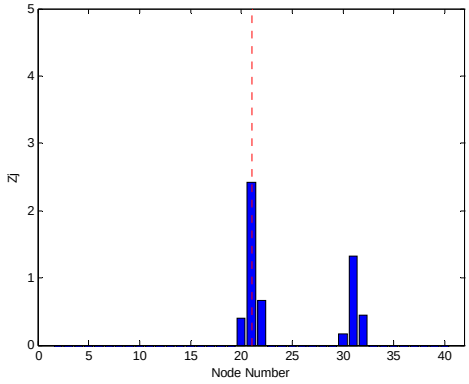

(a) Mode 1

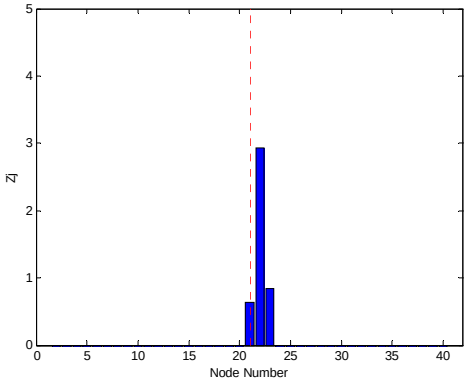

(b) Modes 1+2

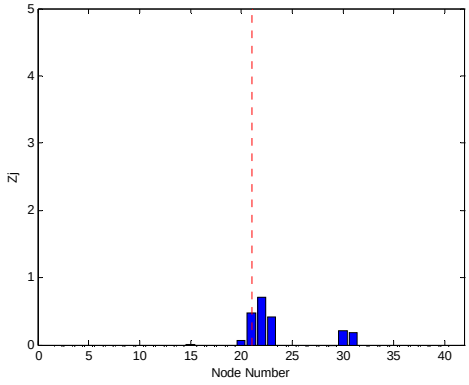

(c) Modes 1+2+3

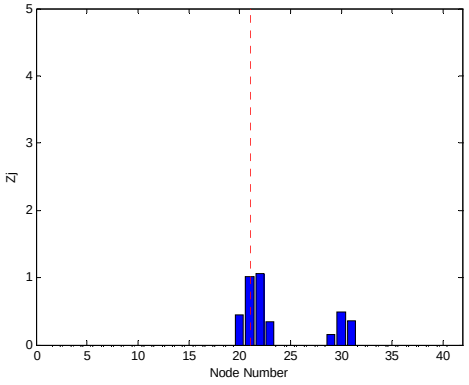

(d) Modes 1+2+3+4

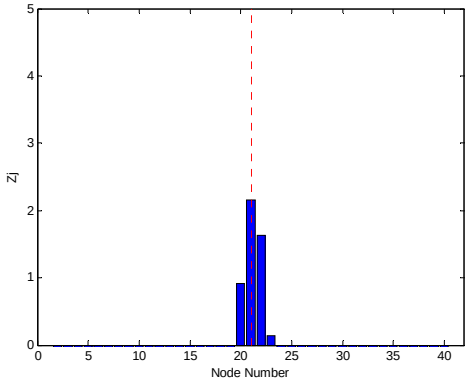

(e) Modes 1+2+3+4+5

Damage Detection of the RC Beams (4M)

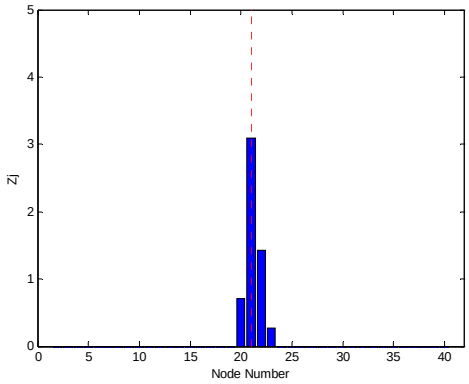

(a) Mode 1

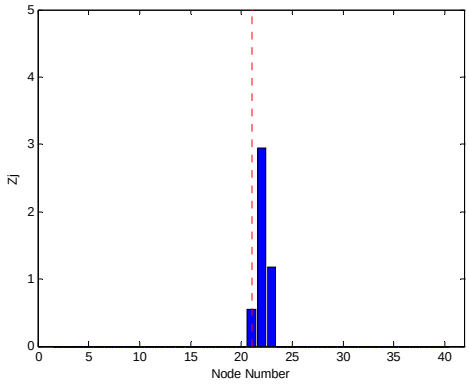

(b) Modes 1+2

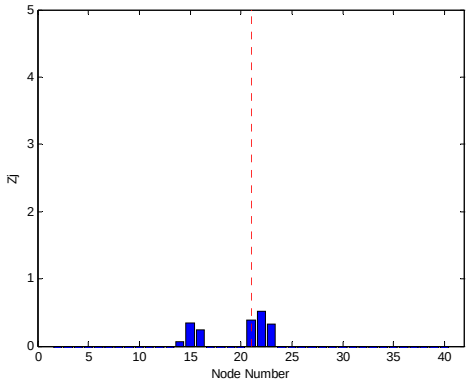

(c) Modes 1+2+3

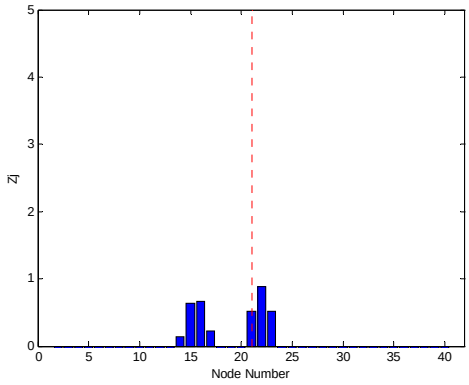

(d) Modes 1+2+3+4

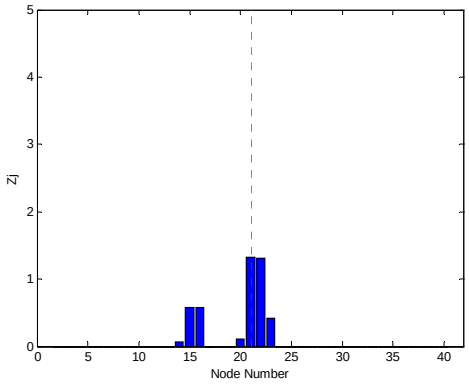

(e) Modes 1+2+3+4+5

Damage Detection of the RC Beams (4S)

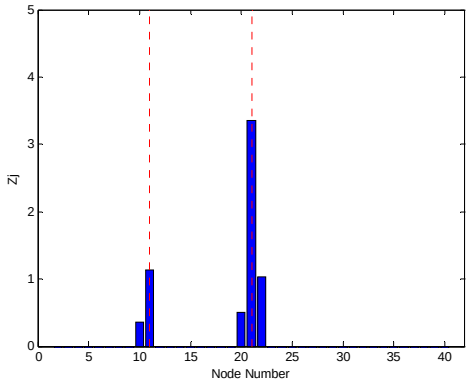

(a) Mode 1

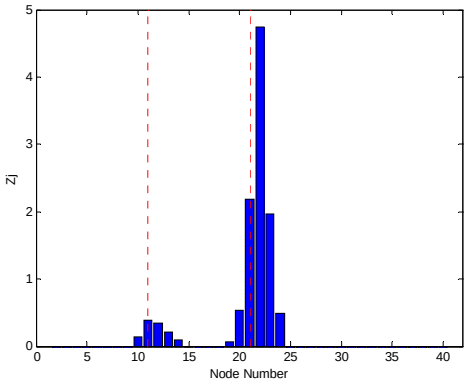

(b) Modes 1+2

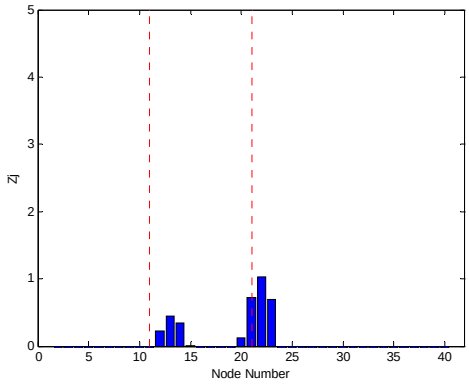

(c) Modes 1+2+3

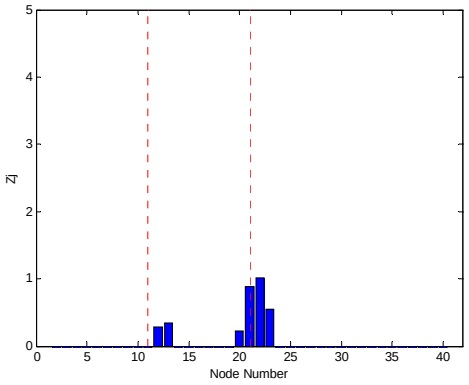

(d) Modes 1+2+3+4

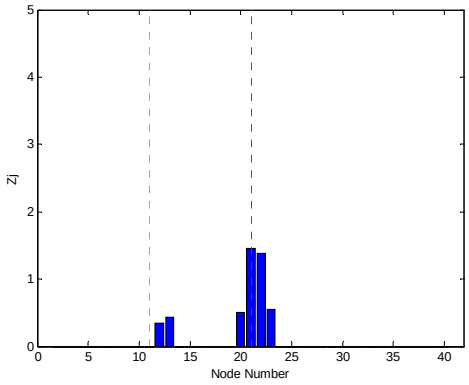

(e) Modes 1+2+3+4+5

Damage Detection of the RC Beams (2S4S)

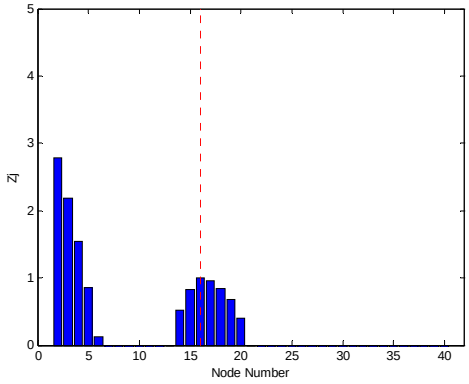

(a) Mode 1

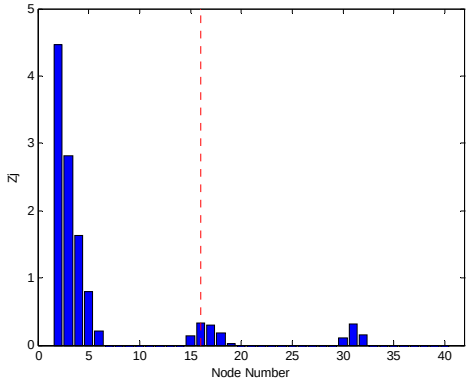

(b) Modes 1+2

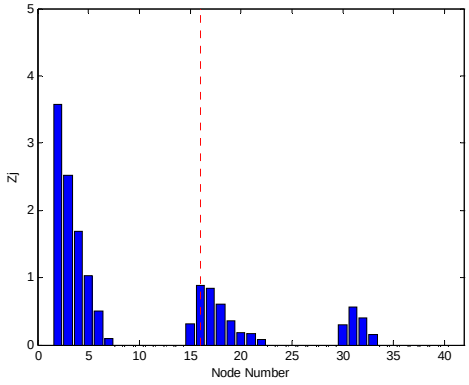

(c) Modes 1+2+3

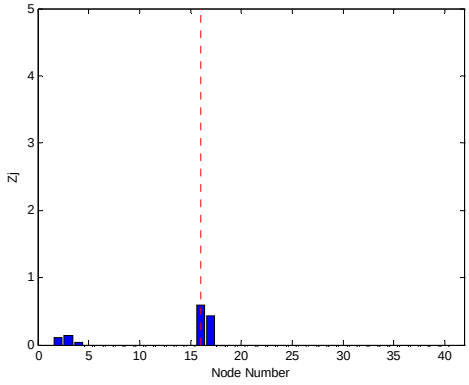

(d) Modes 1+2+3+4

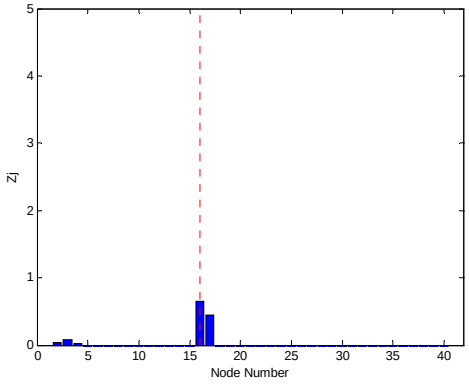

(e) Modes 1+2+3+4+5

Damage Detection of the RC Beams (3L)

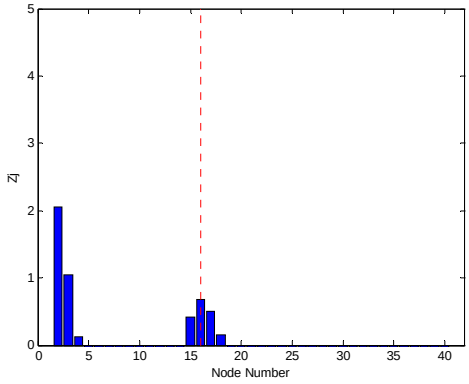

(a) Mode 1

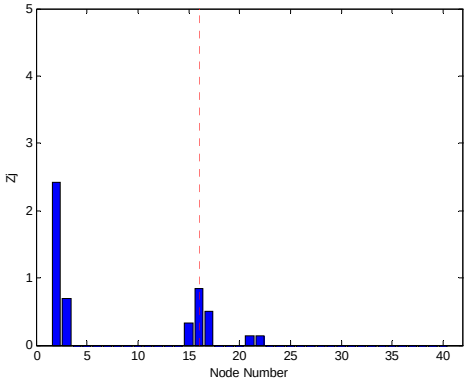

(b) Modes 1+2

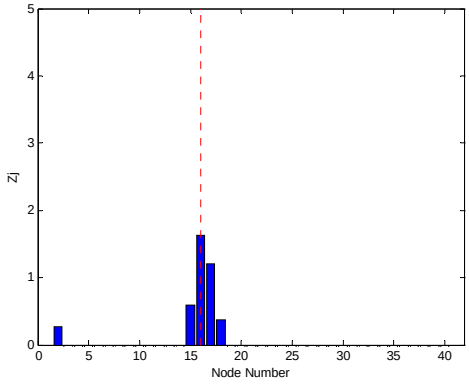

(c) Modes 1+2+3

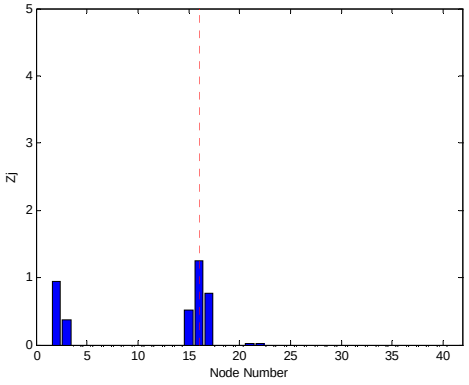

(d) Modes 1+2+3+4

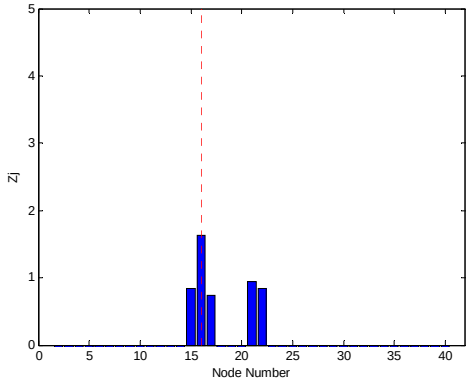

(e) Modes 1+2+3+4+5

Damage Detection of the RC Beams (3M)

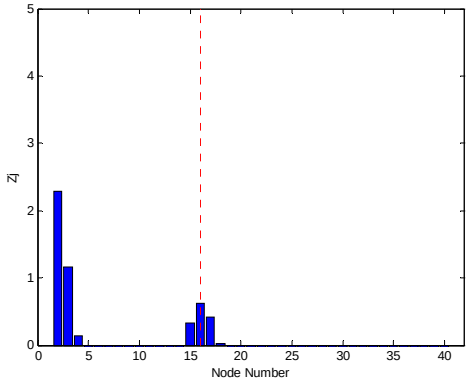

(a) Mode 1

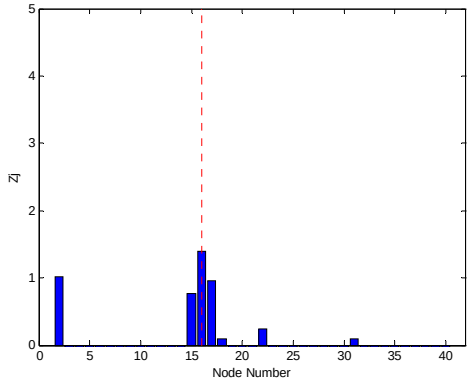

(b) Modes 1+2

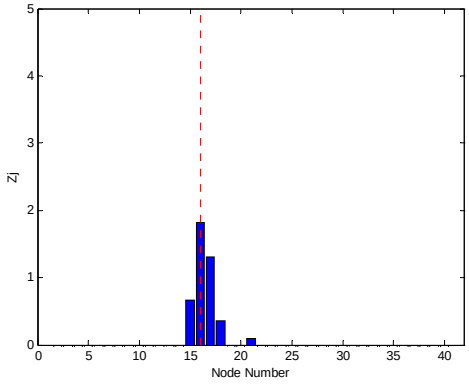

(c) Modes 1+2+3

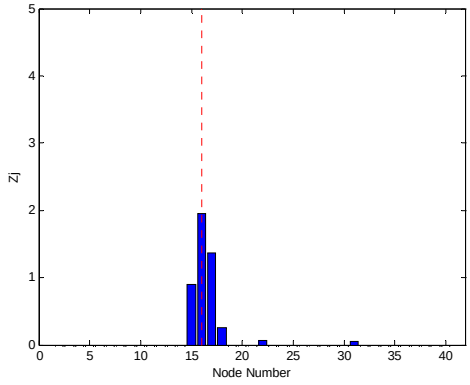

(d) Modes 1+2+3+4

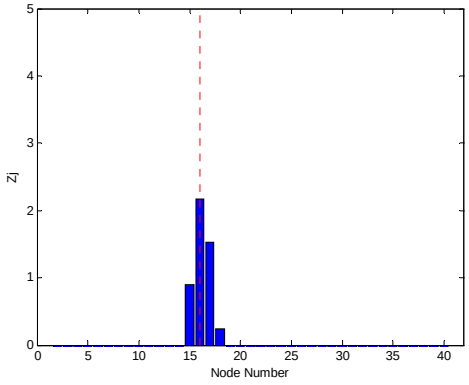

(e) Modes 1+2+3+4+5

Damage Detection of the RC Beams (3S)

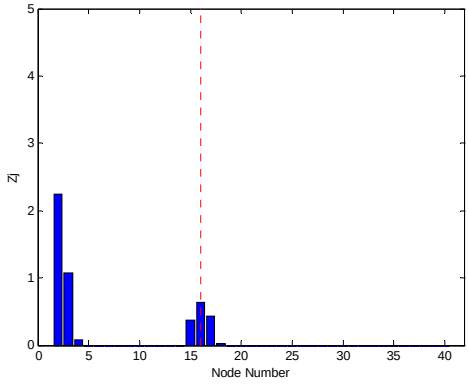

(a) Mode 1

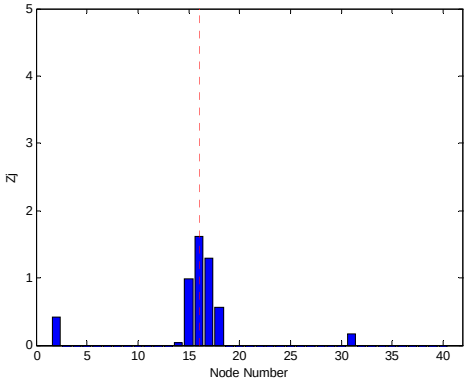

(b) Modes 1+2

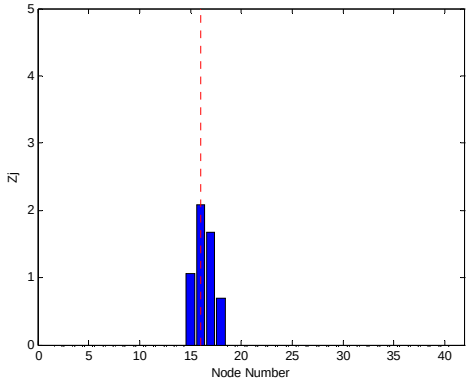

(c) Modes 1+2+3

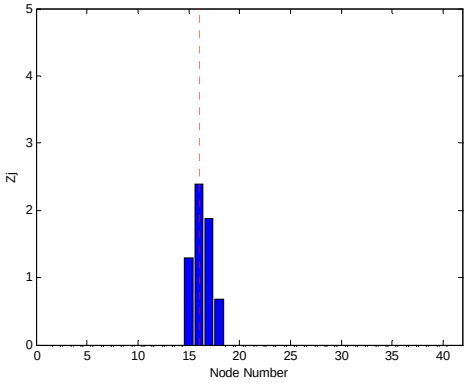

(d) Modes 1+2+3+4

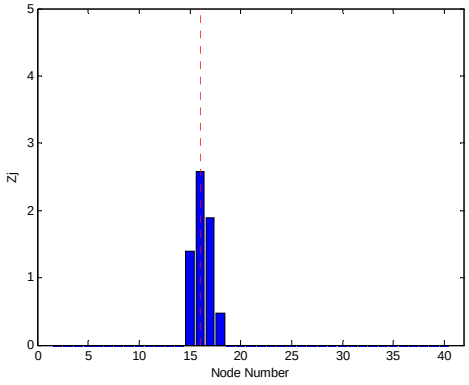

(e) Modes 1+2+3+4+5

Damage Detection of the RC Beams (3SBar)

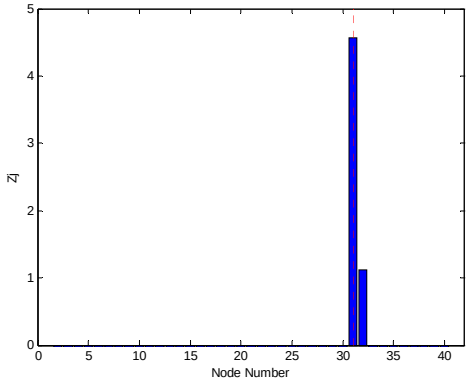

(a) Mode 1

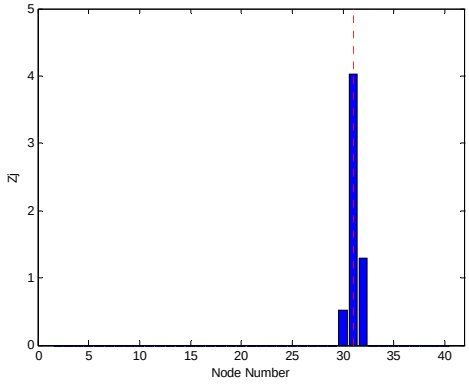

(b) Modes 1+2

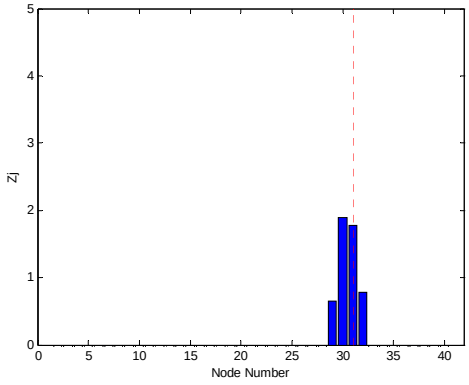

(c) Modes 1+2+3

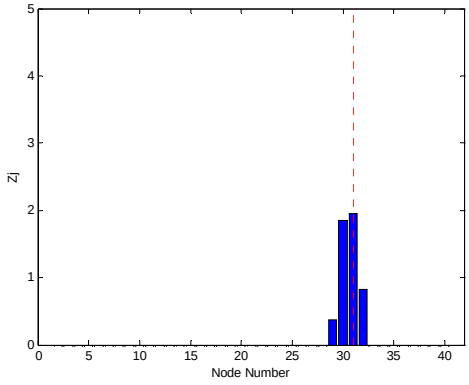

(d) Modes 1+2+3+4

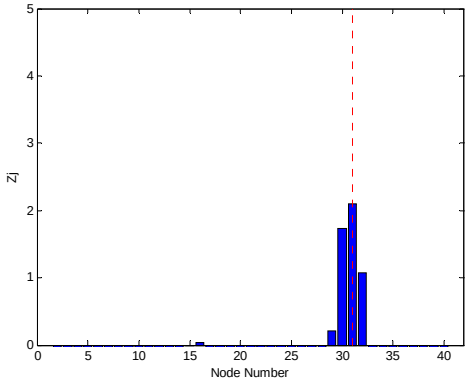

(e) Modes 1+2+3+4+5

Damage Detection of the RC Beams (HB)

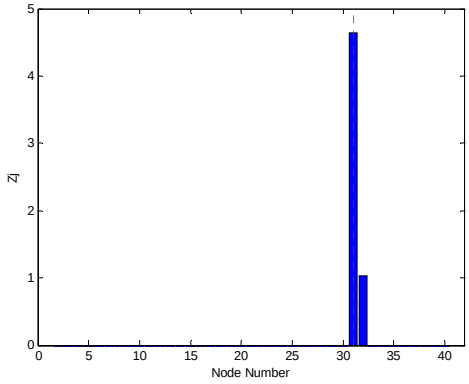

(a) Mode 1

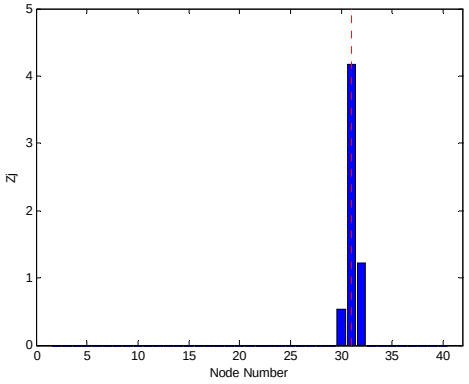

(b) Modes 1+2

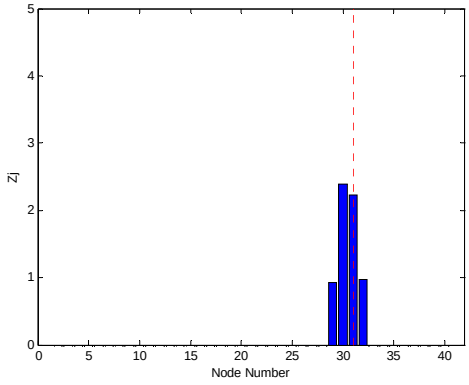

(c) Modes 1+2+3

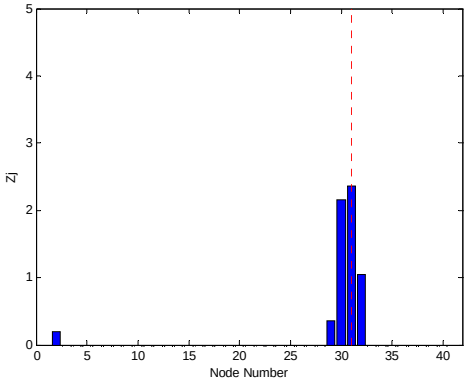

(d) Modes 1+2+3+4

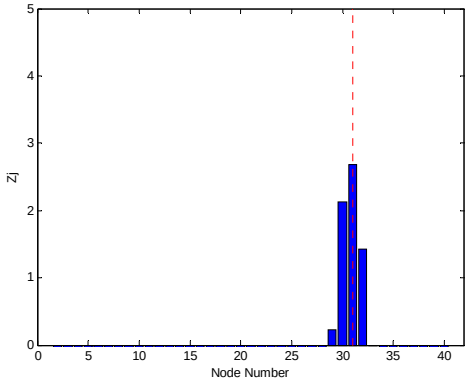

(e) Modes 1+2+3+4+5

Damage Detection of the RC Beams (HT)

C.2 Comparison Results of Damage Detection in the Experimental Work

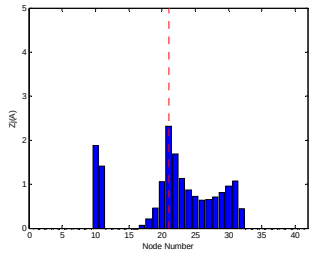

DI-A (1-Mode)

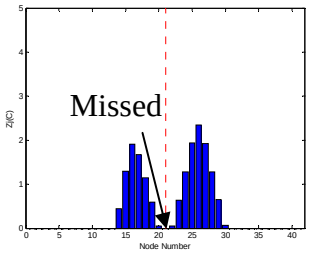

DI-C (1-Mode)

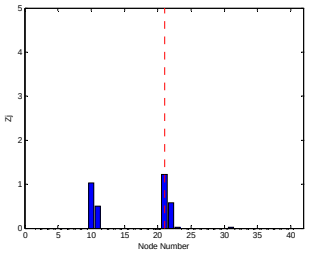

DI-NI (1-Mode)

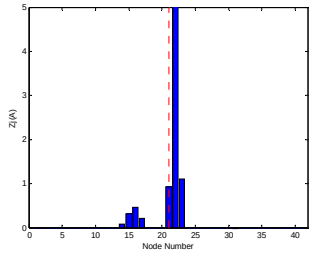

DI-A (2-Modes)

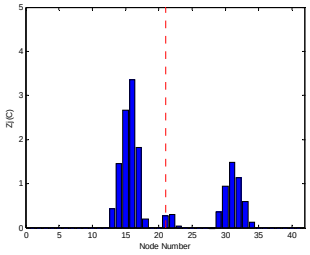

DI-C (2-Modes)

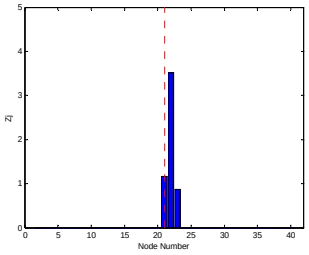

DI-NI (2-Modes)

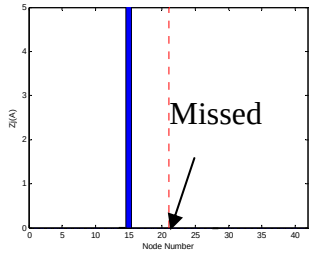

DI-A (3-Modes)

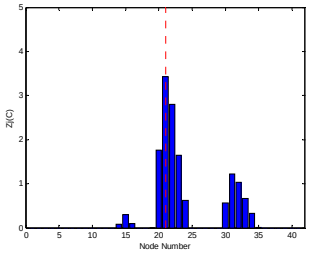

DI-C (3-Modes)

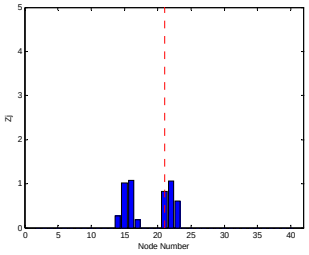

DI-NI (3-Modes)

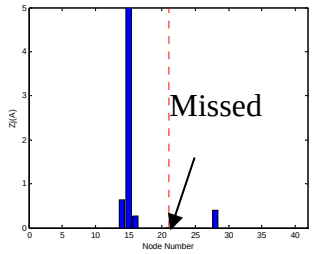

DI-A (4-Modes)

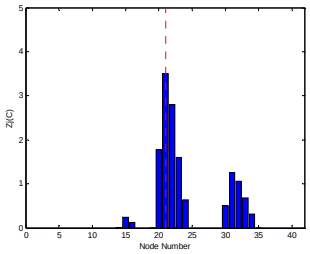

DI-C (4-Modes)

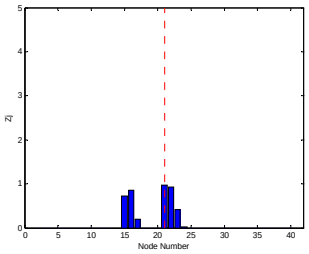

DI-NI (4-Modes)

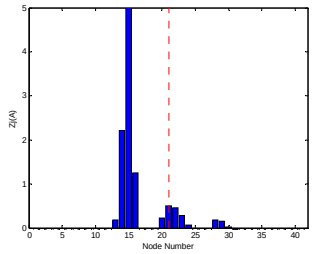

DI-A (5-Modes)

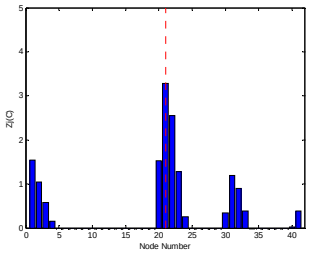

DI-C (5-Modes)

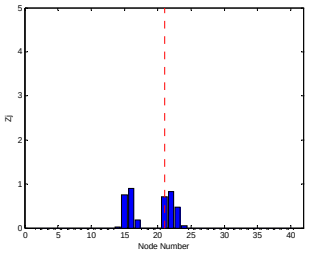

DI-NI (5-Modes)

Comparison Results of Damage Detection (4L)

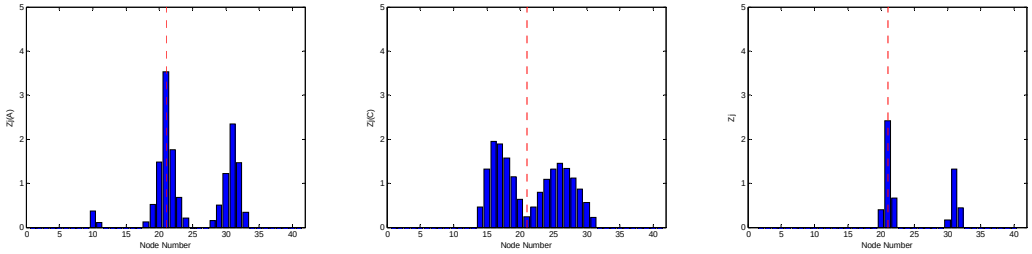

DI-A (1-Mode) DI-C (1-Mode) DI-NI (1-Mode)

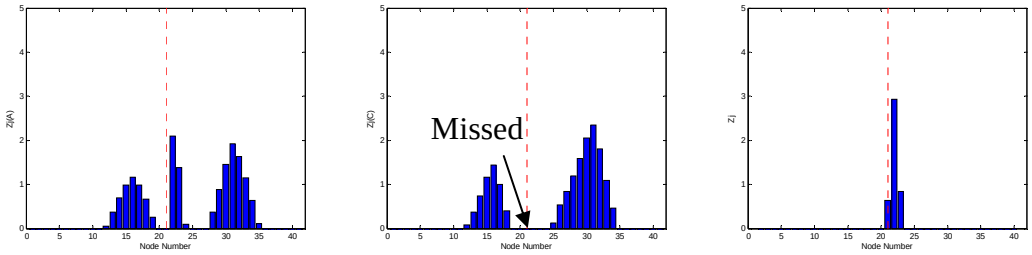

DI-A (2-Modes) DI-C (2-Modes) DI-NI (2-Modes)

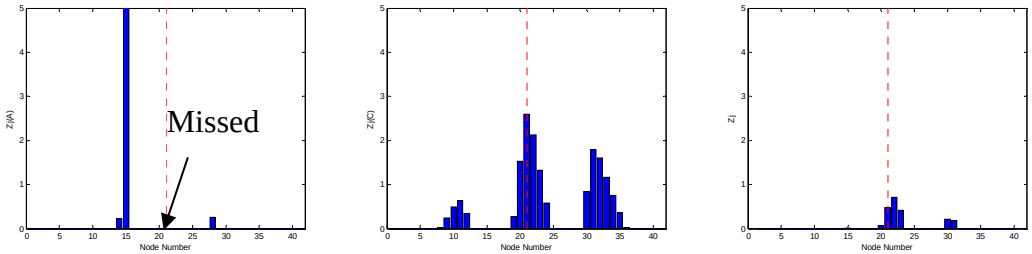

DI-A (3-Modes) DI-C (3-Modes) DI-NI (3-Modes)

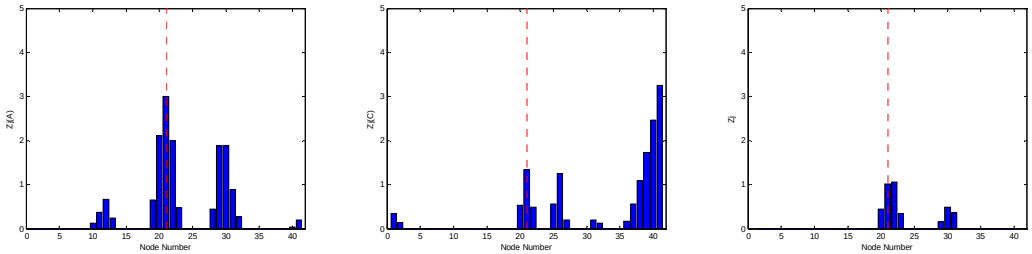

DI-A (4-Modes) DI-C (4-Modes) DI-NI (4-Modes)

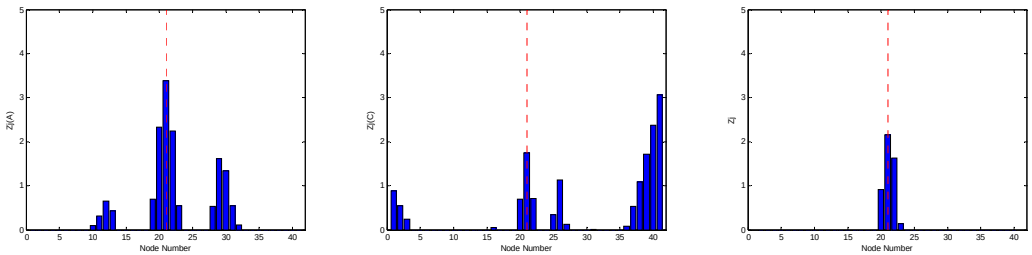

DI-A (5-Modes) DI-C (5-Modes) DI-NI (5-Modes)

Comparison Results of Damage Detection (4M)

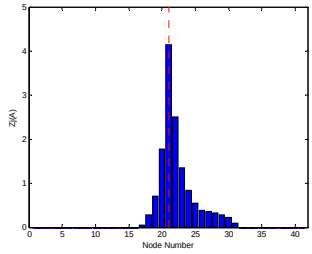

DI-A (1-Mode)

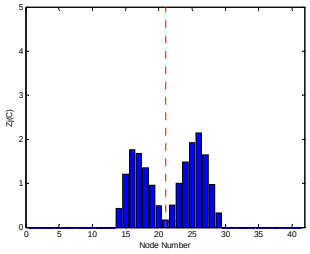

DI-C (1-Mode)

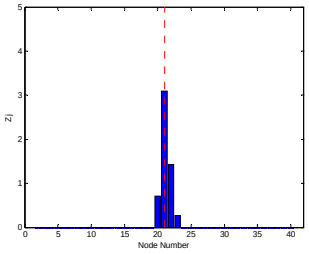

DI-NI (1-Mode)

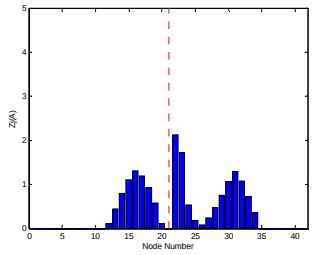

DI-A (2-Modes)

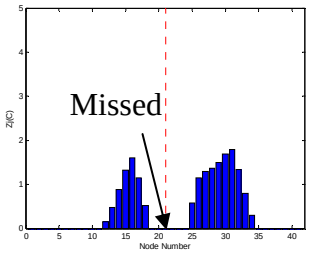

DI-C (2-Modes)

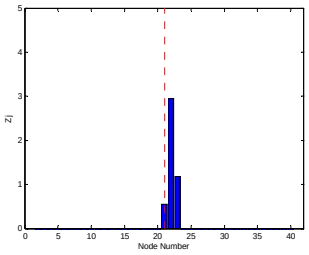

DI-NI (2-Modes)

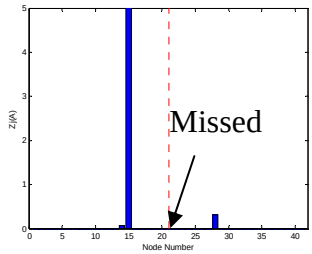

DI-A (3-Modes)

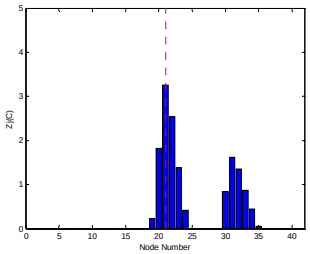

DI-C (3-Modes)

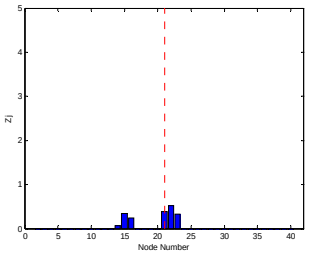

DI-NI (3-Modes)

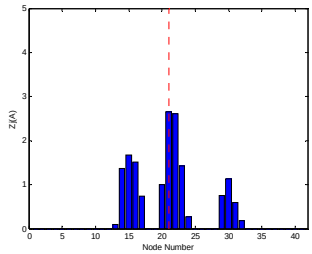

DI-A (4-Modes)

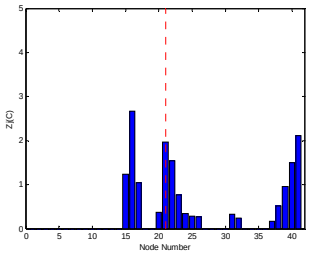

DI-C (4-Modes)

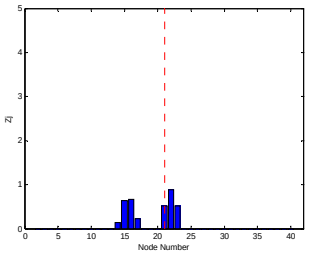

DI-NI (4-Modes)

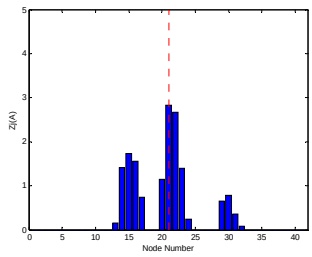

DI-A (5-Modes)

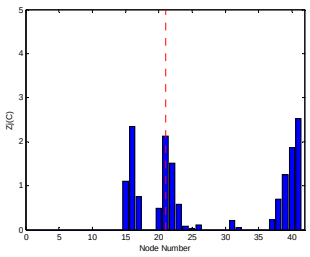

DI-C (5-Modes)

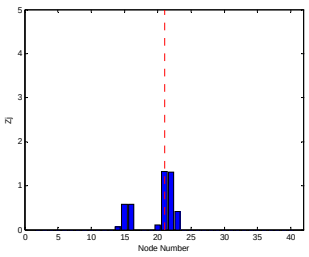

DI-NI (5-Modes)

Comparison Results of Damage Detection (4S)

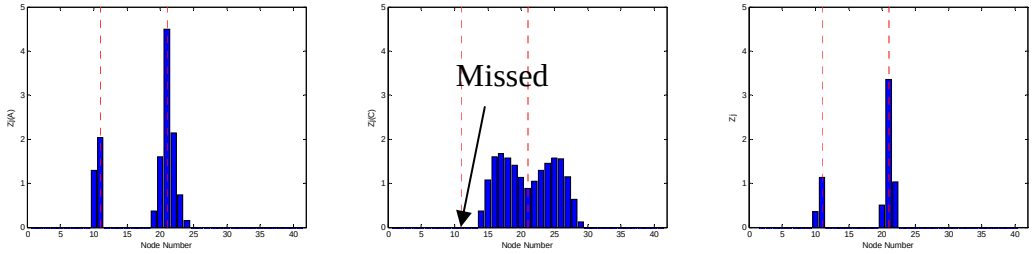

DI-A (1-Mode) DI-C (1-Mode) DI-NI (1-Mode)

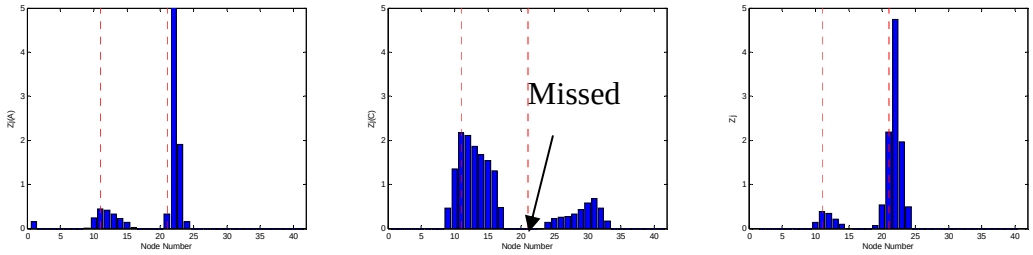

DI-A (2-Modes) DI-C (2-Modes) DI-NI (2-Modes)

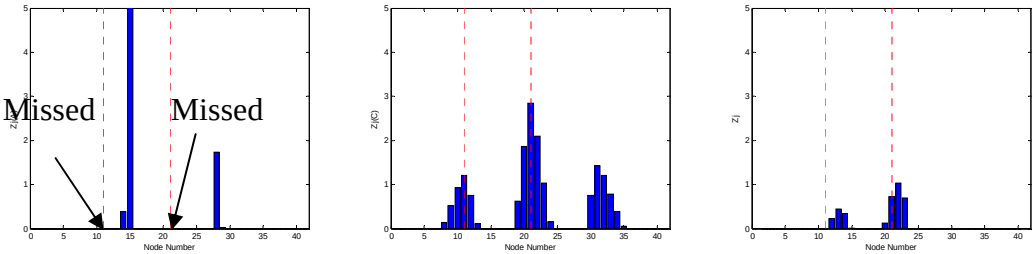

DI-A (3-Modes) DI-C (3-Modes) DI-NI (3-Modes)

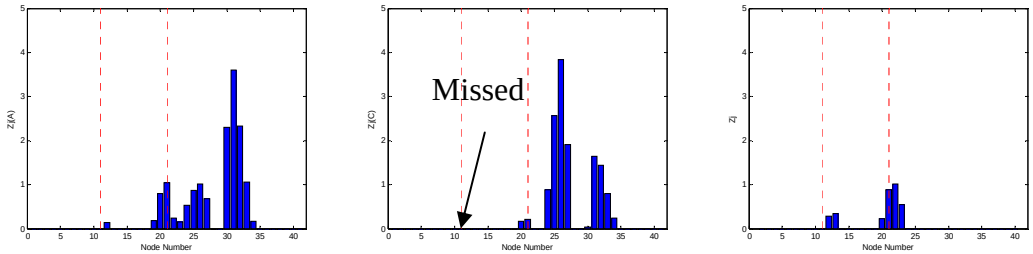

DI-A (4-Modes) DI-C (4-Modes) DI-NI (4-Modes)

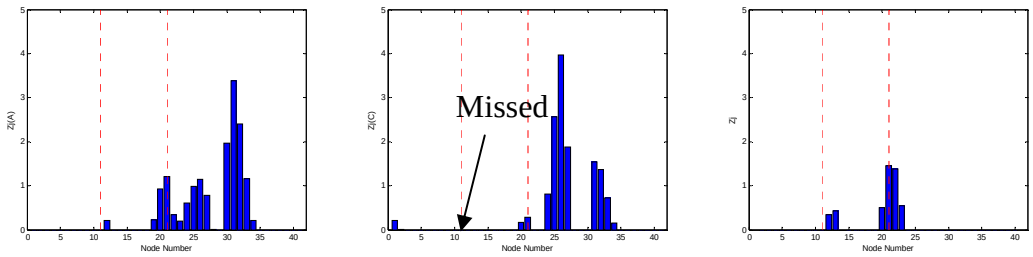

DI-A (5-Modes) DI-C (5-Modes) DI-NI (5-Modes)

Comparison Results of Damage Detection (2S4S)

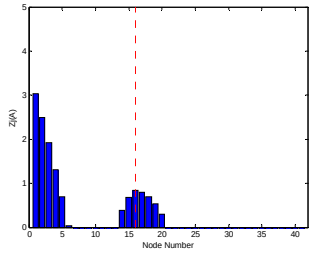

DI-A (1-Mode)

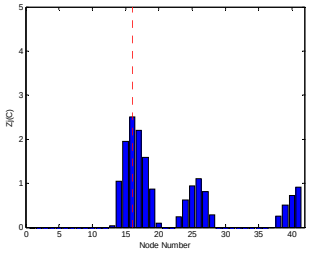

DI-C (1-Mode)

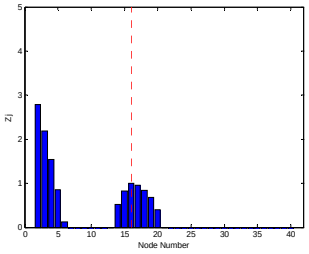

DI-NI (1-Mode)

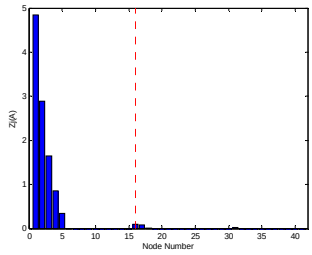

DI-A (2-Modes)

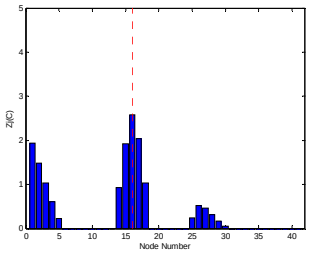

DI-C (2-Modes)

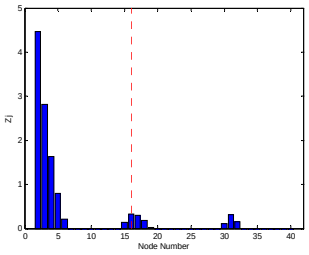

DI-NI (2-Modes)

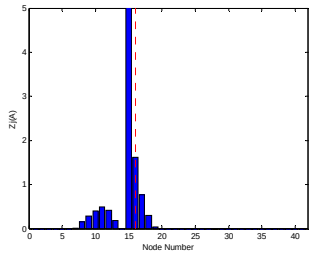

DI-A (3-Modes)

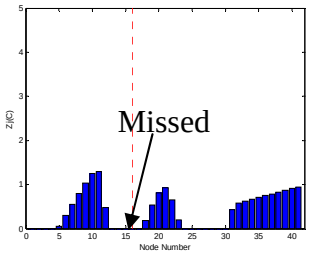

DI-C (3-Modes)

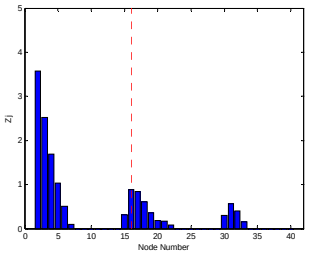

DI-NI (3-Modes)

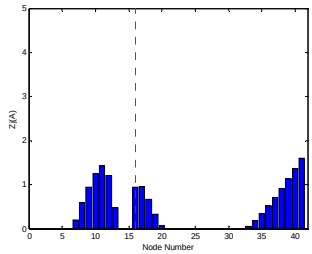

DI-A (4-Modes)

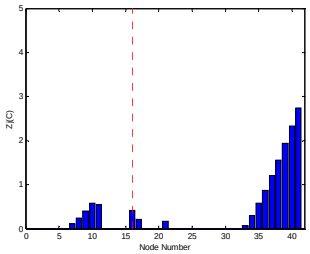

DI-C (4-Modes)

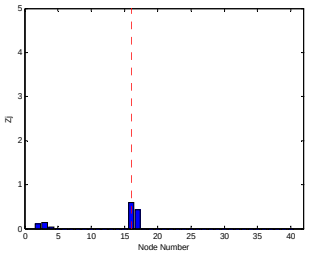

DI-NI (4-Modes)

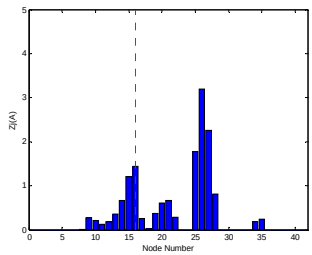

DI-A (5-Modes)

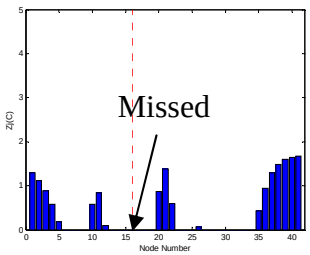

DI-C (5-Modes)

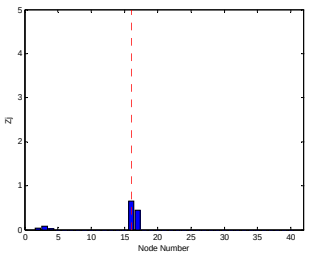

DI-NI (5-Modes)

Comparison Results of Damage Detection (3L)

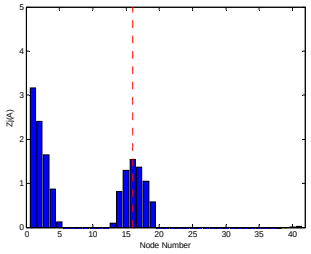

DI-A (1-Mode)

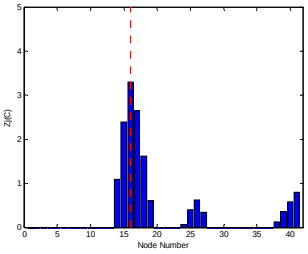

DI-C (1-Mode)

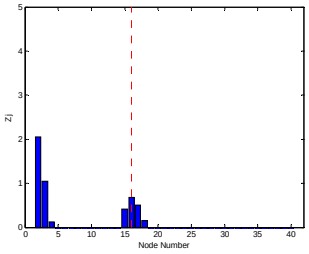

DI-NI (1-Mode)

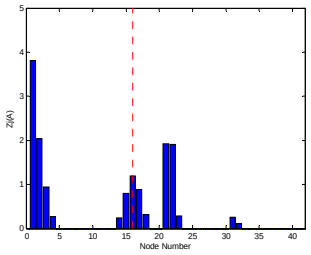

DI-A (2-Modes)

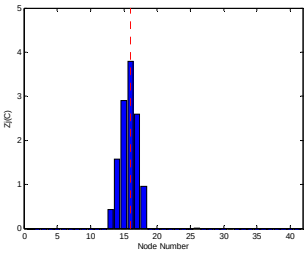

DI-C (2-Modes)

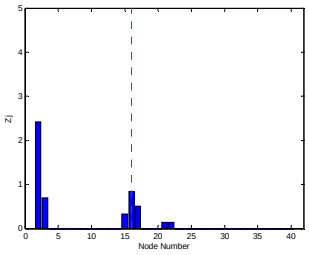

DI-NI (2-Modes)

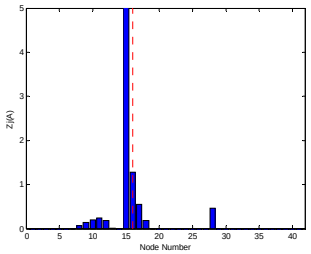

DI-A (3-Modes)

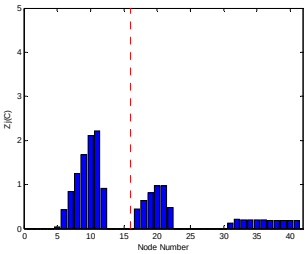

DI-C (3-Modes)

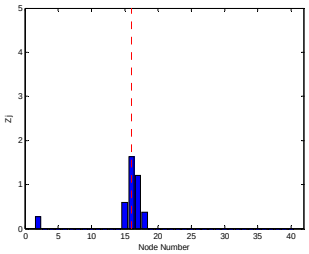

DI-NI (3-Modes)

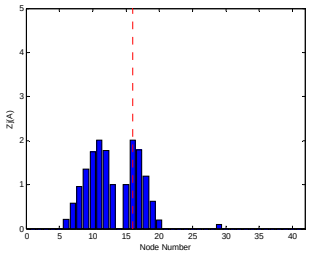

DI-A (4-Modes)

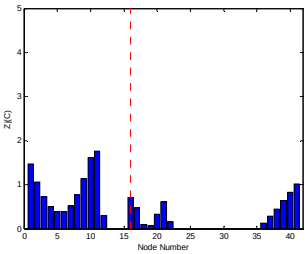

DI-C (4-Modes)

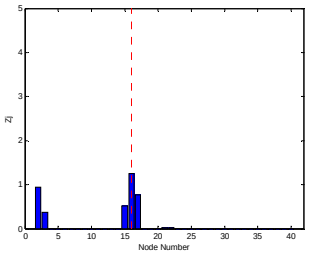

DI-NI (4-Modes)

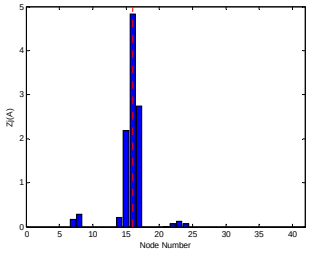

DI-A (5-Modes)

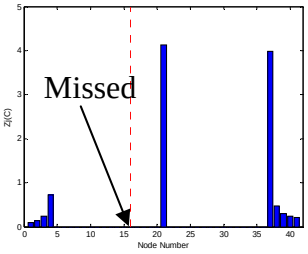

DI-C (5-Modes)

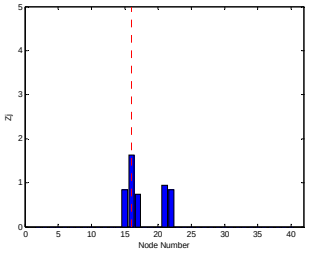

DI-NI (5-Modes)

Comparison Results of Damage Detection (3M)

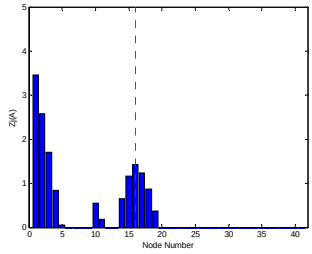

DI-A (1-Mode)

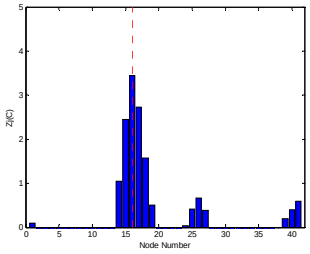

DI-C (1-Mode)

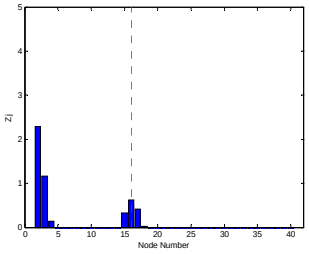

DI-NI (1-Mode)

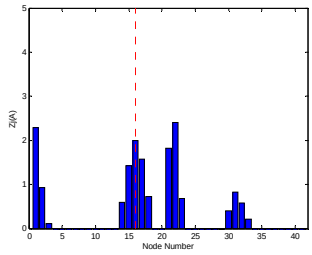

DI-A (2-Modes)

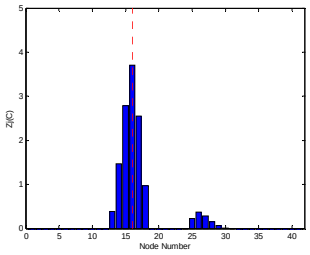

DI-C (2-Modes)

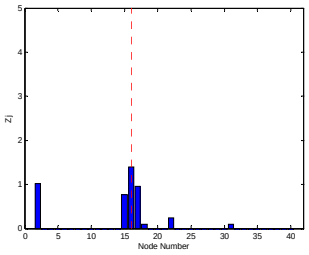

DI-NI (2-Modes)

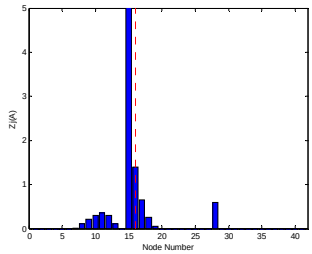

DI-A (3-Modes)

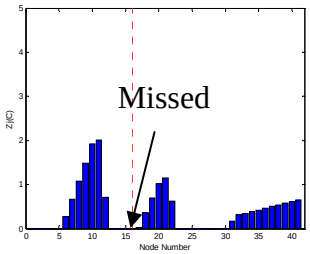

DI-C (3-Modes)

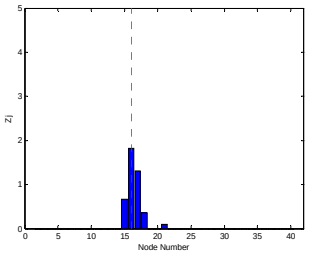

DI-NI (3-Modes)

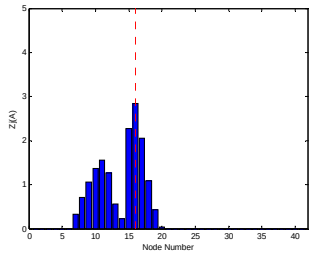

DI-A (4-Modes)

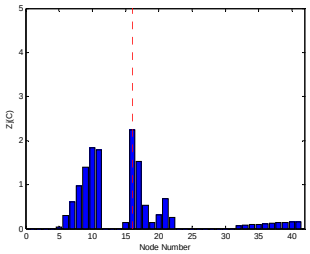

DI-C (4-Modes)

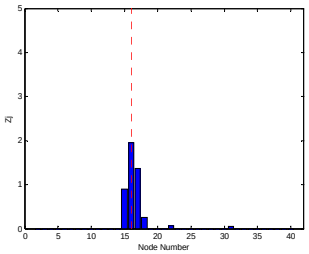

DI-NI (4-Modes)

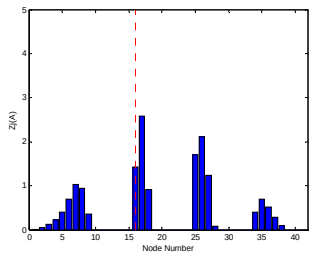

DI-A (5-Modes)

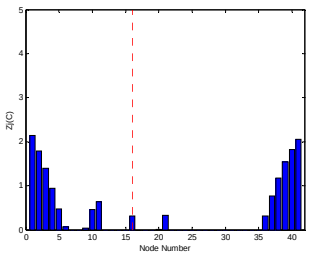

DI-C (5-Modes)

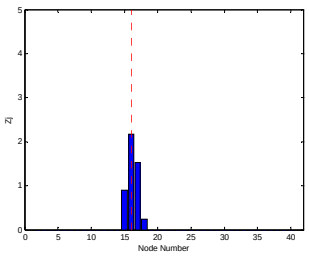

DI-NI (5-Modes)

Comparison Results of Damage Detection (3S)

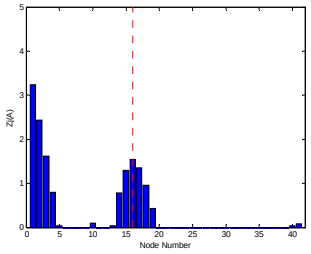

DI-A (1-Mode)

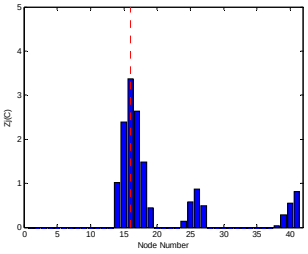

DI-C (1-Mode)

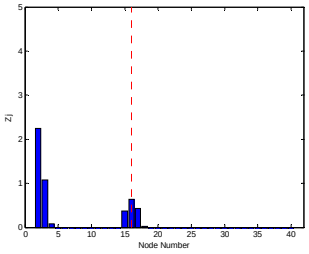

DI-NI (1-Mode)

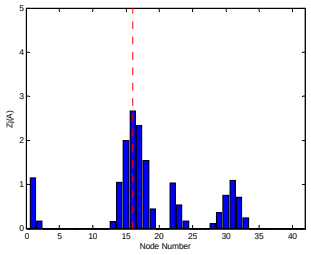

DI-A (2-Modes)

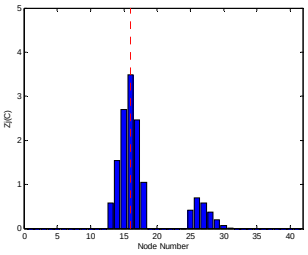

DI-C (2-Modes)

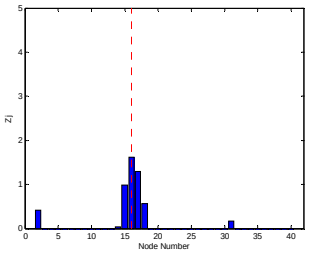

DI-NI (2-Modes)

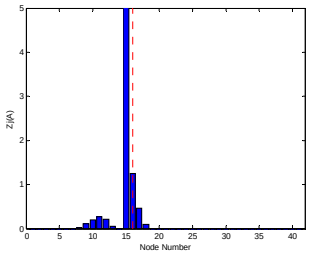

DI-A (3-Modes)

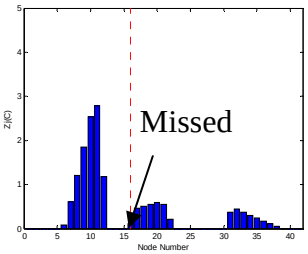

DI-C (3-Modes)

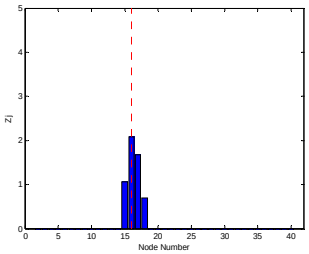

DI-NI (3-Modes)

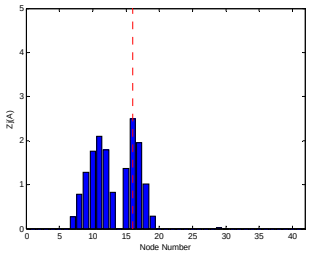

DI-A (4-Modes)

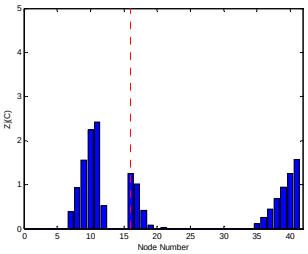

DI-C (4-Modes)

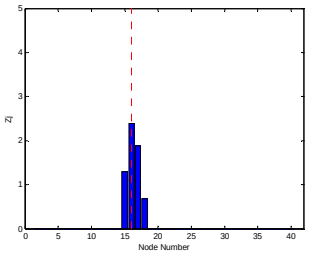

DI-NI (4-Modes)

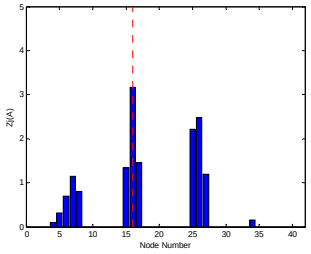

DI-A (5-Modes)

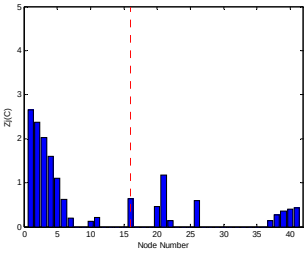

DI-C (5-Modes)

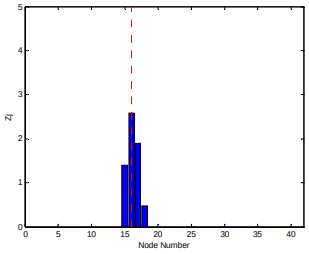

DI-NI (5-Modes)

Comparison Results of Damage Detection (3SBar)

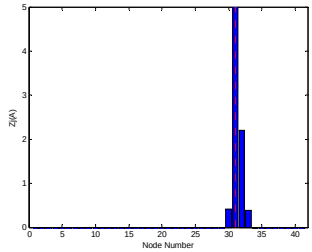

DI-A (1-Mode)

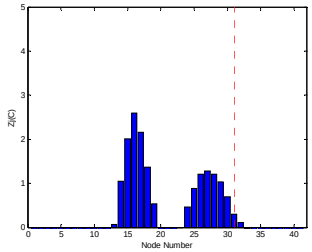

DI-C (1-Mode)

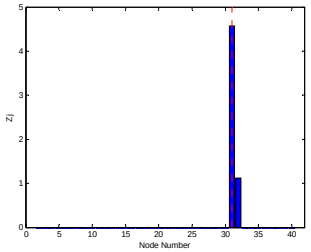

DI-NI (1-Mode)

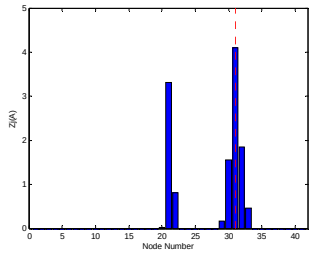

DI-A (2-Modes)

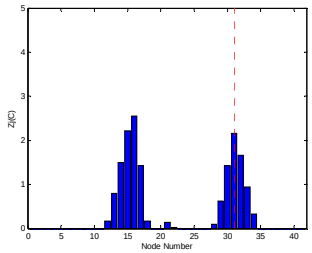

DI-C (2-Modes)

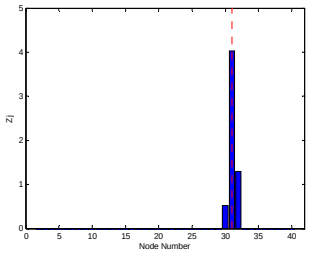

DI-NI (2-Modes)

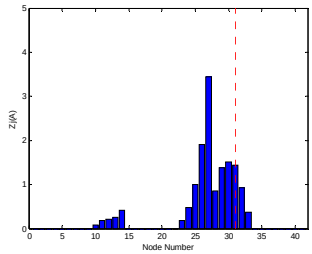

DI-A (3-Modes)

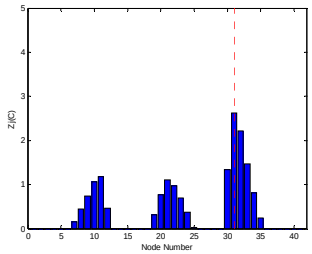

DI-C (3-Modes)

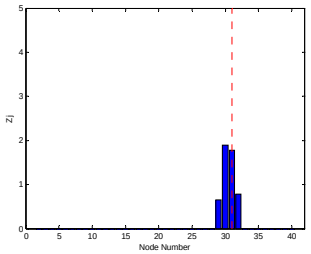

DI-NI (3-Modes)

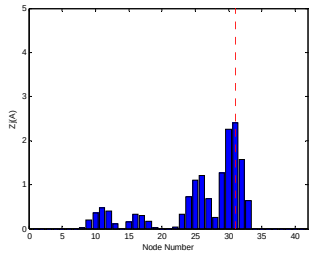

DI-A (4-Modes)

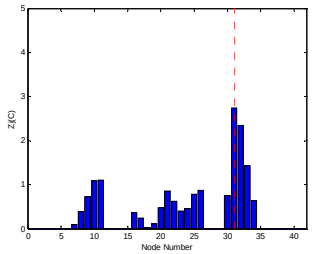

DI-C (4-Modes)

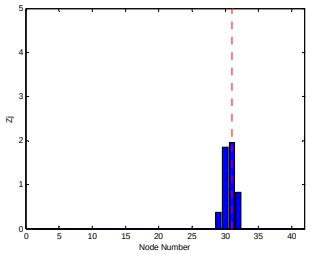

DI-NI (4-Modes)

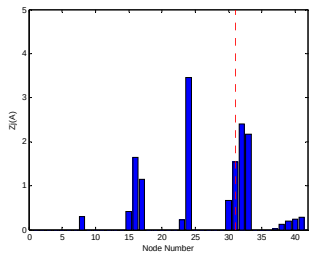

DI-A (5-Modes)

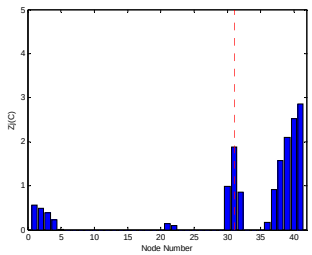

DI-C (5-Modes)

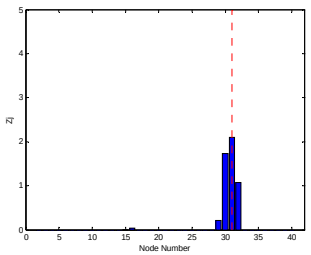

DI-NI (5-Modes)

Comparison Results of Damage Detection (HB)

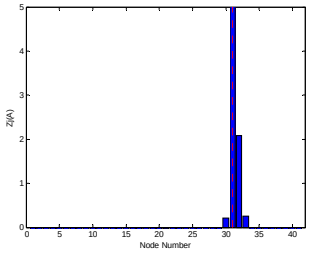

DI-A (1-Mode)

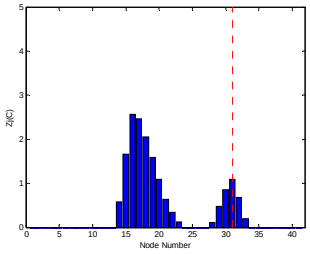

DI-C (1-Mode)

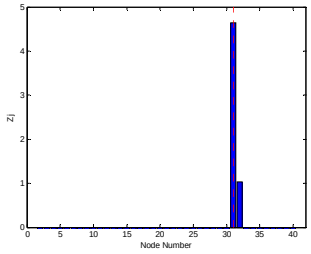

DI-NI (1-Mode)

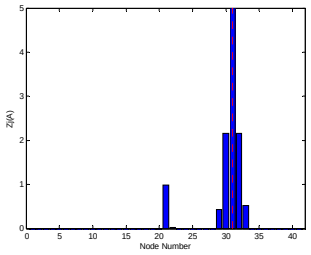

DI-A (2-Modes)

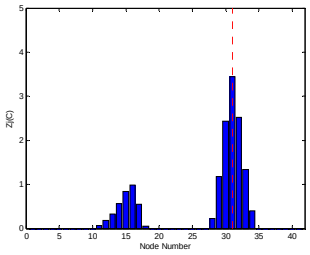

DI-C (2-Modes)

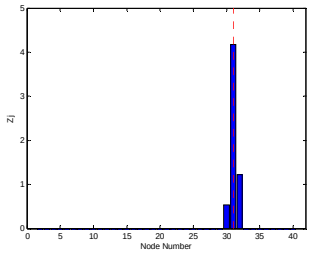

DI-NI (2-Modes)

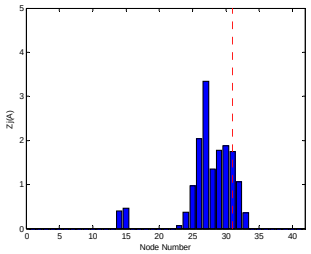

DI-A (3-Modes)

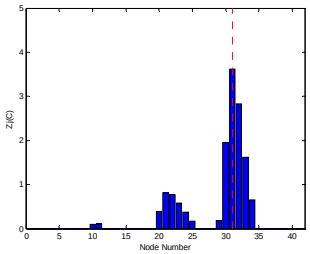

DI-C (3-Modes)

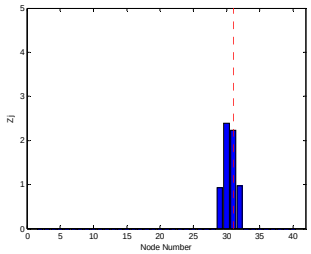

DI-NI (3-Modes)

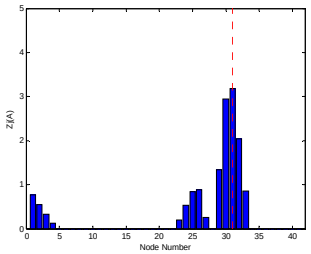

DI-A (4-Modes)

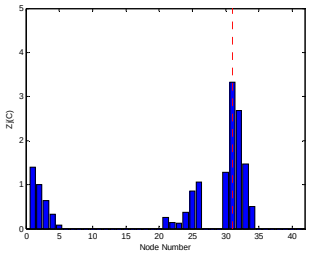

DI-C (4-Modes)

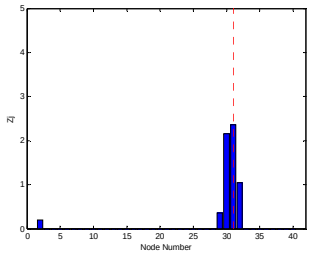

DI-NI (4-Modes)

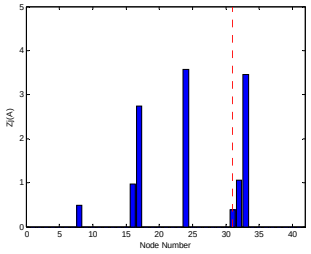

DI-A (5-Modes)

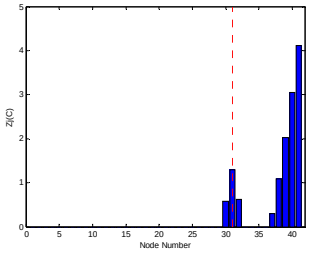

DI-C (5-Modes)

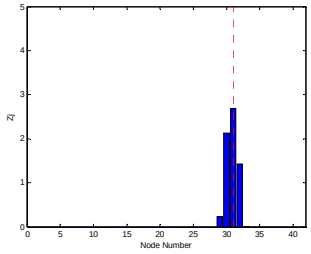

DI-NI (5-Modes)

Comparison Results of Damage Detection (HT)

C.3 Results of Estimation of Damage Severities in the Experimental Work

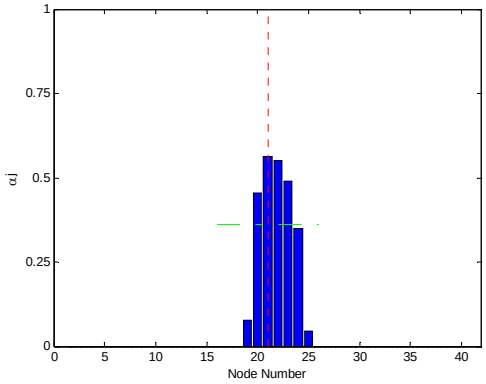

Estimation of Damage Severities (4L 5-Modes)

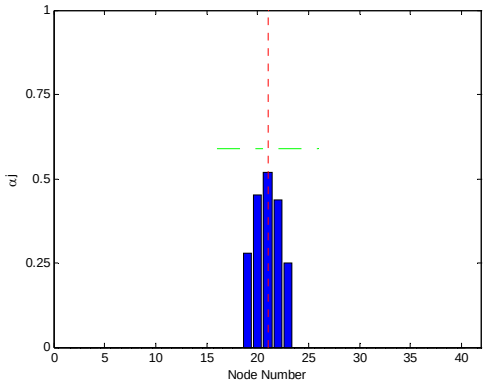

Estimation of Damage Severities (4M 5-Modes)

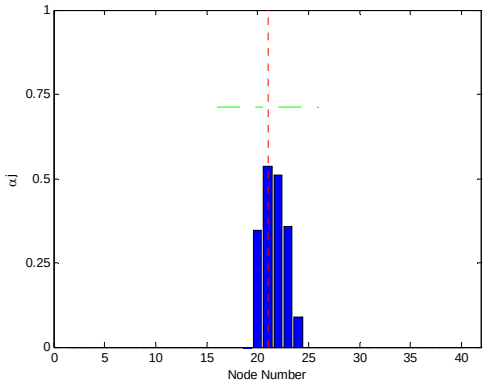

Estimation of Damage Severities (4S 5-Modes)

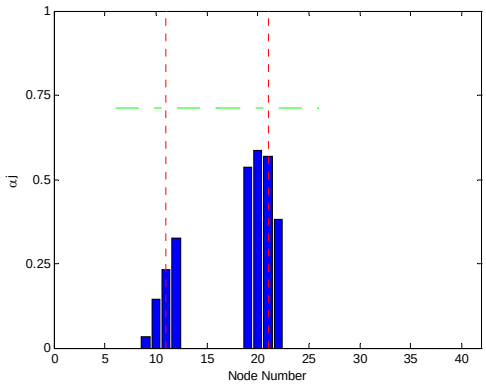

Estimation of Damage Severities (2S4S 5-Modes)

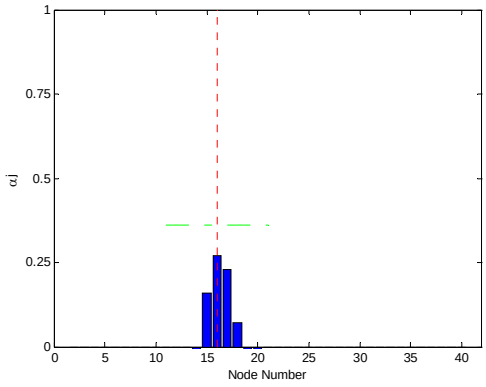

Estimation of Damage Severities (3L 5-Modes)

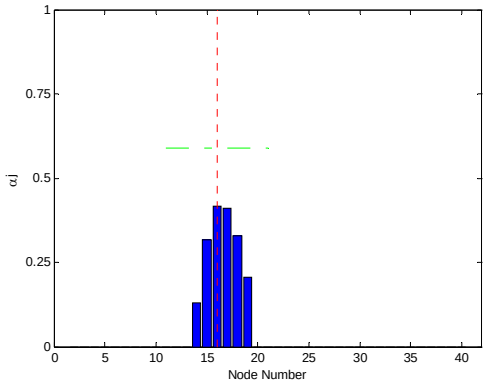

Estimation of Damage Severities (3M 5-Modes)

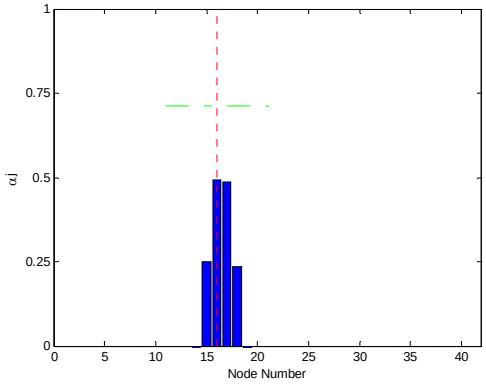

Estimation of Damage Severities (3S 5-Modes)

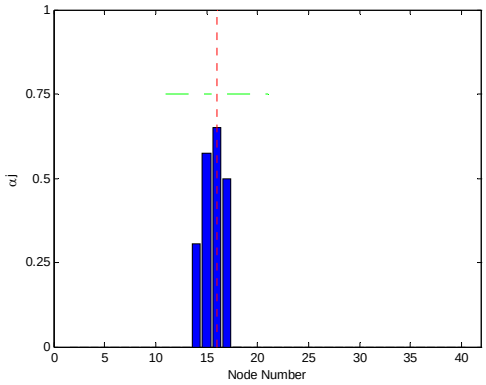

Estimation of Damage Severities (3SBar 5-Modes)

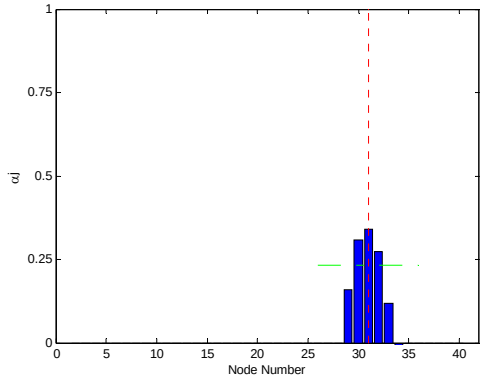

Estimation of Damage Severities (HB 5-Modes)

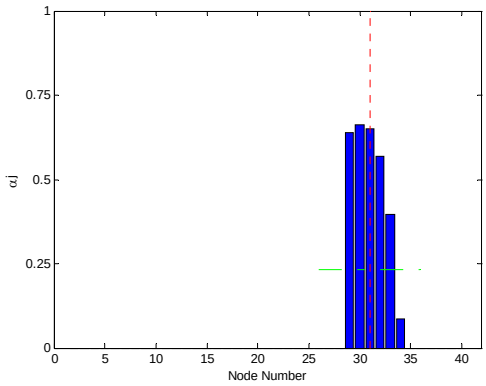

Estimation of Damage Severities (HT 5-Modes)

C.4 Results of Comparison between Numerical (no noise) and Experimental work

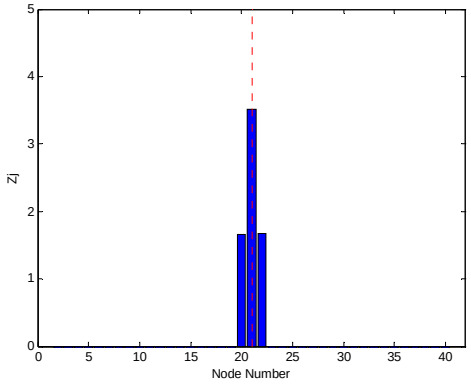

Numerical (1-Mode)

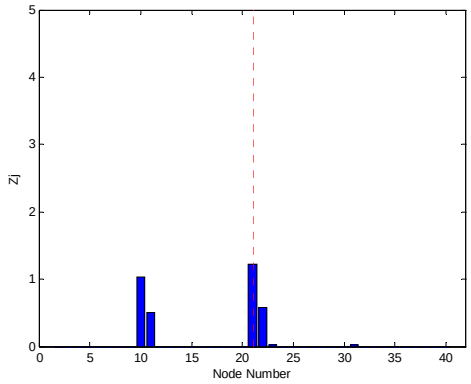

Experimental (1-Mode)

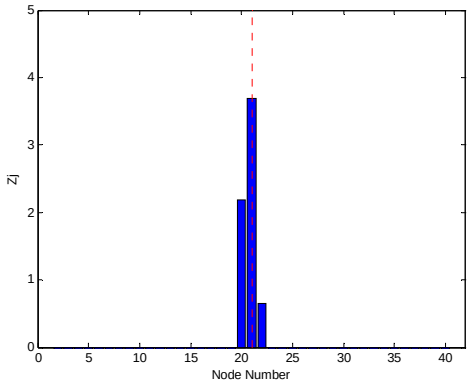

Numerical (2-Modes)

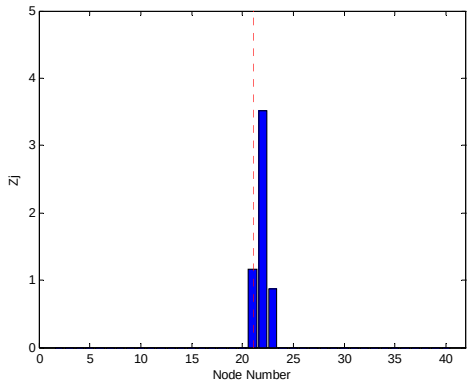

Experimental (2-Modes)

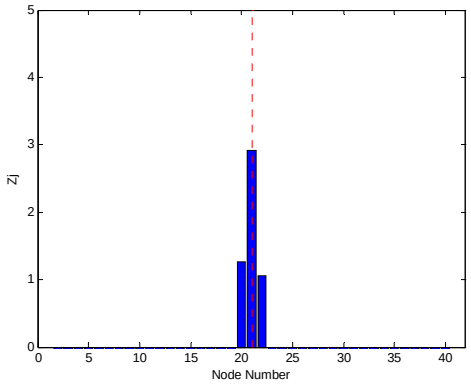

Numerical (3-Modes)

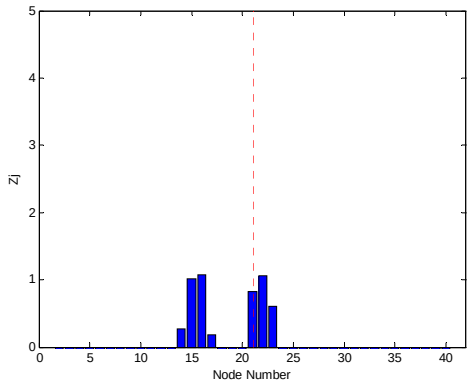

Experimental (3-Modes)

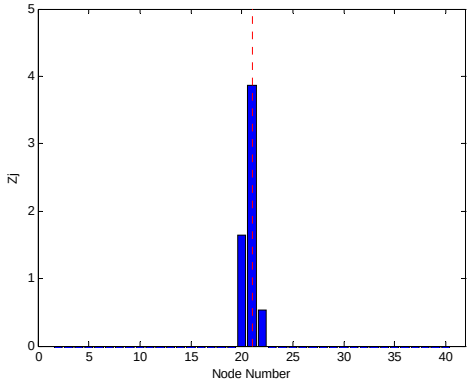

Numerical (4-Modes)

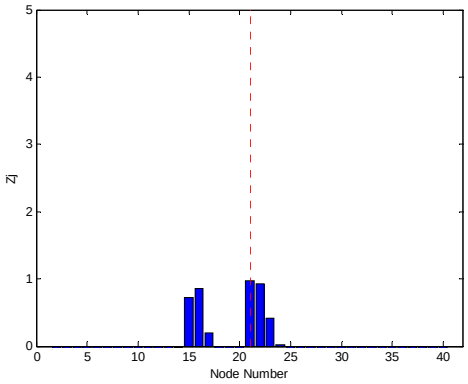

Experimental (4-Modes)

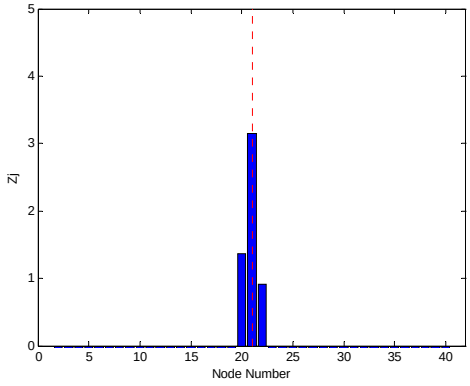

Numerical (5-Modes)

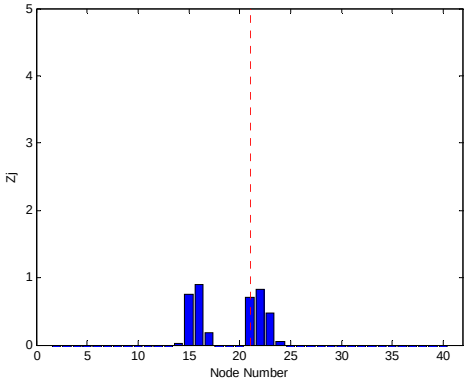

Experimental (5-Modes)

Results of Comparison between Numerical (no noise) and Experimental work (4L)

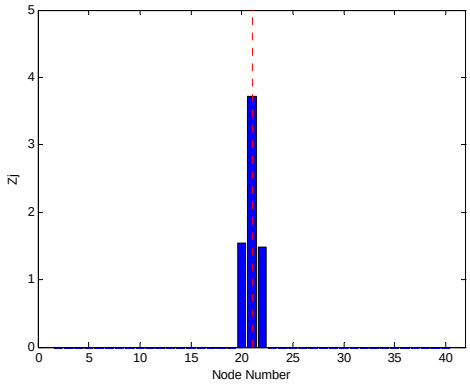

Numerical (1-Mode)

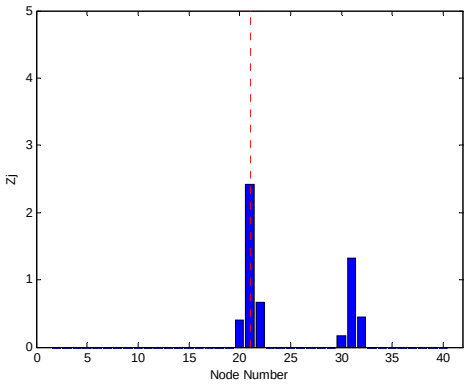

Experimental (1-Mode)

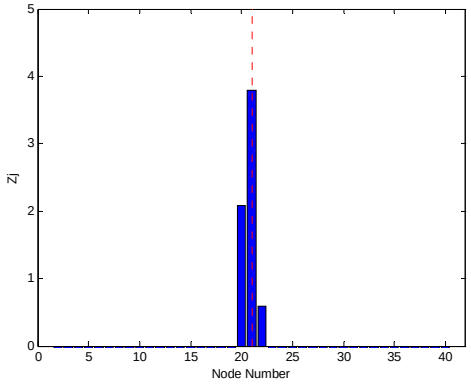

Numerical (2-Modes)

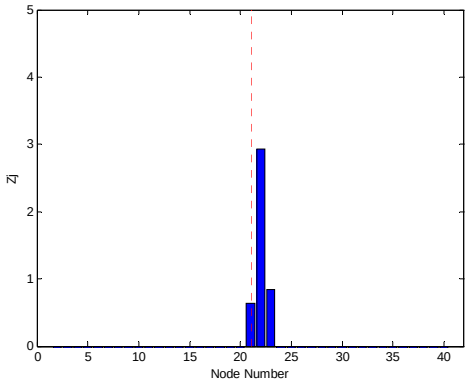

Experimental (2-Modes)

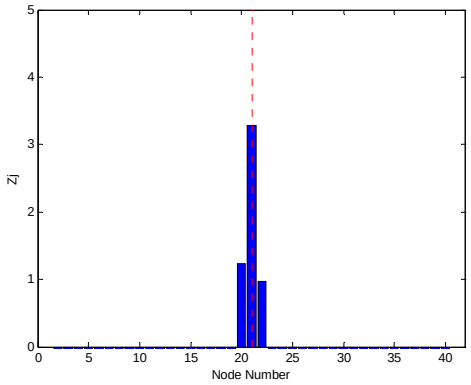

Numerical (3-Modes)

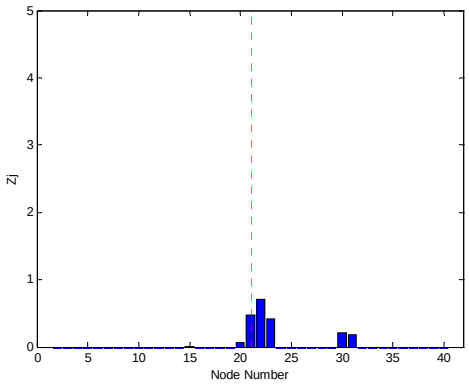

Experimental (3-Modes)

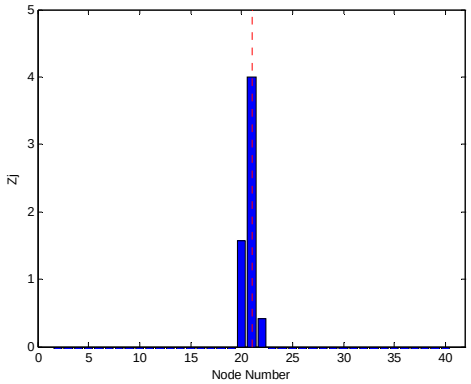

Numerical (4-Modes)

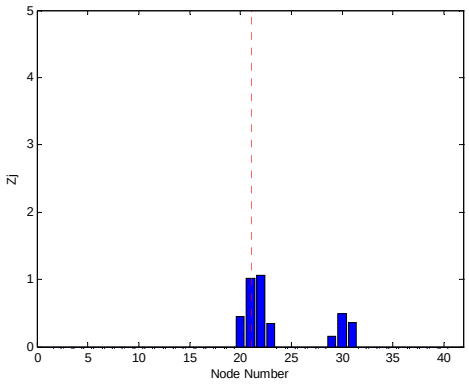

Experimental (4-Modes)

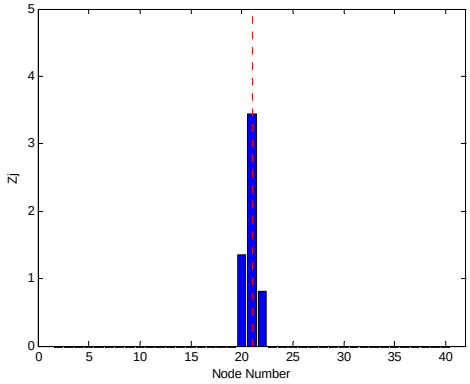

Numerical (5-Modes)

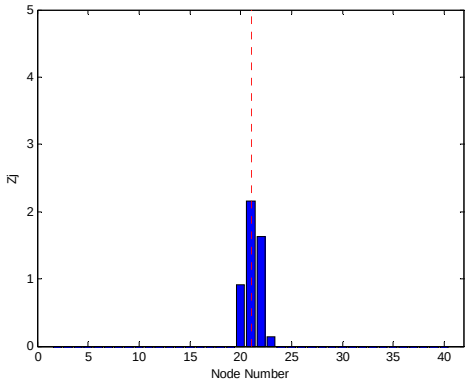

Experimental (5-Modes)

Results of Comparison between Numerical (no noise) and Experimental work (4M)

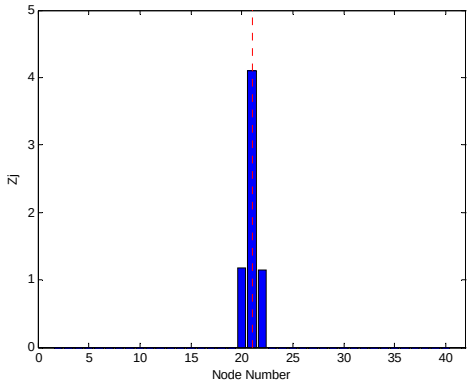

Numerical (1-Mode)

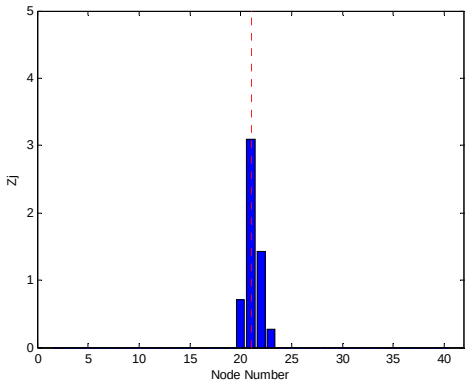

Experimental (1-Mode)

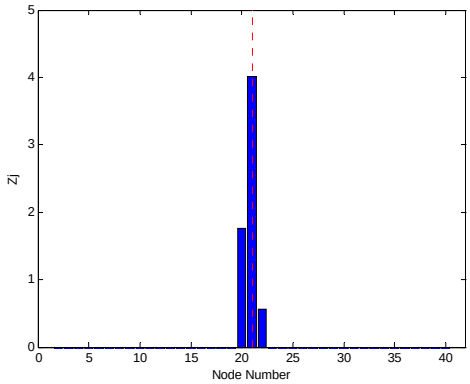

Numerical (2-Modes)

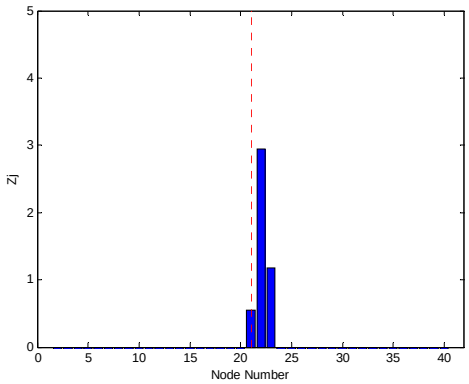

Experimental (2-Modes)

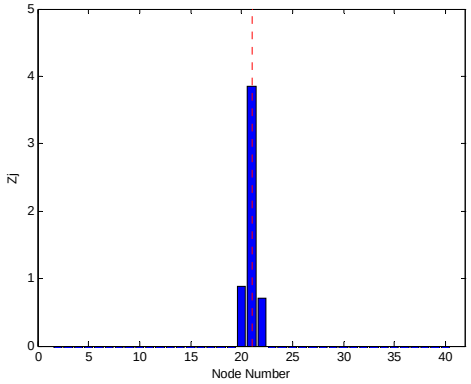

Numerical (3-Modes)

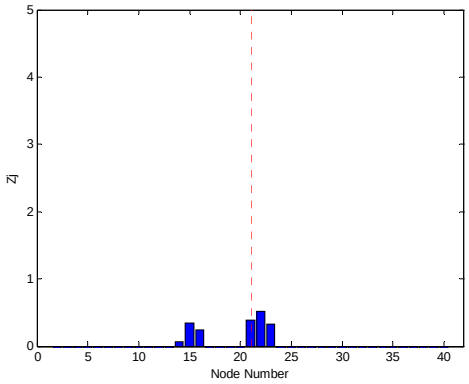

Experimental (3-Modes)

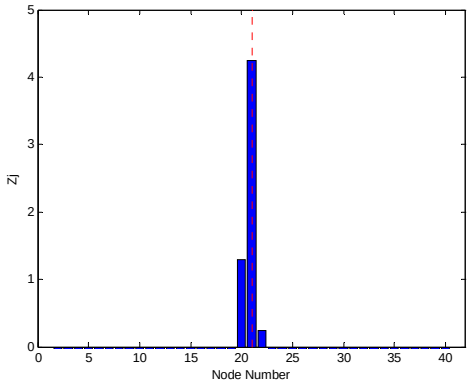

Numerical (4-Modes)

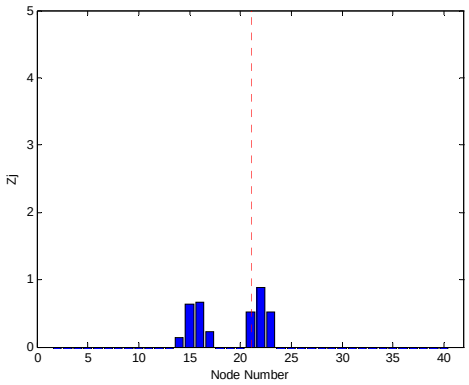

Experimental (4-Modes)

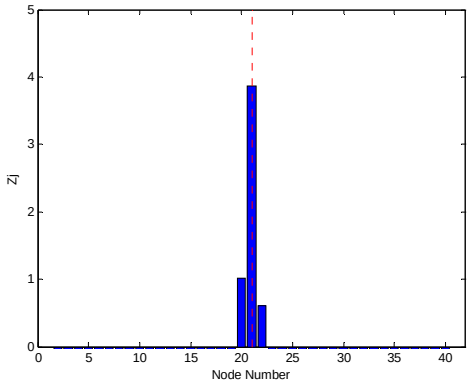

Numerical (5-Modes)

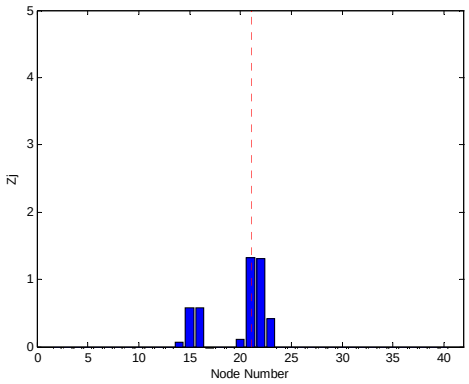

Experimental (5-Modes)

Results of Comparison between Numerical (no noise) and Experimental work (4S)

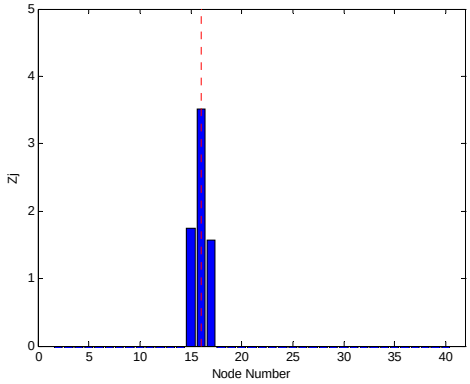

Numerical (1-Mode)

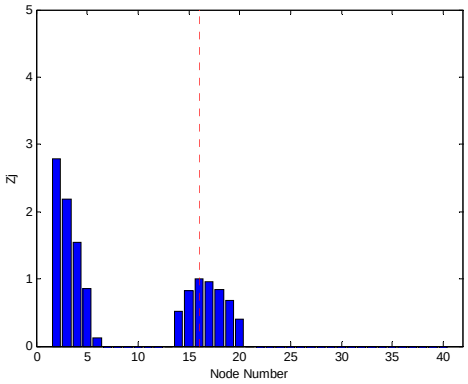

Experimental (1-Mode)

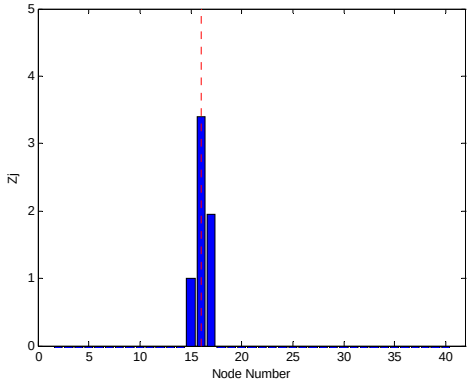

Numerical (2-Modes)

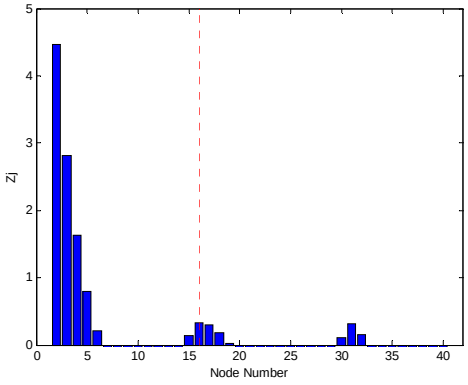

Experimental (2-Modes)

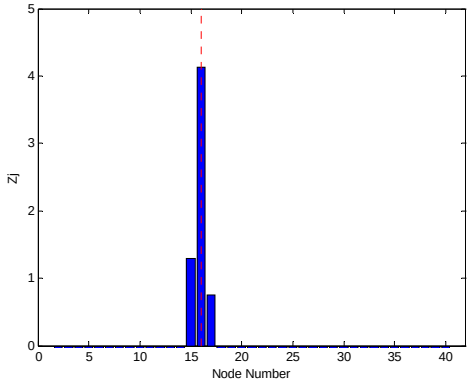

Numerical (3-Modes)

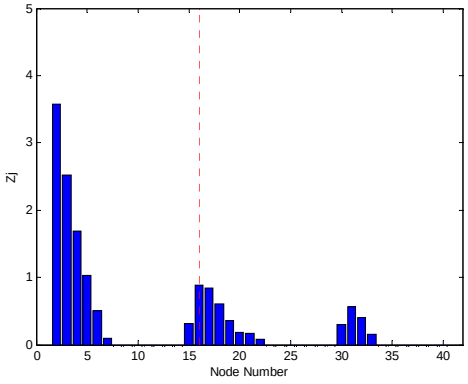

Experimental (3-Modes)

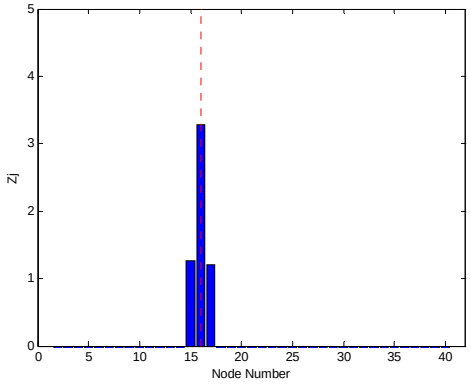

Numerical (4-Modes)

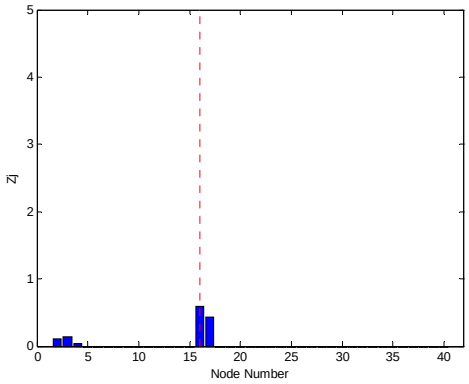

Experimental (4-Modes)

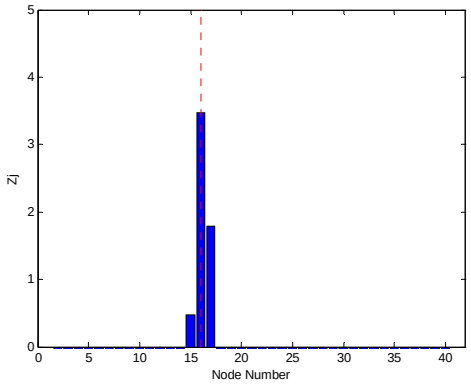

Numerical (5-Modes)

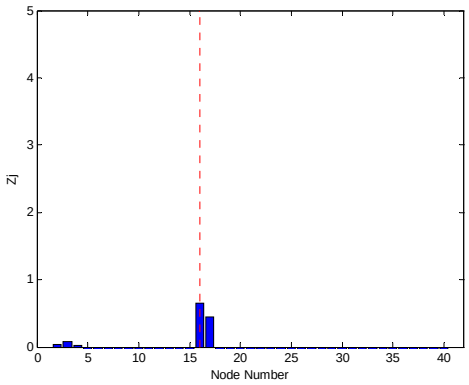

Experimental (5-Modes)

Results of Comparison between Numerical (no noise) and Experimental work (3L)

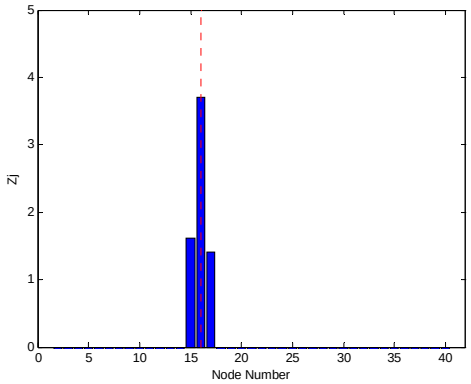

Numerical (1-Mode)

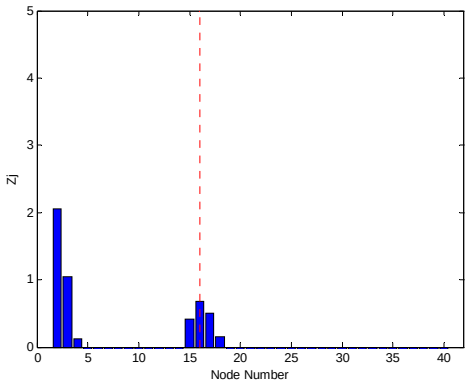

Experimental (1-Mode)

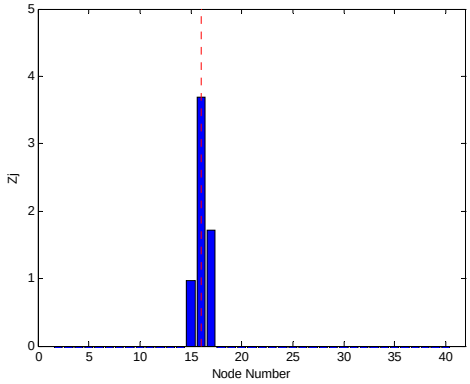

Numerical (2-Modes)

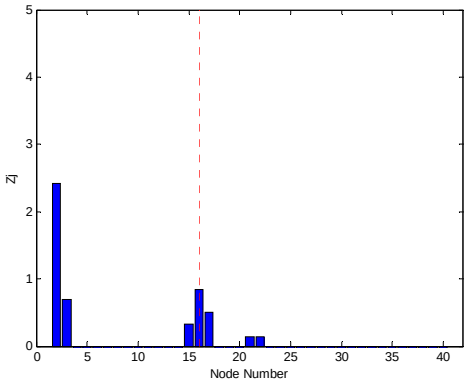

Experimental (2-Modes)

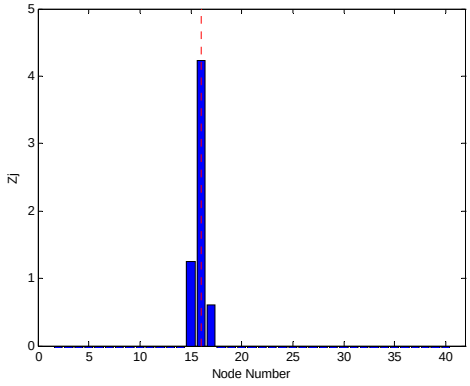

Numerical (3-Modes)

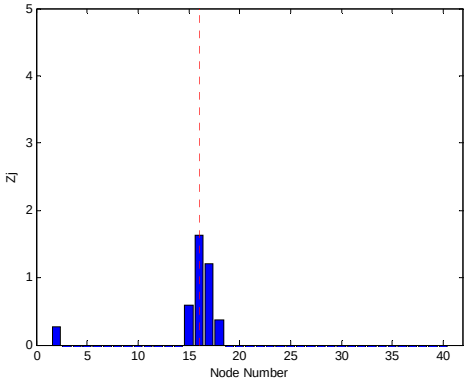

Experimental (3-Modes)

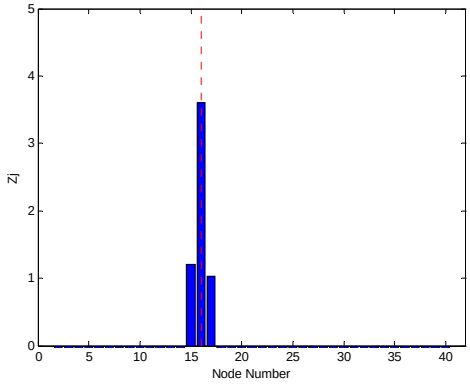

Numerical (4-Modes)

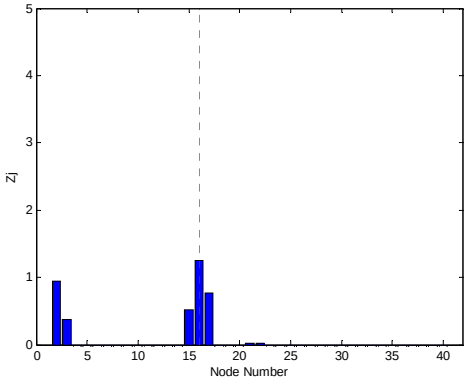

Experimental (4-Modes)

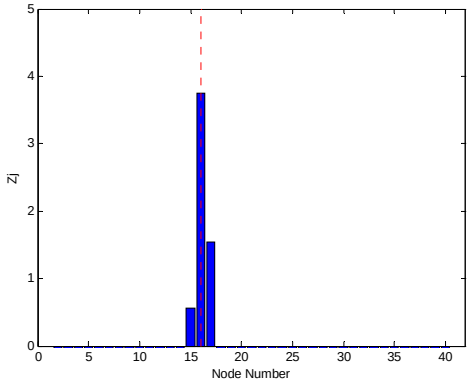

Numerical (5-Modes)

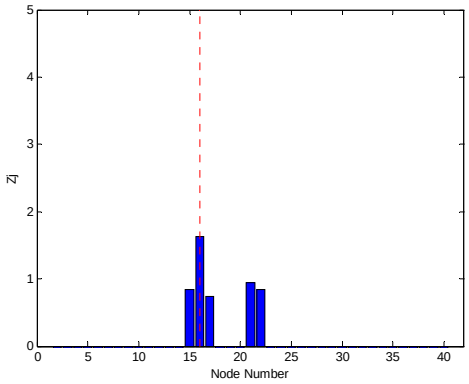

Experimental (5-Modes)

Results of Comparison between Numerical (no noise) and Experimental work (3M)

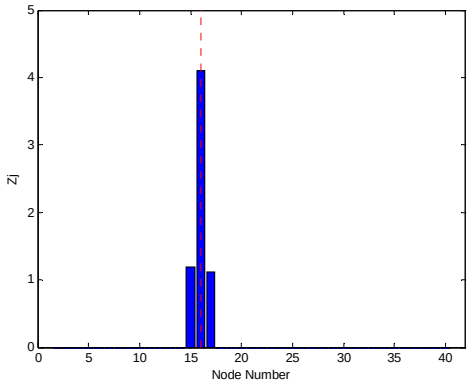

Numerical (1-Mode)

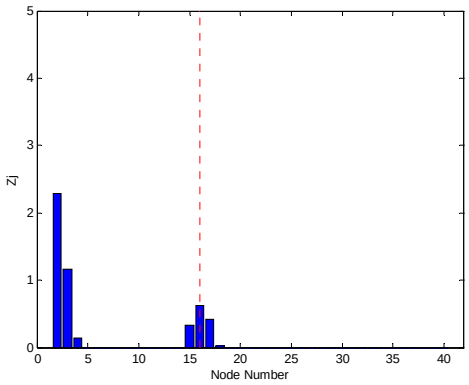

Experimental (1-Mode)

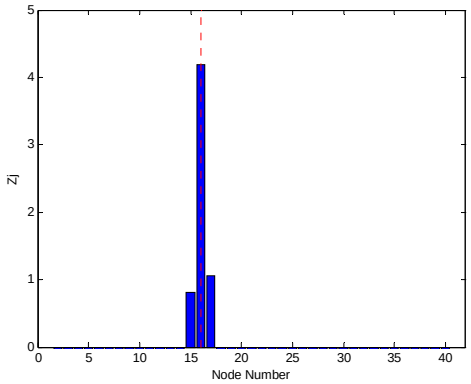

Numerical (2-Modes)

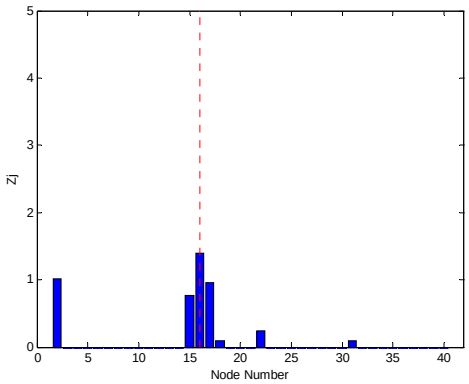

Experimental (2-Modes)

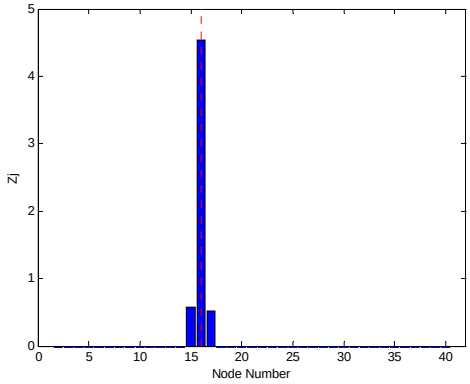

Numerical (3-Modes)

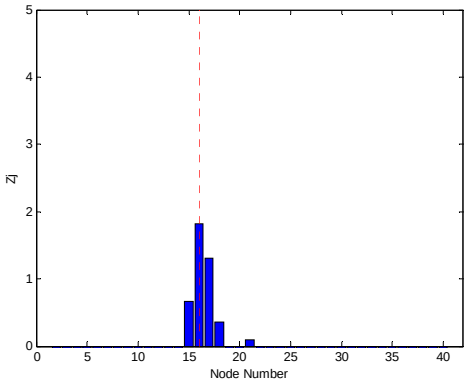

Experimental (3-Modes)

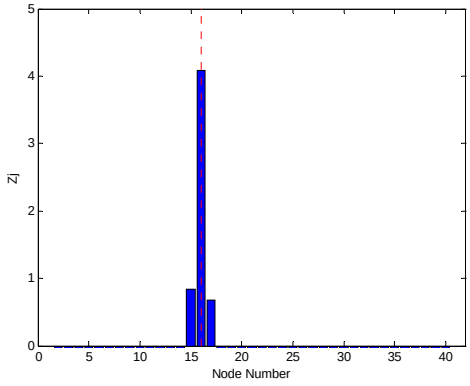

Numerical (4-Modes)

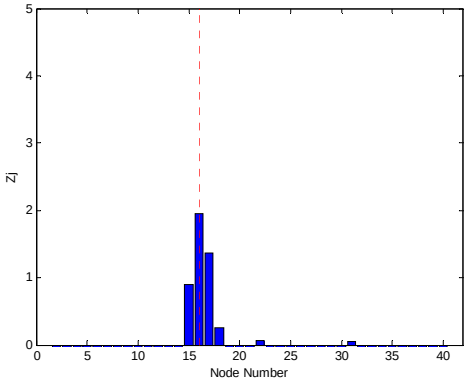

Experimental (4-Modes)

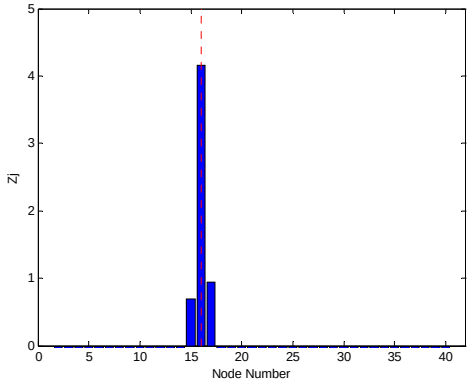

Numerical (5-Modes)

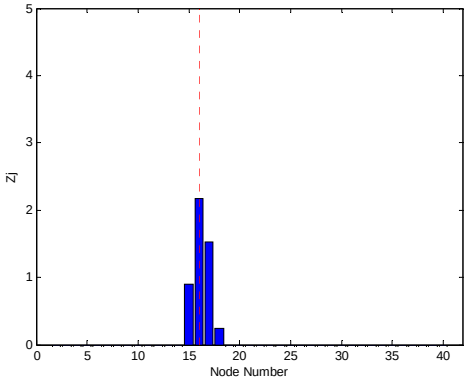

Experimental (5-Modes)

Results of Comparison between Numerical (no noise) and Experimental work (3S)

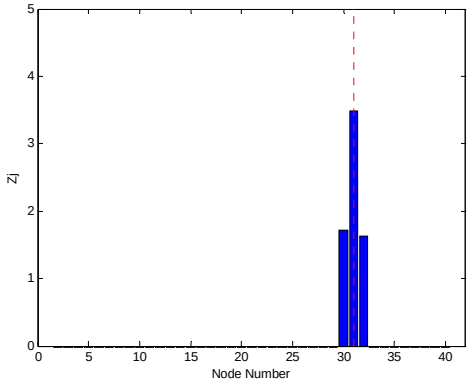

Numerical (1-Mode)

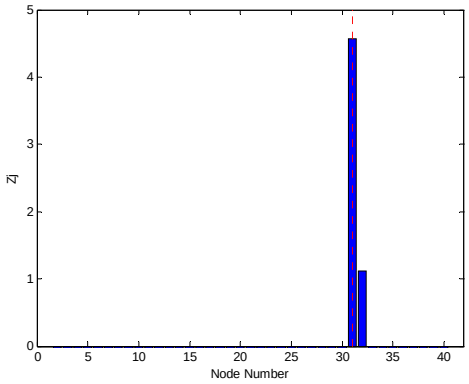

Experimental (1-Mode)

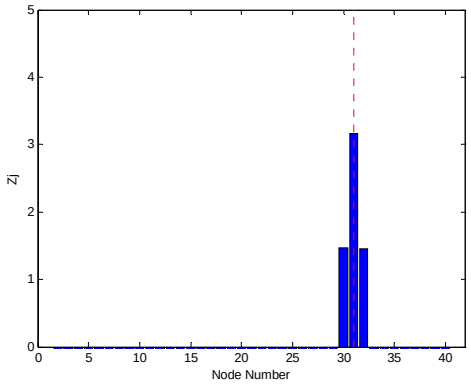

Numerical (2-Modes)

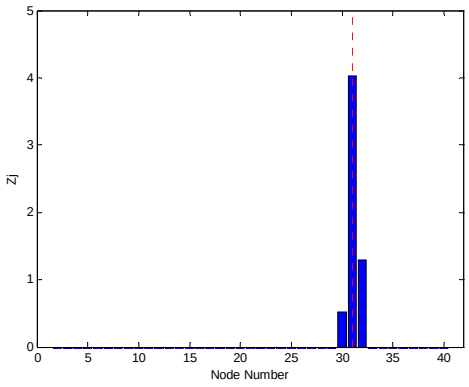

Experimental (2-Modes)

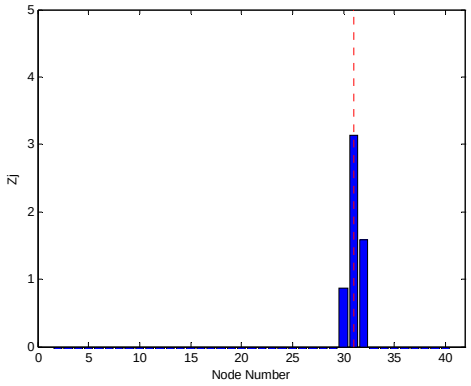

Numerical (3-Modes)

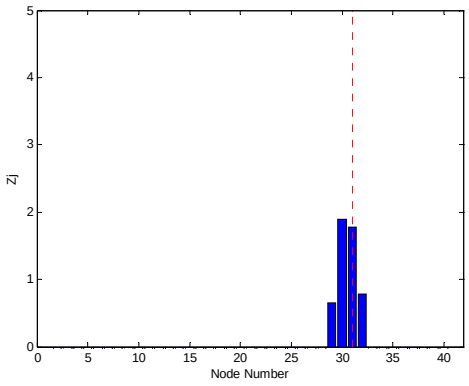

Experimental (3-Modes)

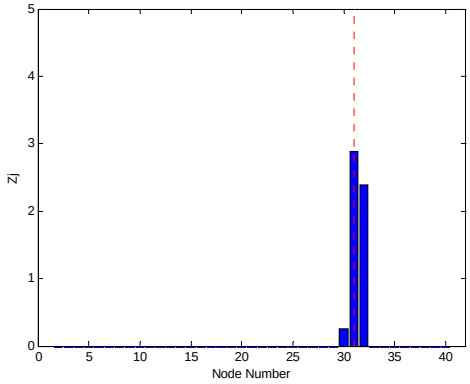

Numerical (4-Modes)

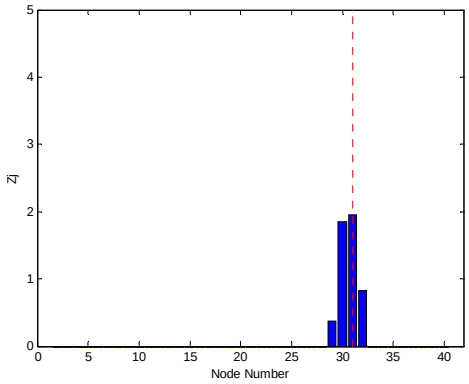

Experimental (4-Modes)

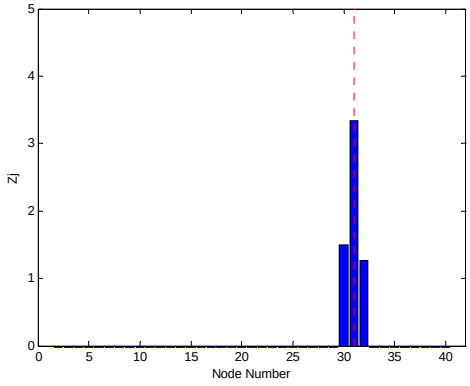

Numerical (5-Modes)

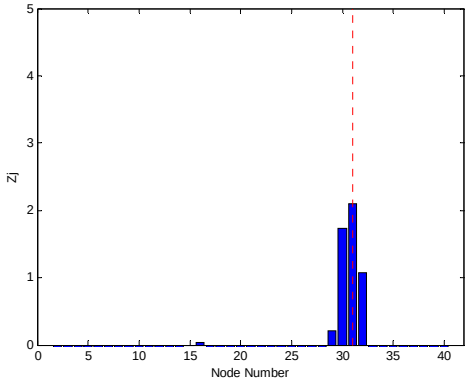

Experimental (5-Modes)

Results of Comparison between Numerical (no noise) and Experimental work (HB)

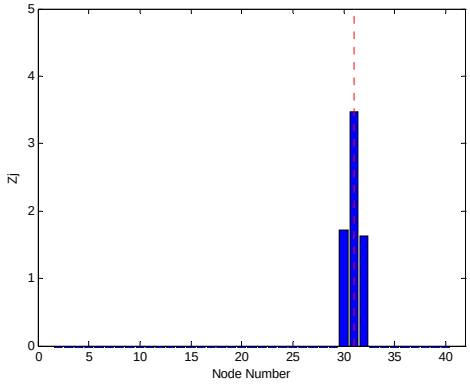

Numerical (1-Mode)

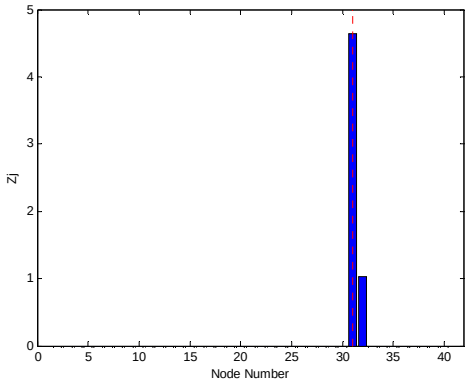

Experimental (1-Mode)

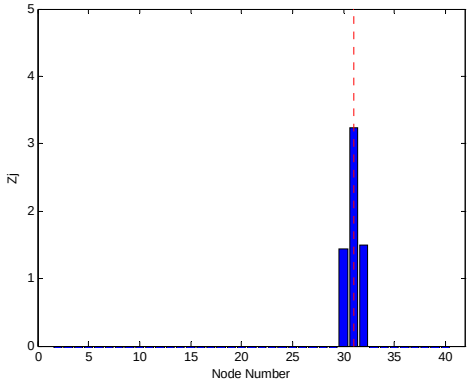

Numerical (2-Modes)

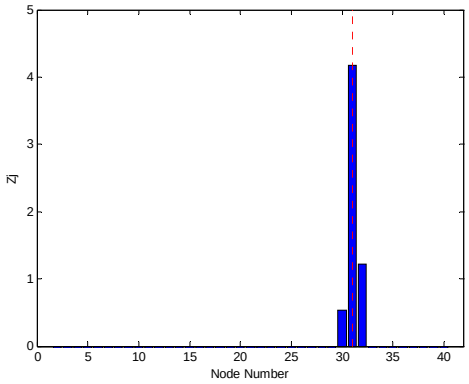

Experimental (2-Modes)

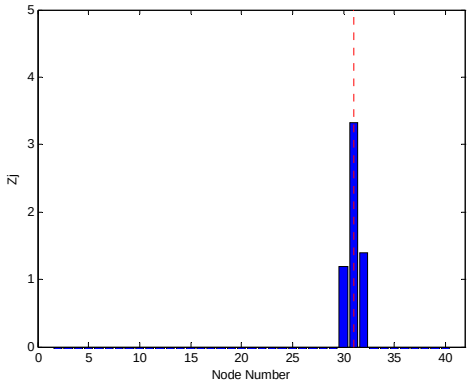

Numerical (3-Modes)

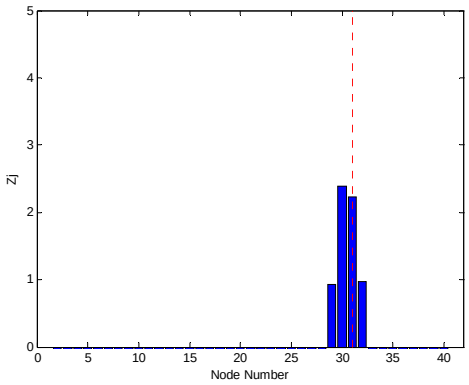

Experimental (3-Modes)

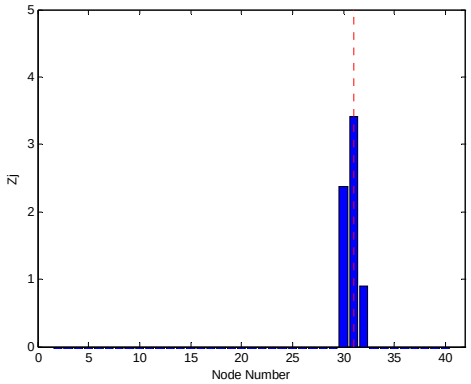

Numerical (4-Modes)

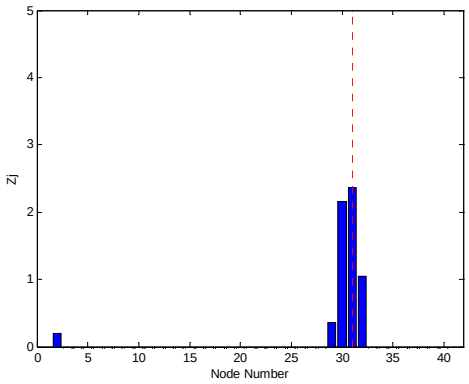

Experimental (4-Modes)

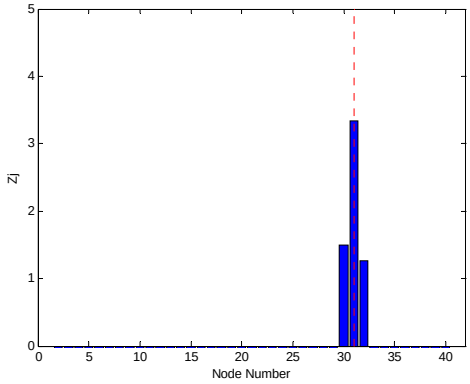

Numerical (5-Modes)

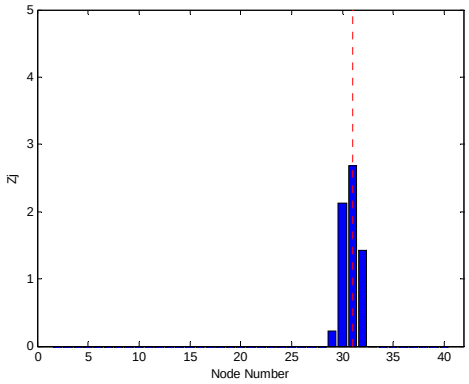

Experimental (5-Modes)

Results of Comparison between Numerical (no noise) and Experimental work (HT)

C.5 Comparison Results of Severity Estimation between Numerical (no noise) and Experimental work

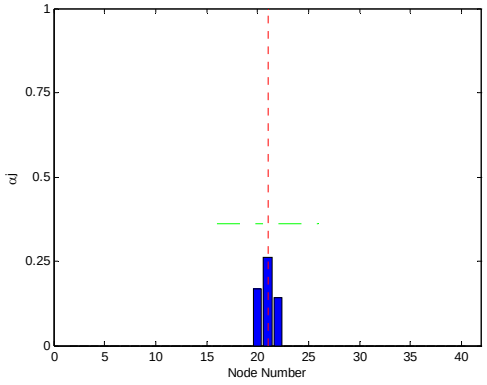

NUM (5-Modes)

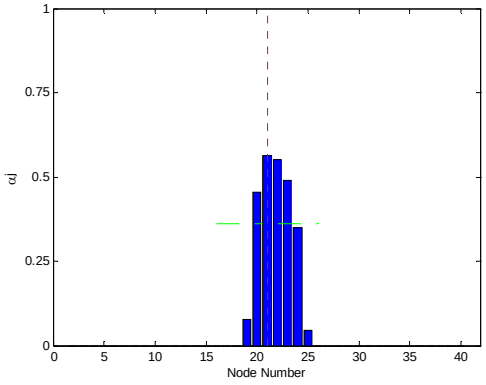

EXP (5-Modes)

Comparison Results of Severity Estimation (4L)

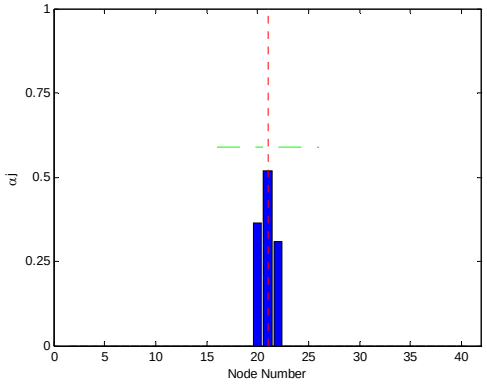

NUM (5-Modes)

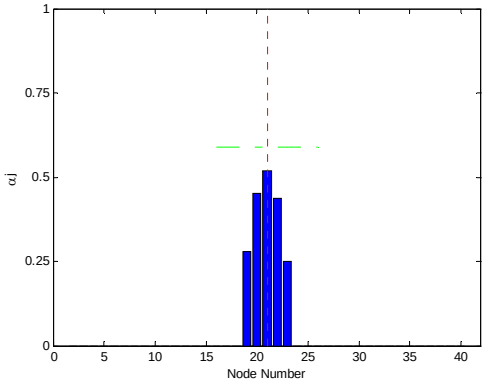

EXP (5-Modes)

Comparison Results of Severity Estimation (4M)

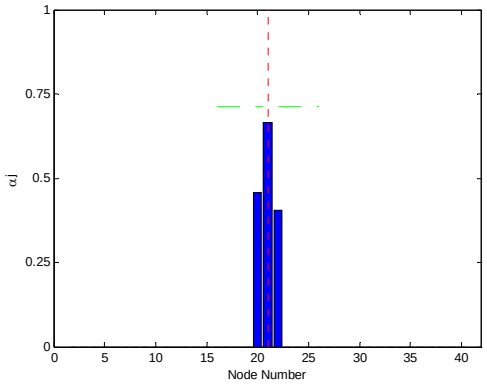

NUM (5-Modes)

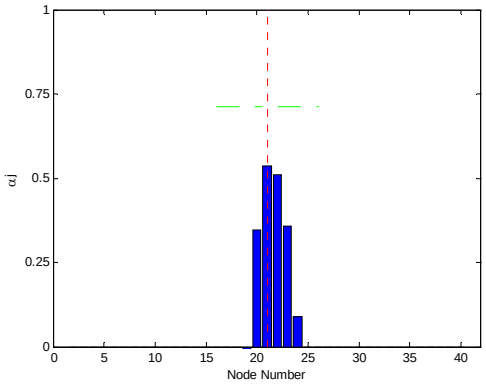

EXP (5-Modes)

Comparison Results of Severity Estimation (4S)

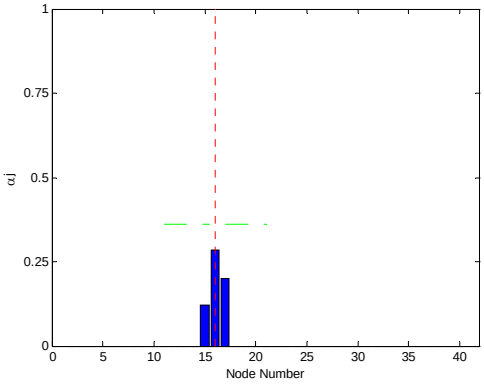

NUM (5-Modes)

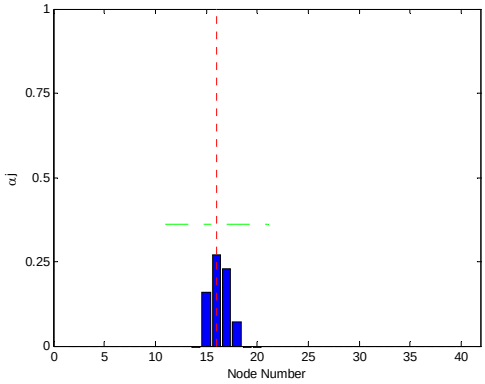

EXP (5-Modes)

Comparison Results of Severity Estimation (3L)

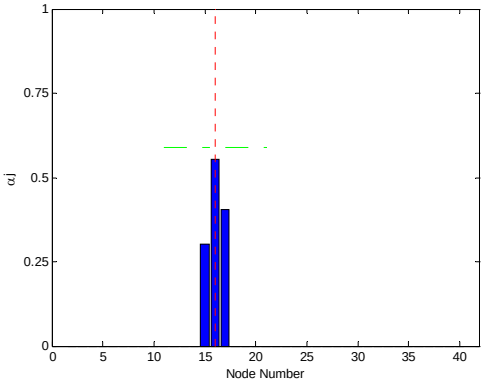

NUM (5-Modes)

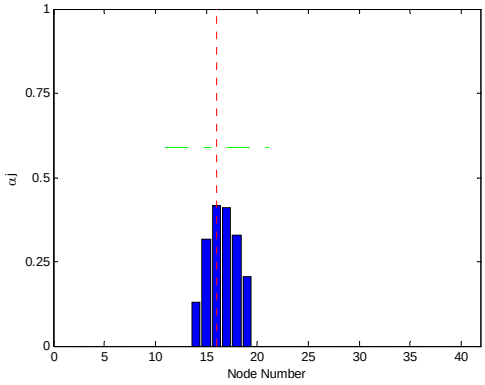

EXP (5-Modes)

Comparison Results of Severity Estimation (3M)

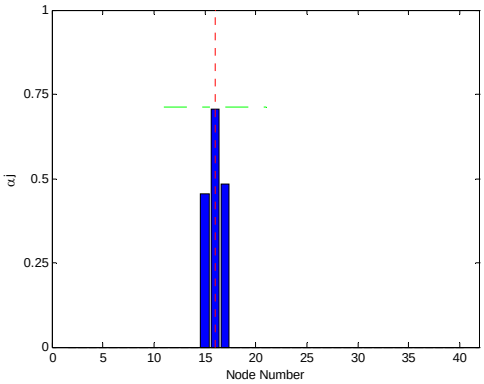

NUM (5-Modes)

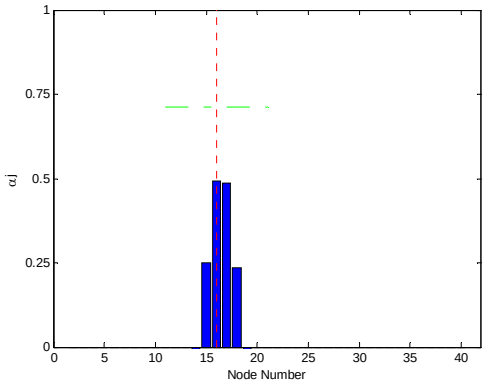

EXP (5-Modes)

Comparison Results of Severity Estimation (3S)